

# The Many Facets of Cosmic Explosions

Thesis by  
Alicia Margarita Soderberg

Advisor  
Shrinivas R. Kulkarni

In Partial Fulfillment of the Requirements  
for the Degree of  
Doctor of Philosophy



California Institute of Technology  
Pasadena, California

2007

(Defended May 18, 2007)

© 2007

Alicia Margarita Soderberg

All rights Reserved

## Acknowledgements

Arriving at Caltech in 2002, I anticipated five years of challenging and rewarding experiences - I have not been disappointed. Working with Professor Shri Kulkarni is a unique opportunity that has been both motivational and maturing. Not only did Shri encourage my independence and dedication, he also showed me (through successes and some infrequent failures) the ingredients that make up a fantastic advisor. To future Caltech graduate students, I cannot recommend a better or more unique Ph.D. advisor, and I will always consider Shri as a mentor, a colleague, and a friend.

The results presented in this thesis would not have been possible without the support of my collaborators. Most notable is Dale Frail, who mirrors Shri's enthusiasm and scientific drive, and has an uncanny knack of steering students in the scientific paths that maximize their success. Next, I thank Roger Chevalier for his mentorship and guidance in the study of radio supernovae. Among the Caltech GRB group, I thank Derek Fox, Edo Berger, Brad Cenko, and Paul Price for their dedication. I also thank Re'em Sari, Doug Leonard, Udi Nakar, and Avishay Gal-Yam for fruitful discussions, and my office mates (Dawn Erb, Naveen Reddy, Joanna Brown, and Brian Cameron) for daily companionship. Finally, I thank Ed Fenimore for first introducing me to the fascinating study of gamma-ray bursts, and Enrico Ramirez-Ruiz for mentorship at the IoA in Cambridge.

I am indebted to the people at the VLA and AOC for their continued support; in particular I thank Joan Wrobel and Barry Clark for their generous allocation of VLA time towards this thesis effort. Along this line, I also thank the CXO team (most notably, Harvey Tannenbaum) and the staff at Palomar and Keck Observatories. I am also indebted to the NSF Graduate Research Fellowship Program and the NASA Graduate Student Research Program for financial support throughout the duration of this five-year thesis effort.

Finally, none of this would have been possible without the support of Edo and my parents, Nancy and Jon, who have each pushed me to be independent and

successful from day one.

# The Many Facets of Cosmic Explosions

by

Alicia Margarita Soderberg

In Partial Fulfillment of the  
Requirements for the Degree of  
Doctor of Philosophy

## Abstract

Over the past few years, long-duration  $\gamma$ -ray bursts (GRBs), including the subclass of X-ray flashes (XRFs), have been revealed to be a rare variety of Type Ibc supernova (SN Ibc). While all these events result from the death of massive stars, the electromagnetic luminosities of GRBs and XRFs exceed those of ordinary Type Ibc SNe by many orders of magnitude. The observed diversity of stellar death corresponds to large variations in the energy, velocity, and geometry of the explosion ejecta. Using multi-wavelength (radio, optical, X-ray) observations of the nearest GRBs, XRFs, and SNe Ibc, I show that GRBs and XRFs couple at least  $\sim 10^{48}$  erg to relativistic material while SNe Ibc typically couple  $\lesssim 10^{47}$  erg to their fastest (albeit non-relativistic) outflows. Specifically, I find that less than 3% of local SNe Ibc show any evidence for association with a GRB or XRF. Interestingly, this dichotomy is not echoed by the properties of their optical SN emission, dominated by the radioactive decay of Nickel-56; I find that GRBs, XRFs, and SNe Ibc show significant overlap in their optical peak luminosity and photospheric velocities. Recently, I identified a new class of GRBs and XRFs that are under-luminous in comparison with the statistical sample of GRBs. Owing to their faint high-energy emission, these sub-energetic bursts are only detectable nearby ( $z \lesssim 0.1$ ) and are likely 10 times more common than cosmological GRBs. In comparison with local SNe Ibc and typical GRBs/XRFs, these explosions are intermediate in terms of both volumetric rate and energetics. Yet the essential physical process that causes a dying star to produce a GRB, XRF, or sub-energetic burst, and not just a SN, remains a crucial open question. Progress requires a detailed understanding of

ordinary SNe Ibc which will be facilitated with the launch of wide-field optical surveys in the near future.

# Contents

<b>1</b>	<b>Introduction and Summary</b>	<b>1</b>
1.1	Introduction: The Death of Massive Stars . . . . .	1
1.1.1	Supernovae . . . . .	1
1.1.2	Gamma-ray Bursts . . . . .	3
1.1.3	GRB 980425/SN 1998bw . . . . .	5
1.1.4	A GRB-SN Connection . . . . .	8
1.1.5	X-ray Flashes . . . . .	9
1.1.6	Off-axis GRBs and SNe Ibc . . . . .	10
1.2	Summary of the Thesis . . . . .	11
1.2.1	The Nature of GRB 980425 and a New Class of GRBs . . . . .	11
1.2.2	The Nature of X-ray Flashes . . . . .	13
1.2.3	An Optical View of the GRB-SN Connection . . . . .	15
1.2.4	A Large Radio Survey of Type Ibc Supernovae . . . . .	16
<b>I</b>	<b>The Discovery of a Class of Sub-energetic GRBs</b>	<b>20</b>
<b>1</b>	<b>Constraints on an Off-Axis jet in GRB-SN 1998bw</b>	<b>22</b>
1.1	Introduction . . . . .	23
1.2	Observations . . . . .	25
1.3	SN 1998bw: Constraining the Off-Axis Jet Model . . . . .	26
1.3.1	The $\epsilon_B - \dot{M}_{-5}/v_{w,3}$ Degeneracy . . . . .	27
1.4	Local Type Ibc Supernovae: Further Constraints . . . . .	28
1.5	Discussion and Conclusions . . . . .	29

<b>2</b>	<b>The Sub-energetic GRB 031203 as a Cosmic Analogue to GRB 980425</b>	<b>34</b>
<b>3</b>	<b>Relativistic Ejecta from XRF 060218 and the Rate of Cosmic Explosions</b>	<b>42</b>
<b>II</b>	<b>The Nature of X-ray Flashes</b>	<b>54</b>
<b>1</b>	<b>The First Redshift for an X-ray Flash: XRF 020903 at <math>z=0.25</math></b>	<b>56</b>
1.1	Introduction . . . . .	57
1.2	Observations . . . . .	58
1.2.1	Ground-based Photometry . . . . .	58
1.2.2	Ground-based Spectroscopy . . . . .	59
1.2.3	Hubble Space Telescope . . . . .	60
1.2.4	Radio Observations of XRF 020903 . . . . .	61
1.3	The Afterglow of XRF 020903 . . . . .	62
1.4	Energetics . . . . .	63
1.5	Conclusions . . . . .	64
<b>2</b>	<b>A Spectacular Radio Flare from XRF 050416a at 40 Days</b>	<b>73</b>
2.1	Introduction . . . . .	75
2.2	Observations . . . . .	76
2.2.1	Early Optical Observations . . . . .	77
2.2.2	Late-time Observations with HST . . . . .	78
2.2.3	Spectroscopic Observations . . . . .	80
2.2.4	Radio Observations . . . . .	80
2.2.5	X-ray Observations . . . . .	81
2.3	Properties of the Early Afterglow . . . . .	82
2.3.1	Preliminary Constraints . . . . .	83
2.3.2	Forward Shock Broadband Model . . . . .	85
2.3.3	Collimation of the Ejecta and Viewing Angle . . . . .	85
2.4	Properties of the Late-time Afterglow . . . . .	86
2.4.1	Off-axis Jet Emission . . . . .	87

2.4.2	Circumburst Density Variations . . . . .	88
2.4.3	Energy Injection . . . . .	89
2.4.4	An Associated Supernova . . . . .	91
2.5	Host Galaxy Properties . . . . .	92
2.6	Is XRF 050416a a Short Burst? . . . . .	94
2.7	Discussion and Conclusions . . . . .	96
 <b>III An Optical View of the GRB-SN Connection</b>		<b>112</b>
 <b>1 An HST Search for Supernovae Accompanying X-ray Flashes</b>		<b>114</b>
1.1	Introduction . . . . .	116
1.2	Supernova Light-curve Synthesis . . . . .	117
1.2.1	SN 1998bw . . . . .	118
1.2.2	SN 1994I . . . . .	118
1.2.3	SN 2002ap . . . . .	118
1.3	Hubble Space Telescope XRF-SN Search . . . . .	119
1.3.1	XRF 020903 . . . . .	121
1.3.2	XRF 040701 . . . . .	123
1.3.3	XRF 040812 . . . . .	126
1.3.4	XRF 040916 . . . . .	128
1.4	A Summary of XRF-SN Searches . . . . .	130
1.5	Discussion . . . . .	133
 <b>2 An HST Study of GRB-SNe</b>		<b>148</b>
2.1	Introduction . . . . .	149
2.2	Supernova Light-curve Synthesis . . . . .	151
2.3	Hubble Space Telescope GRB-SN Search . . . . .	151
2.3.1	GRB 040924 . . . . .	152
2.3.2	GRB 041006 . . . . .	155
2.4	Discussion . . . . .	159

<b>IV</b>	<b>A Large Radio Survey of Type Ibc Supernovae</b>	<b>177</b>
<b>1</b>	<b>The Radio and X-ray Luminous Type Ibc Supernova 2003L</b>	<b>179</b>
1.1	Introduction . . . . .	180
1.2	Radio Observations of SN 2003L . . . . .	181
1.2.1	Very Large Array Data . . . . .	181
1.2.2	Very Long Baseline Array Data . . . . .	182
1.3	X-ray Observations with Chandra . . . . .	183
1.4	Preliminary Constraints . . . . .	184
1.5	Internal Synchrotron Self-absorption . . . . .	186
1.5.1	Hydrodynamical Evolution of the Ejecta . . . . .	187
1.5.2	SSA Model Fit for SN 2003L . . . . .	188
1.5.3	Physical Parameters . . . . .	190
1.6	External Absorption . . . . .	192
1.6.1	Basic FFA Model . . . . .	192
1.6.2	Complex FFA Model . . . . .	193
1.7	Modeling the X-ray emission . . . . .	194
1.7.1	Synchrotron Emission . . . . .	194
1.7.2	Thermal Bremsstrahlung Emission . . . . .	195
1.7.3	Inverse Compton Cooling . . . . .	195
1.8	Discussion and Conclusions . . . . .	196
1.9	The Synchrotron Self-absorption Model . . . . .	198
1.9.1	Physical Assumptions . . . . .	199
1.9.2	Emission Spectrum . . . . .	200
1.9.3	Temporal and Spectral Evolution . . . . .	202
<b>2</b>	<b>The Radio and X-ray Luminous SN 2003bg</b>	<b>215</b>
2.1	Introduction . . . . .	216
2.2	Observations . . . . .	218
2.2.1	Very Large Array Data . . . . .	219
2.2.2	X-ray Observations with Chandra . . . . .	222

2.3	Preliminary Constraints . . . . .	223
2.4	Synchrotron Self-absorption Model . . . . .	226
2.4.1	Hydrodynamical Evolution of the Ejecta . . . . .	227
2.5	SSA Model Fit for SN 2003bg . . . . .	228
2.5.1	The Synchrotron Self-absorption Peak . . . . .	228
2.5.2	Subsequent Light-curve Variations . . . . .	230
2.6	Radio Polarization . . . . .	232
2.7	Modeling the X-ray emission . . . . .	233
2.7.1	Synchrotron Emission . . . . .	233
2.7.2	Thermal Bremsstrahlung Emission . . . . .	234
2.7.3	Inverse Compton Scattering . . . . .	235
2.8	Radio Supernovae and CSM Density Variations . . . . .	236
2.8.1	A Comparison of SN 2003bg and SN 2001ig . . . . .	238
2.9	The Progenitors of SNe 2003bg and 2001ig . . . . .	240
2.10	Conclusions . . . . .	241
<b>3</b>	<b>Strong Constraints on Off-Axis GRBs for 68 SNe Ibc</b>	<b>259</b>
3.1	Introduction . . . . .	260
3.2	Radio Observations . . . . .	262
3.2.1	Type Ic SN 2003jd . . . . .	262
3.2.2	Late-time Data on Local Type Ibc Supernovae . . . . .	263
3.3	Off-Axis Models for Gamma-ray Bursts . . . . .	263
3.3.1	An Analytic Approach . . . . .	263
3.3.2	A Semi-analytic Model . . . . .	265
3.4	SN 2003jd: Constraints on the Off-axis Jet . . . . .	266
3.5	Local Type Ibc Supernovae: Further Constraints . . . . .	267
3.6	Discussion and Conclusions . . . . .	269
<b>4</b>	<b>The Radio Properties of Type Ibc Supernovae</b>	<b>284</b>
4.1	Introduction . . . . .	284
4.2	A Large Radio Survey of SNe Ibc: The Sample . . . . .	285

4.2.1	SNe Ibc: One Class or Two? . . . . .	286
4.2.2	Observation Details . . . . .	287
4.3	The Radio Properties of SNe Ibc . . . . .	288
4.4	Constraints on the Ejecta Velocity and Kinetic Energy . . . . .	288
4.5	Constraints on the Mass Loss Rate . . . . .	290
4.6	Conclusions . . . . .	290
<b>5</b>	<b>Future Directions</b>	<b>325</b>
5.1	The Progenitors of SNe Ibc . . . . .	325
5.2	Large-scale Environment . . . . .	327
5.3	Unique Diagnostics of Ejecta Properties . . . . .	328
5.4	Conclusions . . . . .	331
	<b>Bibliography</b>	<b>333</b>

## List of Figures

1.1	Radial outflow from SN explosions . . . . .	6
1.2	Optical and radio/X-ray constraints on the ejecta. . . . .	7
1.3	Relativistic energy yields for GRBs. . . . .	12
1.4	HST imaging of XRF 020903. . . . .	14
1.5	Peak optical magnitudes for GRB/XRF-SNe and local SNe Ibc. . . . .	16
1.6	Radio observations of all local SNe Ibc . . . . .	17
1.7	Kinetic energy of the fastest ejecta for GRBs and SNe Ibc. . . . .	19
1.1	The radio light-curve of GRB-SN 1998bw. . . . .	31
1.2	Constraints on an off-axis jet in GRB-SN 1998bw. . . . .	32
1.3	Constraints on off-axis GRB jets in local SNe Ibc. . . . .	33
2.1	Radio light-curves of GRB 031203. . . . .	40
2.2	Two-dimensional energy plot for cosmic explosions. . . . .	41
3.1	Radio and X-ray light-curves of XRF 060218. . . . .	49
3.2	Radio observations of SNe Ibc, GRBs, and XRFs. . . . .	50
3.3	Energy vs. velocity for GRBs, XRFs, and SNe Ibc. . . . .	51
1.1	Discovery of the first optical afterglow of an XRF. . . . .	66
1.2	Optical afterglow lightcurve. . . . .	68
1.3	Host galaxy spectrum of XRF 020903. . . . .	69
1.4	HST imaging of XRF 020903. . . . .	70
1.5	Radio light-curve of XRF 020903. . . . .	71
1.6	Histogram of GRB radio afterglow luminosities. . . . .	72

2.1	Discovery of the optical afterglow of XRF 050416a. . . . .	105
2.2	Optical/NIR light-curves of the afterglow of XRF 050416a. . . . .	106
2.3	Photometric spectrum of XRF 050416a. . . . .	107
2.4	<i>HST/ACS</i> images of XRF 050416a. . . . .	108
2.5	Optical spectrum of the host galaxy of XRF 050416a. . . . .	109
2.6	Radio light-curves of XRF 050416a. . . . .	110
2.7	X-ray light-curve of XRF 050416a. . . . .	111
1.1	<i>HST/ACS</i> imaging of XRF 020903. . . . .	137
1.2	Constraints on a supernova associated with XRF 020903. . . . .	138
1.3	Host galaxy spectrum for XRF 020903. . . . .	139
1.4	<i>HST/ACS</i> imaging of XRF 040701. . . . .	140
1.5	Constraints on an optical transient associated with XRF 040701. . . . .	141
1.6	<i>HST/ACS</i> imaging of XRF 040812. . . . .	142
1.7	Constraints on a supernova associated with XRF 040812. . . . .	143
1.8	<i>HST/ACS</i> imaging of XRF 040916. . . . .	144
1.9	Constraints on a supernova associated with XRF 040916. . . . .	145
1.10	Constraints on SNe associated with XRFs. . . . .	146
1.11	Peak optical magnitudes for SNe Ibc, GRBs, and XRFs. . . . .	147
2.1	<i>HST/ACS</i> observations of GRB 040924. . . . .	171
2.2	Constraints on a supernova associated with GRB 040924. . . . .	172
2.3	Host galaxy spectrum of GRB 041006. . . . .	173
2.4	<i>HST/ACS</i> imaging of GRB 041006. . . . .	174
2.5	Constraints on a supernova associated with GRB 041006. . . . .	175
2.6	Peak optical magnitudes for ordinary SNe Ibc and GRB-SNe. . . . .	176
1.1	Optical and radio emission from SN 2003L at $t \sim 35$ days. . . . .	208
1.2	Radio light-curves for SN 2003L. . . . .	209
1.3	Spectral indices for the radio emission of SN 2003L. . . . .	210
1.4	VLBA radio map of SN 2003L. . . . .	211

1.5	<i>Chandra</i> X-ray image of SN 2003L at $t \approx 40$ days. . . . .	212
1.6	Physical parameters for SN 2003L. . . . .	213
1.7	FFA fits for the SN 2003L radio emission. . . . .	214
2.1	Optical and radio emission from SN 2003bg. . . . .	251
2.2	Radio light-curves of SN 2003bg. . . . .	252
2.3	Model light-curves for SN 2003bg. . . . .	253
2.4	Spectral indices for the radio emission of SN 2003bg. . . . .	254
2.5	Radio spectra for SN 2003bg. . . . .	255
2.6	X-ray spectra for SN 2003bg. . . . .	256
2.7	SSA physical parameters for SN 2003bg. . . . .	257
2.8	Comparison of SN 2003bg and SN 2001ig. . . . .	258
3.1	Constraints on off-axis jets in SNe Ibc. . . . .	279
3.2	Constraints on an off-axis GRB associated with SN 2003jd. . . . .	280
3.3	Constraints on $E_{51}$ and $A_*$ for putative off-axis GRBs. . . . .	281
3.4	Regions of $E_{51} - A_*$ parameter space ruled out for off-axis GRBs. . . . .	282
3.5	Constraints on the fraction of SNe Ibc with off-axis GRBs. . . . .	283
4.1	Statistics for SNe Ibc. . . . .	318
4.2	Radio observations of all local SNe Ibc . . . . .	319
4.3	Peak radio luminosity distribution for SNe Ibc. . . . .	320
4.4	Radio luminosity vs peak time for SNe Ibc . . . . .	321
4.5	Kinetic energy vs ejecta velocity for SNe Ibc . . . . .	322
4.6	Mass loss rates for SNe Ibc progenitors . . . . .	323
4.7	Mass loss rates vs ejecta velocity for SNe Ibc . . . . .	324
5.1	Luminosity and metallicity of GRB, XRF, and SNe Ibc host galaxies. . . . .	326
5.2	Host galaxy of SDSS SN 2005hm . . . . .	328
5.3	Radio luminosity of SNe Ibc vs distance . . . . .	330
5.4	X-ray luminosities for nearby GRBs, XRFs, and SNe Ibc . . . . .	331

## List of Tables

2.1	Radio Observations of GRB 031203 . . . . .	39
3.1	Radio Observations of XRF 060218 . . . . .	48
1.1	Optical Observations of the Afterglow of XRF 020903. . . . .	66
1.2	Radio Observations of the Afterglow of XRF 020903. . . . .	67
2.1	Ground-based Optical and NIR Observations of XRF 050416a . . .	100
2.1	Ground-based Optical and NIR Observations of XRF 050416a . . .	101
2.2	<i>HST/ACS</i> Observations of XRF 050416a . . . . .	102
2.3	Spectroscopic lines for XRF 050416a . . . . .	103
2.4	Radio Observations of XRF 050416a . . . . .	104
1.1	<i>HST</i> Observation Log . . . . .	135
1.1	<i>HST</i> Observation Log . . . . .	136
2.1	<i>HST</i> Observation Log . . . . .	162
2.2	Palomar 60-inch <i>R</i> -band Observations of GRB 040924 . . . . .	163
2.2	Palomar 60-inch <i>R</i> -band Observations of GRB 040924 . . . . .	164
2.3	<i>SSO</i> 40-inch and 2.3-meter Observations of GRB 041006 . . . . .	165
2.4	GRB 041006 Spectroscopic Lines . . . . .	166
2.5	Peak Magnitudes and $^{56}\text{Ni}$ Masses for GRB- and XRF-associated SNe167	
2.5	Peak Magnitudes and $^{56}\text{Ni}$ Masses for GRB- and XRF-associated SNe168	
2.6	Peak Magnitudes and $^{56}\text{Ni}$ Masses for Nearby SNe Ibc . . . . .	169
2.6	Peak Magnitudes and $^{56}\text{Ni}$ Masses for Nearby SNe Ibc . . . . .	170

1.1	VLA Radio Flux Density Measurements of SN 2003L . . . . .	205
1.1	VLA Radio Flux Density Measurements of SN 2003L . . . . .	206
1.1	VLA Radio Flux Density Measurements of SN 2003L . . . . .	207
2.1	VLA Radio Flux Density Measurements of SN 2003bg . . . . .	244
2.1	VLA Radio Flux Density Measurements of SN 2003bg . . . . .	245
2.1	VLA Radio Flux Density Measurements of SN 2003bg . . . . .	246
2.1	VLA Radio Flux Density Measurements of SN 2003bg . . . . .	247
2.2	Spectral Models for <i>Chandra</i> ACIS-S Observations of SN 2003bg . . . . .	248
2.3	Radio Light-curve Peaks for SN 2003bg . . . . .	249
2.4	Radio Supernovae with Strong Light-curve Variations . . . . .	250
3.1	Radio Observations of SN 2003jd . . . . .	271
3.2	Late-time Radio Observations of Type Ibc Supernovae . . . . .	272
3.2	Late-time Radio Observations of Type Ibc Supernovae . . . . .	273
3.2	Late-time Radio Observations of Type Ibc Supernovae . . . . .	274
3.2	Late-time Radio Observations of Type Ibc Supernovae . . . . .	275
3.2	Late-time Radio Observations of Type Ibc Supernovae . . . . .	276
3.2	Late-time Radio Observations of Type Ibc Supernovae . . . . .	277
3.3	Physical Parameters for GRBs . . . . .	278
4.1	Radio Observations of SNe Ibc . . . . .	292
4.1	Radio Observations of SNe Ibc . . . . .	293
4.1	Radio Observations of SNe Ibc . . . . .	294
4.1	Radio Observations of SNe Ibc . . . . .	295
4.1	Radio Observations of SNe Ibc . . . . .	296
4.1	Radio Observations of SNe Ibc . . . . .	297
4.1	Radio Observations of SNe Ibc . . . . .	298
4.1	Radio Observations of SNe Ibc . . . . .	299
4.1	Radio Observations of SNe Ibc . . . . .	300
4.1	Radio Observations of SNe Ibc . . . . .	301

4.1	Radio Observations of SNe Ibc . . . . .	302
4.1	Radio Observations of SNe Ibc . . . . .	303
4.1	Radio Observations of SNe Ibc . . . . .	304
4.1	Radio Observations of SNe Ibc . . . . .	305
4.1	Radio Observations of SNe Ibc . . . . .	306
4.1	Radio Observations of SNe Ibc . . . . .	307
4.1	Radio Observations of SNe Ibc . . . . .	308
4.1	Radio Observations of SNe Ibc . . . . .	309
4.1	Radio Observations of SNe Ibc . . . . .	310
4.1	Radio Observations of SNe Ibc . . . . .	311
4.1	Radio Observations of SNe Ibc . . . . .	312
4.2	Radio Observations of SNe Ibc (cont') . . . . .	313
4.3	Radio Observations of SNe Ibc (cont') . . . . .	314
4.4	Radio Observations of SNe Ibc (cont') . . . . .	315
4.5	Peak Radio Flux Densities of SNe Ibc . . . . .	316
4.5	Peak Radio Flux Densities of SNe Ibc . . . . .	317

# Chapter 1

## Introduction and Summary

### 1.1 Introduction: The Death of Massive Stars

It is generally accepted that the most massive stars in the Universe ( $M \gtrsim 10 M_{\odot}$ ) end their lives in a cataclysmic explosion, a supernova (SN), that expels metals and injects energy into the interstellar medium (ISM) of their host galaxies (see Heger et al. 179 for a review). These explosions also give birth to the most extreme compact objects: neutron stars (NS, including pulsars and magnetars) and black holes (BH). Thus, an understanding of the conditions under which massive stars die sheds light on the dynamics of the ISM, galaxy enrichment, the evolution of single and binary stars, and the observed diversity of compact objects. In this PhD thesis, I investigate the nature and diversity of the most massive stellar explosions, including supernovae, gamma-ray bursts, and X-ray flashes.

#### 1.1.1 Supernovae

While the bulk energy released in SN explosions,  $\sim 10^{53}$  erg, is carried away invisibly by neutrinos, a remaining  $10^{51}$  erg of kinetic energy powers the observed emission. Dominated by the radioactive decay of Nickel-56 (half-life of 6.1 days) synthesized in the explosion, the emission peaks on a timescale of days to weeks. The observed spectrum is thermal and peaks in the optical band owing to an electron population thermalized by gamma-rays trapped within the ejecta. With

a maximum luminosity upwards of  $10^{41}$  erg  $s^{-1}$ , supernovae (SNe) outshine their host galaxies for a brief period of time after the explosion. Their strong optical emission and variability timescale are well matched to dedicated search campaigns that monitor nearby ( $d \lesssim 200$  Mpc) galaxies every night in search of new SNe. Thanks to these efforts we now know that SNe occur roughly once per hundred years per galaxy (64). As the efficiency and sensitivity of these searches improves, an ever-increasing number of SNe are discovered each year, with just 15 in 1950 compared to the the current record of 554 in 2006<sup>1</sup>.

With the increase in number of SN discoveries, differences in the optical light-curves and spectral properties were revealed. These distinguishing characteristics enabled several classes of SNe to be identified (see Filippenko 113 for a review). Hydrogen-poor SNe of Type Ia represent the majority of all newly discovered SNe (64) and, unlike all other Types, are believed to result from the thermonuclear explosion of a white dwarf. The remaining SNe are core-collapse explosions, produced by the gravitational collapse of a massive star, with Type IIP SNe being the most common (64). The progenitors of SNe IIP have been directly identified to be red supergiants based on their detection in pre-explosion images (350).

Representing just  $\sim 15\%$  of all new discoveries, Type Ibc supernovae<sup>2</sup> (SNe Ibc) are perhaps the least understood of all the SN types. SNe Ibc were formally recognized as a peculiar class of explosions in the mid 1980s (429). Early indications, especially the lack of Hydrogen and weak or absent Helium features in their optical spectra, suggested a thermonuclear explosion like SNe Ia (108). However, it was noted that they lack a deep 6150 Å Silicon absorption trough, considered the hallmark of Type Ia explosions. SNe Ibc were further differentiated from SNe Ia by their observed strong radio emission ( $L_{\text{rad}} \sim 10^{28}$  ergs $^{-1}$  Hz $^{-1}$ ), produced by the ejecta interacting with a dense circumstellar medium (CSM), most likely

---

<sup>1</sup><http://www.supernovae.net/snimages/>

<sup>2</sup>It has been suggested that the class may be further divided based on the presence and strength of helium absorption features to Type Ib (He-rich) and Ic (He-poor). However, both the observational and physical motivation for this sub-division remain heavily debated (see Part IV), and thus I refer to them collectively as SNe Ibc throughout this thesis.

expelled by a massive progenitor (374). The eventual realization that SNe Ibc are core-collapse explosions from stripped-envelope progenitors was facilitated by a statistical analysis of their host galaxy properties. Unlike SNe Ia, SNe Ibc always reside in star-forming galaxies and are highly concentrated towards star-forming regions (spiral arms, HII regions) (407).

These observational characteristics quickly led to a general consensus that SNe Ibc are produced by two possible progenitor systems: (i) isolated, massive Wolf-Rayet stars (WR;  $M \gtrsim 20 M_{\odot}$ ) stripped by radiation pressure driven winds (13, 438), and/or (ii) lower mass ( $M \sim 8 - 20 M_{\odot}$ ) stars stripped of their Hydrogen-envelope by a close binary companion (429, 295). Unlike SNe IIP, the progenitors of SNe Ibc have not yet been identified in pre-explosion images nor are the existing archival data (e.g., Smartt et al. 351) sufficiently deep to establish which of these two progenitor models dominates the observed population. In parallel efforts, it has been shown that a large fraction ( $\sim 30\%$ ) of massive stars are observed in close binary systems (209), but the rates are not sufficiently constraining to rule out the single-star progenitor model for SNe Ibc.

In an parallel effort, it was soon realized that these “naked” SNe are of specific interest in the study of massive stars (evolution, death) since they offer an unhampered view of the explosion. Yet despite this initial progress, the rarity ( $\sim 10^4 \text{ Gpc}^{-3} \text{ yr}^{-1}$ ; Dahlen et al. 95) and heterogeneity (242) of SNe Ibc did not motivate strong observational programs. As a result, interest waned for the next decade, and the nature of Type Ibc SN progenitors (single vs. binary) remained an open question.

### 1.1.2 Gamma-ray Bursts

In an interesting turn of fate, SNe Ibc have recently enjoyed an explosion of renewed interest thanks to their association with gamma-ray bursts (GRBs). Since their discovery in the early 1970s, the origin of GRBs has been heavily debated (see Piran 293 for a review). With an observed rate of roughly  $0.5 \text{ Gpc}^{-3} \text{ yr}^{-1}$  (346), GRBs are non-thermal bursts of gamma-ray photons at energies of a few

hundred keV, with durations of a few seconds and rapid variability,  $\delta t/t \ll 1$ . These observational properties imply a relativistic outflow powered by a central engine (accreting compact object) which injects energy into the system for many dynamical timescales.

An extragalactic origin for GRBs was first suggested by their isotropic distribution on the sky as observed with the BATSE instrument onboard the Compton Gamma-ray Observatory (CGRO). (255). Thanks to the arcminute localization capability of the BeppoSAX satellite, the cosmological origin of GRBs was confirmed in 1997 with the detection of long-wavelength counterparts (“afterglows”; Costa et al. 90) and their spatial coincidence with intermediate redshift ( $z \sim 1$ ) galaxies (256).

A decade earlier, Paczyński (274) had predicted an extragalactic origin for GRBs, noting that the implied gamma-ray energy release would be roughly comparable to the kinetic energy of core-collapse supernovae. However, as the sample of GRB redshifts increased, the implied gamma-ray energies climbed as high as  $10^{54}$  erg, a serious challenge to existing GRB models. The realization that GRBs are produced in highly collimated jets (opening angles,  $\langle \theta_j \rangle \approx 5$  deg; Rhoads 313), led to the discovery that the beaming-corrected gamma-ray energies are tightly clustered around  $10^{51}$  erg and are thus consistent with the energetics of core-collapse SNe (278, 133).

These observations could be adequately explained in the framework of the “collapsar model” in which a rapidly rotating massive star collapses to a black hole fed by an accretion disk; relativistic jets are then launched along the poles and escape the stellar surface, which has been stripped prior to explosion (234). Turbulence within the jets leads to the observed short pulses of gamma-ray emission while a disk wind disrupts the star in a mildly-aspherical explosion. An optical SN component is seen if the the disk wind is Nickel-rich. With the success of the collapsar model, it became clear that GRBs and core-collapse SNe both represent channels of massive stellar death. However, at the time there was little observational evidence linking the progenitors of GRBs to those of SNe.

### 1.1.3 GRB 980425/SN 1998bw

With the temporal and spatial coincidence of GRB 980425 with Type Ibc SN 1998bw at 36 Mpc came the first observational support for a GRB-SN connection. Yet it was the exceptionally luminous radio emission of SN 1998bw that firmly established this association. While optical SN emission traces the slowest ejecta to which the bulk of the kinetic energy is coupled, radio observations of SNe probe the fastest ejecta as they expand into and accelerate particles in the CSM (Figure 1.1). Hydrodynamic collapse predicts that the coupling of kinetic energy,  $E_K$ , to velocity within the homologously expanding ejecta is quite steep,  $E_K \propto v^{-5.2}$  (388), up to a maximum velocity of  $\sim 0.4c$  (22, 73), such that only  $\sim 0.01\%$  of the kinetic energy is typically coupled to the fastest material (Figure 1.2). The radio emission is characterized by a non-thermal synchrotron spectrum with a spectral peak initially within the radio band and cascading to lower frequencies as the outflow expands.

Based on a simple analysis of the radio data for SN 1998bw, Kulkarni et al. (216) showed that mildly-relativistic expansion velocities (Lorentz factor,  $\Gamma \sim 3$ ) were required for the brightness temperature,  $T_B = c^2 F_\nu / (2\pi k \theta^2 \nu^2)$ , to not violate the inverse Compton catastrophe limit,  $T_B \sim 10^{12}$  K (309). Here,  $F_\nu$  is the radio flux density at frequency  $\nu$  and  $\theta$  is the angular diameter of the radio source on the sky. Moreover, assuming the post-shock energy density was in equipartition between relativistic electrons and magnetic fields, it was argued that a kinetic energy of  $E_K \sim 10^{49}$  erg was coupled to the relativistic ejecta (216, 226). Together, the power and speed implied by the radio data required the presence of a central engine to drive the SN explosion.

The radio emission from SN 1998bw was (and still is; see Part IV) extraordinary in comparison with other radio SNe in the local Universe (e.g., SN 1987A Ball et al. 7). Similarly, a long-lived and luminous X-ray transient was detected in coincidence with the radio source, which is unmatched by X-ray observations of other core-collapse explosions. Finally, the optical lightcurve was as luminous as a SN Ia ( $M_V \approx -19.3$  mag; Galama et al. 151), showing evidence for exceedingly

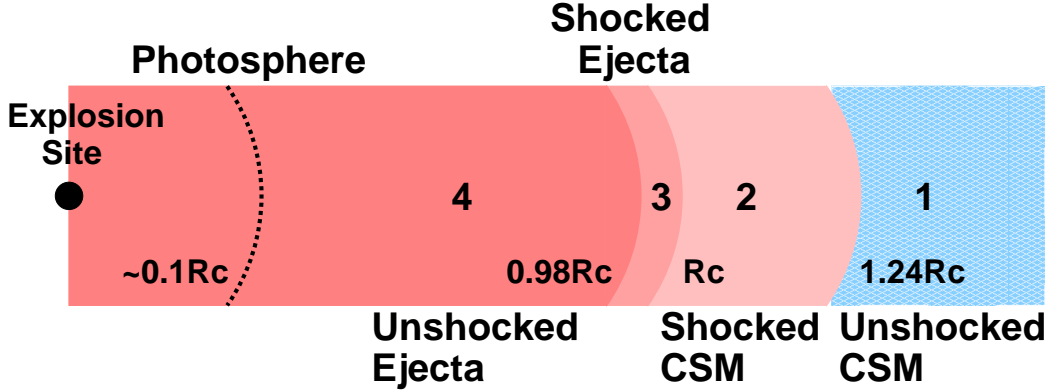


Figure 1.1: The four regions of SN explosions are explained: [1] unshocked CSM, [2] shocked CSM, [3] shocked ejecta, and [4] unshocked ejecta. A contact discontinuity lies between regions [2] and [3] at radius,  $R_c$ . The forward shock at  $1.24 R_c$  races out ahead of the fastest ejecta and accelerates particles in the CSM, while the reverse shock at  $0.98 R_c$  shock heats the dense ejecta. The radio emission is attributed to the shocked material in regions 2 and 3. Meanwhile, optical data trace the evolution of the photosphere ( $\sim 0.1R_c$ ) as it recedes into the slowest (unshocked) ejecta of region [4].

fast photospheric velocities ( $v \approx 60,000 \text{ km s}^{-1}$ ) and pointing to a bulk kinetic energy upwards of  $10^{52} \text{ erg}$  (193).

However, in comparison with cosmological bursts, GRB 980425 was sub-energetic in gamma-ray energy,  $E_\gamma$ , by a factor of  $10^4$ . Similarly, the observed radio and X-ray luminosities were at least two orders of magnitude lower than the afterglows detected from typical GRBs. Afterglow emission is produced by the dynamical interaction of the relativistic jets with particles in the CSM, and is characterized by a non-thermal synchrotron spectrum peaking in the optical at the onset of the burst and cascading to lower frequencies as the outflow decelerates (339).

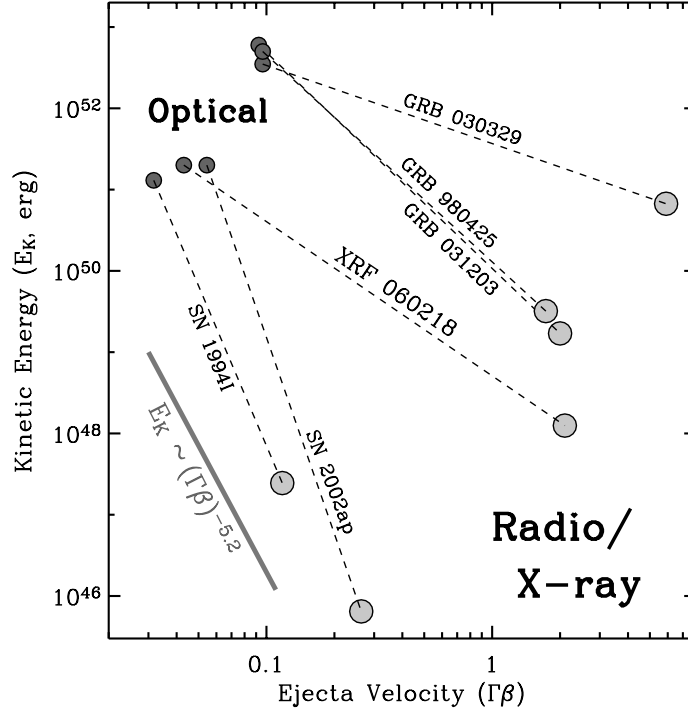


Figure 1.2: Optical data probe the slowest ejecta in SN explosions to which the bulk of the kinetic energy is coupled. Meanwhile, radio and X-ray observations probe the fastest material to which a small fraction of energy is coupled. Hydrodynamic collapse dictates that the velocity profile is steep,  $E_K \propto v^{-5.2}$ , consistent with observations of ordinary SNe Ibc. Engine-driven explosions, including GRBs and XRFs, show flatter profiles (365).

While detailed afterglow modeling revealed narrow jet opening angles for all cosmological GRBs (280, 445), the non-thermal (radio and X-ray) emission from GRB 980425/SN 1998bw showed no evidence for strong collimation (216, 226, 290).

Clearly, the observed properties of GRB 980425 were markedly different from those of previously studied GRBs. This fact motivated two popular explanations: (i) The burst was intrinsically sub-luminous compared to cosmological GRBs and only detected thanks to its proximity. In this scenario, GRB 980425 represented either a  $5\sigma$  outlier in the observed tight distribution of gamma-ray energies or a

member of a distinct class of bursts with significantly less power. (ii) The burst was a typical GRB but viewed far from the collimation axis. In this scenario, the observed radiation from the mildly-relativistic outflow was significantly suppressed because the jet was beamed away from our line-of-sight. For years to come, both the GRB and SN communities were split over the interpretation of the peculiar nature of GRB 980425/SN 1998bw.

#### 1.1.4 A GRB-SN Connection

At the same time, dedicated observational campaigns were focused on finding photometric and/or spectroscopic evidence of optical SNe in coincidence with well-localized cosmological GRBs. The primary method was to search for late-time “bumps” within the optical afterglow light-curves of GRBs, produced by the thermal SN emission peaking roughly  $(10 - 20) \times (1 + z)$  days after the explosion, as observed for SN 1998bw and ordinary SNe Ibc. GRB 980326 provided the first such evidence for an underlying SN component (42) and other examples of late-time optical bumps soon followed (see (435) for a review). With these discoveries, it became clear that at least some GRBs are accompanied by SN explosions. This result was echoed by a study of GRB host galaxy properties where it was found that GRBs, like core-collapse SNe, are always found in star-forming host galaxies (45). Finally, the discovery of GRB 030329 at  $z = 0.17$  provided the first spectroscopic evidence for an underlying Type Ibc SN (2003dh). Given that the observed gamma-ray and afterglow properties of GRB 030329 were roughly similar to those of typical GRBs (27), and the optical properties of SN 2003dh were similar to SN 1998bw, observational evidence for a GRB-SN connection was firmly established (377, 187).

Despite this progress, several questions remained unanswered:

- Are all GRBs associated with a SN of Type Ibc?
- What is the distribution of GRB-SNe optical properties (luminosities, photospheric velocities) and how do they compare with those of ordinary SNe

Ibc?

- Are all SNe Ibc powered by central engines?
- Is there a continuous distribution of ejecta properties between GRBs and ordinary SNe?

### 1.1.5 X-ray Flashes

The latter question directly ties to understanding the nature of X-ray flashes (XRFs), a newly recognized class of high-energy transients characterized by short pulses of non-thermal soft X-ray emission. With observed  $\nu F_\nu$  spectra peaking below 25 keV, a factor of  $\gtrsim 10$  lower than those of GRBs, XRFs were first discovered within the BeppoSAX sample (180) and were later estimated to be 30% of all bursts detected by *HETE-2* (332). At the same time, XRFs and GRBs were shown to share many characteristics, including pulse duration, afterglow emission, and host galaxy properties. Observationally speaking, XRFs appeared to bridge powerful GRBs and ordinary SNe.

Three popular ideas quickly emerged, positing that XRFs are either (i) typical GRBs at high-redshift such that their high-energy emission is redshifted into the soft X-ray band, (ii) a low-energy cousin of GRB explosions characterized by lower Lorentz factor outflows, or (iii) typical GRBs viewed far away from the collimation axis. Redshift measurements easily test model (i), while models (ii) and (iii) can be distinguished with detailed modeling of the afterglow emission.

As discussed in Chapter 4, I have been able to rule out the high-redshift interpretation by setting the distance scale to X-ray flashes. In the context of models (ii) and (iii), the key point is that even the most collimated GRB jets spread sideways as they decelerate, eventually reaching spherical symmetry on a timescale comparable to when they become non-relativistic ( $\sim 1$  year). As the jets spread into our line-of-sight, a rapid rise in the observed afterglow emission is expected on a timescale that scales with viewing angle,  $\theta_v$  (168). Collimated explosions viewed slightly off-axis ( $\theta_v \lesssim 2\theta_j$ ) are expected to show rising afterglow emission for a

few days or weeks, while those viewed significantly off-axis show a rise months to years after the explosion. The temporal evolution of the afterglow therefore constrains the viewing angle with respect to the collimation axis and addresses the fundamental questions:

- What is the nature of X-ray flashes?
- What is the relation (if any) between the progenitors of XRFs and GRBs?

### 1.1.6 Off-axis GRBs and SNe Ibc

In the most extreme case of an off-axis explosion, the GRB jet is oriented nearly perpendicular to our viewing angle such that the gamma-ray emission is completely beamed away from our line-of-sight. The first clue to such an event would be observed thermal SN emission, which is essentially isotropic. Searching for non-thermal emission (radio and X-ray) from optically selected SNe Ibc is therefore a powerful tool to search for off-axis GRBs (287, 275). Given the respective rates of GRBs and SNe and the known distribution of GRB jet opening angles, roughly 1% of SNe Ibc are expected to show evidence for an off-axis GRB. However, this fraction could be significantly higher if there exists a continuum in ejecta properties between GRBs and SNe. Such an observational effort has the ability to answer the following fundamental questions confronting the GRB-SN connection:

- What is the nature of GRB 980425 associated with SN 1998bw?
- What fraction of SNe Ibc show radio emission similar to that of SN 1998bw?
- What fraction of SNe Ibc harbor off-axis GRBs?
- Is there a continuum in the ejecta properties between SNe and GRBs?

Progress required a detailed understanding of the nearest stripped-envelope explosions, including optically-selected SNe Ibc and GRBs. Motivated thus, my PhD thesis addresses each of the questions posed in this section.

## 1.2 Summary of Thesis

The structure of this summary reflects the four main components of my thesis investigation: Part I. The nature of GRB 980425 and the discovery of a class of sub-energetic GRBs; Part II. The nature of X-ray flashes; Part III. An optical view of the GRB-SN connection and its diversity; and Part IV. A large radio survey of Type Ibc supernovae.

### 1.2.1 The Nature of GRB 980425 and a New Class of GRBs

For nearly a decade after the explosion, the nature of the seemingly sub-energetic GRB 980425 and its extraordinary associated SN, was heavily debated. If the burst was a typical GRB viewed far from the collimation axis, the tight clustering of gamma-ray energies would be preserved and at the same time confirm that GRB outflows are strongly collimated. On the other hand, if the burst was intrinsically sub-energetic, it would show no evidence for off-axis ejecta thereby refuting the commonly accepted idea of a standard energy reservoir for GRBs. Late-time radio observations provide the best tool to distinguish between these two models, since they are most sensitive to ejecta initially beamed away from our line-of-sight. This is due to the fact that although the rising afterglow emission from an off-axis jet is achromatic, the synchrotron peak frequency is at or below the radio band on this timescale (months to years).

To test the off-axis jet model proposed for GRB 980425/SN 1998bw, I carried out late-time radio observations at  $t = 5.6$  years, yielding upper limits ( $\lesssim 0.1$  mJy) which are consistent with the continued decay of the early radio emission. Most importantly, the observations are inconsistent with the predictions of an off-axis jet model which posited a strong radio source with  $F_\nu \sim 10$  mJy. I therefore conclude that GRB 980425 was an intrinsically under-luminous burst and a significant outlier in comparison to GRBs at  $z \sim 1$  (357). Furthermore, this result hints that GRB 980425, as the nearest GRB detected to date, likely represents a more common type of burst which is less powerful and not detectable at larger

distances.

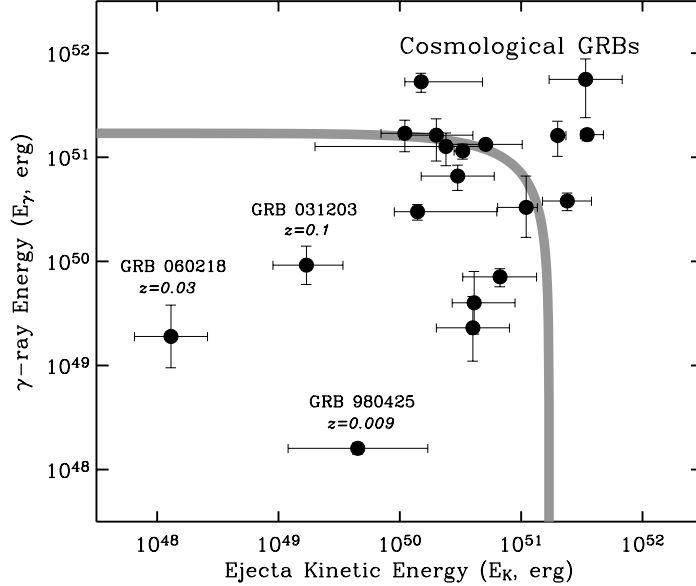


Figure 1.3: The energy released in gamma-rays,  $E_\gamma$ , is compared with the ejecta kinetic energy,  $E_K$  for GRBs. Cosmological GRBs tend to have a total relativistic energy yield,  $E_{\text{rel}} = (E_\gamma + E_K) \approx 2 \times 10^{51}$  erg (arc). The nearest GRBs (labeled) are sub-energetic in one or both axes. Updated from (362).

Soon thereafter, this prediction was confirmed through the *Integral* and *Swift* satellite discoveries of two similarly nearby bursts: GRB 031203 ( $z \approx 0.1$ ) and XRF 060218 ( $z \approx 0.03$ ). Through extensive radio and X-ray follow-up, I show that both are intrinsically sub-energetic bursts in terms of their total relativistic energy yield,  $E_{\text{rel}} = E_K + E_\gamma$ . For these two bursts, the inferred values of  $E_{\text{rel}}$  are at least a factor of 100 lower than those inferred for typical bursts,  $E_{\text{rel}} \approx 2 \times 10^{51}$  erg (including beaming corrections; (27)), therefore implying they are analogues of GRB 980425 (Figure 1.3) (362, 365). Using this newly recognized class of bursts, I estimate that sub-energetic GRBs are more common than standard GRBs by up to a factor of 10. These explosions are further distinguished from ordinary SNe Ibc as they couple at least  $10^{48}$  erg to mildly-relativistic ejecta. Thus, sub-energetic bursts are intermediate between powerful GRBs and ordinary SNe in

terms of relativistic energy, collimation, and volumetric rate, and hint at an overall continuum.

### 1.2.2 The Nature of X-ray Flashes

With prompt emission spectra peaking a factor of 10 below those of GRBs, it is interesting to consider XRFs in the context of sub-energetic bursts. In Part II, I report (i) the discovery of the first optical afterglow associated with an XRF, (ii) the first spectroscopic redshift to an XRF host galaxy, and (iii) the first broadband (radio, optical) afterglow analysis for an XRF (361). Furthermore, using a sample of XRFs, I discuss the nature of these events in the context of off-axis GRBs and sub-energetic bursts.

Discovered two years after launch, XRF 020903 is the softest X-ray flash ever detected by the *HETE-2* satellite (330). Using the Palomar 200-inch telescope, I discovered an optical transient within the 120 square arcmin localization region just 1 day after the burst (Figure 1.4). The source was coincident with a faint star-forming galaxy in an interacting system which I found to be at a redshift of  $z \approx 0.25$  using the Echelle Spectrograph and Imager on Keck II. With this discovery I set the distance scale to X-ray flashes, and in turn, ruled out the popular hypothesis that XRFs are typical GRBs at very high redshift ( $z \sim 10$ ).

Next, through an analysis of the strong radio and optical emission associated with the transient, I showed that the long wavelength counterpart of XRF 020903 was similar to the afterglows of GRBs. Under the framework of GRB afterglow models I further showed that the kinetic energy of the XRF 020903 ejecta was similar to the values inferred for GRBs. Thus, observational evidence for a connection between GRBs and XRFs is firmly established, suggesting similar progenitor. However, unlike typical GRBs, XRF 020903 showed no evidence for strong collimation of the relativistic outflow.

I came to a similar conclusion from broadband (radio, optical, near-IR, X-ray) modeling of the afterglow of XRF 050416a at  $z \approx 0.65$ . Analogous to XRF 020903, XRF 050416a is the softest burst detected to date by the *Swift* satellite (327). A

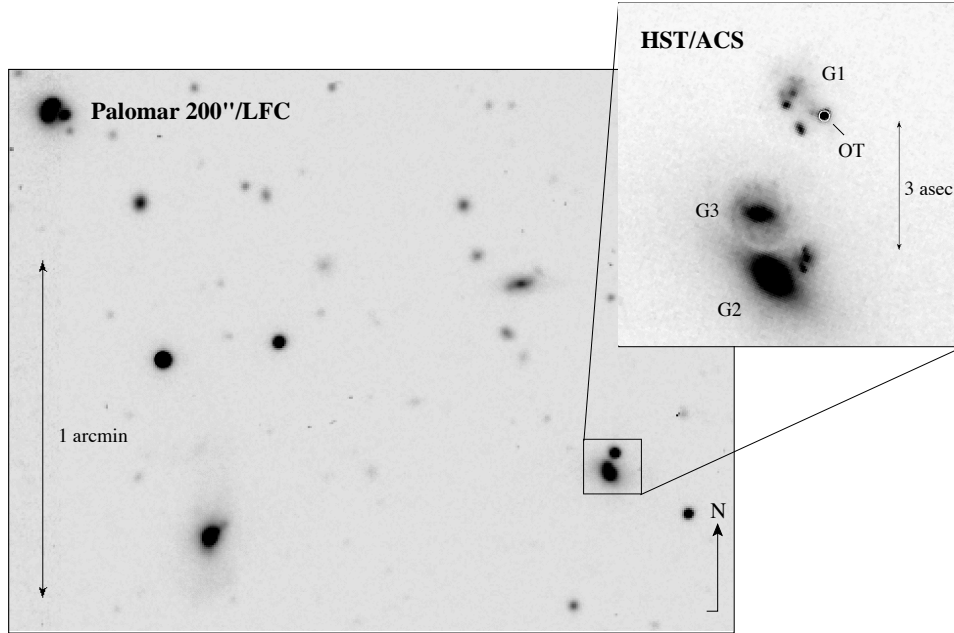


Figure 1.4: I discovered the optical afterglow of XRF 020903 with the Palomar 200-inch telescope. The XRF was later observed with *HST/ACS* on 2002 Dec 3 UT revealing a complicated galaxy morphology for G1, suggesting a system of at least four interacting galaxies similar to the host galaxies of GRBs. The location of the optical transient (OT) is noted on the  $7 \times 7''$  HST cutout and appears to overlap with the SW component of the G1 complex at a redshift of  $z = 0.25$ . Nearby galaxies G2 and G3 are not associated with G1. From (361).

careful analysis of the afterglow evolution shows no evidence that the burst was viewed away from the collimation axis. The implication is that this burst (and perhaps all XRFs) are best explained as GRBs with very wide jet opening angles and perhaps a larger baryonic load (368).

Together with the results from Part I, these conclusions underscore the fact that the initial picture in which GRBs always produce roughly  $10^{51}$  erg in  $\sim 5$  deg relativistic jets is not the complete story. Bursts with significantly less relativistic energy and/or very wide jets exist in large numbers and likely outnumber what we know as “typical” GRBs.

### 1.2.3 An Optical View of the GRB-SN Connection

The discovery of a GRB-XRF connection directly led to the question: do XRFs also show evidence for an association with Type Ibc supernovae? In Part III, I report the results of an optical search for XRF-SNe using deep *HST/ACS* images of four XRFs (including XRF 02093). The images were taken between 20 and 70 days after the burst (rest frame) and are thus well matched to the timescale on which SNe Ibc reach maximum light. The *HST* images reveal evidence for a late-time bump in the optical afterglow light-curve of XRF 020903. Through simultaneous optical spectroscopy, I show that the bump had spectral features consistent with those of SN 1998bw and other Type Ibc supernovae. At the same time, the other three XRFs in this *HST* study showed no evidence for an associated SN. Therefore, I conclude that at least some XRFs are associated with Nickel-rich SNe, thereby reinforcing their connection to GRBs, and in turn, massive stellar death (363). The non-detections indicate, more importantly, that there is a wide diversity in the energetic of the SNe.

I next present a compilation of GRB-SN and XRF-SN optical peak magnitudes (drawn largely from this thesis effort) and compare them with those of ordinary (non-GRB associated) SNe Ibc. This study was motivated by the fact that of all the bursts at  $z \lesssim 1^3$  for which a SN search was undertaken, nearly every one shows an associated SN (447). The following key results came from this study. First, I find a significant dispersion in the properties of GRB- and XRF-SNe; most are not as luminous as GRB-SN 1998bw. Next, the study shows statistically that photospheric velocities do not correlate with peak optical luminosity in either the local or GRB/XRF-SN samples. This result is contrary to early expectations fueled by the broad absorption lines (“broad lined”) and luminous peak magnitude observed for GRB-SN 1998bw. Finally, I show that there is significant overlap in the peak optical luminosities of GRB/XRF-SNe and ordinary SNe Ibc (Figure 1.5). Since the optical emission is dominated by the radioactive decay of Nickel-56, this study

---

<sup>3</sup>I constrain the study to  $z \lesssim 1$  since UV line-blanketing in the rest-frame of the SN suppresses the observed emission in higher redshift bursts.

suggests that these explosions share a similar Nickel-56 production mechanism (366). This result is by no means expected since the collapsar model predicts a different Nickel-56 production mechanism for engine-driven explosions (GRBs and XRFs) than that inferred for standard core-collapse SNe.

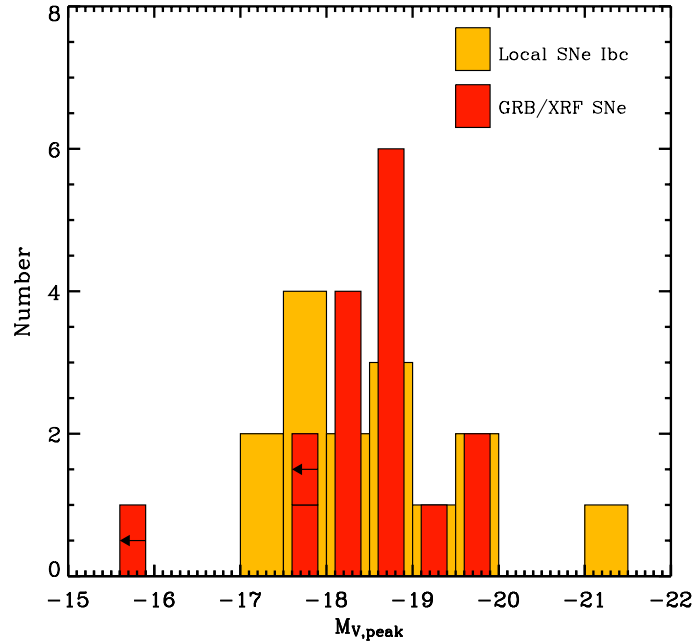


Figure 1.5: A comparison of the peak optical magnitudes for GRB/XRF-SNe and ordinary SNe shows a significant overlap. This study suggests that the two classes may share a similar Nickel-56 production mechanism. From (366).

#### 1.2.4 A Large Radio Survey of Type Ibc Supernovae

Part IV represents the largest component of this PhD thesis effort. Motivated by the extraordinary radio emission from GRB-SN 1998bw, I began in 2002 a dedicated survey with the Very Large Array (VLA) to search for engine-driven SNe in the local Universe. The driving idea is that sub-energetic and/or off-axis GRBs show little or no gamma-ray emission. Radio and X-ray follow-up of optically selected SNe Ibc may therefore represent the most efficient (and perhaps

only) way to identify such explosions. Luminous radio and/or X-ray emission may indicate a mildly-relativistic outflow, which in turn, is a proxy for the presence of a central engine.

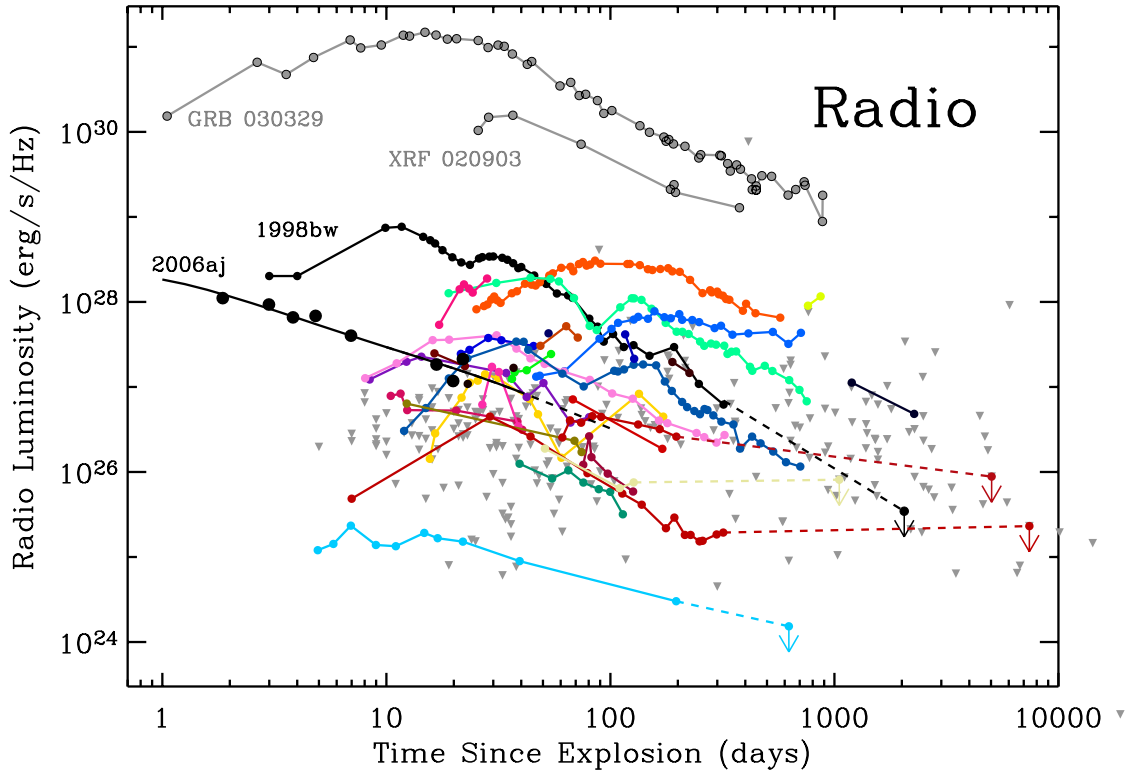


Figure 1.6: To date, 30 local ( $d \lesssim 200$  Mpc) SNe Ibc have been detected at radio wavelengths, the majority of which were found through our dedicated VLA survey. Detections are shown as colored light-curves and  $3\sigma$  upper limits as inverted grey triangles. GRB-SN 1998bw and XRF 2006aj, also within the maximum distance of this sample, are distinguished by their bright early peaking radio emission (black). Both of these events were sub-energetic in comparison with typical GRBs (e.g., GRB 030329; grey) and XRFs (e.g., XRF 020903; grey).

I report radio observations from  $\sim 200$  SNe Ibc within  $\sim 200$  Mpc that span timescales of days to decades after the explosion. Early radio observations are crucial for identifying sub-energetic and/or uncollimated explosions. On the other

hand, late-time radio observations are sensitive to jets initially beamed away from our line-of-sight. Moreover, since radio observations probe the interaction of the ejecta with the CSM, they directly trace the density profile of the local environment thereby revealing the mass loss history of the progenitor star. Through this dedicated VLA survey, I have characterized in a systematic way the environments (density, profile) and ejecta properties (kinetic energy, velocity, geometry) of SNe Ibc for the first time.

Several surprising results have emerged from this effort. First, only  $\sim 15\%$  of local SNe Ibc show detectable radio emission despite the fact that a radio supernova  $10^3$  times fainter than GRB-SN 1998bw can be detected with the current sensitivity of the VLA (Figure 1.6). Next, the thirty radio bright SNe Ibc discovered to date (see Part IV) vary in peak luminosity by four orders of magnitude, with peak times spanning roughly 1 to 1000 days. These observed differences indicate similarly large variations in their CSM densities and/or energy coupled to fast ejecta. Moreover, I find that roughly 40% of well-studied radio SNe show evidence for abrupt fluctuations which may be attributed to density and hence mass loss inhomogeneities (356). Interestingly, I note that a similar fraction of massive stars are expected to die in close binary systems (295).

In the context of the GRB-SN connection, I compare the radio properties of local SNe Ibc with those of GRB 980425/SN 1998bw and XRF 060218/SN 2006aj - the only bursts within this same volume. I find that *none* of the SNe Ibc in this study show evidence for mildly relativistic ejecta, though a few show velocities as high as  $\sim 0.5c$ . Statistically, I constrain the fraction of SNe with radio properties like GRB-SN 1998bw to be less than 1% and those like XRF-SN 060218 to be less than 3%. The latter case is less constrained, owing to the fact that XRF 060218 had a radio light-curve 10 times less luminous and peaking 10 times faster than SN 1998bw.

Focusing on just those radio observations taken  $\gtrsim 100$  days after the explosion, I search for evidence of off-axis GRB jets spreading into our line-of-sight. Of the 68 SNe Ibc in this sub-sample, I find no evidence for off-axis emission and therefore

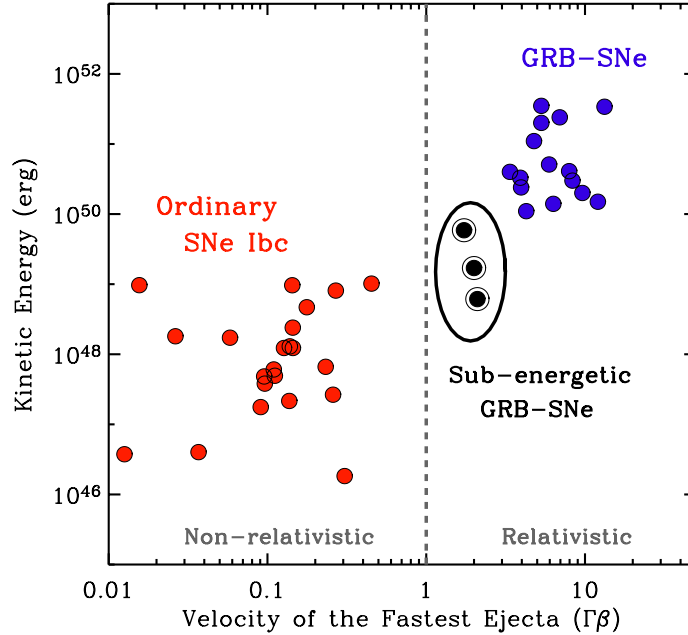


Figure 1.7: Cosmological GRBs show copious energy coupled to relativistic material while ordinary SNe Ibc show less than  $10^{48}$  erg coupled to material no faster than  $\sim 0.5c$ . The new class of sub-energetic bursts bridge the two classes and hint at an overall continuum.

statistically constrain the fraction of SNe Ibc which harbor typical GRB jets to be less than 10% (365). This holds, in particular, for the  $\sim 5\%$  of local SNe that show broad optical absorption lines like GRB-SN1998bw. This result supports my earlier conclusion that neither a high optical luminosity nor fast photospheric velocities are indicators of relativistic ejecta.

Combining these results with those from Parts I and II, I show that there is a clear dichotomy between GRBs and ordinary SNe Ibc with respect to the kinetic energy coupled to fast ejecta. However, the newly discovered class of sub-energetic bursts bridge these two classes and hint at an overall continuum (Figure 1.7).

Finally, I conclude Part IV with a discussion of future prospects for the study of GRBs, XRFs, sub-energetic bursts, and SNe Ibc as we enter the era of wide-field optical transient surveys (e.g., PanSTARRS, LSST).

## Part I

# The Discovery of a Class of Sub-energetic GRBs

The Discovery of a Class of Sub-energetic GRBs

## Chapter 1

# Constraints on Off-Axis GRB Jets in Type Ibc Supernovae From Late-Time Radio Observations<sup>†</sup>

A. M. SODERBERG<sup>a</sup>, D. A. FRAIL<sup>b</sup>, & M. H. WIERINGA<sup>c</sup>

<sup>a</sup>Division of Physics, Mathematics and Astronomy, 105-24, California Institute of Technology,  
Pasadena, CA 91125

<sup>b</sup>National Radio Astronomy Observatory, Socorro, NM 87801

<sup>c</sup>Australia Telescope National Facility, CSIRO, P.O. Box 76, Epping NSW 1710, Australia

## Abstract

It has been suggested that the peculiar properties of the luminous Type Ic supernova SN 1998bw and its low-energy gamma-ray burst GRB 980425 may be understood if they originated in a standard gamma-ray burst explosion viewed far from the axis of the relativistic jet. In this scenario, strong radio emission is predicted from the jet on a timescale 1 to 10 years after the explosion as it decelerates and spreads into our line of sight. To test this hypothesis we have carried out late-time radio observations of SN 1998bw at  $t = 5.6$  years, yielding upper limits which are

---

<sup>†</sup>A version of this chapter was published in *The Astrophysical Journal*, vol. 607, L13-L16, (2004). Reproduced by permission of the AAS.

consistent with the continued fading of the supernova. We find these limits to be consistent with an off-axis jet only if the progenitor mass loss rate is  $\dot{M} \lesssim 4 \times 10^{-7} M_{\odot} \text{ yr}^{-1}$  (for a wind velocity  $v_w = 1000 \text{ km s}^{-1}$ ) or the fraction of the shock energy in magnetic fields is  $\epsilon_B \lesssim 10^{-3}$ . These values are low relative to those inferred for cosmological GRBs. We combine the SN 1998bw measurements with existing observations for a sample of 15 local Type Ibc supernovae to estimate that at most 6% produce collimated, relativistic outflows.

## 1.1 Introduction

GRB 980425 was the first gamma-ray burst (GRB) to be identified with a supernova (SN), SN 1998bw (151, 290). However, this association was not universally accepted since the spatial and temporal coincidence of these events could only be approximated to  $\pm 8'$  and  $\pm 2 \text{ d}$ , respectively. Recently, the detection of spectroscopic features in the light curve of GRB 030329, similar to those seen in SN 1998bw (377, 187), has strengthened the hypothesis of the SN 1998bw/GRB 980425 association. These results have given a powerful impetus to the “collapsar” model (233, 451) in which a Wolf-Rayet progenitor undergoes core collapse, producing a rapidly rotating black hole surrounded by an accretion disk which injects energy into the system and thus acts as a “central engine”. The energy extracted from this system supports a quasi-spherical Type Ibc SN explosion and drives collimated jets through the stellar rotation axis which produce the prompt gamma-ray and afterglow emission (see review by Zhang and Meszaros 449).

Despite this progress, some unresolved issues remain. Foremost among these is understanding the connection between local SNe Ibc and cosmological GRBs. Estimates of the fraction of Type Ibc SNe that produce a GRB range from  $10^{-5}$  (288), to 0.5% (133), and even approaching 100% (218). This uncertainty in the relative rates of Ibc SNe and GRBs is due to different assumptions about the geometry and energetics of GRBs.

As the only local SN observed in association with a GRB, SN 1998bw is the

key to our understanding. At a distance of 38 Mpc, this Type Ic SN was unusually luminous at optical and radio wavelengths (216, 151). The broad absorption lines seen in early spectra of SN 1998bw implied expansion velocities of  $\geq 30,000 \text{ km s}^{-1}$  and (isotropic) kinetic energies of  $\sim 3 \times 10^{52} \text{ erg}$  (193, 436, 388). Likewise, the bright, early-peaked radio emission implied a significant amount of energy ( $\sim 10^{50} \text{ erg}$ ) coupled to mildly ( $\Gamma \approx 2$ ) relativistic ejecta (216). Detailed modeling by Li and Chevalier (226) confirmed this result and also showed the need for a second energy injection episode, indicating the presence of a central engine, similar to the model inferred for GRBs.

However, in contrast to the large energies inferred from the optical and radio emission from SN 1998bw, GRB 980425 was a sub-energetic gamma-ray burst. The prompt emission had an (isotropic) energy release of only  $8 \times 10^{47} \text{ erg}$  (290) – 4 to 6 orders of magnitude below typical GRBs (133).

One popular explanation posits that SN 1998bw/GRB980425 was a typical GRB viewed away from the jet axis (263, 65, 106, 436, 334, 440). This hypothesis can be described by two different scenarios based on the ratio of the off-axis angle,  $\theta_{\text{oa}}$ , to the opening angle of the GRB jet,  $\theta_j$ . In Case 1,  $\theta_{\text{oa}} \sim 3\theta_j$  so the jet emission is detected at early time. Here, the  $\gamma$ -rays originate from the edge of the relativistic jet, causing the inferred (isotropic) energy to be suppressed (168). In Case 2,  $\theta_{\text{oa}}$  is large ( $\gg 10 \theta_j$ ) so the jet emission is only detectable at late time ( $t \sim 1 - 10 \text{ years}$ ) when the jet has reached spherical symmetry. In this case, the prompt  $\gamma$ -ray emission may be due to Compton scattering of photons into our line-of-sight (417).

Granot et al. (168) have investigated Case 1, finding the optical and  $\gamma$ -ray emission to be consistent with an off-axis angle of  $\theta_{\text{oa}} \approx 4^\circ$  (for  $\Gamma \approx 100$ ). This scenario, however, may have difficulty explaining the X-ray and radio evolution. Waxman (417) has recently investigated Case 2, predicting a late-time rise in the observed luminosity which is most easily detectable at radio frequencies (275, 398, 166).

The possibility of Case 2 has given rise to unification models which imply some

fraction of local Ibc SNe can also be described as GRBs viewed off-axis (417, 218). While the off-axis jet model provides a convenient framework in which to unite the GRB and SN phenomena, confirmation of the model requires observational evidence for a GRB jet within a local SN. In this paper we carry out late-time radio observations of SN 1998bw in an effort to detect the putative off-axis jet from GRB 980425. We combine this measurement with existing observations for a sample of nearby Type Ibc SNe to place constraints on the parameters of the off-axis jet and the fraction of local Ibc SNe which could be associated with relativistic jets similar to those seen in cosmological GRBs.

## 1.2 Observations

We observed SN 1998bw with the Australia Telescope Compact Array (ATCA)<sup>1</sup> beginning at 2003 December 4 21:00 UT and ending on 2003 December 5 8:30 UT. Dual frequency observations were made at 1384 and 2368 MHz, using a bandwidth of 128 MHz and two orthogonal linear polarizations for each frequency band. The final synthesized beams were  $8 \times 14''$  and  $5 \times 8''$ , at 1384 and 2368 MHz, respectively.

No emission is detected toward SN 1998bw at either frequency but there is a weak source ( $209 \mu\text{Jy}$ ) detected at 2368 MHz  $1.7''$  west and  $3.1''$  north of the SN. This source is too bright to be due to thermal emission from the complex of HII regions in this area. It is possible that this is the radio counterpart of the ultraluminous X-ray transient (S1b) recently identified by Kouveliotou et al. (2004) but it would be 60-times more luminous than the only other known detection (198). The peak flux density at the position of the SN was  $62 \pm 40$  and  $149 \pm 50 \mu\text{Jy}$  for 1384 and 2368 MHz, respectively. These new upper limits, taken 2049.19 d after GRB 980425 exploded ( $t \simeq 5.6$  yrs), lie just below the extrapolation of a power-law decay from 50 to 790 days (Figure 1.1).

---

<sup>1</sup>The Australia Telescope is funded by the Commonwealth of Australia for operation as a National Facility managed by CSIRO.

### 1.3 SN 1998bw: Constraining the Off-Axis Jet Model

Waxman (417) has made predictions for the evolution of late-time radio emission from a typical GRB jet viewed far from the jet axis. As the off-axis jet sweeps up material and decelerates, it eventually undergoes a dynamical transition to sub-relativistic expansion (135) and spreads sideways into our line-of-sight. This occurs on a timescale  $t_{\text{oa}} \approx E_{51}/(\dot{M}_{-5}/v_{w,3})$  years. Here  $E_{51}$  is the energy of the jet (normalized to  $10^{51}$  erg),  $v_w$  is the velocity of the stellar wind, and  $\dot{M}_{-5}/v_{w,3}$  is the mass loss rate of the progenitor star normalized as  $(\dot{M}/10^{-5} M_{\odot} \text{ yr}^{-1})(v_w/10^3 \text{ km/s})$  and equivalent to  $A_* = 1$  in the notation commonly used for GRBs (75). On this same timescale the radio emission from the SN, which is produced by a spherical shock interacting with the circumstellar medium, will fade significantly with a power-law decay index of  $\alpha \approx 1.3 - 1.6$  (226).

Particle acceleration within the jet produces bright synchrotron emission which causes a rapid rise of the radio luminosity as the jet comes into our line-of-sight. Making the typical assumption that the energy is partitioned between the electrons and the magnetic field, and that these fractions ( $\epsilon_e$  and  $\epsilon_B$ ) are constant throughout the evolution of the jet, the spectral luminosity is given by Waxman (417) as:

$$L_{\nu} = 1.7 \times 10^{30} (3\epsilon_e)(3\epsilon_B)^{3/4} \times \frac{(\dot{M}_{-5}/v_{w,3})^{9/4}}{E_{51}^{1/2}} \left(\frac{\nu}{10 \text{ GHz}}\right)^{-1/2} \left(\frac{t}{t_{\text{oa}}}\right)^{-3/2} \text{ erg/s/Hz} \quad (1.1)$$

On timescales  $t \leq t_{\text{oa}}$  the spectral luminosity of the jet rises steeply as  $t^{+3.9}$  (168) and during  $t \geq t_{\text{oa}}$  it decays as  $t^{-1.5}$ , assuming an electron spectral index  $p = 2$ . As indicated by Eqn 1, an off-axis GRB jet is most easily detected at radio frequencies.

Late-time radio observations of SN 1998bw can therefore be used to impose constraints on the parameter space for an associated off-axis GRB jet. In modeling the evolution of the putative jet emission, we consider four model parameters,  $E_{51}$ ,  $\dot{M}_{-5}/v_{w,3}$ ,  $\epsilon_e$  and  $\epsilon_B$ , for which we adopt values comparable to those inferred for

for cosmological GRBs. The kinetic energy of the jet and the energy fraction in electrons are fairly well constrained by broadband observations of GRB afterglows, so we assume typical values for these parameters of  $E_{51} = 1$  and  $\epsilon_e = 0.1$  (133, 279, 445). The energy fraction in magnetic fields is significantly less constrained, however, showing a typical range of values between  $\epsilon_B = 0.002 - 0.25$  (445). This range imposes a significant uncertainty in the luminosity of an off-axis jet, through Eqn 1.

The model is also strongly dependent on the mass loss rate of the progenitor – generally believed to be a massive Wolf-Rayet (WR) star. Mass loss rates inferred from broadband modeling of GRBs are typically  $\dot{M}_{-5}/v_{w,3} \approx 0.1 - 1$  (75, 280, 445), yet local WR stars have observed mass loss rates significantly larger, on the order of  $\dot{M}_{-5} \approx 0.6 - 9.5$  (62). The uncertainty associated with the progenitor mass loss rate maps to a large range in the predicted peak time and luminosity of an off-axis jet. Thus the uncertainty in  $\dot{M}_{-5}/v_{w,3}$  and  $\epsilon_B$  produces a degeneracy in the model which we are able to constrain using late-time radio observations of local Ibc SNe.

### 1.3.1 The $\epsilon_B - \dot{M}_{-5}/v_{w,3}$ Degeneracy

Figure 1.1 shows the predicted radio luminosity evolution of an off-axis GRB jet based on Eqn 1 and using values of  $\dot{M}_{-5}/v_{w,3} = 0.01, 0.1, 1$  and 10. This plot demonstrates how the uncertainty in  $\epsilon_B$  produces a family of lightcurves for each  $\dot{M}_{-5}/v_{w,3}$  value.

The full set of constraints is derived through investigation of the two-dimensional parameter space of  $\epsilon_B - \dot{M}_{-5}/v_{w,3}$ . Figure 1.2 shows how the predicted spectral luminosity of the putative jet at time,  $t$ , maps to a single contour in this parameter space. By comparing the observed luminosity of SN 1998bw at each epoch with the jet luminosity predicted for that time, we exclude the region of parameter space *rightward* of the corresponding contour since this region produces a jet which is *brighter* than the observed SN 1998bw emission at that epoch.

The region of reasonable parameter space for the putative jet is bracketed by  $\dot{M}_{-5}/v_{w,3} = 0.04 - 6$  as derived from modeling of SN 1998bw radio light curves

(226, 418)<sup>2</sup>, and by  $\epsilon_B = 0.002 - 0.25$  as inferred for most cosmological GRBs. The summed constraints (from  $t = 11$  to 2049 days) rule out the majority of this region.

## 1.4 Local Type Ibc Supernovae: Further Constraints

The search for an off-axis jet can similarly be carried out toward other local ( $d_L < 100$  Mpc) Type Ibc SNe for which there are late-time ( $t \sim 1 - 20$  year) radio observations. Eight type Ibc SNe were taken from Berger et al. (26): seven upper limits (SN 2001B, SN 2001ci, SN 2001ef, SN 2001ej, SN 2001is, SN 2002J, SN 2002bm), and a detection (SN 2002ap) at  $t \approx 0.5$  years. We have supplemented this sample with Very Large Array<sup>3</sup> archival observations of SN 1983N, SN 1984L, SN 1985F, SN 1990B, SN 1994I, and SN 1997X taken at  $t \approx 16.7, 2.9, 7.1, 0.8, 8.0$  and  $2.4$  years, respectively. In addition, we include the recent detection of SN 2001em at  $t \approx 2.4$  years (381) – the only SN within this sample for which there are no early time radio observations. The SNe data are plotted in Figure 1.1. With the exception of SN 2001em, all of the late-time observations are significantly fainter than the  $\dot{M}_{-5}/v_{w,3} = 1$  off-axis jet prediction and nine SNe constrain  $\dot{M}_{-5}/v_{w,3} \leq 0.1$ .

Using the same method applied in §1.3, we derive constraints for these 15 SNe. The resulting contours are plotted with SN 1998bw in Figure 1.3. For SNe with later observations, the constraints on  $\epsilon_B$  values improve, as demonstrated by the contours for SN 1994I and SN 1983N. The more robust constraints are provided by the faintest luminosity limits given by the nearest type Ic supernovae, SN 1994I, SN 2002ap, SN 1983N and SN 1985F, all at  $\lesssim 8$  Mpc. Additional constraints are derived from the SNe for which we detect late-time emission, SN 1994I and SN 2002ap<sup>4</sup>, since they show evidence that the radio luminosity is decaying

---

<sup>2</sup>Li and Chevalier (226) prefer  $\dot{M}_{-5}/v_{w,3} = 6$  for fitting the rise of the radio light curves, while Waxman (418) prefers  $\dot{M}_{-5}/v_{w,3} = 0.04$  for fitting the X-ray light-curve decay.

<sup>3</sup>The Very Large Array is a facility of the National Science Foundation operated under cooperative agreement by Associated Universities, Inc.

<sup>4</sup>This rules out the Totani (2003) model for SN2002ap predicting the radio flux to increase rapidly at  $t \approx 0.46$  years due to an off-axis jet. However, this prediction assumes  $\dot{M}_{-5}/v_{w,3} \approx 0.3$

with respect to earlier lightcurve measurements (see Berger et al. 22) and are thus inconsistent with *rising* off-axis jet emission.

The region of reasonable parameter space for an off-axis jet is roughly bracketed by  $\dot{M}_{-5}/v_{w,3} = A_* = 0.1 - 1$  and  $\epsilon_B = 0.002 - 0.25$  as typically inferred from broadband modeling of cosmological GRBs (280, 75, 445). Figure 1.3 shows that four of the SNe (1994I, 1985F, 1997X, 1990B) have contours that independently rule out this entire parameter space while eleven place significant constraints. The late-time radio emission of SN 2001em is consistent with a typical GRB jet only if the mass loss rate is  $\dot{M}_{-5}/v_{w,3} \approx 1$  (for  $\epsilon_B \approx 0.2$ ). Continued radio monitoring of SN 2001em will reveal the origin of the emission, which may simply result from a late peaking radio SN within a dense circumstellar medium (433).

## 1.5 Discussion and Conclusions

Late-time observations of SN 1998bw ( $t \simeq 5.6$  yrs) have allowed us to test the hypothesis that GRB 980425 was a standard GRB viewed far away from the jet axis. Our measured upper limits at 1384 and 2368 MHz are consistent with the continued power-law decay of the SN emission. These limits imply an off-axis jet is only plausible if the normalized mass loss rate of the progenitor star is  $\dot{M}_{-5}/v_{w,3} \leq 0.04$  (for  $\epsilon_B \geq 0.1$ ). This is  $\sim 20 - 200$  times smaller than the observed mass loss rates for local Wolf-Rayet stars (62) and is below the range typically observed in GRBs. Larger mass loss rates are possible but only if the energy fraction in magnetic fields is low (*i.e.*,  $\epsilon_B \lesssim 10^{-3}$ ).

Even tighter constraints are derived for the off-axis jet model when we examine a larger sample of local Ibc SNe. The low luminosity limits derived for this sample require values of  $\dot{M}_{-5}/v_{w,3} \approx 0.01 - 0.1$  or  $\epsilon_B \lesssim 10^{-3}$  which are below values for typical GRBs. The absence of any late-time radio emission can therefore be used to put a limit on the fraction of core-collapse SNe that produce collimated, relativistic outflows. Our results imply that off-axis jets from nearby SNe are rare whereas lower values could delay the onset of re-brightening.

( $\lesssim 6\%$ ) with the possible exception that the radio emission from SN 2001em is due to a GRB jet.

This conclusion complements the findings of Berger et al. (26) who constrained the GRB/SN fraction through a radio survey of local Ibc SNe at early time. Berger et al. (26) used early, bright radio emission as a proxy for relativistic ejecta, as in the case for SN 1998bw. After studying 33 local SNe with detection limits  $10^3$  times fainter than SN 1998bw, Berger et al. (26) found no evidence for relativistic ejecta in any of the SNe observed, thereby constraining the GRB/SN fraction to  $\lesssim 3\%$ .

Taken together, these results support a view that SN 1998bw was a rare and unusually energetic SN – distinct from local SNe and GRBs. In this scenario, the characteristics of SN 1998bw/GRB 980425 are not dictated by the observer’s viewing angle, but rather by the properties of its central engine. SN 1998bw was an engine-driven explosion (226), in which 99.5% of the kinetic energy ( $\sim 10^{50}$  erg) was coupled to mildly ( $\Gamma \approx 2$ ) relativistic ejecta (216), while a mere 0.5% was detected in the ultra-relativistic ( $\Gamma \approx 100$ ) flow. In contrast, GRBs couple most of their energy to relativistic  $\gamma$ -rays. The observed diversity of cosmic explosions (SNe, X-ray flashes, and GRBs) may therefore be explained with a standard energy yield, but with a varying fraction of that energy given to relativistic ejecta (27).

We thank Edo Berger, Sarah Yost and Eli Waxman for helpful discussions. AMS is supported by the NSFGRFP.

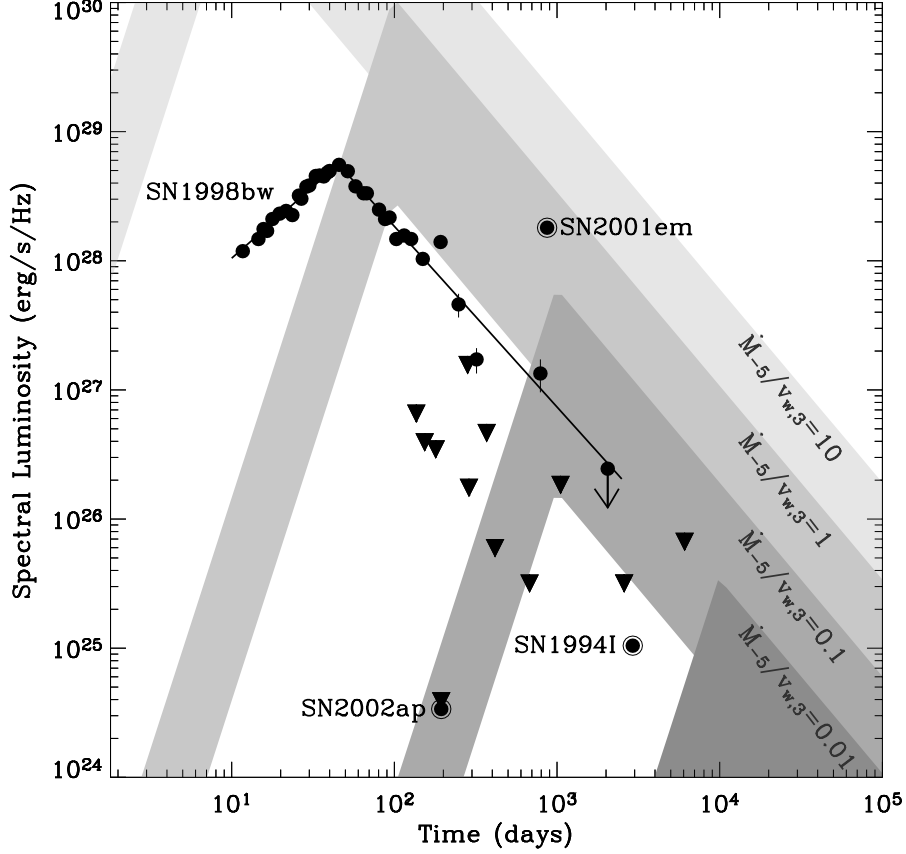


Figure 1.1: The radio luminosity evolution of SN 1998bw is shown with late-time detection limits for 12 nearby Ibc supernovae (triangles) and three late-time detections for SN 1994I, SN 2002ap and SN 2001em. The four shaded regions represent an off-axis GRB jet for  $A_* = \dot{M}_{-5}/v_{w,3} = (0.01, 0.1, 1, 10)$  and assuming a range of values,  $\epsilon_B = 0.002 - 0.25$ . We have assumed typical values of  $E_{51} = 1$  and  $\epsilon_e = 0.1$ . With the exception of SN 2001em, all of these late-time observations are significantly fainter than the  $\dot{M}_{-5}/v_{w,3} = 1$  off-axis jet prediction and nine of the SNe constrain  $\dot{M}_{-5}/v_{w,3} \leq 0.1$ .

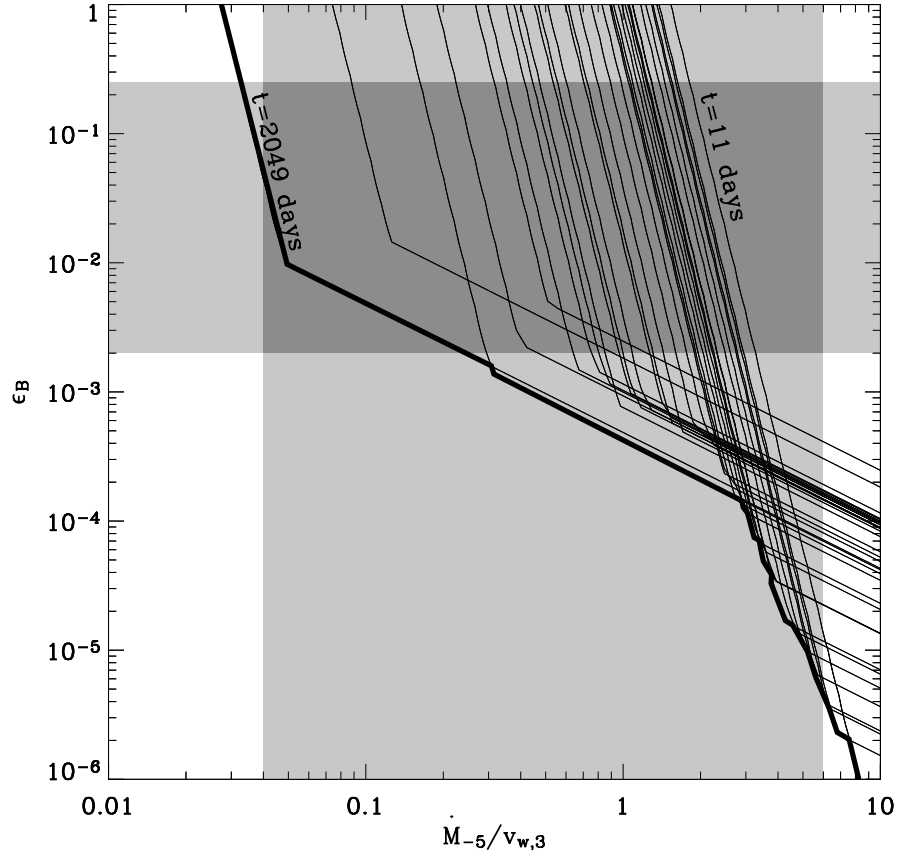


Figure 1.2: Every flux measurement allows us to exclude the region of  $\epsilon_B - \dot{M}$  space *rightward* of the corresponding contour since this region produces a jet which is *brighter* than the observed radio emission at that epoch. The break in each contour marks the  $\epsilon_B$  and  $\dot{M}_{-5}/v_{w,3}$  values that predict a peak jet luminosity equal to that observed. Above the break, a contour constrains a jet with rising flux, while below the break it constrains one with decaying emission. The sum of the excluded regions rules out the area rightward of the thick solid line. The region of reasonable parameter values for the putative jet is bracketed by  $\dot{M}_{-5}/v_{w,3} = 0.04-6$  as derived from modeling of SN 1998bw radio light curves, and by  $\epsilon_B = 0.002-0.25$  as inferred for cosmological GRBs. Our observations of SN 1998bw allow us to rule out the majority of this region.

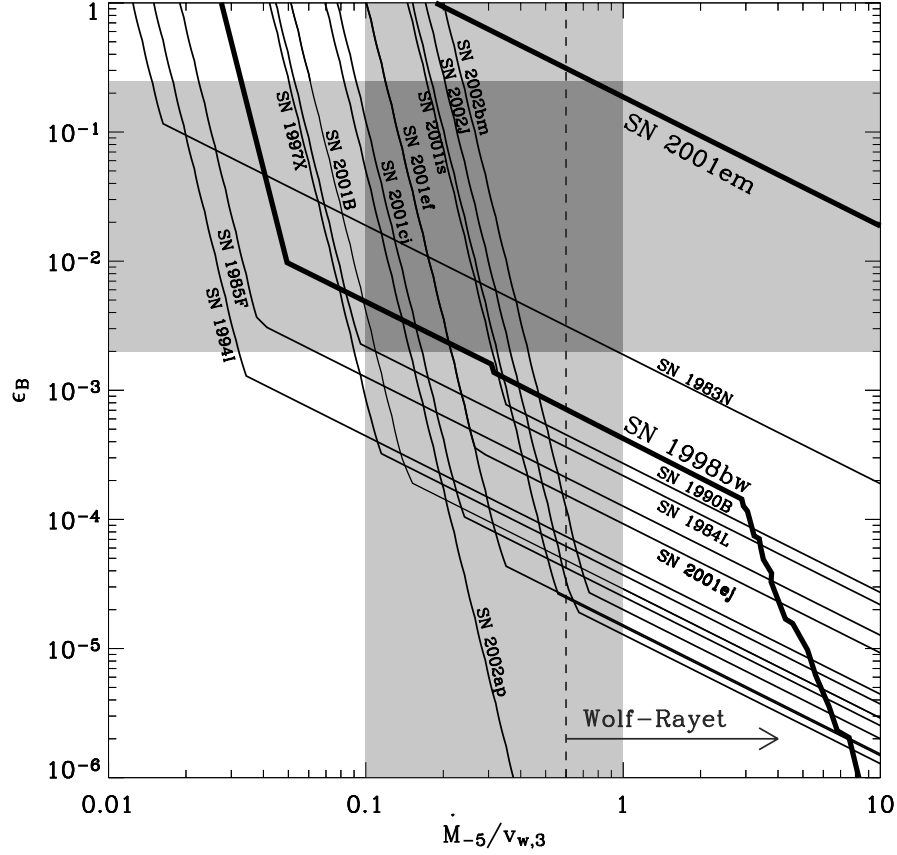


Figure 1.3: Our observations allow us to exclude the region of  $\epsilon_B - \dot{M}$  space *rightward* of each SN contour since this region produces a jet which is *brighter* than the observed limit. The region of reasonable parameter values for an off-axis jet is roughly bracketed by  $\dot{M}_{-5}/v_{w,3} = A_* = 0.1 - 1$  and  $\epsilon_B = 0.002 - 0.25$  as typically inferred from broadband modeling of cosmological GRBs. Four of the SNe contours rule out this entire shaded region while eleven place significant constraints. The recent detection of SN 2001em is consistent with a typical GRB jet only if the mass loss rate is  $\dot{M}_{-5}/v_{w,3} \approx 1$  (for  $\epsilon_B \approx 0.2$ ). The low end of the local distribution of observed Wolf-Rayet mass loss rates is also shown.

## Chapter 2

# The Sub-energetic GRB 031203 as a Cosmic Analogue to GRB 980425<sup>†</sup>

A. M. SODERBERG<sup>a</sup>, S. R. KULKARNI<sup>a</sup>, E. BERGER<sup>a</sup>, D. W. FOX<sup>a</sup>,  
M. SAKO<sup>b</sup>, D. A. FRAIL<sup>c</sup>, A. GAL-YAM<sup>a</sup>, D.-S. MOON<sup>d</sup>, S. B. CENKO<sup>d</sup>,  
S. A. YOST<sup>d</sup>, M. M. PHILLIPS<sup>e</sup>, S. E. PERSSON<sup>e</sup>, W. L. FREEDMAN<sup>e</sup>,  
P. WYATT<sup>e</sup>, R. JAYAWARDHANA<sup>f</sup>, D. PAULSON<sup>f</sup>

<sup>a</sup>Caltech Optical Observatories 105-24, California Institute of Technology, Pasadena, CA 91125,  
USA

<sup>b</sup>Stanford Linear Accelerator Center, 2575 Sand Hill Road M/S 29, Menlo Park, CA 94025, USA

<sup>c</sup>National Radio Astronomy Observatory, P.O. Box 0, Socorro, New Mexico 87801, USA

<sup>d</sup>Space Radiation Laboratory 220-47, California Institute of Technology, Pasadena, CA 91125,  
USA

<sup>e</sup>Carnegie Observatories, 813 Santa Barbara Street, Pasadena, CA 91101, USA

<sup>f</sup>Department of Astronomy, University of Michigan, 830 Dennison Bldg, Ann Arbor MI 48109  
USA

---

<sup>†</sup>A version of this chapter was published in *Nature*, vol. 430, 648–650, (2004).

Over the six years since the discovery (290) of the  $\gamma$ -ray burst GRB 980425, associated (151) with the nearby (distance,  $\sim 40$  Mpc) supernova 1998bw, astronomers have fiercely debated the nature of this event. Relative to bursts located at cosmological distances, (redshift,  $z \sim 1$ ), GRB 980425 was under-luminous in  $\gamma$ -rays by three orders of magnitude. Radio calorimetry (216, 226) showed the explosion was sub-energetic by a factor of 10. Here, we report observations of the radio and X-ray afterglow of the recent  $z = 0.105$  GRB 031203 (164, 304, 341) and demonstrate that it too is sub-energetic. Our result, when taken together with the low  $\gamma$ -ray luminosity (341), suggest that GRB 031203 is the first cosmic analogue to GRB 980425. We find no evidence that this event was a highly collimated explosion viewed off-axis. Like GRB 980425, GRB 031203 appears to be an intrinsically sub-energetic  $\gamma$ -burst. Such sub-energetic events have faint afterglows. Intensive follow-up of faint bursts with smooth  $\gamma$ -ray light curves (46, 267) (common to both GRBs 031203 and 980425) may enable us to reveal their expected large population.

On 3 December 2003 at 22:01:28 UT, the *INTEGRAL* satellite detected (164, 341) a seemingly typical long-duration ( $\Delta t \approx 20$  sec)  $\gamma$ -ray burst. Within 6 hours, the *Newton X-ray Multiple Mirror (XMM)* Observatory detected (335, 415) an X-ray source with flux (2–10 keV band),  $F_X = 3.95 \pm 0.09 \times 10^{-13}$  erg cm $^{-2}$  s $^{-1}$ , fading gradually  $\propto t^\alpha$  with  $\alpha = -0.4$ . Using the Very Large Array (VLA), we discovered a radio source at  $\alpha(\text{J2000}) = 08^{\text{h}}02^{\text{m}}30.18^{\text{s}}$  and  $\delta(\text{J2000}) = -39^\circ 51' 03.51''$  ( $\pm 0.1$  arcsec in each axis), well within the 6-arcsecond radius error circle of the *XMM* source. A subsequent *XMM* observation (320) confirmed the gradual decay of the X-ray source. From our analysis of the *XMM* data we find the flux  $\propto t^{-0.4}$  between the two epochs and the spectral flux density,  $F_{\nu,X} \propto \nu^\beta$ , is fit by  $\beta = -0.81 \pm 0.05$  with an absorbing column density,  $N_{\text{H}} = 6.2 \times 10^{21}$  cm $^{-2}$ . Taken together, the transient X-ray and radio emission are suggestive of afterglow emission.

In addition to monitoring the afterglow in various radio bands (Table 4.1 and discussion below) we obtained an observation of the source with the *Advanced CCD Imaging Spectrometer* (ACIS) instrument aboard the *Chandra* X-ray Observatory

(*CXO*). The *CXO* observations began on 22 January 2004 at 21:35 UT and lasted about 22 ksec. We detected a faint source, count rate in the 2–10 keV band of  $5.6 \times 10^{-4} \text{ s}^{-1}$ , at  $\alpha(\text{J2000})=08^{\text{h}}02^{\text{m}}30.159^{\text{s}}$  and  $\delta(\text{J2000})=-39^{\circ}51'03.51''$  ( $\pm 0.18$  arcsec in each axis), precisely coincident with the VLA source. Using the *XMM* model parameters stated above we obtain  $F_X = 6.4 \times 10^{-15} \text{ erg cm}^{-2} \text{ s}^{-1}$ , implying a faster decline ( $\alpha = -1 \pm 0.1$ ) between the second *XMM* and *Chandra* observations.

The primary interest in this burst is that the radio and X-ray afterglow coincides at the sub-arcsecond level (148) with a nearby ( $z = 0.1055$ ) galaxy (304), making it the nearest GRB with the exception of the peculiar GRB 980425 (151). At this redshift, the isotropic  $\gamma$ -ray energy release is  $10^2$  times smaller (341) than that of the nearest classical event GRB 030329 ( $z = 0.169$ ) (410) and yet a factor of  $10^2$  larger (290, 151) than that of GRB 980425.

The afterglow properties of GRB 031203 also appear to be intermediate between classical cosmological GRBs and GRB 980425: the isotropic X-ray luminosity of GRB 031203 at  $t \approx 10$  hours is  $L_X = 9 \times 10^{42} \text{ erg cm}^{-2} \text{ s}^{-1}$ , nearly  $10^3$  times fainter than that observed (23) for classical GRBs but a factor of  $10^2$  brighter (290) than that of GRB 980425. In the centimetre band, the peak luminosity is  $L_{\nu, 8.5 \text{ GHz}} \approx 10^{29} \text{ erg s}^{-1} \text{ Hz}^{-1}$ , fainter (132) by a factor of  $10^2$  than that of most radio afterglows but comparable (216) to that of GRB 980425. Since  $L_X$  and peak radio luminosity of an afterglow can be used (280, 23) as rough proxies for the afterglow energy, the data suggest that GRBs 031203 and 980425 are sub-energetic in comparison with classical GRBs.

As a next step, we applied the simplest afterglow model (339, 171) (a spherical relativistic blastwave shocking a constant density circumburst medium and accelerating relativistic electrons; the afterglow emission arises from synchrotron emission of shocked electrons) to the afterglow data and we obtain a satisfactory fit (Figure 2.1). On the timescales best probed by the radio data - days to months - we see no evidence for a collimated (jet) geometry commonly seen (133) in the afterglows of cosmological GRBs.

From our modeling we confirm that the blast wave is sub-energetic, find-

ing an inferred afterglow energy of  $E_{\text{AG}} \approx 1.7 \times 10^{49}$  erg. The circumburst particle density  $n \approx 0.6 \text{ cm}^{-3}$ , is not atypical of that inferred (280) for other GRBs. The blastwave is expected to become (417) non-relativistic on a timescale,  $t_{\text{NR}} \approx 34(E_{\text{AG},50}/n_0)^{1/3} \text{ d}$ , where we adopt the notation  $q \equiv 10^x q_x$ . The observational signatures (135) of this transition, a steeper decay of the spectral peak frequency ( $\nu_m \propto t^{-1.5} \rightarrow t^{-3}$ ) and an increase in the spectral peak flux ( $F_{\nu_m} \propto t^0 \rightarrow t^{3/5}$ ) are consistent with the data (Figure 2.1).

Here we use  $E_{\text{AG}}$  to denote the kinetic energy remaining in the blast wave after the prompt  $\gamma$ -ray energy release. In turn, the  $\gamma$ -ray emission arises from ultra-relativistic (bulk Lorentz factor,  $\Gamma \gtrsim 100$ ) ejecta within the blastwave. Thus, a more complete picture of the explosion energy is visualized through a two-dimensional plot of  $E_{\text{prompt}}$ , the beaming-corrected prompt energy release versus  $E_{\text{AG}}$  (Figure 2.2).

The two nearest events, GRBs 031203 and 980425, are clearly sub-energetic outliers in Figure 2.2. Furthermore, we draw the reader’s attention to several additional similarities: GRBs 031203 and 980425 (1) show no evidence for jets (216), (2) possess simple  $\gamma$ -ray light curves (290, 341); and with respect to cosmological (“classical”) bursts the two events (3) violate (341) the  $E_{\text{prompt}} - E_{\text{peak}}$  relation (4) and (4) are outliers in the luminosity-spectral lag relation (267). This discussion motivates the question: *How are these two events related to cosmological GRBs?*

It has been suggested (e.g.,(264)) that all GRB explosions have the same energetics and explosion geometry. In this framework, sub-energetic bursts are simply events viewed away from the jet axis. Such bursts should have a soft  $E_{\text{peak}}$  and also exhibit a rise in the inferred  $E_{\text{AG}}$  as shocked ejecta eventually come into our line of sight. For GRB 031203,  $E_{\text{peak}} > 190 \text{ keV}$  (341), comparable to cosmological GRBs for which we have observational evidence favoring an on-axis viewing angle. Moreover, we see no evidence for an increase in  $E_{\text{AG}}$  during the timescale of the radio observations ( $\sim 150$  days). Similarly, there is no evidence that  $E_{\text{AG}}$  is increasing for GRB 980425 despite dedicated radio monitoring (357) of the source since 1998. With no indication of being off-axis explosions, we presently conclude

that GRBs 031203 and 980425 are intrinsically sub-energetic events.

Astronomers have had to wait six years to discover a sub-energetic event similar to GRB 980425, despite a large population (as implied by their proximity). The bulk of the population has escaped our attention due to their faint  $\gamma$ -ray and afterglow emission which challenge our current detection limits. The *Swift* satellite mission, with its higher  $\gamma$ -ray sensitivity (compared to current missions) and improved localization capability (enabling rapid identification of afterglow counterparts) is expected to revolutionize our understanding of cosmic explosions.

GRB research at Caltech is supported in part by funds from NSF and NASA. We are, as always, indebted to Scott Barthelmy and the GCN. The VLA is operated by the National Radio Astronomy Observatory, a facility of the National Science Foundation operated under cooperative agreement by Associated Universities, Inc.. AMS is supported by an NSF Graduate Research Fellowship. AG acknowledges support by NASA through a Hubble Fellowship grant.

Table 2.1. Radio Observations of GRB 031203

Epoch (UT)	$\Delta t$ (days)	$F_{\nu,1.43}$ ( $\mu\text{Jy}$ )	$F_{\nu,4.86}$ ( $\mu\text{Jy}$ )	$F_{\nu,8.46}$ ( $\mu\text{Jy}$ )	$F_{\nu,22.5}$ ( $\mu\text{Jy}$ )
2003 Dec 5.52	1.60	...	...	$0.540 \pm 0.062$	...
2003 Dec 7.52	3.60	...	...	$0.249 \pm 0.043$	...
2003 Dec 8.35	4.43	...	$0.393 \pm 0.060$	$0.053 \pm 0.052$	...
2003 Dec 12.38	8.46	...	...	$0.280 \pm 0.049$	...
2003 Dec 15.37	11.45	...	...	$0.304 \pm 0.042$	...
2003 Dec 17.38	13.46	...	$0.520 \pm 0.050$	$0.448 \pm 0.039$	$0.483 \pm 0.083$
2003 Dec 21.35	17.43	...	...	$0.457 \pm 0.041$	...
2003 Dec 23.37	19.45	...	...	$0.811 \pm 0.040$	...
2003 Dec 26.40	22.48	...	$0.583 \pm 0.054$	$0.467 \pm 0.046$	...
2003 Dec 31.33	27.41	...	...	$0.675 \pm 0.045$	...
2004 Jan 4.33	31.41	...	$0.728 \pm 0.055$	$0.459 \pm 0.047$	...
2004 Jan 8.26	35.34	...	$0.624 \pm 0.050$	$0.308 \pm 0.043$	...
2004 Jan 12.29	39.37	$1.011 \pm 0.113$	$0.598 \pm 0.063$	$0.647 \pm 0.045$	...
2004 Jan 15.35	42.43	$0.689 \pm 0.136$	$0.749 \pm 0.063$	$0.664 \pm 0.061$	...
2004 Jan 25.24	52.32	$0.710 \pm 0.082$	...	$0.450 \pm 0.044$	...
2004 Jan 26.34	53.42	...	$0.556 \pm 0.058$	...	...
2004 Feb 7.24	65.32	$0.937 \pm 0.112$	$0.751 \pm 0.045$	$0.533 \pm 0.028$	$0.273 \pm 0.066$
2004 Feb 15.22	73.30	$0.756 \pm 0.147$	$0.576 \pm 0.050$	$0.517 \pm 0.042$	...
2004 Feb 28.13	86.21	...	...	$0.517 \pm 0.047$	$0 \pm 0.114$
2004 Mar 6.17	93.25	$0.631 \pm 0.091$	$0.522 \pm 0.058$	$0.304 \pm 0.046$	...
2004 Mar 23.13	110.21	$0.787 \pm 0.169$	$0.593 \pm 0.062$	$0.432 \pm 0.042$	...
2004 Apr 19.07	137.15	...	...	$0.426 \pm 0.037$	...

Radio observations made with the Very Large Array (VLA). Observations commenced on 5 December 2003 UT. For all observations we used the standard continuum mode with  $2 \times 50$  MHz bands. At 22.5 GHz we used referenced pointing scans to correct for the systematic 10 – 20 arcsec pointing errors of the VLA antennas. We used the extra-galactic sources 3C 147 (J0542+498) and 3C 286 (J1331+305) for flux calibration, while the phase was monitored using J0828-375. The data were reduced and analyzed using the Astronomical Image Processing System. The flux density and uncertainty were measured from the resulting maps by fitting a Gaussian model to the afterglow emission.

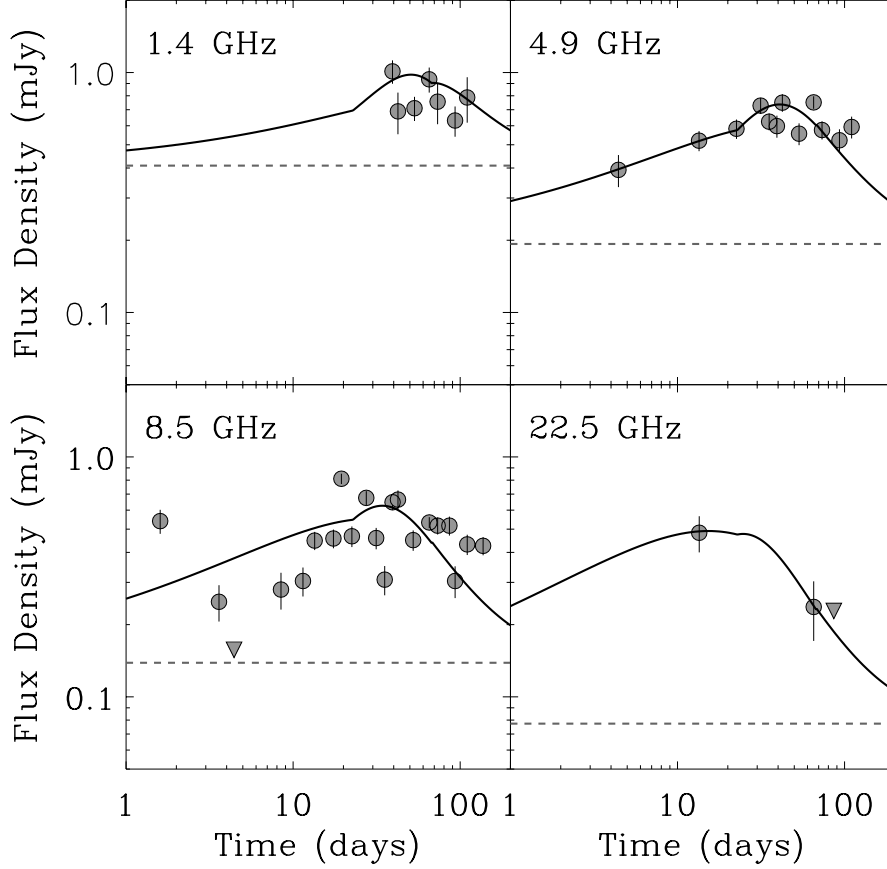


Figure 2.1: The solid lines are models of synchrotron (afterglow) emission from spherical ejecta expanding into a uniform circumburst medium (171). The models include a contribution from the host galaxy, which is well-fit by  $F_{\text{host}} \approx 0.4(\nu/1.4 \text{ GHz})^{-0.6} \text{ mJy}$  (dashed lines) and is consistent with the star formation rate inferred (304) from optical spectroscopy of the host. For our best-fit model, we find  $\chi_r^2 = 8.9$  (38 degrees of freedom), dominated by interstellar scintillation. The blastwave transitions to the non-relativistic regime at  $t_{NR} \approx 23$  d. From the derived synchrotron parameters (at  $t = 1$  d):  $\nu_a \approx 3.2 \times 10^8$  Hz,  $\nu_m \approx 3.6 \times 10^{12}$  Hz, and  $F_{\nu_a} \approx 0.04$  mJy we find an isotropic afterglow energy,  $E_{\text{AG, iso}} \approx 1.7 \times 10^{49} \nu_{c,15.5}^{1/4}$  erg, a circumburst density  $n \approx 0.6 \nu_{c,15.5}^{3/4} \text{ cm}^{-3}$ , and the fractions of energy in the relativistic electrons (energy distribution  $N(\gamma) \propto \gamma^{-p}$  with  $p \approx 2.6$ ) and magnetic field of  $\epsilon_e \approx 0.4 \nu_{c,15.5}^{1/4}$  and  $\epsilon_B \approx 0.2 \nu_{c,15.5}^{-5/4}$ , respectively. Here,  $\nu_c = 3 \times 10^{15} \nu_{c,15.5}$  is the synchrotron cooling frequency which is roughly constrained by the (non-synchrotron) SN 2003lw X-ray emission.

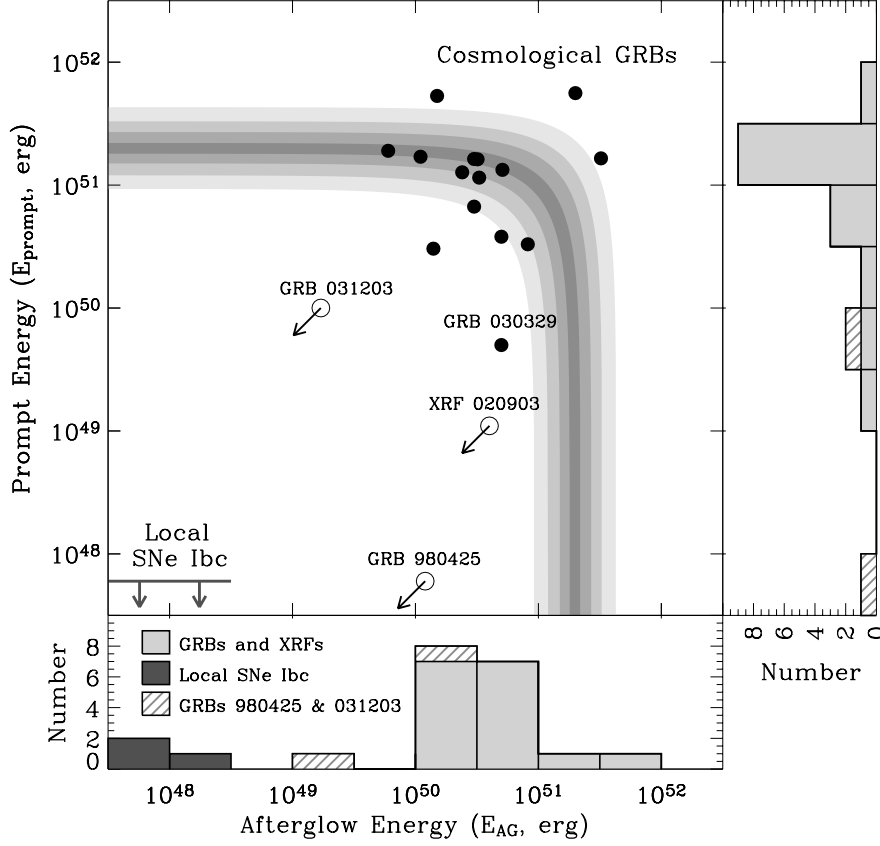


Figure 2.2: The energy in the prompt emission,  $E_{\text{prompt}}$ , and in the afterglow,  $E_{\text{AG}}$ , have been corrected (133, 44, 27) for beaming based on the jet-break time observed for each burst, except in the cases of GRB 980425 (226, 216), XRF 020903 (360) and GRB 031203 for which there is no evidence for a collimated outflow. For these three cases we plot the isotropic values of  $E_{\text{prompt}}$  and  $E_{\text{AG}}$  and use an arrow to indicate they represent upper limits on both axes. The arcs mark lines of constant  $E_{\text{prompt}} + E_{\text{AG}}$  as a guide to the reader. Most cosmological GRBs tend to cluster (27) around  $E_{\text{prompt}} + E_{\text{AG}} \approx 2 \times 10^{51}$  erg while GRBs 031203 and 980425, the nearest two bursts in the sample, are clearly sub-energetic. With the exception of SN 1998bw, associated with GRB 980425, there are no local Ibc supernovae with detected  $\gamma$ -ray emission, however the kinetic energy in the ejecta (excluding the photospheric energy yield), is generally found (26) to be  $E_{\text{AG}} \lesssim 3 \times 10^{48}$  erg (bottom left corner). Histograms of  $E_{\text{AG}}$  and  $E_{\text{prompt}}$  are shown in the bottom and side panels, respectively, for cosmological GRBs and local Ibc SNe. The striped energy bins show the locations of GRBs 980425 and 031203.

## Chapter 3

# Relativistic Ejecta from XRF 060218 and the Rate of Cosmic Explosions<sup>†</sup>

A. M. SODERBERG<sup>a</sup>, S. R. KULKARNI<sup>a</sup>, E. NAKAR<sup>b</sup>, E. BERGER<sup>c</sup>,  
 P. B. CAMERON<sup>a</sup>, D. B. FOX<sup>d</sup>, D. A. FRAIL<sup>e</sup>, A. GAL-YAM<sup>a</sup>, R. SARI<sup>a</sup>,  
 S. B. CENKO<sup>f</sup>, M. KASLIWAL<sup>a</sup>, R. A. CHEVALIER<sup>g</sup>, T. PIRAN<sup>h</sup>, P. A. PRICE<sup>i</sup>,  
 B. P. SCHMIDT<sup>j</sup>, G. POOLEY<sup>k</sup>, D.-S. MOON<sup>f</sup>, B. E. PENPRASE<sup>l</sup>, E. OFEK<sup>a</sup>,  
 A. RAU<sup>a</sup>, N. GEHRELS<sup>m</sup>, J. A. NOUSEK<sup>d</sup>, D. N. BURROWS<sup>d</sup>, S. E. PERSSON<sup>c</sup>,  
 P. J. MCCARTHY<sup>c</sup>

<sup>a</sup>Caltech Optical Observatories 105-24, California Institute of Technology, Pasadena, CA 91125,  
 USA

<sup>b</sup>Theoretical Astrophysics 130-33, California Institute of Technology, Pasadena, CA 91125, USA

<sup>c</sup>Carnegie Observatories, 813 Santa Barbara St., Pasadena, CA 91101, USA

<sup>d</sup>Department of Astronomy, Pennsylvania State University, University Park, PA 16802, USA

<sup>e</sup>National Radio Astronomy Observatory, P.O. Box 0, Socorro, New Mexico 87801, USA

<sup>f</sup>Space Radiation Laboratory 220-47, California Institute of Technology, Pasadena, CA 91125,  
 USA

<sup>g</sup>Department of Astronomy, University of Virginia, PO Box 3818, Charlottesville, VA 22903,  
 USA

---

<sup>†</sup>A version of this chapter was published in *Nature*, vol. 442, 1014–1017, (2006).

<sup>h</sup>Racah Institute of Physics, Hebrew University, Jerusalem 91904, Israel

<sup>i</sup>Institute for Astronomy, University of Hawaii, 2680 Woodlawn Drive, Honolulu, HI 96822, USA

<sup>j</sup>RSAA, ANU, Mt. Stromlo Observatory, via Cotter Rd, Weston Creek, ACT 2611, Australia

<sup>k</sup>Mullard Radio Astronomy Observatory, Cavendish Laboratory, Cambridge CB3 0HE, UK

<sup>l</sup>Pomona College Dept. of Physics & Astronomy, 610 N. College Ave, Claremont, CA 91711,  
USA

<sup>m</sup>NASA Goddard Space Flight Center, Greenbelt, MD 20771, USA

Over the last decade, long-duration  $\gamma$ -ray bursts (GRBs) including the subclass of X-ray flashes (XRFs) have been revealed (151, 216, 243) to be a rare variety of Type Ibc supernova (SN). While all these events result from the death of massive stars, the electromagnetic luminosities of GRBs and XRFs exceed those of ordinary Type Ibc SNe by many orders of magnitude. The essential physical process that causes a dying star to produce a GRB or XRF, and not just an SN, remains the crucial open question. Here we present radio and X-ray observations of XRF 060218 (associated (292) with SN 2006aj), the second nearest (59, 258) GRB identified to-date, which allow us to measure its total energy and place it in the larger context of cosmic explosions. We show that this event is 100 times less energetic but ten times more common than cosmological GRBs. Moreover, it is distinguished from ordinary Type Ibc SNe by the presence of  $10^{48}$  erg coupled to mildly-relativistic ejecta, along with a central engine (an accretion-fed, rapidly rotating compact source) which produces X-rays for weeks after the explosion. This suggests that the production of relativistic ejecta is the key physical distinction between GRBs/XRFs and ordinary SNe, while the nature of the central engine (black hole or magnetar) may distinguish typical bursts from low-luminosity, spherical events like XRF 060218.

On 2006 February 18.15 UT, the Burst Alert Telescope (BAT), a hard X-ray detector aboard the *Swift* satellite, detected (59) an exceedingly long-duration

( $\Delta t \approx 2000$  sec) transient. Within 153 seconds of the  $\gamma$ -ray trigger, the on-board X-ray Telescope (XRT) and Ultra-Violet Optical Telescope (UVOT) identified (59) a counterpart coincident (258) with a dwarf galaxy at  $z = 0.0335$ . The XRT and BAT data show (59) that the event peaked at a photon energy of 4.9 keV, thereby classifying this transient as an X-ray Flash, XRF 060218. Distinguished (181) by their soft X-ray dominated spectrum (peak energy,  $E_p \lesssim 25$  keV versus 250 keV), the subclass of XRFs are otherwise similar (see Soderberg et al. 361 and references therein) to GRBs in their observational properties.

Using the Very Large Array (VLA), we discovered a radio source at  $\alpha(\text{J2000})=03^{\text{h}}21^{\text{m}}39.68^{\text{s}}$  and  $\delta(\text{J2000})=16^{\circ}52'01.82''$  ( $\pm 0.02$  arcsec in each axis), coincident with the UVOT position. Our monitoring of the radio source showed a power-law decay with  $\alpha \approx -0.8$  through  $t \approx 22$  d (Table 4.1), similar to the decay of afterglows seen from GRBs; here  $F_\nu \propto t^\alpha$  is the spectral flux density. Over the same period the XRT undertook intensive observations of the source in the X-ray band (0.3–10 keV). We find the X-ray spectral flux density,  $F_{\nu,X} \propto \nu^{\beta_X}$ , is fit by  $\beta_X = -2.2 \pm 0.2$  with an absorbing column density,  $N_{\text{H}} = 3.9 \pm 0.4 \times 10^{21} \text{ cm}^{-2}$ , consistent with previously reported (59, 98) values.

Separately, we observed the source with the *Advanced CCD Imaging Spectrometer* (ACIS) instrument aboard the *Chandra* X-ray Observatory (*CXO*). These observations began on 2006 February 26.78 and March 7.55 UT ( $t \approx 8.8$  and 17.4 days) and lasted about 20 and 30 ks, respectively. The measured count rates are  $(1.9 \pm 0.3) \times 10^{-3}$  and  $(1.3 \pm 0.3) \times 10^{-3} \text{ s}^{-1}$ , respectively. Using the XRT model parameters stated above we derive  $F_X = (4.5 \pm 1.4) \times 10^{-14}$  and  $(2.8 \pm 0.9) \times 10^{-14} \text{ erg cm}^{-2} \text{ s}^{-1}$  for the unabsorbed flux values. The XRT-*CXO* data spanning the range from a few minutes to 17 d are well fit a simple power-law decay model with temporal index,  $\alpha_X = -1.1$ .

XRF 060218 is most interesting because it is nearby, distance  $d \approx 145$  Mpc. Indeed it is second only to GRB 980425/SN 1998bw (151) at just 36 Mpc. Similar to GRB 980425, XRF 060218 is also associated (292) with a Type Ic supernova explosion, SN 2006aj. The isotropic prompt energy release (59)  $E_{\gamma,\text{iso}} = (6.2 \pm$

$0.3) \times 10^{49}$  erg, is at least 100 times fainter than typical GRBs but comparable to another nearby event, GRB 031203 (341, 362) ( $z = 0.106$ ). Similarly, the radio and X-ray luminosities are  $10^3$  and  $10^2$  times fainter than those of cosmological GRBs, respectively.

Radio observations directly probe the ejecta and environments of stellar explosions since the blastwave (velocity  $v$ ) shocks the circumstellar medium and accelerates relativistic electrons which give rise to radio synchrotron emission. For radio sources dominated by synchrotron-self absorption, the brightness temperature is  $T_B \lesssim 4 \times 10^{10}$  K. As can be seen from Figure 3.1, at day 5 the radio emission peaks between 1.4 GHz and 4.9 GHz. Applying the basic equipartition analysis (see Kulkarni et al. 216) we find, at this epoch, that the radius of the radio emitting region is  $r \approx 3 \times 10^{16}$  cm, the ejecta kinetic energy is  $E_K \approx 2 \times 10^{48}$  erg and the circumburst particle density is  $n \approx 5 \text{ cm}^{-3}$ . The blast wave thus expands with a Lorentz factor  $\Gamma = (1 - \beta^2)^{-1/2} \sim 2.3$ ; here  $\beta \equiv v/c$ .

The early, steady decay of the radio emission indicates (367) that it cannot be attributed to a collimated jet directed away from our line-of-sight. Moreover, on a timescale,  $t_{\text{NR}} \approx 7.3(E_{\text{K},48}/n_0)^{1/3}$  days, the blastwave becomes (418) sub-relativistic ( $\Gamma\beta < 1$ ) at which point it effectively assumes spherical geometry, even if the initial explosion was biconical. Independently, noting the absence of a “jet break” in the radio light-curve (to 22 d) and applying the standard formulation (338) we find the opening angle,  $\theta_j \gtrsim 1.4$  radian. Thus, on several grounds, the radio data argue for a quasi-spherical ejecta with  $10^{48}$  erg coupled to mildly-relativistic material. In addition, our observations at 104 days show no evidence for a late-time increase in the radio flux, thus constraining the presence of additional ejecta components (off-axis jets; Figure 3.2) spreading into our line-of-sight.

As can be seen from Figure 3.1 the above synchrotron model is unable to explain the strong X-ray emission. Attributing the emission to scattering of SN optical photons by the mildly-relativistic ejecta requires an optical depth,  $\tau \sim 10^{-4}$ , too large to be produced by the shocked electrons which provide  $\tau = nr\sigma_T \sim 10^{-7}$ ; here  $\sigma_T$  is the Thomson cross section. We must therefore seek an entirely different

origin for the observed X-rays.

At day 1, the steep X-ray spectrum roughly connects to the peculiar optical/UV component ( $\beta_{OX} \sim -2$ ) observed (59) to peak on this timescale. A similar steep near-IR spectrum was seen (237) in GRB 031203 at  $t = 0.4$  d. Given that both GRB 031203 and XRF 060218 are (362, 341) sub-energetic events, we suggest that this mysterious steep component is ubiquitous among sub-energetic GRBs and speculate that a central engine is the origin of this intense, long-lived emission. One particularly attractive possibility is a rapidly rotating (period,  $P$ ) highly magnetized (field strength,  $B$ ) neutron star, a *magnetar*. The spin down power,  $\dot{E} = 10^{45}(P/10 \text{ ms})^{-4}(B/10^{15} \text{ G})^2 \text{ erg s}^{-1}$ , can explain the peculiar optical to X-ray integrated luminosity at 1 day while the temporal evolution requires a braking index lower than three (magnetic dipole). We note that similarly low braking indices are measured for young Galactic pulsars (e.g., Lyne et al. 232 and references therein).

Combining the sky coverage and detection thresholds of  $\gamma$ -ray missions, we estimate the following sensitivity to the two exemplars of low energy events (GRB 980425 and XRF 060218):  $3.8 \times 10^{-3}$  (*BeppoSAX*),  $1.2 \times 10^{-3}$  (*HETE-2*) and  $3.7 \times 10^{-3} \text{ Gpc}^3 \text{ yr}$  (*Swift*). Thus, the true rate of sub-energetic GRBs is  $230_{-190}^{+490} \text{ Gpc}^{-3} \text{ yr}^{-1}$  (90% confidence range; see Supplementary Information I), about 10 times more abundant than typical bright GRBs (346), for which we use a mean inverse beaming factor of  $\langle f_b^{-1} \rangle \sim 100$ ; here  $f_b \equiv 1 - \cos\theta_j$ . Separately, we note that sub-energetic GRBs could not be strongly beamed or the true rate of such events would exceed the local ( $d \lesssim 100 \text{ Mpc}$ ) rate (64, 95) of Type Ibc supernovae,  $9_{-5}^{+3} \times 10^3 \text{ Gpc}^{-3} \text{ yr}^{-1}$ .

Spectroscopy of the nearest GRB-associated supernovae (SNe 1998bw, 2003dh, 2003lw, and now 2006aj) reveals (see Pian et al. 292 and references therein) remarkably broad absorption lines (indicative of fast ejecta) and may suggest that all GRB-SNe are broad-lined (BL). Locally, BL events comprise (296) five percent of SNe Ibc. Thus, the rate of BL events and sub-energetic GRBs are comparable, suggesting that all BL SNe harbor a long-lived central engine.

Radio observations of an extensive sample of 144 optically-selected local SNe

Ibc, however, suggest (26, 367) a different picture (Figure 3.2). Not a single SN (BL or otherwise) shows strong early radio emission comparable to that seen in SNe 1998bw and 2006aj. Thus, we constrain the volumetric rate of such events to be  $\lesssim 300 \text{ Gpc}^{-3} \text{ yr}^{-1}$  (see Supplementary Information II), consistent with the rate of sub-energetic GRBs inferred above. Focusing on the BL SNe, less than one in three are similar to GRBs, indicating that broad lines cannot be used as a reliable proxy for a central engine.

The commonality between the three nearest events (980425, 060218, 031203) is their substantial ( $E_K \gtrsim 10^{48} \text{ erg}$ ) mildly-relativistic ( $\Gamma \gtrsim 2$ ) ejecta and a smooth pulse profile for the prompt emission. These two clues lead us to suggest that the primary *physical* distinction between GRBs/XRFs and ordinary supernovae is the velocity profile of the ejecta. For the latter, hydrodynamic collapse requires that the ejecta energy is concentrated at low velocities,  $E_K \propto (\Gamma\beta)^{-5.2}$ . In comparison, the shallow velocity profiles inferred for GRBs and XRFs indicate that some other agent (an engine) enables coupling of copious energy to relativistic material (Figure 3.3).

We conclude by noting that magnetars constitute (145) about 10% of the Galactic neutron star birth-rate, and thus a similar fraction of SNe Ibc. This rate is similar to that of the sub-energetic GRBs. Furthermore, magnetars produce long-lived emission (see Hurley et al. 191 and references therein) and have been suggested (404) previously as candidate GRB progenitors. We therefore speculate that a magnetar central engine is what distinguishes sub-energetic GRBs from the cosmological bursts, which are thought to be powered by a black hole.

GRB research at Caltech is supported in part by funds from NSF and NASA. We are, as always, indebted to Scott Barthelmy and the GCN. The VLA is operated by the National Radio Astronomy Observatory, a facility of the National Science Foundation operated under cooperative agreement by Associated Universities, Inc. AMS and SBC are supported by NASA Graduate Research Fellowships. EB and AG acknowledge support by NASA through a Hubble Fellowship grant. DNB and JAN acknowledge support by NASA.

Table 3.1. Radio Observations of XRF 060218

Epoch (UT)	$\Delta t$ (days)	$F_{\nu,1.43}$ ( $\mu\text{Jy}$ )	$F_{\nu,4.86}$ ( $\mu\text{Jy}$ )	$F_{\nu,8.46}$ ( $\mu\text{Jy}$ )	$F_{\nu,15.0}$ ( $\mu\text{Jy}$ )	$F_{\nu,22.5}$ ( $\mu\text{Jy}$ )
2006 Feb 20.02	1.87	—	$78 \pm 70$	$453 \pm 77$	—	—
2006 Feb 21.14	3.00	—	—	$381 \pm 60$	—	$250 \pm 52$
2006 Feb 21.77 <sup>†</sup>	3.62	—	—	—	$350 \pm 350$	—
2006 Feb 21.97	3.83	—	$287 \pm 56$	$269 \pm 40$	—	—
2006 Feb 22.99	4.85	$25 \pm 25$	$328 \pm 61$	$280 \pm 47$	—	—
2006 Feb 25.12	6.97	$134 \pm 145$	$80 \pm 47$	$164 \pm 39$	$46 \pm 141$	—
2006 Feb 26.09	7.94	—	$32 \pm 32$	$30 \pm 30$	—	—
2006 Feb 28.10	9.95	—	—	$39 \pm 25$	—	—
2006 Mar 2.23	12.08	$70 \pm 70$	—	—	—	—
2006 Mar 3.03	12.88	—	—	$15 \pm 15$	—	—
2006 Mar 6.89	16.74	—	—	$75 \pm 13$	—	—
2006 Mar 10.01	19.86	—	—	$48 \pm 14$	—	—
2006 Mar 12.11	21.96	—	—	$87 \pm 39$	—	—
2006 Mar 15.04	24.91	—	—	$20 \pm 20$	—	—
2006 Mar 20.86	30.71	—	—	$32 \pm 20$	—	—
2006 Mar 24.96	34.81	—	—	$15 \pm 18$	—	—
2006 Mar 26.85	36.70	$69 \pm 69$	$5 \pm 37$	—	—	—
2006 Mar 31.89	41.74	—	—	$22 \pm 22$	—	—
2006 Apr 9.84	50.70	—	—	$25 \pm 25$	—	—
2006 Jun 2.67	104.52	—	—	$17 \pm 21$	—	—

Radio observations made with the Very Large Array (VLA) and the Ryle Telescope<sup>†</sup>. We used the standard continuum mode with  $2 \times 50$  MHz bands (VLA) and 350 MHz bandwidth (Ryle).

At 22.5 GHz we used referenced pointing scans to correct for the systematic  $10 - -20$  arcsec pointing errors of the VLA antennas. We used the extra-galactic sources 3C 48 (J0137+331) and 3C 147 (J0542+498) for flux calibration, while the phase was monitored using J0319+190 (VLA) and J0326+1521 (Ryle). The data were reduced and analyzed using the Astronomical Image Processing System. The flux density and uncertainty were measured from the resulting maps by fitting a Gaussian model to the afterglow emission.

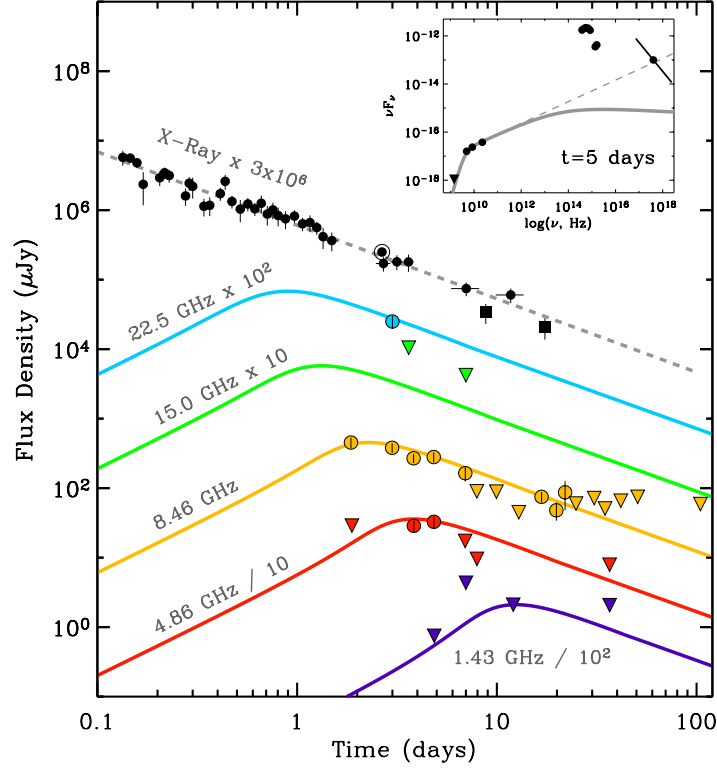


Figure 3.1: Radio measurements are summarized in Table 4.1. Upper limits are given as  $3\sigma$  (inverted triangles). Solid lines are models of synchrotron emission from a spherical shock expanding into a wind-blown circumstellar medium ( $n \propto r^{-2}$ ). At  $t = 5$  d the radio spectrum peaks near 4 GHz due to the synchrotron self-absorption frequency,  $\nu_a$ . We assume that the energy density is partitioned between the relativistic electrons (energy distribution  $N(\gamma) \propto \gamma^{-p}$  with  $p \approx 2.1$ ) and magnetic field as  $\epsilon_e = \epsilon_B = 0.1$ . We find that  $E_K \approx 2 \times 10^{48}$  erg is coupled to ejecta with  $\Gamma \approx 2.3$ . The expansion,  $r \propto t^m$ , appropriate (71) for a core-collapse SN explosion with a distribution of ejecta velocities, is fit with  $m \approx 0.85$ . We infer a progenitor mass loss rate of  $2 \times 10^{-7} M_\odot \text{ yr}^{-1}$  (for wind velocity,  $v_w = 10^3 \text{ km s}^{-1}$ ). These parameters constrain the characteristic synchrotron frequency,  $\nu_m \approx 0.3$  GHz, and the synchrotron cooling frequency,  $\nu_c \approx 10^{14}$  Hz, at  $t = 5$  days and thus  $\nu_m < \nu_a$ ; consistent with the observed radio spectrum (inset, solid grey curve). A nearly identical fit is obtained for a trans-relativistic GRB blastwave expanding into a constant density circumstellar medium (171) for parameters:  $E_K \approx 1.2 \times 10^{48}$  erg,  $n = 10^2 \text{ cm}^{-3}$ ,  $\epsilon_e = \epsilon_B = 0.1$ , and  $p = 2.1$ ; in this case the mildly-relativistic ejecta is assumed to expand with a single bulk Lorentz factor. These values constrain the geometry of the ejecta to be effectively spherical,  $\theta_j \gtrsim 1.4$ . The X-ray flux (XRT=circles; XMM=encircled dot, scaled to XRT spectral model; CXO=squares) is significantly brighter than an extrapolation of the above model as evidenced by the unusually flat radio to X-ray spectral index,  $\beta_{RX} \approx -0.5$  (inset, dashed line), and the steep X-ray spectrum  $\beta_X \approx -2.2$  (inset, black line), instead of  $\beta_X \sim -1.1$  for typical GRBs. We suggest that the integrated optical to X-ray luminosity ( $10^{44} \text{ erg s}^{-1}$ ;  $2 - 10^4 \text{ eV}$ ) can be attributed to the spin-down power of a magnetar. By day 5, the optical/UV spectrum is dominated by the thermal SN emission (inset).

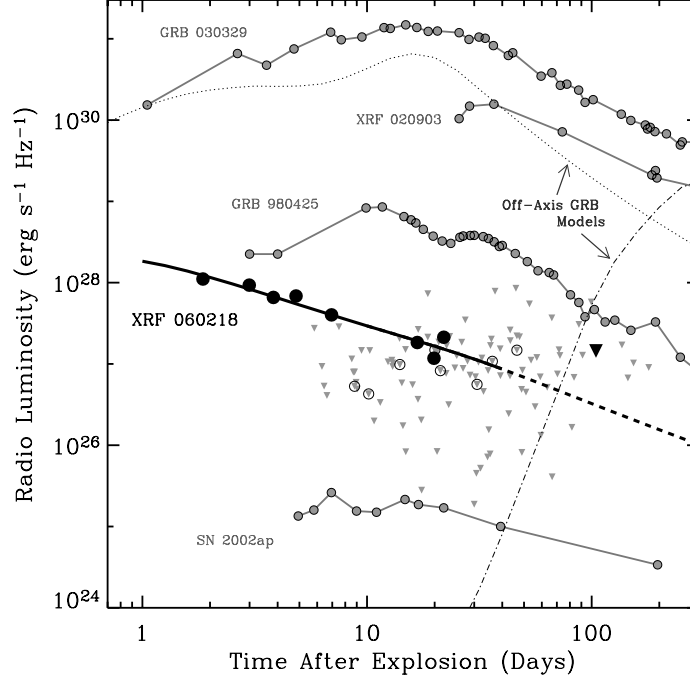


Figure 3.2: Since 1999 we have been monitoring the radio emission from optically-selected SNe Ibc with the Very Large Array. We use radio luminosity as a proxy for mildly-relativistic ejecta to quantify the fraction of SNe Ibc powered by central engines. Our observations of 144 SNe show that most SNe Ibc do not produce strong radio emission and therefore show no evidence for a central engine. For comparison, we include the radio afterglows for nearby ( $z \lesssim 0.25$ ) GRBs 980425 and 030329, and XRF 020903 all three of which show (216, 27, 361) evidence for an engine-driven explosion. XRF 060218 is intermediate between GRBs and BL SN2002ap, demonstrating that broad lines are not a reliable proxy for strong radio emission. Radio limits for other local broad-lined SNe (encircled triangles) show that less than one in three of these events may have a radio luminosity comparable to XRF 060218 or GRB 980425 (90% confidence level). In addition, we show two 8.5 GHz model light-curves for a typical GRB viewed away from the collimation axis. Both models adopt typical GRB parameters (see Soderberg et al. 367 and references therein) of  $\Gamma = 100$ ,  $E_{K,\text{iso}} = 10^{53}$  erg,  $n = 1 \text{ cm}^{-3}$ ,  $\epsilon_e = \epsilon_B = 0.1$ , and  $p = 2.1$ . In the first model we assume that the observed  $\gamma$ -ray and radio emission are produced by a GRB jet viewed from an angle  $\theta_{\text{obs}} = 2\theta_j$ ; here  $\theta_{\text{obs}}$  is the angle between our line-of-sight and the jet axis. Under this framework, the observed prompt emission properties ( $\Delta t$ ,  $E_p$ ,  $E_{\gamma,\text{iso}}$ ) are related to the intrinsic values through the quantity  $D \equiv [\Gamma(\theta_{\text{obs}} - \theta_j)]^{-2}$ . For  $D \sim 0.02$ , the intrinsic properties for XRF 060218 would be typical for GRBs:  $\Delta t \sim 40$  sec,  $E_p \sim 250$  keV,  $E_{\gamma,\text{iso}} \sim 10^{53}$  erg, and  $\theta_j \sim 4^\circ$ . The resulting off-axis model (dotted line) is a factor of  $10^3$  brighter than the observed XRF 060218 radio light-curve and can therefore be ruled out. In the second model, we assume that in addition to the quasi-spherical mildly-relativistic ejecta component producing the observed radio emission, XRF 060218 also harbors a strongly collimated relativistic jet directed significantly away from our line-of-sight. In this scenario, we expect (418, 367) a late-time radio re-brightening as the jet becomes non-relativistic and spreads sideways into our line-of-sight. Adopting  $\theta_j = 4^\circ$  we find that our latest radio limit (104 days; black triangle) rules out an off-axis GRB with  $\theta_{\text{obs}} \lesssim 60^\circ$  (dash-dot line). We conclude that the XRF 060218 ejecta was quasi-spherical and intrinsically sub-energetic.

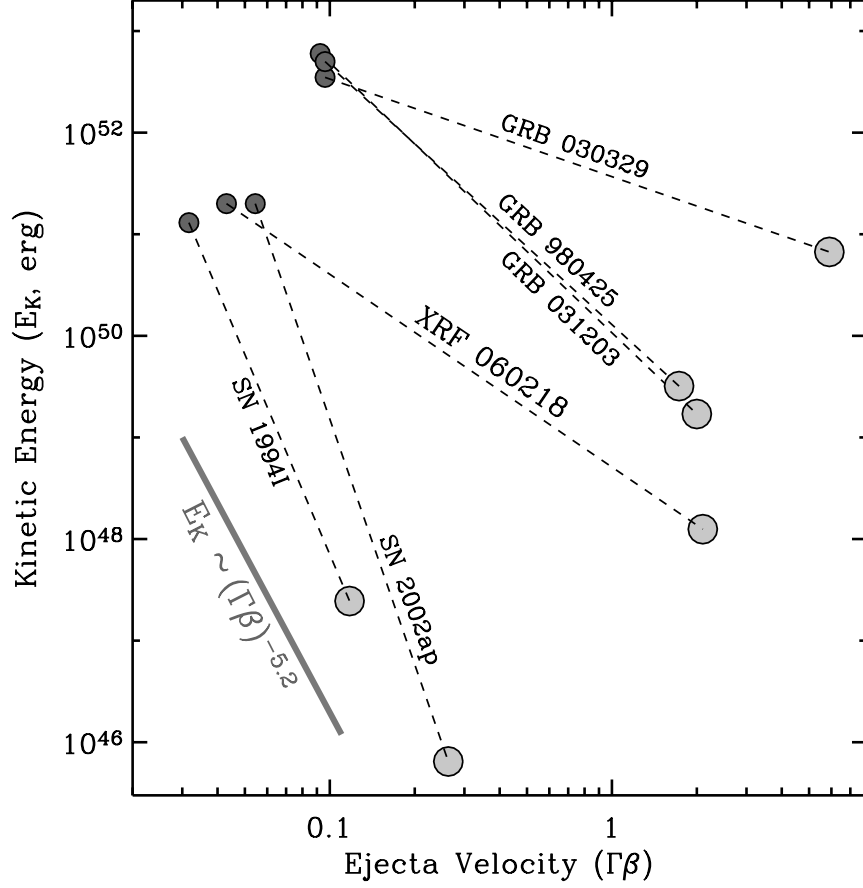


Figure 3.3: Optical data (small dark circles) probe (see Baron et al. 9, Mazzali et al. 250 and references therein) the slowest ejecta in supernova explosions which typically carry the bulk of the kinetic energy ( $E_K = 0.3M_{\text{ej}}v_{\text{ej}}^2 \sim 10^{51}$  erg). On the other hand, radio observations (large light circles) trace (27, 216, 362, 26, 71) only the fastest ejecta in the explosion. For GRBs 030329 and 031203,  $\Gamma \propto t^{-3/8}$ ; we adopt the bulk velocity of the relativistic ejecta at day 1 as inferred from radio modeling. For GRB 980425, XRF 060218, SN 2002ap and SN 1994I the bulk velocity is roughly constant on the timescale probed by the radio observations; we adopt the velocity at the radio peak time. Standard hydrodynamic collapse results (388) in a kinetic energy profile,  $E_K \propto (\Gamma\beta)^{-5.2}$  (grey line), and thus a negligible fraction of the kinetic energy may be coupled to mildly-relativistic ejecta, consistent with the radio observations of local Ibc SNe 1994I and 2002ap. In the case of typical GRBs (e.g., GRB 030329), however, the kinetic energy of the mildly-relativistic ejecta is nearly comparable to that of the slower material indicating the presence of a central engine. Since the origin of the relativistic flow is separate from the SN, there is probably not a continuous distribution of matter between the two data points but rather distinct ejecta components. Sub-energetic bursts such as XRF 060218 are intermediate between these two classes and may indicate that their central engines are different than those of typical GRBs. We conclude that the minimum criteria for producing GRBs and XRFs is a mildly-relativistic ( $\Gamma \gtrsim 2$ ), quasi-spherical ejecta carrying at least  $10^{48}$  erg.

## SUPPLEMENTARY INFORMATION

**I. Estimates for the Rate of Sub-energetic GRBs:** To estimate the rate of sub-energetic events similar to GRB 980425 ( $d = 36.1$  Mpc) and XRF 060218 ( $d = 145$  Mpc), we consider only the satellite instruments with precise localization capability: *BeppoSAX* Wide Field Cameras (WFC), *High Energy Transient Explorer 2 (HETE-2)* Wide Field X-ray Monitor (WXM), and *Swift* Burst Alert Telescope (BAT). Inclusion of *INTEGRAL* would not significantly affect our results due to its low GRB detection rate. For these three instruments we adopt the detection threshold curves calculated by Band (2003, ApJ, 588, 945; 2006, ApJ, 644, 378) in units of peak photon flux per second ( $F_{\text{peak}}$ ; 1-1000 keV) as a function of the  $\nu F_{\nu}$  spectral peak energy,  $E_{\text{peak}}$ . We assume the shape of the prompt emission spectrum is fit by a broken power-law (Band *et al.* 1993, ApJ, 413, 281) such that  $F_{\nu} \propto \nu^{\alpha}$  ( $F_{\nu} \propto \nu^{\beta}$ ) for  $h\nu < E_{\text{peak}}$  ( $h\nu > E_{\text{peak}}$ ). Using the observed spectral parameters ( $F_{\text{peak}}$ ,  $E_{\text{peak}}$ ,  $\alpha$ ,  $\beta$ ) we calculate the sensitivity of each instrument to each of the two events.

For GRB 980425,  $F_{\text{peak}} \approx 3 \times 10^{-7}$  erg cm $^{-2}$  s $^{-1}$  (24-1820 keV; Galama *et al.* 1998, Nature, 395, 670)  $E_{\text{peak}} \approx 160$  keV,  $\alpha \approx -0.27$  and  $\beta \approx -2$  (Jimenez, Band & Piran 2001, ApJ, 561, 171). Extrapolating to the 1-1000 keV band, we find that the peak photon flux is  $F_p \approx 8.4$  ph cm $^{-2}$  s $^{-1}$  and thus the event could be detected to 120 (WFC), 60 (WXM) and 130 (BAT) Mpc.

For XRF 060218,  $F_{\text{peak}} \approx 5 \times 10^{-8}$  erg cm $^{-2}$  s $^{-1}$  (15-150 keV; Campana *et al.* 2006, Nature, submitted)  $E_{\text{peak}} \approx 4.9$  keV,  $\beta \approx -1.5$  and  $\alpha$  is not constrained (15-150 keV; Campana *et al.* 2006, Nature, submitted). We estimate  $F_p \approx 1.9$  ph cm $^{-2}$  s $^{-1}$  and therefore XRF 060218 could be detected to 220 (WFC), 110 (WXM) and 180 (BAT) Mpc. We note that unlike other missions, the BAT detection threshold is significantly lower (factor of  $\sim 3$ ) for unusually long duration events such as XRF 060218.

Next we estimate the effective monitoring time,  $T_m$  of each of the missions assuming their sky coverage,  $S$  and operation time,  $T$ . For the two Wide Field Cameras  $S = 2 \times 0.123 = 0.246$  sr (Band, 2003, ApJ, 588, 945) and  $T = 4$  yrs,

and for WXM  $S = 0.806$  sr and  $T = 3$  yrs (Guetta *et al.*, 2004, ApJ, 615, L73). For BAT,  $S = 2$  sr and  $T = 1$  yr (S. Barthelmy, private communication). Thus we find monitoring times,  $T_m = (T/4\pi)S$ , of 0.08 (WFC), 0.19 (WXM), and 0.16 (BAT) yrs. We estimate the sensitivity of these instruments to each of the events as  $T_m \times V$ ; here  $V$  is the volume to which each event could be detected. Adopting the larger of the two sensitivities for each instrument we find  $3.8 \times 10^{-3}$  (WFC),  $1.2 \times 10^{-3}$  (WXM) and  $3.7 \times 10^{-3}$  (BAT) Gpc<sup>3</sup> yr. Summing the sensitivities, we find that the rate of sub-energetic events is  $230_{-190}^{+490}$  Gpc<sup>-3</sup> yr<sup>-1</sup> where the errors are dominated by the 90% Poisson statistics for two detections (Gehrels, 1986, ApJ, 303, 336).

**II. Estimates for the rate of Type Ibc supernovae like GRB 980425 and XRF 060218:** To estimate the rate of SNe Ibc with strong, early radio emission comparable to that observed for sub-energetic bursts we only consider the 75 events (out of 144 optically-selected local SNe Ibc) with  $3\sigma$  upper limits fainter than the observed GRB 980425 and XRF 060218 light-curves at that same epoch. We then assume various values for the true fraction of SNe Ibc with radio emission comparable (or higher) to that of XRF 060218 and GRB 980425 and determine the probability of finding null-detections for all 75 events for each assumed fraction. Larger fractions are ruled out with higher confidence. At 90% confidence, we rule out the scenario where  $\gtrsim 3\%$  of SNe Ibc are as radio bright as XRF 060218 and GRB 980425. Adopting the local rate of SNe Ibc,  $9_{-5}^{+3} \times 10^3$  Gpc<sup>-3</sup> yr<sup>-1</sup>, as measured by Cappellaro *et al.* (1999, Astr. Astrophysics, 351, 459) and Dahlen *et al.* (2004, ApJ, 613, 189), we conclude that the volumetric rate of events like GRB 980425 and XRF 060218 is less than 3% of the local SNe Ibc sample, or  $\lesssim 300$  Gpc<sup>-3</sup> yr<sup>-1</sup>.

Repeating this analysis for the subset of broad-lined SNe Ibc, we find that at 90% confidence we can rule out the scenario where  $\gtrsim 30\%$  of local, optically selected BL SNe Ibc produce radio emission similar to that observed for GRB 980425 and XRF 060218.

## Part II

# The Nature of X-ray Flashes

The Nature of X-ray Flashes

## Chapter 1

# A Redshift Determination for XRF 020903: First Spectroscopic Observations of an X-ray Flash<sup>†</sup>

A. M. SODERBERG<sup>a</sup>, S. R. KULKARNI<sup>a</sup>, E. BERGER<sup>a</sup>, D. B. FOX<sup>a</sup>,  
P. A. PRICE<sup>a</sup>, S. A. YOST<sup>a</sup>, M. P. HUNT<sup>a</sup>, D. A. FRAIL<sup>b</sup>, M. HAMUY<sup>c</sup>,  
S. A. SHECTMAN<sup>c</sup>, J. P. HALPERN<sup>d</sup>, N. MIRABEL<sup>d</sup>

<sup>a</sup>Division of Physics, Mathematics and Astronomy, MS 105-24, California Institute of  
Technology, Pasadena, CA 91125, USA

<sup>b</sup>National Radio Astronomy Observatory, P.O. Box 0, Socorro, NM 87801, USA

<sup>c</sup>Carnegie Observatories, 813 Santa Barbara Street, Pasadena, CA 91101, USA

<sup>d</sup>Astronomy Department, Mailcode 5246, Columbia University, New York, NY 10027, USA

## Abstract

We report the discovery of optical and radio afterglow emission from the extremely soft X-ray flash, XRF 020903. Our spectroscopic observations provide the first redshift for an X-ray flash, thereby setting the distance scale for these events. At

---

<sup>†</sup>A version of this chapter was published in *The Astrophysical Journal*, vol. 606, 994–999, (2004). Reproduced by permission of the AAS.

$z = 0.251$ , XRF 020903 is one of the nearest cosmic explosions ever detected, second only to the recent GRB 030329 and the unusual GRB 980425/SN 1998bw. Moreover, XRF 020903 is the first X-ray flash for which we detect an optical afterglow. The luminosity of the radio afterglow of XRF 020903 is 1000 times greater than that of Ibc supernovae but similar to those of GRB afterglows. From broadband afterglow modeling we show that the explosion energy of XRF 020903 is not dissimilar from values inferred for typical gamma-ray bursts, suggesting that these cosmological explosions may derive from a similar mechanism.

## 1.1 Introduction

Prior to the detection of afterglows, gamma-ray bursts (GRBs) were enshrouded in mystery for nearly thirty years. Great progress in our understanding of these energetic events came with the first redshift measurement which placed GRBs at cosmological distances (256). In a similar fashion, the mystery of X-ray flashes (XRFs) has been fueled by the absence of confirmed redshifts. These events, identified in the 1990s by *BeppoSAX*, are characterized by a peak energy in  $\nu F_\nu$  of  $E_{\text{peak}} \sim 25$  keV (compared to  $E_{\text{peak}} \sim 250$  keV for GRBs). With a distribution of durations similar to those observed for GRBs, it has been assumed that XRFs are associated with GRBs and therefore share their extragalactic distance scale (181).

The subsequent discovery of XRF X-ray and radio afterglows with properties similar to those observed in GRB afterglows has further strengthened this association (177, 3, 390). Still, the question of whether the difference between GRBs and XRFs is intrinsic or extrinsic remains unanswered. Assuming XRFs are simply GRBs observed away from the jet collimation axis, they would have less  $\gamma$ -ray emission and the difference is extrinsic, based solely on the line-of-sight to the observer. On the other hand, the difference could be intrinsic, namely XRFs may represent a class of explosions which are similar in energetics to GRBs yet characterized by less relativistic ejecta possibly due to a heavier baryonic load. It is clear that by setting the distance scale for XRFs (and hence their energy scale) we

can begin to distinguish between extrinsic and intrinsic effects.

In this paper we present the first spectroscopic redshift for an X-ray flash, XRF 020903, placing this event among the nearest high-energy explosions and offering confirmation that X-ray flashes are cosmological and produce a total energy output similar to that observed in GRBs.

## 1.2 Observations

On 2002 September 3.421 UT the Wide-Field X-ray Monitor (WXM) and Soft X-ray Camera (SXC) aboard the High Energy Transient Explorer-2 (HETE-2) detected an X-ray flash within the 0.5–10 keV energy band. With an exceptionally low peak energy of  $E_{\text{peak}} \sim 5$  keV and a fluence of  $7.2 \times 10^{-8}$  erg cm $^{-2}$ , XRF 020903 is the softest event ever detected by HETE-2 with a ratio of X-ray fluence ( $S_X$ ) to  $\gamma$ -ray fluence ( $S_\gamma$ ) of  $\log(S_X/S_\gamma) = 4.3$  (329). Ground analysis provided a localization for XRF 020903 centered at  $\alpha(\text{J2000}) = 22^{\text{h}}49^{\text{m}}01^{\text{s}}$ ,  $\delta(\text{J2000}) = -20^{\circ}55'47''$  with a  $4' \times 31'$  uncertainty region at  $\Delta t \approx 0.3$  days (318).

### 1.2.1 Ground-based Photometry

We began observing the field of XRF 020903 on 2002 September 4.32 UT ( $\Delta t \approx 0.9$  days) with the Palomar Observatory 200-inch telescope (P200) equipped with the Large Field Camera (LFC). With a total exposure time of 20 minutes under photometric conditions (stellar FWHM  $\sim 1.2''$ ) the observations reached a limiting magnitude of  $R \sim 23$  mag. Visual comparison with Digitized Sky Survey archival images did not reveal an afterglow candidate.

A second epoch was obtained on September 10.30 UT ( $\Delta t \approx 7$  days) using the same observational set-up and in similar observing conditions. Image subtraction between the first and second epochs revealed one variable object within the HETE-2 error region (Figure 1.1) located at  $\alpha(\text{J2000}) = 22^{\text{h}}48^{\text{m}}42.34^{\text{s}}$ ,  $\delta(\text{J2000}) = -20^{\circ}46'09.3''$  and lying  $\sim 4$  arcsec NW of a bright elliptical galaxy (hereafter G2; Soderberg et al. 371).

With an approximate magnitude of  $R \approx 19$  at  $\Delta t \approx 1$  day, the new object decreased in brightness by 1.4 magnitudes between the two epochs, implying a temporal flux decay index of  $\alpha \approx -1$ . As the source proved consistent with a typical GRB afterglow evolution, the optical transient was adopted as a suitable candidate for the optical afterglow of XRF 020903.

We observed the afterglow position on three additional epochs with the P200 and the MDM Observatory 1.3 meter telescope (Table 1.1 and Figure 1.2). These, along with Digitized Sky Survey archival images, reveal the presence of an extended source with  $R \sim 21$  mag coincident with the position of the transient and thereby suggestive of a host galaxy (hereafter G1).

Due to the underlying extended source and the proximity of the transient to G2, accurate magnitude estimates relied on careful PSF photometry of the field. Absolute calibration of field stars was supplied by Henden (182). We used 12 unsaturated field stars in common between the Palomar and Henden images to fully calibrate observations of the variable source. We note that although the transient decreased in brightness quickly between the first two epochs, later epochs ( $\Delta t \approx 30 - 40$  days) appear to indicate a plateau in the light curve which was confirmed by other observers (163) and may originate from unresolved flux contamination from G1.

### 1.2.2 Ground-based Spectroscopy

Initial spectroscopy of the transient was performed on 2002 September 28.1 UT with the Magellan Baade Telescope using the Low Dispersion Survey Spectrograph (LDSS2). A position angle of 168 degrees was used such that spectral information on G1 and G2 was obtained simultaneously. Despite the positional coincidence of G2 and G1, it was found that the systems are not physically associated, separated by 3900 km/s in velocity space (371). In this epoch, the transient source was still significantly bright.

Further spectroscopic observations were made of the putative host (G1) with the Echelle Spectrograph & Imager (ESI) mounted on the Keck II telescope on

2003 July 4 UT ( $\Delta t \approx 300$  days). These observations do not include any flux from the transient source. During a total exposure time of 1 hour, we obtained a spectrum of G1 and G2 with a slit width of 0.75 arcsec.

We find that G2 is a large elliptical galaxy with at least one interacting galaxy companion, G3, located  $< 1''$  to the NE (see Figure 1.4). Observations of G2 exhibit a relatively smooth continuum with features typical of an elliptical galaxy. The Ca II H and K absorption lines give a redshift of  $z = 0.235$ , while G3 is offset by only 240 km/s at a redshift of  $z = 0.236$ .

In contrast, G1 is shown to be an active star-forming galaxy at  $z=0.251$  with a rich set of narrow bright emission lines (Figure 2). The  $[\text{OIII}]/\text{H}\beta$  and  $[\text{NII}]/\text{H}\alpha$  intensity ratios indicate that the galaxy is a low-metallicity and high-excitation starburst galaxy. In addition, the flux ratio of the  $[\text{NeIII}]$  and  $[\text{OII}]$  lines is  $F^{3869}/F^{3727} \approx 0.43$ , similar to the observed value for the host galaxy of GRB 970508 (41) and approximately 10 times higher than typical values for H II regions. The bright  $[\text{NeIII}]$  emission lines observed in GRB hosts are thought to be indicative of a substantial population of massive stars. On the other hand, Chornock and Filippenko (76) note that a spectrum of G1 taken with the Low Resolution Imaging Spectrometer (LRIS) on the Keck I telescope reveals a deficit of emission at rest wavelengths  $< 4000 \text{ \AA}$  which is consistent with a population of older stars.

### 1.2.3 Hubble Space Telescope

The afterglow candidate was observed with the Hubble Space Telescope (HST) using the Advanced Camera for Surveys (ACS) under Program No. 9405 (P.I.: A. Fruchter). Three epochs of imaging were obtained from  $\Delta t \sim 94$  to  $\sim 300$  days with exposure times of 1840 sec in the F606W filter. Following ‘‘On-The-Fly’’ pre-processing the data were drizzled using standard IRAF tools (STSDAS; Fruchter and Hook 141). In drizzling our final images, we retained the native WFC pixel scale of 0.05’’ and used a `pixfrac` of 1.0. The HST images reveal a complex galaxy morphology for G1, suggesting a system of at least four interacting galaxies (see

Figure 1.4).

To locate the optical transient with respect to the host galaxy complex, we performed a source to source comparison of our first-epoch Palomar (2002 September 4) and HST (2002 December 3) images. We found 42 unsaturated, unconfused sources in common between these two images, and were able to match the two coordinate lists with an rms mapping uncertainty of 0.06 arcsec. We derived the position of the transient from the difference image of the 2002 September 4 and September 10 data. Since the optical transient is well-detected in the difference image, the uncertainty in its centroid position is negligible. The uncertainty in the coordinate mapping thus dominates the uncertainty in the position of the source relative to the host galaxy complex. The optical transient appears to overlap with the SW component of the G1 complex (Figure 1.4).

#### 1.2.4 Radio Observations of XRF 020903

##### Very Large Array Data

We began observations of the field of XRF 020903 with the Very Large Array (VLA<sup>1</sup>) on 2002 September 27.22 UT. A radio source was detected in coincidence with the optical transient at a location of  $\alpha(\text{J2000}) = 22^{\text{h}}48^{\text{m}}42.34^{\text{s}}$ ,  $\delta(\text{J2000}) = -20^{\circ}46'08.9''$  with an uncertainty of 0.1 arcsec in each coordinate. The initial observation showed the radio source to have a flux density of  $F_{\nu} = 1.06 \pm 0.02$  mJy at 8.5 GHz. The National Radio Astronomy Observatory VLA Sky Survey (NVSS; Condon et al. 89) did not show any evidence for a pre-existing source at this location down to a limit of 1 mJy. Further observations at 8.5 GHz on September 29.11 ( $\Delta t \approx 26$  days) showed that the source faded to  $F_{\nu} = 0.75 \pm 0.04$  mJy. We continued monitoring the transient source with the VLA over the next  $\approx 370$  days at frequencies of 1.5, 4.9, 8.5, and 22.5 GHz. The lightcurve is displayed in Figure 1.5.

---

<sup>1</sup>The VLA is operated by the National Radio Astronomy Observatory, a facility of the National Science Foundation operated under cooperative agreement by Associated Universities, Inc.

### Very Long Baseline Array Data

The relatively low redshift and strong radio emission of the transient source made it an ideal candidate for Very Long Baseline Array (VLBA) observations. On September 30.23 UT ( $\Delta t \approx 27$  days) we observed the radio transient for a total duration of 6 hours at 8.5 GHz. Using sources J2253+1608 and J2148+0657 we were able to flux calibrate the field and we phase referenced against source J2256-2011 at a distance of  $< 2$  degrees. Data were reduced and processed using standard VLBA packages within the Astronomical Image Processing System (AIPS). We detected the radio transient with a flux of  $0.89 \pm 0.17$  mJy at a position coincident with the VLA and optical observations at a location of  $\alpha(\text{J2000}) = 22^{\text{h}}48^{\text{m}}42.33912^{\text{s}} \pm 0.00003$ ,  $\delta(\text{J2000}) = -20^{\circ}46'08.945'' \pm 0.0005$ . This is our most accurate position measurement for the transient object. The source is unresolved within our VLBA beam size of  $1.93 \times 1.73$  mas. Furthermore, the consistency between the flux measured with VLBA and low resolution VLA observations rules out the presence of diffuse components (e.g., jets).

### 1.3 The Afterglow of XRF 020903

The large error box and the proximity of the optical transient to G2 and G3 delayed rapid identification of the transient (302, 285, 403, 140). As a result there was little optical followup of the transient at early times (see Table 1.1). At later times, the transient is rapidly dominated by the emission from G1. An additional complication was introduced by Gal-Yam (146) who, based on archival photographic plates from 1954 and 1977, proposed that G1 hosted a variable active galactic nucleus (AGN).

In contrast to the above discussion, the extensive radio light curve (Figure 1.5) provides strong evidence that the transient is the afterglow of XRF 020903. The radio light curve is similar to the afterglow of GRBs (132). At 4.9 GHz, the source was observed to rise to a peak flux at  $\Delta t \approx 29$  days and subsequently decay with a characteristic index of  $\alpha \approx -1.1$ . A steeper decline of  $F_{\nu} \propto t^{-1.5}$  was observed at

8.5 GHz where the peak flux precedes the first observational epoch. We note that the dynamic range of the radio afterglow emission clearly distinguishes the source from a radio bright AGN.

The afterglow interpretation is consistent with the optical spectroscopic observations of G1, namely the absence of broad lines or features typical of AGN, as well as the absence of any jet structure in the VLBA images of the radio transient. We proceed, accepting the notion that the optical/radio transient is the afterglow of XRF 020903.

## 1.4 Energetics

At a redshift of  $z = 0.251$ , the X-ray fluence implies an isotropic equivalent energy  $E_{\text{iso}} \approx 1.1 \times 10^{49}$  erg. This value is 3 to 6 orders of magnitude lower than the isotropic energies of gamma-ray bursts (133). Since there is no evidence for a jet break in the afterglow observations, the data are consistent with a wide jet or a spherical explosion. This, along with the early decline of the optical flux ( $F_{\nu} \propto t^{-1.3}$  at  $\Delta t \approx 1$  d; Figure 1.2) rules out the possibility that the inferred low energy is due to a viewing angle significantly away from the jet axis. In such a scenario, the optical flux would rise until the edge of the jet enters the observer's line of sight, peaking at  $\Delta t \geq t_{\text{jet}}$ , where  $t_{\text{jet}}$  is the observed time of the jet break (e.g., Granot et al. 168).

Figure 1.6 shows that although the energy in the prompt emission of XRF 020903 is significantly lower than that observed for typical GRBs, the peak luminosity of the radio afterglow is comparable to that found in GRB afterglows. This indicates that XRF 020903 has a similar kinetic energy to GRB afterglows. To study this in more detail we used standard broadband afterglow models with spherical and collimated ejecta expanding into circumburst media with uniform density and wind density profile,  $\rho \propto r^{-2}$  (e.g. Berger et al. 29). We find that independent of the assumed model, the total kinetic energy is  $E \sim 4 \times 10^{50}$  erg with reasonable values for the circumburst density and energy fractions (electron

and magnetic field) of  $n \approx 100 \text{ cm}^{-3}$ ,  $\epsilon_e \approx 0.6$  and  $\epsilon_B \approx 0.01$ , respectively. Thus we confirm the afterglow energy is similar to values found for GRB afterglows (280, 23).

Recent evidence suggests a standard total energy yield ( $10^{51}$  erg) for all GRBs (27), where the total energy yield ( $E_{\text{tot}}$ ) is defined as the sum of the energy in the prompt emission ( $E_\gamma$ ) plus the mildly relativistic energy as inferred from the afterglow ( $E_{\text{rad}}$ ). Clearly, for XRF 020903 the explosion energy is dominated by the mildly relativistic afterglow, while a minor fraction of energy couples to the high Lorentz factors characterizing the prompt emission.

Figure 1.6 also compares the radio luminosity of XRF 020903 with other spherical explosions - Type Ibc supernovae. With a radio luminosity  $\sim 1000$  times greater than typical Ibc SNe, it is clear that XRF 020903 is a significantly more energetic explosion. This suggests that despite their similar explosion geometries, XRF 020903 and type Ibc supernovae are intrinsically different - possibly due to the presence of a central engine (26).

## 1.5 Conclusions

We present radio and optical observations of the afterglow of XRF 020903 - the first X-ray flash to have a detected optical afterglow and a spectroscopic distance determination. At a redshift of  $z = 0.251$ , this burst has set the distance scale for XRFs and confirmed the assumption that they are cosmological in origin. The host galaxy of XRF 020903 appears to be a typical star-forming galaxy similar to those of GRB host galaxies.

The isotropic energy release of the prompt (X-ray) emission of XRF 020903 is at least two orders of magnitude smaller than those of GRBs. However, from our broadband modeling of the afterglow we determine that the total kinetic energy is about  $10^{50}$  erg, not dissimilar to those inferred for GRBs (280, 23). In comparison with a larger sample of cosmic explosions, XRF 020903 is a clear example where less energy is coupled to high Lorentz factors. This source highlights the diversity

in high-energy transients and underscores the importance of studying spherical explosions.

We thank J. Ulvestad for his help with scheduling the VLBA observation. MH acknowledges support for this work provided by NASA through Hubble Fellowship grant HST-HF-01139.01-A awarded by the Space Telescope Science Institute, which is operated by the Association of Universities for Research in Astronomy, Inc., for NASA, under contract NAS 5-26555. JPH and NM acknowledge support from NSF grant AST-0206051. AMS is supported by an NSF graduate research fellowship. GRB research at Caltech is supported by NASA and NSF.

Table 1.1. Optical Observations of the Afterglow of XRF 020903.

Date (UT)	$\Delta t$ (days)	Telescope	R (mag)
2002 Sep 4.32	0.9	Palomar 200"	$19.23 \pm 0.10$
2002 Sep 10.30	6.9	Palomar 200"	$20.60 \pm 0.10$
2002 Sep 28.25	24.8	MDM 1.3 m	$20.80 \pm 0.2$
2002 Oct 7.17	33.8	Palomar 200"	$20.73 \pm 0.17$
2003 Jul 2.47	302.1	Palomar 200"	$21.00 \pm 0.45$

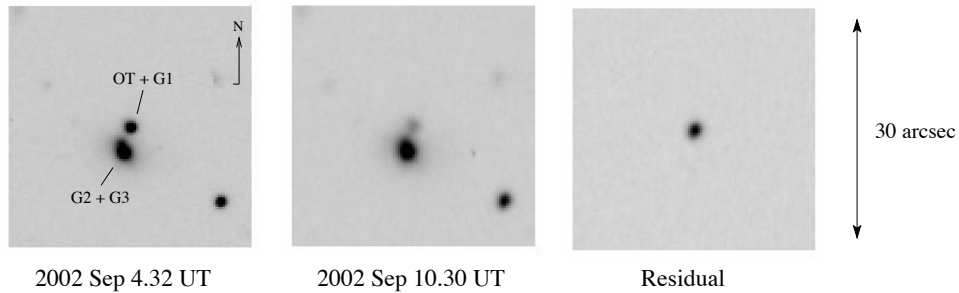


Figure 1.1: The field of XRF 020903 was observed with the Palomar 200-inch telescope equipped with the Large Field Camera on 2002 September 4.32 and September 10.30 UT. Image subtraction techniques revealed one variable object within the HETE-2 error-box lying  $\sim 4$  arcsec NW of a bright elliptical galaxy (G2). The residual image clearly indicates a transient stellar source which decreased in brightness by 1.4 magnitudes between the two epochs.

Table 1.2. Radio Observations of the Afterglow of XRF 020903.

Date (UT)	$\Delta t$ (days)	1.5 GHz ( $\mu\text{Jy}$ )	4.9 GHz ( $\mu\text{Jy}$ )	8.5 GHz ( $\mu\text{Jy}$ )	22.5 GHz ( $\mu\text{Jy}$ )
2002 Sep 27.22	23.8	...	...	1058 $\pm$ 19	...
2002 Sep 29.11	25.7	197 $\pm$ 70	552 $\pm$ 42	746 $\pm$ 37	590 $\pm$ 125
2002 Sep 30.23 <sup>a</sup>	26.8	...	...	892 $\pm$ 166	...
2002 Oct 2.06	28.6	210 $\pm$ 91	788 $\pm$ 45	765 $\pm$ 41	0 $\pm$ 270
2002 Oct 10.13	36.7	294 $\pm$ 91	832 $\pm$ 47	640 $\pm$ 40	...
2002 Nov 13.02	74.0	175 $\pm$ 56	380 $\pm$ 38	190 $\pm$ 30	...
2003 Mar 3.71	181.3	...	215 $\pm$ 59	...	...
2003 Mar 7.72	185.3	...	112 $\pm$ 45	...	...
2003 Mar 14.74	192.3	...	127 $\pm$ 32	...	...
2003 Mar 17.69	195.3	...	103 $\pm$ 40	...	...
2003 Sep 15.22	376.8	43 $\pm$ 66	21 $\pm$ 34	...	...

<sup>a</sup>VLBA observation

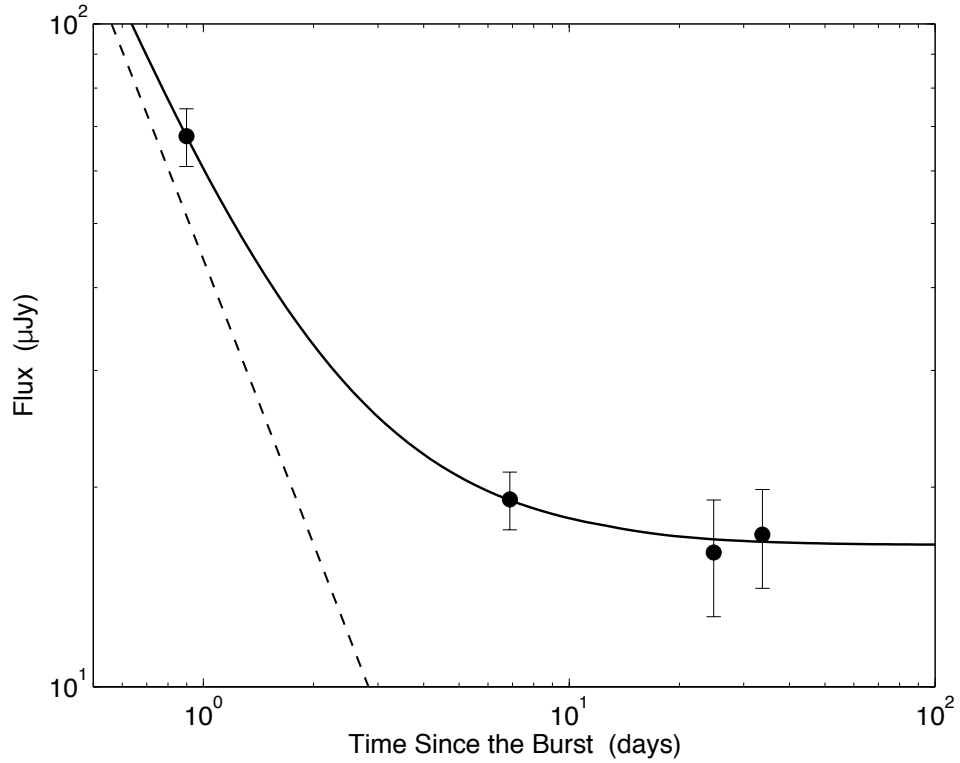


Figure 1.2: Data were obtained from the Palomar 200-inch and MDM 1.3-meter telescopes. The solid line is our best fit to the broadband data, including the afterglow component with a temporal decay of  $\alpha \approx -1.3$  (dashed line) and the host galaxy (G1) contribution of  $R \sim 20.8$  mag. The early decline rules out the possibility that the viewing angle is significantly away from the jet axis (see Granot et al. 168).

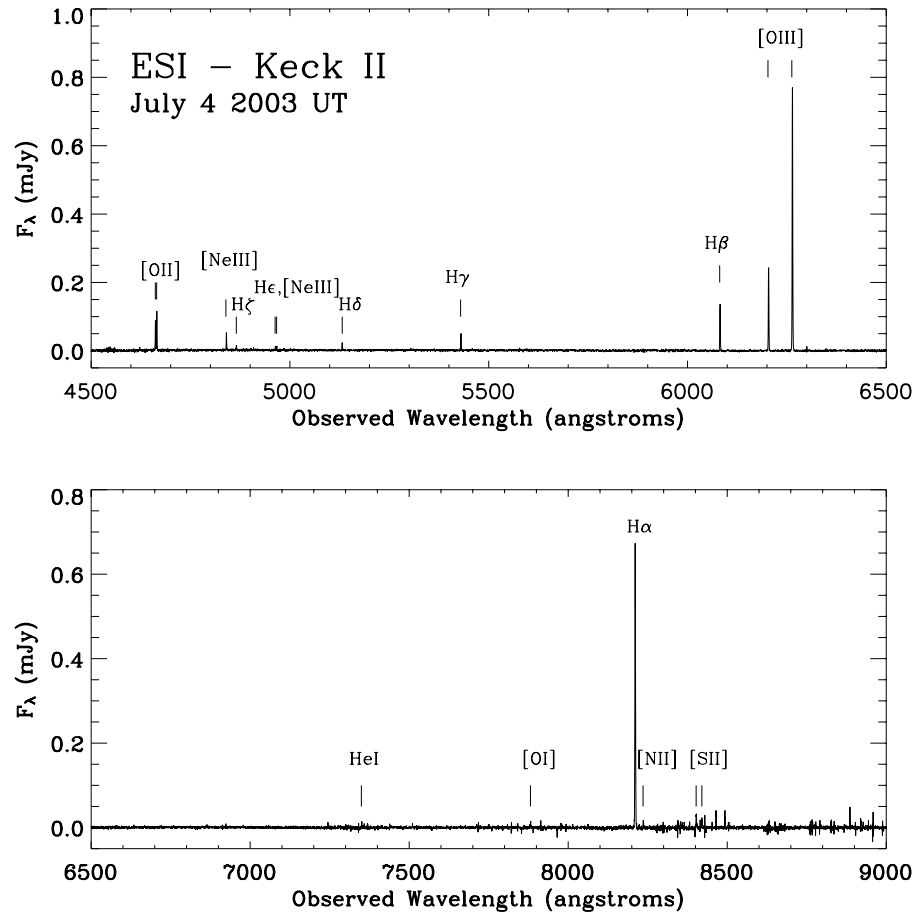


Figure 1.3: On 2003 July 4 UT we obtained spectroscopic observations of the putative host galaxy (G1) underlying the optical transient source associated with XRF 020903. Data were taken with the Echelle Spectroscopic Imager (ESI) mounted on the Keck II telescope. The source is shown to be an active star-forming galaxy at  $z=0.251$  with a rich set of narrow bright emission lines.

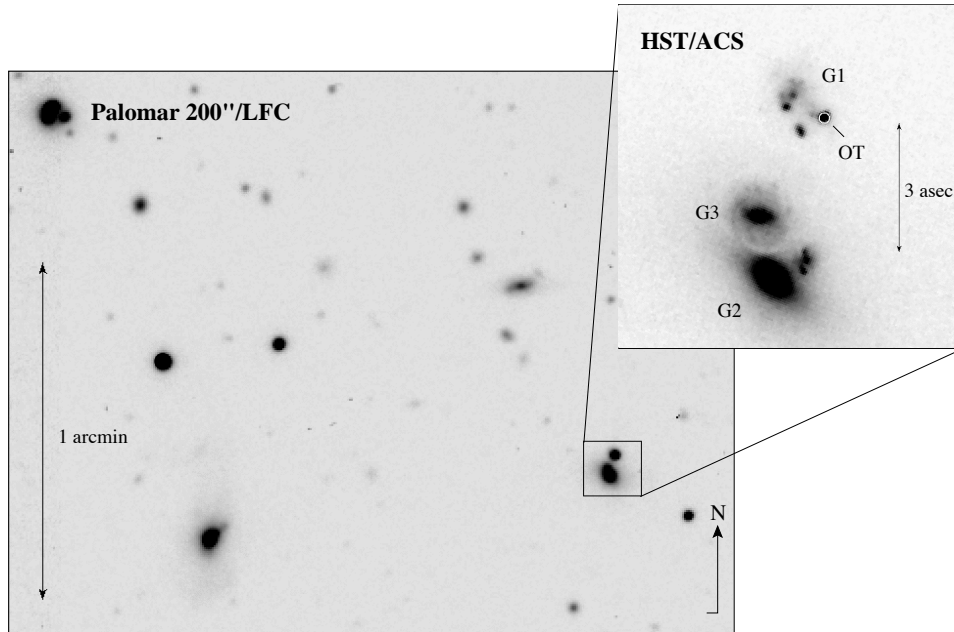


Figure 1.4: The transient discovered within the error-box of XRF 020903 was observed with the Hubble Space Telescope (HST) using the Advanced Camera for Surveys (ACS) on 2002 December 3 UT. The HST image reveals a complicated galaxy morphology for G1, suggesting a system of at least four interacting galaxies. The location of the optical transient is noted on the  $7 \times 7''$  HST cutout with a circle which represents a  $2\sigma$  positional uncertainty of  $0.12''$ . Nearby galaxies G2 and G3 are labeled accordingly on the HST image. The optical transient appears to overlap with the SW component of the G1 complex.

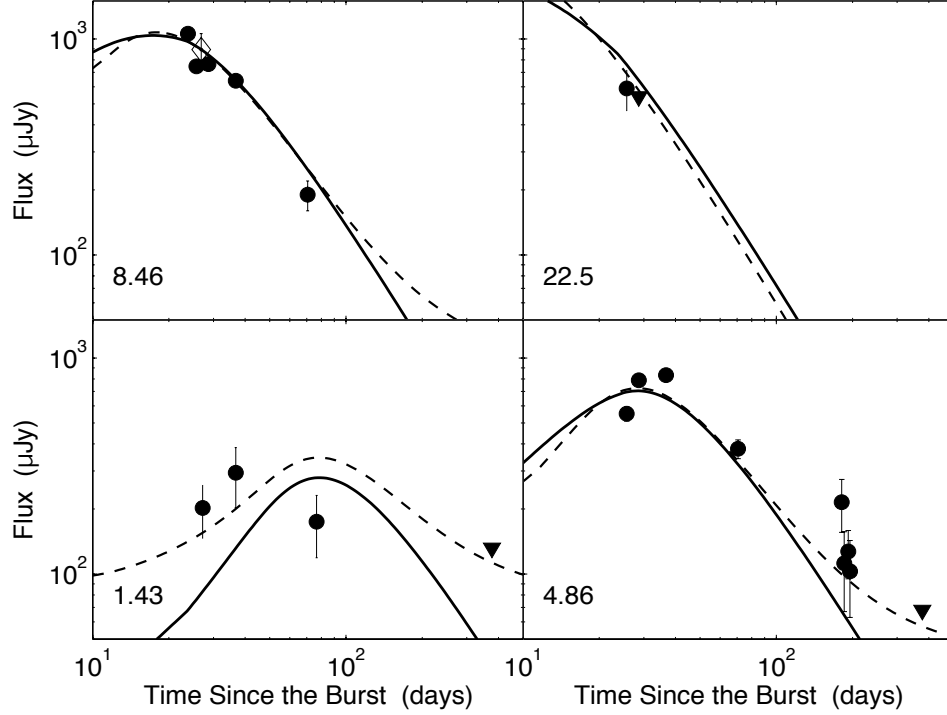


Figure 1.5: We observed the field of XRF 020903 with the Very Large Array over the period  $\Delta t \approx 25 - 370$  days. A bright radio counterpart was detected at a position coincident with the optical transient. We continued monitoring the source with the VLA over the next  $\approx 300$  days at frequencies of 1.5, 4.9, 8.5, and 22.5 GHz. Assuming the transient source is the radio afterglow component associated with XRF 020903, we overplot the best fit broadband model (solid line) which predicts a total kinetic energy of  $4 \times 10^{50}$  erg in the afterglow. Allowing for a host galaxy emission component, we find a better fit assuming a host galaxy flux of  $F_{1.4\text{GHz}} \approx 80 \mu\text{Jy}$  (dashed line). The implied star-formation rate from the host is  $5 M_{\odot}\text{yr}^{-1}$  following the conversion from Yun and Carilli (446). The 8.5 GHz data point marked by the open diamond symbol denotes the VLBA observation of the unresolved transient source (beam size= $1.93 \times 1.73$  mas).

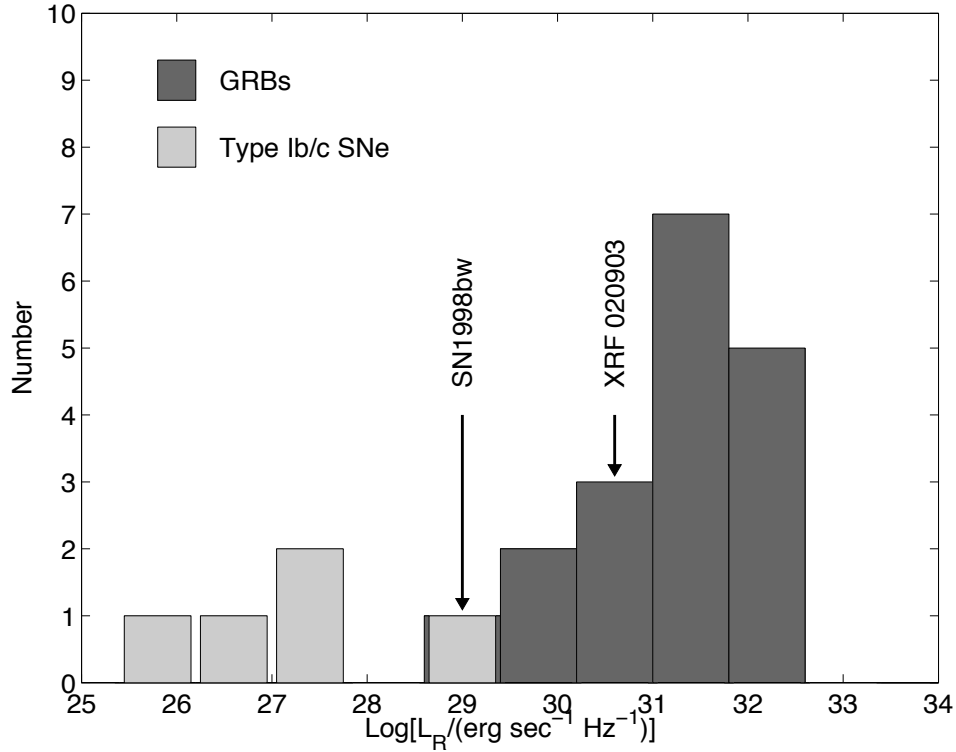


Figure 1.6: The histogram above compares the peak radio luminosity for various cosmic explosions, including type Ib/c supernovae (spherical ejecta geometry) as well as typical long-duration GRBs (collimated ejecta geometry). Although the energy in the prompt emission of XRF 020903 is  $10^2 - 10^3$  times lower than that observed for typical GRBs, the total kinetic energy in the afterglow of XRF 020903 is comparable to that found in typical GRBs afterglows. In comparison with a larger sample of cosmic explosions, XRF 020903 is a clear example where there is less energy coupled to high Lorentz factors.

## Chapter 2

# A Spectacular Radio Flare from XRF 050416a at 40 Days and Implications for the Nature of X-ray Flashes<sup>†</sup>

A. M. SODERBERG<sup>a</sup>, E. NAKAR<sup>b</sup>, S. B. CENKO<sup>c</sup>, P. B. CAMERON<sup>a</sup>,  
D. A. FRAIL<sup>d</sup>, S. R. KULKARNIA, D. B. FOX<sup>e</sup>, E. BERGER<sup>f</sup>, A. GAL-YAM<sup>a</sup>,  
D-S. MOON<sup>c</sup>, P. A. PRICE<sup>g</sup>, G. ANDERSON<sup>h</sup>, B. P. SCHMIDT<sup>h</sup>, M. SALVO<sup>h</sup>,  
J. RICH<sup>h</sup>, A. RAU<sup>a</sup>, E. O. OFEK<sup>a</sup>, R. A. CHEVALIER<sup>i</sup>, M. HAMUY<sup>f</sup>,  
F. A. HARRISON<sup>c</sup>, P. KUMAR<sup>j</sup>, A. MACFADYEN<sup>k</sup>, P. J. MCCARTHY<sup>f</sup>,  
H. S. PARK<sup>l</sup>, B. A. PETERSON<sup>h</sup>, M. M. PHILLIPS<sup>f</sup>, M. RAUCH<sup>f</sup>, M. ROTH<sup>f</sup>,  
S. SHECTMAN<sup>f</sup>

<sup>a</sup>Division of Physics, Mathematics and Astronomy, 105-24, California Institute of Technology,  
Pasadena, CA 91125, USA

<sup>b</sup>Theoretical Astrophysics, 130-33 California Institute of Technology, Pasadena, CA 91125, USA

<sup>c</sup>Space Radiation Laboratory, MS 220-47, California Institute of Technology, Pasadena, CA  
91125, USA

<sup>d</sup>National Radio Astronomy Observatory, Socorro, NM 87801, USA

---

<sup>†</sup>A version of this chapter was published in *The Astrophysical Journal*, vol. 662, (2007). Re-  
produced by permission of the AAS.

<sup>e</sup>Department of Astronomy and Astrophysics, Pennsylvania State University, 525 Davey  
Laboratory, University Park, PA 16802, USA

<sup>f</sup>Observatories of the Carnegie Institution of Washington, 813 Santa Barbara Street, Pasadena,  
CA 91101, USA

<sup>g</sup>Institute for Astronomy, University of Hawaii, 2680 Woodlawn Drive, Honolulu, HI 96822, USA

<sup>h</sup>Research School of Astronomy and Astrophysics, Australian National University, Mt Stromlo  
Observatory, via Cotter Rd, Weston Creek, ACT 2611, Australia

<sup>i</sup>Department of Astronomy, University of Virginia, P.O. Box 3818, Charlottesville, VA  
22903-0818, USA

<sup>j</sup>Astronomy Department, University of Texas, Austin, TX 78731, USA

<sup>k</sup>Institute for Advanced Study, Princeton, NJ 08540, USA

<sup>l</sup>Lawrence Livermore National Laboratory, 7000 East Avenue, Livermore, CA 94550, USA

## Abstract

We present detailed optical, near-infrared, and radio observations of the X-ray flash 050416a obtained with Palomar and Siding Springs Observatories as well as the *Hubble Space Telescope* and Very Large Array, placing this event among the best-studied X-ray flashes to date. In addition, we present an optical spectrum from Keck LRIS from which we measure the redshift of the burst,  $z = 0.6528$ . At this redshift the isotropic-equivalent prompt energy release was about  $10^{51}$  erg, and using a standard afterglow synchrotron model we find that the blastwave kinetic energy is a factor of 10 larger,  $E_{K,\text{iso}} \approx 10^{52}$  erg. The lack of an observed jet break to  $t \sim 20$  days indicates that the opening angle is  $\theta_j \gtrsim 7^\circ$  and the total beaming-corrected relativistic energy is  $\gtrsim 10^{50}$  erg. We further show that the burst produced a strong radio flare at  $t \sim 40$  days accompanied by an observed flattening in the X-ray band which we attribute to an abrupt circumburst density jump or an episode of energy injection (either from a refreshed shock or off-axis

ejecta). Late-time observations with the *Hubble Space Telescope* show evidence for an associated supernova with peak optical luminosity roughly comparable to that of SN 1998bw. Next, we show that the host galaxy of XRF 050416a is actively forming stars at a rate of at least  $2 M_{\odot} \text{ yr}^{-1}$  with a luminosity of  $L_B \approx 0.5L^*$  and metallicity of  $Z \sim 0.2 - 0.8 Z_{\odot}$ . Finally, we discuss the nature of XRF 050416a in the context of short-hard gamma-ray bursts and under the framework of off-axis and dirty fireball models for X-ray flashes.

## 2.1 Introduction

Nearly a decade ago, X-ray flashes (XRFs) were observationally recognized as a subclass within the sample of gamma-ray bursts (GRBs) detected by the *Bep-poSAX* Wide-Field Cameras (180). The events are distinguished by a prompt spectrum that peaks in the soft X-ray range ( $E_p \lesssim 25 \text{ keV}$ ), a factor of  $\sim 10$  below the typical values observed for GRBs (8). Since then, it has been shown that XRFs and GRBs share many observational properties, including prompt emission durations (332), redshifts (361), broadband afterglows (e.g., XRF 050406, Romano et al. 321, Schady et al. 342), and host galaxy properties (43, 196, 308). Moreover, the recent discovery of Type Ic supernovae (SNe) in association with XRFs 020903 (363, 31) and 060218 (292, 258, 259) indicate that XRFs, like GRBs, are produced in massive stellar explosions. Together, these clues strongly suggest that XRFs and GRBs share similar progenitors.

Driven by this progress, several theories have been proposed to explain the soft prompt emission observed for XRFs under the framework of a standard GRB model. One popular idea posits that XRFs are merely typical GRBs viewed away from the collimation axis (e.g., Yamazaki et al. 441). In this scenario the prompt emission is primarily beamed away from our line-of-sight, resulting in lower fluence and  $E_p$  values for the observed burst. An important implication of the off-axis model is that the early afterglow evolution should be characterized by a rising phase as the jet decelerates and spreads sideways into our line-of-sight (168, 418, 367).

Another theory suggests that XRFs are intrinsically different from GRBs in their ability to couple energy to highly-relativistic material. In this scenario, XRFs are produced in explosions characterized by lower bulk Lorentz factors,  $10 \lesssim \Gamma \lesssim 100$ , than those inferred for typical GRBs,  $\Gamma \gtrsim 100$  (450). This may be the result of baryon loading of the high-velocity ejecta, a so-called “dirty fireball” (102). Generally speaking, low Lorentz factor explosions may be identified through an analysis of their prompt emission since an optically thin spectrum at high energies implies a lower limit on the Lorentz factor (230). In the case of X-ray flashes, however, there are generally insufficient high-energy photons for this type of analysis. For these events, detailed modeling of the broadband afterglow may be used to place a lower limit on the Lorentz factor.

Here we present an extensive, multi-frequency data set for XRF 050416a at  $z = 0.6528$  which extends to  $t \sim 220$  days after the burst. By combining near-infrared, optical, ultra-violet, radio, and X-ray data we present an in-depth analysis of the afterglow, energetics, supernova and host galaxy of XRF 050416a, placing it among the best-studied X-ray flashes to date. Moreover, thanks to our dedicated late-time monitoring campaign, we show that XRF 050416a produced a strong radio flare at  $t \sim 40$  days accompanied by a brief plateau phase in the X-ray band. Finally, we discuss the nature of XRF 050416a in the context of off-axis and dirty fireball models for X-ray flashes.

## 2.2 Observations

XRF 050416a was discovered by the *Swift* Burst Alert Telescope (BAT) on 2005 April 16.4616 UT. The ratio of 15 – 25 keV and 25 – 50 keV channel fluences,  $f_{15-25 \text{ keV}}/f_{25-50 \text{ keV}} \approx 1.1$ , classifies the event as an X-ray flash (327). This is consistent with the low peak photon energy,  $E_p = 15.0^{+2.3}_{-2.7}$  keV (327); a factor of  $\sim 10$  lower than the typical values observed for long-duration GRBs (8) and a factor of  $\sim 3$  larger than the values inferred for XRFs 020903 and 060218 (330, 59)

As discussed by Sakamoto et al. (327), the prompt emission light-curve is char-

acterized by a relatively smooth, triangular peak which is only detected at energies below 50 keV. The burst duration is  $T_{90} \approx 2.4$  sec (15–150 keV), placing it between the classes of short- and long-duration GRBs while the hardness ratio shows a clear softening. In addition, Sakamoto et al. (327) note two intriguing features of the data: (1) the rise time of the pulse is longer than the decay time, and (2) the cross-correlation lag function (an indication of the spectral softening) is  $-0.066_{-0.018}^{+0.014}$  sec, apparently inconsistent with the overall softening trend observed for the light-curves. This lag function estimate is significantly different than the typical values inferred for long-duration GRBs and even more extreme than the zero spectral lags inferred for short-hard bursts (268). We note, however, that the spectral lag for XRF 050416a was derived through a comparison of the two softest BAT bands (15–25 and 25–50 keV) and therefore prevents a clear comparison with the spectral lag estimates for other *Swift* GRBs for which 15–25 and 50–100 keV bands are typically used. Given that the temporal evolution is not strongly variable, this may indicate that the prompt emission was produced by another process (e.g.. external shocks, Dermer et al. 102). Finally, we note that this burst is inconsistent with the lag-luminosity correlation for long-duration GRBs which posits that low luminosity bursts such as XRF 050416a have long spectral lags (269).

### 2.2.1 Early Optical Observations

Using the roboticized Palomar 60-inch telescope (P60) we initiated observations of the field of XRF 050416a at 2005 April 16.4634 UT (2.5 minutes after the burst). In our first 120 second image we discovered a new source within the *Swift*/BAT error circle at  $\alpha = 12^{\text{h}}33^{\text{m}}54^{\text{s}}.58$ ,  $\delta = +21^{\circ}03'26''.7$  (J2000) with an uncertainty of 0.5 arcsec in each coordinate based on an astrometric tie to the USNO-B catalog (Figure 2.1). We subsequently monitored the afterglow evolution with the Palomar 60-inch, 200-inch, and Siding Springs 2.3-meter telescopes in the  $R$ -,  $I$ -,  $z'$ -, and  $K_s$ -band through  $t \approx 7$  days.

Aperture photometry was performed on each of the images in the standard

method using the `aphot` package within IRAF. Absolute calibration of  $R$ -,  $I$ -, and  $z'$ -band light-curves was derived using the field calibration of Henden (184) and utilizing the transformation equations of Smith et al. (352). The  $K_s$ -band light-curve was calibrated against 2MASS using 15 unconfused sources. The errors resulting from calibration uncertainty ( $\lesssim 10\%$ ) were added in quadrature to the measurement errors. As shown in Figure 2.2 and Table 2.1, the afterglow was  $I = 18.82 \pm 0.11$  mag at  $t \approx 1.6$  min (mid-exposure).

We supplement these NIR/optical afterglow data with additional measurements from the GCNs (225, 301, 305, 397, 444) and those reported by Holland et al. (188), obtained with the *Swift*/UVOT and 1.54-m Danish Telescope. The resulting dataset spans 1930 Å (*Swift*/UVOT UVW2) to 22000 Å ( $K_s$ ); however, we note that the majority of the UV observations are upper limits. Using this extended dataset we measure the temporal and spectral properties of the NIR/optical afterglow emission. We find the following NIR/optical power-law decay indices ( $\alpha$ , where  $F_\nu \propto t^\alpha$ ) between  $\sim 0.01$  and 1 day:  $\alpha_{K_s} = -0.7 \pm 0.3$ ,  $\alpha_I = -0.7 \pm 0.3$ ,  $\alpha_R = -0.5 \pm 0.3$ ,  $\alpha_V = -1.0 \pm 0.3$ ,  $\alpha_B = -0.5 \pm 0.3$ , consistent with the values reported by Holland et al. (188). These values imply a mean temporal index of  $\bar{\alpha}_{\text{NIR/opt}} = -0.7 \pm 0.2$ .

Finally, we analyze the spectral index ( $\beta$  with  $F_\nu \propto \nu^\beta$ ) within the NIR/optical bands. As shown in Figure 2.5 there are two epochs at which the photometric spectrum is well-sampled:  $t \approx 0.014$  and 0.8 days. We fit each of the observed spectra with a simple power-law and find  $\beta_{\text{NIR/opt}} \approx -1.3$  ( $\chi_r^2 \approx 0.5$ ) and  $-1.5$  ( $\chi_r^2 \approx 0.6$ ) for the first and second epochs, respectively. As will be discussed in §2.3.1, the observed steep spectrum is indicative of extinction within the host galaxy.

## 2.2.2 Late-time Observations with HST

Using the *Wide-Field Camera (WFC)* of the *Advanced Camera for Surveys (ACS)* on-board the *Hubble Space Telescope (HST)*, we imaged the field of XRF 050416a four times, spanning 37 to 219 days after the burst. Each epoch consisted of two

or four orbits during which we imaged the field in filters F775W and/or F850LP, corresponding to SDSS  $i'$ - and  $z'$ - bands, respectively.

The *HST* data were processed using the `multidrizzle` routine (141) within the `stsdas` package of IRAF. Images were drizzled using `pixfrac=0.8` and `pixscale=1.0` resulting in a final pixel scale of 0.05 arcsec/pixel. Drizzled images were then registered to the final epoch using the `xregister` package within IRAF. We astrometrically tied the *HST* and P60 images using 12 unconfused sources in common resulting in a final systematic uncertainty of 0.70 arcsec ( $2\sigma$ ).

To search for source variability and remove host galaxy contamination, we used the *ISIS* subtraction routine by Alard (1) which accounts for temporal variations in the stellar PSF. Adopting the final epoch observations as templates we produced residual images. These residual images were examined for positive sources positionally coincident with the P60 afterglow.

Photometry was performed on the residual sources within a 0.5 arcsec aperture. We converted the photometric measurements to infinite aperture and calculated the corresponding AB magnitudes within the native *HST* filters using the aperture corrections and zero-points provided by Sirianni et al. (349). Here we made the reasonable assumption that the transient flux is negligible in the template images. For comparison with ground-based data, we also converted the F775W measurements to Johnson  $I$ -band (Vega) magnitudes using the transformation coefficients derived by Sirianni et al. (349) and assuming the  $F_\nu$  source spectrum implied by the first epoch *HST* data.

As shown in Table 2.1 and Figure 2.4, the transient is clearly detected in the first epoch *HST* residual images. An astrometric tie between the first and final epochs shows that the residual is offset  $0.02 \pm 0.02$  arcsec from the center of the host galaxy. Our residual images show the source to be F775W=  $24.35 \pm 0.02$  and F850LP=  $23.83 \pm 0.03$  mag in the AB system ( $I = 23.82 \pm 0.02$  mag in the Vega system) at  $t \approx 37$  days. As shown in Figure 2.2, these values are a factor of  $\sim 5$  above an extrapolation of the early afterglow decay. The observed spectral index between the F775W and F850LP filters is  $\beta_{HST} \approx -2.8 \pm 0.3$ , significantly

steeper than the afterglow spectrum observed at early time (§2.2.1 and Figure 2.5) as well as the typical values measured for NIR/optical afterglows ( $\beta_{\text{NIR/opt}} \approx -0.6$ ; Panaitescu and Kumar 280, Yost et al. 445). As will be discussed in §2.4.4, the timescale and spectral signature of the observed flux excess are suggestive of a thermal supernova component.

### 2.2.3 Spectroscopic Observations

We observed the host galaxy of XRF 050416a with the Low Resolution Imaging Spectrograph on Keck I on 2005 June 6.3 UT ( $t \sim 50$  days). We placed a 1.0 arcsec longslit across the host galaxy at a position angle of PA=87°. Data were reduced in standard manner using the `onedspec` and `twospec` packages within IRAF. Flux calibration was performed using the spectrophotometric standard star BD+284211.

As shown in Figure 2.5 and Table 2.3, we detect several strong emission lines in the spectrum including H $\beta$ , H $\gamma$ , [O Roman2] $\lambda$ 3727, and [O Roman3] $\lambda$ 4959, 5006 at a redshift of  $z = 0.6528 \pm 0.0002$ . Adopting the standard cosmological parameters ( $H_0 = 71 \text{ km s}^{-1} \text{ Mpc}^{-1}$ ,  $\Omega_M = 0.27$ ,  $\Omega_\Lambda = 0.73$ ), the isotropic gamma-ray energy release is  $E_{\gamma,\text{iso}} \approx 1.2 \pm 0.2 \times 10^{51} \text{ erg}$  (1 keV – 10 MeV; Sakamoto et al. 327). Compared with typical long-duration bursts, the prompt energy release of XRF 050416a is a factor of  $\sim 100$  lower (Frail et al. 133, Bloom et al. 44, Amati 2 and references therein).

### 2.2.4 Radio Observations

We began observing XRF 050416a with the Very Large Array<sup>1</sup> (VLA) on 2005 April 16.49 UT ( $t \approx 37$  min). No radio source was detected coincident with the optical position to a limit of  $F_\nu < 122 \mu\text{Jy}$  at  $\nu = 8.46 \text{ GHz}$ . However, further observations at  $t \approx 5.6$  days revealed a new radio source with  $F_\nu \approx 101 \pm 34 \mu\text{Jy}$  coincident

---

<sup>1</sup>The Very Large Array and Very Long Baseline Array are operated by the National Radio Astronomy Observatory, a facility of the National Science Foundation operated under cooperative agreement by Associated Universities, Inc.

with the optical and X-ray afterglow positions at  $\alpha = 12^{\text{h}}33^{\text{m}}54.594^{\text{s}} \pm 0.002$ ,  $\delta = 21^{\circ}03'26.27'' \pm 0.04$  (J2000) which we identify as the radio afterglow.

We continued to monitor the radio afterglow at 1.43, 4.86, and 8.46 GHz through  $t \approx 140$  days (Table 4.1). All observations were taken in standard continuum observing mode with a bandwidth of  $2 \times 50$  MHz. We used 3C286 (J1331+305) for flux calibration, while phase referencing was performed against calibrators J1221+282 and J1224+213. The data were reduced using standard packages within the Astronomical Image Processing System (AIPS).

As shown in Figure 2.6, the evolution of the radio afterglow is dissimilar from those of typical GRBs and inconsistent with a standard blastwave model. Between  $t \sim 20$  and 40 days an abrupt rebrightening (factor of  $\sim 3$ ) is observed at all radio bands with a temporal index steeper than  $\alpha_{\text{rad}} \approx 0.9$ . Following this radio flare the emission decays rapidly with an index of  $\alpha_{\text{rad}} \lesssim -1.5$ . The peak radio luminosity at 8.46 GHz,  $L_{\text{rad}} \approx 1.3 \times 10^{31} \text{ erg s}^{-1} \text{ Hz}^{-1}$ , is typical for GRBs (132), a factor of  $\sim 10$  and  $10^3$  larger than those of XRFs 020903 and 060218, respectively (361, 365), and between  $10^2$  and  $10^6$  times higher than the peak radio luminosities observed for optically-selected Type Ibc supernovae (353). By  $t \approx 105$  days the radio afterglow is no longer detected at any frequency.

### 2.2.5 X-ray Observations

The afterglow of XRF 050416a was observed with the *Swift* X-ray Telescope (XRT) beginning 1.2 minutes after the burst and continuing through  $t \sim 69$  days, placing it among the best studied X-ray afterglows to date (270, 271). From their analysis of the XRT data, Mangano et al. (239) report a spectral index of  $\beta_X = -1.04_{-0.05}^{+0.11}$  and evidence for significant absorption in the host galaxy,  $N_H = 6.8_{-1.2}^{+1.0} \times 10^{21} \text{ cm}^{-2}$ , corresponding to  $E(B - V)_{\text{rest}} = 1.2 \pm 0.2$  assuming the conversion of Predehl and Schmitt (299) and a Milky Way extinction curve (286). As shown in Figure 2.7, at  $t = 10$  hours the X-ray luminosity was  $L_{X,\text{iso}}(t = 10 \text{ hrs}) \approx 2.3 \times 10^{45} \text{ erg s}^{-1}$ , placing it at the lower edge of the observed distribution for GRBs (23, 138).

As discussed by Mangano et al. (239) and shown in Figure 2.7, the early evolution of the X-ray afterglow can be characterized by three phases: [1] an initial steep decay, [2] a flattening between  $t \approx 7$  and 20 minutes during which the flux is roughly constant, and [3] a resumed decay through  $t \sim 20$  days. These three phases have been shown to be ubiquitous among *Swift* X-ray afterglows (270). However, at  $t \sim 20$  days there is a second flattening which continues through  $t \sim 40$  days. By 70 days the X-ray afterglow is no longer detected, implying a significant steepening to  $\alpha_X \lesssim -1.8$  between the last two observations. We note that the timescale for the X-ray flattening and subsequent steep decay is coincident with the observed radio flare.

### 2.3 Properties of the Early Afterglow

Using the detailed multi-frequency observations of the XRF 050416a afterglow we can constrain the physical properties of the ejecta and the circumburst density. We adopt a standard relativistic blastwave model in which the afterglow emission is produced through the dynamical interaction of the ejecta with the surrounding medium (the forward shock, FS) with an additional component from shock heating of the ejecta (the reverse shock, RS). In this scenario, the total energy density is partitioned between relativistic electrons,  $\epsilon_e$ , and magnetic fields,  $\epsilon_B$ , while the thermal energy of the shocked protons accounts for the fraction remaining (see Piran 293 for a review). The shocked electrons are accelerated into a power-law distribution,  $N(\gamma) \propto \gamma^{-p}$  above a minimum Lorentz factor,  $\gamma_m$ . The emission resulting from the forward and reverse shock components is described by a synchrotron spectrum characterized by three break frequencies - the self-absorption frequency,  $\nu_a$ , the characteristic frequency,  $\nu_m$ , and the cooling frequency,  $\nu_c$  - and a flux normalization,  $F_{\nu_m}$  (339). In modeling the afterglow spectral and temporal evolution, we adopt the formalism of Granot and Sari (171) for a relativistic forward shock expanding into a constant density circumburst medium.

### 2.3.1 Preliminary Constraints

In fitting the forward shock model to the afterglow data of XRF 050416a we use only observations between 0.014 and 20 days when the afterglow follows a simple power-law evolution. To constrain the spectrum of the forward shock, we first investigate the afterglow evolution in the optical and X-ray bands. As shown in Figure 2.7, the X-ray data between 0.014 and 20 days are reasonably fit with  $\alpha_X \approx -1.1$  ( $\chi_r^2 \approx 0.70$ ). Mangano et al. (239) report that the X-ray spectral index on this same timescale is  $\beta_X \approx -1.04$ , leading to  $\alpha - 3\beta/2 \approx 0.5$ . A comparison to the standard closure relations,  $\alpha - 3\beta/2 = 0$  ( $\nu_m < \nu < \nu_c$ ) and  $\alpha - 3\beta/2 = 1/2$  ( $\nu > \nu_c$ ) indicates that  $\nu_X > \nu_c$ . This conclusion is supported by the near-IR to X-ray spectral slope,  $\beta_{K,X} = -0.47 \pm 0.06$  at  $t \approx 0.6$  days, which is flatter than  $\beta_X$  as expected if  $\nu_{\text{NIR/opt}} < \nu_c < \nu_X$ . Therefore, the X-ray observations suggest that  $p = -2\beta \approx 2.1$ .

Next we consider the spectral index within the NIR/optical bands. As discussed in §2.2.1 and shown in Figure 2.5, the observed NIR/optical spectral index on this timescale is  $\beta_{\text{NIR/opt}} \approx -1.3$  to  $-1.5$ . These values are significantly steeper than  $\beta_{K,X}$  and imply that the optical flux is suppressed by host galaxy extinction. Making the reasonable assumption that  $\nu_m \lesssim \nu_{\text{NIR/opt}}$  on the timescale of our afterglow observations, and adopting  $p \approx 2.1$  as indicated by the X-ray observations, we estimate  $\beta_{\text{NIR/opt}} = -(p - 1)/2 \approx -0.55$  for the intrinsic spectral index of the NIR/optical afterglow. Adopting this value for  $\beta_{\text{NIR/opt}}$ , we find that both NIR/optical spectra are reasonably fit with a Galactic extinction of  $E(B - V) = 0.03$  (343) and a host galaxy component of  $E(B - V)_{\text{rest}} \approx 0.28$  (Figure 2.5). Here we have assumed a Milky Way extinction model for the host (286) but note that a comparable fit may be obtained for an SMC extinction curve. We further note that this optically-derived extinction estimate is lower than that inferred from the X-ray spectrum (239), consistent with the trend observed for long-duration GRBs (152).

With this extinction correction, the near-IR to X-ray spectral index becomes  $\beta_{K,X} \approx -0.5 \pm 0.1$ , consistent with our estimate for the intrinsic spectral in-

dex within the NIR/optical band. Moreover, the extinction-corrected NIR/optical spectral index and observed average temporal index of  $\bar{\alpha}_{\text{NIR/opt}} = -0.7 \pm 0.2$  are consistent with the standard closure relation:  $\alpha - 3\beta/2 = 0 \approx 0.1$ . We also note that this supports our assumption of a constant density medium since, in a wind environment, the expected temporal index is steeper than  $\alpha = -1.25$ , and thus inconsistent with the observed values. Using all the available optical and X-ray observations we estimate that  $\nu_c \approx 1 \times 10^{17}$  Hz at  $t = 1$  day.

Next we compare the near-IR and radio afterglow data to constrain  $\nu_m$  and the peak spectral flux,  $F_{\nu_m}$ . Assuming that  $\nu_m$  passed through the NIR/optical bands near the time of our first  $K_s$ -band observations implies that the peak spectral flux is roughly comparable to the extinction-corrected  $K_s$  flux:  $F_{K_s} \approx 230 \mu\text{Jy}$  at  $t \approx 11$  minutes. Here we focus on the  $K_s$ -band data since they are the least sensitive to host galaxy extinction, which we estimate to be  $A_K \approx 0.24$  mag (a 20% increase in flux) for  $E(B - V)_{\text{rest}} \approx 0.28$ . Scaling these constraints to  $t = 1$  day ( $\nu_m \propto t^{-1.5}$  and  $F_{\nu_m} \propto t^0$ ) and accounting for the smooth shape of the spectral peak, we find  $\nu_m \approx 4.0 \times 10^{11}$  Hz and  $F_{\nu_m} \approx 350 \mu\text{Jy}$ . Here and throughout,  $F_{\nu_m}$  is the asymptotic extrapolation of the smooth spectrum peak and is therefore slightly higher than the intrinsic peak flux. We note that since the NIR/optical data require  $F_{\nu_m} \propto \nu^{-(p-1)/2}$ , lower values of  $\nu_m$  imply increasingly higher values of  $F_{\nu_m}$  at the time of the first  $K_s$ -band observations.

Finally, we test that these constraints are consistent with the radio observations. Given the evolution of  $\nu_m$ , these constraints predict that the spectral peak should pass through the radio band at  $t \approx 13$  days with an extrapolated peak flux density of  $F_{\nu_m} \approx 350 \mu\text{Jy}$ , roughly consistent with the 4.86 GHz observations on this timescale. We emphasize that the early steady decay of the NIR/optical data require that  $\nu_m$  passes through the radio no later than 13 days. Finally, we note that the radio spectrum is optically thin throughout the timescale of VLA monitoring (see Figure 2.6) and thus we observationally constrain  $\nu_a$  to be below 1.43 GHz.

### 2.3.2 Forward Shock Broadband Model

Adopting these constraints we apply a broadband afterglow model fit to the multi-frequency data in order to determine the physical parameters of the burst. The four spectral parameters ( $F_{\nu_m}$ ,  $\nu_a$ ,  $\nu_m$ , and  $\nu_c$ ) are fully determined by four physical parameters: the isotropic ejecta energy,  $E_{K,\text{iso}}$ , the energy density partition fractions,  $\epsilon_e$  and  $\epsilon_B$ , and the circumburst density,  $n$ . Therefore by constraining the four spectral parameters through broad-band observations, we are able to determine a unique solution for the four physical parameters (see Sari et al. 339 and Piran 293 for reviews). Although the radio observations provide only an upper limit on  $\nu_a$ , we are able to define a range of reasonable values by requiring that  $\epsilon_e, \epsilon_B \leq 1/3$ , which accounts for an equal or greater contribution from shocked protons. This requirement excludes unphysical solutions in which the sum of the contributions from shocked electrons, protons, and magnetic fields exceed the total energy density. Combined with the observed constraints for  $F_{\nu_m}$ ,  $\nu_m$ , and  $\nu_c$  we find the following ranges for the physical parameters:

$$E_{K,\text{iso}} \approx (8.2 - 14) \times 10^{51} \text{ erg} \quad (2.1)$$

$$n \approx (0.33 - 4.2) \times 10^{-3} \text{ cm}^{-3} \quad (2.2)$$

$$\epsilon_e \approx (0.20 - 1/3) \quad (2.3)$$

$$\epsilon_B \approx (0.072 - 1/3). \quad (2.4)$$

As shown in Figures 2.2, 2.6, and 2.7, this model provides an adequate fit to the broadband data between  $t \sim 0.01$  and 20 days.

### 2.3.3 Collimation of the Ejecta and Viewing Angle

The lack of an observed jet break in the X-rays to  $t \sim 20$  days, together with the inferred physical parameters constrain the opening angle of the jet (e.g., Sari et al. 338) to  $\theta_j \approx 3.1 t_j^{3/8} E_{K,\text{iso},52}^{-1/8} n_{-3}^{1/8} (1+z)^{-3/8} \gtrsim 6.9$  degrees. Here,  $t_j$  is the

jet break time in days and we have adopted the notation  $10^x Q_x = Q$ . This limit is slightly larger than the median of the jet opening angles inferred for long-duration GRBs,  $\theta_j \sim 5^\circ$  (Bloom et al. 44, Ghirlanda et al. 160, Soderberg et al. 354 and references therein). This indicates that the beaming-corrected ejecta energy release is  $E_K \equiv E_{K,\text{iso}}(1 - \cos\theta) \approx (9.8 \times 10^{49} - 1.4 \times 10^{52})$  erg where the range includes the uncertainty in  $E_{K,\text{iso}}$  and the lower limit on  $\theta_j$ . Moreover, we expect the blastwave to become non-relativistic on a timescale  $t_{\text{NR}} \approx 2.0 E_{51}^{1/3} n_{-3}^{-1/3} \sim (0.6 - 6.8)$  yrs (231). On a similar timescale, the ejecta are predicted to approach spherical symmetry after which the blastwave evolution is well described by the Sedov-von Neumann-Taylor (SNT) solution (448, 135); in this regime the afterglow emission decays with  $\alpha = -9/10$  ( $-1$ ) for frequencies below (above) the cooling frequency.

Next, the early steady decay of the X-ray and NIR/optical afterglow indicates that the jet collimation axis is directed roughly along our line-of-sight. In comparison, GRBs viewed significantly off-axis ( $\theta_{\text{obs}} > 2\theta_j$ ) are predicted to show a rising afterglow light-curve as the jet spreads sideways and intersects our viewing angle (168, 418, 367). Here,  $\theta_{\text{obs}}$  is the angle between our line-of-sight and the jet collimation axis. We conclude that the ejecta are viewed roughly on-axis and therefore the inferred beaming-corrected energies are not affected significantly (if at all) by viewing angle effects.

## 2.4 Properties of the Late-time Afterglow

Next we address the nature of the late-time broadband afterglow evolution with special attention to the strong radio flare observed at  $\sim 40$  days. Radio flares have been noted for several other GRBs, though only at early times (e.g., GRB 990123 at  $t \lesssim 1$  day; Kulkarni et al. 215). Based on their observed timescale and evolution, radio flares are typically attributed to emission from the reverse shock (337). Here we present detailed radio observations for XRF 050416a which show for the first time a strong radio flare at late time. Possible causes for a late-time radio

rebrightening include the emission from a decelerating jet initially directed away from our line-of-sight (418, 227), circumburst density variations (432, 306), and energy injection from a slow shell catching up to and refreshing the afterglow shock (311). We discuss each of these possibilities below.

### 2.4.1 Off-axis Jet Emission

It has been shown that the observational signature of a relativistic jet viewed significantly away from our line-of-sight is a rapid achromatic rise in the early afterglow light-curves (275, 168, 418). In this scenario, the observed peak of the afterglow emission occurs as the spreading jet crosses our viewing angle. The timescale for this peak is  $\sim 100$  days for a GRB jet with typical parameters ( $E_K = 10^{51}$  erg,  $n = 1 \text{ cm}^{-3}$ ,  $\epsilon_e = \epsilon_B = 0.1$ ,  $\theta_j = 5^\circ$ ) viewed from an angle  $\theta_{\text{obs}} = 30^\circ$  (367). The subsequent afterglow evolution is the same as that seen by an on-axis observer, decaying steeply with  $\alpha = -p \approx [-2 \text{ to } -3]$  for frequencies above  $\nu_m$  (338). The observed timescale and evolution of the XRF 050416a radio flare are therefore roughly consistent with the predictions of an off-axis relativistic jet.

However, as noted by Mangano et al. (239) and discussed in §2.3.3, the early and steady decay of the XRF 050416a broadband afterglow implies the presence of relativistic ejecta directed along our line-of-sight. These ejecta are also responsible for the production of the observed prompt emission. Attributing the strong late-time radio flare to an energetic off-axis relativistic jet therefore implies that multiple relativistic ejecta components were produced in the explosion. Moreover, the steep rise and peak flux of the radio flare imply sharp edges for the off-axis jet and a kinetic energy 2 to 3 times larger than that of the on-axis ejecta. While this scenario cannot be ruled out, we consider it unlikely given the complicated ejecta geometry required.

### A Receding Jet

Li and Song (227) describe a related scenario in which a strong late-time radio flare is observed from a receding jet initially directed anti-parallel to our line-of-

sight. In this case, early afterglow emission is expected from the approaching jet while emission from the receding jet is expected on a timescale  $5 \times t_{\text{NR}}$  due to the light travel time delay. This scenario is appealing in that it may explain both the early and late-time afterglow emission observed for XRF 050416a within the standard framework of engine-driven (accretion-fed compact source; Piran 293) double-sided jets. However, as discussed in §2.3.3, broadband modeling of the afterglow emission predicts the non-relativistic transition to occur no earlier than 0.6 yrs - too late to explain the radio flare at 40 days. Moreover, the peak emission from a receding jet should be comparable to the radio flux at  $t_{\text{NR}}$  and decay with a temporal index given by the Sedov solution,  $\alpha_{\text{rad}} = -9/10$  (227); both of these predictions are inconsistent with the observations. We conclude that afterglow emission from a receding jet is unlikely to produce the observed radio flare.

#### 2.4.2 Circumburst Density Variations

It has been argued that abrupt variations in the circumburst medium can produce a strong rebrightening in the radio afterglows of GRBs. Specifically, the dynamical interaction of the forward shock with a wind-termination shock at  $r \sim 1$  pc is predicted to cause a rebrightening of the radio afterglow on a timescale of a few years (432, 306, 307). Here it is assumed that the blastwave is expanding non-relativistically when it encounters the density jump, overall consistent with the observed timescales for non-relativistic transitions (135, 24, 134). For comparison, the interaction of a relativistic blastwave with an abrupt (step function) density jump is not expected to cause strong variations in the afterglow light-curves, where here it has been assumed that the post-jump expansion is also relativistic (266).

In the case of XRF 050416a, the strong radio flare and X-ray plateau phase occur on a timescale when the blastwave is still relativistic, and therefore an abrupt circumburst density jump appears an unlikely explanation. This is supported by the fact that during the relativistic regime, the flux at frequencies above  $\nu_c$  should be unaffected by circumburst density variations (171). We speculate, however, that a very large density jump may be able to decelerate the blastwave to non-

relativistic speeds on a very short timescale and may therefore be able to explain the unusual late-time afterglow evolution. The increase in density would cause a shift in  $\nu_a$  which may explain the peculiar evolution of the spectral index in the radio band (Figure 2.6). Based on our afterglow modeling (§2.3.2), we estimate that the circumburst radius of the forward shock at the onset of the radio flare was roughly  $\sim 1$  pc, roughly consistent with the radius of a wind-termination shock (154, 74). In this scenario, we expect a post-jump self-similar evolution consistent with the Sedov-Taylor solution. Since the late-time radio and X-ray data are not sufficiently sensitive to trace the post-flare evolution, we cannot rule out this possibility.

Finally, we investigated a scenario where the radio/X-ray flare is produced by the dynamical interaction of the quasi-spherical, non-relativistic SN ejecta with a CSM density enhancement. In fact, density jumps have been invoked to explain radio modulations observed for local (non-relativistic) SNe Ibc (e.g., SN 2003bg; Soderberg et al. 355). Adopting a simple minimum energy calculation (216) and requiring that the shock energy is equally partitioned between magnetic fields and relativistic electrons, we find that attributing the strong radio emission to the quasi-spherical SN component requires that the SN ejecta is relativistic ( $\Gamma \sim 10$ ) at the time of the radio/X-ray flare. However, as discussed above, strong flux variations are not expected while the blastwave is relativistic. Combined with the fact that the flare is at least a factor of  $10^2$  more radio luminous than any other SN Ibc ever observed (including GRB-SN 1998bw, Kulkarni et al. 216), we conclude that the radio/X-ray flare can not be attributed to the quasi-spherical SN ejecta.

### 2.4.3 Energy Injection

An episode of energy injection may also cause a rebrightening of the afterglow flux. Energy injection may arise from long-lived central engine activity or under the framework of a “refreshed” shock where a slow moving shell ejected during the initial burst eventually catches up with the afterglow shock (311, 167). The observed ratio of the settling time to the epoch of injection,  $\delta t/t$ , can distinguish

between these two scenarios. For  $\delta t/t < 1$  the injection is produced by engine activity, while  $\delta t/t \gtrsim 1$  indicates a refreshed shock. In the case of XRF 050416a, the X-ray and radio data after 20 days imply  $\delta t/t > 1$ , suggesting that the ejecta were refreshed on this timescale.

As shown in Figure 2.6, an extrapolation of the early radio evolution lies a factor of  $\sim 3$  below the observed flux at the onset of the radio flare. An energy increase affects the spectral parameters according to the following scalings:  $\nu_a \propto E_{K,\text{iso}}^{1/5}$ ,  $\nu_m \propto E_{K,\text{iso}}^{1/2}$ ,  $F_{\nu_m} \propto E_{K,\text{iso}}$ , and  $\nu_c \propto E_{K,\text{iso}}^{-1/2}$  (171). Given that  $\nu_m$  is within the radio band on this timescale we have  $F_{\nu,\text{rad}} \propto E_{K,\text{iso}}$  and thus the radio flare corresponds to an energy injection of a comparable factor,  $\sim 3$ . For the X-ray band,  $F_{\nu,X} \propto E_{K,\text{iso}}^{(p+2)/4}$ , thus for  $p \approx 2.1$  an energy injection of a factor of  $\sim 3$  corresponds to a comparable increase in the X-ray flux. The *Swift*/XRT observations suggest a flattening on this timescale. Here we adopt the conservative assumption that the shock microphysics ( $\epsilon_e$ ,  $\epsilon_B$  and  $p$ ) do not evolve during the energy injection.

One important implication of the energy injection model is that the post-injection asymptotic temporal decay should be the same as that before the injection. This prediction is consistent with the energy injection episodes invoked for GRBs 021004 and 030329 (38, 167). However, in the case of XRF 050416a, the late-time radio and X-ray data suggest a steep post-injection decay,  $\alpha \gtrsim -2$ , significantly steeper than that observed pre-injection. Moreover, the afterglow should asymptotically approach a flux normalization larger by a factor of  $\sim 3$  in both the radio and X-ray bands. As shown in Figures 2.6 and 2.7, this appears inconsistent with the observations which suggest that the late-time afterglow is comparable (or fainter) than an extrapolation of the early afterglow model. We note, however, that the faintness of the late-time afterglow and the steep post-injection decay may be explained if a jet break occurred on roughly the same timescale as the energy injection.

In comparison with other late-time afterglow studies (135, 393, 24, 212, 134), the radio flare and X-ray flattening observed for XRF 050416a are clearly atypical for long-duration GRBs. We therefore attribute the observed evolution to an

unusual scenario involving either a large circumburst density jump or a late-time injection of energy (from a slow shell or off-axis ejecta).

#### 2.4.4 An Associated Supernova

The *HST* measurements at late-time can be used to constrain any possible contribution from an associated supernova. Based on previous studies of GRB-SNe, the thermal emission from an associated supernova is predicted to reach maximum light on a timescale of  $20 \times (1 + z)$  days with a peak magnitude of  $M_{V,\text{rest}} \approx -20$  mag or fainter (Zeh et al. 447, Soderberg et al. 366 and references therein). Observationally, the emergence of a SN component produces a steepening of the optical spectrum as the supernova nears maximum light and dominates the afterglow emission.

An extrapolation of the broadband afterglow model to 40 days shows that the *HST* data are brighter by a factor of  $\sim 5$ . For comparison, the radio flare and X-ray plateau on this same timescale represent flux density enhancements by factors of roughly  $\sim 3$  and 2, respectively.

As discussed in §2.2.2 we measure the spectrum of the optical transient within the *ACS* bands and find  $\beta_{HST} \approx -2.8 \pm 0.3$  at 37 days. After correction for extinction (see §2.2.1), the implied spectral index becomes  $\beta_{HST} \approx -1.9$ . For comparison, the spectral index between the radio and X-ray bands on this timescale (coincident with the radio flare and X-ray flattening) is  $\beta_{\text{radX}} \approx -0.56 \pm 0.04$  and the indices within the bands are  $\beta_{\text{rad}} \approx -0.6 \pm 0.2$  (Figure 2.6) and  $\beta_X \approx -1.0$  (239), respectively. Given that the *HST*-derived spectral index, even after correction for extinction, is (1) significantly steeper than the NIR/optical index observed at early time,  $\beta_{\text{NIR/opt}} \approx -1.4$ , (2) significantly steeper than  $\beta_{\text{radX}}$  measured at a comparable epoch, and (3) inconsistent with the range of synchrotron spectral indices predicted for a relativistic blastwave ( $\beta = [-1.5, 2.5]$ , Sari et al. 339), we conclude that the optical flux at  $t \sim 40$  days is dominated by another emission process, likely an associated SN.

Next, to determine if the late-time optical data are consistent with the temporal

evolution of a typical GRB/XRF-associated supernova, we compare the *HST* flux values with synthesized SN light-curves. We compiled *UBVRIJHK* observations of SN 1998bw from the literature (151, 254, 282) and smoothed the extinction-corrected (Galactic component of  $E(B-V)=0.059$ , Schlegel et al. 343) light-curves. Here we assume that the SN 1998bw host-galaxy extinction is negligible, consistent with the findings of Patat et al. (282) based on a spectroscopic analysis of the host galaxy. We then produced  $k$ -corrected NIR/optical light-curves of SN 1998bw at the redshift of XRF 050416a by interpolating over the photometric spectrum and stretching the arrival time of the photons by a factor of  $(1+z)$ .

Shown in Figure 2.2 are the synthesized light-curves for SN 1998bw at  $z = 0.6528$ , summed together with the afterglow model. The *HST* data are roughly comparable with the flux normalization and evolution of the summed model. Therefore, the temporal and spectral properties of the *HST* data suggest that XRF 050416a was associated with a supernova similar to SN 1998bw. However, we caution that the temporal coincidence of the SN peak with the radio flare makes it difficult to estimate the relative contributions of the SN and afterglow.

## 2.5 Host Galaxy Properties

We now turn to the properties of the GRB host galaxy. We measure the brightness of the host galaxy in the final *HST* epoch to be  $F775W = 23.1 \pm 0.1$  mag ( $I = 22.7 \pm 0.1$  mag). These values are not corrected for extinction. At  $z = 0.6528$  the rest-frame  $B$ -band is traced by the observed F775W band, leading to an absolute magnitude,  $M_B \approx -20.3 \pm 0.1$  mag, or a luminosity  $L_B \approx 0.5L^*$ . This host luminosity is similar to that inferred for XRF 030528 (308) and the hosts of typical GRBs (219). At  $z = 0.6528$ , the measured offset of the optical transient (§2.2.1) relative to the center of the host galaxy corresponds to  $140 \pm 140$  pc. This offset is a factor of  $\sim 10$  smaller than the median value for long-duration GRBs (45).

As shown in Figure 2.5, the host exhibits several emission lines typical of star-forming galaxies. We estimate the star formation rate in the host galaxy from the

observed fluxes of the various emission lines. Using the flux of the [O Roman2] $\lambda$ 3727 line,  $F_{[\text{OII}]} \approx 9.6 \times 10^{-17} \text{ erg cm}^{-2} \text{ s}^{-1}$  (Table 2.3), and the conversion of Kennicutt (205),  $\text{SFR} = (1.4 \pm 0.4) \times 10^{-41} L_{[\text{OII}]} \text{ M}_{\odot} \text{ yr}^{-1}$ , we find a star formation rate of about  $2.5 \pm 0.7 \text{ M}_{\odot} \text{ yr}^{-1}$ . From the  $\text{H}\beta$  line flux,  $F_{\text{H}\beta} \approx 3.7 \times 10^{-17} \text{ erg cm}^{-2} \text{ s}^{-1}$ , and assuming the Case-B recombination ratio of  $F_{\text{H}\alpha}/F_{\text{H}\beta} = 2.87$  and the conversion of Kennicutt (205), we infer a star formation rate of  $\text{SFR} = 7.9 \times 10^{-42} L_{\text{H}\alpha} \approx 1.5 \pm 0.2 \text{ M}_{\odot} \text{ yr}^{-1}$ . Thus, we conclude that the star formation rate (not corrected for extinction) is roughly  $2 \text{ M}_{\odot} \text{ yr}^{-1}$ . We note that the observed ratio of  $\text{H}\gamma/\text{H}\beta = 0.3 \pm 0.1$  compared to the theoretical value of about 0.47 (273) suggests a significant extinction correction (factor of  $\sim 10$ ) following the method of (58). We conclude that the star formation rate for the host of XRF 050416a is similar to those inferred for long-duration GRBs (77, 17) and at least an order of magnitude larger than that inferred for XRF 020903 (361, 31).

The combination of the inferred star formation rate and host luminosity provides a measure of the specific star formation rate. We find a value of  $4 \text{ M}_{\odot} \text{ yr}^{-1} L^*/L$  (uncorrected for extinction), which is about a factor of two lower than the mean specific star formation rate for the hosts of long-duration GRBs (77).

Next, we use the relative strengths of the oxygen and hydrogen emission lines to infer the ionization state and oxygen abundance. The relevant indicators are  $R_{23} \equiv \log(F_{[\text{OII}]} + F_{[\text{OIII}]} / F_{\text{H}\beta}) \approx 0.74$  and  $O_{32} \equiv \log(F_{[\text{OIII}]} / F_{[\text{OII}]}) \approx 0.055$ . Using the calibrations of McGaugh (253) and Kobulnicky and Kewley (210) we find that for the upper branch the metallicity is  $12 + \log(\text{O}/\text{H}) \approx 8.6$  while for the lower branch it is about 7.9; the two branches are due to the double-valued nature of  $R_{23}$  in terms of metallicity. Thus, the host metallicity of XRF 050416a is  $0.2 - 0.8 Z_{\odot}$ , larger than that inferred for XRF 060218 (259, 430) and comparable to that for XRF 030528 (308). Moreover, this range is somewhat higher than the typical metallicities for GRB hosts, some of which have metallicities that are  $\sim 1/10$  solar (e.g., Prochaska et al. 303).

## 2.6 Is XRF 050416a a Short Burst?

With a prompt emission duration of just  $T_{90} \approx 2.4$  sec (327), it is interesting to consider XRF 050416a as a member of the short-hard class of gamma-ray bursts, popularly believed to result from the coalescence of neutron stars or black holes (e.g., Eichler et al. 107). Based on the bi-modal BATSE duration distribution, bursts with  $T_{90} \gtrsim 2$  seconds are assumed to belong to the long-duration class (213), although a decomposition of the overlapping distributions suggests that a small fraction of short-hard bursts (SHBs) have durations longer than this cut-off. The distinction between short-hard and long-duration bursts is further complicated by the detection of soft X-ray tails lasting several seconds following SHBs 050709 and 050724 (411, 12). This suggests that SHBs are not necessarily characterized by a pure hard emission spectrum (326). Related to this issue is the use of spectral lags to distinguish between long and short bursts. As discussed by Norris and Bonnell (268), long-duration bursts typically have longer lags that correlate with isotropic equivalent prompt gamma-ray luminosity (269). On the other hand, SHBs have negligible (or even negative) spectral lags.

In the case of XRF 050416a, the prompt duration places it between the long- and short-duration classes. The low value of  $E_p$  may suggest that it belongs to the long-duration class, however, it is becoming clear that hardness cannot be used to reliably distinguish between the two classes (see Nakar 265). Similarly, while the negative lag inferred for XRF 050416a may suggest a SHB classification, examples do exist of long-duration BATSE bursts with negative lags (268).

Afterglow modeling may provide additional clues. The range of values we infer for the XRF 050416a beaming-corrected energies are overall consistent with those of long-duration GRBs, including the subclass of sub-energetic bursts. At the same time, they are roughly consistent with the values inferred for SHBs (129, 28, 354). However, the low circumburst density,  $n \sim 10^{-3}$ , is a factor of 10 to  $10^4$  smaller than the typical values inferred for long-duration GRBs (e.g., Panaitescu and Kumar 280, Yost et al. 445, Chevalier et al. 74) but comparable

to those of SHBs (129, 28, 49, 55, 277, 354). The observed radio flare and X-ray flattening at 20 days are atypical for both long- and short- duration GRBs and therefore cannot be used to classify this event. However, it is interesting to note that large variations in the circumburst density are more naturally explained in the context of a massive stellar progenitor with interacting stellar winds (154, 306).

Next is a discussion of the XRF 050416a host galaxy since long- and short-bursts may also be distinguished by their environments (see Berger 16 for a recent review). As discussed in §2.5, the host is a star-forming galaxy with an inferred SFR and metallicity comparable to those of long-duration GRBs. Moreover, XRF 050416a is located near the center and brightest part of its host galaxy. It is thus consistent with the locations of long-duration bursts with respect to their hosts (45, 142). For comparison, SHBs are typically localized to low SFR hosts with significant old stellar populations at radial offsets up to a factor of 10 larger than those of typical long-duration bursts (28, 129, 48, 354).

Finally, the discovery of an associated Type Ic supernova is perhaps one of the best methods to distinguish between long- and short-bursts. The discovery of several long-duration bursts and X-ray flashes at  $z \lesssim 0.3$  in the last few years has firmly established that GRBs and XRFs are accompanied by supernovae of Type Ic (151, 377, 237, 363, 292). A study of the luminosity distribution for GRB/XRF-SNe reveals a significant dispersion, implying a spread of (at least) an order of magnitude in peak optical luminosity (447, 366). At the same time, deep imaging of SHBs has constrained any associated SN emission to be up to  $\sim 100$  times less luminous as SN 1998bw (129, 354). In the case of XRF 050416a, the temporal and spectral properties of the *HST* data suggest that XRF 050416a was accompanied by a supernova with a peak luminosity roughly similar to SN 1998bw. We stress, however, that the temporal coincidence of the radio flare with the SN peak complicates any study of the SN properties.

Based on the associated SN and large-scale environmental properties, we conclude that XRF 050416a is a member of the long-duration class of gamma-ray bursts. This event highlights the difficulty in classifying bursts based on their

prompt emission properties alone.

## 2.7 Discussion and Conclusions

We present extensive broad-band NIR/optical and radio data for the afterglow of the X-ray flash 050416a and show that it is localized to a star-forming ( $\gtrsim 2 M_{\odot} \text{ yr}^{-1}$ ) host galaxy at  $z = 0.6528$ . Along with XRFs 020903, 030723, and 060218, this burst is one of the best-studied X-ray flashes to date. Moreover, XRF 050416a is only the third XRF with a spectroscopic redshift for which a broadband afterglow study has been performed and the physical parameters have been constrained. The isotropic-equivalent prompt and kinetic energy releases are  $E_{\gamma,\text{iso}} \approx 1.2 \times 10^{51}$  (327) and  $E_{K,\text{iso}} \approx 10^{52}$  erg respectively. These values are a factor of  $10^2$  times larger than those of XRF 020903 (330, 361) and up to  $10^4$  times larger than those inferred for sub-energetic GRBs 980425, 031203, and XRF 060218 (290, 216, 341, 362, 59, 365).

Adopting the results of our standard synchrotron model and  $t_j \gtrsim 20$  days we constrain the collimation of the ejecta to  $\theta_j \gtrsim (6.9 - 9.7)^\circ$ , slightly larger than the median value of  $5^\circ$  for typical GRBs (Bloom et al. 44, Ghirlanda et al. 160 and references therein). This indicates that the beaming-corrected energy release is  $E_K \approx (9.8 \times 10^{49} - 1.4 \times 10^{52})$  erg and  $E_\gamma \approx (8.6 \times 10^{48} - 1.2 \times 10^{51})$  erg, implying a total relativistic energy yield of  $E_{\text{tot}} \approx (1.1 \times 10^{50} - 1.5 \times 10^{52})$  erg, which straddles the median value for cosmological GRBs,  $E_{\text{tot}} \approx 2 \times 10^{51}$  erg (27). However, the efficiency in converting the energy in the ejecta into  $\gamma$ -rays is  $\eta_\gamma \equiv E_\gamma / (E_K + E_\gamma) \approx (0.04 - 0.08)$ , significantly lower than the typical values for GRBs (280, 445) and comparable to that inferred for XRF 020903 ( $\eta_\gamma \approx 0.03$ , Soderberg et al. 361). This strengthens the idea that XRFs and GRBs are distinguished by their ability to couple significant energy to highly-relativistic material (361, 450).

In addition to the burst energetics, several key results emerge from our broad-band analysis of XRF 050416a. First is the detection of a bright, late-time radio flare accompanied by an observed flattening in the X-ray bands which we attribute

to a large circumburst density enhancement or episode of energy injection (refreshing shell or off-axis ejecta) at  $t \sim 20$  days. In the context of a density jump, it is interesting to note that the inferred pre-jump circumburst density is several orders of magnitude lower than the values typically inferred for long-duration GRBs (see Soderberg et al. 367 for a recent compilation). Moreover, radio observations of local (optically-selected) core-collapse SNe show similar flux modulations (factor of 2 to 3) attributed to abrupt variations in the circumstellar medium (423, 325, 355).

Next, the temporal and spectral evolution of the optical afterglow suggests the contribution from a supernova component with peak luminosity and light-curve shape comparable to SN 1998bw. Given the temporal coincidence of the radio flare and X-ray flattening with the SN peak, XRF 050416a highlights the need for full spectral coverage in late-time GRB/XRF-SN searches. This is illustrated by the optical rebrightening observed for XRF 030723 at  $\sim 15$  days and interpreted as a thermal SN component (144) while the X-ray and radio data show similar rebrightenings at late-time suggesting a CSM density jump or energy injection (Butler et al. 57, Soderberg *et al.* in prep).

With the addition of XRF 050416a, there are three XRFs (020903, 060218, and now 050416a) with spectroscopic redshifts observed in association with supernovae with peak luminosities varying by up to a factor of 10 compared to SN 1998bw (363, 31, 292). However, deep *HST* observations of XRF 040701 at  $z = 0.21$  revealed that any associated SN was at least a factor of 10 (and likely  $\gtrsim 100$ ) times fainter than SN 1998bw (363). It is therefore clear that most XRFs produce Nickel-rich supernova explosions, but that there is a significant dispersion in the peak luminosities of XRF-associated SNe. A similar result is found for GRB-associated SNe (447, 366) and further strengthens the idea that GRBs and XRFs are intimately related.

Finally, we address XRF 050416a within the framework of off-axis and dirty fireball models for XRFs. As discussed in §2.3.3, the evolution of the early afterglow indicates that the ejecta are being viewed along the collimation axis. Similarly, on-axis viewing angles are inferred from afterglow studies of XRFs 020903

(361), 050215B (223), 050406 (321), and 060218 (59, 365). Unification models in which X-ray flashes are understood as typical GRBs viewed away from the burst collimation axis (e.g., Granot et al. 168, Yamazaki et al. 441) are therefore inconsistent with the observations for these five events. To date, such models are only consistent with the observations of one X-ray flash: XRF 030723 (144, 57, 170).

While the lack of high-energy photons prevents a direct constraint on the Lorentz factor of the burst, our detailed afterglow modeling allows us to place a lower limit on the initial bulk Lorentz factor,  $\Gamma_0 \gtrsim 110$ , by extrapolating  $\Gamma \propto t^{-3/8}$  back to the first XRT observation at  $\sim 100$  sec. This value is somewhat lower than the typical values inferred for cosmological GRBs (280) and consistent with the upper range of values predicted for a dirty fireball. Given that some dirty fireball models predict XRFs to have wider jets than typical GRBs (e.g., Zhang et al. 451), it is interesting to note that there are no X-ray flashes for which an achromatic jet break has been observed. This may suggest that their ejecta are not strongly collimated. In fact, detailed radio observations of XRFs 020903 and 060218 spanning  $\gtrsim 100$  days imply a quasi-spherical ejecta geometry in both cases (361, 365).

While the basic properties of X-ray flashes (redshifts, hosts, isotropic  $\gamma$ -ray energies) are now available for several events, it is clear that broadband afterglow observations are required for a complete understanding of the burst properties. With the addition of XRF 050416a to the existing sample of only a few well-studied events, we continue to work towards a systematic comparison of the global characteristics of XRFs and GRBs. While limited, the current sample suggests that the two classes share similar ejecta energies, associated SNe, and viewing angles. Further studies of XRF afterglows will be used to confirm whether the two classes differ in their collimation angles.

The authors thank Re'em Sari and Don Lamb for helpful discussions. As always, the authors thank Jochen Greiner for maintaining his GRB page. A.M.S. and S.B.C. are supported by the NASA Graduate Student Research Program. E.B. and A.G. acknowledge support by NASA through Hubble Fellowship grants awarded by STScI, which is operated by AURA, Inc., for NASA. GRB research at

Caltech is supported through NASA.

Table 2.1. Ground-based Optical and NIR Observations of XRF 050416a

Date Obs (UT)	$\Delta t^a$ (days)	Telescope	Filter	magnitude <sup>b</sup>
2005 April 16.4641	0.0025	Palomar 60-inch	<i>I</i>	$18.82 \pm 0.11$
2005 April 16.4659	0.0043	Palomar 60-inch	<i>I</i>	$18.86 \pm 0.11$
2005 April 16.4677	0.0061	Palomar 60-inch	<i>I</i>	$19.16 \pm 0.13$
2005 April 16.4696	0.0080	Palomar 60-inch	<i>I</i>	$19.35 \pm 0.23$
2005 April 16.4692	0.0076	Palomar 200-inch	$K_s$	$16.37 \pm 0.21$
2005 April 16.4714	0.0098	Palomar 60-inch	<i>I</i>	$19.01 \pm 0.12$
2005 April 16.4731	0.0116	Palomar 60-inch	<i>I</i>	$19.53 \pm 0.18$
2005 April 16.4772	0.0156	Palomar 60-inch	$z'$	$19.16 \pm 0.27^c$
2005 April 16.4763	0.0147	Palomar 200-inch	$K_s$	$16.64 \pm 0.20$
2005 April 16.4833	0.0217	Palomar 60-inch	<i>I</i>	$19.09 \pm 0.20$
2005 April 16.4828	0.0212	Palomar 200-inch	$K_s$	$16.79 \pm 0.20$
2005 April 16.4880	0.0264	Palomar 60-inch	<i>I</i>	$19.34 \pm 0.23$
2005 April 16.4895	0.0279	Palomar 200-inch	$K_s$	$16.89 \pm 0.24$
2005 April 16.4960	0.0344	Palomar 200-inch	$K_s$	$16.99 \pm 0.25$
2005 April 16.5026	0.0410	Palomar 200-inch	$K_s$	$16.98 \pm 0.29$
2005 April 16.5089	0.0473	ANU 2.3-meter	<i>R</i>	$20.92 \pm 0.05$
2005 April 16.5502	0.0886	ANU 2.3-meter	<i>R</i>	$21.18 \pm 0.12$
2005 April 16.5543	0.0927	ANU 2.3-meter	<i>R</i>	$21.40 \pm 0.15$
2005 April 16.5585	0.0969	ANU 2.3-meter	<i>R</i>	$21.16 \pm 0.08$
2005 April 16.5626	0.1010	ANU 2.3-meter	<i>R</i>	$21.43 \pm 0.11$
2005 April 16.5669	0.1053	ANU 2.3-meter	<i>R</i>	$21.44 \pm 0.26$
2005 April 16.5702	0.1086	ANU 2.3-meter	<i>R</i>	$21.39 \pm 0.16$

Table 2.1—Continued

Date Obs (UT)	$\Delta t^a$ (days)	Telescope	Filter	magnitude <sup>b</sup>
2005 April 16.5744	0.1128	ANU 2.3-meter	<i>R</i>	$21.37 \pm 0.16$
2005 April 16.5779	0.1163	ANU 2.3-meter	<i>R</i>	$21.18 \pm 0.17$
2005 April 16.5816	0.1200	ANU 2.3-meter	<i>R</i>	$21.35 \pm 0.16$
2005 April 16.5850	0.1234	ANU 2.3-meter	<i>R</i>	$21.36 \pm 0.10$
2005 April 16.5893	0.1277	ANU 2.3-meter	<i>R</i>	$21.44 \pm 0.27$
2005 April 16.5924	0.1308	ANU 2.3-meter	<i>R</i>	$21.46 \pm 0.22$
2005 April 16.5975	0.1359	ANU 2.3-meter	<i>R</i>	$21.63 \pm 0.34$
2005 April 16.6092	0.1476	ANU 2.3-meter	<i>R</i>	$21.71 \pm 0.30$
2005 April 16.6187	0.1571	ANU 2.3-meter	<i>R</i>	$21.87 \pm 0.46$
2005 April 17.3895	0.9279	Palomar 60-inch	<i>R</i>	$22.62 \pm 0.30$
2005 April 17.4006	0.9390	Palomar 60-inch	<i>z'</i>	$< 20.38^c$
2005 April 17.4087	0.9467	Palomar 60-inch	<i>I</i>	$22.05 \pm 0.30$
2005 April 18.2884	1.8264	Palomar 60-inch	<i>R</i>	$< 23.46$
2005 April 18.4031	1.9411	Palomar 60-inch	<i>I</i>	$< 22.83$
2005 April 23.3511	6.8896	Palomar 200-inch	<i>K<sub>s</sub></i>	$< 19.70$

<sup>a</sup>Days since explosion have been calculated for the mid-point of each exposure.

<sup>b</sup>Magnitudes have not been corrected for extinction. Limits are given as  $3\sigma$ .

<sup>c</sup>AB system.

Table 2.2. *HST/ACS* Observations of XRF 050416a

Date Obs (UT)	$\Delta t$ (days)	Exp. Time (sec)	Filter	<i>HST</i> mag <sup>a</sup> (AB)	Johnson mag <sup>b</sup> (Vega)
2005 May 23.38	36.92	3282	F775W	$24.35 \pm 0.02$	$23.82 \pm 0.02$
2005 May 23.46	37.00	3430	F850LP	$23.83 \pm 0.03$	—
2005 June 16.17	60.71	3986	F775W	$25.88 \pm 0.10$	$25.36 \pm 0.10$
2005 July 11.15	85.69	4224	F775W	$26.44 \pm 0.22$	$25.92 \pm 0.22$
2005 November 21.06	218.60	4224	F850LP	—	—
2005 November 21.19	218.73	4224	F775W	—	—

<sup>a</sup>AB system magnitudes in the *HST* filters given in column 4. Photometry was done on residual images (see §2.2.2). We have assumed the source flux to be negligible in the final (template) epoch. Magnitudes have not been corrected for extinction.

<sup>b</sup>We convert the F775W magnitudes in column 5 to Johnson *I*-band (Vega system) as described in §2.2.2. Magnitudes have not been corrected for extinction.

Table 2.3. Spectroscopic lines for XRF 050416a

Line	$\lambda$ (rest) ( $\text{\AA}$ )	$\lambda$ (observed) <sup>a</sup> ( $\text{\AA}$ )	Redshift	Flux <sup>b</sup> ( $\times 10^{-17} \text{erg cm}^{-2} \text{s}^{-1}$ )
[OII]	3728.38	6162.08	0.6528	$9.6 \pm 0.4$
H $\gamma$	4341.72	7174.64	0.6525	$1.2 \pm 0.2$
H $\beta$	4862.72	8037.14	0.6528	$3.7 \pm 0.5$
[OIII]	4960.30	8198.79	0.6529	$2.5 \pm 0.3$
[OIII]	5008.24	8277.57	0.6528	$8.4 \pm 0.4$

<sup>a</sup>Observed wavelengths have been corrected to vacuum.

<sup>b</sup>Flux values have not been corrected for Galactic extinction.

Table 2.4. Radio Observations of XRF 050416a

Date Obs (UT)	$\Delta t$ (days)	$F_{\nu, 1.43 \text{ GHz}}^a$ ( $\mu\text{Jy}$ )	$F_{\nu, 4.86 \text{ GHz}}$ ( $\mu\text{Jy}$ )	$F_{\nu, 8.46 \text{ GHz}}$ ( $\mu\text{Jy}$ )
2005 April 16.49	0.026	—	—	$20 \pm 51$
2005 April 22.03	5.57	—	$200 \pm 46$	$101 \pm 34$
2005 April 28.29	11.83	—	$188 \pm 42$	$132 \pm 30$
2005 May 1.35	14.89	—	$201 \pm 43$	—
2005 May 31.10	44.64	—	—	$431 \pm 46$
2005 June 3.99	48.53	—	$585 \pm 48$	—
2005 June 8.03	52.57	$420 \pm 190$	$562 \pm 51$	$398 \pm 33$
2005 June 16.97	61.51	—	$505 \pm 49$	$330 \pm 35$
2005 June 20.16	64.70	—	—	$286 \pm 33$
2005 July 1.92	76.46	$843 \pm 214$	$321 \pm 48$	$189 \pm 36$
2005 July 30.02	104.56	$0 \pm 192$	$68 \pm 36$	$93 \pm 41$
2005 August 14.97	120.51	—	—	$72 \pm 42$
2005 August 21.89	127.42	—	—	$41 \pm 47$
2005 September 19.90	156.44	—	$0 \pm 54$	—
2005 October 15.73	182.27	—	$33 \pm 47$	$89 \pm 38$

<sup>a</sup>All errors are given as  $1\sigma$  (rms).

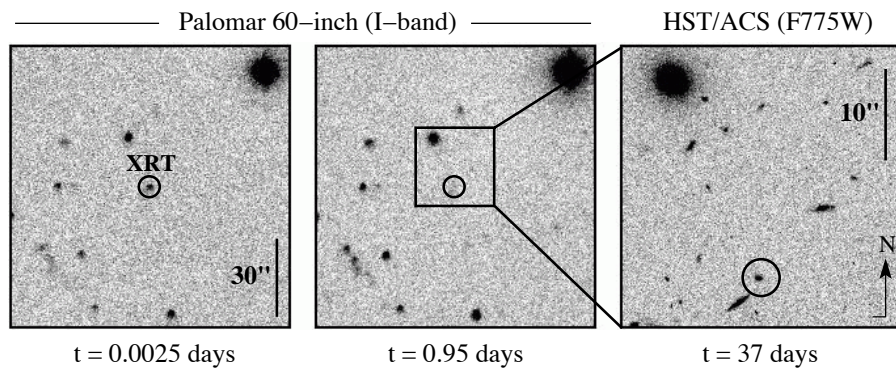


Figure 2.1: We began observing the field of XRF 050416a with the Palomar 60-inch telescope in the  $I$ -band about 2.5 minutes after the burst. We discovered a fading source within the 3.0 arcmin (radius) *Swift*/BAT error circle. Subsequent localizations of the XRT (circle) and UVOT afterglow positions were shown to be coincident with the P60 source. Our late-time *HST* images reveal a host galaxy coincident with the optical afterglow position.

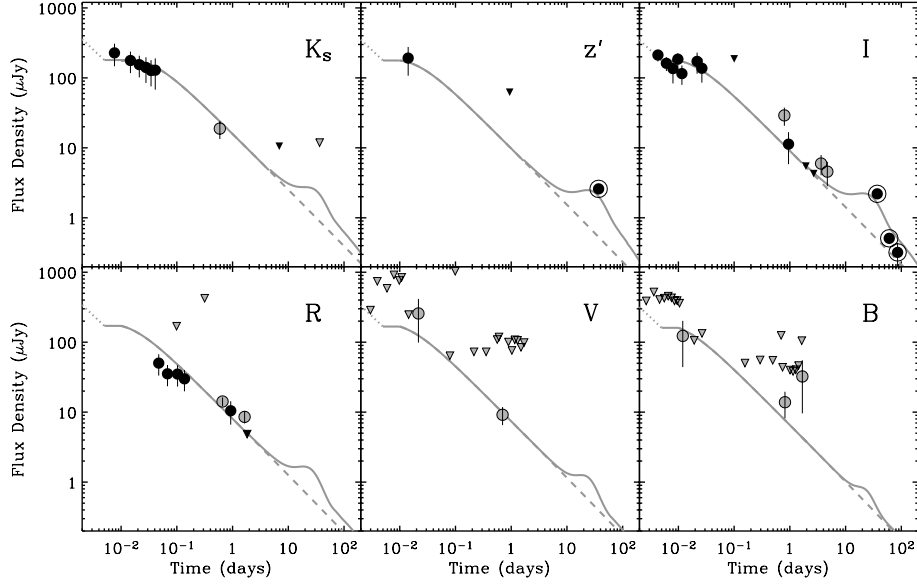


Figure 2.2: We supplement our measurements from Table 2.1 (black symbols) with data from the GCNs (225, 301, 305, 397, 444) and Holland et al. (188) (grey symbols). Detections are shown as circles and upper limits as inverted triangles. *R*-band data from the ANU 2.3-meter have been binned for clarity. All data have been corrected for host galaxy extinction (see §2.2.1). Between  $t \approx 0.01$  and 1 day the NIR/optical afterglow shows an average decay index of  $\bar{\alpha}_{\text{NIR/opt}} \approx -0.75$ . As described in §2.3.2, we find a reasonable fit to the spectral and temporal evolution of the broadband data with a standard afterglow model. Our *HST* measurements are shown as encircled dots; the implied steep spectral index suggests the contribution from an supernova component at  $t \sim 40$  days (§2.4.4). We sum the flux from a SN 1998bw-like supernova at  $z = 0.6528$  with our afterglow model to produce the final fits (grey solid lines). For comparison, we also show the afterglow model alone (dashed grey line). We note that this model does not apply to the very early afterglow evolution at  $t \lesssim 0.01$  days. The dotted grey lines at early time represent the evolution of the NIR/optical assuming these bands track the X-ray evolution on this timescale.

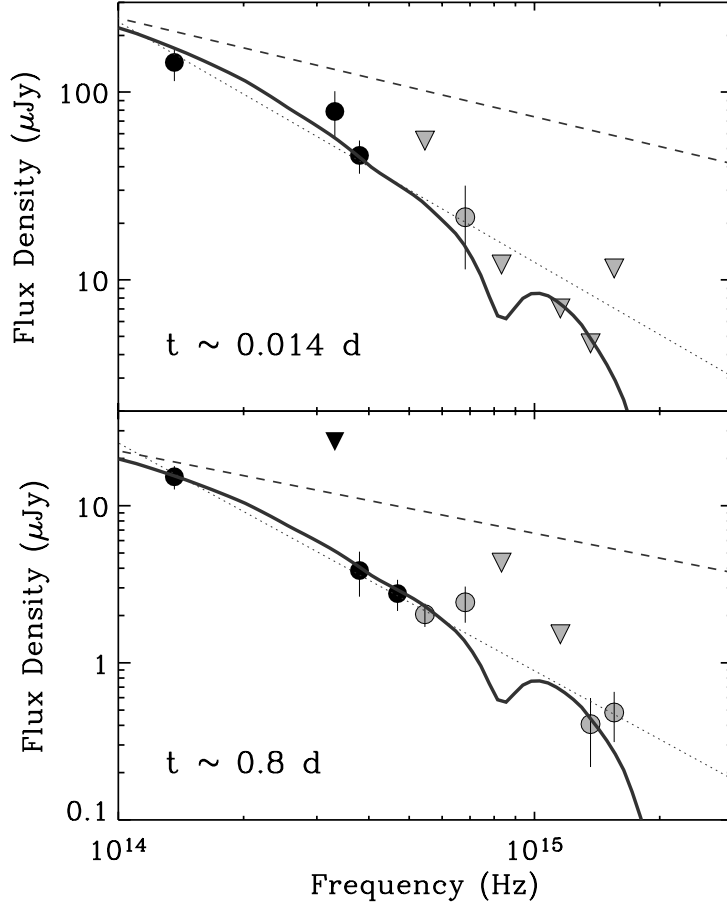


Figure 2.3: The observed photometric spectrum for XRF 050416a is shown at  $t \approx 0.014$  (top) and 0.8 days (bottom). The  $K_s$ -,  $z'$ -,  $I$ -, and  $R$ -band data (black symbols) are from Table 2.1 while the  $V$ ,  $B$ ,  $U$ ,  $UVW1$ ,  $UVM2$ , and  $UVW2$  data (grey symbols) are from Holland et al. (188). Detections are shown as circles and upper limits as inverted triangles. The observed spectrum is fit by  $\beta_{\text{NIR/opt}} \approx -1.3$  and  $-1.5$  in the top and bottom panels, respectively (dotted line). We fit the data with an extinction model (solid line) which includes  $E(B - V) = 0.03$  from the Galaxy (343) and a rest-frame host galaxy extinction of  $E(B - V)_{\text{rest}} = 0.28$  assuming an intrinsic spectral index of  $\beta_{\text{NIR/opt}} \approx -0.55$  (dashed line).

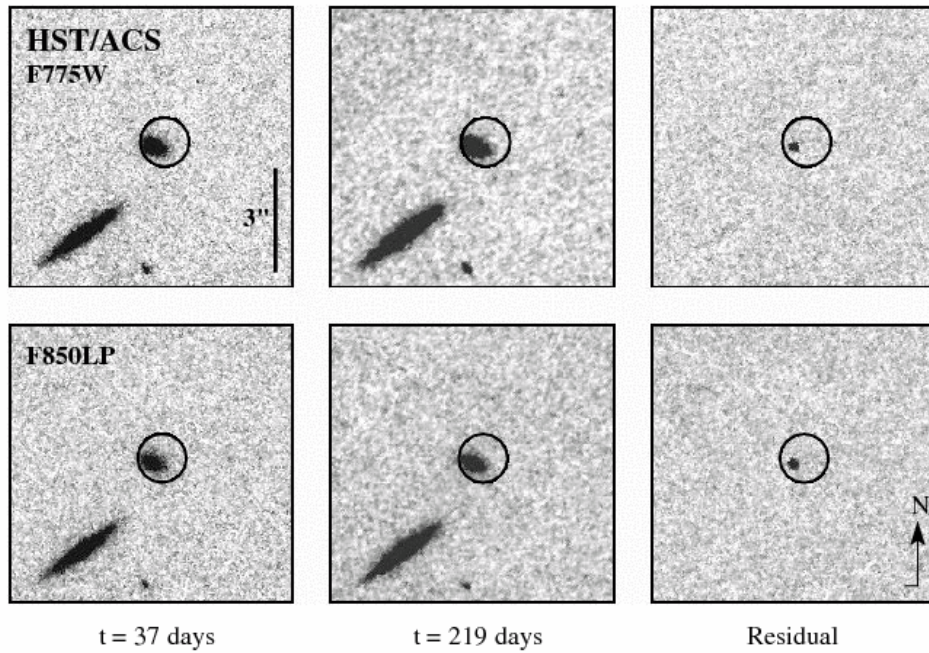


Figure 2.4: Images were obtained in filters F775W and F850LP spanning  $t \approx 37$  to 219 days after the explosion. The host galaxy emission dominates that of the afterglow throughout this timescale. Relative astrometry between the P60 and the *HST* images provides an optical afterglow position accurate to 0.70 arcsec (circle,  $2\sigma$ ). Residual images of the afterglow were produced through image subtraction techniques (§2.2.2). The position of the afterglow is offset by  $0.02 \pm 0.02$  arcsec with respect to the host galaxy center.

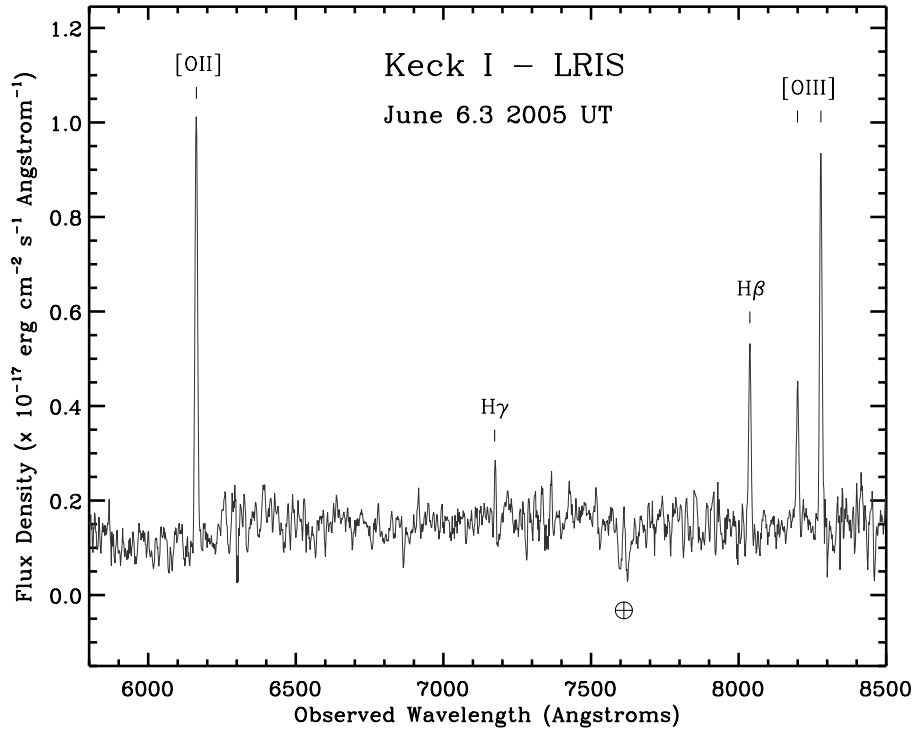


Figure 2.5: The spectrum was obtained with the Low Resolution Imaging Spectrograph on Keck I on 2005 June 6.3 UT. Several bright emission lines are detected, indicating that the host is a star-forming galaxy at redshift  $z = 0.6528 \pm 0.0002$ . As discussed in §2.5 we find that the host is actively forming stars with a rate of  $\gtrsim 2 M_{\odot} \text{ yr}^{-1}$  and an inferred metallicity of  $Z \sim 0.2 - 0.8 Z_{\odot}$ .

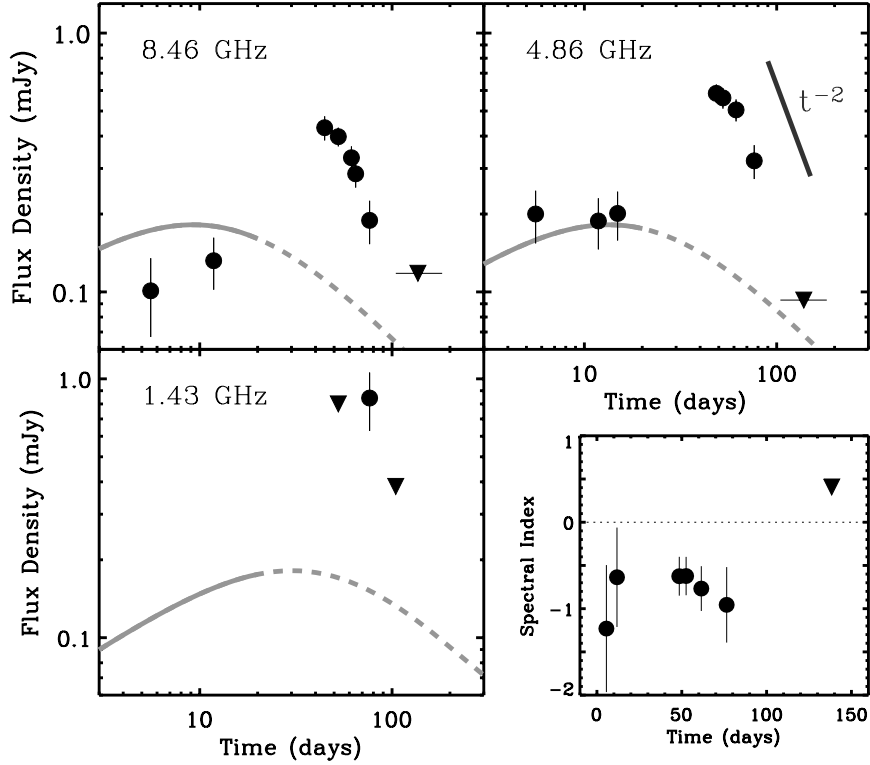


Figure 2.6: Radio observations of XRF 050416a from the Very Large Array as listed in Table 4.1. We have summed the late-time limits in each frequency for clarity. The radio evolution is characterized by an unusual flare at  $t \sim 40$  days which rapidly fades below our detection limits. This radio flare occurs roughly on the same timescale as the observed X-ray flattening. (Figure 2.7). We attribute both the radio flare and the X-ray flattening to an episode of late-time energy injection (refreshing shell or off-axis ejecta) or a large circumburst density jump. Our early afterglow model fit is shown (solid grey lines) and extrapolated to the epoch of the radio flare (dashed grey lines). The spectral index between 8.46 and 4.86 GHz is optically thin throughout our radio monitoring, including the late-time flare (lower right panel).

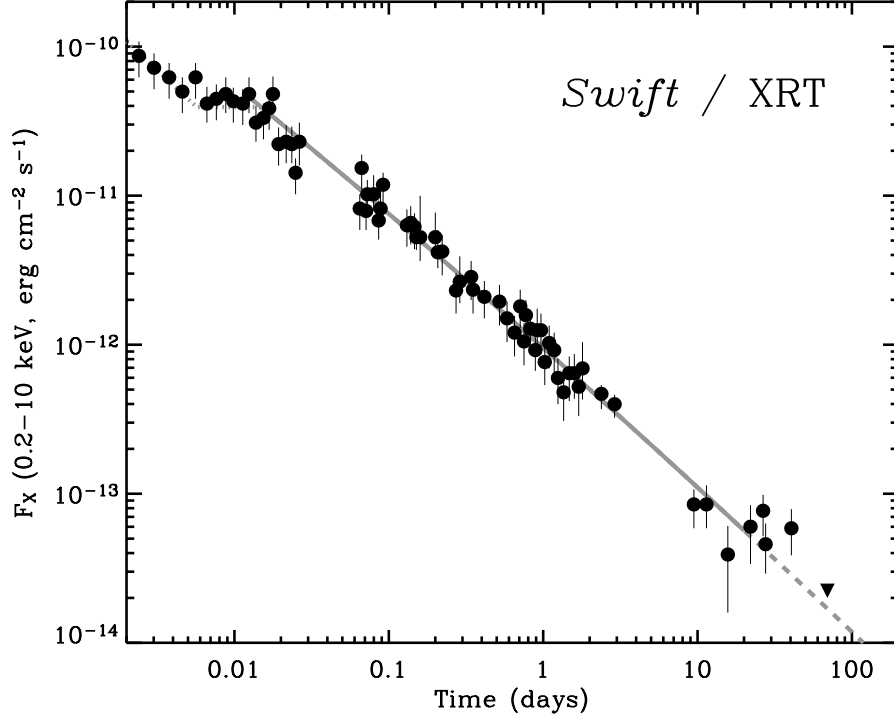


Figure 2.7: X-ray observations of XRF 050416a from the *Swift*/XRT as reported by Mangano et al. (239). The X-ray light-curve is characterized by four phases: (1) a initial step decay, (2) a flattening between  $t \approx 0.005 - 0.01$  days, (3) a subsequent decay, and (4) a second flattening between  $t \approx 20 - 40$  days. The final measurement at 70 days implies a rapid steepening following the second flattening. We attribute the late-time flattening to energy injection (refreshing shell or off-axis ejecta) or a large circumburst density jump. Overplotted is our afterglow model fit between 0.014 and 20 days (solid grey line) and extrapolated to late time (dashed grey line). We do not attempt to fit the data prior to 0.01 days (dotted line) due to insufficient broadband data.

## Part III

# An Optical View of the GRB-SN Connection

An Optical View of the GRB-SN Connection

## Chapter 1

# An HST Search for Supernovae Accompanying X-ray Flashes<sup>†</sup>

A. M. SODERBERG<sup>a</sup>, S. R. KULKARNI<sup>a</sup>, D. B. FOX<sup>a</sup>, E. BERGER<sup>b</sup>, P. A. PRICE<sup>c</sup>, S. B. CENKO<sup>d</sup>, D. A. HOWELL<sup>e</sup>, A. GAL-YAM<sup>a</sup>, D. C. LEONARD<sup>a</sup>,  
D. A. FRAIL<sup>f</sup>, D.-S. MOON<sup>d</sup>, R. A. CHEVALIER<sup>g</sup>, M. HAMUY<sup>b</sup>, K. C. HURLEY<sup>h</sup>, D. KELSON<sup>b</sup>, K. KOVIK<sup>b</sup>, W. KRZEMINSKI<sup>b</sup>, P. KUMAR<sup>i</sup>, A. MACFADYEN<sup>a</sup>, P. J. MCCARTHY<sup>b</sup>, H. S. PARK<sup>j</sup>, B. A. PETERSON<sup>k</sup>, M. M. PHILLIPS<sup>b</sup>, M. RAUCH<sup>b</sup>, M. ROTH<sup>b</sup>, B. P. SCHMIDT<sup>k</sup>, S. SHECTMAN<sup>b</sup>

<sup>a</sup>Division of Physics, Mathematics and Astronomy, 105-24, California Institute of Technology,  
Pasadena, CA 91125, USA

<sup>b</sup>Observatories of the Carnegie Institution of Washington, 813 Santa Barbara St., Pasadena, CA  
91101, USA

<sup>c</sup>University of Hawaii, Institute of Astronomy, 2680 Woodlawn Drive, Honolulu, HI 96822-1897,  
USA

<sup>d</sup>Space Radiation Laboratory 220-47, California Institute of Technology, Pasadena, CA 91125,  
USA

<sup>e</sup>Department of Astronomy and Astrophysics, University of Toronto, 60 St. George Street,  
Toronto, ON M5S 3H8, Canada

---

<sup>†</sup>A version of this chapter was published in *The Astrophysical Journal*, vol. 627, 877–887, (2005). Reproduced by permission of the AAS.

<sup>f</sup>National Radio Astronomy Observatory, Socorro, NM 87801, USA

<sup>g</sup>Department of Astronomy, University of Virginia, P.O. Box 3818, Charlottesville, VA  
22903-0818, USA

<sup>h</sup>University of California, Berkeley, Space Sciences Laboratory, Berkeley, CA 94720-7450, USA

<sup>i</sup>Astronomy Department, University of Texas, Austin, TX 78731, USA

<sup>j</sup>Lawrence Livermore National Laboratory, 7000 East Avenue, Livermore, CA 94550, USA

<sup>k</sup>Research School of Astronomy and Astrophysics, The Australian National University, Weston  
Creek, ACT 2611, Australia

## Abstract

We present the results from an *Hubble Space Telescope/ACS* search for supernovae associated with X-ray flashes 020903, 040701, 040812, and 040916. We find strong evidence that XRF 020903 ( $z = 0.25$ ) was associated with a SN 1998bw-like supernova and confirm this using optical spectroscopy at  $t \sim 25$  days. We find no evidence, however, for SN 1998bw-like supernovae associated with the other three events. In the case of XRF 040701 ( $z = 0.21$ ), we rule out even a faint supernova similar to SN 2002ap, using template light-curves for several local Type Ic supernovae. For the two cases in which the redshift is not known, XRFs 040812 and 040916, we derive robust redshift limits assuming they were accompanied by supernovae similar to SN 1998bw and compare these limits with photometric redshift constraints provided by their host galaxies. We supplement this analysis with results for three additional events (XRFs 011030, 020427, and 030723) and discuss the observed diversity of supernovae associated with X-ray flashes and gamma-ray bursts. We conclude that XRF-SNe exist, but can be significantly fainter than SN 1998bw, possibly consistent with the observed spread in local Type Ibc supernovae.

## 1.1 Introduction

Observational evidence for a connection between gamma-ray bursts (GRBs) and supernovae (SNe) was first established with the discovery of the highly luminous type Ic SN 1998bw in spatial and temporal coincidence with GRB 980425 (290, 151). In the seven years since this extraordinary event, several possible GRB-SN associations have been reported based on red “bumps” observed in optical afterglow light-curves (e.g., Bloom et al. 42). Moreover, in two cases (GRBs 030329 and 031203) there is unambiguous spectroscopic evidence of high velocity SN features (187, 377, 244, 237). These observations provide conclusive evidence that at least some gamma-ray bursts are produced in the explosions of massive stars.

In recent years, a new class of high-energy transients has been identified, characterized by an emission spectrum peaking in the X-ray band, an order of magnitude softer than the peak energies observed for GRBs (181). These so-called X-ray flashes (XRFs) are thought to be related to GRBs since the two classes share several observational properties, including prompt emission profiles (Sakamoto et al. 328, and references therein), broadband afterglows (56, 361, 144) and star-forming host galaxies at cosmological distances (43, 221, 222).

Several hypotheses on the physical connection between XRFs and GRBs have been proposed. One popular model posits that XRFs are simply GRBs viewed away from the jet collimation axis (439, 450, 170). In this scenario, the observed prompt emission is dominated by the mildly relativistic material in the “wings” of the jet, rather than the highly relativistic ( $\Gamma \gtrsim 100$ ) ejecta beamed away from the line-of-sight. Another popular model suggests that XRFs are produced in a “dirty fireball,” where the ejecta carry a more substantial baryonic load (and hence less relativistic material) than typical GRBs (450). In both scenarios XRFs are expected to be associated with SNe, whose properties and detectability should not be affected by the viewing angle or baryonic load.

The discovery of a SN in association with an XRF would therefore conclusively

associate XRFs with the death of massive stars and hence GRBs. Motivated thus, we undertook a systematic search for SNe associated with XRFs using the *Hubble Space Telescope* (*HST*). As part of our XRF-SN analysis, we synthesized supernova light-curves at various redshifts utilizing as templates the well-sampled optical light-curves of several local SNe (§2.2). Comparison of the synthesized SNe with our *HST* observations enabled us to study the diversity of XRF associated SNe. Details on the individual *HST* targets and observations follow in §2.3. By including results from other XRF-SN searches, we compile an extended sample of seven events (XRFs 011030, 020427, 020903, 030723, 040701, 040812, and 040916), and present a global summary of XRF-SN detection limits in §2.4. A discussion on the observed spread in the peak optical luminosities of GRB- and XRF-associated SNe follows as §1.5.

## 1.2 Supernova Light-curve Synthesis

In modeling the XRF-associated SNe, we adopted optical data for the local SNe 1994I, 1998bw, and 2002ap as templates. These three SNe were selected based on their well-sampled optical light-curves which represent an overall spread in the observed properties of Type Ibc supernovae. To produce synthesized light-curves for each of these template SNe, we compiled optical *UBVRI* observations from the literature and smoothed the extinction-corrected (foreground plus host galaxy) light-curves. We then redshifted the light-curves by interpolating over the photometric spectrum and stretching the arrival time of the photons by a factor of  $(1 + z)$ . Since observed spectra of local ( $d \lesssim 100$  Mpc) Type Ibc SNe show a steep drop-off in flux blue-ward of  $\sim 4000$  Å due to heavy line-blanketing and since good-quality UV data are currently not available below 3000 Å we do not attempt to extrapolate the rest-frame spectra blue-ward of the rest-frame *U*-band observations. This limits the synthesized light-curves to  $z \leq 0.80$  and  $z \leq 1.20$  for the observed *R*- and *I*-bands, respectively. Below we discuss the compiled optical datasets for each of the template SNe.

### 1.2.1 SN 1998bw

The well-sampled *UBVRI* light-curves for SN 1998bw were taken from Galama et al. (151) and McKenzie and Schaefer (254) and corrected for galactic extinction ( $A_V = 0.19$ ; Schlegel et al. 344). We assume negligible host galaxy extinction, consistent with the spectroscopic analysis Patat et al. (282). The broadband optical dataset spans a timescale from  $t \approx 0.7$  to 417 days. Here, the explosion time is set by the *Beppo-SAX* detection of GRB 980425 on 1998 April 25.91 UT (290). In calculating optical luminosities for SN 1998bw, we assume a distance,  $d_L \approx 36.1$  Mpc ( $H_0 = 71$  km/s/Mpc,  $\Omega_M = 0.27$ ,  $\Omega_\Lambda = 0.73$ ), based on the observed redshift to the host galaxy, ESO 184-G82 (150).

### 1.2.2 SN 1994I

Richmond et al. (317) provide a large compilation of multi-color light-curves for SN 1994I. We adopt a large host galaxy extinction of  $A_V = 1.4$  and negligible Galactic extinction as derived through the spectroscopic analysis (317). Using an explosion date of 1994 March 30 UT from radio light-curve modeling (380), the *BVRI* data span from  $t \approx 1.4$  to 130 days, while the *U*-band data extend only as far as  $t \approx 47.4$  days. In an effort to extend the *U*-band light-curve, we scale the late-time linear decay of the *B*-band light-curve to match the last epoch of *U*-band observations and assume the  $U - B$  color is constant thereafter. We note that this scaling introduces a source of uncertainty in our late-time [ $t \gtrsim 47(1+z)$ ] high- $z$  synthesized light-curves of SN 1994I. In calculating optical luminosities, we adopt a distance of  $d_L \approx 8.5$  Mpc for host galaxy, M51, as given by Richmond et al. (317).

### 1.2.3 SN 2002ap

*UBVRI* light-curves were taken from Foley et al. (122) and scaled to an explosion date of 2002 January 28.9 UT (249). We adopt the spectroscopic derived total extinction (foreground plus host galaxy) of  $A_V = 0.26$  (122). Data span  $t \approx 1.3$  to

317.3 days after the explosion in *BVRI* filters while the *U*-band data extend only to  $t \sim 35.2$  days. In a manner similar to that for SN 1994I, we extend the *U*-band light-curve by scaling the late-time *B*-band data and note that this introduces uncertainty in the synthesized light-curves at high- $z$ . We assume the distance to the host galaxy, M74, is  $d_L \approx 7.3$  Mpc (347, 372).

We emphasize the striking differences between the three SN light-curves when the extinction-corrected rest-frame *V*-band light-curves are compared. With regard to the luminosity at peak time, SN 1998bw is a factor of  $\sim 2.2$  more luminous than SN 1994I and  $\sim 6$  times more luminous than SN 2002ap. Moreover, the time of *V*-band peak vary by a factor of two: while SN 1998bw peaks at  $t \sim 16$  days, SN 1994I and SN 2002ap both peak at just  $t \sim 9$  days. Such early peak times present a challenge for GRB-SN searches, since the optical afterglow typically dominates on these timescales.

### 1.3 Hubble Space Telescope XRF-SN Search

Since the activation of our Cycle-13 *HST* program to study the supernovae associated with X-ray flashes and gamma-ray bursts (GO-10135; PI: Kulkarni), three XRFs have been discovered and localized by their afterglow emission: XRFs 040701, 040812, and 040916. In an effort to study the SNe possibly associated with these XRFs, we observed each of these objects with *HST* at late-time, when an associated supernova is most likely to dominate the optical emission. To supplement our sample of XRF observations, we investigated archival *HST* images of XRF 020903 (GO-9405; PI: Fruchter). We describe our data analysis techniques below.

Using the *Wide-Field Camera (WFC)* of the *Advanced Camera for Surveys (ACS)* on-board *HST*, we imaged the fields of XRFs 040701, 040812 and 040916. For each target we undertook observations at two epochs,  $t \sim 30$  and  $\sim 60$  days, in order to search for optical emission associated with an underlying supernova. Each epoch consisted of two orbits during which we imaged the field in two filters,

F625W and F775W, corresponding to SDSS  $r'$ - and  $i'$ - bands, respectively.

We retrieved archival images of XRF 020903 from the *HST* archive<sup>1</sup>. Similar to the other bursts in our sample, the XRF 020903 data were obtained with *HST/ACS* using *WFC*. We analyze the images from two epochs at  $t \sim 91$  and  $\sim 300$  days to search for the signature of an associated supernova. These data were taken in the broad  $V$ -band filter, F606W.

The *HST* data were processed using the `multidrizzle` routine within the `stsdas` package of IRAF (141). Images were drizzled using `pixfrac=0.8` and `pixscale=1.0` resulting in a final pixel scale of 0.05 arcsec/pixel. Drizzled images were then registered to the first epoch using the `xregister` package within *IRAF*.

To search for source variability, we used the *ISIS* subtraction routine by Alard (1) which accounts for temporal variations in the stellar PSF. Residual images (Epoch 1 – Epoch 2) were examined for positive sources positionally coincident with the afterglow error circle. To test our efficiency at recovering transient sources, false stars with a range of magnitudes were inserted into the first epoch images using *IRAF* task `mkobject`. An examination of the false stellar residuals provided an estimate of the magnitude limit ( $3\sigma$ ) to which we could reliably recover transients.

Photometry was performed on the residual sources within a 0.5 arcsec aperture. We converted the photometric measurements to infinite aperture and calculated the corresponding AB magnitudes within the native *HST* filters using the aperture corrections and zero-points provided by Sirianni et al. (349). For comparison with ground-based data, we also converted the photometric measurements to Johnson  $R$ - and  $I$ -band (Vega) magnitudes using the transformation coefficients derived by Sirianni et al. (349) and assuming a flat  $F_\nu$  source spectrum.

In the following sections we summarize the afterglow properties for each of the targets and the photometry derived from our *HST* SN search. A log of the *HST* observations for the four XRFs follows in Table 2.1.

---

<sup>1</sup><http://archive.stsci.edu/hst/search.php>

### 1.3.1 XRF 020903

#### Prompt Emission and Afterglow Properties

XRF 020903 was detected by the Wide-Field X-ray Monitor (*WXM*) on-board the High Energy Transient Explorer (*HETE-2*) satellite on 2002 September 3.421 UT. With a spectral energy distribution peaking below 5 keV, XRF 020903 is the softest burst detected during the lifetime of the instrument (331). Despite the large  $4 \times 31$  arcmin localization region, an optical afterglow was discovered (361) at  $\alpha = 22^{\text{h}}48^{\text{m}}42^{\text{s}}.34$ ,  $\delta = -20^{\circ}46'09''.3$  (J2000). At  $t \approx 0.9$  days, the afterglow had  $R \approx 19.5$  mag and continued to fade as  $F_{\text{opt}} \propto t^{-1.1}$  until  $t \sim 30$  days when the decay flattened to a plateau. Optical spectroscopy showed the transient source to be associated with a galaxy complex at  $z = 0.251$  (371).

#### *HST* Observations

XRF 020903 was observed using *HST/ACS* on 2002 December 3.79 and 2003 June 30.65 UT, corresponding to  $t \sim 91$  and 300 days after the burst. Imaging was carried out in the broad F606W filter for total exposure times of 1840 sec (Epoch 1) and 1920 sec (Epoch 2). Relative astrometry was performed using an early-time ( $t \sim 0.9$  day) image from the Palomar 200-inch telescope (361). Using 42 unsaturated, unconfused stars in common between the two images, we registered the *HST* data with a systematic uncertainty of 0.12 arcsec ( $2\sigma$ ).

The *HST* images reveal that the afterglow localization circle coincides with the southwest knot of the host galaxy complex (Figure 1.1). Through image subtraction, we find a positive residual coincident with the optical afterglow position at  $\alpha = 22^{\text{h}}48^{\text{m}}42.293^{\text{s}}$ ,  $\delta = -20^{\circ}46'08''.47$  (J2000). Photometry of the residual source gives F606W  $\approx 24.53 \pm 0.03$  mag ( $R \approx 24.32 \pm 0.03$  mag). Correcting for galactic extinction ( $A_R = 0.09$ ; Schlegel et al. 344), the true magnitude of the source is  $R \approx 24.23 \pm 0.03$  mag. To estimate our photometric uncertainty, we placed random apertures near other galaxy residuals and calculated the standard deviation of the resulting values.

Figure 1.2 shows the extinction-corrected *HST* photometry along with ground-based *R*-band data for the optical afterglow associated with XRF 020903. Ground-based data have been compiled from the GCNs (91, 163) as well as from Table 1 of Soderberg et al. (361). We have numerically subtracted the host galaxy contribution from the ground-based data, assuming an extinction-corrected host galaxy brightness of  $R \approx 20.90$  mag based on late-time observations (163, 221). From the compiled *R*-band afterglow light-curve, it is evident that the temporal decay flattens significantly around  $t \sim 30$  days and subsequently steepens toward the *HST* measurement at  $t \sim 91$  days. This flattening (or plateau phase) occurs on the same timescale that a SN 1998bw-like supernova at  $z = 0.25$  would reach maximum light (see also Bersier et al. 30).

### Associated Supernova

Over-plotted in Figure 1.2 are the synthesized light-curves of SNe 1998bw, 1994I and 2002ap at a redshift of  $z = 0.25$ . It is clear that an associated SN 1998bw-like supernova would be  $\sim 1$  magnitude brighter than the *HST* observation at  $t \sim 91$  days, while SN 1994I and SN 2002ap-like light-curves are each fainter by 1.4 magnitudes. By taking the weighted average of the ground-based data between  $t \sim 20 - 40$  days, we predict that the supernova was  $0.6 \pm 0.5$  magnitudes fainter than SN 1998bw at maximum light. We note that this uncertainty is dominated by “aperture effects” (see Price et al. 300) which cause variable contribution from the host galaxy complex in different epochs.

We obtained optical spectroscopy of the transient source using the Magellan 6.5-meter telescope equipped with the Low Dispersion Survey Spectrograph (LDSS2) on 2002 September 28.06 UT ( $t \approx 24.6$  days), during the observed plateau phase. The data were reduced and calibrated using standard techniques. The spectrum is characterized by a faint continuum dominated by narrow, bright emission lines typical of star-forming galaxies (Figure 1.3; Soderberg et al. 371, Chornock and Filippenko 76).

To search for high velocity SN features within the observed spectrum, we uti-

lized the supernova classification techniques of Howell et al. (190), designed for identification of SNe in the presence of host galaxy contamination. Host galaxy light must be subtracted from the observed spectrum to reveal the SN flux. We fit a range of starburst host galaxy templates from Kinney et al. (206), consistent with the continuum shape and narrow lines in the observed spectrum. After sigma-clipping the narrow emission lines and subtracting the best-fit galaxy template (model SB1), the residual spectrum shows broad features resembling those of SN 1998bw near maximum light. Figure 1.3 presents a comparison of our galaxy subtracted spectrum with SN 1998bw at  $t \approx 20.5$  days (rest-frame; Patat et al. 282), redshifted to  $z = 0.25$  and dimmed by  $\sim 0.3$  magnitudes. The resemblance is striking.

Taken together, the spectroscopic and photometric data strongly suggest that XRF 020903 was associated with a supernova that is  $\sim 0.6 \pm 0.5$  magnitudes fainter than SN 1998bw at maximum light. Moreover, the SN light-curve fades faster than SN 1998bw, falling  $\sim 1$  mag below the synthesized SN 1998bw light-curve at late-time. A dimmer, faster fading supernova was also interpreted for SN 2003dh/GRB 030329 (Lipkin et al. 229, Deng et al. 100; c.f. Matheson et al. 244) and is consistent with the luminosity-stretch relation for GRB-SNe (47, 375).

### 1.3.2 XRF 040701

#### Prompt Emission and Afterglow Properties

XRF 040701 was localized on 2004 July 1.542 UT by the *HETE-2* WXM to an 8 arcmin radius error circle centered at  $\alpha = 20^{\text{h}}47^{\text{m}}46.3^{\text{s}}$ ,  $\delta = -40^{\circ}14'13''$  (J2000; Barraud et al. 11).

We observed the error circle with the *Chandra* X-ray Observatory (CXO) using the AXAF CCD Imaging Spectrometer (ACIS) for 22.3 ksec beginning at 2004 July 9.32 UT ( $t \approx 7.9$  days) and 20.4 ksec on 2004 July 18.05 ( $t \approx 16.6$  days). Comparison of the two epochs revealed the most variable source to be at position  $\alpha = 20^{\text{h}}48^{\text{m}}16^{\text{s}}.097$ ,  $\delta = -40^{\circ}11'08''.83$  (J2000), with an uncertainty of 0.5 arc-

sec in each coordinate ( $2\sigma$ ; Fox 128) which we interpret as the X-ray afterglow. Assuming galactic absorption, the X-ray flux of the source was  $7.75 \times 10^{-14}$  and  $4.06 \times 10^{-14}$  erg cm $^{-2}$  s $^{-1}$  (2 – 10 keV), in the first and second epochs, respectively. This implies a temporal decay,  $F_X \sim t^\alpha$  with  $\alpha = -1.15$ , between the two observations, comparable to the typical observed values of GRB X-ray afterglows,  $\alpha \sim -1.1$  (Berger et al. 23, and references therein).

Inspection of Digital Sky Survey (DSS) images revealed that the X-ray afterglow is associated with a resolved galaxy complex whose redshift we determined to be  $z = 0.2146$  (204). At this relatively low redshift, the X-ray afterglow is sensitive to absorption within the host galaxy. We fit an absorbed power-law model to the afterglow spectrum where the column density,  $N_H$ , was a combination of foreground and host galaxy extinction. We find that the column density within the host galaxy must be  $N_H \lesssim 5 \times 10^{21}$  cm $^{-2}$  (90% confidence) in order to reproduce the observed low energy ( $< 1$  keV) X-ray photons. Utilizing the  $N_H$  to  $A_V$  conversion of Predehl and Schmitt (299), this limit corresponds to a rest-frame host galaxy extinction of  $A_{V,\text{host}} \lesssim 2.8$  mag.

Despite deep searches, no optical afterglow candidate was discovered through ground-based monitoring of the *Chandra* error circle (99, 21, 291). This non-detection could be the result of the large host-galaxy extinction, consistent with the observed X-ray afterglow absorption.

### ***HST* observations**

*HST/ACS* imaging was carried out on 2004 August 9.66 and 30.52 UT ( $t \approx 39.1$  and 60.0 days after the burst). Each epoch had a total exposure time of 1840 and 1920 sec in the F625W and F775W filters, respectively. We astrometrically tied the *HST* and *Chandra* images by first registering the X-ray source list to our *I*-band images from the Las Campanas Observatory (LCO) 40-inch telescope (21) using three sources in common. We then tied the LCO images to those from *HST* resulting in a final positional uncertainty of 1.06 arcsec ( $2\sigma$ ).

Our *HST* observations reveal that the afterglow error circle coincides with

the northeast galaxy of the host complex. Inspection of the images reveals that there are no transient sources within this localization region. Figure 1.4 shows the images from both epochs in addition to the residual images produced from the subtraction routine. We found that the false stellar residuals recovered at our detection threshold correspond to limits of  $F625W > 27.8$  and  $F775W > 26.8$  mag ( $R > 27.6$  and  $I > 26.4$  mag). Correcting for Galactic extinction ( $A_R = 0.13$ ; Schlegel et al. 344), the actual limits are  $R > 27.5$  and  $I > 26.3$  mag. We note that the slightly elevated flux of the bipolar galaxy residual are consistent with these limits.

Figure 1.5 shows the *HST* limits along with early-time data compiled from the GCNs (99, 291), corrected for galactic extinction. To estimate the flux of the optical afterglow, we extrapolated the observed *Chandra* data to the *R*- and *I*-bands. Following Sari et al. (339) for the case of a constant density medium, the observed X-ray afterglow decay ( $F_X \propto t^{-1.15}$ ) implies that the electron energy index ( $dN/dE \propto E^{-p}$ ) is  $p \approx 2.5$  in the case where the synchrotron cooling frequency,  $\nu_c$ , is above the X-ray band, and  $p \approx 2.2$ , if it is below. We therefore extrapolate the observed X-ray flux by adopting a spectral index ( $F_\nu \propto \nu^\beta$ ) with  $\beta = -(p - 1)/2 \approx -0.75$  in the case of  $\nu_{\text{opt}} < \nu_X < \nu_c$  and  $\beta = -p/2 \approx -1.1$  for  $\nu_c < \nu_{\text{opt}} < \nu_X$ . These two scenarios bracket the whole range of optical flux values implied by the possible location of the  $\nu_c$  at the time of the *CXO* observations.

By extrapolating the predicted optical decay to the first *HST* epoch, we conclude that the afterglow should have been  $\gtrsim 3.0$  magnitudes brighter than our *HST* detection limit. Even in the most extreme scenario, a jet break occurred coincident with the second *Chandra* epoch, forcing the temporal decay to steepen to  $F_\nu \propto t^{-p}$  (338). Still, the afterglow would have been  $\gtrsim 1.7$  magnitudes brighter than the *HST* limit. Under the assumption that the observed X-ray flux was dominated by synchrotron emission, these limits imply that there is significant extinction from the host galaxy. However, in a scenario where the X-ray emission is dominated by other processes (e.g. ,inverse Compton), this extrapolation over-predicts the brightness of the optical afterglow, thereby reducing the implied host

galaxy extinction.

### Supernova Limits

Over-plotted in Figure 1.5 are synthesized light-curves for SNe 1998bw, 1994I, and 2002ap at  $z = 0.21$ . From the figure, it is clear that a SN 1998bw-like supernova would have been  $\sim 6$  magnitudes brighter than our *HST* limits. A faint supernova similar to SN 2002ap would still be  $\sim 3.4$  magnitudes above our detection threshold. Our constraints on the column density imply that host galaxy extinction cannot account for this difference; even in an extreme scenario, given by  $A_{V,\text{host}} \approx 2.8$  mag, our limits are still  $\sim 3.2$  magnitudes fainter than SN 1998bw. We conclude that an XRF 040701-associated supernova must be  $\sim 3$  mag fainter than SN 1998bw, making it significantly fainter than all GRB-SNe known to date.

### 1.3.3 XRF 040812

#### Prompt Emission and Afterglow Properties

XRF 040812 was discovered on 2004 August 12.251 UT by the Imager on Board the Integral Satellite (IBIS). Preliminary analysis indicated a spectrum that was X-ray rich. The event was localized to a 2-arcmin radius circle centered at  $\alpha = 16^{\text{h}}26^{\text{m}}05^{\text{s}}$ ,  $\delta = -44^{\circ}42'32''$  (J2000; Gotz et al. 165).

Patel et al. (284) observed the field of XRF 040812 with *Chandra*/ACIS beginning on 2004 August 17.30 UT ( $t \approx 5$  days) and on 2004 August 22.41 UT ( $t \approx 10$  days) for 10 ksec each. Comparison of the two epochs revealed a variable source at position  $\alpha = 16^{\text{h}}26^{\text{m}}2^{\text{s}}.25$ ,  $\delta = -44^{\circ}43'49''.4$  (J2000) which faded as  $F_X \propto t^{-1.4}$  between the observations (283). The unabsorbed flux in the first and second epochs was  $2.53 \times 10^{-13}$  and  $9.30 \times 10^{-14}$  erg cm $^{-2}$  s $^{-1}$  (0.5–10 keV), respectively (60, 61).

Due to high galactic extinction in the direction of the burst ( $A_R = 3.6$  mag; Schlegel et al. 344) and the presence of an extremely bright star  $\sim 20$  arcsec from the *CXO* position, optical/IR campaigns could neither observe the optical

afterglow nor obtain spectroscopy of the host galaxy (15, 19, 88, 96). As a result, a spectroscopic redshift is not available for XRF 040812.

### *HST* Observations

*HST/ACS* imaging for XRF 040812 was carried out on 2004 September 13.4 and October 4.8 UT ( $t \approx 32.1$  and 53.6 days after the burst). Each epoch had a total exposure time of 2000 and 2120 sec in the F625W and F775W filters, respectively. Observations were taken with orientation angles chosen to minimize contamination from diffraction spikes and saturated columns resulting from the bright foreground star. Using the *Chandra* source list provided by Patel et al. (284), we identified five unconfused, unsaturated sources in common between the *Chandra* observations and our *I*-band Las Campanas Observatory (LCO) 40-inch observations (19) and used these to tie the X-ray afterglow position to ground-based images. The LCO and *HST* images were then registered, resulting in a final positional uncertainty of 0.91 arcsec ( $2\sigma$ ).

Through examination of the *HST* images, we find an extended source  $\sim 0.33$  arcsec ( $< 1\sigma$ ) from the nominal *CXO* position and interpret it as the host galaxy of XRF 040812. We find the galaxy to be relatively bright, F625W  $\approx 24.50 \pm 0.06$  mag, corresponding to  $R \approx 20.68 \pm 0.05$  mag after correcting for the large foreground extinction. Comparison with the set of GRB host galaxy magnitudes compiled by Berger et al. (25) suggests that XRF 040812 is at a relatively low redshift,  $z \lesssim 0.5$ . At this redshift, the host galaxy extinction is constrained to be  $A_{V,\text{host}} \lesssim 6.1$ , (90% confidence) based on our independent analysis of the lowest energy X-ray afterglow emission.

Image subtraction reveals no transient sources that could be attributed to an optical afterglow or associated supernova within the *CXO* localization circle (Figure 1.6). We find  $3\sigma$  detection limits on the residual image of F625W  $> 27.0$  and F775W  $> 26.4$  mag ( $R > 26.8$  and  $I > 25.9$  mag). Due to the large Galactic extinction, however, the true limits are significantly shallower,  $R > 23.2$  and  $I > 23.3$  mag.

Figure 1.7 displays the Galactic extinction-corrected *HST* limits along with the predicted optical afterglow extrapolated from the X-ray flux in a manner similar to that for XRF 040701 (§1.3.2). Given the observed X-ray decay, we extrapolate with  $\beta \approx -0.96$  for  $p \approx 2.92$  and  $\beta \approx -1.29$  for  $p \approx 2.59$ . As evident from the figure, the *HST* *I*-band limit is 1.9 magnitudes fainter than the predicted optical afterglow, assuming the flux continued evolving as  $F_{\text{opt}} \propto t^{-1.4}$  to the *HST* epoch. If, instead, a jet break occurred at the second *Chandra* epoch, the predicted optical afterglow could be consistent with the *HST* non-detection.

### Supernova Limits

Since the redshift of XRF 040812 is not known, we over-plot synthesized light-curves for SNe 1998bw, 1994I, and 2002ap at the appropriate redshift such that the SN curves match the residual image *HST* detection limit. Supernovae placed above these redshift limits would not be detected. Due to the heavy foreground extinction toward XRF 040812, the *I*-band limits provide deeper constraints on an associated supernova. As shown in Figure 1.7, a SN 1998bw-like supernova is ruled out for  $z \lesssim 0.90$  while SN 1994I-, and SN 2002ap-like SNe are ruled out for  $z \lesssim 0.34$  and  $z \lesssim 0.35$ , respectively. To be consistent with the estimated low- $z$  inferred from the host galaxy brightness, an associated SN must be significantly fainter than SN 1998bw or suppressed due to host galaxy extinction.

#### 1.3.4 XRF 040916

##### Prompt Emission and Afterglow Properties

On 2004 September 16.002 UT the *HETE-2* satellite discovered XRF 040916. Preliminary spectral analysis revealed a dearth of photons at  $\gtrsim 10$  keV, suggestive that the event was an X-ray flash (442). The initial localization error region was 18 arcmin in radius centered at  $\alpha = 23^{\text{h}}01^{\text{m}}44^{\text{s}}$ ,  $\delta = -05^{\circ}37'43''$  (J2000). A refined error box with half the original size (545 square arcmin) was released later (443). Using SuprimeCam mounted on the Subaru 8.2m telescope, Kosugi et al. (211)

discovered a faint optical afterglow at  $\alpha = 23^{\text{h}}00^{\text{m}}55^{\text{s}}.1$ ,  $\delta = -05^{\circ}38'43''$  (J2000) with a magnitude of  $Rc \approx 22.3 \pm 0.2$  at  $t \approx 0.23$  days. The afterglow subsequently decayed as  $F_{\text{opt}} \propto t^{-1.0}$ . In comparison to GRB optical afterglows compiled by Fox et al. (130) and Berger et al. (20), XRF 040916 is the faintest optical afterglow ever detected on this timescale. We note that no spectroscopic redshift has been reported for this event.

### *HST* Observations

XRF 040916 was imaged with *HST/ACS* on 2004 October 18.38 and November 30.30 UT ( $t \approx 32.4$  and  $75.3$  days after the burst) for a total exposure time of 1930 (2058) sec in Epoch 1 and 1928 (2056) sec in Epoch 2 in the F625W (F775W) filter. For astrometry, we used early-time ( $t \sim 0.16$  day) *R*- and *I*-band data from the Palomar Robotic 60-inch telescope (*P60*; Cenko et al., in prep) in which the optical afterglow is clearly detected. Twelve stars in common between the Palomar and *HST* images provided an astrometric uncertainty of 0.29 arcsec ( $2\sigma$ ).

Within the afterglow position error circle, we find a faint source near the detection limit of our first epoch F625W and F775W images at  $\alpha = 23^{\text{h}}00^{\text{m}}55.141^{\text{s}}$ ,  $\delta = -05^{\circ}38'42''.70$  (J2000). Figure 1.8 shows the source is too faint to be recovered in the residual images, implying it is just below our  $3\sigma$  detection threshold of F625  $> 27.9$  mag and F775W  $> 27.2$  mag ( $R > 27.7$  and  $I > 26.7$  mag). Correcting for galactic extinction ( $A_R = 0.15$ ; Schlegel et al. 344), the true limits are  $R > 27.5$  and  $I > 26.6$  mag.

In Figure 1.9 we show the *HST* limits along with early-time data from *P60* and from the GCNs (211, 208, 183), all corrected for Galactic extinction. The early data are well fit with a  $F_{\text{opt}} \propto t^{-1.0}$  decay. We note that the early detection by Henden (183) is inconsistent with our *I*-band data. The *HST* limits are consistent with the extrapolated optical afterglow, assuming the flux decayed without steepening until the epoch of *HST* observations.

## Supernova Limits

Since the redshift of XRF 040916 is not known, we over-plot synthesized light-curves for SNe 1994I and 2002ap each at the appropriate redshift such that the SN curves match the residual image *HST* detection limit. Supernovae with light-curves similar to SNe 1994I and 2002ap would not be detected above  $z \approx 1.02$  and  $z \approx 0.82$ , respectively. Synthesized light-curves for SN 1998bw at  $z = 0.8$  and  $z = 1.2$  represent the limits to which we can confidently extrapolate the rest-frame SN spectrum. These light-curves are  $\sim 3$  and  $\sim 1.5$  magnitudes brighter than the observed *HST* limits in the *R*- and *I*- bands, and therefore suggest that either XRF 040916 is at higher redshift (e.g.  $z > 1.2$ ) or it is associated with a lower luminosity SN.

We note that XRF 040916 is the only event within our *HST* survey for which we do not detect the host galaxy. Given our *HST* detection limit and the small foreground extinction, this implies the host galaxy is fainter than  $R \approx 27.5$  mag. We compare this limit with faint GRB host galaxies; *all* of the GRB hosts with  $R > 26$  mag are at redshift  $z > 1.4$  (25). Assuming the GRB host galaxy luminosity function also applies to XRFs, this implies that XRF 040916 is at a similarly high redshift, far beyond the  $z \sim 1.2$  redshift limit out to which we can detect an associated SN.

## 1.4 A Summary of XRF-SN Searches

We now present a global summary of all SN searches in XRFs to date, including *HST* campaigns for XRFs 011030, 020427, 020903, 040701, 040812, 040916 and a deep ground-based effort for XRF 030723. In compiling these results, we also discuss the available constraints on host galaxy extinction, which could suppress any emission from an associated SN.

The only XRF for which we find evidence suggestive of an accompanying supernova is XRF 020903 ( $z = 0.25$ ). Based on the observed flattening of the optical light-curves at  $t \sim 30$  days, and the identification of broad features in the optical

spectrum, we propose that XRF 020903 was associated with a supernova up to  $\sim 1$  magnitude fainter than SN 1998bw at maximum light.

In the case of XRF 040701, our foreground extinction-corrected *HST* detection limit is  $\sim 6$  mag fainter than SN 1998bw at this redshift. Our analysis of the X-ray afterglow spectra reveals that the rest-frame host galaxy extinction is constrained to  $A_{V,\text{host}} \lesssim 2.8$ , implying a conservative upper limit on the brightness of the associated SN to be  $\sim 3.2$  mag fainter than SN 1998bw and fainter than all of the GRB-SN studied to date. Taken together, XRFs 020903 and 040701 (the only two XRFs with redshifts in our sample) imply that at least some of the XRF-associated SNe are considerably fainter than SN 1998bw.

Due to the heavy foreground extinction toward XRF 040812, our ability to detect a SN 1998bw-like event would only be possible for  $z \lesssim 0.7$ . In this case, analysis of the X-ray afterglow does not provide a strong constraint on the host galaxy extinction, since the lowest energy photons are absorbed by the Galaxy. Our limits are more constraining for the case of XRF 040916, where we would be sensitive to a SN 1998bw-like supernova beyond  $z \sim 1.2$ . The lack of a SN detection, however, is consistent with a high redshift as possibly suggested by the faintness of the host galaxy and optical afterglow.

Deeper constraints have previously been reported based on *HST/STIS* data for two additional XRFs without known redshifts, XRFs 011030 and 020427 (222). Thanks to the broad throughput of the STIS Clear filter, the sensitivity extends red-ward of *I*-band, thereby enabling SN detection to  $z \approx 1.5$  before UV blanketing suppresses the observed emission. Levan et al. (222) showed that a SN 1998bw-like supernova would be detectable to  $z \sim 1.5$  for both XRFs 011030 and 020427. Using the X-ray afterglow data for these two bursts, Levan et al. (222) estimated their host galaxy extinction to be  $A_V \lesssim 1.7$  and  $A_V \lesssim 2.5$ , respectively, assuming a moderate redshift of  $z \sim 0.5$ . At lower redshift, the host galaxy extinction required to suppress a SN 1998bw-like supernova is inconsistent with the X-ray limits, suggesting that these two bursts are either located at higher redshift or associated with low luminosity SNe. We note that a firm redshift limit of  $z \lesssim 2.3$

has been reported for XRF 020427 based on the lack of Ly $\alpha$  absorption down to 3800 Å within the optical spectrum (406).

While there were no *HST* observations taken for XRF 030723, we utilize the deep ground-based afterglow observations reported by Fynbo et al. (144) to constrain the emission from an underlying supernova. Despite claims that the optical rebrightening at  $t \sim 10$  days is due to an associated supernova (394, 144), we conclude that the observed optical/NIR variability is dominated by afterglow emission since neither the  $R - K$  color nor the optical to X-ray spectral index vary on this timescale (Fox et al., in prep.; Butler et al. 56). We therefore adopt the  $R$ -band afterglow light-curve as an effective upper limit on the flux of an accompanying SN. We derive the most robust constraint from an observation at  $t = 24.78$  days with  $R = 25.08 \pm 0.09$ . This limit is sufficiently deep to rule out a SN 1998bw-like supernova at  $z \lesssim 0.8$ . We note that while the redshift of XRF 030723 is not known, the lack of Ly $\alpha$  absorption in optical spectra limits the redshift to  $z \lesssim 2.3$  (144).

We summarize the limits on XRF-associated supernovae for these seven XRFs in Figure 1.10. Also shown are the peak SN magnitudes (relative to SN 1998bw) for limits (GRB 010921, Price et al. 300) and secure detections of GRB-associated supernovae compiled from the literature (GRBs 970228, 980703, 990712, 991208, 000911, 011121, 020405, 021211 Zeh et al. 447; GRB 030329, Lipkin et al. 229, Deng et al. 100; GRB 031203, Malesani et al. 237; GRB 041006, Stanek et al. 375). This figure highlights the spread of luminosities implied for the supernovae associated with high-energy cosmic explosions. The GRB-SNe clearly show a spread in their peak brightness. Based on XRFs 020903 and 040701, XRF-SNe appear to show a similar spread. Assuming a modest redshift of  $z \sim 1$  for the other five XRF-SNe implies an even larger spread and might suggest that XRFs are associated with systematically fainter SNe.

## 1.5 Discussion

We presented results from our *HST/ACS* search for the supernovae associated with the XRFs 020903, 040701, 040812, 040916 and extended this sample by including published results for SN searches in XRFs 011030, 020427, and 030723. We find strong evidence (photometric and spectroscopic) for a SN 1998bw-like supernova (dimmed by  $\lesssim 1$  mag) in association with XRF 020903 ( $z = 0.25$ ). This finding conclusively associates XRFs with the death of massive stars for the first time. In the case of XRF 040701 ( $z = 0.21$ ), our *HST* limit is  $\sim 6$  magnitudes fainter than SN 1998bw which cannot be accounted for by host galaxy extinction. Based on these two events (XRFs 020903 and 040701), we conclude that at least some XRF-associated SNe exist but can be significantly fainter than SN 1998bw.

In Figure 1.11 we compile peak magnitudes for local Type Ibc supernovae and GRB-associated SNe. While the GRB-SN population tend to lie at the bright end of the local SN luminosity distribution there is a pronounced  $\sim 2$  magnitude spread in their observed peak brightness which produces significant overlap with the local SNe. We emphasize that the SN associated with XRF 020903 is consistent with this observed spread, however, a supernova associated with XRF 040701 would be considered faint even in the context of the local SN population.

Since peak luminosity correlates roughly with the mass of  $^{56}\text{Ni}$  synthesized in the explosion, these observations imply a significant spread in the Nickel yield from GRB and XRF explosions. Most importantly, as revealed from low luminosity GRB/XRF SNe, engine-driven relativistic explosions do not necessarily produce more  $^{56}\text{Ni}$  than local SNe Ibc, which are not associated with relativistic ejecta (26). This result is bracketed by two extremes: events with a large Nickel output can be associated with weak engine-driven explosions harboring only a small amount of relativistic ejecta (e.g., SN 1998bw/GRB 980425), and those with a low Nickel yield can be produced in strong engine-driven explosions characterized by copious amounts of energy coupled to highly relativistic jetted material. In conclusion, we find evidence that Nickel production and engine activity represent indepen-

dent parameters of the GRB/XRF explosion mechanism, each of which can be individually tuned.

The authors are grateful for support under the Space Telescope Science Institute grant HST-GO-10135. A.M.S. acknowledges support by the NASA Graduate Research Fellowship Program Research. E.B. is supported by NASA through Hubble Fellowship grant HST-HF-01171.01 awarded by the STScI, which is operated by the Association of Universities for Research in Astronomy, Inc., for NASA, under contract NAS 5-26555. A.G. acknowledges support by NASA through Hubble Fellowship grant #HST-HF-01158.01-A awarded by STScI. D.C.L. is supported by an NSF Astronomy and Astrophysics Postdoctoral Fellowship under award AST-0401479.

Table 1.1. *HST* Observation Log

Target	Date Obs (UT)	$\Delta t$ (days)	Exp. Time (sec)	Filter	<i>HST</i> mag <sup>a</sup> (AB)	Extinction <sup>b</sup> $A_\lambda$	Johnson mag <sup>c</sup> (Vega)
XRF 020903	2002 December 3.8	91.4	1840	F606W	$24.53 \pm 0.03$	$A_R = 0.09$	$R = 24.23 \pm 0.03$
—	2003 June 30.6	300.2	1920	F606W	—	—	—
XRF 040701	2004 August 9.6	39.1	1820	F625W	$> 27.81$	$A_R = 0.13$	$R > 27.48$
—	2004 August 30.5	60.0	1820	F625W	—	—	—
—	2004 August 9.7	39.1	1940	F775W	$> 26.83$	$A_I = 0.09$	$I > 26.30$
—	2004 August 30.5	60.0	1940	F775W	—	—	—
XRF 040812	2004 September 13.3	32.0	2000	F625W	$> 26.99$	$A_R = 3.61$	$R > 23.18$
—	2004 October 4.8	53.5	2000	F625W	—	—	—
—	2004 September 13.4	32.1	2120	F775W	$> 26.38$	$A_I = 2.62$	$I > 23.32$
—	2004 October 4.8	53.5	2120	F775W	—	—	—
XRF 040916	2004 October 18.4	32.4	1930	F625W	$> 27.89$	$A_R = 0.15$	$R > 27.54$
—	2004 November 30.3	75.3	1928	F625W	—	—	—

Table 1.1—Continued

Target	Date Obs (UT)	$\Delta t$ (days)	Exp. Time (sec)	Filter	<i>HST</i> mag <sup>a</sup> (AB)	Extinction <sup>b</sup> $A_\lambda$	Johnson mag <sup>c</sup> (Vega)
—	2004 October 18.4	32.4	2058	F775W	> 27.19	$A_I = 0.64$	$I > 26.64$
—	2004 November 30.4	75.4	2056	F775W	—	—	—

<sup>a</sup>From residual image. Observed magnitude, not corrected for foreground extinction.

<sup>b</sup>Galactic extinction from Schlegel et al. (344).

<sup>c</sup>From residual image. Corrected for foreground extinction using  $A_\lambda$  given in column 7.

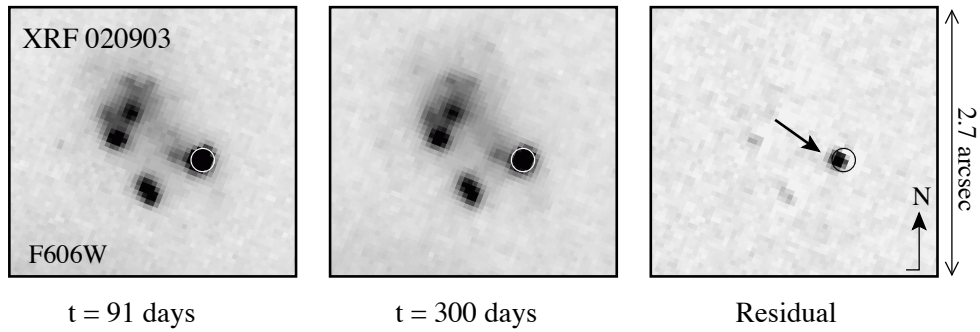


Figure 1.1: Three-panel frame showing *HST/ACS* imaging for XRF 020903 at  $t \sim 91$  days (Epoch 1) and  $t \sim 300$  days (Epoch 2) in the F606W filter. By subtracting the Epoch 2 image from Epoch 1, we produced the residual image, above. We apply the same stretch to all frames. As clearly shown in this residual image, a transient source is detected coincident with the 0.12 arcsec ( $2\sigma$ ) optical afterglow position (circle), lying on the southwest knot of the host galaxy complex.

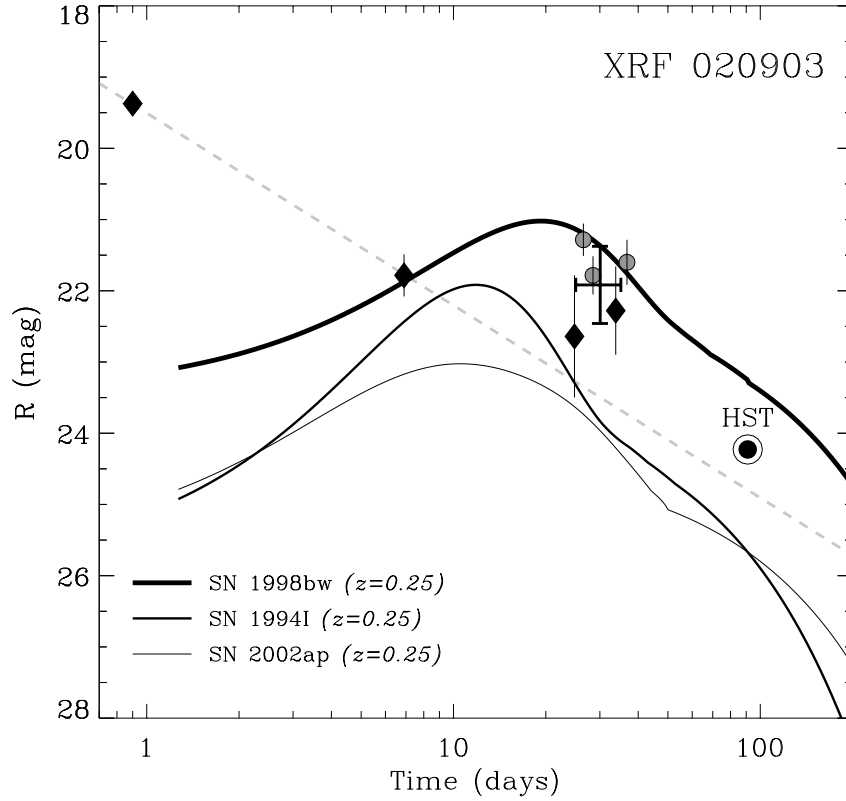


Figure 1.2: Extinction-corrected ground-based  $R$ -band observations of the optical afterglow have been compiled from Soderberg et al. (361) and the GCNs (91, 163), and are shown as diamonds and grey circles, respectively. The temporal decay of the (host galaxy subtracted) optical afterglow is described by  $t^{-1.1}$  (dashed grey line) at early time followed by a plateau phase at  $t \sim 30$  days. The weighted mean of the points between  $t \sim 20 - 40$  days (black cross) indicates that at peak the supernova was  $0.6 \pm 0.5$  magnitudes fainter than the synthesized SN 1998bw light-curve (thick line). At  $t \sim 91$  days, however, the *HST* transient (encircled dot) is  $\sim 1$  magnitude fainter than the synthesized curve, implying the supernova faded faster than SN 1998bw. SN 1994I- and 2002ap-like supernovae (medium and thin lines, respectively) would be significantly fainter than the *HST* residual.

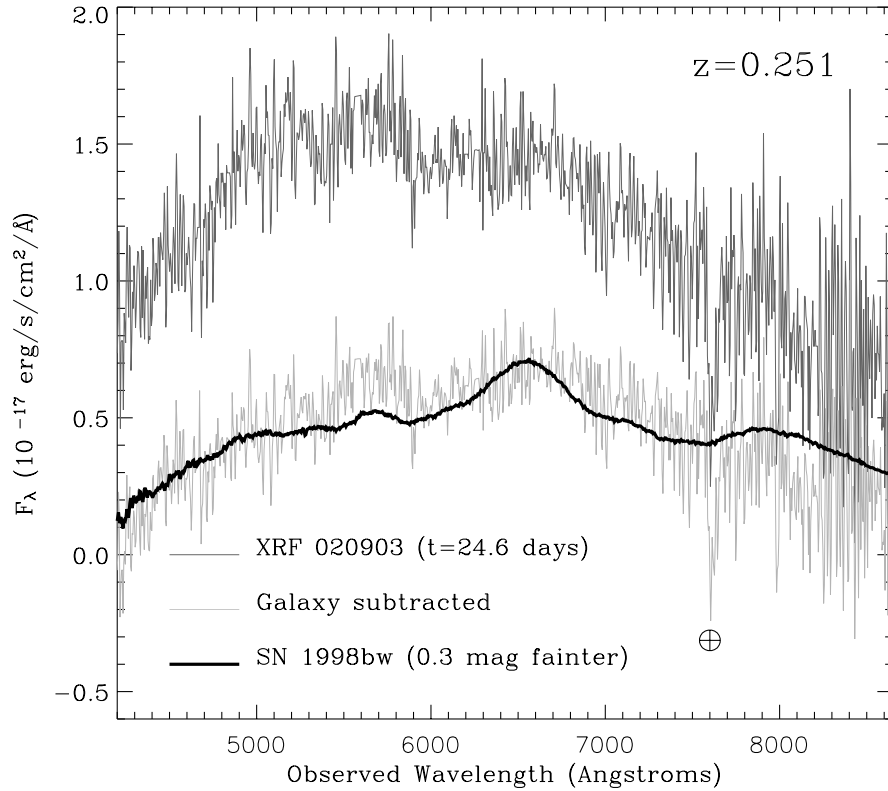


Figure 1.3: Magellan/LDSS2 spectrum of XRF 020903, taken at  $t \approx 24.6$  days. Host galaxy emission lines were sigma-clipped (top) and we remove the host galaxy contribution using a starburst template (bottom; light grey). The galaxy subtracted spectrum has broad SN features, in clear resemblance to SN 1998bw at  $t \sim 20$  days (rest-frame), redshifted to  $z = 0.25$  and dimmed by 0.3 magnitudes (bottom; black). The telluric band is marked with an encircled cross.

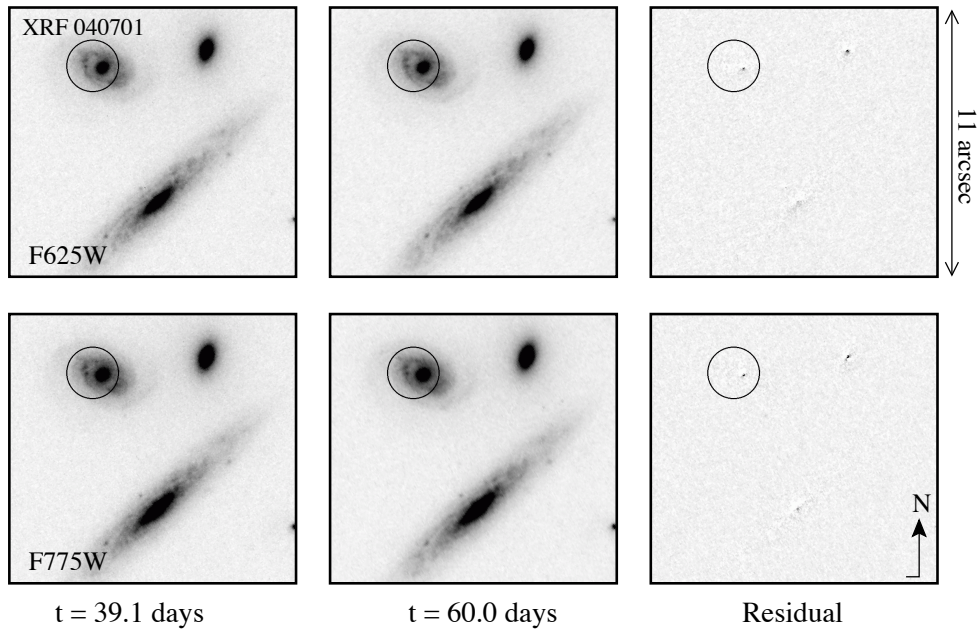


Figure 1.4: Six-panel frame showing *HST/ACS* imaging for XRF 040701 at  $t \sim 39.1$  days (Epoch 1) and  $t \sim 60.0$  days (Epoch 2) in the F625W and F775W filters. By subtracting Epoch 2 images from Epoch 1, we produced the residual images, above. We apply the same stretch to all frames. As shown in these residual images, there is no evidence of an optical transient within the *Chandra* X-ray afterglow position ( $2\sigma$ ; circle) down to our *HST/ACS* detection limits.

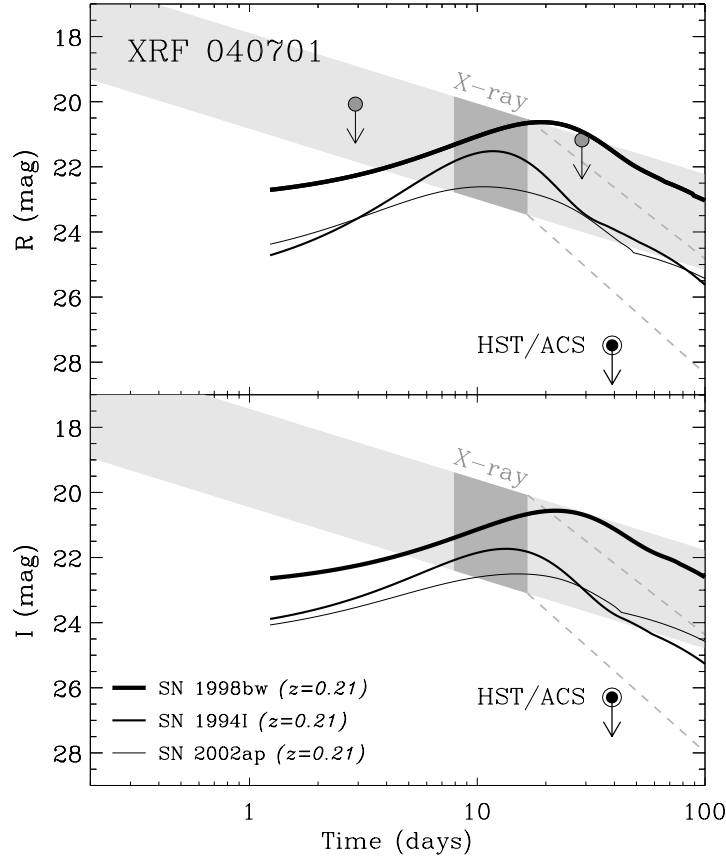


Figure 1.5: Ground-based optical limits (grey circles) have been compiled from the GCNs (99, 291), corrected for Galactic extinction and are plotted for the  $R$ - (upper panel) and  $I$ -band (lower panel). By extrapolating the observed X-ray afterglow to the optical bands, we predict a range of magnitudes for the optical afterglow on these same timescales (dark shaded polygon). Assuming the temporal decay can be extrapolated outside the X-ray observation window produces the light shaded bands. Dashed lines represent the extreme case where a jet break occurs at the second *Chandra* epoch. Simulated SN light-curves for SNe 1998bw (thick line), 1994I (medium line), and 2002ap (thin line), redshifted to  $z = 0.21$ , are overlaid. Image subtraction of our two *HST/ACS* epochs in F625W and F775W, provide deep limits on an associated SN at  $t \sim 32.1$  days (encircled dots).

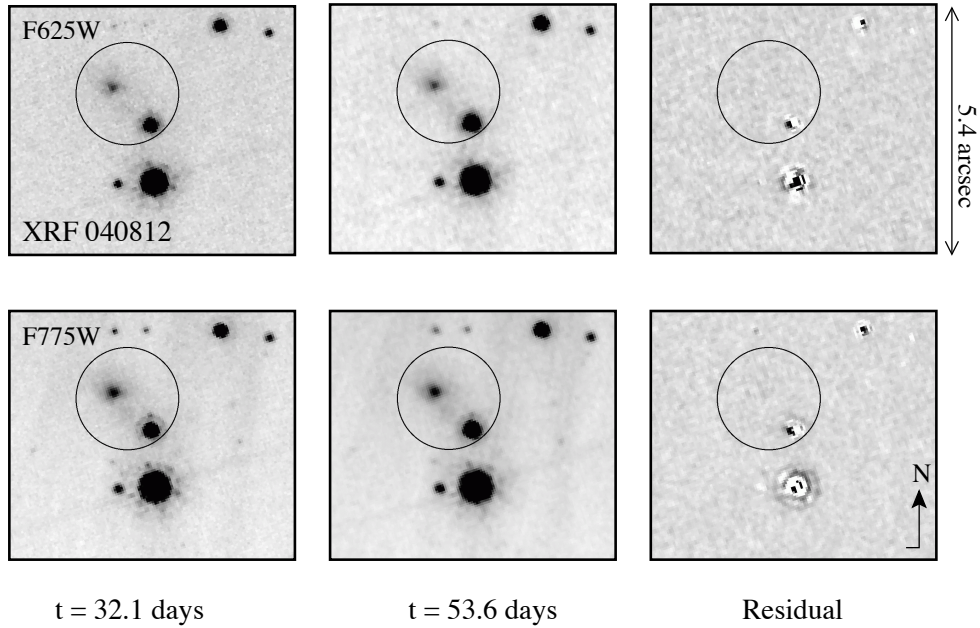


Figure 1.6: Six-panel frame showing *HST/ACS* imaging for XRF 040812 at  $t \sim 32.1$  days (Epoch 1) and  $t \sim 53.6$  days (Epoch 2) in the F625W and F775W filters. Within the X-ray afterglow position ( $2\sigma$ ; circle) a host galaxy is clearly detected. By subtracting Epoch 2 images from Epoch 1, we produced the residual images, above. We apply the same stretch to all frames. As shown in the residual images, there is no evidence of an optical transient within the host galaxy down to our *HST/ACS* detection limits.

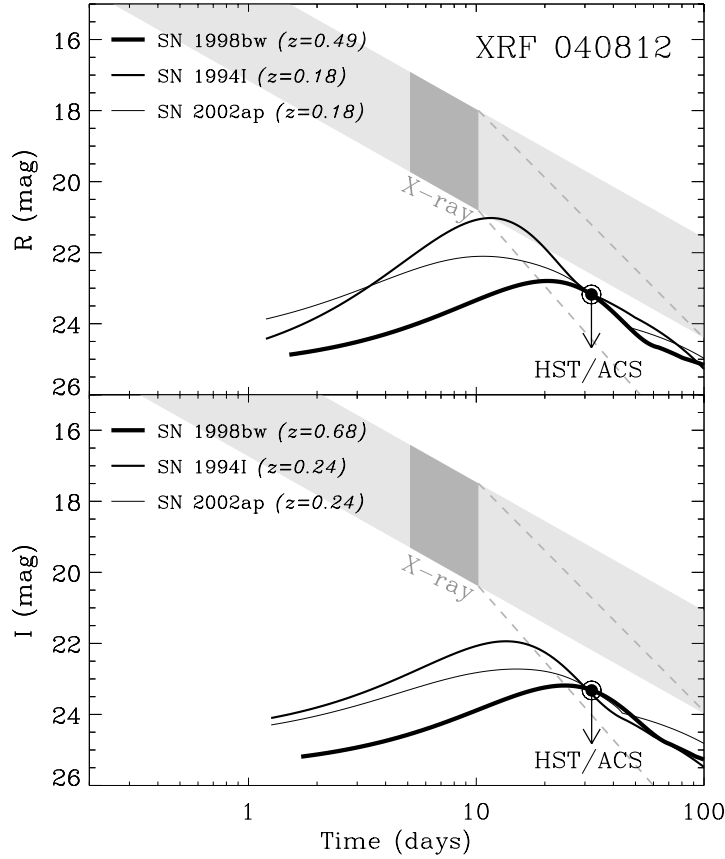


Figure 1.7: Constraints on a supernova associated with XRF 040812 are shown for the  $R$ - and  $I$ -bands. By extrapolating the observed X-ray afterglow to the optical bands, we predict a range of magnitudes for the optical afterglow on these same timescales (dark shaded polygon). Assuming the temporal decay can be extrapolated outside the X-ray observation window produces the light shaded bands. Dashed lines represent the case where a jet break occurs at the second *Chandra* epoch. The marked arrows show the (galactic extinction-corrected) *HST* constraints derived from image subtraction techniques described in Section 1.3.3. Synthesized light-curves for SNe 1998bw (thick), 1994I (medium), and 2002ap (thin), are shown each at the redshift limit to which they could be detected within our residual *HST* observations (encircled dots).

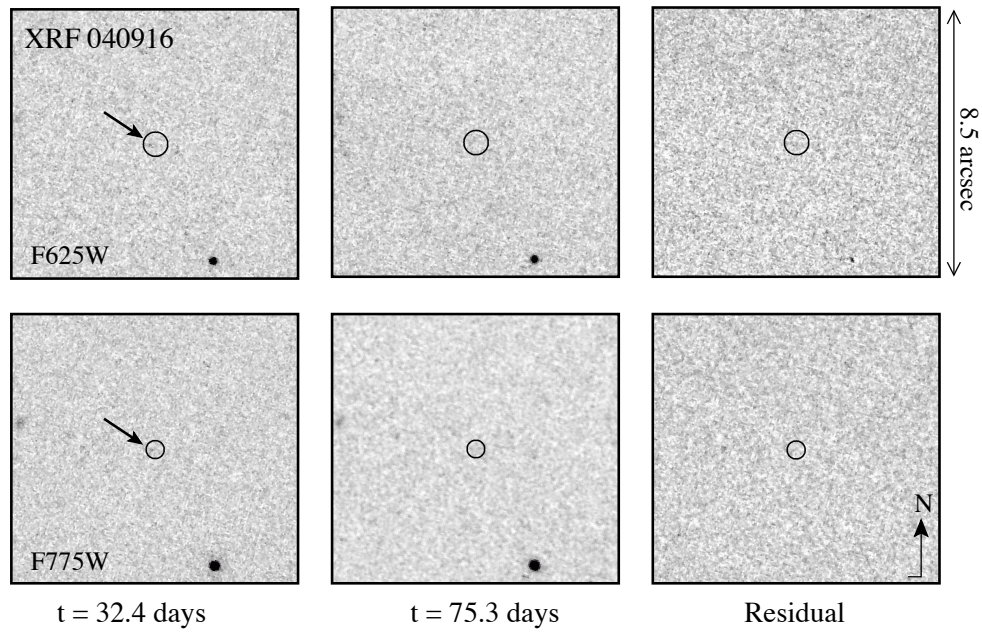


Figure 1.8: Six-panel frame showing *HST/ACS* imaging for XRF 040916 at  $t \sim 32.4$  days (Epoch 1) and  $t \sim 75.3$  days in the F625W and F775W filters. By subtracting Epoch 2 images from Epoch 1, we produced the residual images, above. We apply the same stretch to all frames. As shown in the residual images, a faint source is detected in Epoch 1, coincident with the astrometrically derived optical afterglow position ( $2\sigma$ ; circle).

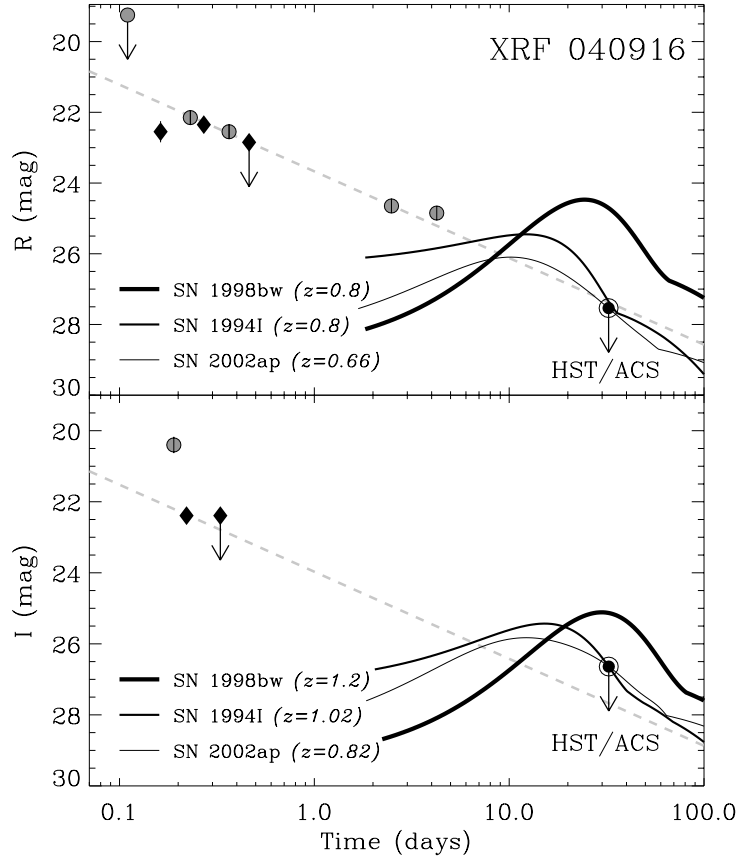


Figure 1.9: Extinction-corrected measurement for the optical afterglow include data from the robotic Palomar 60-inch telescope (diamonds) and from the GCNs (grey circles) and are plotted for the  $R$ - (upper panel) and  $I$ -band (lower panel). The temporal decay of the  $R$ -band afterglow is well fit by  $t^{-1.0}$  (grey dashed line) which we scale to fit the  $I$ -band Palomar 60-inch data as well. The observed magnitude of the faint *HST* transient (encircled dot) is consistent with the extrapolated OT decay. Synthesized light-curves for SNe 1994I (medium line) and 2002ap (thin line) are shown at the redshift for which the SN brightness matches that of the residual source. At  $z = 1.2$  (the redshift limit for our  $I$ -band light-curve synthesis) SN 1998bw (thick line) would still be  $\gtrsim 3$  magnitudes brighter than the *HST* residual source (encircled dot). We note this non-detection is consistent with a higher redshift, as possibly suggested by the faintness of the optical afterglow and host galaxy (§1.3.4).

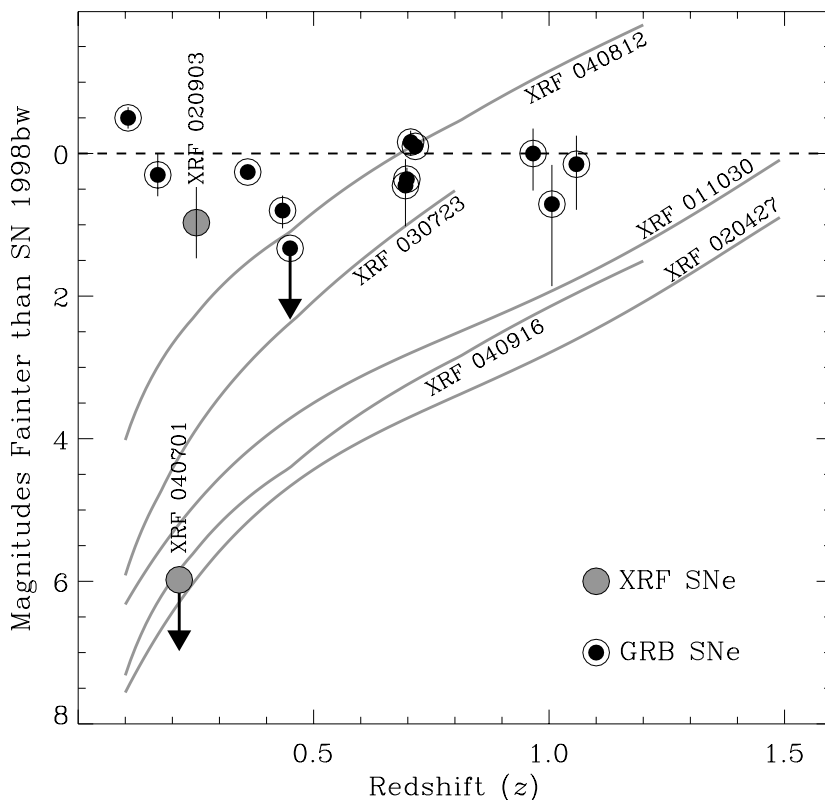


Figure 1.10: A compilation of constraints for SN 1998bw-like supernovae associated with X-ray flashes. For each XRF we adopt the (galactic extinction-corrected) *HST* limit for the brightness of an associated supernova. At a given redshift, the difference between the observed *HST* limit and the synthesized SN 1998bw light-curve represents how faint the supernova must be (with respect to SN 1998bw) in order to go undetected in our images. We plot this magnitude difference against redshift for the seven XRFs with deep, late-time observations. Results for XRFs 011030 and 020427 have been taken from Levan et al. (222). For XRF 040701 we show the limit including negligible host galaxy extinction, but note that this could be as high as  $A_{V,\text{host}} \sim 3$  magnitudes. For XRF 020903 we plot the value based on late-time *HST* observations but note that the peak magnitude could be considerably brighter (see §1.3.1 and Fig. 1.2). Also shown are the confirmed GRB-SN detections compiled from the literature (see §2.4).

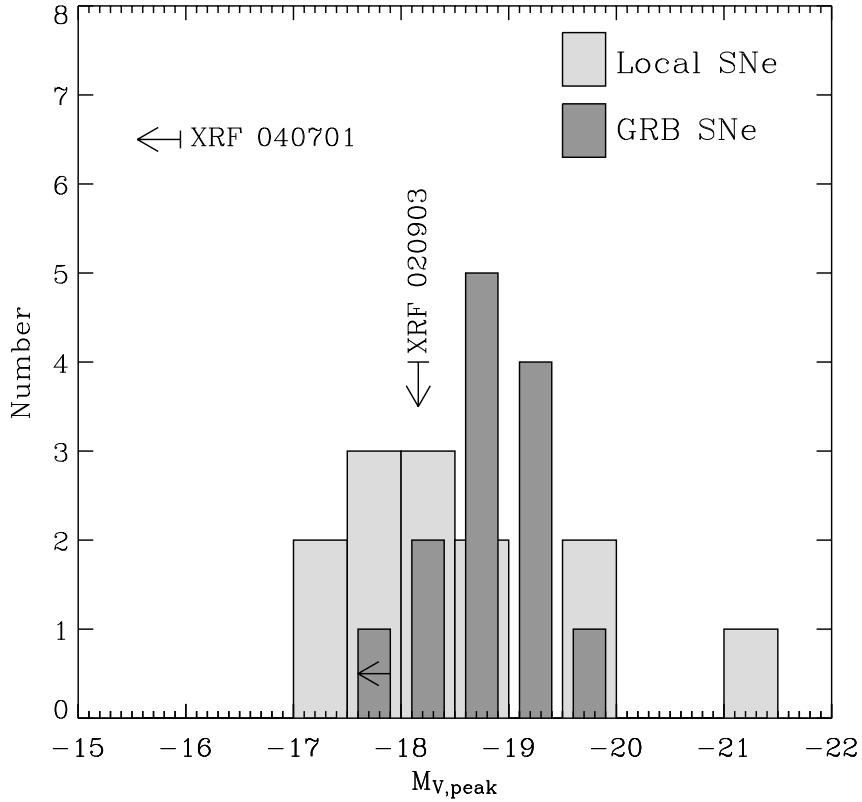


Figure 1.11: Histogram of peak optical magnitudes (rest frame  $M_V$ ) for local Type Ibc supernovae (light grey) and GRB associated SNe (dark grey). Locations of the SNe associated with XRFs 020903 and 040701 (with  $A_{V,\text{host}} = 2.8$  mag) are marked with arrows. There is a significant spread in peak brightness demonstrated by the local SNe and the GRB-SNe samples. The SN associated with XRF 020903 is consistent with this observed diversity. GRB-SNe have been compiled from the literature (see §2.4). Local SNe include SN 1983N (86), SN 1983V (87), SN 1984L (400), SN 1987M (118), SN 1990B (85), SN 1991D (14), SN 1992ar (84), SN 1994I (317), SN 1997ef (194), SN 1999as (178), SN 1999ex (383), SN 2002ap (122), and SN 2003L (Soderberg *et al.*, in prep).

## Chapter 2

### An HST Study of the Supernovae

### Accompanying GRB 040924 and GRB 041006<sup>†</sup>

A. M. SODERBERG<sup>a</sup>, S. R. KULKARNI<sup>a</sup>, P. A. PRICE<sup>b</sup>, D. B. FOX<sup>a</sup>,  
 E. BERGER<sup>c</sup>, D.-S. MOON<sup>d</sup>, S. B. CENKO<sup>d</sup>, A. GAL-YAM<sup>a</sup>, D. A. FRAIL<sup>e</sup>,  
 R. A. CHEVALIER<sup>f</sup>, L. COWIE<sup>b</sup>, G. S. DA COSTA<sup>g</sup>, A. MACFADYEN<sup>a</sup>,  
 P. J. MCCARTHY<sup>c</sup>, N. NOEL<sup>h</sup>, H. S. PARK<sup>i</sup>, B. A. PETERSON<sup>g</sup>,  
 M. M. PHILLIPS<sup>c</sup>, M. RAUCH<sup>c</sup>, A. REST<sup>j</sup>, J. RICH<sup>g</sup>, K. ROTH<sup>k</sup>, M. ROTH<sup>c</sup>,  
 B. P. SCHMIDT<sup>g</sup>, R. C. SMITH<sup>j</sup>, P. R. WOOD<sup>g</sup>,

<sup>a</sup>Division of Physics, Mathematics and Astronomy, 105-24, California Institute of Technology,  
 Pasadena, CA 91125, USA

<sup>b</sup>University of Hawaii, Institute of Astronomy, 2680 Woodlawn Drive, Honolulu, HI 96822-1897,  
 USA

<sup>c</sup>Observatories of the Carnegie Institution of Washington, 813 Santa Barbara St., Pasadena, CA  
 91101, USA

<sup>d</sup>Space Radiation Laboratory 220-47, California Institute of Technology, Pasadena, CA 91125,  
 USA

<sup>e</sup>National Radio Astronomy Observatory, Socorro, NM 87801, USA

---

<sup>†</sup>A version of this chapter was published in *The Astrophysical Journal*, vol. 636, 391–391,  
 (2006). Reproduced by permission of the AAS.

<sup>f</sup>Department of Astronomy, University of Virginia, P.O. Box 3818, Charlottesville, VA  
22903-0818, USA

<sup>g</sup>Research School of Astronomy and Astrophysics, The Australian National University, Weston  
Creek, ACT 2611, Australia

<sup>h</sup>Instituto de Astrofísica de Canarias, C/Vía Lactea s/n, E-38200, La Laguna, Tenerife, Spain

<sup>i</sup>Lawrence Livermore National Laboratory, 7000 East Avenue, Livermore, CA 94550, USA

<sup>j</sup>Cerro Tololo Inter-American Observatory, Casilla 603, La Serena, Chile

<sup>k</sup>Gemini Observatory, 670 N. Aohoku Place, Hilo, HI 96720, USA

## Abstract

We present the results from a *Hubble Space Telescope/ACS* study of the supernovae associated with gamma-ray bursts 040924 ( $z = 0.86$ ) and 041006 ( $z = 0.71$ ). We find evidence that both GRBs were associated with a SN 1998bw-like supernova dimmed by  $\sim 1.5$  and  $\sim 0.3$  magnitudes, respectively, making GRB 040924 the faintest GRB-associated SN ever detected. We study the luminosity dispersion in GRB/XRF-associated SNe and compare to local Type Ibc supernovae from the literature. We find significant overlap between the two samples, suggesting that GRB/XRF-associated SNe are not necessarily more luminous nor produce more  $^{56}\text{Ni}$  than local SNe. Based on the current (limited) datasets, we find that the two samples may share a similar  $^{56}\text{Ni}$  production mechanism.

## 2.1 Introduction

Gamma-ray burst (GRB) explosions harbor both spherical supernova (SN) ejecta and highly collimated engine-driven jets (151, 243, 187). This “spherical+jet” paradigm for the geometry of GRBs implies that both explosion components must be studied independently. Early ( $t \lesssim$  few days) optical observations trace the

synchrotron radiation produced from the engine-driven relativistic jets, while late-time ( $t \gtrsim 20$  days) observations probe the optical emission from the non-relativistic spherical SN ejecta, powered by the decay of  $^{56}\text{Ni}$ . Such observations allow us to address the following fundamental questions regarding the GRB/SN connection: what is the diversity among GRB-associated SNe, and how does the sample compare to local Type Ibc supernovae (SNe Ibc)?

Three of the best studied events, SNe 1998bw, 2003dh, and 2003lw (associated with GRBs 980425, 030329, and 031203, respectively) were strikingly similar, with brighter optical luminosities and faster photospheric velocities than local SNe Ibc (151, 282, 243, 187, 237). These events suggested that the supernovae associated with GRBs belong to a distinct sub-class of “hyper-energetic” supernovae. However, there are also several counter-examples: under-luminous SNe associated with GRBs and X-ray flashes (XRFs; events very similar to GRBs but differentiated by a soft prompt energy release peaking in the X-ray band; Heise et al. 180) with optical luminosities significantly fainter than SN 1998bw. The most extreme examples are GRB 010921 (Price et al. 300; but see Zeh et al. 447) and XRF 040701 (363), for which the associated SNe are at least 1.3 and 3.2 magnitudes fainter than SN 1998bw, respectively.

Motivated by our fundamental questions, we began a *Hubble Space Telescope* (*HST*) program to study the diversity in supernovae associated with GRBs and XRFs (GO-10135; PI: Kulkarni). In Soderberg et al. (363), we presented the results of our *HST* supernova search in XRFs 020903, 040701, 040812 and 040916. We showed that at least some XRFs are associated with SNe, but that there may be a significant dispersion in their optical peak magnitudes.

Here we present the results from our *HST* study of the supernovae associated with GRBs 040924 ( $z = 0.86$ ) and 041006 ( $z = 0.71$ ). In §2.3 we show that each is associated with a SN 1998bw-like supernova dimmed by  $\sim 1.5$  and  $\sim 0.3$  magnitudes, respectively, making GRB 040924 the faintest GRB-associated SN detected to date. These two events suggest a notable dispersion of peak optical magnitudes for GRB-associated SNe.

Finally, we compile optical peak magnitudes and  $^{56}\text{Ni}$  mass estimates for all GRB/XRF-associated SNe and local SNe Ibc to study the diversity among these two samples. In §2.4 we address the question of whether both samples are drawn from the same parent population of core-collapse supernovae.

## 2.2 Supernova Light-curve Synthesis

In modeling the GRB-associated SNe, we adopted optical data for the local SNe 1994I (317), 1998bw (151, 254), and 2002ap (122) as templates. These three SNe were selected based on their well-sampled optical light-curves which represent an overall spread in the observed properties of Type Ibc supernovae. To produce synthesized light-curves for each of these template SNe, we compiled optical *UBVRI* observations from the literature and smoothed the extinction-corrected (foreground plus host galaxy) light-curves. We then redshifted the light-curves by interpolating over the photometric spectrum and stretching the arrival time of the photons by a factor of  $(1+z)$ . The details of each template dataset are described in Soderberg et al. (363).

## 2.3 Hubble Space Telescope GRB-SN Search

Using the *Wide-Field Camera (WFC)* of the *Advanced Camera for Surveys (ACS)* on-board *HST*, we imaged the fields of GRBs 040924 and 041006. For each target we undertook observations at several epochs, spanning  $t \sim 30$  and  $\sim 150$  days, in order to search for optical emission associated with an underlying supernova. Each epoch consisted of 2 to 4 orbits during which we imaged the field in filters, F775W and/or F850LP, corresponding to SDSS  $i'$ - and  $z'$ - bands, respectively.

The *HST* data were processed using the `multidrizzle` routine (141) within the `stsdas` package of IRAF. Images were drizzled using `pixfrac=0.8` and `pixscale=1.0` resulting in a final pixel scale of 0.05 arcsec/pixel. Drizzled images were then registered to the first epoch using the `xregister` package within IRAF.

To search for source variability and remove host galaxy contamination, we used

the *ISIS* subtraction routine by Alard (1) which accounts for temporal variations in the stellar PSF. Adopting the final epoch observations as template images, we produced residual images. These residual images were examined for positive sources positionally coincident with the afterglow error circle. To test our efficiency at recovering faint transient sources, false stars with a range of magnitudes were inserted into the first epoch images using *IRAF* task `mkobject`. The false stars were overlaid on top of the diffuse host galaxy emission at radial distances similar to that measured for the afterglow. An examination of the false stellar residuals provided an estimate of the magnitude limit ( $3\sigma$ ) to which we could reliably recover faint transients.

Photometry was performed on the residual sources within a 0.5 arcsec aperture. We converted the photometric measurements to infinite aperture and calculated the corresponding AB magnitudes within the native *HST* filters using the aperture corrections and zero-points provided by Sirianni et al. (349). For comparison with ground-based data, we also converted the photometric measurements to Johnson *I*- and *z*-band (Vega) magnitudes using the transformation coefficients derived by Sirianni et al. (349) and adopting the source color given by the first epoch F775W and F850LP observations.

In the following sections we summarize the afterglow properties for both targets and the photometry derived from our *HST* SN study. A log of the *HST* observations for the GRBs follows in Table 2.1.

### 2.3.1 GRB 040924

#### Prompt Emission and Afterglow Properties

GRB 040924 was detected by the Wide-Field X-ray Monitor (*WXM*) on-board the High Energy Transient Explorer (*HETE-2*) satellite on 2004 September 24.4951 UT. Preliminary analysis showed the peak of the spectral energy distribution was soft,  $E_{\text{peak}} \approx 42 \pm 6$  keV, and the ratio of X-ray (7 – 30 keV) to  $\gamma$ -ray (30 – 400 keV) fluence,  $S_X/S_\gamma \approx 0.6$ , classifying this event as an X-ray rich burst (111).

Using the Roboticized Palomar 60-inch telescope (*P60*; Cenko *et al.*, in prep), we discovered the optical afterglow at position  $\alpha = 02^{\text{h}}06^{\text{m}}22^{\text{s}}.55$ ,  $\delta = +16^{\circ}06'48''.8$  (J2000) with an uncertainty of 0.2 arcsec in each coordinate (126), well within the 6.4 arcsec (radius) localization region. As shown by our extensive *P60* monitoring, the afterglow was  $R \approx 18.0$  mag at  $t \approx 16$  minutes and subsequently decayed.

We continued to monitor the afterglow emission from  $t \approx 0.01$  to 1 day after the burst (Table 2.2), producing a well-sampled *R*-band light-curve. As shown in Figure 2.2, these data show a shallow initial decay, followed by a steepening at  $t \sim 0.02$  days. In an effort to characterize the light-curve behavior, we fit a smoothed, broken power-law model (e.g., Beuermann *et al.* 32) of the form

$$F_{\nu}(t) = 2F_{\nu,0} \left[ \left( \frac{t}{t_b} \right)^{\alpha_1 s} + \left( \frac{t}{t_b} \right)^{\alpha_2 s} \right]^{-1/s} \quad (2.1)$$

where  $t_b$  is the break time in days,  $F_{\nu,0}$  is the normalized flux density at  $t = t_b$ , and  $\alpha_1$  and  $\alpha_2$  are the asymptotic indices at  $t \ll t_b$  and  $t \gg t_b$ , respectively. Here  $s$  is used to parameterize the sharpness of the break. A best fit ( $\chi_r^2 = 3.3$ ) is found for the following parameters:  $F_{\nu,0} \approx 90.4 \mu\text{Jy}$ ,  $\alpha_1 \approx 0.39$ ,  $\alpha_2 \approx 1.22$ ,  $t_b \approx 0.021$  days, and  $s \approx 10$ . To interpret this steepening as a jet break (315, 338) would imply a electron spectral index,  $N \propto \gamma^{-p}$  with  $p \approx 1.2$ . This value is significantly lower than those typically observed ( $p \approx 2.2$ ; Yost *et al.* 445) and far below the range predicted by the standard blastwave model,  $p = [2 - 3]$  (339). We therefore ascribe this early afterglow phase (and steepening) to another process, perhaps similar to that observed for the initial slow decay of GRB 021004 (131), interpreted as interaction with a stellar wind medium (228).

Terada and Akiyama (391) report that the afterglow was  $K \approx 17.5 \pm 0.1$  mag at  $t \approx 0.1$  days. Comparison with the *R*-band afterglow model at the same epoch provides a spectral index,  $F_{\nu} \propto \nu^{\beta}$  with  $\beta \approx -0.7$ , between the *R*- and *K*-bands. Adopting this spectral index, we interpolate our *R*-band afterglow model to the *I*- and *z*-bands for comparison with our late-time *HST* observations (§ 2.3.1).

Optical spectroscopy later revealed that the burst was located at a redshift of

$z = 0.859$ , based on identification of several host galaxy emission lines (431).

### ***HST* observations**

*HST/ACS* imaging was carried out on 2004 November 2.4, 26.5, and 2005 February 19.0 UT ( $t \approx 39, 63,$  and 147 days after the burst). For the first and third epochs, we observed with both the F775W and F850LP filters, while the second epoch consisted of just F775W observations. We astrometrically tied the *HST* and *P60* images using four sources in common resulting in a final systematic uncertainty of 0.22 arcsec ( $2\sigma$ ).

Our *HST* observations reveal that the optical afterglow error circle coincides with a strongly variable source at  $\alpha = 02^{\text{h}}06^{\text{m}}22^{\text{s}}.552$ ,  $\delta = +16^{\circ}06'49''.11$  (J2000), lying  $\sim 0.3$  arcsec NW of the host galaxy nucleus. We interpret this source as a combination of afterglow plus supernova emission. Figure 2.1 shows the first epoch, template image and first epoch residual for both the F775W and F850LP filter observations. There is no evidence for a point source in our third epoch (template) images. We therefore make the reasonable assumption that the transient source flux is negligible at that time. The resulting *HST* photometry is listed in Table 2.1.

Figure 2.2 shows the *HST* photometry along with our *I*- and *z*-band afterglow models (see §2.3.1) and some early-time data compiled from the GCNs (348), all corrected for galactic extinction. By comparing the afterglow models with the *HST* photometry, we find evidence for a  $\sim 1.9$  magnitude rebrightening at  $t \sim 39$  days. We note that the timescale of this rebrightening is roughly consistent with the peak time of SN 1998bw at  $z = 0.86$ .

### **Associated Supernova**

We interpret the observed late-time rebrightening as an associated supernova component. Comparison with our synthesized (redshifted) supernova light-curves reveals that an associated SN 1998bw-like supernova would be  $\sim 1.5$  magnitudes brighter than the *HST* observation at  $t \sim 39$  days, while SN 1994I and SN 2002ap-like light-curves are fainter by  $\sim 0.8$  and  $\sim 1.5$  magnitudes, respectively. To fit the

*HST* observations, we add the contribution from a template SN light-curve (see §2.2) to the afterglow model. We allow the brightness of the synthesized template to be scaled but do not allow for the light-curve to be stretched. Moreover, we assume the GRB and SN exploded at the same time. By fitting the *HST* *I*- and *z*-band data simultaneously, we find a best fit solution ( $\chi_r^2 \approx 0.8$ ) for a SN 1998bw-like supernova dimmed by  $\sim 1.5$  magnitudes (Figure 2.2). We note that on this timescale, the supernova emission clearly dominates that of the afterglow model. Therefore, even if the afterglow underwent a late-time ( $t > 2$  days) jet break, our supernova fits would not be significantly affected.

Host galaxy extinction could affect our SN light-curve fits since it implies the associated SN was more luminous than the observations suggest. Fortunately, we can constrain the host galaxy extinction using optical/IR afterglow observations, since extinction will produce an artificial steepening of the synchrotron spectrum. Making the reasonable assumption that the synchrotron cooling frequency was above the optical/IR bands at early-time, we have  $\beta_{\text{opt/IR}} \approx -0.7 = -(p - 1)/2$  and thus  $p \approx 2.4$ . For  $p < 2$  the standard blastwave model is violated, therefore implying the spectral index must be steeper than  $\beta_{\text{opt/IR}} = -0.5$ . Adopting this limit for the intrinsic spectral index of the afterglow implies a constraint on the host-galaxy extinction of  $A_{V,\text{host}} \lesssim 0.16$  mag. This corresponds to limits on the observed extinction of  $A_I \approx A_z \lesssim 0.20$  mag, implying the associated SN was at least 1.3 magnitudes fainter than SN 1998bw. We therefore conclude that the supernova associated with GRB 040924 was between 1.3 and 1.5 magnitudes fainter than SN 1998bw at maximum light, making this event the faintest GRB-associated SN ever detected.

### 2.3.2 GRB 041006

#### Prompt Emission and Afterglow Properties

GRB 041006 was discovered by the *HETE-2/WXM* on 2004 October 6.513 UT. The ratio of 2 – 30 keV and 30 – 400 keV channel fluences showed the event was

an X-ray rich burst. The event was localized to a 5.0 arcmin (radius) localization region centered at  $\alpha = 00^{\text{h}}54^{\text{m}}53^{\text{s}}$ ,  $\delta = +01^{\circ}12'04''$  (J2000; Galassi et al. 153).

Using the Siding Springs Observatory (*SSO*) 40-inch telescope, we discovered the optical afterglow at  $\alpha = 00^{\text{h}}54^{\text{m}}50^{\text{s}}.17$ ,  $\delta = +01^{\circ}14'07''.0$  (J2000; Da Costa et al. 94), consistent with the *HETE-2* error circle. As our early time ( $t \approx 0.024$  to 0.122 days; Table 2.3) *SSO* 40-inch and 2.3 meter observations show, the afterglow was  $V \approx 18.1$  mag at  $t \approx 35$  minutes and subsequently faded in the *B*-, *V*-, and *H*-bands.

Stanek et al. (375) have presented an extensive compilation of (extinction-corrected) *R*-band afterglow data from  $t \approx 0.03$  to 64 days, primarily from the Multiple Mirror Telescope (MMT) and from the GCNs (see references therein). They fit the evolution of the early light-curve (up to  $t \sim 4$  days) with the broken power-law model given in Equation 1, finding best fit parameters of  $F_{\nu,0} \approx 50.0 \mu\text{Jy}$ ,  $\alpha_1 \approx 0.57$ ,  $\alpha_2 \approx 1.29$ ,  $t_b \approx 0.14$  days, and  $s \approx 2.59$ . As in the case of GRB 040924 (§ 2.3.1), this observed steepening is too shallow to be interpreted as a jet break under the standard blastwave model. We instead interpret this early afterglow phase as due to another process, possibly the result of an off-axis viewing angle as proposed by Granot et al. (170).

Combining our early-time *SSO* data with those compiled by Stanek et al. (375), we estimate the spectral index of the optical/IR afterglow to be  $\beta_{\text{opt/IR}} \approx -0.5$  by fitting a power-law to the *B*-, *V*-, *R*-, and *H*-band data. Adopting this spectral index, we interpolate the *R*-band model to the *I*- and *z*-bands for comparison with our late-time *HST* observations (§ 2.3.2).

Optical spectroscopy at  $t \approx 0.6$  days revealed that the burst was located at  $z \geq 0.712$ , based on tentative identification of several absorption lines in the low signal-to-noise spectrum (143). To confirm this redshift measurement, we acquired a spectrum of the optical afterglow with the Gemini Multi-Object Spectrograph (GMOS) on Gemini North (GN-2004B-Q-5; PI: Price) commencing at 2004 October 7.36 UT ( $t \approx 0.85$  days). Using the R400 grating and a 1 arcsec slit, we obtained four individual 1800 sec exposures. Data were reduced and extracted us-

ing the `gemini.gmos` package within IRAF. We identify four absorption lines and one emission line (Table 2.4 and Figure 2.3), which we interpret as arising from Mg II, Ca II and [O II] at a redshift of  $z = 0.716$ , in broad agreement with the earlier measurement by Fugazza et al. (143). Based on the high equivalent widths and the presence of [O II], this is likely the redshift of the host galaxy, and not due to an intervening system along the line of sight. Using the  $R$ -band afterglow model and the photometrically derived spectral index, we flux calibrate the spectrum and obtain an approximate [O II] emission line flux of  $1.3 \times 10^{-17}$  erg/cm<sup>2</sup>/s. Adopting the conversion factor of Kennicutt (205), this line flux corresponds to a star formation rate of  $0.5 M_{\odot}$ /yr at the redshift of the host galaxy.<sup>1</sup>

### ***HST* observations**

*HST/ACS* imaging was carried out on 2004 November 2.3, 27.4, December 23.4 and 2005 February 10.5 UT ( $t \approx 27, 52, 78$  and 127 days after the burst). For the first and fourth epochs, we observed with both the F775W and F850LP filters, while the second, and third epochs consisted of just F775W observations. We astrometrically tied the *HST* and *SSO* images using five sources in common resulting in a final systematic uncertainty of 0.53 arcsec ( $2\sigma$ ).

Our *HST* observations reveal that the optical afterglow error circle coincides with a strongly variable source at  $\alpha = 00^{\text{h}}54^{\text{m}}50^{\text{s}}.229$ ,  $\delta = +01^{\circ}14'05''.82$  (J2000). The source is situated directly on top of a faint host galaxy which is at the detection limit of our *HST* images. We note the presence of a brighter galaxy  $\sim 1$  arcsec from the afterglow position which was misidentified as the host galaxy by Covino et al. (92) based on ground-based images.

Figure 2.4 shows the first epoch, template image, and first epoch residual for both the F775W and F850LP filter observations. From the figure, it is clear that the source is still faintly detected in our final epoch (template) observations. To assume negligible source flux in the template images is therefore not valid. We estimate the flux of the source in our template images by performing PSF

---

<sup>1</sup>We have adopted a cosmology with  $H_0 = 65$  km/s/Mpc and  $(\Omega_M, \Omega_{\Lambda}) = (0.3, 0.7)$ .

photometry on the object. In calculating the magnitude of the source in the first, second and third epochs, we add the template epoch flux to the residual image photometry. The resulting *HST* photometry is given in Table 2.1.

Figure 2.5 shows the *HST* photometry along with our *I*- and *z*-band afterglow model (see §2.3.2) and some early-time data compiled from the GCNs (112, 189), all corrected for galactic extinction. By comparing the afterglow model with the *HST* data, we find evidence for a  $\sim 2.1$  magnitude rebrightening at  $t \sim 27$  days, roughly consistent with the peak time of a SN 1998bw-like supernova at  $z = 0.71$ . We note that this rebrightening was discovered earlier ( $t \sim 12$  days) using ground-based facilities and interpreted as the emerging flux from an associated supernova (36, 156, 375).

### Associated Supernova

As discussed in §2.3.2, Stanek et al. (375) presented an extensive compilation of *R*-band observations which span the epoch of rebrightening. By removing the contribution from the afterglow, they find evidence for an associated SN with a peak magnitude  $\sim 0.1$  mag brighter than SN 1998bw and with a light-curve stretched by a factor of 1.35 in time.

To confirm this result, we compared our redshifted template SN light-curves with our late-time *HST* observations and found that an associated SN 1998bw-like supernova would be  $\sim 0.2$  mag brighter than the *HST* observation at  $t \sim 27$  days, while SN 1994I- and SN 2002ap-like supernova light-curves are fainter by  $\sim 1.4$  and  $\sim 2.3$  magnitudes, respectively. In an effort to characterize the light-curve of the associated SN, we fit the *HST* observations in a manner similar to that done for GRB 040924 (§2.3.1). By fitting the *HST* *I*- and *z*-band data simultaneously, we find a best fit solution ( $\chi_r^2 \approx 0.4$ ) for a SN 1998bw-like supernova dimmed by  $\sim 0.3$  magnitudes. We emphasize that this fit does not include any stretching of the light-curve. Moreover, we find no improvement in the quality of the fit when template stretching is included. This result is inconsistent with the findings of Stanek et al. (375). We attribute this discrepancy to contamination from the host

and nearby galaxy (see Figure 2.4) which plagues the Stanek et al. (375) late-time photometry.

We note that the presence of host galaxy extinction would imply that the associated SN was brighter than our estimates. We use the optical/IR afterglow observations to constrain the host galaxy extinction in a manner similar to that performed for GRB 040924 (§2.3.1). However, in this case, the observed spectral index ( $\beta_{\text{opt/IR}} \approx -0.5$ ) is comparable to the theoretical limit and is therefore consistent with negligible host galaxy extinction. We conclude that the supernova associated with GRB 041006 was  $\sim 0.3$  magnitudes fainter than SN 1998bw at maximum light and decayed at a comparable rate.

## 2.4 Discussion

In the sections above, we showed that GRBs 040924 and 041006 were each associated with a supernova similar to SN 1998bw but dimmed by  $\sim 1.5$  and  $\sim 0.3$  magnitudes, respectively. These two events clearly show that there is a significant spread in the luminosity of GRB-associated SNe, suggesting a dispersion in the production of  $^{56}\text{Ni}$ . Such a dispersion has already been observed for local SNe Ibc (316).

To better study this dispersion, we compile optical peak magnitudes (rest-frame) and  $^{56}\text{Ni}$  mass estimates for GRB/XRF-associated SNe and local SNe Ibc from the literature (Tables 2.5 and 2.6). In this compilation we consider all the GRB/XRF-associated SNe with spectroscopic redshifts of  $z \lesssim 1$ ; SN searches at higher redshifts are plagued by UV (rest-frame) line-blanketing. Since spectroscopic confirmation of the SN component is only available for the four nearest events in this sample (GRBs 980425, 020903, 031203, and 030329; see Table 2.5), photometric data is used to constrain the brightness of an associated SN. We note, however, that uncertainty associated with host galaxy extinction and decomposition of the afterglow emission from the SN can impose a non-negligible uncertainty in the estimated SN peak magnitude. For the local sample, we include only the

events with published photometry. The latter may impose a slight bias in favor of brighter and peculiar SNe<sup>2</sup>.

In Figure 2.6 (top panel), we show <sup>56</sup>Ni mass estimates and peak optical magnitudes for GRB/XRF-associated SNe and local SNe Ibc. From the figure, it is clear that (1) peak magnitude scales roughly with <sup>56</sup>Ni mass, and (2) GRB-associated SNe do not necessarily synthesize more <sup>56</sup>Ni than ordinary SNe Ibc.

We next compare their peak optical magnitudes, since the correlation between <sup>56</sup>Ni mass and peak optical magnitudes should manifest itself as a similar dispersion. In Figure 2.6 (bottom panel) we show a histogram of peak optical magnitudes for all GRB/XRF-associated SNe and local SNe Ibc. Examination of the two samples reveals noticeable overlap; while GRB/XRF-associated SNe tend to cluster toward the brighter end of the distribution, some of the faintest SNe Ibc observed are in fact associated with GRBs and XRFs (e.g., GRBs 010921, 040924, XRF 040701) and the most luminous events are actually drawn from the local sample. Apparently, GRB/XRF-associated SNe are not necessarily over-luminous in comparison with local SNe Ibc. Moreover, by assuming a rough scaling of <sup>56</sup>Ni production with peak optical magnitude, this implies a notable overlap between the two samples with respect to their dispersion in synthesized material, consistent with the data shown in the upper panel.

The following question naturally arises: are both GRB/XRF-associated SNe and local SNe Ibc drawn from the same population of events? To address this issue, we performed a Kolmogorov-Smirnov (K-S) test on the two sets of SN peak magnitudes. Our K-S test reveals that the probability the two samples have been drawn from the same parent population is  $\sim 91\%$ . It is therefore conceivable that both SNe Ibc and GRB/XRF-associated SNe belong to the same SN population, and thus share a common <sup>56</sup>Ni production mechanism.

This result may imply that GRB/XRF-associated SNe and local SNe Ibc share

---

<sup>2</sup>Three of the thirteen local SNe Ibc included in this compilation were published as “luminous” events. By removing them from the local sample, the probability that both GRB/XRF-associated SNe and local SNe are drawn from the same parent population is reduced to  $\sim 50\%$ .

a common progenitor system and/or explosion mechanism. Yet we know from radio observations of local SNe that most Type Ibc's lack the engine-driven relativistic ejecta observed in GRBs (26, 357, 369). This may be accounted for in the spherical+jet paradigm where the production of  $^{56}\text{Ni}$  and relativistic ejecta are independent parameters of the explosion, each of which can be individually tuned. Additional studies of both GRB/XRF-associated SNe and local SNe Ibc will enable us to better map out this two-dimensional parameter space and address in detail the nature of the progenitors and explosion mechanisms.

The authors are grateful for support under the Space Telescope Science Institute grant HST-GO-10135. A.M.S. acknowledges support by the NASA Graduate Student Researchers Program. E.B. is supported by NASA through Hubble Fellowship grant HST-HF-01171.01 awarded by the STScI, which is operated by the Association of Universities for Research in Astronomy, Inc., for NASA, under contract NAS 5-26555. A.G. acknowledges support by NASA through Hubble Fellowship grant #HST-HF-01158.01-A awarded by STScI. KR is supported by the Gemini Observatory, which provided observations presented in this paper, and which is operated by the Association of Universities for Research in Astronomy, Inc., under a cooperative agreement with the NSF on behalf of the Gemini partnership: the National Science Foundation (United States), the Particle Physics and Astronomy Research Council (United Kingdom), the National Research Council (Canada), CONICYT (Chile), the Australian Research Council (Australia), CNPq (Brazil), and CONICET (Argentina).

Table 2.1. *HST* Observation Log

Target	Date Obs (UT)	$\Delta t$ (days)	Exp. Time (sec)	Filter	<i>HST</i> mag <sup>a</sup> (AB)	Extinction <sup>b</sup> $A_\lambda$	Johnson mag <sup>c</sup> (Vega)
GRB040924	2004 November 2.4	38.9	3064	F775W	$26.44 \pm 0.23$	$A_I = 0.113$	$I = 25.75 \pm 0.23$
—	2004 November 2.5	39.0	3211	F850LP	$25.60 \pm 0.11$	$A_z = 0.106$	$z = 24.96 \pm 0.11$
—	2004 November 26.5	63.0	3932	F775W	$> 27.59$	$A_I = 0.113$	$I > 26.90$
—	2005 February 18.5	147.0	3932	F775W	—	—	—
—	2005 February 19.5	148.0	3932	F850LP	—	—	—
GRB041006	2004 November 2.3	26.7	3832	F775W	$24.01 \pm 0.05$	$A_I = 0.044$	$I = 23.47 \pm 0.05$
—	2004 November 2.3	26.7	3430	F850LP	$23.58 \pm 0.04$	$A_z = 0.041$	$z = 23.01 \pm 0.04$
—	2004 November 27.4	51.9	4224	F775W	$25.11 \pm 0.10$	$A_I = 0.044$	$I = 24.57 \pm 0.10$
—	2004 December 23.4	77.8	4224	F775W	$25.83 \pm 0.19$	$A_I = 0.044$	$I = 25.29 \pm 0.19$
—	2005 February 10.3	126.8	4224	F775W	$26.26 \pm 0.25$	$A_I = 0.044$	$I = 25.73 \pm 0.25$
—	2005 February 11.2	127.7	4224	F850LP	$25.90 \pm 0.21$	$A_z = 0.041$	$z = 25.32 \pm 0.21$

<sup>a</sup>AB system magnitudes in the *HST* filters given in column 5. Photometry was done on residual images (see §2.3). We have assumed the source flux to be negligible in the final (template) epoch for GRB040924. For GRB041006, we estimated the source flux in the template epoch using PSF photometry and corrected the residual photometry accordingly. All represent observed magnitudes, not corrected for foreground extinction.

<sup>b</sup>Galactic extinction from Schlegel et al. (344).

<sup>c</sup>Magnitudes from column 6, converted to the Vega system and corrected for foreground extinction using  $A_\lambda$  given in column

7.

Table 2.2. Palomar 60-inch *R*-band Observations of GRB 040924

Date Obs (UT)	$\Delta t$ (days)	Magnitude <sup>a</sup>
2004 September 24.506	0.011	$17.8 \pm 0.1$
2004 September 24.509	0.014	$17.9 \pm 0.1$
2004 September 24.512	0.017	$18.0 \pm 0.1$
2004 September 24.513	0.018	$18.1 \pm 0.1$
2004 September 24.514	0.019	$18.0 \pm 0.1$
2004 September 24.517	0.022	$18.1 \pm 0.1$
2004 September 24.519	0.024	$18.2 \pm 0.1$
2004 September 24.526	0.030	$18.5 \pm 0.1$
2004 September 24.527	0.032	$18.5 \pm 0.1$
2004 September 24.530	0.035	$18.6 \pm 0.1$
2004 September 24.539	0.044	$19.0 \pm 0.1$
2004 September 24.875	0.380	$21.9 \pm 0.1$
2004 September 24.894	0.399	$22.1 \pm 0.1$
2004 September 24.909	0.414	$22.2 \pm 0.1$
2004 September 24.926	0.430	$22.1 \pm 0.1$
2004 September 24.942	0.447	$22.2 \pm 0.1$
2004 September 24.957	0.462	$22.3 \pm 0.1$
2004 September 24.972	0.477	$22.3 \pm 0.1$
2004 September 24.988	0.493	$22.2 \pm 0.1$
2004 September 25.003	0.508	$22.4 \pm 0.1$
2004 September 25.018	0.523	$22.5 \pm 0.1$

Table 2.2—Continued

Date Obs (UT)	$\Delta t$ (days)	Magnitude <sup>a</sup>
2004 September 25.036	0.540	$22.5 \pm 0.1$
2004 September 25.050	0.555	$22.7 \pm 0.1$
2004 September 25.066	0.571	$22.6 \pm 0.1$
2004 September 25.081	0.586	$22.4 \pm 0.1$
2004 September 25.097	0.602	$22.4 \pm 0.1$
2004 September 25.224	0.729	$22.6 \pm 0.1$

<sup>a</sup>Corrected for Galactic extinction according to Schlegel et al. (344).

Table 2.3. *SSO* 40-inch and 2.3-meter Observations of GRB 041006

Date Obs (UT)	$\Delta t$ (days)	Filter	Telescope	Magnitude <sup>a</sup>
2004 October 6.537	0.024	<i>V</i>	40-inch	$18.11 \pm 0.02$
2004 October 6.541	0.028	<i>V</i>	40-inch	$18.20 \pm 0.04$
2004 October 6.546	0.033	<i>V</i>	40-inch	$18.29 \pm 0.02$
2004 October 6.550	0.037	<i>V</i>	40-inch	$18.38 \pm 0.03$
2004 October 6.555	0.042	<i>V</i>	40-inch	$18.48 \pm 0.03$
2004 October 6.582	0.069	<i>B</i>	40-inch	$19.18 \pm 0.07$
2004 October 6.586	0.073	<i>B</i>	40-inch	$19.24 \pm 0.06$
2004 October 6.590	0.077	<i>B</i>	40-inch	$19.29 \pm 0.07$
2004 October 6.595	0.082	<i>V</i>	40-inch	$18.99 \pm 0.03$
2004 October 6.605	0.092	<i>H</i>	2.3-meter	$17.16 \pm 0.07$
2004 October 6.612	0.099	<i>H</i>	2.3-meter	$17.12 \pm 0.06$
2004 October 6.620	0.107	<i>H</i>	2.3-meter	$17.19 \pm 0.06$
2004 October 6.627	0.114	<i>H</i>	2.3-meter	$17.47 \pm 0.06$
2004 October 6.635	0.122	<i>H</i>	2.3-meter	$17.43 \pm 0.07$

<sup>a</sup>Corrected for Galactic extinction according to Schlegel et al. (344). *B*- and *V*-band photometry is relative to the field calibration by Henden (183) while the *H*-band photometry is relative to 2MASS.

Table 2.4. GRB 041006 Spectroscopic Lines

Observed Wavelength ( $\text{\AA}$ )	Equivalent Width ( $\text{\AA}$ )	Line ID	Rest Wavelength ( $\text{\AA}$ )
4798.16	4.4	Mg II	$\lambda$ 2796
4810.35	3.9	Mg II	$\lambda$ 2803
6396.31	1.7	[O II]	$\lambda$ 3727
6750.32	1.4	Ca II	$\lambda$ 3935
6810.06	1.1	Ca II	$\lambda$ 3970

Table 2.5. Peak Magnitudes and  $^{56}\text{Ni}$  Masses for GRB- and XRF-associated SNe

GRB Name	Redshift ( $z$ )	$M_{V,\text{peak}}^a$ (mag)	Ref.	$^{56}\text{Ni}$ Mass ( $M_{\odot}$ )	Ref.
GRB 970228	0.695	$-18.16^{+0.54}_{-0.52}$	Zeh et al. (447)	—	—
GRB 980425	0.0085	$-19.13 \pm 0.05$	Galama et al. (151)	$0.6 \pm 0.1$	Iwamoto et al. (193), Woosley et al. (1999)
GRB 980703	0.966	$-19.68^{+1.44}_{-0.60}$	Zeh et al. (447)	—	—
GRB 990712	0.434	$-18.02^{+0.23}_{-0.19}$	Zeh et al. (447)	—	—
GRB 991208	0.706	$-18.86^{+0.72}_{-0.29}$	Zeh et al. (447)	—	—
GRB 000911	1.058	$-18.26^{+0.12}_{-0.14}$	Zeh et al. (447)	—	—
GRB 010921	0.45	$< -17.80$	Price et al. (300)	—	—
GRB 011121	0.36	$-18.83^{+0.07}_{-0.10}$	Zeh et al. (447)	—	—
GRB 020405	0.698	$-18.63^{+0.19}_{-0.14}$	Zeh et al. (447)	—	—
XRF 020903	0.251	$-18.53 \pm 0.5$	Soderberg et al. (363)	—	—
GRB 021211	1.006	$-18.42^{+1.15}_{-0.55}$	Zeh et al. (447)	—	—

Table 2.5—Continued

GRB Name	Redshift ( $z$ )	$M_{V,\text{peak}}^a$ (mag)	Ref.	$^{56}\text{Ni}$ Mass ( $M_{\odot}$ )	Ref.
GRB 030329	0.169	$-18.83 \pm 0.30$	Deng et al. (100), Lipkin et al. (229)	$0.40^{+0.15}_{-0.10}$	Deng et al. (100)
GRB 031203	0.1055	$-19.63 \pm 0.15$	Malesani et al. (237)	—	—
XRF 040701	0.2146	$< -15.95$	Soderberg et al. (363)	—	—
GRB 040924	0.859	$-17.63 \pm 0.10$	this paper	—	—
GRB 041006	0.716	$-18.83 \pm 0.05$	this paper	—	—

<sup>a</sup>Assuming a SN 1998bw-like light-curve with no additional stretching.

Table 2.6. Peak Magnitudes and  $^{56}\text{Ni}$  Masses for Nearby SNe Ibc

SN Name	$M_{V,\text{peak}}$ (mag)	Ref.	$^{56}\text{Ni}$ Mass ( $M_{\odot}$ )	Ref.
SN 1983N	$-18.89 \pm 0.57^{\text{a}}$	Clocchiatti et al. (86)	0.25	Gaskell et al. (157)
SN 1983V	$-18.61 \pm 0.41$	Clocchiatti et al. (87)	—	—
SN 1984L	$-18.50 \pm 0.10$	Tsvetkov (400)	$0.20 \pm 0.05$	Baron et al. (10)
SN 1987M	$-19.40 \pm 0.5$	Filippenko et al. (118)	0.26	Swartz et al. (386)
SN 1990B	$-17.91 \pm 0.3$	Clocchiatti et al. (85)	—	—
SN 1991D	$-19.6 \pm 0.6$	Benetti et al. (14)	0.7	Benetti et al. (14)
SN 1992ar	$-19.7 \pm 0.5$	Clocchiatti et al. (84)	$0.5^{+0.25}_{-0.18}$	Clocchiatti et al. (84)
SN 1994I	$-17.69 \pm 0.58^{\text{b}}$	Richmond et al. (317)	$0.07 \pm 0.035$	Iwamoto et al. (195)
SN 1997ef	$-17.1 \pm 0.2$	Iwamoto et al. (194)	$0.15 \pm 0.03$	Iwamoto et al. (194)
SN 1999as	$-21.4 \pm 0.2$	Hatano et al. (178)	$4.0 \pm 0.5^{\dagger}$	Hatano et al. (178)
SN 1999ex	$-17.86 \pm 0.26$	Stritzinger et al. (383)	0.16	Hamuy et al. (176)
SN 2002ap	$-17.4 \pm 0.4^{\text{c}}$	Foley et al. (122)	$0.07 \pm 0.02$	Mazzali et al. (249)

Table 2.6—Continued

SN Name	$M_{V,\text{peak}}$ (mag)	Ref.	$^{56}\text{Ni}$ Mass ( $M_{\odot}$ )	Ref.
SN 2003L	$-18.18 \pm 0.2$	Soderberg <i>et al.</i> , (in prep)	—	—

<sup>a</sup>Absolute magnitude brightened by 1.22 mag to be in agreement with the distance assumed by Gaskell et al. (157).

<sup>b</sup>Absolute magnitude dimmed by 0.4 mag to be in agreement with the distance assumed by Iwamoto et al. (195).

<sup>c</sup>Absolute magnitude brightened by 0.2 mag to be in agreement with the distance assumed by Mazzali et al. (249).

<sup>d</sup>Given the similarity of the SN 1999as light-curve to Type IIIn events, it has been suggested that circumstellar interaction contributes to the bright peak luminosity observed for this SN. While there is still no direct indication of such interaction from optical spectra (no narrow emission lines), it is estimated that the explosion must have produced at least  $\sim 1 M_{\odot}$  even after correcting for any CSM interaction (Daniel Kasen, PhD thesis).

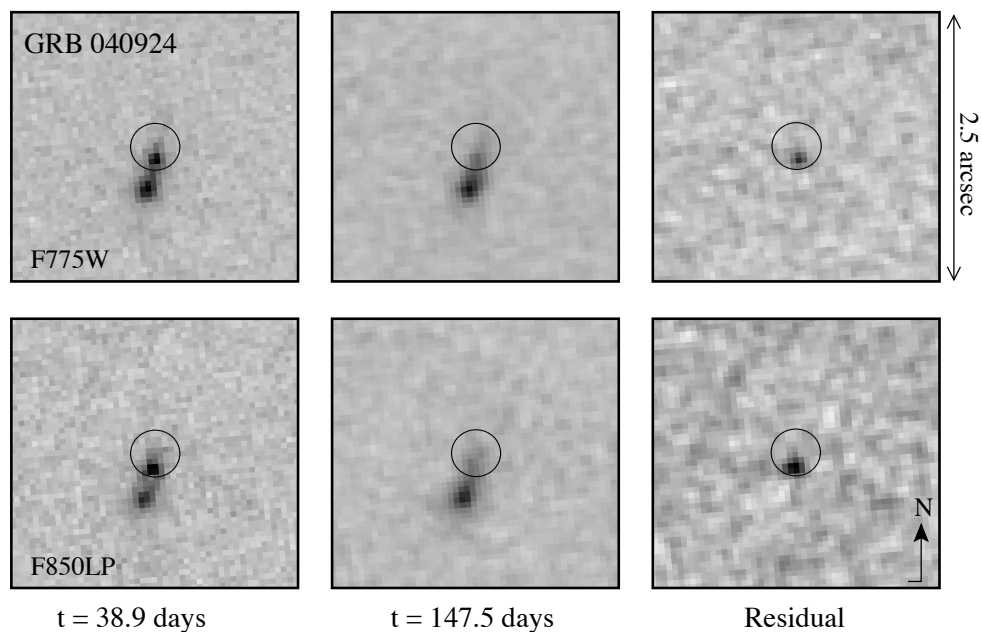


Figure 2.1: Six-panel frame showing *HST/ACS* imaging for GRB 040924 at  $t \sim 38.9$  days (Epoch 1) and  $t \sim 147.5$  days (Epoch 3) in the F775W and F850LP filters. By subtracting Epoch 3 images from those of Epoch 1, we produced the residual images shown above. We have applied the same stretch to all frames. As clearly shown in the residual images, a transient source is detected coincident with the 0.22 arcsec ( $2\sigma$ ) optical afterglow position (circle).

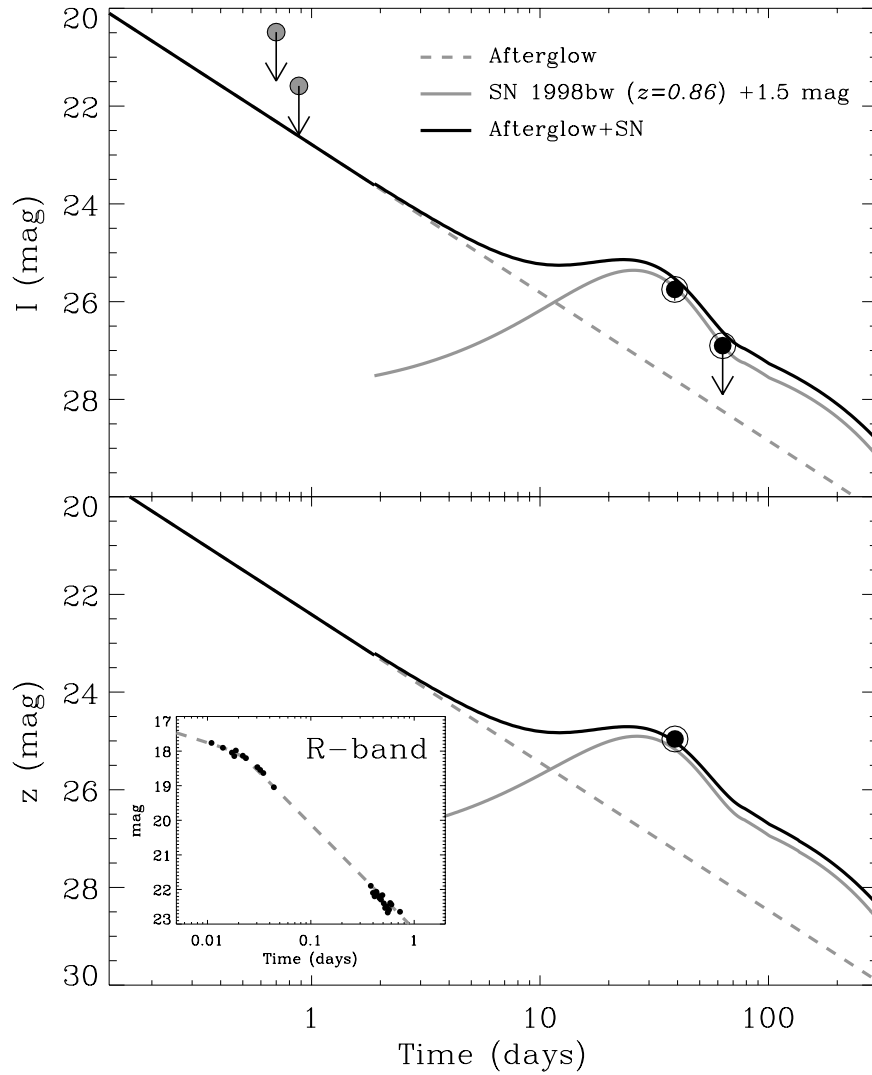


Figure 2.2: As discussed in §2.3.1, we fit a broken-power law model to our Palomar 60-inch  $R$ -band afterglow data reported in Table 2.2 (inset). Adopting a spectral index of  $\beta \approx -0.7$  we then extrapolate the  $R$ -band afterglow fit to the  $I$ - and  $z$ -bands (grey dashed lines). Extinction-corrected data compiled from the GCNs and are overplotted (grey arrows; Silvey et al. 348). We fit the late-time  $HST$  data (encircled black dots) by summing the contribution from the afterglow model plus that from a supernova. We find a best fit (solid black lines) by including a SN 1998bw-like supernova (grey solid lines) redshifted to  $z = 0.86$  and dimmed by  $\sim 1.5$  magnitudes.

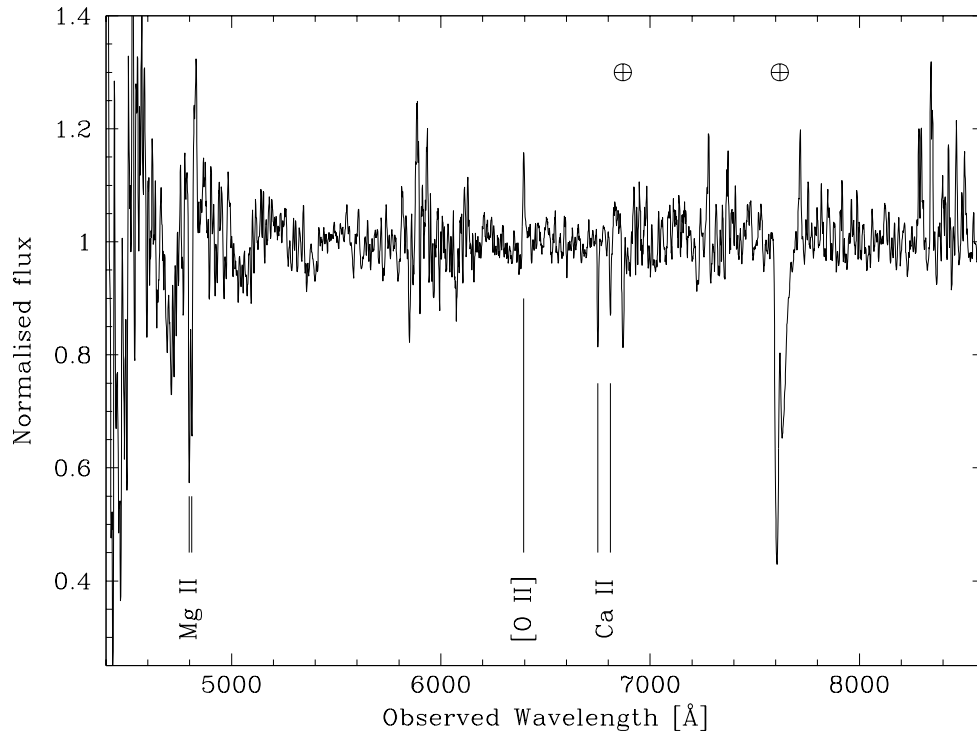


Figure 2.3: Gemini/GMOS spectrum of the optical afterglow for GRB 041006 at  $t \approx 0.85$  days. Based on three absorption features and one emission line, we determine the redshift of the host galaxy to be  $z = 0.716$ , consistent with the earlier report of  $z = 0.712$  by Fugazza et al. (143).

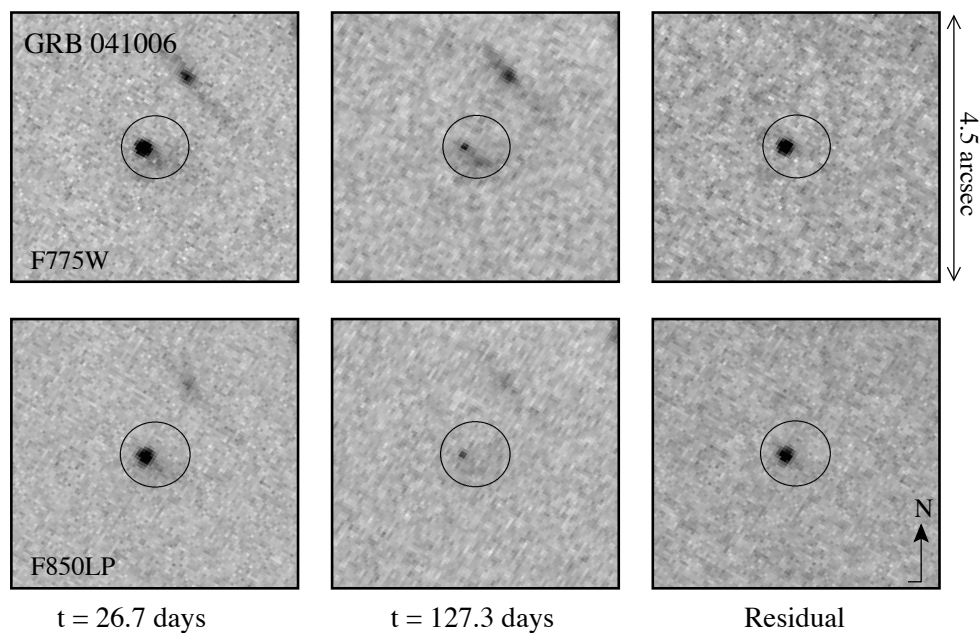


Figure 2.4: Six-panel frame showing *HST/ACS* imaging for GRB041006 at  $t \sim 26.7$  days (Epoch 1) and  $t \sim 127.3$  days (Epoch 4) in the F775W and F850LP filters. By subtracting Epoch 4 images from those of Epoch 1, we produced the residual images shown above. We have applied the same stretch to all frames. As clearly shown in the residual images, a transient source is detected coincident with the 0.53 arcsec ( $2\sigma$ ) optical afterglow position (circle).

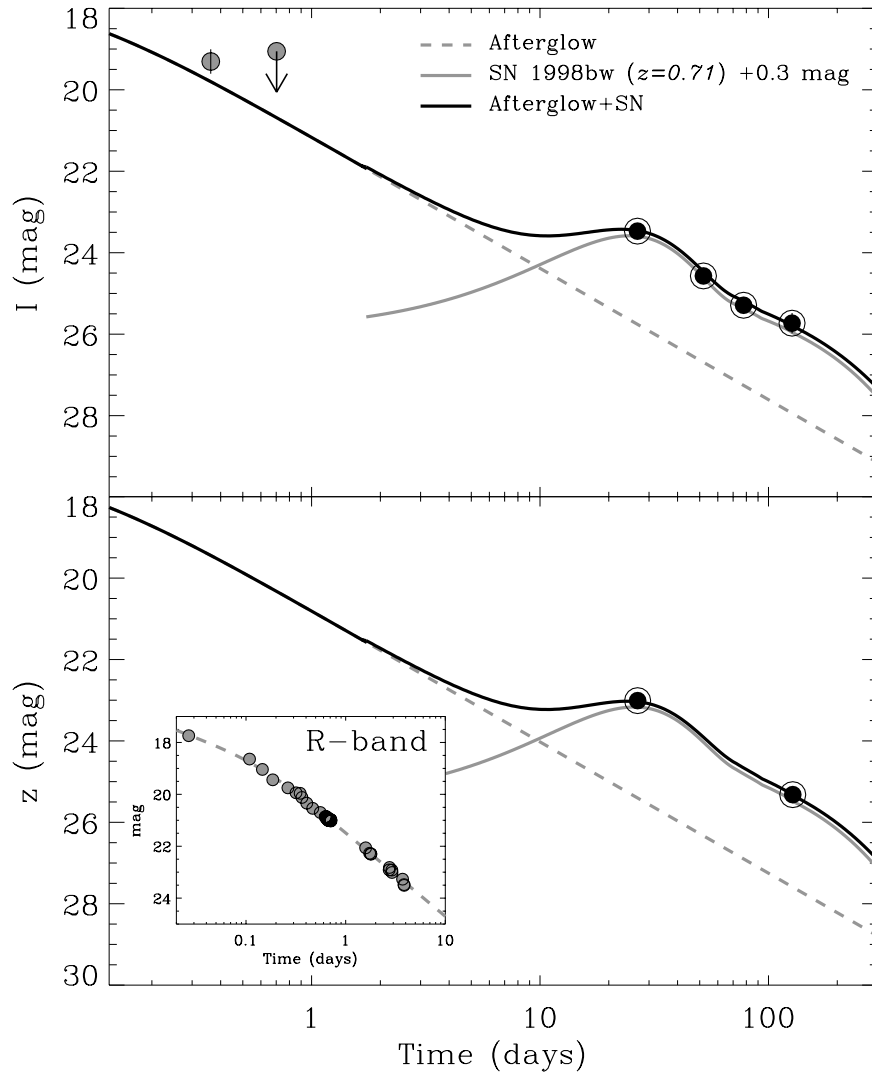


Figure 2.5: Adopting the  $R$ -band afterglow data reported in Stanek et al. (375), we reproduce their broken-power law fit (inset). Adopting a spectral index of  $\beta \approx -0.5$  we then extrapolate the  $R$ -band afterglow fit to the  $I$ - and  $z$ -bands (grey dashed lines). Extinction-corrected data have been compiled from the GCNs are overplotted (grey circles; Ferrero et al. 112, Hoversten et al. 189). We fit the late-time  $HST$  data (encircled black dots) by summing the contribution from the afterglow model plus that from a supernova. We find a best fit (solid black lines) by including a SN 1998bw-like supernova (grey solid lines) redshifted to  $z = 0.71$  and dimmed by  $\sim 0.3$  magnitudes.

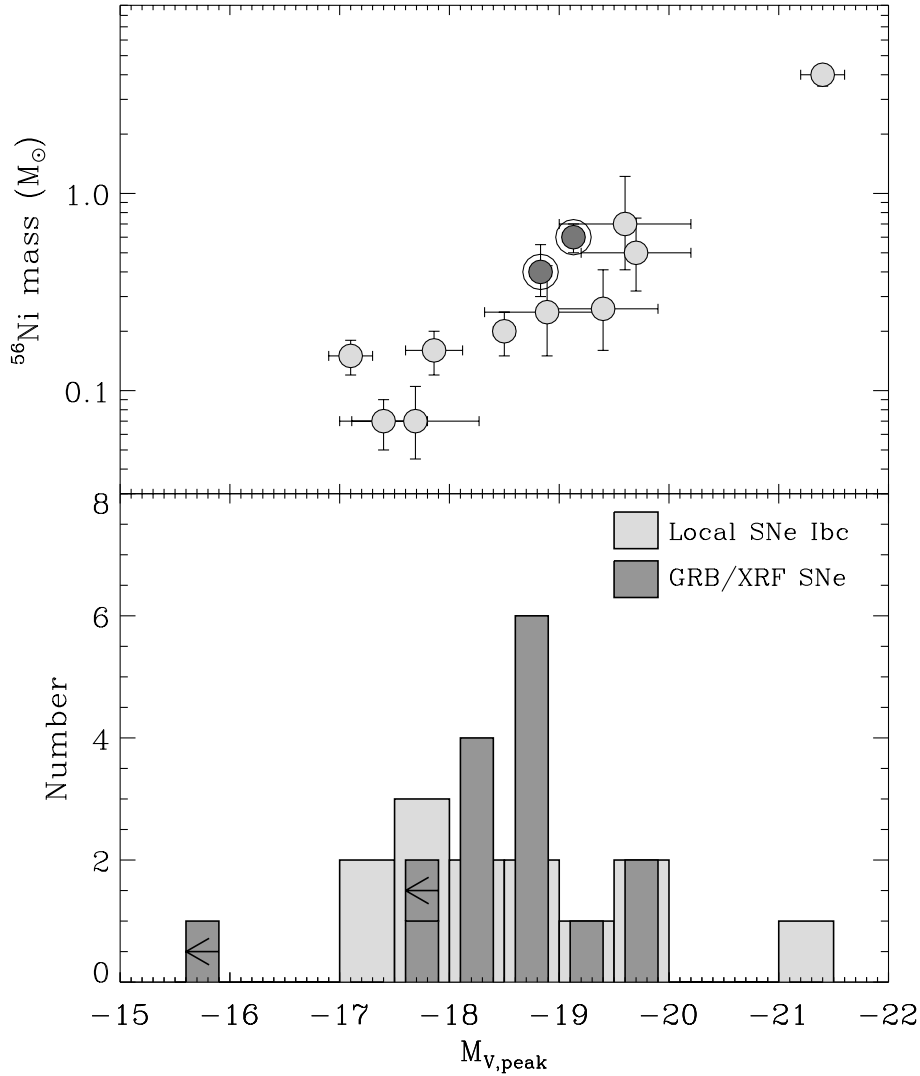


Figure 2.6: Top panel: rest-frame optical peak magnitudes for GRB-associated SNe (encircled dots) and local SNe Ibc (grey circles) have been compiled from the literature (Tables 2.5 and 2.6) and are plotted against the mass of  $^{56}\text{Ni}$  synthesized in the explosion. For  $^{56}\text{Ni}$  estimates without errors, we adopt the fractional uncertainty associated with the peak luminosity. Peak optical magnitudes clearly trace the mass of  $^{56}\text{Ni}$  ejected. Apparently, GRB-associated SNe do not necessarily produce more  $^{56}\text{Ni}$  than ordinary local SNe Ibc. Bottom panel: histogram of peak optical magnitudes for GRB/XRF-associated SNe and local SNe Ibc. There is a significant overlap between the two samples. Our K-S test reveals that there is a  $\sim 91\%$  probability the two samples are drawn from the same population.

Part IV

A Large Radio Survey of Type  
Ibc Supernovae

A Large Radio Survey of Type Ibc Supernovae

## Chapter 1

# The Radio and X-ray Luminous Type Ibc Supernova 2003L<sup>†</sup>

A. M. SODERBERG<sup>a</sup>, S. R. KULKARNI<sup>a</sup>, E. BERGER<sup>b</sup>, R. A. CHEVALIER<sup>c</sup>,  
D. A. FRAIL<sup>d</sup>, D. B. FOX<sup>a</sup>, R. C. WALKER<sup>d</sup>

<sup>a</sup>Division of Physics, Mathematics and Astronomy, 105-24, California Institute of Technology,  
Pasadena, CA 91125, USA

<sup>b</sup>Observatories of the Carnegie Institution of Washington, 813 Santa Barbara St., Pasadena, CA  
91101, USA

<sup>c</sup>Department of Astronomy, University of Virginia, P.O. Box 3818, Charlottesville, VA  
22903-0818, USA

<sup>d</sup>National Radio Astronomy Observatory, Socorro, NM 87801, USA

## Abstract

We present extensive radio observations of SN 2003L, the most luminous and energetic Type Ibc radio supernova with the exception of SN 1998bw (associated with GRB 980425). Observations from the Very Large Array are well described by a fitting a synchrotron self-absorption model to the emission spectrum. This model

---

<sup>†</sup>A version of this chapter was published in *The Astrophysical Journal*, vol. 621, 908–920, (2005). Reproduced by permission of the AAS.

implies a sub-relativistic ejecta velocity,  $\bar{v} \approx 0.2c$ , and a size of  $r \approx 4.3 \times 10^{15}$  cm at  $t \approx 10$  days. The circumstellar density is suitably fit with a stellar wind profile,  $n_e \propto r^{-2}$  cm $^{-3}$  and a constant mass loss rate of  $\dot{M} \approx 7.5 \times 10^{-6}$  M $_{\odot}$  yr $^{-1}$ . Moreover, the magnetic field follows  $B \propto r^{-1}$  and the kinetic energy of the radio bright ejecta is roughly  $E \approx 10^{48}$  erg assuming equipartition of energy between relativistic electrons and magnetic fields. Furthermore, we show that free-free absorption does not contribute significantly to the radio spectrum, since it implies ejecta velocities which are inconsistent with size constraints derived from Very Long Baseline Array observations. In conclusion, we find that although SN 2003L has a radio luminosity comparable to that seen in SN 1998bw, it shows no evidence for a significant amount of energy coupled to relativistic ejecta. Using SN 2003L as an example, we comment briefly on the coupling of ejecta velocity and energy in Type Ibc supernovae.

## 1.1 Introduction

Radio emission from core-collapse supernovae (SNe) have been sought primarily to study the circumstellar medium (421, 71). However, starting with Type Ibc SN 1998bw, associated with the under-luminous gamma-ray burst GRB 980425 (290, 151, 216), radio observations have also been used a tracer of relativistic ejecta (216, 226). This event prompted a storm of publications: SN 1998bw was the most luminous radio supernova (at early times), showed strong variability and produced copious gamma-ray emission relative to ordinary SNe Ibc. These data provided the first observational evidence that at least some SNe Ibc are associated with GRBs (e.g., Bloom et al. 42, Bloom et al. 47, Stanek et al. 377, c.f. Price et al. 300).

To further explore the connection between GRBs and SNe Ibc, we began a radio survey of local Type Ibc supernovae. Our survey was motivated by two simple phenomenological questions: [1] What is the prevalence of SN 1998bw-like supernovae?, [2] Is there a continuum between ordinary SNe and GRBs as traced

by their relativistic ejecta?

In Berger et al. (26) we reported the first three years of the survey. We found that most SNe Ibc are not detectable with current radio sensitivity, with limits reaching  $10^{-3}$  that of the peak brightness of SN 1998bw. Clearly, luminous SN 1998bw-like supernovae are rare (less than 3%) and those within an order of magnitude of SN 1998bw are uncommon (less than 10%).

Here, we present radio observations of SN 2003L, the first SN Ibc with a radio luminosity comparable to SN 1998bw. While there is no evidence for mildly-relativistic ejecta, the radio emitting ejecta of SN 2003L are unusually energetic. This discovery suggests the existence of a sub-class of SNe Ibc with similar energetics to SN 1998bw and even weaker central engines, if any.

The organization of this paper is as follows: observations from the Very Large Array (VLA), the Very Long Baseline Array (VLBA) and the *Chandra* X-ray Observatory (CXO) are described in §3.2 and §1.3. Preliminary estimates of the energy and velocity are presented in §2.3. Modeling of the radio light-curves is discussed in §2.5 and §1.6 assuming the dominant absorption is from internal synchrotron self-absorption and external free-free absorption, respectively. Modeling of the X-ray emission follows as §2.7. In the Discussion (§3.6) we conclude by addressing the nature of SN 2003L.

## 1.2 Radio Observations of SN 2003L

### 1.2.1 Very Large Array Data

SN 2003L was optically discovered on 2003 January 12.15 UT, offset  $9''.0$  W and  $1''.5$  N from the center of NGC 3506 (50) and at a distance of  $d \approx 92$  Mpc (405). In our first observation with the Very Large Array<sup>1</sup> (VLA), on 2003 January 26.2 UT, we detected a radio source coincident with the optical position at  $\alpha(\text{J2000}) =$

---

<sup>1</sup>The Very Large Array and Very Long Baseline Array are operated by the National Radio Astronomy Observatory, a facility of the National Science Foundation operated under cooperative agreement by Associated Universities, Inc.

$11^{\text{h}}03^{\text{m}}12.3^{\text{s}}, \delta(\text{J2000}) = +11^{\circ}04'38.1''$  ( $\pm 0.1$  arcsec in each coordinate) with flux density of  $f_{\nu} = 743 \pm 39 \mu\text{Jy}$  at 8.5 GHz. This, and subsequent observations at 4.9, 8.5, 15.0, and 22.5 GHz, are summarized in Table 1.

All observations were taken in standard continuum observing mode with a bandwidth of  $2 \times 50$  MHz. We used 3C286 for flux calibration, and for phase referencing we used calibrators J1118+125, J1120+134, and J1103+119. Data were reduced using standard packages within the Astronomical Image Processing System (AIPS).

As seen in Table 1, observations were taken in each of the four VLA configurations. The decreased spatial resolution of the C and D configurations resulted in detection of diffuse host galaxy emission surrounding the supernova, primarily affecting the low ( $\leq 8.5$  GHz) frequency observations (Figure 1.1). At 8.5 GHz the host galaxy extends  $45 \times 45$  arcsec, but is resolved away on baselines  $\geq 10$  k $\lambda$ . By restricting the UV range to exclude shorter baselines, we measured the flux density of the supernova with minimal contribution from the host galaxy. Measurements at higher frequencies and in other VLA configurations were made by fitting a Gaussian to the SN emission and solving for the integrated intensity.

Figure 2.3 shows the SN 2003L radio light-curves assuming an approximate explosion date of 2003 January 1.0 UT as derived from optical data (W. Li, private communication). The radio light-curves evolve as  $f_{\nu} \propto t^{1.2}$  before the peak, exhibit a broad maximum and fade as  $f_{\nu} \propto t^{-1.2}$ . The spectral index ( $\beta$  with  $f_{\nu} \propto \nu^{\beta}$ ) is observed as  $\beta \approx -1.1$  in the optically thin regime (Figure 1.3).

### 1.2.2 Very Long Baseline Array Data

Complimentary to our VLA campaign, we obtained a single observation of SN 2003L using the Very Large Baseline Array (VLBA). The six hour observation began on 2003 March 7.30 UT ( $t \approx 65$  days), and was taken in standard continuum mode with a bandwidth of  $4 \times 8$  MHz centered on the observing frequency of 4.9 GHz. Fringe calibrations were applied using 3C273 and phase referencing was conducted using J1103+1158 at an angular distance of 0.9 degrees from the SN.

We detect SN 2003L at a position of  $\alpha = 11^{\text{h}}03^{\text{m}}12^{\text{s}}.3008$ ,  $\delta = +11^{\circ}04'38''.08$  (J2000.0) with a positional uncertainty of 10 mas in each coordinate (Figure 1.4). We note that these errors are dominated by the positional uncertainty of J1103+1158, assumed to be at  $\alpha = 11^{\text{h}}03^{\text{m}}03^{\text{s}}.5299$ ,  $\delta = +11^{\circ}58'16''.61$  (J2000.0). Using the VLBA utilities within AIPS, we find a flux density for the supernova of  $F_{4.9 \text{ GHz}} = 848 \pm 64 \mu\text{Jy}$  within the  $3.158 \times 1.285$  mas beam. We note that there is no emission from the host galaxy at this resolution. At a distance of 92 Mpc, this unresolved VLBA detection places a direct constraint on the size of the expanding ejecta of  $r \lesssim 9.1 \times 10^{17}$  cm and an average expansion speed of  $\bar{v} \leq 5.4c$  during the first 65 days after the explosion.

### 1.3 X-ray Observations with Chandra

We observed SN 2003L with the *Chandra* ACIS-S detector beginning at 2003 February 10.15 UT ( $t \approx 40$  days). During the 30 ksec observation, we detected  $30 \pm 6$  counts from the supernova (214). For spectral extraction we adopt a source aperture of 2.46 arcsec, which encloses approximately 98% of the flux of an on-axis point-source at 1 keV (the peak of our raw photon counts spectrum). Our aperture correction is therefore minimal by comparison to our  $\sim 20\%$  flux uncertainties (see below). Background counts are selected from an annular region extending from 2.46 arcsec to 7.38 arcsec from the source; in general larger background regions are preferred for *Chandra* data analysis but the extended emission from the host galaxy makes a more local selection preferable in this case (see Figure 1.5).

Schlegel et al. (344) dust maps give  $E(B - V) = 0.021$  mag for the location of SN 2003L. Dickey and Lockman (103) suggest an average  $N_{\text{H}}$  of  $2.25 \times 10^{20} \text{cm}^{-2}$ , while a direct conversion from the Schlegel et al. optical reddening suggests  $1.13 \times 10^{20} \text{cm}^{-2}$  (299). We fix  $N_{\text{H}}$  for our fits at  $2.5 \times 10^{20} \text{cm}^{-2}$ .

For a power-law spectral fit we find the power-law photon index  $\Gamma = 1.53 \pm 0.4$  (range is 0.86 to 2.24 at 90% confidence). For a thermal bremsstrahlung spectral fit we find the plasma temperature has  $kT > 1.7$  keV at 90% confidence, with a best-

fit value of 6.7 keV that is unconstrained from higher energies. The relatively small number of counts enables satisfactory fits (reduced chi-squared values of  $\chi_r^2 \approx 1.3$ ; 5 degrees of freedom) for both models, with the neutral hydrogen absorption applied to either a power-law or thermal bremsstrahlung continuum.

Our source count rate is  $1.0 \pm 0.2$  cts/ksec in the ACIS-S3 detector. This corresponds to a 0.5–5.0 keV flux for our spectral models of approximately  $5.3 \times 10^{-15}$  erg/cm<sup>2</sup>/s in either case. Extrapolating to the full 2–10 keV X-ray band, the corresponding fluxes are  $9.2 \times 10^{-15}$  erg/cm<sup>2</sup>/s for the power law model and  $7.6 \times 10^{-15}$  erg/cm<sup>2</sup>/s for the thermal bremsstrahlung model. The associated X-ray luminosity is thus  $L_{2-10 \text{ keV}} \approx 9.2 \times 10^{39}$  erg/s and  $7.2 \times 10^{39}$  erg/s for the power-law and thermal models, respectively. In comparison with other X-ray supernovae, SN 2003L is among the most luminous ever detected, only a factor of  $\sim 10$  fainter than SN 1998bw at a comparable epoch (290).

## 1.4 Preliminary Constraints

We are interested in the energy and expansion velocity of the ejecta producing the radio emission. As a preliminary constraint, we estimate the brightness temperature,  $T_B$ , of SN 2003L and compare it with robust constraints imposed by the Inverse Compton Catastrophe (ICC; Kellermann and Pauliny-Toth 203). The brightness temperature of a source with angular radius,  $\theta$  is given by

$$T_B = \left( \frac{c^2}{2\pi k} \right) \left( \frac{f_\nu}{\theta^2} \right) \nu^{-2} \text{ K} \quad (1.1)$$

Compact sources with  $T_B \gtrsim 10^{12}$  K cool rapidly via inverse Compton scattering. As an initial estimate for the physical size of the supernova, we first assume that the optical expansion velocity of 12000 km s<sup>-1</sup> (241) can be used as an average speed to describe the motion of the radio bright ejecta. Using our approximate explosion date, we estimate the shock radius to be  $r \approx 2.9 \times 10^{15}$  cm at  $t \approx 28$  days. For an observed flux density of  $f_\nu \approx 3.1$  mJy at  $\nu \approx 22.5$  GHz, the brightness temperature is  $T_B \approx 6.3 \times 10^{11}$  K, just below that of the inverse Compton catastrophe (ICC)

limit. This exercise provides no evidence for relativistic ejecta, therefore suggesting that SN 2003L expands with a modest sub-relativistic velocity.

For radio sources dominated by synchrotron-self absorption (SSA), the brightness temperature can be further constrained to  $T_B < 4 \times 10^{10}$  K. By assuming equipartition between the energy in electrons ( $\epsilon_e$ ) and magnetic fields ( $\epsilon_B$ ), we derive an estimate of the velocity and a lower limit on the kinetic energy of radio emitting material. This approach has been used extensively in discussion of extra-galactic sources and was more recently applied to supernovae (71, 216). The method requires three observables at any single epoch: the spectral peak frequency,  $\nu_p$ , the peak flux density,  $f_p$ , and the spectral index of the optically thin emission,  $f_\nu \propto \nu^\beta$ . Here,  $\beta \equiv -(p-1)/2$  for electrons accelerated into a power-law distribution,  $N(\gamma) \propto \gamma^{-p}$  above a minimum Lorentz factor,  $\gamma_m$ . Following Kulkarni et al. (216) and Berger et al. (22), the angular radius of the radiosphere,  $\theta_{\text{ep}}$ , and the equipartition energy,  $E_{\text{ep}}$ , are given by

$$\theta_{\text{ep}} \approx 120 \left( \frac{d}{\text{Mpc}} \right)^{-1/17} \left( \frac{f_p}{\text{mJy}} \right)^{8/17} \left( \frac{\nu_p}{1 \text{ GHz}} \right)^{(-2\beta-35)/34} \mu\text{as} \quad (1.2)$$

$$E_{\text{ep}} \approx 1.1 \times 10^{56} \left( \frac{d}{\text{Mpc}} \right)^2 \left( \frac{f_p}{\text{mJy}} \right)^4 \left( \frac{\nu_p}{1 \text{ GHz}} \right)^{-7} \left( \frac{\theta_{\text{ep}}}{\mu\text{as}} \right)^{-6} \text{erg}. \quad (1.3)$$

At  $t \approx 30$  days (our first epoch) the peak flux density is  $f_p \approx 3.2$  mJy at  $\nu_p \approx 22.5$  GHz. Using the observed optically thin spectral index of  $\beta \approx -1.1$ , Equations 1.2 and 1.3 give  $\theta_{\text{ep}} \approx 7.7 \mu\text{as}$  implying an equipartition radius of  $r_{\text{ep}} \approx 1.1 \times 10^{16}$  cm and an average expansion speed of  $\bar{v}_{\text{ep}} \approx 0.15c$ . The minimum energy of the ejecta is thus  $E_{\text{ep}} \approx 1.5 \times 10^{47}$  erg and the magnetic field is  $B_{\text{ep}} \approx 1.1$  G. These constraints alone demand that SN 2003L is among the most energetic Type Ibc supernovae in terms of radio-emitting ejecta, second only to SN 1998bw. We note that additional absorption terms (e.g., free-free absorption) and the inclusion of shocked protons serve to increase the equipartition energy estimate.

Equipartition analyses may also be used to roughly constrain the minimum

electron Lorentz factor and the characteristic synchrotron frequency,  $\nu_m$ . Equating particle kinetic energy across the shock discontinuity, we find

$$\epsilon_e \left(\frac{v}{c}\right)^2 m_p c^2 \approx \bar{\gamma} m_e c^2 \quad (1.4)$$

where  $\bar{\gamma}$  is the average Lorentz factor of the electrons and  $v$  is the velocity of the ejecta. Assuming roughly  $\bar{\gamma} \approx \gamma_m$  and substituting Equation 1.24 for  $\gamma_m$ , we derive the following estimate for the characteristic synchrotron frequency,  $\nu_m$ ,

$$\nu_m \approx \epsilon_e^2 \left(\frac{v}{c}\right)^4 \left(\frac{m_p}{m_e}\right)^2 \left(\frac{eB}{2\pi m_e c}\right) \text{ Hz.} \quad (1.5)$$

Adopting the values derived from equipartition analyses ( $v \approx 0.15c$ ,  $B = 1.1 \text{ G}$  and  $\epsilon_e = 0.5$ ), we find roughly  $\nu_m \approx 1 \text{ GHz}$  at  $t \approx 30 \text{ days}$  which is below our observing band.

## 1.5 Internal Synchrotron Self-absorption

In the Appendix we present a rigorous formulation of the temporal and spectral evolution of synchrotron emission arising from sub-relativistic supernova ejecta. This prescription, based on the formalism of Frail et al. (135), is generalized to include the cases where  $\nu_m$ , is greater than the self-absorption frequency,  $\nu_a$ , and where  $\epsilon_e \neq \epsilon_B$ .

The observed flux density and radio spectrum at any single epoch are determined by three parameters:  $C_f$ ,  $C_\tau$ , and  $\nu_{m,0}$ . Here,  $C_f$  and  $C_\tau$  are normalization constants of the flux density and optical depth, respectively, while  $\nu_{m,0}$  is the value of  $\nu_m$  at epoch  $t_0$ . The parameters  $C_f$ ,  $C_\tau$ , and  $\nu_{m,0}$  are in turn determined by the values of four physical parameters at  $t = t_0$ : the magnetic field,  $B_0$ , the shock radius,  $r_0$ , the minimum electron Lorentz factor,  $\gamma_{m,0}$ , and the ratio of energy densities,  $\mathfrak{F}_0 \equiv \epsilon_e/\epsilon_B$ . With four physical parameters ( $B_0$ ,  $r_0$ ,  $\gamma_{m,0}$ ,  $\mathfrak{F}_0$ ) and only three constraints ( $C_f$ ,  $C_\tau$ ,  $\nu_{m,0}$ ), we must assume an additional constraint in order to find a unique solution. An additional constraint is obtained by adopting a value

for  $\mathfrak{F}_0$ . Inverting the equations for  $C_f$ ,  $C_\tau$ , and  $\nu_{m,0}$  (Equations 1.31, 1.32, and 1.33, respectively) we derive the following expressions for  $B_0$ ,  $r_0$ , and  $\gamma_{m,0}$ .

$$B_0 = \left[ 1.3 \times 10^8 \pi^{15} (2+p)^{-6} (p-2)^{-4} \frac{m_e^{19} c^{21}}{e^{17}} \frac{\eta^4}{\mathfrak{F}_0 d^4} \right]^{1/17} \times C_f^{-2/17} C_\tau^{4/17} \nu_{m,0}^{-2(p-2)/17} \text{ G} \quad (1.6)$$

$$r_0 = \left[ 1.5 \times 10^{-2} \pi^{-9} (2+p)^7 (p-2)^{-1} \frac{c}{m_e^8} \frac{\eta d^{16}}{\mathfrak{F}_0} \right]^{1/17} \times C_f^{8/17} C_\tau^{1/17} \nu_{m,0}^{-(p-2)/34} \text{ cm} \quad (1.7)$$

$$\gamma_{m,0} = \left[ 3.1 \times 10^{-2} \pi \frac{(2+p)^3 (p-2)^2}{m_e c^2} \frac{\mathfrak{F}_0^2 d^2}{\eta^2} \right]^{1/17} \times C_f^{1/17} C_\tau^{-2/17} \nu_{m,0}^{(13+2p)/34} \quad (1.8)$$

Here, we define  $d$  as the distance to the supernova and  $\eta$  characterizes the thickness of the radiating electron shell as  $r/\eta$ . We make the standard assumption of a thin shell with  $\eta = 10$  (226, 135).

### 1.5.1 Hydrodynamical Evolution of the Ejecta

Evolutionary models governing the hydrodynamics of the SN ejecta provide additional constraints. As discussed by Chevalier (70), there are several different models that can be used to describe the hydrodynamic evolution of the ejecta. These models allow the temporal indices,  $\alpha_r$ ,  $\alpha_B$ ,  $\alpha_\gamma$ , and  $\alpha_\mathfrak{F}$  to be constrained. Here, we adopt the standard model of Chevalier 70 for our basic SSA fit.

The first assumption of the standard model is that the hydrodynamic evolution of the ejecta is self-similar across the shock discontinuity. This implies  $r \propto t^{\alpha_r}$  with  $\alpha_r = (n-3)/(n-s)$  where  $n$  is the density profile of the outer SN ejecta ( $\rho \propto r^{-n}$ ) and  $s$  is the density profile of the radiating electrons within the shocked circumstellar medium ( $n_e \propto r^{-s}$ ). In addition, the standard model assumes that the magnetic energy density ( $U_B \propto B^2$ ) and the relativistic electron energy density ( $U_e \propto n_e \gamma_m$ ) scale as the total post-shock energy density ( $U \propto n_e v^2$ ). In this scenario, the magnetic field is amplified by turbulence near the shock discontinuity, implying fixed energy fractions,  $\epsilon_e$  and  $\epsilon_B$ , and thus a constant value of  $\mathfrak{F}$

throughout the evolution of the ejecta.

Adopting this evolutionary model, the temporal indices are constrained as follows. The self-similar solution requires that the total energy density scales as  $U \propto t^{\alpha_{n_e} + 2\alpha_v}$  where  $\alpha_{n_e}$  defines the temporal evolution of the electron density. For a radial dependence of  $s$ , we have  $\alpha_{n_e} = -s\alpha_r$ . Using the scaling for the shock velocity (Equation 1.20), we then have  $U \propto t^{-s\alpha_r + 2(\alpha_r - 1)}$ . Similarly,  $U_e \propto t^{-s\alpha_r + \alpha_\gamma}$ . In a model where  $\epsilon_e$  and  $\epsilon_B$  are constant, it follows that  $\alpha_{\mathfrak{F}} = 0$  and  $U_e \propto U_B \propto U$ . This results in the following constraints,

$$\alpha_\gamma = 2(\alpha_r - 1) \quad (1.9)$$

$$\alpha_B = \frac{(2-s)}{2}\alpha_r - 1. \quad (1.10)$$

With the standard assumption that the circumstellar medium is characterized by a wind density profile,  $s = 2$ , Equation 1.10 simplifies to  $\alpha_B = -1$ .

### 1.5.2 SSA Model Fit for SN 2003L

Using the SN 2003L multi-frequency radio light-curves and a chosen value of  $\mathfrak{F}_0$ , we fit for the constants  $C_f$  and  $C_\tau$  as well as the temporal index  $\alpha_r$ . As discussed in §2.3,  $\nu_m$  is estimated to be below our radio observing band and we therefore adopt  $\nu_{m,0} \approx 1$  GHz. We note that the uncertainty in  $\nu_{m,0}$  corresponds to minimal uncertainty in the derived physical parameters as shown by Equations 1.6 – 1.8.

Adopting a reference time of  $t_0 = 10$  days, we find a best-fit solution ( $\chi_r^2 = 7.5$ ; 105 degrees of freedom) for parameters:  $C_f = 7.2 \times 10^{-53}$ ,  $C_\tau = 4.5 \times 10^{38}$ , and  $\alpha_r = 0.96$ . According to Equations 1.9 – 1.10, these values imply  $\alpha_\gamma = 0.075$  and  $\alpha_B = -1.0$ . Here, we have used  $\mathfrak{F}_0 = 1$  with  $\alpha_{\mathfrak{F}} = 0$  and an electron energy index,  $p = (-2\beta + 1) = 3.2$ , based on the observed optically thin spectral index,  $\beta \approx -1.1$  (see §3.2 and Figure 1.3). As discussed in the Appendix, we parameterize the sharpness of the  $\nu_a$  spectral break with  $\zeta = [0, 1]$  and find  $\zeta \approx 0.5$  for our best-fit solution. The model provides a reasonable fit to the light-curves as seen in

Figure 2.3. We note that the large  $\chi_r^2$  is dominated by scintillation, primarily affecting the lower frequency observations.

Better fits can be obtained by relaxing the assumptions of the standard model (hereafter Model 1) as described in Section 2.4.1. In Model 2, we remove the assumption of a wind density profile and effectively fit for  $s$ . For this model we find a best-fit solution ( $\chi_r^2 = 5.7$ ; 104 degrees of freedom) for  $C_f = 1.2 \times 10^{-52}$ ,  $C_\tau = 2.5 \times 10^{38}$ ,  $\alpha_r = 0.85$ , and  $\alpha_B = -0.84$ . By Equation 1.10, this solution implies a shallow CSM density profile of  $s = 1.6$ . As in the case of Model 1, we have adopted  $\mathfrak{F}_0 = 1$ ,  $\alpha_{\mathfrak{F}} = 0$ ,  $p = 3.2$ , and  $\zeta = 0.5$  for this fit.

A similar fit is obtained by fixing the density profile as  $s = 2$  and removing the assumption of constant energy density fractions,  $\epsilon_e$  and  $\epsilon_B$ . In this case, Model 3, the constraints given by Equations 1.9 and 1.10 do not apply since  $\alpha_{\mathfrak{F}}$  is non-zero. By definition,  $\mathfrak{F} \propto U_e/U_B$ , resulting in the constraint

$$\alpha_{\mathfrak{F}} = -s\alpha_r + \alpha_\gamma - 2\alpha_B \quad (1.11)$$

which gives  $\alpha_{\mathfrak{F}} = -2\alpha_r + \alpha_\gamma - 2\alpha_B$  for  $s = 2$ . For Model 3, we find a best-fit solution ( $\chi_r^2 = 5.7$ ; 103 degrees of freedom) for  $C_f = 1.2 \times 10^{-52}$ ,  $C_\tau = 2.4 \times 10^{38}$ ,  $\alpha_r = 0.78$ ,  $\alpha_B = -1.1$  and  $\alpha_\gamma = 0.16$ . The implied evolution of  $\mathfrak{F}$  is given by  $\alpha_{\mathfrak{F}} = 0.88$  with  $\epsilon_e \propto t^{0.61}$  and  $\epsilon_B \propto t^{-0.27}$ . Consistent with Models 1 and 2,  $\mathfrak{F}_0 = 1$ ,  $p = 3.2$  and  $\zeta = 0.5$  were used for this fit.

A comparison of the best-fit solutions from Models 1-3 are shown in Figure 2.3. It should be noted that Models 2 and 3 produce the same light-curve fit since they both allow for one extra degree of freedom. While these two models provide a slightly better representation of the SN 2003L data, we adopt Model 1 as our best SSA solution since these assumptions have been shown to be consistent with the full physical model for SN 1993J (136), currently the best-studied radio SN.

### 1.5.3 Physical Parameters

Using our solution for Model 1, we find the following values and evolution for  $B$ ,  $r$ , and  $\gamma_m$ . The temporal evolution of the magnetic field is  $B \approx 4.5(t/t_0)^{-1.0}$  G with an associated radial dependence,  $B \propto r^{-1.04}$ , similar to that found for the Type IIb SN 1993J ( $B \propto r^{-1}$ ; Fransson and Björnsson 136). The shock radius is well described by  $r \approx 4.3 \times 10^{15}(t/t_0)^{0.96}$  cm implying a sub-relativistic velocity of  $\bar{v} \approx 0.20(t/t_0)^{-0.04} c$ . We note that this radial evolution is faster to that of SN 1983N ( $r \propto t^{0.86}$ ; Chevalier 71) and is within the expected range,  $0.67 \leq \alpha_r \leq 1.0$  (70, 71). The minimum Lorentz factor of the electrons follows  $\gamma_m \approx 8.9(t/t_0)^{-0.08}$  and the implied evolution of  $\nu_m$  (see Equation 1.28) is  $\nu_m \approx 1.0(t/t_0)^{-1.16}$  GHz which is nearly comparable to the evolution observed for SN 1998bw ( $\nu_m \propto t^{-1.0}$ ; Li and Chevalier 226) and significantly slower than the decay rate in the adiabatic Sedov-Neumann-Taylor solution ( $\nu_m \propto t^{-3}$ ; Zel'dovich and Raizer 448, Frail et al. 135).

Using these derived values, additional physical parameters can be computed. The number density of emitting electrons within the circumstellar ejecta,  $n_e$ , is thus

$$n_e = \frac{p-2}{p-1} \frac{B_0^2}{8\pi} \frac{\mathfrak{F}_0}{m_e c^2 \gamma_{m,0}} \left(\frac{t}{t_0}\right)^{2\alpha_B - \alpha_\gamma + \alpha_\mathfrak{F}} \text{ cm}^{-3}. \quad (1.12)$$

Using our above values for  $\mathfrak{F}_0$ ,  $B$  and  $\gamma_{m,0}$ , we find  $n_e \approx 6.1 \times 10^4 (r/r_0)^{-2.0} \text{ cm}^{-3}$ . For  $\alpha_r \approx 0.96$  and  $s = 2$ , the density profile of the ejecta scales steeply as  $\rho \propto r^{-27}$ .

The associated progenitor mass loss rate is

$$\dot{M} = \frac{8\pi}{\eta} n_e m_p r_0^2 v_w \left(\frac{t}{t_0}\right)^{2\alpha_B - \alpha_\gamma + 2\alpha_r + \alpha_\mathfrak{F}} M_\odot \text{ yr}^{-1} \quad (1.13)$$

where we have assumed a nucleon-to-proton ratio of 2 and  $v_w$  is the velocity of the stellar wind. Assuming a typical wind velocity of  $v_w = 1000 \text{ km s}^{-1}$ , we find a progenitor mass loss rate of  $\dot{M} \approx 7.5 \times 10^{-6} M_\odot \text{ yr}^{-1}$  for SN 2003L. We note that this derived mass loss rate is a factor of  $\sim 30$  larger than that of the Type

Ic SN 1998bw and SN 2002ap and yet falls at the low end of values observed for Galactic Wolf-Rayet (WR) stars (62), the favored progenitor model for Type Ibc SNe and gamma-ray bursts.

The total ejecta energy,  $E$ , is then given as

$$E = \frac{4\pi}{\eta} r_0^3 \frac{\mathfrak{F}_0}{\epsilon_{e,0}} \frac{B_0^2}{8\pi} \left(\frac{t}{t_0}\right)^{2\alpha_B + 3\alpha_r + \alpha_{\mathfrak{F}} - \alpha_{\epsilon_e}} \text{ erg.} \quad (1.14)$$

It should be noted that the total energy depends not only on the ratio  $\mathfrak{F}_0$ , but also on assumed value of  $\epsilon_{e,0}$ . For  $\epsilon_{e,0} = 0.1$  (consistent with Li and Chevalier 226, Berger et al. 22) we find an ejecta energy of  $E_0 \approx 8.2 \times 10^{47} (t/t_0)^{0.89}$  erg, just a factor of two below that of SN 1998bw and 300 times larger than that of SN 2002ap at similar epochs. As discussed by Li and Chevalier (226), a larger  $\mathfrak{F}_0$  would increase the energy budget further.

For comparison, we derive the physical parameters implied by Models 2 and 3 here. Model 2 shows a slower temporal evolution of radius,  $r \approx 5.3 \times 10^{15} (t/t_0)^{0.85}$  cm, and thus a more rapid decline in velocity,  $\bar{v} \approx 0.20(t/t_0)^{-0.15}c$ . The radio bright ejecta scales as  $E \approx 1.0 \times 10^{48} (t/t_0)^{0.88}$  erg and the magnetic field evolves with radius as  $B \approx 3.7(r/r_0)^{-0.99}$  G, similar to Model 1. The main difference of Model 2 is that the electron density shows a radial dependence of  $n_e \approx 3.7 \times 10^4 (r/r_0)^{-1.63}$  cm<sup>-3</sup>, significantly shallower than that associated with a constant circumstellar wind. The density profile of the ejecta is thus given by  $\rho \propto r^{-10.7}$  and is similar to that found for the Type II SN 1987A ( $\rho \propto r^{-9}$ ; Arnett 6). This implies an evolution of the mass loss rate,  $\dot{M} \approx 6.8 \times 10^{-6} (r/r_0)^{0.37} M_{\odot} \text{ yr}^{-1}$ .

Model 3 shows an even faster deceleration of the ejecta with  $\bar{v} \approx 0.20(t/t_0)^{-0.22}c$  and radial evolution of  $r \approx 5.3 \times 10^{15} (t/t_0)^{0.78}$  cm. In this case, the energy increases relatively slowly as  $E \approx 1.0 \times 10^{48} (t/t_0)^{0.34}$  erg and the magnetic field falls off more steeply as  $B \approx 3.7(r/r_0)^{-1.46}$  G. The density profile is fixed at  $s = 2$ , giving an evolution of  $n_e \approx 3.6 \times 10^4 (r/r_0)^{-2}$  cm<sup>-3</sup> and a constant mass loss rate of  $\dot{M} \approx 6.8 \times 10^{-6} M_{\odot} \text{ yr}^{-1}$ . We note that Model 3 predicts a relatively shallow ejecta density profile with  $\rho \propto r^{-6.25}$ . Figure 2.7 compares the physical parameters

predicted by Models 1-3.

## 1.6 External Absorption

In the analysis presented above we did not account for the possible effects of external absorption on the observed radio light-curves. For low mass loss rates such as the value we derived through SSA modeling of SN 2003L (Section 2.5), it has generally been found that free-free absorption (FFA) contributes only minimally to the observed light-curves. Consistent with the SSA model, FFA models assume that the intrinsic radio emission spectrum is due to non-thermal synchrotron processes. The observable signature of FFA is a steepening of the optically thick light-curves at early time (due to contributions from both SSA and FFA processes), as was seen in the case of the Type IIb SN 1993J (136).

### 1.6.1 Basic FFA Model

To begin, we fit a basic external absorption model in which the dominant absorption process is assumed to be thermal FFA from a uniform ionized circumstellar medium located external to the ejecta. Following (421), this FFA dominated model is given by

$$f_\nu(t) = K_1 \left( \frac{\nu}{5 \text{ GHz}} \right)^\beta \left( \frac{t}{1 \text{ day}} \right)^{\alpha_f} e^{-\tau_\nu} \text{ mJy}, \quad (1.15)$$

with

$$\tau_\nu(t) = K_2 \left( \frac{\nu}{5 \text{ GHz}} \right)^{-2.1} \left( \frac{t}{1 \text{ day}} \right)^{\alpha_\tau}. \quad (1.16)$$

where  $\alpha_f$  and  $\alpha_\tau$  describe the temporal evolution of the flux density and optical depth, respectively;  $K_1$  and  $K_2$  are normalization constants and  $\beta$  is the optically thin spectral index.

As shown in Figure 1.7, the basic FFA model fit (thin solid line) provides a poor match to the data, underestimating the slow turn-on of the radio emission with  $\chi_r^2 \approx 14.0$  (two times worse than the SSA model fit, §2.5). The fitted parameter

values are  $K_1 \approx 597$ ,  $\beta \approx -1.0$ ,  $\alpha_f \approx -0.97$ ,  $K_2 \approx 1710$ , and  $\alpha_\tau \approx -1.5$ .

According to this FFA dominated model, we estimate the predicted mass loss rate of the progenitor star using Equation 17 of Weiler et al. (419). We find a high mass loss rate of  $\dot{M} \approx 1.4 \times 10^{-2} M_\odot \text{ yr}^{-1}$  (for  $v_w = 1000 \text{ km s}^{-1}$ ). This value is three orders of magnitude above the typical mass loss rate for Galactic Wolf-Rayet stars, which show  $\dot{M} \approx 10^{-5} M_\odot \text{ yr}^{-1}$  with  $v_w \approx 1000$  to  $2000 \text{ km s}^{-1}$  (62).

### 1.6.2 Complex FFA Model

Better light-curve fits are obtained by applying the complex FFA model of Weiler et al. (419) which includes multiple external absorption processes, each characterized by the distribution of absorbing material (uniform vs. clumpy) and the location of the material with respect to the radiating electrons (within the CSM vs. distant). We note that this FFA model also allows for both internal SSA and FFA components to contribute to the shape of the observed radio light-curves.

Applying this model to the SN 2003L radio light-curves, we find that the two dominant absorption processes are internal SSA and external FFA due to a clumpy CSM. In the notation of Weiler et al. (419) this corresponds to  $K_1 \approx 2.80 \times 10^3$ ,  $\alpha \approx -1.11$ ,  $\beta \approx -1.24$ ,  $K_3 \approx 7.66 \times 10^4$ ,  $\delta' \approx -2.15$ ,  $K_5 \approx 1.28 \times 10^3$ ,  $\delta'' \approx -1.60$ , with all other parameters effectively insignificant. As shown in Figure 1.7, the complex FFA solution (thick solid line) provides an reasonable fit to the data with  $\chi_r^2 = 4.5$  for 96 dof.

To estimate the physical parameters of the SN in this model we remove the external absorption due to the clumpy CSM component leaving only the intrinsic synchrotron self-absorbed spectrum. As shown in Figure 1.7, at  $t \approx 2$  days the peak flux density is  $f_p \approx 102.1 \text{ mJy}$  at  $\nu_p \approx 22.5 \text{ GHz}$  and  $\beta \approx -1.1$ . For these values, Equations 1.2 and 1.3 give an equipartition radius of  $r_{\text{ep}} \approx 5.7 \times 10^{16} \text{ cm}$ , an expansion velocity of  $\bar{v}_{\text{ep}} \approx 14c$ , and an ejecta energy of  $E_{\text{ep}} \approx 7.0 \times 10^{48} \text{ erg}$ . With this velocity, the ejecta radius would be  $r \approx 2.4 \times 10^{18} \text{ cm}$  at  $t \approx 65$  days, in violation of the VLBA limit of  $r \leq 9.1 \times 10^{17} \text{ cm}$ . To match the observed VLBA limit, we relax the assumption of equipartition, but this results in a steep increase

in the total ejecta energy by a factor of  $\sim 300$ , giving  $E \approx 3 \times 10^{51}$ . Moreover, we note that the model is parameterized for the case of non-relativistic ejecta speeds and is therefore inconsistent with the implied relativistic velocity. A consistent, non-relativistic solution to the Weiler et al. (419) model could not be found for the case of SN 2003L.

## 1.7 Modeling the X-ray emission

X-ray emission in supernovae can be produced by three processes (137): (1) non-thermal synchrotron emission from radiating electrons, (2) thermal (free-free) bremsstrahlung emission from material in the circumstellar shock and/or the ejecta reverse shock, and (3) inverse Compton scattering of photospheric photons by relativistic electrons. We examine each of these scenarios in the context of the bright X-ray emission of SN 2003L.

### 1.7.1 Synchrotron Emission

Extrapolating the (optically thin) synchrotron emission at  $t \approx 40$  days from the radio to the X-ray band as  $f_\nu \propto \nu^\beta$  with  $\beta \approx -1.1$ , we find that the synchrotron emission under-predicts the observed X-ray flux by a factor of  $\sim 50$ . The discrepancy is significantly larger when a synchrotron cooling break,  $\nu_c$ , is included, beyond which the spectrum steepens by  $\Delta\beta = -0.5$  (see the Appendix). Using Equation 1.34 together with the magnetic field evolution derived in Section 2.5, the cooling frequency at  $t \approx 40$  days is  $\nu_c \approx 1.1 \times 10^{11}$  Hz. Including this synchrotron break and extrapolating from  $\nu_c$  to  $\nu_{\text{X-ray}}$  as  $f_\nu \propto \nu^{-1.6}$ , the synchrotron emission in the X-ray grossly under-predicts the observed flux by 5 orders of magnitude. We also note that the flat spectrum,  $\beta \approx -0.5$ , of the observed X-rays is inconsistent with the steep synchrotron spectral index observed in the radio bands,  $\beta \approx -1.1$ . We therefore conclude that the X-ray emission is not due to synchrotron processes.

### 1.7.2 Thermal Bremsstrahlung Emission

In a scenario dominated by thermal bremsstrahlung processes, the X-ray emission is produced by the forward shock plowing into circumstellar material and/or the reverse shock heating of the ejecta. In this case, the strength of the X-ray emission depends of the density of the emitting material. The shocked material then cools by free-free emission processes. For an  $n_e \propto r^{-2}$  wind density profile, free-free luminosity from the forward or reverse shock is generalized (72, 385) roughly by

$$L_X \approx 7.5 \times 10^{34} C_L \left( \frac{\dot{M}}{10^{-5} M_\odot \text{ yr}^{-1}} \right)^2 \left( \frac{1000 \text{ km/s}}{v_w} \right)^2 \left( \frac{t}{40 \text{ days}} \right)^{-1} \text{ erg s}^{-1} \quad (1.17)$$

where  $C_L$  is a constant such that  $C_L = C_{\text{FS}} = 1$  for the forward shock and  $C_L = C_{\text{RS}} = (n - 3)(n - 4)^2 / (4n - 8)$  for the reverse shock. For SSA Model 1 (Section 2.5), we find  $\alpha_r \approx 0.96$  and thus  $n \approx 27$  and  $C_{\text{RS}} \approx 127$ . Using the mass loss rate derived from Model 1, the *combined* free-free luminosity from the forward and reverse shocks is therefore  $L_{X,\text{FS+RS}} \approx 5.4 \times 10^{36} \text{ erg s}^{-1}$ , and a factor  $\sim 10^3$  fainter than that observed. On the other hand, if we assume the X-ray emission *must* be dominated by free-free processes, then this implies a mass loss rate of  $2.7 \times 10^{-4} M_\odot \text{ yr}^{-1}$  ( $v_w = 1000 \text{ km s}^{-1}$ ), which is inconsistent with both the rate predicted by radio SSA models as well as that associated with FFA modeling (Section 1.6).

### 1.7.3 Inverse Compton Cooling

X-ray emission from supernovae can also be produced by inverse Compton (IC) cooling of the relativistic electrons by the optical photons as was claimed to be important for the X-ray emission of SN 2002ap (37). In this scenario, the ratio of

energy densities in magnetic fields,  $U_B$ , and photons,  $U_{\text{ph}}$ , is given roughly by

$$\frac{f_{\text{radio}}}{f_{\text{X-ray}}} \approx \frac{U_B}{U_{\text{ph}}} \quad (1.18)$$

where  $f_{\text{radio}} \equiv \nu f_\nu$  is the optically thin synchrotron flux in the radio band and  $f_X$  is the corresponding X-ray flux. At  $t \approx 40$  days, the observed radio flux was  $f_{\text{radio}} \approx 6.7 \times 10^{-16} \text{ erg cm}^{-2} \text{ s}^{-1}$  and the X-ray flux was  $f_{\text{X-ray}} \approx 9.2 \times 10^{-15} \text{ erg cm}^{-2} \text{ s}^{-1}$ , giving a ratio of  $f_{\text{radio}}/f_{\text{X-ray}} \approx 0.074$ .

Assuming the timescale for Compton cooling is comparable to the epoch *Chandra* observations,  $t_{\text{comp}} \approx 40$  days, and using Equations (14–18) of Björnsson and Fransson (37), we are able to roughly match the observed X-ray luminosity. Since we see no evidence for IC cooling affects within our radio light-curves, we place a lower limit of  $\nu_{\text{IC}} \geq 22$  GHz. This implies constraints on the magnetic field and shock velocity of  $B \geq 0.4$  G and  $v \geq 0.09c$ , consistent with the values predicted from SSA radio analyses (§ 2.5). The corresponding limit on the energy density in magnetic fields is thus  $U_B \gtrsim 0.0048 \text{ erg cm}^{-3}$  and is therefore consistent with the value found through SSA Model 1 (§ 2.5). We note that in these estimates, a bolometric luminosity of  $L_{\text{bol},42} \approx 1.5$  has been very roughly estimated based on fitting the SN 2003L optical light-curve (Soderberg *et al.*, in prep.).

While inverse Compton cooling appears to be a feasible process to produce the luminous X-ray emission of SN 2003L, it predicts a steep spectral index,  $\beta_{\text{X-ray}} \approx \beta_{\text{radio}} \approx -1.1$ , which is inconsistent with the observed value of  $\beta \approx -0.5$  ( $2 - \sigma$ ). We note, however, that the poor photon statistics may be responsible for this discrepancy.

## 1.8 Discussion and Conclusions

As the first Type Ibc supernova with a radio and X-ray luminosity within an order of magnitude of SN 1998bw, SN 2003L is clearly an unusual event. Here, we summarize our findings. Both SSA and FFA models (Sections 2.5 and 1.6) show that the energy of the ejecta is  $\gtrsim 10^{48}$  erg and nearly comparable to that

of SN 1998bw at a similar epoch. In Case 1 the equipartition and SSA analyses predict a sub-relativistic velocity,  $\bar{v} \approx 0.2c$ , and a relatively low mass loss rate,  $\dot{M} \approx 7.5 \times 10^{-6} M_{\odot} \text{ yr}^{-1}$  which are roughly consistent with a scenario where inverse Compton scattering produces the observed X-ray emission. In Case 2, the complex FFA models reproduce the observed radio light-curves well, yet they imply a highly relativistic ejecta speed,  $\bar{v} \approx 14c$ , or a huge energy output of  $E \geq 10^{51}$  erg, as well as a high mass loss rate of  $\dot{M} \approx 10^{-2} M_{\odot} \text{ yr}^{-1}$  which over-predicts the observed X-ray emission assuming a thermal bremsstrahlung emission model.

Our VLBA observation at  $t \approx 65$  days implies an ejecta size which is inconsistent with the extreme velocities required by the complex FFA model in Case 2. Only by deviating far from equipartition and significantly increasing the total energy of the ejecta can this inconsistency be resolved. Moreover, the predicted mass loss rate is at least two orders of magnitude above the observed rates from Wolf-Rayet stars. In conclusion, we find Case 2 to be infeasible and we therefore adopt Case 1 as the most likely scenario. We note that Case 1 predicts a mass loss rate comparable to the low end of values observed for local Wolf-Rayet stars.

While similar to SN 1998bw in radio luminosity and ejecta energy, a main distinguishing characteristic between SN 2003L and SN 1998bw is their shock velocity: while the radio ejecta of SN 1998bw attained mildly-relativistic speeds, that of SN 2003L was clearly sub-relativistic as shown in Section 2.5. This discrepancy is echoed by optical spectroscopy which showed photospheric velocities in excess of  $3 \times 10^4 \text{ km s}^{-1}$  for SN 1998bw (282) and  $10^4 \text{ km s}^{-1}$  for SN 2003L (405, 241). Therefore, we see that for SN 1998bw, mildly-relativistic ejecta was coupled with bright radio emission, while for SN 2003L the emission is bright *despite* the modest ejecta velocities. The question is thus, why is the radio ejecta of SN 2003L especially luminous and energetic?

One hypothesis considers the distribution of kinetic energy according to ejecta velocity. SN 1998bw is a clear case where a significant fraction of the explosion energy has been deposited into mildly-relativistic material. For SN 2003L, however, the bulk of the energy is coupled to sub-relativistic ejecta. Tan et al. (388)

have shown that in some cases, high velocity ejecta can be produced from a whip effect racing down the ejecta. The observed diversity in the coupling between velocity and energy could therefore be intrinsic to the SN Ibc population. A similar situation is observed for gamma-ray bursts which partition their energy into ultra-relativistic emission ( $\gamma$ -rays) and mildly-relativistic afterglow emission (X-rays, optical, radio) by variable fractions.

Through our ongoing radio surveys of local SNe Ibc and cosmological gamma-ray bursts, we continue to map out the energetics of these explosions. Our goal is to understand the link between Type Ibc supernovae and GRBs by studying properties of the explosion (ejecta velocity and kinetic energy) in addition to those of the progenitor star (CSM density profile and evolutionary mass loss rate). Through these further studies, we aim to shed light on the illusive bridge between these two classes of cosmic explosions.

We are indebted to Barry Clark for his generous scheduling of the VLA for this project, and to Jim Ulvestad for enabling the VLBA observations. The authors thank Re'em Sari, Claes Fransson, Eli Waxman, Dick Sramek and Michael Ruppen for useful discussions. Caltech SN research is supported by NSF and NASA grants. AMS acknowledges support by the National Radio Astronomy Observatory Graduate Summer Student Research Assistantship program. Research by EB is supported by NASA through Hubble Fellowship grant HST-HF-01171.01 awarded by the Space Telescope Science Institute, which is operated by the Association of Universities for Research in Astronomy, Inc., for NASA, under contract NAS 5-26555. RAC thanks NSF grant AST-0307366.

## Appendix

### 1.9 The Synchrotron Self-absorption Model

Here we describe the SSA model prescription applied in Section 2.5. The model was adapted from the formalism of (135), designed to describe gamma-ray burst radio emission following the transition to sub-relativistic, adiabatic expansion. We

replace the assumption of Sedov-Neumann-Taylor (SNT) dynamics (448) with a general parameterization of the shock evolution. This substitution enables us to study the early supernova synchrotron emission, while the ejecta is in the free-expansion phase. We note that by adopting the scalings given by the SNT dynamics into our generalized equations, the formalism of Frail et al. (135) is fully recovered.

### 1.9.1 Physical Assumptions

To first order, we assume that the supernova ejecta is undergoing spherical, homologous expansion at sub-relativistic velocity,  $v$ . At any time,  $t$ , the observed synchrotron emission originates from a thin shell of radiating electrons with radius,  $r$ , and thickness,  $r/\eta$  (with  $\eta \approx 10$ ). The electrons are accelerated into a power-law energy distribution,  $N(\gamma) \propto \gamma^{-p}$ , above a minimum Lorentz factor,  $\gamma_m$ . We adopt the standard assumption that the energy density of the ejecta is partitioned between the fraction in relativistic electrons,  $\epsilon_e$ , and the fraction in magnetic fields,  $\epsilon_B$ . For simplicity, we denote the ratio of these energies as  $\mathfrak{F} \equiv \epsilon_e/\epsilon_B$  and further assume that it evolves as  $\mathfrak{F} \propto t^{\alpha_{\mathfrak{F}}}$ .

The temporal evolution of the radius, velocity, minimum Lorentz factor, and magnetic field are then parameterized as

$$r = r_0 \left( \frac{t}{t_0} \right)^{\alpha_r} \quad (1.19)$$

$$v = v_0 \left( \frac{t}{t_0} \right)^{\alpha_r - 1} \quad (1.20)$$

$$\gamma_m = \gamma_{m,0} \left( \frac{t}{t_0} \right)^{\alpha_\gamma} \quad (1.21)$$

$$B = B_0 \left( \frac{t}{t_0} \right)^{\alpha_B} \quad (1.22)$$

where the subscript 0 corresponds to the parameter values at an (arbitrary) reference time,  $t_0$ . Here, the indices  $\alpha_r$ ,  $\alpha_\gamma$ ,  $\alpha_B$ , and  $\alpha_{\mathfrak{F}}$  are determined by the hydrodynamic evolution of the ejecta, and are constrained according to the assumed

evolutionary model (see §2.4.1).

### 1.9.2 Emission Spectrum

In characterizing the synchrotron emission spectrum, we use the standard formalism of Rybicki (323). Within this framework, the synchrotron power per unit frequency emitted by a single electron is given by

$$P(\nu, \gamma) = \frac{e^3 B}{m_e c^2} F\left(\frac{\nu}{\nu_{\text{crit}}(B, \gamma)}\right) \quad (1.23)$$

where  $\gamma$ ,  $e$ , and  $m_e$  are the Lorentz factor, charge, and mass of the electron, respectively. The critical frequency,  $\nu_{\text{crit}}$ , is defined as

$$\nu_{\text{crit}} \equiv \gamma^2 \left(\frac{eB}{2\pi m_e c}\right) \quad (1.24)$$

(323). Adopting the notation  $x \equiv (2/3)(\nu/\nu_{\text{crit}})$ , the function  $F(x)$  describes the total synchrotron power spectrum.

$$F(x) \equiv x \int_x^\infty K_{5/3}(\xi) d\xi \quad (1.25)$$

where  $K_{5/3}$  is the modified Bessel function of 2/3 order (323). This function peaks at  $x = 0.29$  and decays rapidly for  $x > 1$ .

Applying the temporal scalings for  $r$ ,  $\beta$ ,  $B$ , and  $\gamma_m$  (Equations 1.19 - 1.22), the flux density from a uniform shell of radiating electrons is then given by

$$f_\nu(t) = C_f \left(\frac{t}{t_0}\right)^{(4\alpha_r - \alpha_B)/2} [(1 - e^{-\tau_\nu^\zeta(t)})]^{1/\zeta} \nu^{5/2} F_3(x) F_2^{-1}(x) \text{ erg/s/Hz/cm}^2 \quad (1.26)$$

where the optical depth,  $\tau_\nu(t)$ , is defined

$$\tau_\nu(t) = C_\tau \left(\frac{t}{t_0}\right)^{(p-2)\alpha_\gamma + (3+p/2)\alpha_B + \alpha_r + \alpha_\beta} \nu^{-(p+4)/2} F_2(x) \quad (1.27)$$

and  $\zeta = [0, 1]$  parameterizes the sharpness of the spectral break between opti-

cally thick and thin regimes. We adopt  $\nu_m \equiv \nu_{\text{crit}}(\gamma = \gamma_m)$  as the characteristic synchrotron frequency,

$$\nu_m(t) = \nu_{m,0} \left( \frac{t}{t_0} \right)^{2\alpha_\gamma + \alpha_B} \text{ Hz}, \quad (1.28)$$

and for  $x = (2/3)(\nu/\nu_m(t))$ , the functions,  $F_2(x)$  and  $F_3(x)$ , are defined

$$F_2(x) \equiv \sqrt{3} \int_0^x F(y) y^{(p-2)/2} dy, \quad F_3(x) \equiv \sqrt{3} \int_0^x F(y) y^{(p-3)/2} dy \quad (1.29)$$

where  $y$  is a simple integration variable representing the range  $y = [0, x]$ . The temporal dependencies of  $F_2(x)$  and  $F_3(x)$  can be computed numerically. For  $\nu \ll \nu_m$ , we find the following scalings

$$F_2(x) \propto t^{0.49(p+0.73)}, \quad F_3(x) \propto t^{0.47(p-0.14)} \quad (1.30)$$

and for  $\nu \gg \nu_m$ , neither function evolves. Therefore, using equations 1.26 through 1.30, the model flux density at any time is strictly determined by three parameters:  $C_f$ ,  $C_\tau$ , and  $\nu_{m,0}$ :

$$C_f \equiv \frac{2\pi}{2+p} m_e \left( \frac{r_0}{d} \right)^2 \left( \frac{2\pi m_e c}{e B_0} \right)^{1/2} \quad (1.31)$$

$$C_\tau \equiv \frac{(p+2)(p-2)}{4\pi\eta} \gamma_{m,0}^{(p-1)} \left( \frac{B_0^2}{8\pi} \mathfrak{F}_0 \right) \left( \frac{e^3 B_0 r_0}{m_e^3 c^4 \gamma_{m,0}} \right) \left( \frac{e B_0}{2\pi m_e c} \right)^{p/2} \quad (1.32)$$

$$\nu_{m,0} \equiv \frac{1}{2\pi} \gamma_{m,0}^2 \frac{e B_0}{m_e c} \quad (1.33)$$

where  $d$  is the distance to the source and  $\mathfrak{F}_0$  is the value of  $\mathfrak{F}$  at  $t_0$ . Equations 1.31 - 1.33 above show that  $C_f$ ,  $C_\tau$ , and  $\nu_{m,0}$  are in turn determined by four physical parameters:  $B_0$ ,  $r_0$ ,  $\gamma_{m,0}$ , and  $\mathfrak{F}_0$ .

### 1.9.3 Temporal and Spectral Evolution

We use the above formalism to determine the spectral evolution of the synchrotron emission for a given ordering of the synchrotron break frequencies,  $\nu_a$  and  $\nu_m$ . Here, we define the self-absorption frequency,  $\nu_a$ , as the frequency at which the optical depth is unity:  $\tau_{\nu_a} \equiv \tau(\nu = \nu_a) = 1$ .

For completeness, we give the temporal and spectral evolution for higher frequencies near the synchrotron cooling frequency,  $\nu_c$ , defined as the the frequency above which electrons cool efficiently. This frequency is given by

$$\nu_c = \frac{18\pi m_e c e}{t^2 \sigma_T^2 B^3} \text{ Hz} \quad (1.34)$$

and is typically located between the radio and optical observing bands during the first few years after the supernova explosion.

#### Case 1: $\nu_a \ll \nu_m$

In Case 1, the self-absorption frequency is well below the characteristic synchrotron frequency,  $\nu_a \ll \nu_m$ . In this scenario, the spectrum peaks at  $\nu_p \approx \nu_m$ . It can be shown that the temporal scalings associated with the peak are then given by

$$\nu_p \approx \nu_m \propto t^{2\alpha_\gamma + \alpha_B}, \quad f_{\nu_p} \approx f_{\nu_m} \propto t^{3\alpha_r + 3\alpha_B - \alpha_\gamma + \alpha_\mathfrak{F}}. \quad (1.35)$$

Here,  $\nu_a \ll \nu_m$  so the evolution of  $\nu_a$  and  $f_{\nu_a}$  depend on the temporal scaling of  $F_2(x)$  (Equation 1.30). We find

$$\nu_a \propto t^{(2(p-136)\alpha_\gamma + (p+264)\alpha_B + 100\alpha_r + 100\alpha_\mathfrak{F})/(p+164)}, \quad f_{\nu_a} \propto t^{(9\alpha_r + 8\alpha_B - 5\alpha_\gamma + \alpha_{\nu_a} + 3\alpha_\mathfrak{F})/3} \quad (1.36)$$

where, for simplicity, we use  $\alpha_{\nu_a}$  to denote the temporal dependence of  $\nu_a$ . For all

frequencies, the temporal and frequency dependence of  $f_\nu$  is then generalized by

$$f_\nu \propto \begin{cases} \nu^2 t^{(9\alpha_r + 8\alpha_B - 5\alpha_\gamma - 5\alpha_{\nu_a} + 3\alpha_{\mathfrak{F}})/3} & \nu < \nu_a \\ \nu^{1/3} t^{(9\alpha_r + 8\alpha_B - 5\alpha_\gamma + 3\alpha_{\mathfrak{F}})/3} & \nu_a < \nu < \nu_m \\ \nu^{-(p-1)/2} t^{(6\alpha_r + (5+p)\alpha_B + 2(p-2)\alpha_\gamma + 2\alpha_{\mathfrak{F}})/2} & \nu_m < \nu < \nu_c \\ \nu^{-p/2} t^{(6\alpha_r + (8-5p)\alpha_B + 2(p-2)\alpha_\gamma + 2\alpha_{\mathfrak{F}} - 4p + 2)/2} & \nu_c < \nu \end{cases} \quad (1.37)$$

where the temporal scalings associated with the synchrotron cooling frequency are

$$\nu_c \propto t^{-3\alpha_B - 2}, \quad f_{\nu_c} \propto t^{3\alpha_r + (4-p)\alpha_B + (p-2)\alpha_\gamma + \alpha_{\mathfrak{F}} - p + 1}. \quad (1.38)$$

### Case 2: $\nu_m \ll \nu_a$

In Case 2, the characteristic synchrotron frequency is below the self-absorption frequency,  $\nu_m \ll \nu_a$ . In this case, the spectral peak occurs at  $\nu_p \approx \nu_a$ . Since  $F_2(x)$  is constant for  $\nu \gg \nu_m$ , the scalings simplify to

$$\nu_p \approx \nu_a \propto t^{(2(p-2)\alpha_\gamma + 2(3+p/2)\alpha_B + 2\alpha_r + 2\alpha_{\mathfrak{F}})/(p+4)}, \quad f_{\nu_p} \approx f_{\nu_a} \propto t^{(4\alpha_r - \alpha_B + 5\alpha_{\nu_a})/2}. \quad (1.39)$$

In this scenario, the evolution of  $\nu_m$  is given by Equation 1.28 while  $F_{\nu_m}$  scales as

$$f_{\nu_m} \propto t^{2\alpha_r + 2\alpha_B + 5\alpha_\gamma}. \quad (1.40)$$

For all frequencies, the temporal and frequency dependence of  $f_\nu$  is then generalized

by

$$f_\nu \propto \begin{cases} \nu^2 t^{2\alpha_r + \alpha_\gamma} & \nu < \nu_m \\ \nu^{1/3} t^{(4\alpha_r - \alpha_B)/2} & \nu_m < \nu < \nu_a \\ \nu^{-(p-1)/2} t^{(4\alpha_r - \alpha_B + (4+p)\alpha_{\nu_a})/2} & \nu_a < \nu < \nu_c \\ \nu^{-p/2} t^{(2\alpha_r + (1-3p)\alpha_B + (2+p/2)\alpha_{\nu_a} - 2p + 1)} & \nu_c < \nu \end{cases} \quad (1.41)$$

where the temporal scalings associated with the synchrotron cooling frequency are

$$\nu_c \propto t^{-3\alpha_B - 2}, \quad f_{\nu_c} \propto t^{(4\alpha_r + (3-3p)\alpha_B + (4+p)\alpha_{\nu_a} - 2p + 2)/2}. \quad (1.42)$$

Table 1.1. VLA Radio Flux Density Measurements of SN 2003L

Date (UT)	$\Delta t$ (days)	$F_{4.9 \text{ GHz}} \pm \sigma$ ( $\mu\text{Jy}$ )	$F_{8.5 \text{ GHz}} \pm \sigma$ ( $\mu\text{Jy}$ )	$F_{15.0 \text{ GHz}} \pm \sigma$ ( $\mu\text{Jy}$ )	$F_{22.5 \text{ GHz}} \pm \sigma$ ( $\mu\text{Jy}$ )	Array Config.
2003 Jan 26.2	25.2	—	743 $\pm$ 39	—	—	DnC
2003 Jan 28.3	27.3	—	810 $\pm$ 63	—	3179 $\pm$ 85	DnC
2003 Jan 29.3	28.3	—	848 $\pm$ 65	—	3119 $\pm$ 86	DnC
2003 Jan 30.4	29.4	—	966 $\pm$ 60	—	3122 $\pm$ 75	DnC
2003 Jan 31.3	30.3	—	1051 $\pm$ 62	—	3080 $\pm$ 86	DnC
2003 Feb 1.2	31.2	—	947 $\pm$ 52	—	3252 $\pm$ 70	DnC
2003 Feb 2.3	32.3	—	883 $\pm$ 53	—	2973 $\pm$ 99	DnC
2003 Feb 3.3	33.3	—	—	2287 $\pm$ 121	—	DnC
2003 Feb 6.3	36.3	—	1147 $\pm$ 47	—	—	DnC
2003 Feb 8.3	38.3	—	1211 $\pm$ 39	—	—	D
2003 Feb 11.6	41.6	—	1483 $\pm$ 76	2686 $\pm$ 156	2956 $\pm$ 96	D
2003 Feb 14.5	44.5	—	1448 $\pm$ 62	2753 $\pm$ 153	2684 $\pm$ 124	D
2003 Feb 16.4	46.4	—	1413 $\pm$ 55	2719 $\pm$ 144	—	D
2003 Feb 18.4	48.4	—	1546 $\pm$ 45	—	—	D
2003 Feb 22.3	52.3	—	—	3014 $\pm$ 137	2714 $\pm$ 68	D
2003 Feb 23.3	53.3	—	1854 $\pm$ 41	—	—	D
2003 Feb 25.3	55.3	—	1969 $\pm$ 53	2799 $\pm$ 149	2838 $\pm$ 99	D
2003 Feb 26.3	56.3	—	—	2865 $\pm$ 131	—	D
2003 Mar 2.3	60.3	—	2283 $\pm$ 51	2924 $\pm$ 132	—	D
2003 Mar 7.3	65.3	848 $\pm$ 64 <sup>a</sup>	—	—	2263 $\pm$ 73	D
2003 Mar 8.4	66.4	—	2351 $\pm$ 47	2857 $\pm$ 123	2486 $\pm$ 66	D

Table 1.1—Continued

Date (UT)	$\Delta t$ (days)	$F_{4.9 \text{ GHz}} \pm \sigma$ ( $\mu\text{Jy}$ )	$F_{8.5 \text{ GHz}} \pm \sigma$ ( $\mu\text{Jy}$ )	$F_{15.0 \text{ GHz}} \pm \sigma$ ( $\mu\text{Jy}$ )	$F_{22.5 \text{ GHz}} \pm \sigma$ ( $\mu\text{Jy}$ )	Array Config.
2003 Mar 10.3	68.3	—	2081±52	2966±115	—	D
2003 Mar 14.4	72.4	—	2527±52	2901±150	2422±70	D
2003 Mar 17.4	75.4	—	2673±57	3055±173	—	D
2003 Mar 20.3	78.3	—	2422±61	—	2130±223	D
2003 Mar 23.3	81.3	—	2500±43	2664±118	—	D
2003 Mar 27.4	85.4	—	2776±51	—	1833±100	D
2003 Apr 1.2	90.2	—	2551±54	—	—	D
2003 Apr 2.1	91.1	—	—	—	1819±141	D
2003 Apr 10.4	99.4	—	—	2581±320	—	D
2003 Apr 30.0	119.0	—	2532±75	—	1078±173	D
2003 May 3.1	122.1	—	2534±80	—	1327±114	D
2003 May 16.3	135.3	—	2455±96	1925±282	1146±165	D
2003 May 28.1	147.0	1989±41	2200±47	1452±235	941±161	D
2003 Jun 4.0	154.0	2410±114	2151±77	—	—	A
2003 Jun 17.1	167.1	2555±83	2210±68	1279±226	—	A
2003 Jul 1.1	181.1	—	2262±63	—	—	A
2003 Jul 9.0	189.0	2485±90	2075±61	1135±125	—	A
2003 Jul 24.0	204.0	2380±81	2048±66	1177±166	—	A
2003 Aug 11.9	222.9	—	—	—	670±148	A
2003 Aug 15.8	226.8	2346±84	1646±74	824±237	—	A
2003 Sep 15.7	257.7	2177±87	1151±53	768±165	—	A

Table 1.1—Continued

Date (UT)	$\Delta t$ (days)	$F_{4.9 \text{ GHz}} \pm \sigma$ ( $\mu\text{Jy}$ )	$F_{8.5 \text{ GHz}} \pm \sigma$ ( $\mu\text{Jy}$ )	$F_{15.0 \text{ GHz}} \pm \sigma$ ( $\mu\text{Jy}$ )	$F_{22.5 \text{ GHz}} \pm \sigma$ ( $\mu\text{Jy}$ )	Array Config.
2003 Oct 6.7	278.6	2140±40	1244±58	—	—	BnA
2003 Oct 11.7	283.7	2177±79	1176±45	612±122	—	BnA
2003 Oct 27.7	299.7	1937±70	1200±42	520±124	—	B
2003 Nov 1.7	304.7	—	1115±55	—	—	B
2003 Nov 14.6	317.6	1713±73	1075±52	—	—	B
2003 Nov 25.5	328.5	1689±67	981±49	148±148	—	B
2003 Dec 6.6	339.6	1980±69	961±42	506±149	—	B
2004 Jan 26.4	390.4	—	714±38	—	—	B
2004 Feb 8.3	403.3	—	863±42	—	—	CnB
2004 Mar 6.4	430.4	1281±42	—	—	—	C
2004 Mar 20.2	444.2	—	668±30	—	—	C
2004 Apr 21.0	476.0	—	—	125±137	—	C
2004 May 21.0	506.0	—	—	—	280±53	D
2004 Jul 27.0	573.0	—	592±48	—	—	D

<sup>a</sup>VLBA observation

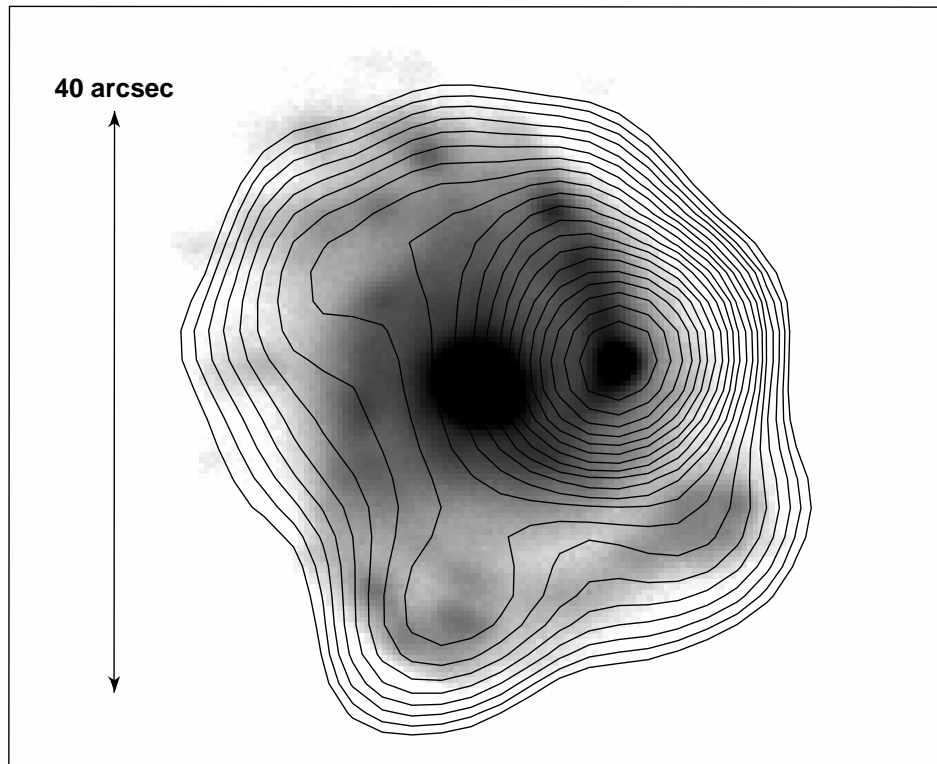


Figure 1.1: A Palomar 60-inch  $R$ -band image (greyscale) shows the SN located within a spiral arm of host galaxy NGC 3506. Twenty-five radio (8.5 GHz) map contours are over-plotted from 0.15 mJy (3-sigma) to 4.0 mJy in equally spaced logarithmic intervals. The radio emission peaks at the optical position of SN 2003L and diffuse emission from the host galaxy extends to a size of approximately 45 by 45 arcsec.

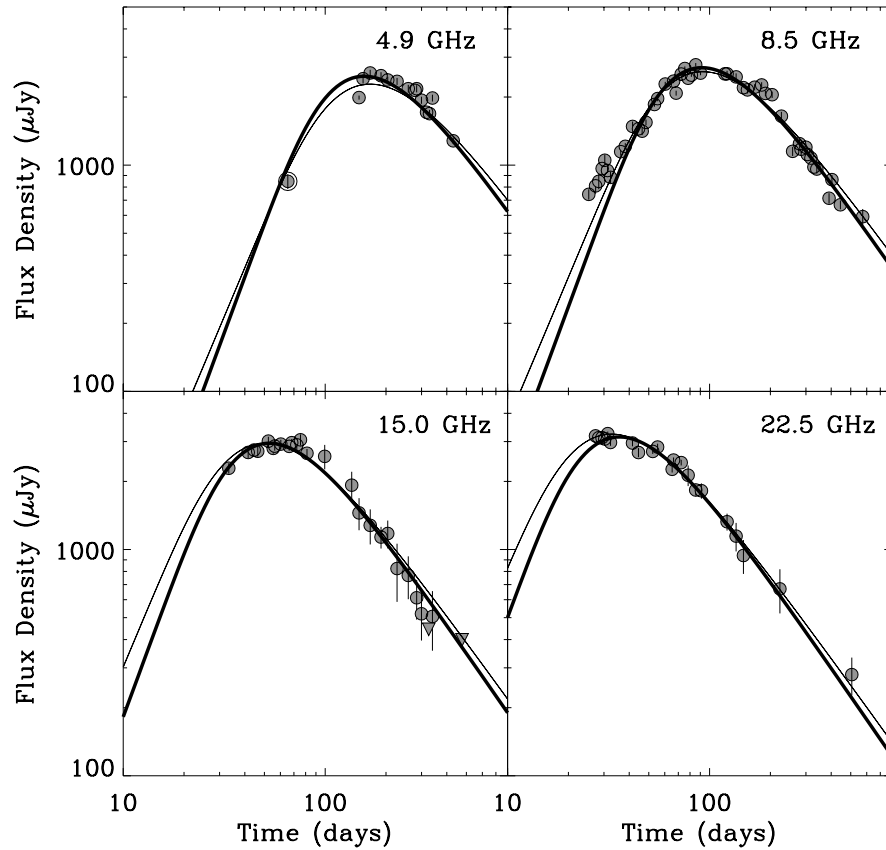


Figure 1.2: Radio light-curves of for the Type Ic SN 2003L were taken with the VLA at frequencies 4.9, 8.5, 15.0, and 22.5 GHz between January 2003 and July 2004. The single VLBA observation (5 GHz) is shown as an encircled dot. SSA Model 1 (thick solid line), and Models 2 and 3 (thin solid line) as described in §2.5 are over-plotted.

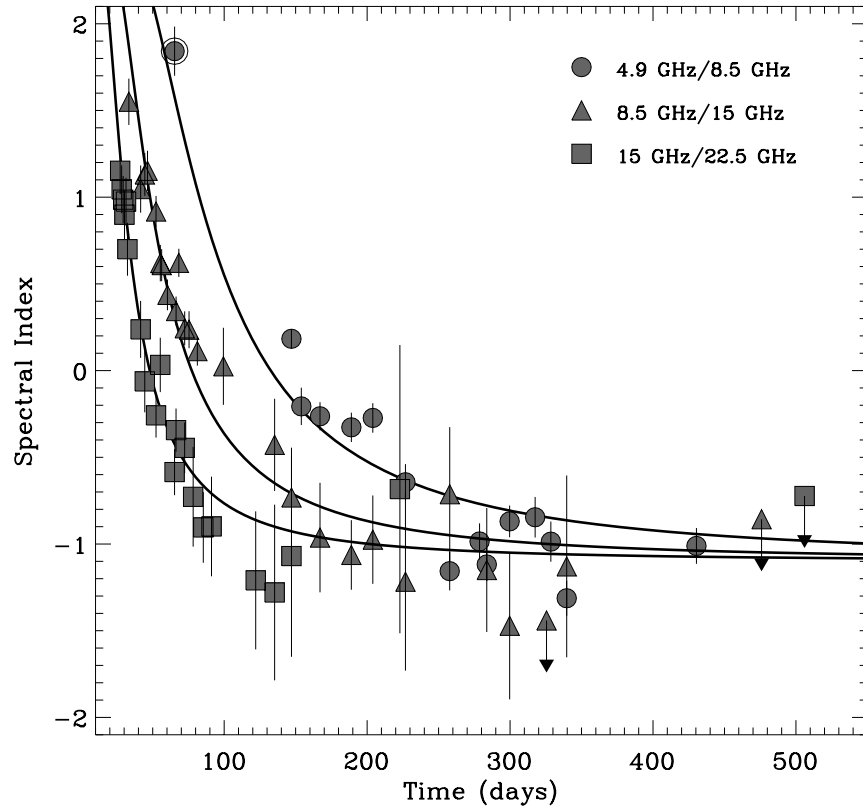


Figure 1.3: The temporal evolution of 4.9/8.5 GHz, 8.5/15.0 GHz, and 15.0/22.5 GHz spectral indices are shown and SSA Model 1 (§2.5) is over-plotted. We highlight the VLBA observation with an encircled dot.

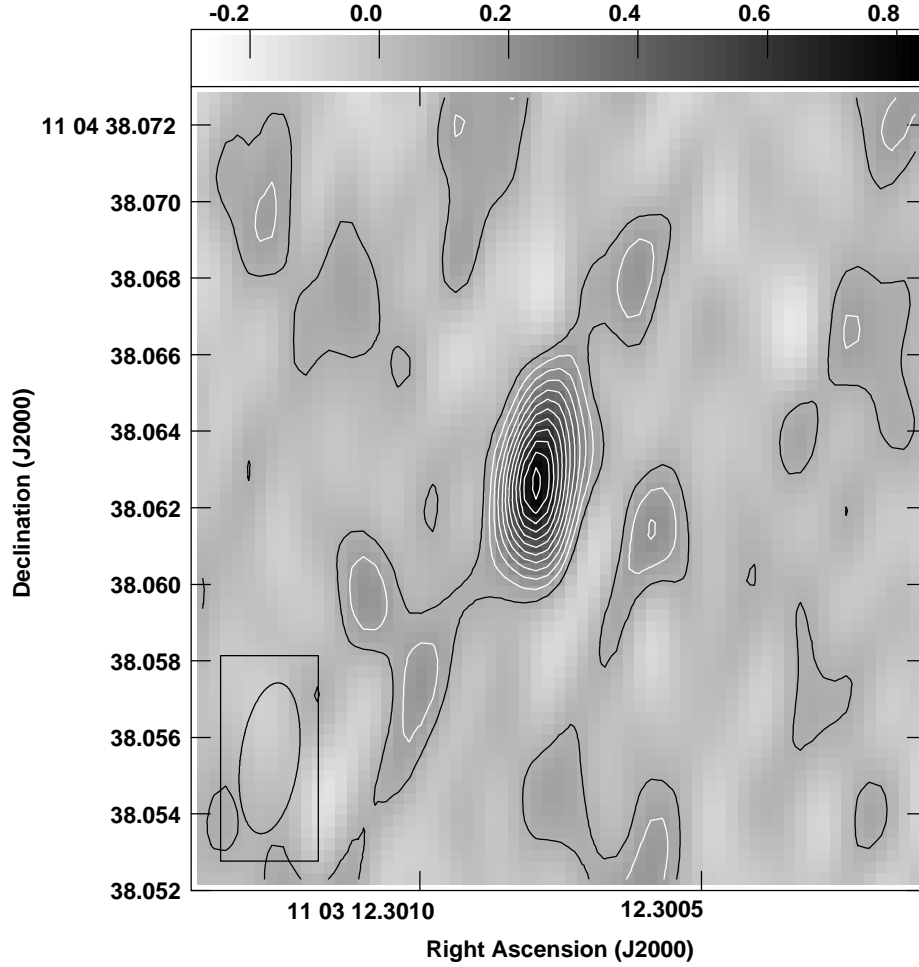


Figure 1.4: VLBA image of SN2003L at 4.9 GHz at  $t \approx 65$  days after the explosion. We find a flux density for the supernova of  $F_{4.9 \text{ GHz}} = 848 \pm 64 \mu\text{Jy}$  within a  $3.158 \times 1.285$  mas beam. Contours define  $1 \sigma$  increments of  $67 \mu\text{Jy}$ . At a distance of 92 Mpc, this unresolved VLBA detection places a direct constraint on the size of the expanding ejecta of  $r \lesssim 9.1 \times 10^{17}$  cm at  $t \approx 65$  days.

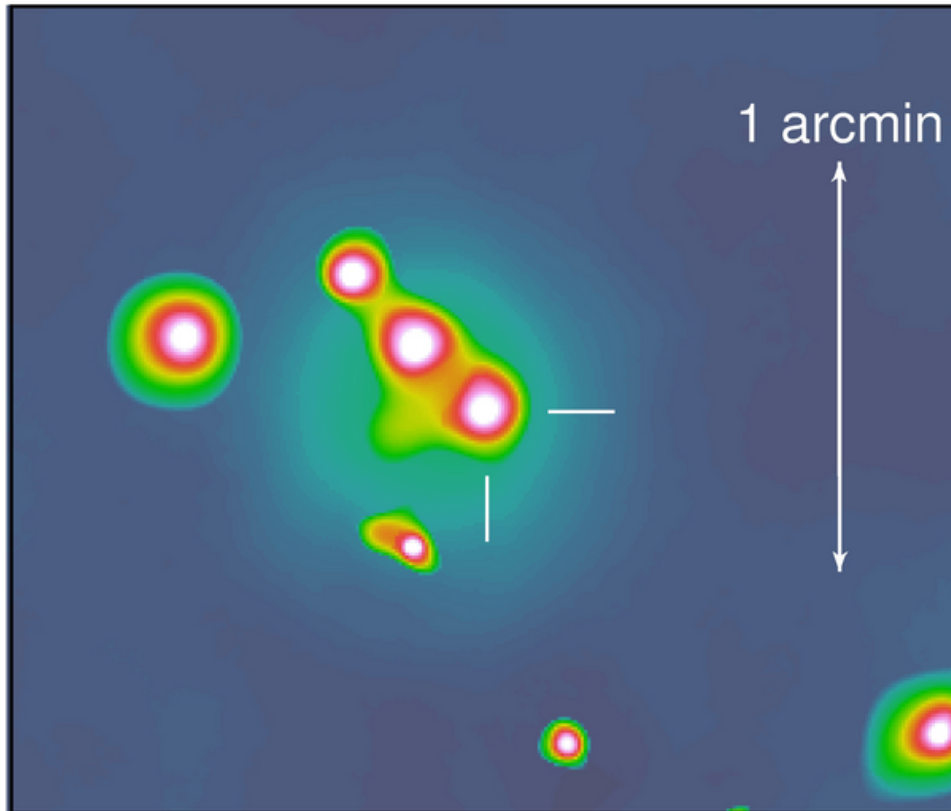


Figure 1.5: The 2–10 keV luminosity of SN 2003L is  $L_X \approx 9.2 \times 10^{39}$  erg/s/Hz for a power-law spectral model. SN 2003L is therefore the most luminous X-ray SN Ibc (on this timescale) with the exception of SN 1998bw.

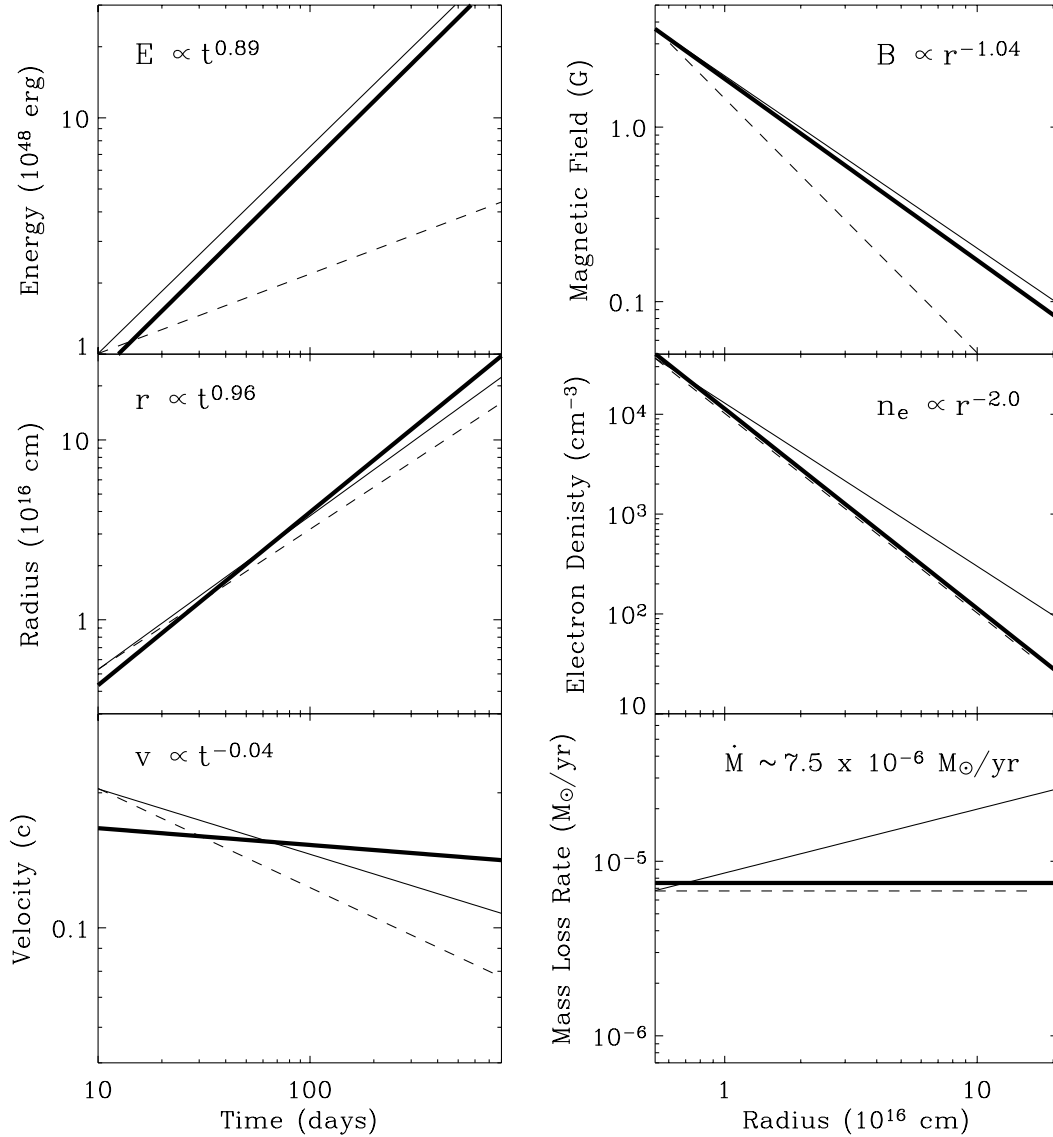


Figure 1.6: Physical parameters for SN2003L based on SSA Model 1 (thick solid line), Model 2 (thin solid line), and Model 3 (thin dashed line) as described in §2.5. Left column: the temporal evolution from  $t = 10 - 800$  days is shown for the ejecta energy, shock radius, and average velocity (top to bottom). Right column: the radial profile of the magnetic field, electron number density, and mass loss rate are shown from  $r = 5 \times 10^{15}$  to  $2.1 \times 10^{17}$  cm. The scalings appearing at the top of each plot correspond to Model 1.

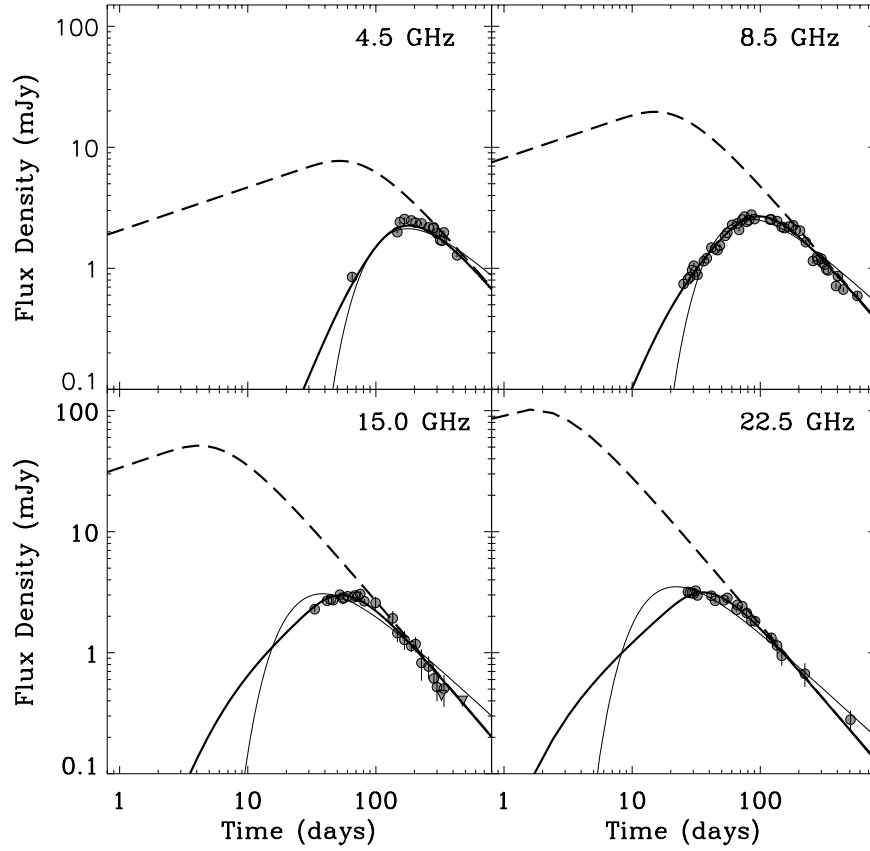


Figure 1.7: Free-free absorption fits for SN 2003L based on formalism from Weiler et al. (421) (basic model; thin solid line) and Weiler et al. (419) (complex model; solid line). The basic model provides a poor fit to the data while the complex model provides a significantly better fit by including additional absorption processes. The intrinsic (de-absorbed) synchrotron spectrum of the complex model (dashed line) implies a relativistic velocity which violates the VLBA constraint at  $t \approx 65$  days.

## Chapter 2

# The Radio and X-ray Luminous SN 2003bg and the Circumstellar Density Variations Around Radio Supernovae<sup>†</sup>

A. M. SODERBERG<sup>a</sup>, R. A. CHEVALIER<sup>b</sup>, S. R. KULKARNI<sup>a</sup>, D. A. FRAIL<sup>c</sup>,

<sup>a</sup>Division of Physics, Mathematics and Astronomy, 105-24, California Institute of Technology,  
Pasadena, CA 91125, USA

<sup>b</sup>Department of Astronomy, University of Virginia, P.O. Box 3818, Charlottesville, VA  
22903-0818, USA

<sup>c</sup>National Radio Astronomy Observatory, Socorro, NM 87801, USA

## Abstract

We report extensive radio and X-ray observations of SN 2003bg whose spectroscopic evolution shows a transition from a broad-lined Type Ic to a hydrogen-rich Type II and later to a typical hydrogen-poor Type Ibc. We show that the extraordinarily luminous radio emission is well described by a self-absorption dominated synchrotron spectrum while the observed X-ray emission at  $t \approx 30$  days is adequately fit by Inverse Compton scattering of the optical photons off of the

---

<sup>†</sup>A version of this chapter was published in *The Astrophysical Journal*, vol. 651, 1005–1018, (2006). Reproduced by permission of the AAS.

synchrotron-emitting electrons. Our radio model implies a sub-relativistic ejecta velocity,  $\bar{v} \approx 0.24c$ , at  $t_0 \approx 10$  days after the explosion which emphasizes that broad optical absorption lines do not imply relativistic ejecta. We find that the total energy of the radio-emitting region evolves as  $E \approx 7.3 \times 10^{48} (t/t_0)^{0.4}$  erg, assuming equipartition of energy between relativistic electrons and magnetic fields ( $\epsilon_e = \epsilon_B = 0.1$ ). The circumstellar density is well described by a stellar wind profile with modest (factor of  $\sim 2$ ) episodic density enhancements which produce abrupt achromatic flux variations. We estimate an average mass loss rate of  $\dot{M} \approx 3 \times 10^{-4} M_\odot \text{ yr}^{-1}$  (assuming a wind velocity of  $v_w = 10^3 \text{ km s}^{-1}$ ) for the progenitor, consistent with the observed values for Galactic Wolf-Rayet stars. Comparison with other events reveals that  $\sim 50\%$  of radio supernovae show similar short timescale flux variations attributable to circumstellar density irregularities. Specifically, the radio light-curves of SN 2003bg are strikingly similar to those of the Type IIb SN 2001ig, suggestive of a common progenitor evolution for these two events. Based on the relative intensity of the inferred density enhancements, we conclude that the progenitors of SNe 2003bg and 2001ig experienced quasi-periodic mass loss episodes just prior to the SN explosion. Finally, this study emphasizes that abrupt radio light-curve variations cannot be used as a reliable proxy for an engine-driven explosion, including off-axis gamma-ray bursts.

## 2.1 Introduction

Accounting for  $\sim 10\%$  of the nearby supernova population, Type Ibc supernovae (hereafter SNe Ibc) are identified by their lack of spectroscopic hydrogen and silicon features (see Filippenko 113 for a review). Recognized as a rare subclass of core-collapse supernova  $\sim 20$  years ago (108), SNe Ibc have recently enjoyed a revitalized interest. Beginning with the discovery of Type Ic SN 1998bw in temporal and spatial coincidence with gamma-ray burst (GRB) 980425 (151, 290), we now know that most long-duration GRBs (e.g., Stanek et al. 377) and X-ray flashes (XRFs; Soderberg et al. 363) are associated with SNe Ibc. However, radio

observations of local SNe Ibc indicate that the inverse is *not* true; there is a strict limit of  $\lesssim 10\%$  on the fraction of SNe Ibc that could be accompanied by a GRB or XRF (370). The lack of hydrogen features in both SNe Ibc and GRB/XRF-associated SNe imply that they represent the explosion of massive stripped-core progenitors (429, 436).

The popular models for SNe Ibc progenitors include massive Wolf-Rayet (WR) stars that eject their envelopes through strong dense winds, and close binary systems where the progenitor star is stripped of its hydrogen-rich layer by the companion (109). Despite dedicated archival searches, the progenitors of SNe Ibc are still poorly constrained by pre-explosion images. The best photometric constraints are currently associated with SN 2002ap and SN 2004gt which exclude WR progenitors in the top  $\sim 30\%$  and  $\sim 50\%$  of the population, respectively (351, 147, 247). While intriguing, these archival observations lack the sensitivity to clearly discriminate between the WR and binary progenitor models.

By studying the circumstellar medium around the supernova, however, it is possible to place independent constraints on the progenitor. Observations show that galactic Wolf-Rayet stars are embedded in wind stratified media (78) while binary systems are associated with disrupted circumstellar media, possibly including an outflow during a common envelope phase (295).

Radio observations provide the most direct probe of the circumstellar density structure around supernovae (421, 71). By observing the dynamical interaction of the ejecta with the surrounding medium we are able to map out the mass loss history of the progenitor star. The identification of irregular density profiles may therefore distinguish between Wolf-Rayet and binary progenitor systems.

Here we present extensive radio observations of SN 2003bg, discovered as part of our ongoing radio survey of local Type Ibc supernovae. The peculiar SN 2003bg spectroscopically evolved from a broad-lined Type Ic to a hydrogen-rich Type II and later to a typical Type Ibc (Hamuy *et al.*, in prep), thereby bridging the hydrogen-rich and poor divisions of the core-collapse classification system. Our densely-sampled radio light-curves show that the extraordinarily luminous radio

emission for a SN Ibc is characterized by episodic short-timescale variations. We show that these variations are well described by abrupt density enhancements in the circumstellar medium. Comparison with other radio supernovae shows that  $\sim 50\%$  of all well-studied events similarly show evidence for abrupt light-curve variations. We review the mass loss evolution observed (and inferred) for the progenitors of these core-collapse SNe. Using the observed radio properties for the peculiar SN 2003bg, we place constraints on the nature of its progenitor system.

The organization of this paper is as follows: observations from the Very Large Array (VLA) and the *Chandra* X-ray Observatory (CXO) are described in §3.2. Preliminary estimates of the energy, velocity, and density of the radio-emitting region are presented in §2.3. Modeling of the radio light-curves are presented in §3.3 and §2.5, while a discussion of the radio polarization mechanism follows as §2.6. Our modeling of the X-ray emission is discussed in §2.7. In §2.8 we present a compilation of radio supernovae with abrupt light-curve variations and review their circumstellar irregularities. Finally, in §2.9 we discuss the possible causes of the density enhancements surrounding SN 2003bg and the implications for the progenitor system.

## 2.2 Observations

SN 2003bg was optically discovered on 2003 February 25.7 UT, offset  $16''.3$  W and  $24''.6$  S from the center of host galaxy, MCG -05-10-15, at  $d \approx 19.6$  Mpc (434). Early spectroscopy on 2003 February 28 UT indicated that SN 2003bg was a peculiar Type Ic supernova with broad optical absorption lines, indicative of fast photospheric velocities and comparable to those seen in SN 1998bw (115). Soon thereafter, SN 2003bg developed strong, broad H $\alpha$  emission with a P-Cygni absorption component indicating an expansion velocity of  $-17,110$  km s $^{-1}$  (174). P-Cygni components were additionally observed for H $\beta$  and H $\gamma$ , prompting the reclassification of SN 2003bg as an unusual Type II supernova. Nebular spectra taken several months later revealed that all evidence of hydrogen had disappeared,

suggestive that the SN had transitioned back to a Type Ibc event (Hamuy et al., in prep).

The peak time of the optical light-curves suggests that SN 2003bg was discovered within just a few days of explosion (Hamuy, private communication). Throughout this paper we therefore assume an approximate explosion date of 2003 February 22 UT.

### 2.2.1 Very Large Array Data

Motivated by the spectroscopic similarity of SN 2003bg to the radio luminous SN 1998bw, we initiated radio observations of SN 2003bg on 2003 March 4.07 UT with the Very Large Array<sup>1</sup> (VLA). At 8.46 GHz we detected a radio source coincident with the optical position at  $\alpha(\text{J2000}) = 04^{\text{h}}10^{\text{m}}59.42^{\text{s}}$ ,  $\delta(\text{J2000}) = -31^{\circ}24'50.3''$  ( $\pm 0.1$  arcsec in each coordinate) with flux density of  $f_{\nu} = 2.51 \pm 0.05$  mJy (Figure 2.1). We subsequently began an intense follow-up campaign to study the temporal and spectral evolution of the radio emission.

Radio data were collected at 1.43, 4.86, 8.46, 15.0, 22.5, and 43.3 GHz spanning 2003 March through 2005 October and are summarized in Table 4.1. All VLA observations were taken in standard continuum observing mode with a bandwidth of  $2 \times 50$  MHz. At 22.5 and 43.3 GHz we included referenced pointing scans to correct for the systematic 10-20 arcsec pointing errors of the VLA antennas. We used 3C48, 3C147, and 3C286 (J0137+331, J0542+498, and J1331+305) for flux calibration, while phase referencing was performed against calibrators J0407-330 and J0453-281. Data were reduced using standard packages within the Astronomical Image Processing System (AIPS). No diffuse radio emission from the host galaxy was detected in any of our observations. Flux density measurements were obtained by fitting a Gaussian model to the SN. In addition to the *rms* noise in each measurement, we include a systematic uncertainty of 2% due to the uncertainty in the

---

<sup>1</sup>The Very Large Array and Very Long Baseline Array are operated by the National Radio Astronomy Observatory, a facility of the National Science Foundation operated under cooperative agreement by Associated Universities, Inc.

absolute flux calibration.

The SN 2003bg radio light-curves are compiled in Figures 2.2 and 2.3, spanning  $\sim 10$  to  $\sim 1000$  days after the explosion. The radio evolution of SN 2003bg is characterized by several achromatic short timescale ( $\delta t/t \lesssim 1$ ) variations. As will be discussed in §2.8, light-curve variations have also been observed for  $\sim 50\%$  of well-sampled radio supernovae including Type IIL SN 1979C (423), Type Ic SN 1998bw (216, 419), and more recently for Type IIb SN 2001ig (325).

### Radio Spectrum

Shown in Figure 2.4 are the spectral indices between each of the adjacent radio frequencies. A spectral turnover is clearly observed for the lower frequencies at early time; at later time the spectral slope converges to  $\beta \approx -1.1$ . The observed spectral shape is overall consistent with a non-thermal synchrotron spectrum with a significant absorption component that suppresses the low frequency emission. In the case of radio supernovae, a low frequency turn-over may be attributed to internal synchrotron self-absorption (SSA; Chevalier 71) or free-free absorption (FFA; Weiler et al. 421) from the external medium. The observed spectral index of the optically-thick spectrum enables us to distinguish between these two processes. For radio supernovae dominated by SSA, the radio spectrum is approximated by

$$F_\nu = 1.582 F_{\nu_p} \left( \frac{\nu}{\nu_p} \right)^{5/2} \times \left( 1 - \exp \left[ - \left( \frac{\nu}{\nu_p} \right)^{-\frac{(5-2\beta_{\text{thin}})}{2}} \right] \right), \quad (2.1)$$

where  $\nu_p$  is the peak spectral frequency,  $F_{\nu_p}$  is the flux density at  $\nu_p$ , and  $\beta_{\text{thin}}$  is the optically-thin spectral index (71). On the other hand, for FFA dominated emission, the optically-thick radio spectrum steepens to

$$F_\nu = K_1 \left( \frac{\nu}{5 \text{ GHz}} \right)^{\beta_{\text{thin}}} \times \exp \left[ -K_2 \left( \frac{\nu}{5 \text{ GHz}} \right)^{-2.1} \right] \text{ mJy} \quad (2.2)$$

where  $K_1$  and  $K_2$  are normalization constants (421).

We fit these functions to two well-sampled radio spectra collected on 2003

March 17 and 2004 February 8 ( $t \approx 23$  and 351 days). As shown in Figure 2.5, the optically-thick spectral component in each epoch is best described with a spectral index of  $\beta \approx 2.5$ , and thus entirely consistent with the index predicted by the SSA dominated model. Specifically, we find the following best-fit SSA parameters:  $F_{\nu_p} \approx 110$  mJy (50 mJy) and  $\nu_p \approx 25$  GHz (2.2 GHz) with  $\chi_r^2 \approx 1.5$  (4.5) for the early (late) spectrum. The FFA dominated models produce steeper optically-thick spectra ( $\beta > 2.5$ ) and thus provide a significantly worse fit to the data. We find the following best-fit FFA parameters:  $K_1 \approx 550$  (35) and  $K_2 \approx 11$  (0.12) with  $\chi_r^2 \approx 180$  (8.2) for the early (late) spectra. Here we have adopted  $\beta_{\text{thin}} \approx -1.1$  for both models, consistent with the observed optically-thin spectral indices from  $t \sim 10$  to 1000 days (Figure 2.4). Clearly the SSA model fit is preferred over the FFA fit in both epochs. We conclude that internal SSA dominates the absorption on the timescale probed by the radio data.

### Radio Polarization of SN 2003bg

Since synchrotron emission is inherently polarized, the magnetic field geometry of radio SNe can be directly probed through polarization measurements. In order to measure the polarization for SN 2003bg, we carried out a full polarization calibration of our 8.46 GHz VLA observations taken on 2003 October 7.4 UT ( $t \approx 227$  days). This run was chosen for polarization calibration based on the high dynamic range of the radio image. To correct for the instrumental polarization, we observed calibrator J0403+260 over a wide range in parallactic angle and computed the leakage terms with AIPS task PCAL. We used 3C147 to calibrate the absolute polarization angle.

We do not find any significant polarization for SN 2003bg. In particular, we place a limit on the linear polarization intensity ( $I_{\text{pol}} = \sqrt{Q^2 + I^2}$ , where  $Q$  and  $I$  are the Stokes parameters) of  $I_{\text{pol}} < 0.071$  mJy, corresponding to a fractional polarization limit of  $\lesssim 0.8\%$  ( $3\sigma$ ). In comparison with other radio SN linear polarization measurements this is one of the deepest limits obtained to date: a factor of  $\sim 4$  deeper than the limit for SN 1993J ( $\lesssim 3.3\%$ , Bietenholz et al. 35)

and comparable to that for SN 1979C ( $\lesssim 1\%$ , Weiler et al. 422).

### 2.2.2 X-ray Observations with Chandra

SN 2003bg was observed with the *Chandra* ACIS-S detector on 2003 March 24.5 UT ( $t \sim 30$  days after the explosion) for 50.5 ksec. Pooley and Lewin (297) reported the detection of an X-ray source at  $\alpha(\text{J2000}) = 04^{\text{h}}10^{\text{m}}59.42^{\text{s}}$ ,  $\delta(\text{J2000}) = -31^{\circ}24'50.3''$  ( $\pm 0.5$  arcsec in each coordinate), coincident with the optical SN position. The source was re-observed with ACIS-S on 2003 June 22.3 UT ( $t \sim 120$  days) for 40.5 ksec to search for variability between the two epochs.

We retrieved the SN 2003bg data from the *Chandra* data archive<sup>2</sup> and reduced them following the CIAO science threads<sup>3</sup>. The source is clearly detected in both epochs and we note that no diffuse emission is detected from the host galaxy. For spectral extraction of the SN emission, we adopt a source aperture of 4.92 arcsec and a large background region located  $\sim 20$  arcsec from the source. After subtracting off the background emission, we measure count rates of  $0.0117 \pm 0.0005$  and  $0.0020 \pm 0.0003$  cps (0.3-10 keV) in the first and second epochs, respectively.

Pooley and Lewin (297) report that the first epoch data can be reasonably fit with several different spectral models and propose a MEKAL hot plasma model for the best fit. Given that the small number of counts prevents the model fits from being distinguished, we fit the extracted SN spectra with only two basic models: absorbed power-law and thermal bremsstrahlung. Table 2.2 lists the parameter values for our resulting spectral fits, where we have adopted both fixed and variable  $N_{\text{H}}$  values for comparison. Schlegel et al. (344) dust maps give  $E(B - V) = 0.022$  mag for the position of SN 2003bg. Using the standard conversion of Predehl and Schmitt (299), we find  $N_{\text{H}} = 1.3 \times 10^{20} \text{ cm}^{-2}$  for the Galactic column density along our line-of-sight. The relatively few X-ray counts enable satisfactory fits ( $\chi_r^2 \sim 1$ ) for each of the models.

Given the significantly fewer counts in the second epoch, we fit the spectrum

---

<sup>2</sup><http://cda.harvard.edu/chaser/>

<sup>3</sup><http://cxc.harvard.edu/ciao/threads/>

with a fixed (galactic) absorption. Moreover, for the power-law fit we adopt the best-fit spectral index from our first epoch. The resulting flux values appear in Table 2.2 for both power-law and thermal bremsstrahlung fits. As in the case of the first epoch, both models provide an equally good representation of the data.

In Figure 2.6 we show the absorbed power-law model fits for Epochs 1 and 2, assuming a fixed Galactic  $N_H$ . Using the associated spectral parameters in Table 2.2, we find unabsorbed flux values of  $F_X \approx (9.3 \pm 0.4) \times 10^{-14}$  and  $(1.2 \pm 0.4) \times 10^{-14}$  erg cm $^{-2}$  s $^{-1}$  (0.3–10 keV) for these fits, respectively.

The observed temporal evolution is  $F_X \propto t^{\alpha_X}$  with  $\alpha_X \approx -1.5 \pm -0.3$  and the implied spectral indices between the optically thin radio and X-ray band are nearly constant at  $\beta_{RX} \approx -0.94$  and  $0.89$ , for the first and second *Chandra* epochs, respectively. At a distance of 19.6 Mpc, the observed X-ray luminosity values are thus  $L_X \approx (4.3 \pm 0.2) \times 10^{39}$  and  $(5.5 \pm 1.9) \times 10^{38}$  erg s $^{-1}$ , placing SN 2003bg among the most X-ray luminous SNe ever detected and a factor of  $\sim 10$  fainter than SN 1998bw on a comparable timescale.

### 2.3 Preliminary Constraints

Readhead (310) showed that there is an upper limit to the brightness temperature,  $T_B$ , for SSA dominated radio sources. This limit corresponds to the scenario where the fractions of post-shock energy density in relativistic electrons ( $\epsilon_e$ ) and magnetic fields ( $\epsilon_B$ ) are in equipartition, and the shocked electrons are accelerated into a power-law distribution,  $N \propto \gamma^{-p}$ , above a minimum Lorentz factor,  $\gamma_m$ . Under these assumptions, the equipartition brightness temperature,  $T_{\text{ep}} \equiv c^2 f_{\nu_p} / (2\pi k \theta_{\text{ep}}^2 \nu_p^2) \approx 5 \times 10^{10}$  K, defines the upper bound on  $T_B$  (310, 216). Here,  $\theta_{\text{ep}}$  is the equipartition size (radius) of the radio source. It is noted that  $T_{\text{ep}}$  depends only weakly on the observed peak frequency and flux density.

Under the assumption that  $T_B = T_{\text{ep}}$ , we can estimate the radius and energy of the radio-emitting material for SN 2003bg. Our first VLA epoch in which the spectral turnover is observed is 2003 March 29 ( $t \sim 35$  days). In this epoch

we observed a peak flux density of  $f_{\nu_p} \approx 85$  mJy at  $\nu_p \approx 22.5$  GHz and an optically thin spectral index of  $\beta = -(p - 1)/2 \approx -1.1$  (Figure 2.4). As shown in Figure 2.5, on the timescale probed by our observations the SN 2003bg radio spectrum is well fit with a SSA model and we therefore identify the spectral peak as the synchrotron self-absorption frequency,  $\nu_a$  (defined as the frequency where the optical depth due to SSA is unity;  $\tau_{\text{SSA}} = 1$ ). Using Equations 2 and 3 of Soderberg et al. (359) (hereafter S05) the observed source properties ( $f_{\nu_p}$ ,  $\nu_p$ ,  $\beta$ , and  $d$ ) imply an equipartition radius of  $\theta_{\text{ep}} \approx 40$   $\mu\text{as}$  ( $r_{\text{ep}} \approx 1.2 \times 10^{16}$  cm) and a total energy for the radio-emitting material of  $E_{\text{ep}} \approx 1.7 \times 10^{48}$  erg, where we have assumed  $\epsilon_e = \epsilon_B = 0.1$ . The average velocity of the radio shell is therefore roughly  $\bar{v}_{\text{ep}} \approx 0.13c$  and the magnetic field is  $B_{\text{ep}} \approx 2.8\epsilon_B^{1/2} E_{\text{ep}}^{1/2} r_{\text{ep}}^{-3/2} \approx 0.9$  G.

A comparison with the ejecta velocities compiled for core-collapse SNe (71) shows that SN 2003bg resembles more closely a Type Ibc (typical ejecta velocities,  $\bar{v} \sim 0.1c$ ) rather than a Type II event ( $\bar{v} \sim 0.01c$ ). Moreover, the inferred ejecta velocity for SN 2003bg is a factor of  $\sim 10$  slower than the mildly relativistic speed inferred for SN 1998bw. This analysis emphasizes that broad optical absorption lines cannot be used as a proxy for relativistic ejecta, consistent with the radio analysis for broad-lined SNe 2002ap (22) and SN 2003jd (370).

Our preliminary constraint on the minimum energy for SN 2003bg places it among the most energetic radio SNe Ibc ever observed, second only to SN 1998bw and comparable to SN 2003L (S05). We note that additional absorption processes (e.g., FFA) and departures from equipartition (e.g., SN 1993J; Fransson and Björnsson 136) increase the energy budget further.

Equipartition analysis may also be used to roughly constrain the characteristic synchrotron frequency,  $\nu_m$ . Equating particle kinetic energy across the shock discontinuity, S05 show that  $\nu_m \approx 9.2 \times 10^3 \epsilon_e^2 (v/c)^4 B$  GHz, which gives  $\nu_m \approx 0.02$  GHz for  $\epsilon_e = 0.1$  with the values of  $v_{\text{ep}}$  and  $B_{\text{ep}}$  given above. At  $t \sim 35$  days,  $\nu_m$  is therefore already below our radio observing band and the synchrotron break frequencies are ordered such that  $\nu_m < \nu_a$ .

Finally, we use these equipartition results at  $t \approx 35$  days to estimate the mass

loss rate of the progenitor star. From Chevalier (71), the mass loss rate of the star,  $\dot{M}$ , can be derived from the post-shock energy density in magnetic fields:

$$U_B = \frac{B^2}{8\pi} \approx \frac{\epsilon_B}{4\pi} \left( \frac{\dot{M}}{v_w} \right) r^{-2} v^2 \quad (2.3)$$

where we have assumed a stellar wind-blown medium ( $n \propto r^{-2}$ ). We find  $\dot{M} \approx 6.1 \times 10^{-5} M_\odot \text{ yr}^{-1}$  (assuming a Wolf-Rayet wind velocity of  $v_w = 10^3 \text{ km s}^{-1}$ ).

For comparison, we estimate the mass loss rate assuming FFA dominates the absorption. In this scenario, the shock radius is larger than the equipartition estimate and so our equipartition parameters provide only a lower limit on the mass loss rate of the progenitor star. Using Equation 2.3 of (137) we find:

$$\frac{\dot{M}_{-5}}{v_{w,3}} > 4.3 \times 10^3 \tau_{\text{FFA}}^{1/2} \frac{\nu_p}{\text{GHz}} T_5^{3/4} \left( \frac{v}{c} \right)^{3/2} \left( \frac{t}{35 \text{ days}} \right)^{3/2} \quad (2.4)$$

where  $\tau_{\text{FFA}}$  is the optical depth to FFA processes and  $T_5$  is the temperature normalized to  $10^5 \text{ K}$ . Here we have adopted the notation  $10^x Q_x = Q$  where  $\dot{M}$  is given in units of  $M_\odot \text{ yr}^{-1}$  and  $v_w$  is given in  $\text{km s}^{-1}$ . Setting  $\tau_{\text{FFA}} = 1$  and  $T_5 = 1$  we find  $\dot{M}_{-5}/v_{w,3} > 4.5 \times 10^3$  corresponding to a mass loss rate of  $0.045 M_\odot \text{ yr}^{-1}$  ( $v_w = 10^3 \text{ km s}^{-1}$ ) at  $t \approx 35 \text{ days}$ . This is three orders of magnitude larger than that derived from the SSA interpretation. Moreover, this would imply that the total energy of the radio-emitting material (a proxy for the kinetic energy of the fastest ejecta,  $v \gtrsim 0.13c$ ) exceeds  $1.5 \times 10^{51} \text{ erg}$ . Since hydrodynamic collapse distributes the ejecta kinetic energy as  $E_K \propto v^{-5}$  (245), this would imply that the optical data (with  $v \approx 0.06c$ ) have  $E_K > 10^{53} \text{ erg}$ , larger than any other core-collapse SN to date. This result, taken together with the fact that a SSA model provides a significantly better fit to the radio spectra, leads us to conclude that the observed spectral turn-over is due to internal synchrotron self-absorption.

## 2.4 Synchrotron Self-absorption Model

In modeling the radio light-curves of SN 2003bg, we adopt the formalism of S05 where we presented a rigorous formulation of the temporal and spectral evolution of synchrotron emission arising from sub-relativistic supernova ejecta. S05 show how the observed SN radio emission spectrum at any single epoch is determined by three parameters:  $C_f$ ,  $C_\tau$ , and  $\nu_m$ . Here,  $C_f$  and  $C_\tau$  are normalization constants of the flux density and optical depth with cgs units of  $\text{g s}^{1/2}$  and  $\text{s}^{-(2+p/2)}$ , respectively. The parameters  $C_f$ ,  $C_\tau$  and  $\nu_m$  are in turn determined by the values of four physical parameters: the magnetic field,  $B$ , the shock radius,  $r$ , the minimum electron Lorentz factor,  $\gamma_m$ , and the ratio  $\mathfrak{F} \equiv \epsilon_e/\epsilon_B$ . With four physical parameters ( $B$ ,  $r$ ,  $\gamma_m$ ,  $\mathfrak{F}$ ) and only three constraints ( $C_f$ ,  $C_\tau$ ,  $\nu_m$ ), we must assume an additional constraint to find a unique solution. This constraint is obtained by adopting a value for  $\mathfrak{F}$ . By inverting the equations for  $C_f$ ,  $C_\tau$ , and  $\nu_m$ , S05 derive the following expressions for  $B$ ,  $r$ , and  $\gamma_m$ :

$$B = 9.0 \times 10^{-8} (2+p)^{-6/17} (p-2)^{-4/17} \eta^{4/17} \mathfrak{F}^{-1/17} \times \left(\frac{d}{\text{cm}}\right)^{-4/17} \left(\frac{C_f}{\text{g s}^{1/2}}\right)^{-2/17} \left(\frac{C_\tau}{\text{s}^{-(2+p/2)}}\right)^{4/17} \left(\frac{\nu_m}{\text{Hz}}\right)^{-2(p-2)/17} \text{ G} \quad (2.5)$$

$$r = 9.3 \times 10^{12} (2+p)^{7/17} (p-2)^{-1/17} \eta^{1/17} \mathfrak{F}^{-1/17} \times \left(\frac{d}{\text{cm}}\right)^{16/17} \left(\frac{C_f}{\text{g s}^{1/2}}\right)^{8/17} \left(\frac{C_\tau}{\text{s}^{-(2+p/2)}}\right)^{1/17} \left(\frac{\nu_m}{\text{Hz}}\right)^{-(p-2)/34} \text{ cm} \quad (2.6)$$

$$\gamma_m = 2.0 (2+p)^{3/17} (p-2)^{2/17} \eta^{-2/17} \mathfrak{F}^{2/17} \times \left(\frac{d}{\text{cm}}\right)^{2/17} \left(\frac{C_f}{\text{g s}^{1/2}}\right)^{1/17} \left(\frac{C_\tau}{\text{s}^{-(2+p/2)}}\right)^{-2/17} \left(\frac{\nu_m}{\text{Hz}}\right)^{(13+2p)/34}. \quad (2.7)$$

Here,  $d$  is the distance to the supernova and  $\eta$  characterizes the thickness of the radiating electron shell as  $r/\eta$ . The number density of the synchrotron emitting electrons then follows directly as

$$n_e = \frac{p-2}{p-1} \frac{B^2}{8\pi} \frac{\mathfrak{F}}{m_e c^2 \gamma_m} \quad (2.8)$$

where it is assumed that the contribution from electrons in a thermal distribution is negligible. The circumstellar density can be expressed in terms of a progenitor mass loss rate

$$\dot{M} = \frac{8\pi}{\eta} n_e m_p r^2 v_w \quad (2.9)$$

by adopting a value for the wind velocity. The total energy of the radio-emitting material at a given epoch is then given by

$$E = \frac{4\pi}{\eta} r^3 \frac{\mathfrak{F} B^2}{\epsilon_e 8\pi} \quad (2.10)$$

where it should be noted that  $E$  depends not only on  $\mathfrak{F}$  but also on an assumed value of  $\epsilon_e$ .

#### 2.4.1 Hydrodynamical Evolution of the Ejecta

As discussed by Chevalier (70), several models have been proposed for hydrodynamic evolution of the sub-relativistic supernova ejecta. Based on separate assumptions, these analytic models constrain the temporal behavior of the shock radius, magnetic field, electron Lorentz factor, and energy partition fractions. Here, we adopt the standard SSA model (Model 1 of Chevalier 70) for the hydrodynamical evolution of the ejecta. This model assumes that the evolution is self-similar across the shock discontinuity, and thus  $r \propto t^{\alpha_r}$  with  $\alpha_r = (n-3)/(n-s)$  where  $n$  characterizes the density profile of the outer SN ejecta ( $\rho \propto r^{-n}$ ) and  $s$  characterizes the density profile of the radiating electrons within the shocked circumstellar material ( $n_e \propto r^{-s}$ ). In addition, the standard SSA model assumes that the magnetic energy density ( $U_B \propto B^2$ ) and the relativistic electron energy density ( $U_e \propto n_e \gamma m$ ) scale as the total post-shock energy density ( $U \propto n_e v^2$ ). In this scenario, the magnetic field is amplified by turbulence near the shock discontinuity, implying fixed energy fractions,  $\epsilon_e$  and  $\epsilon_B$ , and thus a constant value of  $\mathfrak{F}$  throughout the evolution of the ejecta.

The evolution of the magnetic field is determined by the CSM density profile and the expansion of the shock radius:  $B \propto t^{\alpha_B}$  with  $\alpha_B = \alpha_r(2-s)/2 - 1$ . We note that for a wind-stratified medium,  $s = 2$  and  $\alpha_B = -1$ . The minimum Lorentz factor evolves as  $\gamma_m \propto t^{\alpha_\gamma}$  with  $\alpha_\gamma = 2(\alpha_r - 1)$ . From the scalings of Equation 2.10 it follows that  $E \propto t^{3\alpha_r - 2}$ , and therefore the total post-shock energy increases with time until the swept up circumstellar mass is comparable to the rest mass of the SN ejecta.

## 2.5 SSA Model Fit for SN 2003bg

As shown in Figure 2.2 and briefly discussed in §3.2, the radio light-curves for SN 2003bg are characterized by achromatic short timescale variability, inconsistent with the strict power-law evolution prescribed by the standard model. In an effort to model the overall evolution of the radio ejecta we therefore divide the multi-frequency light-curves into four subsections, each defined by the observed time of abrupt variation. We then apply the SSA model described in §3.3 to each subsection.

### 2.5.1 The Synchrotron Self-absorption Peak

Figure 2.3 shows that the first peak observed for each of the radio frequencies is chromatic, and therefore produced by a cascading spectral break. We define the time range for this chromatic evolution phase to be  $t < 110$  days, extending until just before the first achromatic variation is observed. As discussed in §3.2 the radio emission is well described by a SSA dominated spectrum and we therefore attribute this chromatic subsection to the passage of  $\nu_a$  through the observed frequencies. The evolution of the spectral indices (Figure 2.4) indicate that the self-absorption frequency cascades as  $\nu_a \propto t^{-1.1}$ , consistent with typical values observed for other SSA dominated radio supernovae (71).

Using our multi-frequency radio data collected during the time range of the first peak and adopting  $\mathfrak{F} = 1$ , we fit for the constants  $C_f$  and  $C_\tau$  as well as the

temporal indices  $\alpha_r$  and  $\alpha_B$ . As discussed in Section 2.3,  $\nu_m$  is estimated to be below the radio band during our observations and thus is unconstrained by the data. We therefore estimate  $\nu_{m,0} \approx 0.1$  GHz at our chosen reference time of  $t_0 = 10$  days<sup>4</sup>, consistent with the preliminary value calculated in §2.3. We find a best-fit solution ( $\chi_r^2 \approx 46$ ; dominated by interstellar scintillation) for parameters:  $p \approx 3.2$ ,  $C_f \approx 3.1 \times 10^{-51}$  g s<sup>1/2</sup>,  $C_\tau \approx 6.2 \times 10^{38}$  s<sup>-3.6</sup>,  $\alpha_r \approx 0.8$ , and  $\alpha_B \approx -1$ . These values imply  $s \approx 2$ ,  $n \approx 7$  and  $\alpha_\gamma \approx -0.4$ . As explained within the Appendix of S05, we parameterize the sharpness of the  $\nu_a$  spectral break with  $\zeta = [0, 1]$  and find  $\zeta \approx 0.6$  for our final solution. This SSA model provides a reasonable fit to the chromatic subsection of the light-curves as shown in Figures 2.2 and 2.3.

With this SSA model fit, the physical parameters of the ejecta and CSM are uniquely determined by Equations 2.5 - 2.10. Chevalier (67) shows that for  $s \approx 2$  and  $n \approx 7$ ,  $\eta \approx 4$ . Adopting this value, we find that the expansion of the ejecta is described by  $r \approx 6.2 \times 10^{15}(t/t_0)^{0.8}$  cm, and the average velocity is  $\bar{v} \approx 0.24(t/t_0)^{-0.2}c$ . The radio ejecta therefore expand with a modest sub-relativistic velocity comparable to that observed for SN 2002ap (22), and significantly slower than SN 1998bw (bulk Lorentz factor,  $\Gamma \sim 2$  on a similar timescale (216, 226). Adopting  $\epsilon_e = \epsilon_B = 0.1$  we find that the total energy of the radio emitting material is given by  $E \approx 7.3 \times 10^{48}(t/t_0)^{0.4}$  erg, comparable to that of SN 1998bw. The magnetic field evolves radially as  $B \approx 4.9(r/r_0)^{-1.25}$  G, slightly steeper than that observed for Type Ic SNe 2003L (S05), 2002ap (22) and the Type IIb SN1993J (136). The electron number density and associated mass loss rate are thus given by  $n_e \approx 2.2 \times 10^5(r/r_0)^{-2}$  cm<sup>-3</sup> and  $\dot{M} \approx 1.4 \times 10^{-4}$  M<sub>⊙</sub> yr<sup>-1</sup> where we have assumed a Wolf-Rayet wind velocity of  $v_w = 1000$  km s<sup>-1</sup> and adopted a nucleon-to-electron density ratio of two (appropriate for WR winds). This mass loss rate is consistent with the values observed for Galactic Wolf-Rayet stars (62).

---

<sup>4</sup>Here (and throughout) we use subscript “0” to denote the values of parameters at the reference time.

### 2.5.2 Subsequent Light-curve Variations

Shortly after the observed SSA peak cascades through 8.46 GHz, an abrupt rise was observed at the optically thin frequencies. By  $t \sim 120$  days the radio emission reached an *achromatic* second peak. Subsequent achromatic light-curve variations were later observed at  $t \sim 300$  and 600 days and are most pronounced at frequencies above  $\nu_a$ . As shown in Figure 2.4 these variations were associated with abrupt changes in the spectral indices, most notably for those indices which straddle  $\nu_a$ .

Possible causes for these abrupt light-curve variations include energy injection from a central engine, interaction of the reverse shock with density structures in the ejecta, and interaction of the forward shock with CSM density enhancements. Kulkarni et al. (216) invoke energy injection to explain the achromatic second peak in the radio light-curves of SN 1998bw at  $t \sim 40$  days. This interpretation was supported by the inferred mildly relativistic ejecta speeds and associated prompt gamma-ray emission, suggestive that SN 1998bw was powered by a GRB-like central engine. In the case of SN 2003bg, however, the inferred ejecta speed is merely sub-relativistic and therefore there is no evidence for an engine-driven explosion. We conclude that the variations observed for SN 2003bg cannot be attributed to long-lived engine activity.

Mioduszewski et al. (257) show that the late-time flattening observed for the SN 1993J radio light-curves can be produced through the interaction of the reverse shock with density inhomogeneities within the ejecta. While the 1-D hydrodynamical simulations provide a reasonable fit to the smooth evolution of SN 1993J at  $t \gtrsim 1000$  days, it is not clear that they could produce the abrupt rise at  $t \sim 100$  days observed for SN 2003bg. Moreover, any abrupt features in the ejecta would likely be smoothed by instabilities in a 3-D simulation.

In the third scenario, the interaction between the forward shock and strong density variations in the circumstellar material produces abrupt changes in the temporal evolution of the radio light-curves. For a wind-stratified medium with constant progenitor mass loss rate, the circumstellar density is predicted to follow a smooth  $r^{-2}$  profile. Abrupt deviations from a wind density profile have been

inferred for several radio supernovae (e.g., SN 1979C; Weiler et al. 423) and are argued to be the result of a variable mass loss history and/or the effects of a binary companion on the structure of the CSM. These density-induced variations are more pronounced at optically thin frequencies than for optically thick. Here we show that the light-curve variations observed for SN 2003bg are similarly due to CSM density enhancements.

We model the SN 2003bg radio light-curves with a simple density enhancement model under the following assumptions: (a) the density variations can be approximated by modest abrupt jumps in the CSM such that the density profile returns to  $n_e \propto r^{-2}$  after each enhancement, (b) the hydrodynamical evolution of the ejecta returns to the self-similar solution after each jump, thereby maintaining the same values of  $\alpha_r$ ,  $\alpha_B$ , and  $\alpha_\gamma$  both before and after each density enhancement, (c) the microphysics of the shock are not affected by the density jumps and therefore  $\epsilon_e$  and  $\epsilon_B$  remain constant throughout the evolution of the ejecta, (d) the bulk motion of the ejecta is not significantly affected by the density jumps since the slower, more massive material behind the shock continues to plow forward, and (e) the minimum Lorentz factor of the radiating electrons is not affected by the CSM enhancements, although the number of electrons participating in the radio emission increases.

Maintaining a self-similar evolution throughout the density variations requires that the magnetic field is enhanced by each of the CSM jumps. Moreover, since  $\epsilon_e$  and  $\epsilon_B$  are assumed to be fixed constants, the additional thermal energy produced by these enhancements causes an increase in the total energy of the radio emitting region. Therefore, in fitting the subsequent peaks in the SN 2003bg radio light-curves, we assume that the evolution of  $r$  and  $\gamma_m$  remain effectively unchanged while  $B$  and  $E$  vary according to the strength of the CSM density enhancements.

We recognize that this simple density enhancement model is not fully consistent with the hydrodynamic evolution of the ejecta. In fact, a small change in the radial expansion is expected as the shock wave reaches the higher-density region. For the  $n \approx 7$  self-similar solution adopted here and the modest density enhancements we

infer, we estimate this to be a minor effect ( $\sim 10\%$ ). Therefore, the variations in ejecta parameters ( $B$  and  $E$ ) are primarily the result of the CSM density enhancements rather than the minor variations in radial expansion. However, the series of density jumps that we infer cause the evolution of the radio ejecta to gradually deviate from the initial radial evolution, making our model less accurate at very late time (after several years). In addition, we note that the outflow does not immediately settle on the new self-similar solution following each density variation, but instead settles on a timescale comparable for the radius to double (i.e. the ratio of the settling time to the age of the blastwave is of order unity). Thus the sharp features appearing in our light-curve fits are merely an artifact of our model assumptions.

As discussed in §3.3,  $C_f$ ,  $C_\tau$ , and  $\nu_m$  are functions of just three physical parameters:  $r$ ,  $\gamma_m$ , and  $B$ . Of these, only  $B$  responds significantly to the CSM density variations. From the Appendix of S05 we have  $C_f \propto B^{-1/2}$ ,  $C_\tau \propto B^{3+p/2}$ , and  $\nu_m \propto B$ . By fitting for  $B$  at each density variation, the new values of  $C_f$ ,  $C_\tau$ , and  $\nu_m$  are thus directly determined.

The observed timescales and estimated circumstellar radii for each density enhancement are given in Table 2.3. We note that we do not fit the short rise time of each phase during which the ejecta are settling to the new self-similar solution. As shown in Figure 2.3, we find reasonable fits for each of the light-curve phases by invoking modest (factor of  $\lesssim 2$ ) density enhancements. In Table 2.3 we list the values of  $C_f$ ,  $C_\tau$  and  $\nu_m$  and the associated enhancement factors for the density, magnetic field, and ejecta energy for each phase. It is interesting to note that the strength of the enhancements decay with time.

## 2.6 Radio Polarization

As discussed in §3.2, our VLA observations constrain the linear polarization of the radio emission to less than  $\sim 0.8\%$ . Although the synchrotron emission from the radio ejecta is inherently polarized, the observed polarization level can

be significantly suppressed for two reasons. First, since the SN 2003bg radiosphere is not resolved in the VLA data our polarization limit applies to the *integrated* polarization of the ejecta emission. As shown for supernova remnant Cas A, the integrated polarization can be significantly suppressed due to the approximate circular symmetry of the radio ejecta (322). Second, the radio emission can be depolarized due to internal Faraday dispersion within the ejecta (53, 68). For the density and magnetic field values we derive from our SSA model, we predict the integrated linear polarization of the SN 2003bg radio emission to be negligible, consistent with the observations.

## 2.7 Modeling the X-ray emission

X-ray emission in supernovae can be produced by three processes (137): [1] non-thermal synchrotron emission from radiating electrons, [2] thermal (free-free) bremsstrahlung emission from material in the circumstellar shock and/or the ejecta reverse shock, and [3] inverse Compton scattering of photospheric photons by relativistic electrons. We examine each of these scenarios in the context of the bright X-ray emission observed for SN 2003bg.

### 2.7.1 Synchrotron Emission

As shown in Table 2.2, the spectral index between the optically thin radio and X-ray emission is  $\beta \approx -0.9$  for both *Chandra* epochs. Assuming a constant injection spectral index from the radio to X-ray bands we extrapolate the observed radio spectral index of  $\beta \approx 1.1$  to the X-ray and find that the synchrotron emission under-predicts the observed X-ray flux by a factor of  $\sim 10$  in both epochs. This discrepancy grows significantly larger when the synchrotron cooling break,  $\nu_c = 18\pi m_e c e / (t^2 \sigma_T^2 B^3)$ , is included, beyond which the spectrum steepens by  $\Delta\beta = -0.5$ . Using the magnetic field derived in §2.5, the cooling frequency at  $t \approx 30$  (120) days is  $\nu_c \approx 6.1 \times 10^{10}$  ( $2.3 \times 10^{11}$ ) Hz. Including the cooling break and extrapolating from  $\nu_c$  to  $\nu_{\text{X-ray}}$  as  $f_\nu \propto \nu^{-1.6}$ , the synchrotron flux falls five orders

of magnitude below the observed X-ray emission. We therefore conclude that the X-ray emission is not dominated by synchrotron emission.

### 2.7.2 Thermal Bremsstrahlung Emission

In a scenario dominated by thermal bremsstrahlung processes, the X-ray emission is produced by the forward shock plowing into circumstellar material and/or the reverse shock heating of the ejecta. In this case, the strength of the X-ray emission depends strongly on the density of the CSM and unshocked ejecta. The shocked material then cools by free-free emission processes. For a wind-stratified density profile, the summed free-free luminosity from the forward and reverse shock is generalized (72, 385) roughly by

$$L_{X,\text{FS+RS}} \approx 8.6 \times 10^{34} C_{L,\text{FS+RS}} \dot{M}_{-5}^2 v_{w,3}^{-2} t_1^{-1} \text{ erg s}^{-1} \quad (2.11)$$

where  $C_{L,\text{FS+RS}}$  is a constant such that  $C_{L,\text{FS+RS}} = 1 + (n-3)(n-4)^2/(4n-8)$ . From our SSA radio model we find  $\alpha_r \approx 0.8$  and  $\dot{M}_{-5} \approx 14$  ( $v_{w,3} = 1$ ), thus  $C_{L,\text{FS+RS}} \approx 2.8$  and  $L_{X,\text{FS+RS}} \approx 1.6 \times 10^{37} \text{ erg s}^{-1}$ . The predicted X-ray luminosity is therefore a factor of  $\sim 10^2$  fainter than the first epoch observation.

On the other hand, if we assume the X-ray emission must be dominated by free-free processes, then this implies a significantly higher mass loss rate of  $\dot{M}_{-5} \approx 230$  ( $v_{w,3} = 1$ ). However, we reiterate that a high-density model dominated by external absorption processes is inconsistent with the observed radio spectrum (Figure 2.5). A possible compromise could be that the X-ray emission is produced by dense CSM clumps distributed with a very low filling factor ( $f \ll 1$ ) such that the radio emission is optically thin. This scenario was invoked for the radio luminous Type IIn SN 1986J (420). However, the dense CSM clumps inferred for Type IIn's also give rise to bright nebular H $\alpha$  emission lines which are not present in the nebular spectra of SN 2003bg. Moreover, it would be difficult to sustain the ejecta velocities inferred from our radio modeling in such a high density environment (Chevalier & Fransson, *in prep*). We conclude that the radio and optical emission

do not support a scenario in which the observed X-ray flux is dominated by thermal bremsstrahlung emission.

### 2.7.3 Inverse Compton Scattering

X-ray emission from supernovae can also be produced by inverse Compton scattering (ICS) of the relativistic electrons by the optical photons. This process was observed to be important in explaining the observed X-ray emission for SN 2002ap (37) and SN 2003L (S05) on timescales comparable to the optical maximum. In this scenario the ratio of flux measured in the radio and X-ray bands, respectively is given by

$$\frac{F_{\text{radio}}}{F_X} \approx \frac{U_B}{U_{\text{ph}}} \quad (2.12)$$

where  $U_B$  and  $U_{\text{ph}}$  are the energy densities in magnetic fields and up-scattered photons, respectively. We note that Equation 2.12 is relatively insensitive to the spectral energy index of the electrons. Björnsson and Fransson (37) show that

$$U_{\text{ph}} \approx 0.4 L_{\text{bol},42} \left( \frac{t_d v}{c} \right)^{-2} \text{ erg cm}^{-3} \quad (2.13)$$

where  $t_d$  is the time in days,  $L_{\text{bol},42}$  is the optical luminosity at  $t = t_d$  normalized to  $10^{42}$  erg  $\text{s}^{-1}$  and  $v$  is the shock velocity.

At the time at the first X-ray observation,  $t_d \approx 30$ , the optically thin radio flux was  $F_{\text{radio}} \approx 2.2 \times 10^{-14}$  erg  $\text{cm}^{-2}$   $\text{s}^{-1}$  and the unabsorbed X-ray flux was  $F_X \approx 9.3 \times 10^{-14}$  erg  $\text{cm}^{-2}$   $\text{s}^{-1}$ ; therefore  $F_{\text{radio}}/F_X \approx 0.24$ . From our SSA radio modeling (§2.5) we estimate  $B \approx 1.6$  G and  $v \approx 0.19c$  at  $t \approx 30$  days. Based on the optical peak magnitude (Hamuy et al., private communication) we find  $L_{\text{bol},42} \approx 2.3$  at  $t_d \approx 30$ , coincident with the time of optical maximum. Therefore,  $U_B = B^2/8\pi \approx 0.10$  erg  $\text{cm}^{-3}$ , and  $U_{\text{ph}} \approx 0.028$  erg  $\text{cm}^{-3}$ . Thus  $U_B/U_{\text{ph}} \approx 0.28$ , comparable to the observed ratio for  $F_{\text{radio}}/F_X$ . We conclude that inverse Compton emission can produce the bright X-ray luminosity in the first epoch.

The second epoch, however, cannot be explained through ICS. From our radio

model at  $t_d \approx 120$ ,  $B \approx 0.41$  G,  $v \approx 0.15c$  and  $F_{\text{radio}} \approx 1.5 \times 10^{-15}$  erg cm $^{-2}$  s $^{-1}$ . The optical light-curve implies  $L_{\text{bol},42} \approx 0.23$  at this time. Therefore we estimate  $U_B/U_{\text{ph}} \approx 24$  and a predicted IC X-ray flux of  $6.3 \times 10^{-17}$  erg cm $^{-2}$  s $^{-1}$  which is a factor of  $\sim 200$  fainter than that observed. We conclude that the X-ray flux observed at 120 days is dominated by a separate process, possibly due to a cosmic ray dominated SN shock which produces a late-time flattening of X-ray light-curves in SNe Ibc (Chevalier & Fransson, *in prep.*)

## 2.8 Radio Supernovae and CSM Density Variations

We have shown that the abrupt radio light-curve variations observed for SN 2003bg can be attributed to density enhancements in the circumstellar medium. In comparison with well-sampled radio supernovae compiled from previous studies<sup>5</sup> including our ongoing survey of Type Ibc events (Soderberg *et al.*, *in prep.*), we find that  $\sim 50\%$  of radio supernovae similarly show evidence for abrupt achromatic variations. At the same time, there are several examples of well-studied radio supernovae with smooth light-curve evolutions including Type IIb SN 1993J (409, 35) and Type Ic SN 2003L (S05), among others. In Table 2.4, we compile the light-curve properties for radio supernovae with abrupt variability. We emphasize that this compilation contains core-collapse SNe from nearly all spectroscopic classifications, including hydrogen-rich Type IIL, IIIn, and IIb, in addition to hydrogen-poor Type Ibc.

Table 2.4 shows that the short timescale variability observed for radio supernovae can be qualitatively divided into three types. The most common effect is an abrupt steepening of the radio light-curves as observed for SN 1988Z (433). On the other hand, an abrupt rise in the optically thin flux has been observed for a couple of events (e.g., SN 1987A, Manchester *et al.* 238). More intriguingly, episodic (and perhaps periodic) light-curve bumps are observed for SNe 1979C (425, 260, 261), 2001ig (325), 1998bw (216, 419), and 2003bg, all of which are characterized by

---

<sup>5</sup><http://rsd-www.nrl.navy.mil/7213/weiler/sne-home.html>

modest flux deviations (factor of  $\lesssim 2$ ).

These three types of radio variability are generally attributed to dynamical interaction of the ejecta with irregularities in the circumstellar medium. Abrupt density variations in the media surrounding core-collapse supernovae are known to be produced in a variety of ways, including: [1] fluctuations in the progenitor mass loss rate and/or wind velocity. This scenario is supported through observations of local supernova remnants and massive stars which collectively suggest a complex picture for mass loss during the final stage of stellar evolution. [2] Termination shocks between stellar winds ejected during the evolution of the progenitor star may produce abrupt density enhancements at radii of  $R \gtrsim 0.1$  pc (154, 155, 74, 307). Case 2 is observationally motivated by the circumstellar nebulae associated with local Wolf-Rayet stars, which are produced by interacting stellar winds (78). [3] a clumpy stellar wind perhaps resulting from fragmentation of circumstellar shells by Rayleigh-Taylor instabilities (154). This scenario is motivated by narrow  $H\alpha$  line profiles observed for Type II<sub>n</sub> supernovae. In the case of SN 1988Z, Chugai and Danziger (81) propose a shocked dense wind component at  $R \sim 5 \times 10^{16}$  cm to explain the low-velocity line emission. [4] the effects of a binary companion on the circumstellar wind profile. This case is observationally motivated by the binary companion for Type II<sub>b</sub> SN 1993J (246) and the dense circumstellar ring around SN 1987A at  $R \sim 8 \times 10^{17}$  cm (54) commonly attributed to the effects of a companion star (294). In this scenario, the binary system parameters determine the circumstellar radii at which the progenitor wind is most affected. [5] a close binary progenitor system embedded in a common envelope (295). Given that the rate of SN progenitors in common envelope binary systems is predicted to be low ( $\sim 1\%$  of SNe Ibc; Chugai 79) this scenario is expected to be rare. As an example, a common envelope system has been argued to explain the large inferred density enhancement at  $R \sim 7 \times 10^{16}$  cm responsible for strong radio (381), X-ray (298), and optical ( $H\alpha$ ; Soderberg et al. 358) emission in the unusual Type Ic SN 2001em at  $t \sim 2.5$  years (80).

To summarize, the strength and location of circumstellar density variations

depend on the method by which the density profile was disturbed. We note that Cases 3 and 5 are generally associated with hydrogen-rich events whereas Cases 1, 2, and 4 are applicable to all classes of core-collapse supernovae.

Finally, in light of this compilation it is interesting to note that an abrupt rise in the optically thin radio emission of Type Ibc supernovae can also be attributed to the presence of an off-axis gamma-ray burst jet (275, 418). As the jet sweeps up circumstellar material and decelerates, it eventually undergoes a dynamical transition to sub-relativistic expansion on a timescale of  $t \sim 1$  yr (135). Once sub-relativistic, the jet spreads sideways and the ejecta rapidly approach spherical symmetry. The observational signature of an off-axis GRB is therefore an abrupt optically thin rise as the jet sweeps through our line-of-sight. Due to the location of the synchrotron spectral peak, this signature is most easily detected in the radio band on a timescale of  $t \sim 1$  to 10 years (370). Yet as we have shown here, many radio supernovae show evidence for density induced variability on this same timescale. We therefore emphasize that abrupt flux variations in radio supernovae may not be used as a reliable proxy for an off-axis GRB jet and/or energy injection from a central engine.

### 2.8.1 A Comparison of SN 2003bg and SN 2001ig

A comparison of the radio light-curves represented in Table 2.4 shows that the variations are generally unique to each supernova. However, as Figure 2.8 shows, the separation and intensity of the observed variations in SN 2003bg and the Type IIb SN 2001ig are strikingly similar. By simply scaling our SN 2003bg light-curve fits by a factor of  $\sim 0.1$  we obtain a reasonable match to the SN 2001ig radio evolution. With this scaling we derive the following physical parameters for the SN 2001ig radio-emitting ejecta:  $r \approx 4.2 \times 10^{15}(t/t_0)^{0.8}$  cm,  $\bar{v} \approx 0.16c(t/t_0)^{-0.2}$ ,  $B \approx 3.8(t/t_0)^{-1}$  G, and  $E \approx 1.3 \times 10^{48}(t/t_0)^{0.4}$  erg for  $\epsilon_e = \epsilon_B = 0.1$ . The electron number density is thus given by  $n_e \approx 3.0 \times 10^5(r/r_0)^{-2}$  cm $^{-3}$ , with successive peaks of relative intensity comparable to those observed in SN 2003bg (Table 2.3) and an associated mass loss rate of  $\dot{M} \approx 8.6 \times 10^{-5} M_\odot \text{ yr}^{-1}$  ( $v_w = 1000 \text{ km s}^{-1}$ ). We

note that this mass loss estimate is comparable to that reported by Ryder et al. (325), but they adopt free-free absorption for the dominant absorption process and a progenitor wind velocity of  $10 \text{ km s}^{-1}$ , typical of red supergiant Type II SN progenitors. Our SSA modeling, however, shows the ejecta velocity of SN 2001ig is consistent with those of SNe Ibc and the mass loss rate is in fact comparable to Galactic Wolf-Rayet stars, similar to the case of SN 2003bg.

Figure 2.8 shows that strong light-curve deviations are observed for both SNe on timescales of  $\sim 120$  and  $300$  days with evidence for a weaker feature at  $t \sim 600$  days. Making the reasonable approximation that the ejecta evolve as  $r \sim 5 \times 10^{15} (t/t_0)^{0.8}$  cm, these variations correspond to density enhancements at radial distances of  $R \sim 4 \times 10^{16}$  and  $8 \times 10^{16}$  cm. Assuming a progenitor wind velocity of  $v_w = 1000 \text{ km s}^{-1}$ , we infer ejection timescales of  $\sim 12$  and  $24$  years before the SN explosion. Moreover, as shown in the Figure 2.8 the strength of the light-curve variations decreases with time implying that the largest enhancements are closest to the explosion site.

In addition to their radio light-curves, the optical evolution for SNe 2003bg and 2001ig are also similar. In both cases there was spectroscopic evidence for a thin layer of hydrogen near the time of optical maximum (289, 174); however nebular spectra revealed no hydrogen emission in either event (Filippenko and Chornock 114; Hamuy, private communication)<sup>6</sup>. This evolution is characteristic of Type IIb supernovae (e.g., SN 1993J; Filippenko et al. 117). However, their inferred ejecta velocities resemble more closely those of SNe Ibc and therefore imply compact (Wolf-Rayet) progenitors. We conclude that these two events are intermediate between Types IIb and Ibc, and show more overall similarities to hydrogen-poor events. Moreover, the likeness of their observed radio and optical evolution may indicate similar environments and progenitor evolutions.

---

<sup>6</sup>Given the similarity between the two SNe, it is natural to question whether earlier observations of SN 2001ig would have revealed a Type Ic spectrum as was observed for SN 2003bg at  $t \sim 6$  days past explosion.

## 2.9 The Progenitors of SNe 2003bg and 2001ig

The overall resemblance of SN 2003bg and SN 2001ig, as outlined in the previous section, suggests that a similar process is responsible for the observed density variations. Based on the location ( $R \gtrsim 5 \times 10^{16}$  cm) and relative intensity (factor of  $\lesssim 2$ ) of the density enhancements, we find that Cases 1 and 4 (a variable mass loss rate and the tidal effects of a binary companion, respectively) provide the most likely explanations for the inferred circumstellar structure.

Noting the abrupt fluctuations in the SN 2001ig radio light-curves, Ryder et al. (325) recently proposed a binary induced pinwheel nebula for the inferred episodic density enhancements. In this scenario, the colliding stellar winds produce a smooth dusty plume that spirals in the plane of the binary orbit. A highly eccentric orbit is required to produce structure at well-defined intervals and a favorable viewing angle is necessary to reproduce the observed flux variations. Here the location and intensity of the pinwheel structure is determined by the binary parameters. Ryder et al. (324) argue further support for this model based on the discovery of a late-B - late-F supergiant coincident (rms uncertainty of 0.03 arcsec, corresponding to 1.7 pc at  $d \approx 11.5$  Mpc) with the SN 2001ig optical position which they interpret as the putative binary companion. However, in cases of observed pinwheel nebulae (e.g., Tuthill et al. 402), the dust plumes are attributed to the strong wind-wind interaction between a Wolf-Rayet and O- or early-B star companion. Taken together with the substantial uncertainty in the position of the putative companion, this suggests that a binary induced pinwheel nebula for SN 2001ig is not clearly substantiated.

Adopting a pinwheel model for both SNe 2003bg and 2001ig would imply that the geometry of their circumstellar nebulae are nearly identical and thus they share remarkably similar binary systems. Moreover, this model would imply that our viewing angle with respect to their circumstellar nebulae must also be very similar. While this scenario cannot be ruled out, it is clearly unlikely.

Assuming a single star progenitor model, the mass loss rates derived through

our SSA modeling for SNe 2003bg and 2001ig imply massive Wolf-Rayet progenitors. Broadband observations of Galactic WR stars show that the circumstellar media for these events are often significantly disturbed. In particular, X-ray observations show evidence for colliding stellar winds and dense clumps (e.g., Hillier 186). If the progenitors of SNe 2003bg and 2001ig were single WR stars then the observed density variations could be produced by a series of enhanced mass loss episodes. To be consistent with the radio data, the mass loss ejections must ramp up as the star nears explosion. In this scenario, the observed variation timescale and the lack of CSM structure at radii inward of  $R \sim 4 \times 10^{16}$  cm may be explained by a quasi-periodic mechanism which drives enhanced mass loss episodes every  $\sim 12$  years. If accompanied by wind velocity variations, these episodes could produce shells of circumstellar material, overall consistent with the circularly symmetric density structures we infer for SNe 2003bg and 2001ig. The observed similarity between SNe 2003bg and 2001ig implies that these mass loss episodes may be common among some fraction of hydrogen-poor events.

These clues suggest that episodic variations in the progenitor mass loss rate and/or wind velocity provide a reasonable explanation to the radio light-curve variations observed for both SNe 2003bg and 2001ig. Given the predicted timescale for the mass ejections, these two SNe provide some of the best evidence for unusual mass loss evolution immediately preceding the supernova explosion. While the presence of a binary companion cannot be ruled out for either of these hydrogen-poor events, additional studies of short timescale variability in radio supernovae will enable discrimination between single and binary progenitor models.

## 2.10 Conclusions

We report extensive radio and X-ray observations of SN 2003bg. The spectroscopic evolution of this unusual supernova shows a transition from a broad-lined Type Ic to a hydrogen-rich Type II and later to a typical hydrogen-poor Type Ibc. This evolution strengthens the connection between Type II and Type Ibc (including

broad-lined) events. We show that the extraordinarily luminous radio emission for a SN Ibc is well described by a self-absorption dominated synchrotron spectrum while the observed X-ray emission at  $t \approx 30$  days is adequately fit by inverse Compton scattering of the optical photons off of the synchrotron emitting electrons. Our radio model implies a sub-relativistic ejecta velocity,  $\bar{v} \approx 0.24c$ , and a size of  $r \approx 6.2 \times 10^{15}$  cm at  $t_0 \approx 10$  days. This analysis emphasizes that broad optical absorption lines do not imply relativistic ejecta. We find that the total energy of the radio emitting region evolves as  $E \approx 7.3 \times 10^{48} (t/t_0)^{0.4}$  erg assuming equipartition of energy between relativistic electrons and magnetic fields ( $\epsilon_e = \epsilon_B = 0.1$ ). The circumstellar density is well described by stellar wind profile,  $\propto r^{-2}$ , with modest (factor of  $\sim 2$ ) episodic enhancements which produce abrupt achromatic flux variations. We show that free-free absorption does not contribute significantly to the radio spectrum and estimate an average mass loss rate of  $\dot{M} \approx 3 \times 10^{-4} M_\odot \text{ yr}^{-1}$ , consistent with observed values for local Wolf-Rayet stars.

Comparison with other events reveals that  $\sim 50\%$  of radio supernovae show similar short timescale light-curve variations which are attributable to circumstellar density irregularities. This compilation emphasizes that abrupt radio light-curve variations cannot be used as a reliable proxy for an engine-driven explosion, including off-axis gamma-ray bursts.

Finally, the radio light-curves and spectroscopic evolution for SN 2003bg are strikingly similar to those of SN 2001ig, suggestive of a common progenitor evolution for these two events. The overall similarity of SNe 2003bg and 2001ig to radio SNe Ibc is suggestive of a compact Wolf-Rayet progenitor model. Based on the relative intensity of the inferred density enhancements, we conclude that the progenitors of hydrogen-poor SNe 2003bg and 2001ig experienced quasi-periodic mass loss episodes just prior to the SN explosion.

We are indebted to Barry Clark for his generous scheduling of the VLA for this project. We thank M. Hamuy and A. Filippenko for making their optical SN 2003bg data available to us during this study. The authors thank Re'em Sari, Doug Leonard, Edo Berger, Michael Rupen, Paolo Mazzali, Avishay Gal-Yam, P.

Brian Cameron, Derek Fox, Ehud Nakar, and Kurt Weiler for useful discussions. Caltech SN research is supported by NSF and NASA grants. AMS acknowledges support by the National Radio Astronomy Observatory Graduate Summer Student Research Assistantship program and the NASA Graduate Student Research Program. RAC acknowledges NSF grant AST-0307366.

Table 2.1. VLA Radio Flux Density Measurements of SN 2003bg

Date (UT)	$\Delta t$ (days) <sup>†</sup>	$F_{\nu,1.43}$ GHz (mJy)	$F_{\nu,4.86}$ GHz (mJy)	$F_{\nu,8.46}$ GHz (mJy)	$F_{\nu,15.0}$ GHz (mJy)	$F_{\nu,22.5}$ GHz (mJy)	$F_{\nu,43.3}$ GHz (mJy)	Array Config.
2003 Mar 4	10	—	—	$2.51 \pm 0.07$	—	—	—	D
2003 Mar 6	12	$0.42 \pm 0.28$	—	$3.86 \pm 0.10$	—	$30.77 \pm 0.71$	—	D
2003 Mar 17	23	$0.55 \pm 0.20$	$2.75 \pm 0.11$	$12.19 \pm 0.26$	$47.03 \pm 0.98$	$106.30 \pm 2.16$	—	D
2003 Mar 29	35	—	$8.87 \pm 0.20$	$24.72 \pm 0.50$	$62.11 \pm 1.26$	$85.39 \pm 1.72$	$64.07 \pm 1.95$	D
2003 Apr 11	48	—	$14.88 \pm 0.32$	$40.34 \pm 0.81$	$71.51 \pm 1.46$	$74.58 \pm 1.53$	$31.75 \pm 1.43$	D
2003 Apr 21	58	—	$22.37 \pm 0.46$	$51.72 \pm 1.04$	$69.31 \pm 1.41$	$39.91 \pm 0.89$	$20.56 \pm 5.87$	D
2003 Apr 26	63	—	$24.62 \pm 0.50$	$49.64 \pm 1.00$	$64.75 \pm 1.32$	$32.48 \pm 0.71$	$15.62 \pm 2.53$	D
2003 May 6	73	—	$28.85 \pm 0.59$	$46.20 \pm 0.93$	$41.18 \pm 0.87$	$30.53 \pm 0.67$	$10.18 \pm 2.55$	D
2003 May 18	85	—	$31.14 \pm 0.68$	$38.648 \pm 0.79$	$19.39 \pm 0.54$	$9.63 \pm 1.13$	—	DnA
2003 May 24	91	—	$32.42 \pm 0.69$	$33.85 \pm 0.71$	$17.34 \pm 0.83$	$10.70 \pm 2.10$	—	DnA
2003 Jun 17	115	—	$39.07 \pm 0.79$	$45.74 \pm 0.92$	$32.14 \pm 0.68$	$21.07 \pm 0.44$	—	A
2003 Jun 31	129	$9.27 \pm 0.30$	$47.37 \pm 0.95$	$53.94 \pm 1.08$	$41.02 \pm 0.84$	$30.19 \pm 1.70$	—	A

Table 2.1—Continued

Date (UT)	$\Delta t$ (days) <sup>†</sup>	$F_{\nu,1.43}$ GHz (mJy)	$F_{\nu,4.86}$ GHz (mJy)	$F_{\nu,8.46}$ GHz (mJy)	$F_{\nu,15.0}$ GHz (mJy)	$F_{\nu,22.5}$ GHz (mJy)	$F_{\nu,43.3}$ GHz (mJy)	Array Config.
2003 Jul 4	132	$8.77 \pm 0.36$	$48.81 \pm 0.98$	$54.27 \pm 1.09$	$40.92 \pm 0.83$	—	—	A
2003 Jul 14	142	$10.10 \pm 0.48$	$52.69 \pm 1.06$	$54.83 \pm 1.10$	$39.24 \pm 0.81$	—	—	A
2003 Jul 29	157	$11.27 \pm 0.39$	$52.81 \pm 1.06$	$48.43 \pm 0.97$	$30.88 \pm 0.63$	—	—	A
2003 Aug 2	161	$11.38 \pm 0.44$	$50.84 \pm 1.02$	$47.43 \pm 0.95$	$29.17 \pm 0.61$	—	—	A
2003 Aug 22	181	$12.79 \pm 0.35$	$45.19 \pm 0.91$	$35.76 \pm 0.72$	$21.06 \pm 0.48$	$11.00 \pm 0.61$	—	A
2003 Sep 11	201	$14.07 \pm 0.37$	$40.10 \pm 0.81$	$31.35 \pm 0.63$	$16.58 \pm 0.44$	$6.59 \pm 0.43$	—	BnA
2003 Sep 24	214	$17.07 \pm 0.40$	$39.65 \pm 0.80$	$28.67 \pm 0.58$	$16.54 \pm 0.39$	$10.13 \pm 0.48$	—	BnA
2003 Oct 7	227	$15.94 \pm 0.34$	$36.45 \pm 0.73$	$27.38 \pm 0.55$	$15.58 \pm 0.35$	$7.84 \pm 0.47$	—	BnA
2003 Oct 22	242	$19.31 \pm 0.49$	$36.53 \pm 0.74$	$24.57 \pm 0.50$	—	$9.38 \pm 0.23$	—	B
2003 Nov 4	255	$19.23 \pm 0.48$	$34.56 \pm 0.70$	$22.30 \pm 0.46$	$12.71 \pm 0.35$	$7.86 \pm 0.31$	—	B
2003 Nov 15	266	$23.05 \pm 0.59$	$33.37 \pm 0.68$	$21.67 \pm 0.44$	$11.31 \pm 0.30$	$7.79 \pm 0.25$	—	B
2003 Dec 4	285	$22.99 \pm 0.54$	$33.12 \pm 0.67$	$21.31 \pm 0.43$	$12.02 \pm 0.28$	$7.74 \pm 0.19$	—	B

Table 2.1—Continued

Date (UT)	$\Delta t$ (days) <sup>†</sup>	$F_{\nu,1.43}$ GHz (mJy)	$F_{\nu,4.86}$ GHz (mJy)	$F_{\nu,8.46}$ GHz (mJy)	$F_{\nu,15.0}$ GHz (mJy)	$F_{\nu,22.5}$ GHz (mJy)	$F_{\nu,43.3}$ GHz (mJy)	Array Config.
2003 Dec 19	300	24.13 ± 0.54	33.19 ± 0.67	20.88 ± 0.42	11.67 ± 0.28	7.76 ± 0.19	—	B
2004 Jan 14	326	24.50 ± 0.59	32.90 ± 0.66	20.33 ± 0.41	11.36 ± 0.28	6.84 ± 0.19	—	B
2004 Jan 25	337	28.30 ± 0.61	31.66 ± 0.64	19.85 ± 0.40	9.08 ± 0.26	5.96 ± 0.18	—	CnB
2004 Feb 8	351	23.88 ± 0.62	30.90 ± 0.63	18.84 ± 0.38	9.65 ± 0.26	6.72 ± 0.16	3.36 ± 0.57	CnB
2004 Feb 25	368	31.99 ± 0.76	28.73 ± 0.58	17.14 ± 0.35	9.72 ± 0.25	5.72 ± 0.17	—	C
2004 Apr 2	405	—	—	14.61 ± 0.30	—	7.48 ± 0.39	—	C
2004 Apr 7	410	33.27 ± 0.72	23.88 ± 0.50	14.49 ± 0.31	—	—	—	C
2004 Apr 21	424	27.93 ± 0.63	22.96 ± 0.47	14.16 ± 0.29	6.41 ± 0.25	2.73 ± 0.13	0 ± 0.39	C
2004 Apr 31	434	24.82 ± 0.57	20.98 ± 0.43	13.25 ± 0.27	5.75 ± 0.21	3.05 ± 0.24	—	C
2004 May 2	435	—	—	13.08 ± 0.27	—	—	0.38 ± 0.23	C
2004 Jun 29	493	26.60 ± 0.76	16.20 ± 0.34	10.04 ± 0.21	6.59 ± 0.36	3.78 ± 0.51	1.31 ± 0.38	D
2004 Aug 8	533	23.65 ± 0.74	14.60 ± 0.33	8.92 ± 0.22	5.72 ± 0.40	3.25 ± 0.58	—	D

Table 2.1—Continued

Date (UT)	$\Delta t$ (days) <sup>†</sup>	$F_{\nu,1.43}$ GHz (mJy)	$F_{\nu,4.86}$ GHz (mJy)	$F_{\nu,8.46}$ GHz (mJy)	$F_{\nu,15.0}$ GHz (mJy)	$F_{\nu,22.5}$ GHz (mJy)	$F_{\nu,43.3}$ GHz (mJy)	Array Config.
2004 Nov 15	632	—	—	6.23 ± 0.41	4.47 ± 1.08	2.74 ± 0.57	—	A
2004 Nov 29	646	23.70 ± 0.51	10.82 ± 0.23	—	—	—	—	A
2005 Jan 24	702	23.23 ± 0.603	10.21 ± 0.23	6.18 ± 0.14	3.43 ± 0.19	—	—	BnA
2005 Jan 31	709	—	—	—	—	1.86 ± 0.10	—	BnA
2005 Mar 19	756	—	—	4.62 ± 0.16	2.52 ± 0.21	—	—	B
2005 Apr 11	779	23.15 ± 0.78	8.49 ± 0.21	—	—	—	—	B
2005 May 22	820	21.43 ± 0.93	7.56 ± 0.21	3.93 ± 0.13	2.69 ± 0.85	0.85 ± 0.23	—	B
2005 Aug 12	902	21.71 ± 1.42	8.23 ± 0.20	4.69 ± 0.12	2.56 ± 0.23	2.22 ± 0.35	1.31 ± 0.32	C
2005 Oct 27	978	21.84 ± 0.29	7.83 ± 0.08	4.48 ± 0.07	—	—	—	DnC

<sup>†</sup>Days since explosion assuming an explosion date of 2003 February 22 UT.

Table 2.2. Spectral Models for *Chandra* ACIS-S Observations of SN 2003bg

Date (UT)	$\Delta t$ (days)	Model	$N_{\text{H}}^{\dagger}$ ( $10^{22} \text{ cm}^{-2}$ )	$\Gamma^{\dagger}$	$kT^{\ddagger}$ (keV)	$\chi^2/dof$	Flux (0.3-10 keV) $^{\ddagger}$ ( $\text{erg cm}^{-2} \text{ s}^{-1}$ )	$\beta_{RX}^*$
2003 March 24.5	30	Power Law	$0.013^{\dagger}$	$1.7 \pm 0.2$	—	24/20	$(9.3 \pm 0.4) \times 10^{-14}$	-0.94
—	—	—	$0.054 \pm 0.033$	$1.9 \pm 0.3$	—	24/19	$(9.6 \pm 0.4) \times 10^{-14}$	-0.94
—	—	Th. Brem.	$0.013^{\dagger}$	—	$4.3 \pm 0.9$	26/20	$(7.8 \pm 0.9) \times 10^{-14}$	-0.95
—	—	—	$< 0.018$	—	$4.5 \pm 0.9$	25/19	$(7.7 \pm 0.9) \times 10^{-14}$	-0.95
2003 June 22.3	120	Power Law	$0.013^{\dagger}$	1.7	—	5/7	$(1.2 \pm 0.4) \times 10^{-14}$	-0.89
—	—	Th. Brem.	$0.013^{\dagger}$	—	$4.4 \pm 1.6$	4/7	$(1.2 \pm 0.2) \times 10^{-14}$	-0.97

$^{\ddagger}$ All errors represent 90% confidence levels.

$^{\dagger}N_{\text{H}}$  fixed to the Galactic value (see §2.2.2).

\*Spectral index between optically thin radio and X-ray flux density.

Table 2.3. Radio Light-curve Peaks for SN 2003bg

Phase	$\Delta t$ (days)	$r$ ( $\times 10^{16}$ cm)	$C_f^\dagger$ ( $\times 10^{-51}$ g s $^{1/2}$ )	$C_\tau^\dagger$ ( $\times 10^{38}$ s $^{-3.6}$ )	$\nu_m^\dagger$ (GHz)	$n_e^\ddagger$ (jump)	$B^\ddagger$ (jump)	$E^\ddagger$ (jump)
1	$\lesssim 110$	$\lesssim 6.2$	3.1	6.2	0.11	—	—	—
2	120-250	6.7-12	2.7	23	0.15	1.8	1.3	1.8
3	300-500	14-21	2.5	46	0.18	1.4	1.2	1.4
4	$\gtrsim 600$	$\gtrsim 24$	2.4	67	0.19	1.2	1.1	1.2

$^\dagger$ Values computed at the reference time of  $t_0 = 10$  days.

$^\ddagger$ Factor by which the parameter is enhanced with respect to an extrapolation of the parameters from the previous phase.

Table 2.4. Radio Supernovae with Strong Light-curve Variations

SN	Type	$t_{\text{peak}}$ (years)	$\nu_{\text{peak}}$ ( $\nu$ GHz)	Variation Type	Ref. <sup>†</sup>
1957D	II	< 27	4.9	Abrupt Steepening	1,2,3
1978K	IIn	2.6	4.9	Abrupt Steepening	4
1979C	III	1.2	5.0	Episodic Bumps	1,5,6
1980K	III	0.4	5.0	Abrupt Steepening	1,7
1986J	IIn	3.8	4.9	Abrupt Steepening	8
1987A	II	0.0093	0.84	Abrupt Rise	9,10
1988Z	IIn	2.5	4.9	Abrupt Steepening	11
1998bw	Ic	0.030	4.9	Episodic Bumps	12,13,14
2001em	Ic/II	< 2.5	4.9	Abrupt Rise	15,16
2001ig	IIf	0.20	5.0	Episodic Bumps	17
2003bg	Ic/II	0.27	4.9	Episodic Bumps	18
2004C	Ic	< 0.24	4.9	Abrupt Rise	19
2004cc	Ic	0.068	8.5	Abrupt Steepening	19

<sup>†</sup>References: 1 - Weiler et al. (421); 2 - Cowan et al. (93), 3 - Stockdale et al. (379); 4 - Schlegel et al. (345); 5 - Weiler et al. (425); 6 - Montes et al. (261); 7 - Montes et al. (260); 8 - Bietenholz et al. (34); 9 - Ball et al. (7); 10 - Chevalier (71); 11 - Williams et al. (433); 12 - Kulkarni et al. (216); 13 - Li and Chevalier (226); 14 - Weiler et al. (419); 15 - Stockdale et al. (381); 16 - Chugai and Chevalier (80); 17 - Ryder et al. (325); 18 - this paper; 19 - Soderberg *et al.*, in prep.

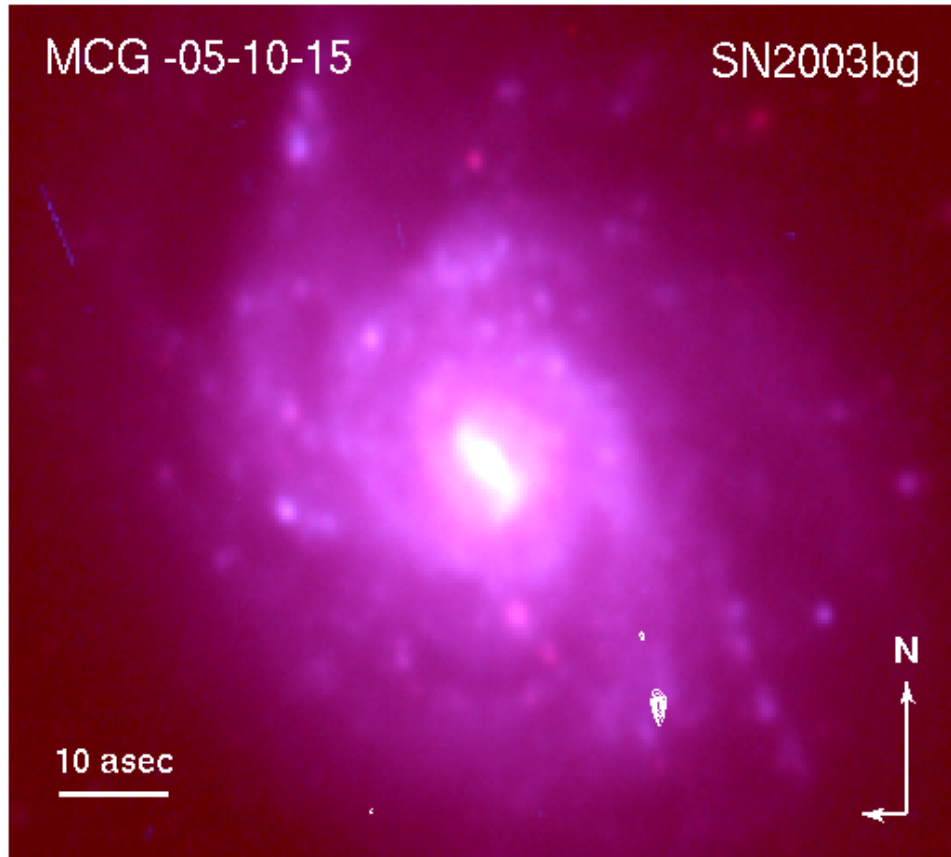


Figure 2.1: Composite color ( $g'r'$ ) image of host galaxy MCG -05-10-15 taken with the Palomar 200-inch telescope with the Large Field Camera. White contours map the radio emission from SN 2003bg detected with the Very Large Array at 8.46 GHz on 2005 May 31 (VLA B-array configuration). Contours are linearly spaced and correspond to flux density values between 0.5 and 4.0 mJy. The SN was located in a star-forming spiral arm of the host galaxy at position  $\alpha(\text{J2000}) = 04^{\text{h}}10^{\text{m}}59.42^{\text{s}}$ ,  $\delta(\text{J2000}) = -31^{\circ}24'50.3''$  ( $\pm 0.1$  arcsec in each coordinate). We note that no diffuse emission from the host galaxy was detected in any of our radio observations.

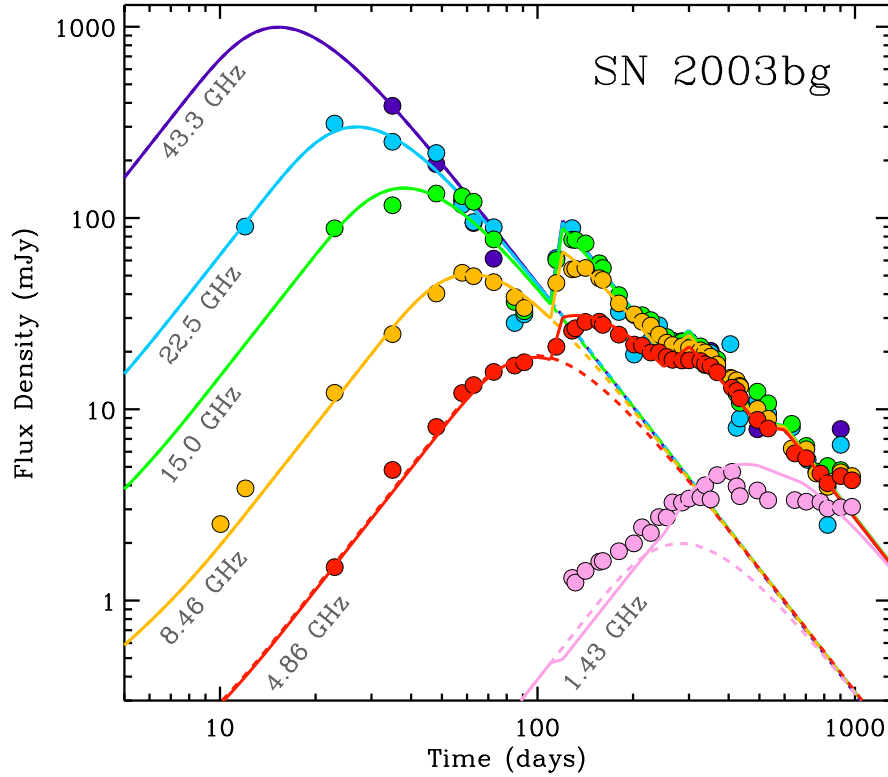


Figure 2.2: From bottom to top, the measurements were taken with the VLA at 1.43 GHz (pink), 4.86 GHz (red), 8.46 GHz (orange), 15.0 GHz (green), 22.5 GHz (blue), and 43.3 GHz (purple) between 2003 March and 2005 October UT ( $t \sim 10 - 1000$  days after the explosion). The data have been scaled to the 8.46 GHz measurements by  $\nu^\beta$  where  $\beta \approx -1.1$  is the observed optically thin spectral index. An abrupt, achromatic light-curve deviation is observed at  $t \sim 120$  days and additional, weaker deviations are suggested at  $t \sim 300$  and 600 days. The synchrotron self-absorption model described in §2.5 is overplotted (solid lines). An extrapolation of the early fit ( $t \lesssim 110$  days) is shown for comparison (dashed lines).

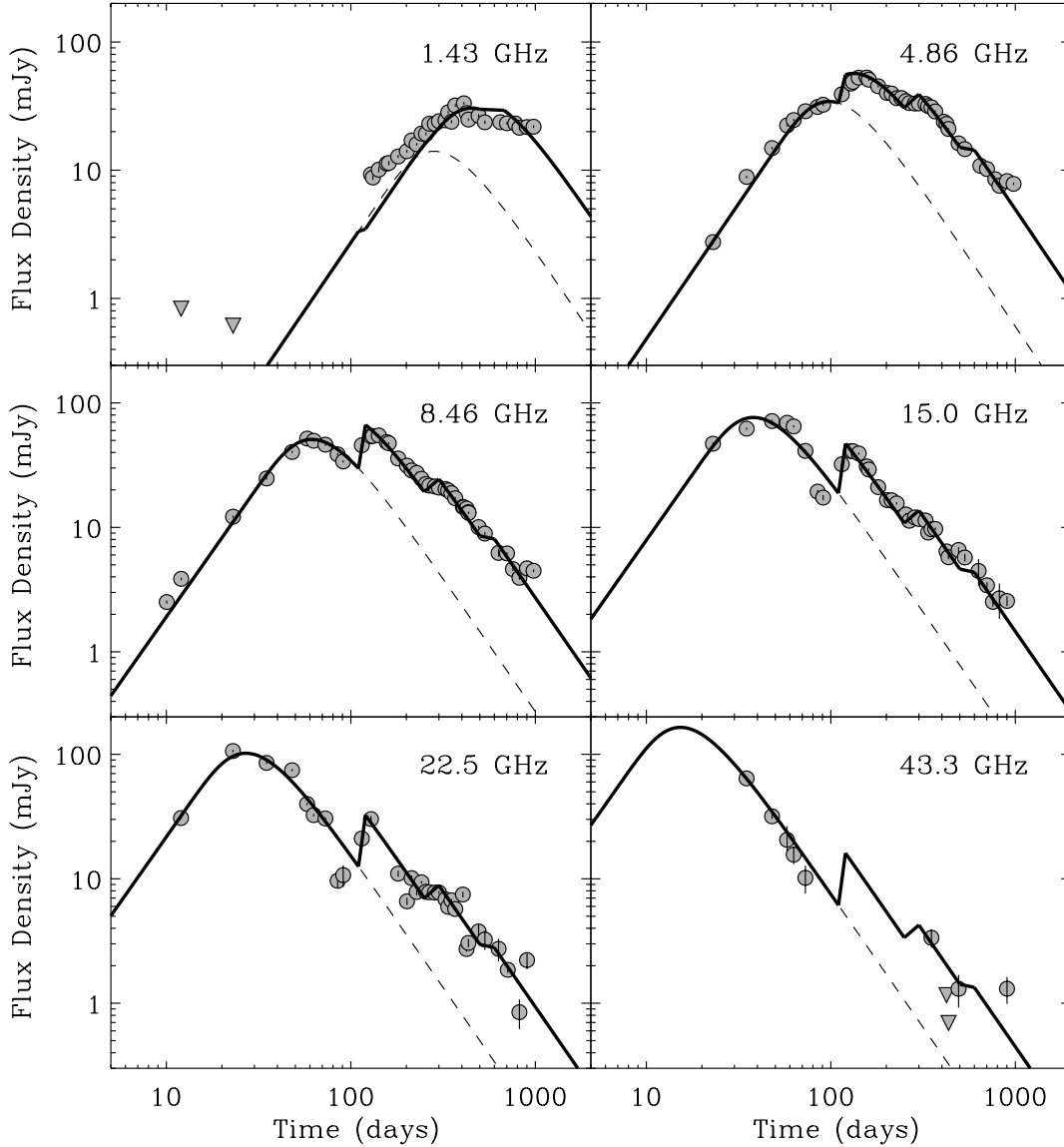


Figure 2.3: Radio light-curves of SN 2003bg were taken with the VLA at frequencies 1.43, 4.86, 8.46, 15.0, 22.5, and 43.3 GHz between 2003 March and 2005 October UT. The synchrotron self-absorption model fits described in §2.5 are overplotted (solid line). An extrapolation of our SSA model with no density variations is shown for comparison (dashed line).

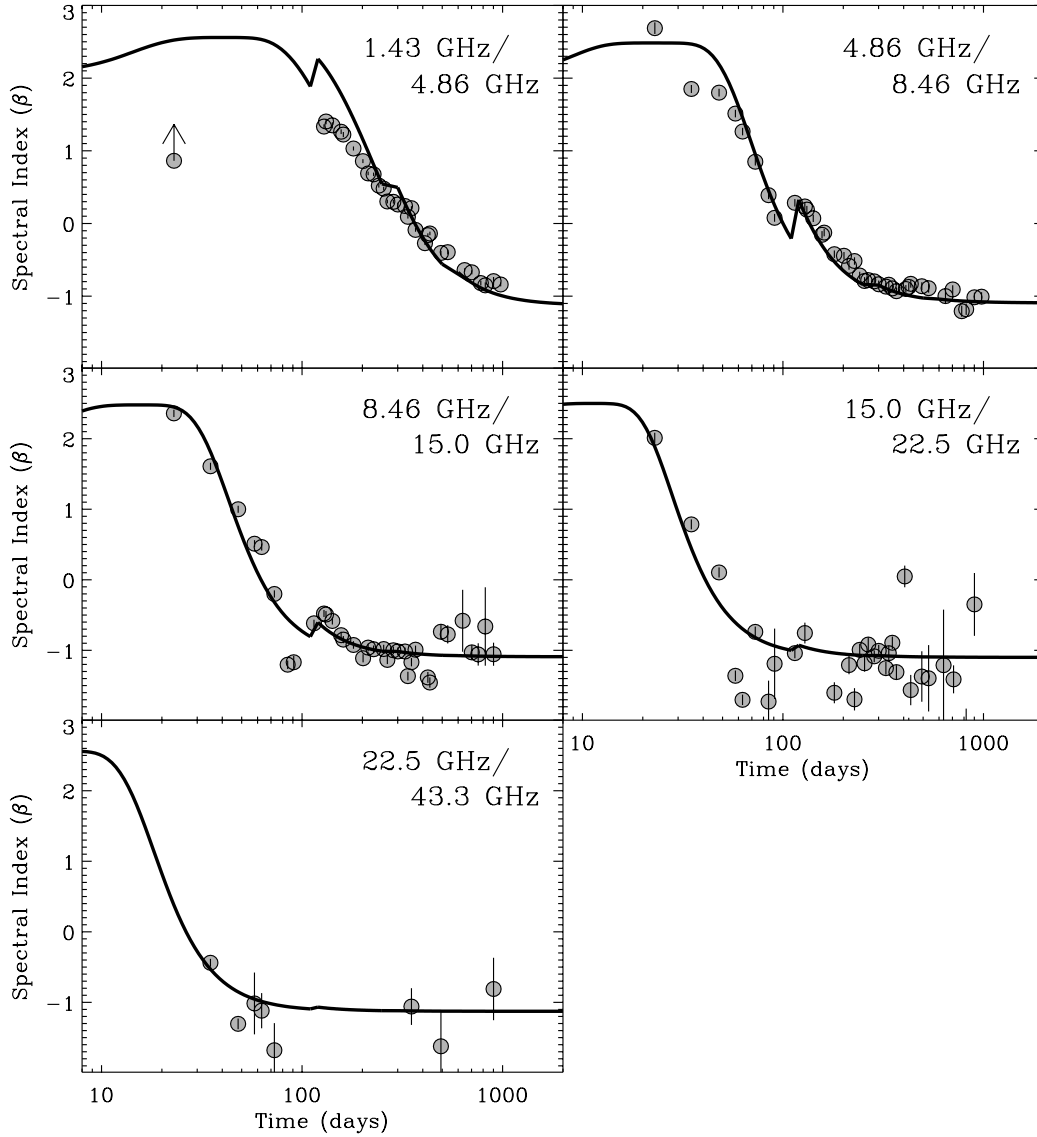


Figure 2.4: The temporal evolution of 1.43/4.86 GHz, 4.86/8.46 GHz, 8.46/15.0 GHz, 15.0/22.5 GHz, and 22.5/43.3 GHz spectral indices are shown along with our SSA model fits (solid lines). The abrupt variations in the spectral indices are overall consistent with our CSM density jump model (§2.5).

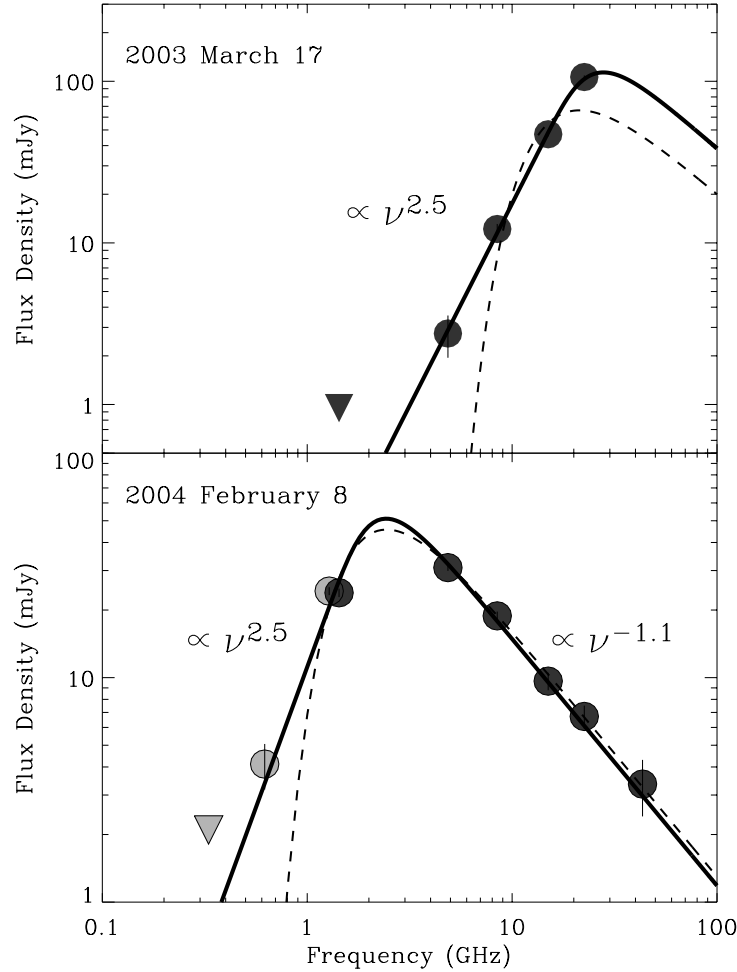


Figure 2.5: Radio spectra for SN 2003bg on 2003 Mar 17 ( $t \approx 23$  days; top) and 2004 Feb 8 UT ( $t \approx 351$  days; bottom). Detections are indicated by filled points and upper limits as inverted triangles. In the later spectrum, we supplement our Very Large Array data (dark grey points) with simultaneous observations from the Giant Meterwave Radio Telescope (light grey points; P. Chandra, 2005, PhD thesis, <http://www.tifr.res.in/~poonam>). The low frequency GMRT observations at 0.33, 0.62, and 1.28 GHz confirm that the absorbed spectral index is not steeper than  $\beta \approx 2.5$  (66). Both spectra are best-fit with a synchrotron self-absorbed spectrum (thick black lines) as described in §2.2.1. For comparison, we show best-fit FFA models (dashed black lines) which are clearly inconsistent with the observed spectrum. We conclude that internal SSA dominates the observed absorption.

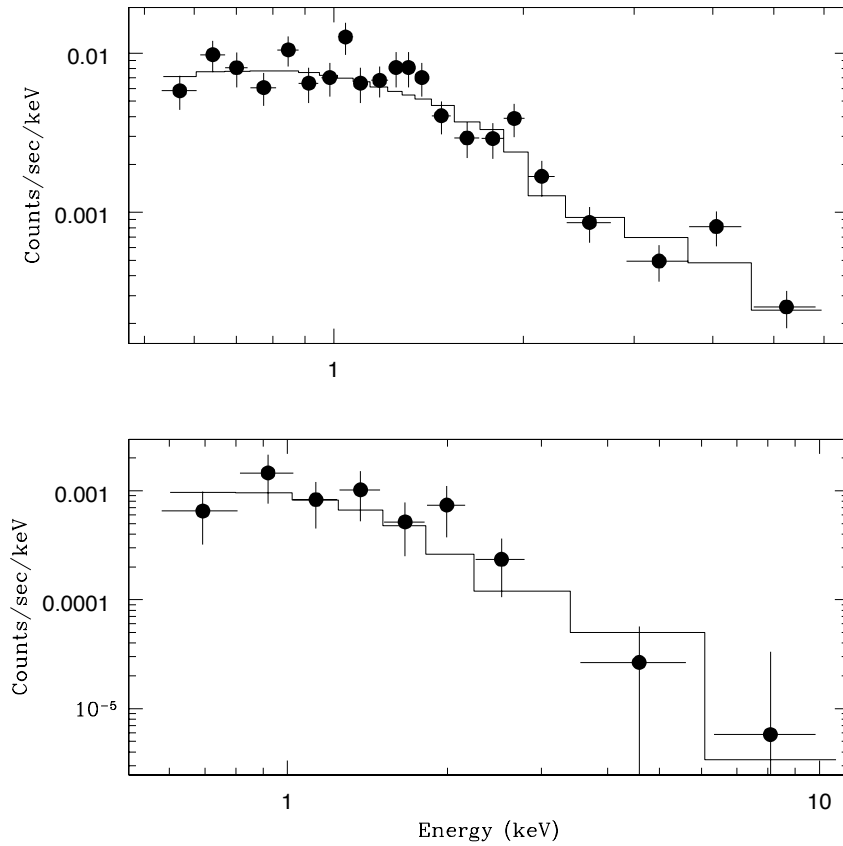


Figure 2.6: *Chandra* ACIS-S spectra for SN 2003bg at  $t \approx 30$  days (upper panel) and at  $t \approx 120$  days (bottom panel). Overplotted in both panels is an absorbed power-law fit with fixed (Galactic)  $N_{\text{H}}$  as described in §2.2.2 and Table 2.2. In §2.7 we argue that the X-ray emission is produced by inverse Compton scattering of the optical photons in the first epoch.

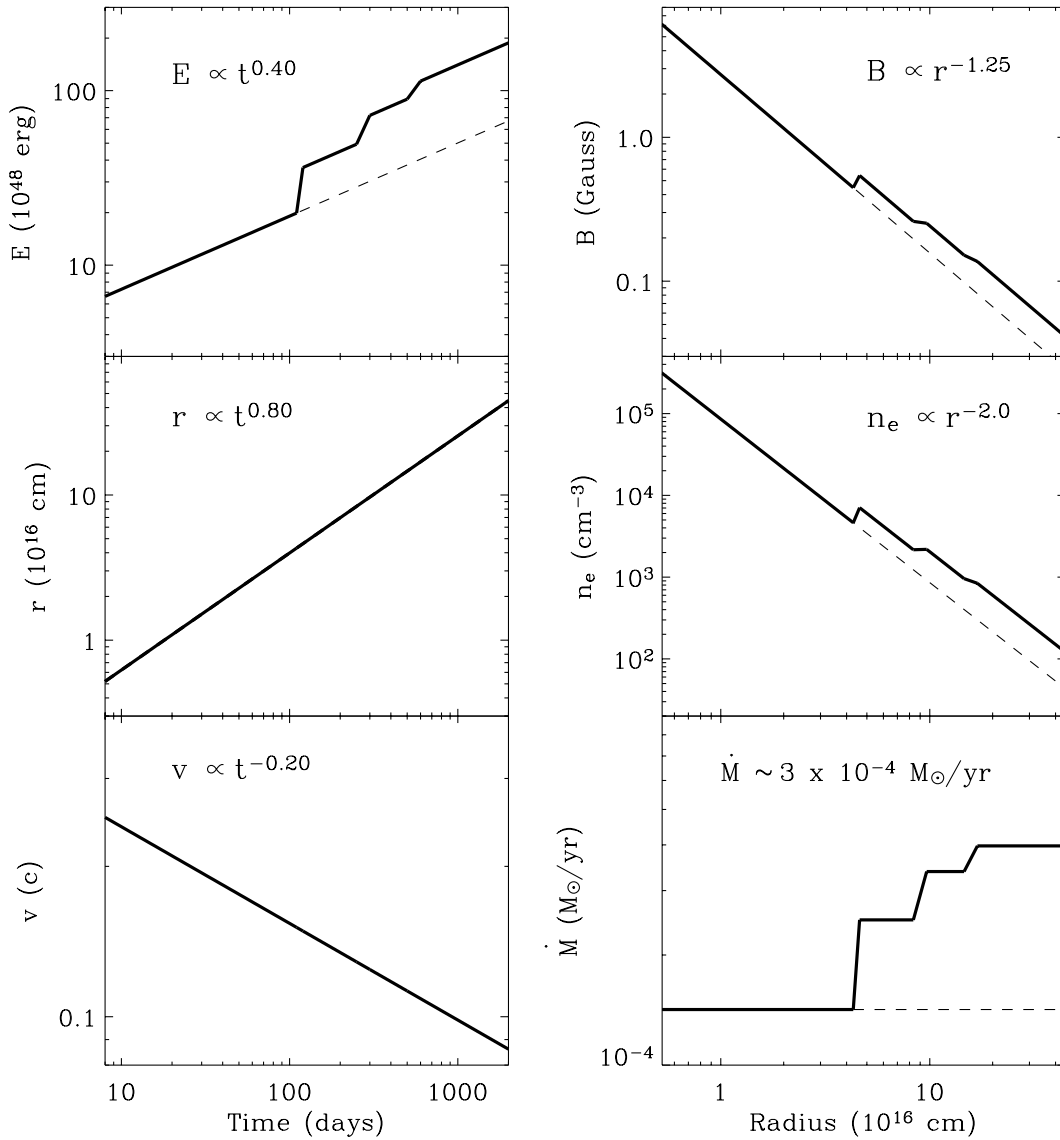


Figure 2.7: Physical parameters for SN 2003bg based on our synchrotron self-absorption model described in §3.3 and applied in §2.5. Left column: the temporal evolution from  $t \approx 10$  to 2000 days is shown for the energy of the emitting region, shock radius, and average velocity (top to bottom). Right column: the radial profile of the magnetic field, electron number density, and mass loss rate are shown from  $r \approx 5 \times 10^{15}$  to  $4 \times 10^{17}$  cm. An extrapolation of our SSA model with no density variations is shown for comparison (dashed line).

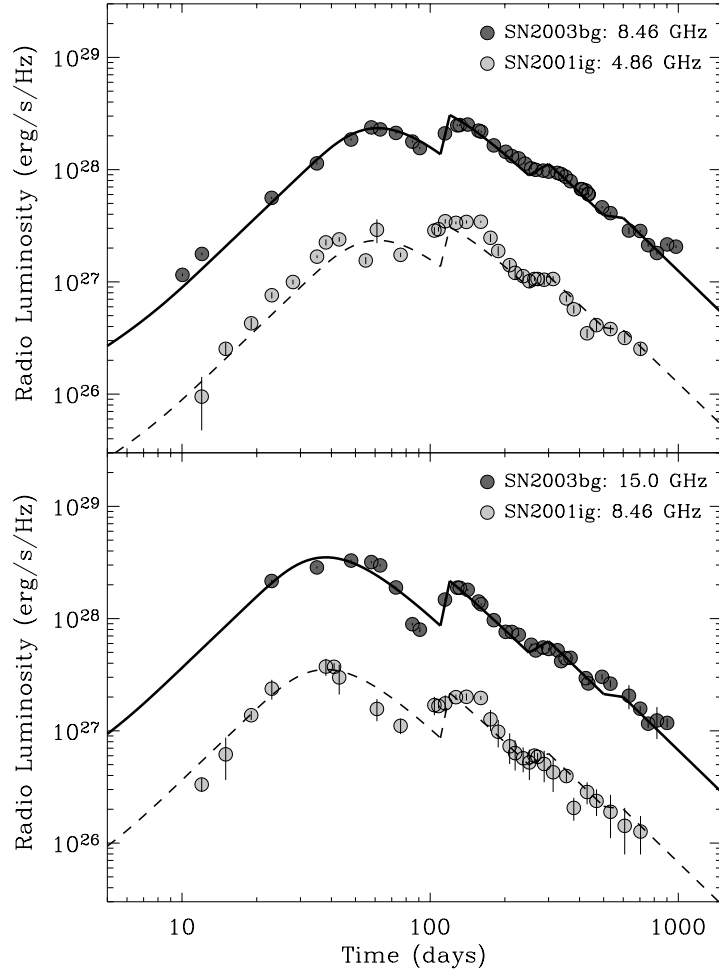


Figure 2.8: Radio light-curves for SN 2003bg (dark grey circles) and the Type IIb SN 2001ig (light grey circles; Ryder et al. 325) are compared. While SN 2003bg is overall a factor of  $\sim 10$  more luminous than SN 2001ig, the shape of the radio light-curves are strikingly similar. Specifically, the SNe show evidence for light-curve variations on similar timescales, perhaps indicative of similar CSM density structures and progenitor system evolution. Our radio modeling fits (thick black lines) for SN 2003bg are shown at 8.46 (top panel) and 15.0 GHz (bottom panel). By dimming the SN 2003bg fits by a factor of  $\sim 10$  we obtain a suitable match to the SN 2001ig light-curves.

## Chapter 3

# Late-time Radio Observations of 68 Type Ibc Supernovae: Strong Constraints on Off-Axis Gamma-ray Bursts<sup>†</sup>

A. M. SODERBERG<sup>a</sup>, E. NAKAR<sup>b</sup>, E. BERGER<sup>c</sup>, S. R. KULKARNI<sup>a</sup>

<sup>a</sup>Division of Physics, Mathematics and Astronomy, 105-24, California Institute of Technology, Pasadena, CA 91125, USA

<sup>b</sup>Theoretical Astrophysics, 130-33 California Institute of Technology, Pasadena, CA 91125, USA

<sup>c</sup>Observatories of the Carnegie Institution of Washington, 813 Santa Barbara St., Pasadena, CA 91101, USA

## Abstract

We present late-time radio observations of 68 local Type Ibc supernovae, including six events with broad optical absorption lines (“hypernovae”). None of these objects exhibit radio emission attributable to off-axis gamma-ray burst jets spreading into our line-of-sight. Comparison with our afterglow models reveals the following conclusions: (1) Less than  $\sim 10\%$  of Type Ibc supernovae are associated with typical gamma-ray bursts initially directed away from our line-of-sight; this places

---

<sup>†</sup>A version of this chapter was published in *The Astrophysical Journal*, vol. 638, 930–937, (2006). Reproduced by permission of the AAS.

an empirical constraint on the GRB beaming factor of  $\langle f_b^{-1} \rangle \lesssim 10^4$  corresponding to an average jet opening angle,  $\theta_j \gtrsim 0.8$  degrees. (2) This holds in particular for the broad-lined supernovae (SNe 1997dq, 1997ef, 1998ey, 2002ap, 2002bl, and 2003jd) which have been argued to host GRB jets. Our observations reveal no evidence for typical (or even sub-energetic) GRBs and rule out the scenario in which every broad-lined SN harbors a GRB at the 84% confidence level. Their large photospheric velocities and asymmetric ejecta (inferred from spectropolarimetry and nebular spectroscopy) appear to be characteristic of the non-relativistic supernova explosion and do not necessarily imply the existence of associated GRB jets.

### 3.1 Introduction

It is now generally accepted that long duration gamma-ray bursts (GRBs) give rise to engine-driven relativistic jets as well as non-relativistic spherical supernova (SN) explosions. The first example of this GRB-SN connection came with the discovery of the Type Ic supernova, SN 1998bw, associated with GRB 980425 ( $d \sim 36$  Mpc; Galama et al. 151, Pian et al. 290). The unusually fast photospheric velocities and exceptionally bright radio emission of SN 1998bw indicated  $\sim 10^{52}$  erg of kinetic energy and mildly relativistic ejecta (bulk Lorentz factor,  $\Gamma \sim 3$ ; Kulkarni et al. 216, Iwamoto et al. 193, Li and Chevalier 226, Woosley et al. 436). In comparison with other core-collapse events ( $E_{KE} \sim 10^{51}$  erg and ejecta speeds,  $v \lesssim 0.1c$ ), SN 1998bw was considered a hyper-energetic supernova (“hypernova”; Iwamoto et al. 193). Broad optical absorption lines were also observed in the Type Ic SNe 2003dh and 2003lw, associated with the cosmological GRBs 030329 and 031203, indicative of comparably large photospheric velocities (243, 237). Together, these observations appear to suggest that broad spectral features are characteristic of GRB-associated SNe.

In addition to events with prompt gamma-ray emission, the GRB-SN connection also implies the existence of “orphan” supernovae whose relativistic jets are initially beamed away from our line of sight (314, 275). Since the discovery of

SN 1998bw, several broad-lined SNe have been identified locally ( $d \lesssim 100$  Mpc) and are currently estimated to represent  $\sim 5\%$  of the Type Ibc supernova (SNe Ibc) population (296). Given their spectral similarity to the GRB-associated SNe, it has been argued that local broad-lined supernovae can be used as signposts for GRBs.

Thus, associations with poorly-localized BATSE bursts have been invoked for the broad-lined SNe 1997cy, 1997ef, and 1999E<sup>1</sup> (159, 401, 414, 251, 319). In addition, association with off-axis GRBs have also been claimed. In the case of SN 2002ap, broad optical absorption lines and evidence for mildly asymmetric ejecta (based on spectropolarimetry measurements) were interpreted to support an off-axis GRB jet (Kawabata et al. 201, Totani 398, but see Leonard et al. 220).

More recently, an off-axis GRB model has been proposed for SN 2003jd, for which photospheric velocities upward of  $40,000 \text{ km s}^{-1}$  were measured at early time (116, 241). More intriguingly, late-time ( $t \sim 400$  days) spectra showed double-peaked emission lines of light-elements, attributed to an asymmetric explosion (202). Mazzali et al. (252) argue that these observations can be understood if SN 2003jd was accompanied by a highly collimated GRB jet initially directed  $\sim 70$  degrees away from our line-of-sight.

Regardless of viewing angle, however, strong afterglow emission eventually becomes visible as the decelerating GRB jets spread laterally and the emission becomes effectively isotropic. As the jets spread into our line-of-sight, a rapid increase of broadband synchrotron emission is observed on a timescale of a few weeks to several years. This late-time emission is most easily detected at long wavelengths (287, 224, 418). Targeting local Type Ibc supernovae with late-time radio observations has thus become the preferred method to search for evidence of off-axis GRBs (382, 357).

Using early radio observations ( $t \lesssim 100$  days) we have already limited the

---

<sup>1</sup>We note that SNe 1997cy and 1999E were initially classified as Type IIn supernovae, however Hamuy et al. (175) later showed convincing evidence that they are hydrogen-rich Type Ia events similar to SN 2002ic.

fraction of SNe Ibc harboring on-axis (or mildly off-axis) GRBs to be  $\lesssim 3\%$  (26). In this paper, we present late-time ( $t \sim 0.5$  to 20 yr) radio observations for 68 local Type Ibc supernovae, including SN 2003jd and five additional broad-lined events, making this the most comprehensive study of late-time radio emission from SNe Ibc. We use these data to constrain the SN fraction associated with GRB jets regardless of viewing angle assumptions, constraining even those initially beamed perpendicular to our line-of-sight.

## 3.2 Radio Observations

### 3.2.1 Type Ic SN 2003jd

SN 2003jd was discovered on 2003 October 25.2 UT within host galaxy MCG - 01-59-021 ( $d_L \sim 81$  Mpc; Burket et al. 52). In Table 3.1 we summarize our radio observations for SN 2003jd, spanning 8 – 569 days after the explosion<sup>2</sup>. All observations were conducted with the Very Large Array<sup>3</sup> (VLA) in the standard continuum mode with a bandwidth of  $2 \times 50$  MHz centered at 4.86, 8.46, or 22.5 GHz. We used 3C48 and 3C147 (J0137+331 and J0542+498) for flux calibration, while J2323-032 was used to monitor the phase. Data were reduced using standard packages within the Astronomical Image Processing System (AIPS).

No radio emission was detected at the optical SN position during our early observations. Our radio limits imply that SN 2003jd was a factor of  $\gtrsim 100$  less luminous than SN 1998bw on a comparable timescale. We conclude that SN 2003jd, like the majority of SNe Ibc, did not produce relativistic ejecta along our line-of-sight.

We re-observed SN 2003jd at  $t \sim 1.6$  yrs to search for radio emission from an off-axis GRB jet. No emission was detected, implying a limit of  $F_\nu < 45 \mu\text{Jy}$  ( $3\sigma$ ) at 8.46 GHz.

---

<sup>2</sup>Here we assume an approximate explosion date of 2003 October 21 UT, based on pre-explosion images (52).

<sup>3</sup>The Very Large Array is a facility of the National Science Foundation operated under cooperative agreement by Associated Universities, Inc.

### 3.2.2 Late-time Data on Local Type Ibc Supernovae

We supplement these data with late-time ( $t \sim 0.5 - 20$  year) radio observations for 67 local ( $d_L \lesssim 200$  Mpc) SNe Ibc, summarized in Table 4.1. Eleven objects were observed at moderately late-time as part of our on-going VLA program to characterize the early ( $t \lesssim 100$  days) radio emission from SNe Ibc (Soderberg *et al.*, in prep). The remaining 54 objects were observed on a later timescale ( $t \gtrsim 1$  year) and were taken from the VLA archive<sup>4</sup>. We note that five of these supernovae (SNe 1997dq, 1997ef, 1998ey, 2002ap, 2002bl) were spectroscopically observed to have broad optical absorption lines, similar to SN 1998bw.

All VLA observations were conducted at 8.46 GHz (except for SN 1991D at 4.86 GHz) in the standard continuum mode with a bandwidth of  $2 \times 50$  MHz. Data were reduced using AIPS, and the resulting flux density measurements for this sample of SNe Ibc is given in Table 4.1. With the exception of SN 2001em, from which radio emission from the non-relativistic, spherical supernova ejecta is still detected at late-time (Stockdale et al. 378, Bietenholz and Bartel 33, but see Granot and Ramirez-Ruiz 169), none of the SNe Ibc show radio emission above our average detection limit of  $\sim 0.15$  mJy ( $3\sigma$ ). In comparison with SN 1998bw, only SN 2001em shows a comparable radio luminosity on this timescale. These results are consistent with the earlier report by Stockdale et al. (382).

In Figure 3.1 we plot the radio observations for this sample of SNe Ibc, in addition to late-time radio data for SN1954A (105) and SN 1984L (357).

## 3.3 Off-Axis Models for Gamma-ray Bursts

### 3.3.1 An Analytic Approach

Waxman (418) present an analytic model for the late-time radio emission from a typical GRB viewed significantly away from the collimation axis. In this model, the GRB jet is initially characterized by a narrow opening angle,  $\theta_j \sim$  few degrees, while the viewing angle is assumed to be large,  $\theta_{\text{obs}} \gtrsim 1$  radian. As the jet

---

<sup>4</sup><http://e2e.nrao.edu/archive/>

sweeps up circumstellar material (CSM) and decelerates, it eventually undergoes a dynamical transition to sub-relativistic expansion (135). The timescale for this non-relativistic transition is estimated at  $t_{NR} \approx 0.2(E_{51}/n_0)^{1/3}$  yr ( $\approx 0.3E_{51}/A_*$  yr) in the case of a homogeneous (wind-stratified) medium (418). Here,  $E_{51}$  is the beaming-corrected ejecta energy normalized to  $10^{51}$  erg and  $n_0$  is the circumstellar density of the homogeneous medium (interstellar medium; ISM) normalized to 1 particle  $\text{cm}^{-3}$ . For a wind-stratified medium,  $A_*$  defines the circumstellar density in terms of the progenitor mass loss rate,  $\dot{M}$ , and wind velocity,  $v_w$ , such that  $\dot{M}/4\pi v_w = 5 \times 10^{11} A_* \text{ g cm}^{-1}$ , and thus  $A_* = 1$  for  $\dot{M} = 10^{-5} M_\odot \text{ yr}^{-1}$  and  $v_w = 10^3 \text{ km s}^{-1}$  (226).

Once sub-relativistic, the jets spread sideways, rapidly intersecting our line-of-sight as the ejecta approach spherical symmetry. At this point the afterglow emission is effectively isotropic and appears similar to both on-axis and off-axis observers. The broadband emission observed from the sub-relativistic ejecta is described by a standard synchrotron spectrum, characterized by three break frequencies: the synchrotron self-absorption frequency,  $\nu_a$ , the characteristic synchrotron frequency,  $\nu_m$ , and the synchrotron cooling frequency,  $\nu_c$ . On timescales comparable to the non-relativistic transition,  $\nu_a$  and  $\nu_m$  are typically below the radio band while  $\nu_c$  is generally near the optical (135, 24, 134). Making the usual assumption that the kinetic energy is partitioned between relativistic electrons and magnetic fields ( $\epsilon_e$  and  $\epsilon_B$ , respectively), and that these fractions are constant throughout the evolution of the jet, Waxman (418) estimate the radio luminosity of the sub-relativistic, isotropic emission to be

$$L_\nu \approx 8.0 \times 10^{29} \left(\frac{\epsilon_e}{0.1}\right) \left(\frac{\epsilon_B}{0.1}\right)^{3/4} n_0^{3/4} E_{51} \times \left(\frac{\nu}{10\text{GHz}}\right)^{-1/2} \left(\frac{t}{t_{NR}}\right)^{-9/10} \text{ erg s}^{-1} \text{ Hz}^{-1} \quad (3.1)$$

for the ISM case, while for a wind-stratified medium

$$\begin{aligned}
L_\nu \approx & 2.1 \times 10^{29} \left(\frac{\epsilon_e}{0.1}\right) \left(\frac{\epsilon_B}{0.1}\right)^{3/4} A_*^{9/4} E_{51}^{-1/2} \\
& \times \left(\frac{\nu}{10\text{GHz}}\right)^{-(p-1)/2} \left(\frac{t}{t_{\text{NR}}}\right)^{-3/2} \text{erg s}^{-1} \text{Hz}^{-1}.
\end{aligned} \tag{3.2}$$

Here it is assumed that the electrons are accelerated into a power-law distribution,  $N(\gamma) \propto \gamma^{-p}$  with  $p = 2.0$ . These equations reveal that the strength of the non-relativistic emission is strongly dependent on the density of the circumstellar medium (especially in the case of a wind) and is best probed at low frequencies.

While this analytic model provides robust predictions for the afterglow emission at  $t > t_{\text{NR}}$ , it does not describe the early evolution or the transition from relativistic to sub-relativistic expansion. At early time, the observed emission from an off-axis GRB is strongly dependent on the viewing angle and dynamics of the jet. To investigate this early afterglow evolution and the transition to sub-relativistic expansion, we developed a detailed semi-analytic model, described below.

### 3.3.2 A Semi-analytic Model

In modeling the afterglow emission from an off-axis GRB jet, we adopt the standard framework for a adiabatic blastwave expanding into either a uniform or wind stratified medium (336, 171). We assume a uniform, sharp-edged jet such that Lorentz factor and energy are constant over the jet surface. The hydrodynamic evolution of the jet is fully described in Oren et al. (272). As the bulk Lorentz factor of the ejecta approaches  $\Gamma \sim 1$ , the jets begin to spread laterally at the sound speed<sup>5</sup>. Our off-axis light-curves are obtained by integrating the afterglow emission over equal arrival time surface. We note that these resulting light-curves are in broad agreement with Model 2 of Granot et al. (168) and are consistent with Waxman’s analytic model (§3.3.1) on timescales,  $t \gtrsim t_{\text{NR}}$ .

---

<sup>5</sup>Since the spreading behavior of relativistic GRB jets is poorly constrained by observations, we assume negligible spreading during this phase. We adopt this conservative assumption since it produces the faintest off-axis light-curves.

Over-plotted in Figure 3.1 are our off-axis models calculated for both wind-stratified and homogeneous media at an observing frequency of  $\nu_{\text{obs}} = 8.46$  GHz. We assume standard GRB parameters of  $E_{51} = A_* = n = 1$ ,  $\epsilon_B = \epsilon_e = 0.1$ ,  $p = 2.2$  and  $\theta_j = 5^\circ$ , consistent with the typical values inferred from broadband modeling of GRBs (280, 445, 74). We compute model light-curves for off-axis viewing angles between 30 and 90 degrees. As clearly shown in the figure, the majority of our late-time SNe Ibc limits are significantly fainter than *all* of the model light-curves, constraining even the extreme case where  $\theta_{\text{obs}} = 90^\circ$ .

### 3.4 SN 2003jd: Constraints on the Off-axis Jet

Based on the double-peaked profiles observed for the nebular lines of neutral oxygen and magnesium, Mazzali et al. (252) argue that SN 2003jd was an aspherical, axisymmetric explosion viewed near the equatorial plane. They suggest that this asymmetry may be explained if the SN explosion was accompanied by a tightly collimated and relativistic GRB jet, initially directed  $\sim 70$  degrees from our line-of-sight. This hypothesis is consistent with the observed lack of prompt gamma-ray emission (192) as well as the absence of strong radio and X-ray emission at early time (364, 416).

Our radio observation of SN 2003jd at  $t \sim 1.6$  years imposes strong constraints on the putative off-axis GRB jet. While the early data constrain only mildly off-axis jets ( $\theta_{\text{obs}} \lesssim 30^\circ$ ), our late-time epoch constrains even those jets initially directed perpendicular to our line-of-sight. As shown in Figure 3.1, our radio limit is a factor of  $\gtrsim 200$  ( $\gtrsim 20$ ) fainter than that predicted for a typical GRB expanding into a homogeneous (wind-stratified) medium, even in the extreme case where  $\theta_{\text{obs}} \sim 90^\circ$ . Given the assumption of typical GRB parameters, we conclude that our late-time radio limit is inconsistent with the presence of an off-axis GRB jet. We note that the model assumptions and physical parameters of our off-axis afterglow light-curves are identical to those adopted by Mazzali et al. (252).

We next explore the range of parameters ruled out by our deep radio limits.

As shown in Equations 1 and 2, the luminosity of the late-time emission is a function of the ejecta energy, the density of the circumstellar medium and the equipartition fractions. To investigate the effect of energy and density on the late-time radio luminosity, we fix the equipartition fractions to  $\epsilon_e = \epsilon_B = 0.1$ , chosen to be consistent with the values typically inferred from afterglow modeling of cosmological GRBs (280, 445).

In Figure 3.2, we illustrate how each radio epoch for SN 2003jd maps to a curve within the two-dimensional parameter space of kinetic energy and circumstellar density for an off-axis GRB. Here we adopt our semi-analytic model (§3.3.2) for a wind-stratified medium, along with a typical electron index of  $p = 2.2$ , and a viewing angle of  $\theta_{\text{obs}} = 90^\circ$ ; the faintest model for a given set of equipartition fractions. By comparing the luminosity limit for SN 2003jd at a particular epoch with the off-axis model prediction for that time, we exclude the region of parameter space *rightward* of the curve since this region produces a jet which is *brighter* than the observed limit. The union of these regions represents the total parameter space ruled out for an associated GRB. As shown in this figure, the total excluded parameter space extends from  $A_* \gtrsim 0.03$  and  $E \sim 10^{47}$  to  $10^{52}$ .

We compare these constraints with the beaming-corrected kinetic energies and CSM densities for 18 cosmological GRBs (Table 3.3). Here we make the rough approximation that  $A_* \approx n_0$ ; a reasonable assumption for circumstellar radii near  $\sim 10^{18}$  cm. As shown in Figure 3.2, these GRBs span the region of parameter space roughly bracketed by  $A_* \sim 0.002$  to 100 and  $E \sim 2 \times 10^{49}$  to  $4 \times 10^{51}$ . The majority of the bursts (13 out of 18) fall within the excluded region of parameter space for SN 2003jd. We conclude that SN 2003jd was not likely associated with a typical GRB at a confidence level of  $\sim 72\%$ .

### 3.5 Local Type Ibc Supernovae: Further Constraints

While physical parameters atypical of the cosmological GRB population can be invoked to hide an off-axis GRB for SN 2003jd, it is exceedingly unlikely for atypical

parameters to dominate a large statistical sample of SNe Ibc. Motivated thus, we searched for off-axis GRBs in the 67 local Type Ibc SNe for which we have compiled late-time ( $t \sim 0.5 - 30$  yr) radio observations. Applying the method described in §3.4 we produce exclusion regions in the  $E_{51} - A_*$  parameter space for each SN. Figure 3.3 shows the resulting contours for all 68 SNe, including SN 2003jd and five broad-lined events. For the twenty SNe with early radio limits (26, 22) we combine late- and early-time data to provide further constraints.

In Figure 3.4 we compile all 68 exclusion regions to quantify the  $E_{51} - A_*$  parameter space constrained by this statistical sample. Contours map the regions excluded by incremental fractions of our sample. As in the case of SN 2003jd, all curves rule out bursts with  $A_* \gtrsim 1$  and  $E \gtrsim 10^{50}$  erg. Moreover, 50% exclude  $A_* \gtrsim 0.1$  and  $E \gtrsim 10^{49}$  erg. For comparison, the mean ejecta energy and CSM density values for cosmological GRBs are  $E \approx 4.4 \times 10^{50}$  erg and  $A_* = n_0 \approx 1.2$ .

Focusing on the subsample of broad-lined SNe, we emphasize that our deep limits rule out both putative GRB jets directed along our line-of-sight (e.g., SN 1997ef) as well as those which are initially beamed off-axis (e.g., SN 2002ap and SN 2003jd). In particular, the large exclusion region for SN 2002ap (see Figure 3.3) implies that an extremely low CSM density, less than  $A_* \sim 3 \times 10^{-3}$ , is needed to suppress the emission from an associated GRB. This is a factor of  $\sim 10$  below the density inferred from modeling of the early radio emission (22) and we therefore conclude that an off-axis GRB model is inconsistent with our late-time observations of SN 2002ap. In Figure 3.4 we show that this entire sample of six broad-lined SNe rule out bursts with energies  $E \gtrsim 10^{49}$  erg, and 50% even rule out  $E \sim 10^{47}$  erg (all assuming a typical  $A_* = 1$ ).

We next address the limits on an association with GRBs defined by the cosmological sample (Table 3.3). For each SN in our sample we calculate the fraction of observed GRBs that lie in its exclusion region. We then determine the probability of finding null-detections for our entire sample by calculating the product of the individual probabilities. We find that the probability that *every* Type Ibc supernova has an associated GRB is  $1.1 \times 10^{-10}$ . We further rule out a scenario

in which one in ten SNe Ibc is associated with a GRB at a confidence level of  $\sim 90\%$ . For the broad-lined events alone we rule out the scenario that every event is associated with a GRB at a confidence level of  $\sim 84\%$ . Confidence levels are shown as a function of GRB/SN fraction in Figure 3.5.

### 3.6 Discussion and Conclusions

We present late-time radio observations for 68 local Type Ibc supernovae, including six broad-lined SNe (“hypernovae”), making this the most comprehensive study of late-time radio emission from SNe Ibc. None of these objects show evidence for bright, late-time radio emission that could be attributed to off-axis jets coming into our line-of-sight. Comparison with our most conservative off-axis GRB afterglow models reveals the following conclusions:

[1] Less than  $\sim 10\%$  of Type Ibc supernovae are associated with GRBs. These data impose an empirical constraint on the GRB beaming factor,  $\langle f_b^{-1} \rangle$ , where  $f_b = (1 - \cos \theta_j)$ . Assuming a local GRB rate of  $\sim 0.5 \text{ Gpc}^{-3} \text{ yr}^{-1}$  (346, 288, 172) and an observed SNe Ibc rate of  $\sim 4.8 \times 10^4 \text{ Gpc}^{-3} \text{ yr}^{-1}$  (240, 64, 124), we constrain the GRB beaming factor to be  $\langle f_b^{-1} \rangle \lesssim \times 10^4$ . Adopting a lower limit of  $\langle f_b^{-1} \rangle > 13$  (224), the beaming factor is now observationally bound by  $\langle f_b^{-1} \rangle \approx [13 - 10^4]$ , consistent with the observed distribution of jet opening angles (133, 172).

[2] Despite predictions that most or all broad-lined SNe Ibc harbor GRB jets (296), our radio observations for six broad-lined events (SNe 1997dq, 1997ef, 1998ey, 2002ap, 2002bl, and 2003jd) reveal no evidence for association with typical (or even sub-energetic) GRBs. While unusual physical parameters can suppress the radio emission from off-axis jets in any one SN, it is unlikely that all six broad-lined events host atypical GRBs. We observationally rule out the scenario in which every broad-lined SN harbors GRB jets with a confidence level of  $\sim 84\%$ .

[3] While low CSM densities (e.g.,  $A_* \lesssim 0.1$ ) can suppress the emission from off-axis GRB jets, such values are inconsistent with the mass loss rates measured from local Wolf-Rayet stars ( $0.6 - 9.5 \times 10^{-5} M_\odot \text{ yr}^{-1}$ ; Cappa et al. 62), thought

to be the progenitors of long-duration gamma-ray bursts.

[4] While we have so far considered only the signature from a highly collimated GRB jet, these late-time radio data also impose constraints on the presence of broader jets and/or jet cocoons. As demonstrated by GRBs 980425 and 030329, the fraction of energy coupled to mildly relativistic and mildly collimated ejecta can dominate the total relativistic energy budget (216, 27). Less sensitive to the effects of beaming and viewing geometry, broad jets are more easily probed at early time ( $t \sim 100$  days) when the emission is brightest. Still, we note that the majority of our late-time radio limits are significantly fainter than GRBs 980425 and 030329 on a comparable timescale, thus constraining even mildly relativistic ejecta.

These conclusions, taken together with the broad spectral features observed for GRB-associated SNe 1998bw, 2003dh, and 2003lw, motivate the question: what is the connection between GRBs and local Type Ibc supernovae? While current optical data suggest that all GRB-SNe are broad-lined, our late-time radio observations clearly show that the inverse is *not* true: broad optical absorption lines do not serve as a reliable proxy for relativistic ejecta. This suggests that their observed large photospheric velocities and asymmetric ejecta are often merely characteristics of the non-relativistic SN explosion and thus manifestations of the diversity within SNe Ibc.

The authors thank Doug Leonard, Paolo Mazzali, Dale Frail, Brian Schmidt, and Avishay Gal-Yam for helpful discussions. As always, the authors thank Jochen Greiner for maintaining his GRB page. A.M.S. is supported by the NASA Graduate Student Research Program. E.B. is supported by NASA through Hubble Fellowship grant HST-HF-01171.01 awarded by the STScI, which is operated by the Association of Universities for Research in Astronomy, Inc., for NASA, under contract NAS 5-26555.

Table 3.1. Radio Observations of SN 2003jd

Date Obs (UT)	$\Delta t^a$ (days)	$F_{\nu,4.96 \text{ GHz}}^b$ ( $\mu\text{Jy}$ )	$F_{\nu,8.46 \text{ GHz}}$ ( $\mu\text{Jy}$ )	$F_{\nu,22.5 \text{ GHz}}$ ( $\mu\text{Jy}$ )
2003 Oct 29	8	$\pm 52$	$\pm 34$	$\pm 58$
2003 Nov 4	14	—	$\pm 77$	—
2003 Nov 15	25	—	$\pm 74$	—
2005 May 12	569	—	$\pm 15$	—

<sup>a</sup>Assuming an explosion date of 2003 October 21 UT, based on pre-explosion images (52).

<sup>b</sup>All flux densities are given as  $1\sigma$  (rms).

Table 3.2. Late-time Radio Observations of Type Ibc Supernovae

SN name	Host Galaxy	Distance <sup>a</sup> (Mpc)	Explosion Date <sup>b</sup> (UT)	IAUC (#)	Date Obs (UT)	$\Delta t^c$ (days)	Flux density <sup>d</sup> ( $\mu\text{Jy}$ )
1983N	NGC 5236	7.2	1983 Jun 26	3835	2003 Oct 17	7416	$\pm 124$
1985F	NGC 4618	7.7	1985 May 14	4042	2003 Oct 17	6730	$\pm 37$
1987M	NGC 2715	18.9	1987 Aug 31	4451	2003 Oct 17	5891	$\pm 34$
1990B	NGC 4568	32.0	1989 Dec 23-1990 Jan 20	4949	2003 Oct 17	5032	$\pm 24$
1990U	NGC 7479	33.7	1990 Jun 28-Jul 27	5063	2003 Oct 17	4845	$\pm 44$
1991A	IC 2973	45.5	1990 Dec 6-13	5178	2003 Oct 17	4695	$\pm 35$
1991D	Anon.	173	1991 Jan 16	5153	1992 Oct 11	633	$\pm 49$
1991N	NGC 3310	14.0	1991 Feb 20-Mar 29	5227	2003 Oct 17	4604	$\pm 59$
1991ar	IC 49	65.0	1991 Aug 3	5334	2003 Oct 17	4458	$\pm 30$
1994I	NGC 5194	6.5	1994 Apr 1-2	5961	2003 Oct 17	3486	$\pm 42$
1994ai	NGC 908	21.3	1994 Dec 8-16	6120	2003 Oct 17	3336	$\pm 40$
1996D	NGC 1614	68.1	1996 Jan 28	6317	2003 Oct 15	2818	$\pm 153$
1996N	NGC 1398	19.7	1996 Feb 16-Mar 13	6351	2003 Oct 15	2787	$\pm 36$

Table 3.2—Continued

SN name	Host Galaxy	Distance <sup>a</sup> (Mpc)	Explosion Date <sup>b</sup> (UT)	IAUC (#)	Date Obs (UT)	$\Delta t^c$ (days)	Flux density <sup>d</sup> ( $\mu\text{Jy}$ )
1996aq	NGC 5584	23.2	1996 Jul 30	6465	2003 Oct 17	2635	$\pm 32$
1997B	IC 438	44.3	1996 Dec 14	6535	2003 Oct 15	2498	$\pm 33$
1997C	NGC 3160	99.2	1996 Dec 18-1997 Jan 14	6536	2003 Oct 17	2481	$\pm 37$
1997X	NGC 4691	15.7	1997 Jan 16-Feb 2	6552	2003 Oct 17	2457	$\pm 22$
1997dc	NGC 7678	49.6	1997 Jul 22	6715	2003 Oct 17	2278	$\pm 36$
1997dq*	NGC 3810	14.0	1997 Oct 16	6770	2003 Oct 17	2192	$\pm 30$
1997ef*	UGC 4107	49.8	1997 Nov 16-26	6778	2003 Oct 17	2156	$\pm 33$
1998T	NGC 3690	44.3	1998 Feb 8-Mar 3	6830	2003 Oct 17	2066	$\pm 482$
1998ey*	NGC 7080	69.0	1998 Nov 1-Dec 5	6830	2003 Oct 17	1794	$\pm 32$
1999bc	UGC 4433	90.2	1999 Jan 30	7133	2003 Oct 15	1721	$\pm 25$
1999di	NGC 776	70.2	1999 Jul 6	7234	2003 Oct 17	1564	$\pm 35$
1999dn	NGC 7714	39.7	1999 Aug 10-20	7241	2003 Oct 17	1524	$\pm 42$
1999ec	NGC 2207	38.9	1999 Aug 24	7268	2003 Oct 15	1515	$\pm 45$

Table 3.2—Continued

SN name	Host Galaxy	Distance <sup>a</sup> (Mpc)	Explosion Date <sup>b</sup> (UT)	IAUC (#)	Date Obs (UT)	$\Delta t^c$ (days)	Flux density <sup>d</sup> ( $\mu$ Jy)
1999eh	NGC 2770	27.6	1999 Jul 26	7282	2003 Oct 17	1544	$\pm 19$
2000C <sup>†</sup>	NGC 2415	53.8	1999 Dec 30-2000 Jan 4	7348	2003 Oct 17	1385	$\pm 35$
2000F	IC 302	84.5	1999 Dec 30-2000 Jan 10	7353	2003 Oct 15	1383	$\pm 26$
2000S	MCG -01-27-2	85.8	1999 Oct 9	7384	2003 Oct 17	1469	$\pm 30$
2000de	NGC 4384	35.6	2000 Jul 13	7478	2003 Oct 17	1191	$\pm 40^e$
2000ds	NGC 2768	19.4	2000 May 28	7507	2003 Oct 17	1237	$\pm 34$
2000dv	UGC 4671	57.7	2000 Jul 4	7510	2003 Oct 17	1200	$\pm 32$
2001B <sup>†</sup>	IC 391	22.0	2000 Dec 25-2001 Jan 4	7555	2003 Oct 15	1021	$\pm 30$
2001M <sup>†</sup>	NGC 3240	50.6	2001 Jan 3-21	7568	2003 Oct 17	1008	$\pm 54$
2001bb <sup>†</sup>	IC 4319	66.3	2001 Apr 15-29	7614	2003 Oct 17	908	$\pm 35$
2001ch	MCG -01-54-1	41.6	2001 Mar 23	2003 Oct 17	7637	938	$\pm 32$
2001ci <sup>†</sup>	NGC 3079	15.8	2001 Apr 17-25	7638	2003 Oct 17	909	$\pm 188$
2001ef <sup>†</sup>	IC 381	35.1	2001 Aug 29-Sep 9	7710	2003 Oct 17	774	$\pm 33$

Table 3.2—Continued

SN name	Host Galaxy	Distance <sup>a</sup> (Mpc)	Explosion Date <sup>b</sup> (UT)	IAUC (#)	Date Obs (UT)	$\Delta t^c$ (days)	Flux density <sup>d</sup> ( $\mu$ Jy)
2001ej <sup>†</sup>	UGC 3829	57.4	2001 Aug 30	7719	2003 Oct 15	778	$\pm 36$
2001em	UGC 11794	83.6	2001 Sep 10-15	7722	2003 Oct 17	765	$907 \pm 58$
2001is <sup>†</sup>	NGC 1961	56.0	2001 Dec 14-23	7782	2003 Oct 15	668	$\pm 31$
2002J <sup>†</sup>	NGC 3464	53.0	2002 Jan 15-21	7800	2003 Oct 17	637	$\pm 23$
2002ap <sup>*†</sup>	NGC 628	9.3	2002 Jan 28-29	7810	2003 Oct 17	626	$\pm 29$
2002bl <sup>*†</sup>	UGC 5499	67.8	2002 Jan 31	7845	2003 Oct 17	624	$\pm 39$
2002bm <sup>†</sup>	MCG -01-32-1	78.0	2002 Jan 16-Mar 6	7845	2003 Oct 17	630	$\pm 39$
2002cp <sup>†</sup>	NGC 3074	73.4	2002 Apr 11-28	7887	2003 Oct 17	547	$\pm 29$
2002hf <sup>†</sup>	MCG -05-3-20	80.2	2002 Oct 22-29	8004	2003 Oct 17	357	$\pm 48$
2002ho <sup>†</sup>	NGC 4210	38.8	2002 Sep 24	8011	2003 Oct 17	389	$\pm 35$
2002hy <sup>†</sup>	NGC 3464	53.0	2002 Oct 13-Nov 12	8016	2003 Oct 17	354	$\pm 23$
2002hz <sup>†</sup>	UGC 12044	77.8	2002 Nov 2-12	8017	2003 Oct 17	344	$\pm 29$
2002ji <sup>†</sup>	NGC 3655	20.8	2002 Oct 20	8025	2003 Oct 17	362	$\pm 18$

Table 3.2—Continued

SN name	Host Galaxy	Distance <sup>a</sup> (Mpc)	Explosion Date <sup>b</sup> (UT)	IAUC (#)	Date Obs (UT)	$\Delta t^c$ (days)	Flux density <sup>d</sup> ( $\mu\text{Jy}$ )
2002jj <sup>†</sup>	IC 340	60.1	2002 Oct 22	8026	2003 Oct 15	360	$\pm 30$
2002jp <sup>†</sup>	NGC 3313	52.7	2002 Oct 20	8031	2003 Oct 17	362	$\pm 37$
2003A	UGC 5904	94.4	2002 Nov 23-2003 Jan 5	8041	2003 Jun 15	182	$\pm 69$
2003I	IC 2481	76.0	2002 Dec 14	8046	2003 Jun 15	183	$\pm 60$
2003aa	NGC 3367	43.1	2003 Jan 24-31	8063	2003 Jun 15	138	$\pm 70$
2003bm	UGC 4226	113.7	2003 Feb 20-Mar 3	8086	2003 Jun 15	109	$\pm 57$
2003bu	NGC 5393	86.1	2003 Feb 10-Mar 11	8092	2003 Jun 15	110	$\pm 71$
2003cr	UGC 9639	155.2	2003 Feb 24-Mar 31	8103	2003 Nov 2	233	$\pm 59$
2003dg	UGC 6934	79.1	2003 Mar 24-Apr 8	8113	2003 Nov 2	215	$\pm 90$
2003dr	NGC 5714	31.7	2003 Apr 8-12	8117	2003 Nov 2	206	$\pm 58$
2003ds	NGC 3191	132.9	2003 Mar 25-Apr 14	8120	2003 Nov 2	212	$\pm 67$
2003el	NGC 5000	80.2	2003 Apr 19-May 22	8135	2003 Nov 2	180	$\pm 65$
2003ev	Anonymous	103.3	2003 Apr 9-Jun 1	8140	2003 Nov 2	180	$\pm 61$

Table 3.2—Continued

SN name	Host Galaxy	Distance <sup>a</sup> (Mpc)	Explosion Date <sup>b</sup> (UT)	IAUC (#)	Date Obs (UT)	$\Delta t^c$ (days)	Flux density <sup>d</sup> ( $\mu\text{Jy}$ )
2003jd* <sup>†</sup>	MCG -01-59-21	80.8	2003 Oct 16-25	8232	2005 May 12	569	$\pm 15$

<sup>a</sup>Distances have been calculated from the host galaxy redshift. We assume  $H_0 = 72 \text{ km s}^{-1} \text{ Mpc}^{-1}$ ,  $\Omega_M = 0.27$ , and  $\Omega_\Lambda = 0.73$ .

<sup>b</sup>Explosion dates are given as a range constrained by the date of discovery and the most recent pre-discovery image in which the SN is not detected. In the cases where pre-discovery images are not available (or not constraining), we adopt the spectroscopically derived age estimate with respect to maximum light and assume a typical light-curve rise time of  $\sim 21$  days to provide a rough estimate of the explosion date.

<sup>c</sup>Calculated using the average of the explosion date range in Column 4.

<sup>d</sup>All observations were conducted at 8.46 GHz (except for SN 1991D at 4.86 GHz) and uncertainties represent  $1\sigma$  rms noise.

<sup>e</sup>We detect a  $\sim 0.7$  mJy source located  $\sim 2$  arcsec from the optical position for SN 2000de. Due to the significant positional offset, we assume the radio source is not associated with the SN.

\*Broad absorption lines observed spectroscopically.

<sup>†</sup>Early radio limits reported in Berger et al. (26)

<sup>‡</sup>Early radio data for SN 2002ap was reported by Berger et al. (22)

Table 3.3. Physical Parameters for GRBs

GRB	$z$	Ejecta Energy <sup>a</sup> ( $\times 10^{51}$ erg)	Density <sup>b</sup> ( $A_* = n$ )	Density Profile	Reference <sup>c</sup>
970508	0.835	$2.4_{-0.9}^{+1.4}$	$2.4_{-0.9}^{+1.4}$	ISM	1
980329	$\lesssim 3.9$	$1.1_{-0.46}^{+0.26}$	$20_{-10}^{+10}$	ISM	2
980425	0.0085	0.012	0.04	Wind	3
980519	1 <sup>†</sup>	$0.41_{-0.14}^{+0.48}$	$0.14_{-0.14}^{+0.48}$	ISM	4
980703	0.966	$3.5_{-0.42}^{+1.26}$	$28_{-6}^{+8}$	ISM	2
990123	1.60	$0.15_{-0.04}^{+0.33}$	$0.0019_{-0.0015}^{+0.0005}$	ISM	4
990510	1.619	$0.14_{-0.05}^{+0.49}$	$0.29_{-0.15}^{+0.11}$	ISM	4
991208	0.706	$0.24_{-0.22}^{+0.28}$	$18_{-6}^{+22}$	ISM	4
991216	1.02	$0.11_{-0.04}^{+0.1}$	$4.7_{-1.8}^{+6.8}$	ISM	4
000301c	2.03	$0.33_{-0.05}^{+0.03}$	$27_{-5}^{+5}$	ISM	4
000418	1.118	3.4	0.02	ISM	5
000926	2.066	$2.0_{-0.2}^{+0.34}$	$16_{-6}^{+6}$	ISM	2
010222	1.477	0.51	1.7	ISM	4
011121	0.36	0.2	0.015	Wind	6
020405	0.69	0.3	$\lesssim 0.07$	Wind	6
020903	0.251	0.4	100	ISM	7
030329	0.168	0.67	3.0	ISM	8
031203	0.105	0.017	0.6	ISM	9

<sup>a</sup>Corrected for beaming. Errors bracket the 90% confidence interval.

<sup>b</sup>Errors bracket the 90% confidence interval.

<sup>c</sup>References: 1. Berger et al. (24); 2. Yost et al. (445); 3. Li and Chevalier (226); 4. Panaitescu and Kumar (280); 5. Berger et al. (18); 6. Chevalier et al. (74); 7. Soderberg et al. (361); 8. Berger et al. (27); 9. Soderberg et al. (362)

<sup>†</sup>Redshift Unknown;  $z=1$  was assumed.

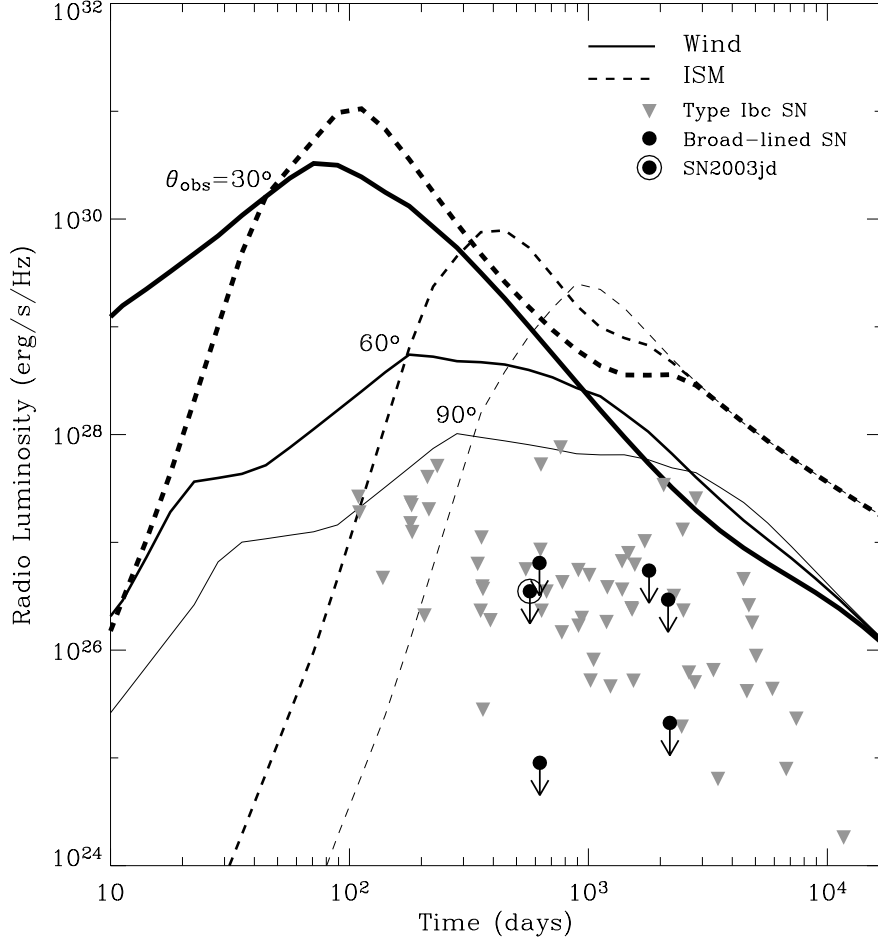


Figure 3.1: Late-time radio limits ( $3\sigma$ ) are shown for 62 local Type Ibc supernovae (grey triangles) and six broad-lined SNe (circles/arrows) including SN 2003jd (encircled dot). For SN 2001em, we adopt the spherical SN emission as an upper limit on the emission from an off-axis GRB jet. Afterglow models for a typical GRB ( $E_{51} = A_* = n_0 = 1$ ,  $\epsilon_e = \epsilon_B = 0.1$ ,  $\theta_j = 5^\circ$ ,  $p = 2.2$ ) are shown for both wind-stratified (solid lines) and homogeneous (dashed lines) media at viewing angles of  $\theta_{\text{obs}} = 30^\circ$  (thickest),  $60^\circ$  (thick), and  $90^\circ$  (thin) away from the initial collimation axis of the jet. As discussed in §3.3.2, we make the conservative assumption that lateral jet spreading does not begin until after the non-relativistic transition, at which point the jets spread sideways at the sound speed. All of the broad-lined SNe, including SN 2003jd, are significantly fainter than the model light-curves, regardless of the CSM density profile or viewing angle.

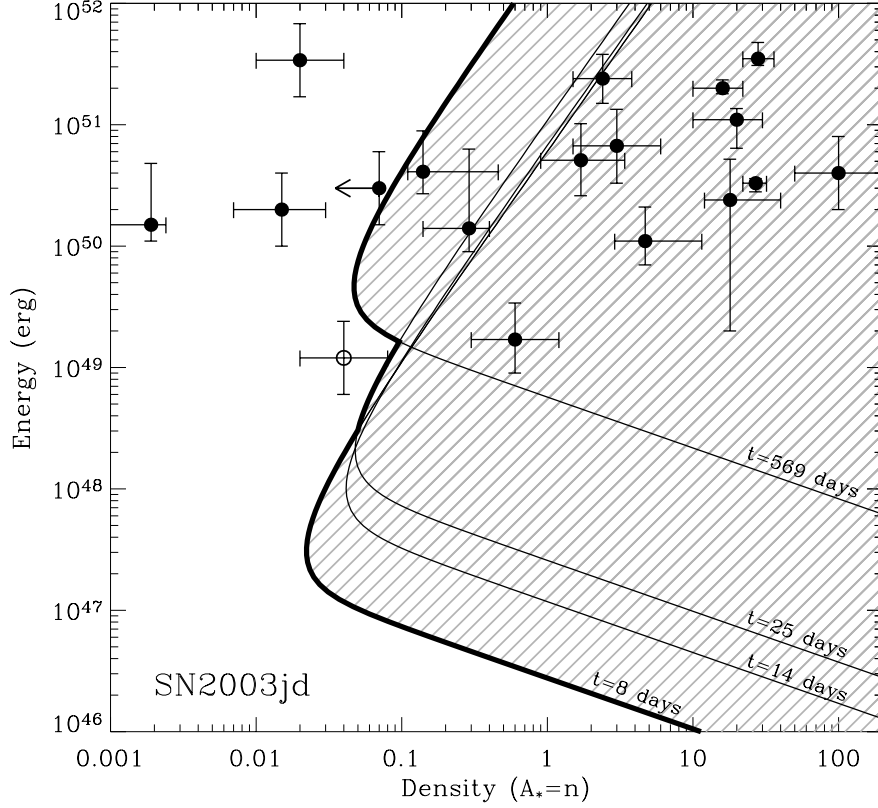


Figure 3.2: Each of the four 8.46 GHz observations is mapped to a contour (thin black lines) in the two-dimensional parameter space of kinetic energy and CSM density for an off-axis GRB. As discussed in §3.4, we adopt a conservative off-axis model (wind-stratified CSM,  $\epsilon_e = \epsilon_B = 0.1$ ,  $p = 2.2$ ,  $\theta_{\text{obs}} = 90^\circ$ ) which produces the faintest light-curves in Figure 1. We exclude the grey hatched region of parameter space *rightward* of each contour since this region produces a jet which is *brighter* than the observed  $3\sigma$  limit. The union of these regions (thick black line) represents the total parameter space ruled out for an associated GRB. For comparison, we also show are the energy and density values for 17 GRBs (filled circles) from Table 3.3, inferred from broadband modeling of the afterglow emission. For the GRBs without reported error estimates, we adopt a factor of two for the uncertainty of both parameters. We also include the parameters for GRB 980425 (unfilled circle) derived from the early radio emission emitted from the quasi-spherical SN component, but note that the lack of strong radio emission from SN 2003jd at early time indicates that it is not similar to GRB 980425.

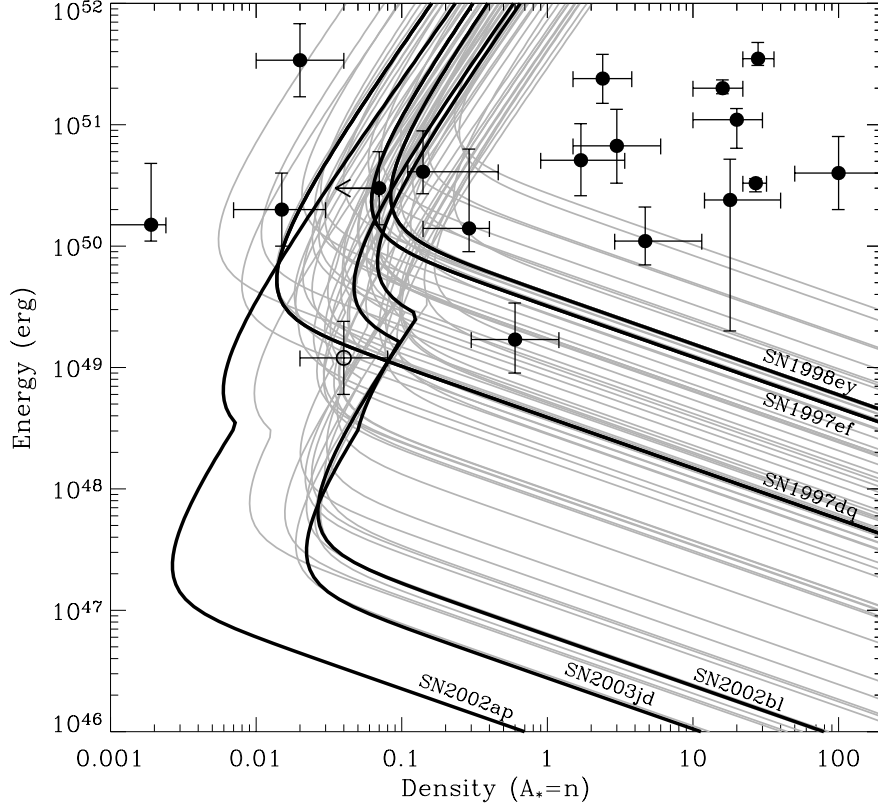


Figure 3.3: Late-time radio limits for 62 SNe Ibc (grey contours) and six broad-lined SNe (black contours, labels) are used to constrain the parameters ( $E_{51}$  and  $A_*$ ) of putative off-axis GRBs as discussed in §3.5. For SN 2001em, we adopt the spherical SN emission as an upper limit on the emission from an off-axis GRB jet. As discussed in §3.4, we adopt a conservative off-axis model (wind-stratified CSM,  $\epsilon_e = \epsilon_B = 0.1$ ,  $p = 2.2$ ,  $\theta_{\text{obs}} = 90^\circ$ ) which produces the faintest light-curves in Figure 1. The region rightward of each SN contour is ruled out since it implies an off-axis GRB which is brighter than the observed  $3\sigma$  limit. For the 21 SNe with additional early-time radio observations, we determine the union of parameter space which is excluded (see Figure 3.2). Energy and density values for 17 cosmological GRBs (filled circles) and GRB 980425 (unfilled circle) are shown for comparison. For the GRBs without reported error estimates, we adopt a factor of two for the uncertainty of both parameters. It is clear that most of the GRBs lie in the excluded regions for each SN, implying that if these events are associated with off-axis GRBs, their densities are unusually low.

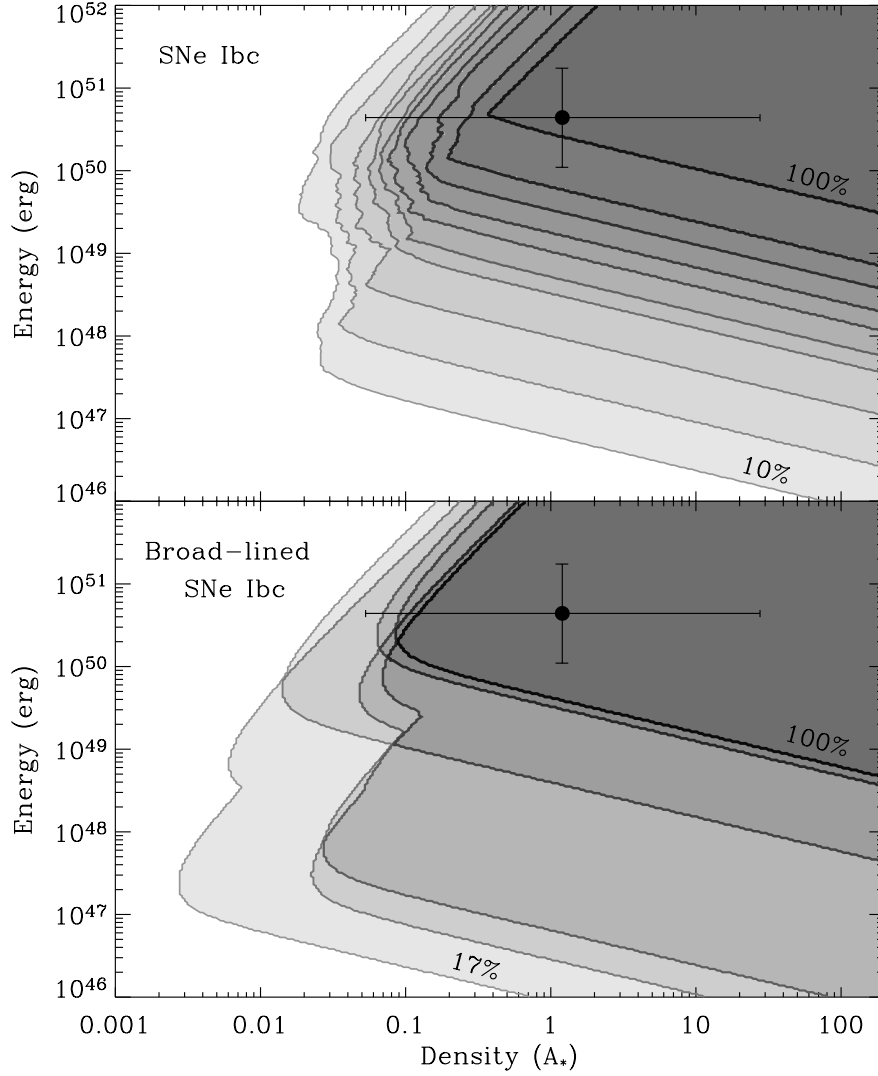


Figure 3.4: Top panel: Regions of  $E_{51} - A_*$  parameter space for off-axis GRBs ruled out by the SNe Ibc sample in Figure 3.3. Contours/shading depict the regions ruled out by fractions of the sample, labeled in increments of 10%. The darkest shading corresponds to the region excluded by 100% of the sample. The statistical mean  $E_{51}$  and  $A_*$  values for cosmological GRBs is shown as a barred point. Bottom panel: Same as above, except only including the broad-lined SNe.

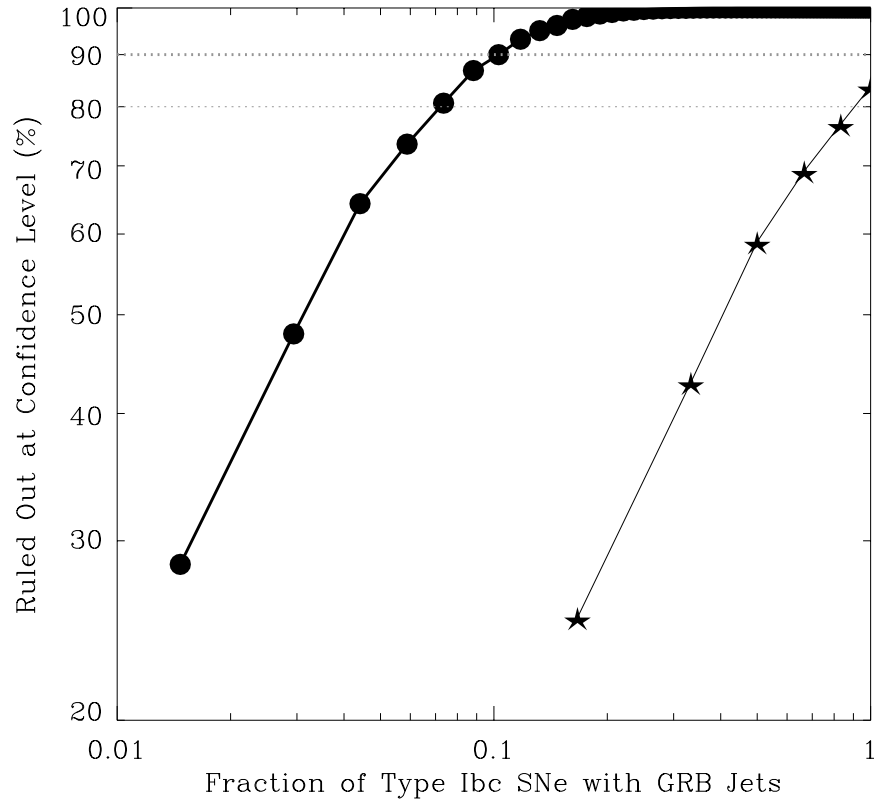


Figure 3.5: Using late-time radio data for 68 local SNe Ibc (Table 4.1) and the physical parameters inferred for cosmological GRBs (Table 3.3) we constrain the fraction of SNe harboring GRBs. We find that we can rule out the the scenario in which every supernova (circles) has an associated GRB (GRBs/SNe=1) at a confidence level of  $\sim 100\%$  and can rule out a fraction of  $\gtrsim 0.1$  with a confidence level of  $\sim 90\%$ . For the broad-lined supernovae (stars) we rule out the scenario in which every event harbors a GRB with a confidence level of  $\sim 84\%$ .

## Chapter 4

# The Radio Properties of Type Ibc Supernovae

A. M. SODERBERG<sup>a</sup>, S. R. KULKARNI<sup>a</sup>, D. A. FRAIL<sup>b</sup>

<sup>a</sup>Division of Physics, Mathematics and Astronomy, 105-24, California Institute of Technology,  
Pasadena, CA 91125m USA

<sup>b</sup>National Radio Astronomy Observatory, Socorro, NM 87801, USA

### 4.1 Introduction

The discovery of several gamma-ray bursts (GRBs) and X-ray flashes (XRFs) at  $z \lesssim 0.3$  in the last few years has firmly established that GRBs and XRFs are accompanied by supernovae of Type Ibc (SNe Ibc) (see Woosley and Bloom 435 for a review). While the distribution of GRB/XRF-SN optical luminosities is indistinguishable from local samples of SNe Ibc (366), spectroscopy reveals unusually broad absorption lines (“broad-lined”, BL) in every case (292). However, the two classes are easily distinguished through the production of mildly-relativistic ejecta, which gives rise to strong non-thermal “afterglow” emission. Radio observations are critical in this analysis since they provide the best calorimetry of the fastest ejecta.

Furthermore, we have identified a population of GRBs/XRFs that are sub-energetic by a factor of  $\sim 10^2$  and about 10 times more common than typical bursts (362, 365). Given their under-luminous prompt energy release, current satellites

can only detect them nearby ( $z \lesssim 0.1$ ). These sub-energetic explosions are intermediate between GRBs/XRFs and local SNe Ibc with respect to gamma-ray release, jet collimation, and volumetric rate, and thus hint at an overall continuum.

Motivated by the GRB/XRF-SN connection and the discovery of sub-energetic GRBs, in 2002 we embarked on a dedicated survey of optically-selected local SNe Ibc with the Very Large Array. The goal is to determine the fraction of SNe Ibc that produce mildly-relativistic ejecta. This survey is well-suited to recognizing bursts for which no gamma-ray emission is detected, either because the jets are pointed away from our line-of-sight (“off-axis”) or the emission is below the detection thresholds of current satellites.

Since then we have observed  $\sim 200$  optically-selected local ( $d \lesssim 200$  PC) SNe Ibc with the VLA, on timescales of days to years after the explosion. This dedicated effort has served to characterize in a systematic way the environments and ejecta properties of SNe Ibc for the first time. Early radio observations are crucial for identifying sub-energetic and/or uncollimated explosions. On the other hand, late-time radio observations are sensitive to jets initially beamed away from our line-of-sight. Through this intense VLA program, we have established that (i) roughly 15% of SNe Ibc show detectable radio emission, (ii) less than  $\sim 3\%$  show radio luminosities comparable to those observed for GRB/XRF afterglows (26, 367, 365), and (iii) basic optical properties (peak magnitude, photospheric velocities) are not reliable indicators of strong radio emission.

## 4.2 A Large Radio Survey of SNe Ibc: The Sample

Beginning in 2002, we obtained radio observations of every newly discovered spectroscopically identified SN Ibc within a maximum distance of  $\sim 200$  Mpc and accessible to the VLA (declination limit,  $\gtrsim 40$  deg). All of the targets were drawn from the IAUC, CBET, or ATEL circulars which typically report  $\sim 20$  new SNe Ibc each year, of which  $\sim 90\%$  are accessible to the VLA. Almost all of the reported SNe Ibc are found through “targeted” SN search campaigns which monitor

only the most luminous local galaxies drawn from the RC3 catalog.

Upon spectral classification, we immediately triggered radio follow-up under our VLA Target-of-Opportunity program resulting in first epoch observations typically within a few days of the initial circular. Since most SNe Ibc are discovered near maximum light, the first epoch observations correspond to days to weeks after the explosion. Follow-up observations for each SN were scheduled logarithmically in time since the explosion.

We supplement this sample with radio data of SNe Ibc discovered before 2002. The majority of these data were extracted from the VLA archive and combined with data in the literature. The archival data were primarily taken for radio studies of nearby galaxies, while some were taken specifically for SN follow-up. As a result, the archival data generally probe significantly later timescales: months to years after the explosion. This is highlighted in Figure 1 where we compare the discovery rate of SNe Ibc with the fraction observed with the VLA. Early observations ( $d \lesssim 150$  days) were uncommon in the years preceding our VLA survey.

#### 4.2.1 SNe Ibc: One Class or Two?

The resulting dataset includes *all* VLA observations of local SNe Ibc to date. In Table 4.1, we list the relevant properties of each SN Ibc included in this sample along with the radio measurements. In particular, we include the spectroscopic classification(s) of each SN as reported in the circulars to search for broad correlations between spectroscopic and radio properties. Since the 1980s, it has been heavily debated whether SNe Ibc represent one class of explosions or two, Types Ib and Ic, distinguished based on the strength of weak helium absorption features (428, 113). Related to this issue is the fact that sub-classification is observationally challenging: the optical helium lines are often (i) weak, (ii) blended with other features, and (iii) evolve with time such that sub-classification is time-dependent (e.g., SN 1999ex; Hamuy et al. 173). To further complicate the issue several “transition” events have been identified which show an unusual evolution of the helium

features (e.g., SN 2005bf; Anupama et al. 5, Tominaga et al. 395, Folatelli et al. 121).

Table 4.1 shows that roughly half of the SNe Ibc are classified as Ib or Ic with the other half as Ibc. More importantly, we focus on the 35% of cases where multiple classifications were made (either by different observers/data or by the same observer using a time series of data). Of these, more than half were shown to be inconsistent with the initial classification. This compilation emphasizes that there currently exists no strong observational motivation for SNe Ibc to be sub-classified as Ib and Ic; the dispersion in helium line strength may simply represent a broad distribution of progenitor properties. As an interesting aside, we also note that 13 (7%) of SNe Ibc in this dataset were initially classified as Type Ia supernovae, underscoring the need for multiple spectral classifications and suggesting that a small fraction of SNe Ia are actually misidentified SNe Ibc.

#### 4.2.2 Observation Details

Radio observations are summarized in Table 4.1. Most of the VLA observations were conducted at 8.46 GHz while frequencies of 1.43, 4.86, 15.0, and 22.5 GHz were also used. All of the data were obtained in the standard continuum mode with a bandwidth of  $2 \times 50$  MHz. Phase referencing was performed against a bright, ( $\gtrsim 0.2$  Jy), nearby ( $\lesssim 10$  deg) source and flux calibration was performed using a short ( $\sim 1$  min) observation of 3C48, 3C147, and/or 3C286. Data were reduced using AIPS, and the resulting flux density measurements for this sample of SNe Ibc are given in Table 4.1. For those SNe with detected radio emission, we list in Table 1 only the first epoch in which the emission is detected. In Table 4.2, we list the peak flux density measurements of the thirty SNe Ibc detected to date. For those SNe not detected in the radio, we list all available upper limits in Table 4.1.

### 4.3 The Radio Properties of SNe Ibc

As shown in Table 4.1 and Figure 4.2, the fraction of SNe Ibc with detectable radio emission is small,  $\sim 15\%$ . Compared with their spectroscopic classification(s), SNe sub-classified as Ib show a somewhat higher detection rate than SNe Ic, indicating that Helium-rich explosions may be stronger radio emitters than Helium-poor. In turn, since optical sub-classification is often difficult, as discussed in section §4.2.1, we propose that radio luminosity may enable a more reliable sub-classification.

Of those with positive detections, the majority ( $\sim 70\%$ ) are discovered before radio maximum with well-constrained spectral peaks. As shown in Table 4.2 and Figures 4.2 and 4.3, the peak radio luminosities span four orders of magnitude,  $L_{\nu,\text{radio}} \approx 10^{26} - 10^{30} \text{ erg s}^{-1} \text{ Hz}^{-1}$ . Normalizing by the distance to which each SN could be detected and the effective monitoring time of the survey, we produce the radio luminosity function in Figure 4.3. Clearly, sub-luminous radio SNe Ibc are the most common, though least often detected.

### 4.4 Constraints on the Ejecta Velocity and Kinetic Energy

As discussed by Chevalier (71), the radio emission from SNe Ibc is produced as the fastest ejecta shock accelerate particles in the CSM. Turbulence amplifies the magnetic field and the accelerated (relativistic) electrons produce synchrotron radiation which peaks near the radio band at the time of the explosion. The spectral peak, defined by the low-frequency turn-over, is dominated by synchrotron self-absorption (SSA). This is different from most Type II SNe which are dominated by external free-free absorption due to an exceedingly dense CSM.

As shown by Readhead (310), for radio sources dominated by SSA the brightness temperature,  $T_B = c^2 F_\nu / (2\pi k \theta^2 \nu^2)$ , is constrained to  $5 \times 10^{10}$  K, assuming the post-shock energy density is in equipartition between magnetic fields,  $\epsilon_B$ , and relativistic electrons,  $\epsilon_e$ . With this assumption, robust constraints on the radius

and internal energy of the radio emitting material,  $E_i$ , are derived (71, 216, 73). These constraints scale simply as observable quantities including the peak spectral frequency,  $\nu_p$ , the flux at the spectral peak,  $f_p$ , and the luminosity distance,  $d$  (see Soderberg et al. 359 356 for a detailed discussion). Here we adopt a simple model (see Chevalier and Fransson 73), assuming  $\epsilon_e = \epsilon_B = 0.1$  which provides the following relations:

$$r = 4 \times 10^{14} (f_p/\text{mJy})^{9/19} (d/\text{Mpc})^{18/19} (\nu_p/5 \text{ GHz})^{-1} \text{ cm} \quad (4.1)$$

$$E_i = 1.5 \times 10^{41} (d/\text{Mpc})^8 (f_p/\text{mJy})^4 (\nu_p/5 \text{ GHz})^{-7} (r/10^{15} \text{ cm})^{-6} \text{ erg.} \quad (4.2)$$

Together with the observed peak time,  $t_p$ , the velocity of the shock is easily constrained from Equation 4.1 and is shown for these SNe Ibc in Figure 4.4. SNe with early bright radio emission indicate the fastest ejecta. Of the thirty radio bright SNe Ibc in this sample, the inferred velocities range from 0.01 to 0.5c.

Next, the inferred energy of the radio-emitting material for these SNe Ibc is constrained to  $10^{45}$  to  $10^{48}$  erg. Here we have adopted a values of 0.1 for both the fraction of energy coupled to magnetic fields,  $\epsilon_B$ , and that coupled to relativistic electrons,  $\epsilon_e$ . As shown in Chevalier (69), the internal energy of the shocked CSM is  $\sim 20\%$  of the total energy, which is in turn equal to the kinetic energy of the fastest ejecta. Including this factor of  $\sim 5$ , we find that the kinetic energy of the fastest ejecta,  $E_K = 5E_i$ , spans  $10^{46} - 10^{49}$  erg for SNe Ibc, a factor of  $10^2$  to  $10^5$  times less than that traced by the optical emission.

Finally, we compare these ejecta parameters (velocity, kinetic energy) with those of GRB and XRFs, including the class of sub-energetic bursts (Figure 4.5). We find that evidence of a clear dichotomy between ordinary SNe Ibc and typical GRBs/XRFs: ordinary SNe couple roughly  $10^{47}$  erg to their fastest (but still non-relativistic) ejecta,  $v \sim 0.15c$ . Meanwhile, typical GRBs/XRFs couple  $10^{51}$  erg to relativistic jets,  $\Gamma \sim 10$ . Sub-energetic explosions bridge these two classes, coupling

at least  $10^{48}$  erg to mildly-relativistic outflows,  $\Gamma \sim 3$ .

## 4.5 Constraints on the Mass Loss Rate

With the assumption that SSA dominates the observed radio spectrum, robust constraints on the CSM density and profile are easily extracted. As shown in Chevalier and Fransson (73), the mass loss rate of the progenitor can be estimated using the radio spectral parameters together with an assumed values of  $\epsilon_B$ ,  $\epsilon_e$ , and the progenitor wind velocity,  $v_w$ . In the simple model adopted here we have

$$\dot{M} = 10^{-5} (f_p/\text{mJy})^{-4/19} (d/\text{Mpc})^{-8/19} (\nu_p/5 \text{ GHz})^2 (t_p/10 \text{ days})^2 \text{ M}_\odot \text{ yr}^{-1} \quad (4.3)$$

where we have adopted  $\epsilon_e = \epsilon_B = 0.1$  and a progenitor wind velocity of  $1000 \text{ km s}^{-1}$ , typical for Galactic Wolf-Rayet stars (63). As shown in Figure 4.6, the inferred distribution of progenitor mass loss rates for SNe Ibc span  $10^{-7} - 10^{-2} \text{ M}_\odot \text{ yr}^{-1}$ . In comparison with the observed mass loss rates of local WR stars (63), these values are largely consistent.

Next, we compare the inferred mass loss rates with the velocity of the fastest ejecta. As shown in Figure 4.7, SNe Ibc with a denser CSM typically show evidence for faster ejecta. Moreover, in comparison with GRB-SN 1998bw and XRF-SN 2006aj which are within the distance limit of this survey, ordinary SNe Ibc show significantly higher mass loss rates. This result suggests that binary progenitor systems may be required to further strip the progenitors of GRB/XRF-SNe.

## 4.6 Conclusions

In conclusion, based on our large survey of optically selected local SNe Ibc, we find that (i) roughly 15% show detectable radio emission with Helium-rich explosions showing a slightly higher detection rate, (ii) the peak radio luminosities of SNe Ibc span four orders of magnitude with peak times between 1 and 1000 days,

(iii) the kinetic energy and fastest velocity of these explosions are significantly different from those of typical GRBs and XRFs, (iv) compared with the sample of sub-energetic GRBs,  $\lesssim 3\%$  of SNe Ibc show ejecta properties indicative of an engine-driven explosion, and (v) the inferred range of progenitor mass loss rates for ordinary SNe Ibc are consistent with those of galactic WRs but higher than those of GRB-SNe.

As discussed in the next chapter, with the emergence of wide-field optical surveys, SNe Ibc from “blind” search campaigns will soon begin to dominate new discoveries. In an investigation of the relation between the large-scale environment (host galaxy characteristics) and ejecta properties, these unbiased surveys will play an important role. In particular, host galaxy metallicity is argued to be a critical parameter as a proxy for the progenitor metallicity. Numerical models suggest that only low metallicity progenitors are able to produce the accretion-disk powered outflows inferred for GRBs (437). Therefore, these models predict that engine-driven explosions are unlikely to be hosted in the luminous, high-metallicity galaxies monitored by targeted SN searches (376). Looking forward, a radio survey focused exclusively on the SNe Ibc discovered through blind surveys will directly address and answer this question.

Table 4.1. Radio Observations of SNe Ibc

SN	Host Galaxy	Disc. Ref. (3)	Spec. Type (4)	Spec. Ref. (5)	$d_L$ (Mpc) (6)	$t_0$ (UT) (7)	Date Obs. (UT) (8)	$\Delta t$ (days) (9)	Detected? (10)	$F_\nu$ ( $\mu$ Jy) (11)	$\nu$ (GHz) (12)	Array Config. (13)	Ref. (14)
1954A	NGC 4214	I1453	Ib	I1453	2.9 <sup>a</sup>	1954 Mar 27 <sup>b</sup>	1986 May 3	$\sim 11725$	N	$\pm 23$	1.43	A	1
—	—	—	—	—	—	—	2005 Dec 26	$\sim 18889$	N	$\pm 14$	8.46	D	—
1962L	NGC 1073	I1809	Ib/Ic**	— <sup>c</sup>	11	1962 Nov 14 <sup>b</sup>	1989 Mar 14	$\sim 9610$	N	$\pm 236$	4.86	B	—
—	—	—	—	—	—	—	1990 Jul 30	$\sim 10113$	N	$\pm 134$	4.86	B	—
1964L	NGC 3938	I1882	Ib/Ic**	— <sup>c</sup>	14	1964 Nov 21 <sup>b</sup>	1989 Mar 14	$\sim 8873$	N	$\pm 66$	4.86	B	—
—	—	—	—	—	—	—	1990 Jul 30	$\sim 9376$	N	$\pm 87$	4.86	B	—
—	—	—	—	—	—	—	2003 Nov 11	$\sim 14225$	N	$\pm 62$	1.43	B	—
1983I	NGC 4051	I3813	Ib/Ic**	— <sup>d</sup>	13	1983 Apr 11 <sup>b</sup>	1986 Mar 18	$\sim 1072$	N	$\pm 236$	1.43	A	—
—	—	—	—	—	—	—	1991 Jun 25	$\sim 3030$	N	$\pm 50$	8.46	A	—
—	—	—	—	—	—	—	2001 Feb 1	$\sim 6536$	N	$\pm 32$	8.46	A	—
1983N	NGC 5236	I3825	Ib	— <sup>e</sup>	4.5 <sup>f</sup>	1983 Jun 28 <sup>b</sup>	1983 Jul 6	$\sim 8$	Y	$2000 \pm 500$	4.86	D	2
1983V	NGC 1365	I3895	Ib/Ic**	— <sup>g</sup>	18 <sup>h</sup>	1983 Nov 10 <sup>b</sup>	1983 Nov 6	$\sim -4$	N	$\pm 53$	1.43	A	—
—	—	—	—	—	—	—	1988 Feb 1	$\sim 1543$	N	$\pm 176$	4.86	B	—
—	—	—	—	—	—	—	1993 Feb 3	$\sim 3370$	N	$\pm 92$	1.43	A	—
—	—	—	—	—	—	—	1999 Feb 20	$\sim 5577$	N	$\lesssim 332$	4.86	DnC	—
1984L	NGC 991	I3979	Ib	I4014	15	1984 Jul 29-Aug 29	1984 Oct 2	34-65	Y	$700 \pm 170$	4.86	D	3
1985F	NGC 4618	I4042	Ib*	— <sup>i</sup>	11	1984 May 22 <sup>j</sup>	1985 Mar 18	$\sim 300$	N	$\pm 31$	4.86	BnA	—
—	—	—	—	—	—	—	1985 Mar 18	$\sim 300$	N	$\pm 78$	1.43	BnA	—
—	—	—	—	—	—	—	1986 Apr 4	$\sim 682$	N	$\pm 48$	4.86	A	—

Table 4.1—Continued

SN	Host Galaxy	Disc. Ref.	Spec. Type	Spec. Ref.	$d_L$ (Mpc)	$t_0$ (UT)	Date Obs. (UT)	$\Delta t$ (days)	Detected?	$F_\nu$ ( $\mu$ Jy)	$\nu$ (GHz)	Array Config.	Ref.
(1)	(2)	(3)	(4)	(5)	(6)	(7)	(8)	(9)	(10)	(11)	(12)	(13)	(14)
—	—	—	—	—	—	—	1987 Jun 10	~ 1114	N	$\pm 48$	4.86	A	—
—	—	—	—	—	—	—	1991 Jun 16	~ 2580	N	$\pm 112$	1.43	A	—
—	—	—	—	—	—	—	2003 Oct 17	~ 7088	N	$\pm 37$	8.46	A	4
1986M	NGC 7499	I4282	Ib	I4288	165	1986 Nov 2 <sup>†</sup>	2003 Jun 1	~ 6051	N	$\pm 281$	1.43	A	—
1987M	NGC 2715	I4451	Ib/Ic**	4459	18	1987 Sep 7 <sup>†</sup>	1987 Nov 7	~ 61	N	$\pm 51$	4.86	BnA	—
—	—	—	—	—	—	—	1987 Nov 7	~ 61	N	$\pm 129$	1.43	BnA	—
—	—	—	—	—	—	—	1988 Jan 26	~ 141	N	$\pm 67$	4.86	B	293
—	—	—	—	—	—	—	1989 Mar 14	~ 553	N	$\pm 176$	4.86	B	—
—	—	—	—	—	—	—	1992 Oct 17	~ 1865	N	$\pm 55$	4.86	A	—
—	—	—	—	—	—	—	2003 Oct 17	~ 5884	N	$\pm 34$	8.46	A	4
1988L	NGC 5480	I4590	Ia/Ib**	I4590	30	1988 Mar 21 <sup>†</sup>	1991 Jun 16	~ 1182	N	$\pm 132$	1.43	A	—
1989E	MCG +5-32-45	I4736	Ib	I4759	121	1988 Dec 21 <sup>†</sup>	1991 Jun 16	~ 907	N	$\pm 130$	1.43	A	—
1990B	NGC 4568	I4949	Ib/Ic**	I4953	16 <sup>k</sup>	1989 Dec 23-1990 Jan 20	1990 Feb 6	17-45	Y	600 $\pm$ 60	8.46	D	5
1990U	NGC 7479	I5111	Ib/Ic**	I5069	30	1990 Jun 28-Jul 27	1991 Jun 17	325-354	N	$\pm 51$	4.86	A	—
—	—	—	—	—	—	—	1992 Oct 16	811-840	N	$\pm 186$	4.86	A	—
—	—	—	—	—	—	—	1996 Nov 4	2290-2319	N	$\pm 42$	4.86	A	—
—	—	—	—	—	—	—	1999 Nov 27	3408-3437	N	$\pm 39$	4.86	B	—
—	—	—	—	—	—	—	2003 Oct 17	4830-4859	N	$\pm 44$	8.46	A	4
1990aa	UGC 540	I5087	Ia/Ibc/Ic**	I5090	66	1990 Aug 19-25	1991 Jun 17	296-302	N	$\pm 107$	4.86	A	—

Table 4.1—Continued

SN	Host Galaxy	Disc. Ref.	Spec. Type	Spec. Ref.	$d_L$ (Mpc)	$t_0$ (UT)	Date Obs. (UT)	$\Delta t$ (days)	Detected?	$F_\nu$ ( $\mu$ Jy)	$\nu$ (GHz)	Array Config.	Ref.
(1)	(2)	(3)	(4)	(5)	(6)	(7)	(8)	(9)	(10)	(11)	(12)	(13)	(14)
—	—	—	—	—	—	—	1992 Oct 16	782-788	N	$\pm 104$	1.43	A	—
—	—	—	—	—	—	—	—	—	N	$\pm 87$	4.86	A	—
1990ai	Anon.	I5147	Ibc	I5147	150 <sup>l</sup>	$\sim 1990$ Nov 12	1991 Jun 16	$\sim 216$	N	$\pm 62$	4.86	A	—
—	—	—	—	—	—	—	1992 Oct 17	$\sim 704$	N	$\pm 37$	1.43	A	—
1990aj	NGC 1640	I5178	Ib	I5178	18	1989 Dec 17 <sup>†</sup>	1991 Jun 17	$\sim 547$	N	$\pm 77$	4.86	A	—
—	—	—	—	—	—	—	1992 Oct 16	$\sim 1033$	N	$\pm 27$	4.86	A	—
—	—	—	—	—	—	—	1992 Oct 17	$\sim 1034$	N	$\pm 61$	1.43	A	—
1991A	IC 2973	I5153	Ic	I5155	49	1990 Dec 6-13	1992 Oct 17	673-680	N	$\pm 67$	4.86	A	—
—	—	—	—	—	—	—	2003 Oct 17	4691-4698	N	$\pm 35$	8.46	A	4
1991D	Anon.	I5182	Ibc/Ib**	I5200	176 <sup>m</sup>	1991 Jan 12 <sup>m</sup>	2002 Oct 11	$\sim 637$	N	$\pm 49$	4.86	A	4
1991L	MCG +7-34-134	I5200	Ibc	I5204	136	1991 Jan 17 <sup>†</sup>	1992 Oct 17	$\sim 638$	N	$\pm 92$	4.86	A	—
1991N	NGC 3310	I5227	Ibc	I5234	23 <sup>n</sup>	1991 Feb 20-Mar 29	1992 Oct 17	567-604	N	$\pm 41$	4.86	A	—
—	—	—	—	—	—	—	1994 May 8	1135-1172	N	$\pm 131$	4.86	A	—
—	—	—	—	—	—	—	1994 Mar 2	1068-1105	N	$\pm 246$	8.46	A	—
—	—	—	—	—	—	—	2002 Feb 16	3974-4011	N	$\pm 15$	8.46	A	—
—	—	—	—	—	—	—	2002 Nov 3	4240-4277	N	$\lesssim 314$	22.5	C	—
—	—	—	—	—	—	—	2003 Oct 17	4585-4622	N	$\pm 59$	8.46	A	4
—	—	—	—	—	—	—	2003 Nov 15	4617-4654	N	$\pm 68$	8.46	B	—
—	—	—	—	—	—	—	—	—	N	$\lesssim 529$	4.86	B	—

Table 4.1—Continued

SN	Host Galaxy	Disc. Ref.	Spec. Type	Spec. Ref.	$d_L$ (Mpc)	$t_0$ (UT)	Date Obs. (UT)	$\Delta t$ (days)	Detected?	$F_\nu$ ( $\mu\text{Jy}$ )	$\nu$ (GHz)	Array Config.	Ref.
(1)	(2)	(3)	(4)	(5)	(6)	(7)	(8)	(9)	(10)	(11)	(12)	(13)	(14)
—	—	—	—	—	—	—	—	—	N	$\pm 88$	15.0	B	—
—	—	—	—	—	—	—	2004 Nov 2	4970-5007	N	$\pm 168$	15.0	A	—
—	—	—	—	—	—	—	—	—	N	$\pm 43$	4.86	A	—
—	—	—	—	—	—	—	2005 Mar 17	5105-5142	N	$\lesssim 317$	4.86	B	—
—	—	—	—	—	—	—	—	—	N	$\pm 60$	8.46	B	—
1991R	Anon.	I5237	Ibc	I5237	15.2 <sup>o</sup>	1991 Mar 2 <sup>†</sup>	1992 Oct 16	$\sim 593$	N	$\pm 59$	4.86	A	—
1991ar	IC 49	I5334	Ib*	I5346	59	1991 Aug 3 <sup>†</sup>	1991 Sep 26	$\sim 54$	N	$\pm 21$	4.86	A	—
—	—	—	—	—	—	—	—	—	N	$\pm 16$	8.46	A	—
—	—	—	—	—	—	—	1991 Oct 6	$\sim 64$	N	$\pm 89$	8.46	A	—
—	—	—	—	—	—	—	1991 Oct 21	$\sim 79$	N	$\pm 80$	8.46	A	—
—	—	—	—	—	—	—	1992 Mar 4	$\sim 213$	N	$\pm 30$	4.86	C	—
—	—	—	—	—	—	—	—	—	N	$\pm 20$	8.46	C	—
—	—	—	—	—	—	—	1992 Oct 10	$\sim 433$	N	$\pm 69$	4.86	A	—
—	—	—	—	—	—	—	—	—	N	$\pm 45$	8.46	A	—
—	—	—	—	—	—	—	2003 Oct 17	$\sim 4458$	N	$\pm 30$	8.46	A	4
1994I	NGC 5194	I5961	II/IIb/Ia/Ibc**	I5962	7.9 <sup>p</sup>	1994 Mar 29-31 <sup>q</sup>	1994 Apr 3	3-5	Y	$550 \pm 70$	8.46	A	6
1994ai	NGC 908	I6120	Ic	I6120	18 <sup>n</sup>	1994 Dec 8-16	1995 Jan 9	24-32	N	$\lesssim 205$	8.46	C	—
—	—	—	—	—	—	—	—	—	N	$\lesssim 461$	4.86	C	—
—	—	—	—	—	—	—	—	—	N	$\pm 131$	15.0	C	—

Table 4.1—Continued

SN	Host Galaxy	Disc. Ref.	Spec. Type	Spec. Ref.	$d_L$ (Mpc)	$t_0$ (UT)	Date Obs. (UT)	$\Delta t$ (days)	Detected?	$F_\nu$ ( $\mu\text{Jy}$ )	$\nu$ (GHz)	Array Config.	Ref.
(1)	(2)	(3)	(4)	(5)	(6)	(7)	(8)	(9)	(10)	(11)	(12)	(13)	(14)
—	—	—	—	—	—	—	1996 Jun 23	554-562	N	$\pm 53$	4.86	A	—
—	—	—	—	—	—	—	2003 Oct 17	3227-3235	N	$\pm 40$	8.46	A	4
1996D	NGC 1614	I6317	Ic*	I6317	63	1996 Jan 28 <sup>†</sup>	1998 Sep 17	$\sim 597$	N	$\lesssim 289$	4.86	B	—
—	—	—	—	—	—	—	2003 Jul 9	$\sim 2717$	N	$\pm 39$	8.46	A	—
—	—	—	—	—	—	—	2003 Oct 15	$\sim 2817$	N	$\pm 153$	8.46	A	4
1996N	NGC 1398	I6351	Ibc/Ib**	I6351	15	1996 Feb 16-Mar 13	1996 Apr 2	20-45	Y	$150 \pm 30$	8.46	C	7
1996aq	NGC 5584	I6454	Ic	I6454	29	1996 Jul 30 <sup>†</sup>	1996 Oct 6	$\sim 68$	Y	$329 \pm 26$	8.46	D	—
—	—	—	—	—	—	—	2003 Oct 17	$\sim 2634$	N	$\pm 32$	8.46	A	4
1997B	IC 438	I6535	Ic*	I6535	41	1996 Dec 14 <sup>†</sup>	2003 Oct 15	$\sim 2497$	N	$\pm 33$	8.46	A	4
1997C	NGC 3160	I6536	Ic	I6536	101	1996 Dec 18-23	2003 Oct 17	2490-2495	N	$\pm 37$	8.46	A	4
1997X	NGC 4691	I6552	Ic/Ibc**	I6552	16 <sup>k</sup>	1997 Jan 16-Feb 2	1997 Feb 6	4-21	Y	$1117 \pm 47$	8.46	DnA	—
1997dc	NGC 7678	I6715	Ib/Ic**	I6717	45	1997 Jul 21 <sup>†</sup>	2003 Oct 17	$\sim 2280$	N	$\pm 36$	8.46	A	4
1997dq	NGC 3810	I6770	Ib/Ic-BL**	I6770	18	1997 Oct 16 <sup>†</sup>	1998 Feb 10	$\sim 117$	N	$\pm 24$	8.46	D	—
—	—	—	—	—	—	—	1998 Jun 10	$\sim 237$	N	$\pm 42$	8.46	BnA	—
—	—	—	—	—	—	—	2000 Oct 17	$\sim 1096$	N	$\pm 81$	4.86	A	—
—	—	—	—	—	—	—	2002 Jun 26	$\sim 1713$	N	$\pm 80$	1.43	B	—
—	—	—	—	—	—	—	2003 Oct 17	$\sim 2193$	N	$\pm 30$	8.46	A	4
1997ef	UGC 4107	I6778	Ib/Ic/Ic-BL**	I6786	49	1997 Nov 20 <sup>r</sup>	2000 Dec 4	$\sim 1109$	N	$\pm 30$	8.46	A	—
—	—	—	—	—	—	—	—	—	N	$\pm 40$	4.86	A	—

Table 4.1—Continued

SN	Host Galaxy	Disc. Ref.	Spec. Type	Spec. Ref.	$d_L$ (Mpc)	$t_0$ (UT)	Date Obs. (UT)	$\Delta t$ (days)	Detected?	$F_\nu$ ( $\mu\text{Jy}$ )	$\nu$ (GHz)	Array Config.	Ref.
(1)	(2)	(3)	(4)	(5)	(6)	(7)	(8)	(9)	(10)	(11)	(12)	(13)	(14)
—	—	—	—	—	—	—	2003 Oct 17	$\sim 2158$	N	$\pm 33$	8.46	A	4
1997ei	NGC 3963	I6795	Ia/Ic**	I6796	47	1997 Dec 5-23	1998 Jan 16	24-42	N	$\pm 28$	8.46	D	—
—	—	—	—	—	—	—	1998 Feb 11	50-68	N	$\lesssim 149$	8.46	D	—
—	—	—	—	—	—	—	1998 Jun 10	169-187	N	$\pm 38$	8.46	BnA	—
1998T	NGC 3690	I6830	Ib	I6830	46	1997 Feb 8-Mar 3	1999 Jan 21	689-712	N	$\pm 131$	8.46	C	—
—	—	—	—	—	—	—	1999 Oct 29	970-993	N	$\pm 103$	8.46	B	—
—	—	—	—	—	—	—	2000 Oct 25	1331-1354	N	$\pm 87$	4.86	A	—
—	—	—	—	—	—	—	2002 Apr 29	1882-1905	N	$\pm 182$	8.46	A	—
—	—	—	—	—	—	—	2003 Oct 17	2420-2443	N	$\pm 482$	8.46	A	4
1998ey	NGC 7080	I7065	Ic-BL	I7066	67	1998 Nov 1-Dec 5	1999 Apr 25	141-175	N	$\lesssim 86$	8.46	D	—
—	—	—	—	—	—	—	—	—	N	$\pm 66$	15.0	D	—
—	—	—	—	—	—	—	2003 Oct 17	1777-1811	N	$\pm 32$	8.46	A	4
1999bc	UGC 4433	I7133	Ic	I7133	90	1999 Jan 30 <sup>†</sup>	2003 Oct 15	$\sim 1719$	N	$\pm 25$	8.46	A	4
1999bu	NGC 3786	I7145	Ic	I7149	42	1999 Mar 7-13	2003 Feb 28	1447-1453	N	$\lesssim 5500$	4.86	D	—
—	—	—	—	—	—	—	2003 Jun 20	1559-1569	N	$\pm 66$	8.46	A	—
1999bv	MCG +10-25-14	I7148	Ibc/II-Ibc**	I7150	82	1999 Mar 11 <sup>†</sup>	1999 Apr 3	$\sim 23$	N	$\pm 71$	8.46	D	—
—	—	—	—	—	—	—	1999 Apr 26	$\sim 46$	N	$\pm 86$	4.86	D	—
1999cn	MCG +2-38-43	I7202	Ic	I7202	102	1999 May 25 <sup>†</sup>	1999 Jun 17	$\sim 23$	N	$\pm 111$	8.46	A	—
—	—	—	—	—	—	—	—	—	N	$\pm 114$	1.43	A	—

Table 4.1—Continued

SN	Host Galaxy	Disc. Ref.	Spec. Type	Spec. Ref.	$d_L$ (Mpc)	$t_0$ (UT)	Date Obs. (UT)	$\Delta t$ (days)	Detected?	$F_\nu$ ( $\mu$ Jy)	$\nu$ (GHz)	Array Config.	Ref.
(1)	(2)	(3)	(4)	(5)	(6)	(7)	(8)	(9)	(10)	(11)	(12)	(13)	(14)
1999di	NGC 776	I7234	Ib	I7239	64	1999 Jul 6 <sup>†</sup>	2003 Oct 17	~ 1564	N	±35	8.46	A	4
1999dm	NGC 7714	I7241	Ia/Ic/Ibc/Ib**	I7244	35	1999 Aug 10-20	1999 Nov 27	99-109	N	±53	4.86	B	—
—	—	—	—	—	—	—	2001 Jul 10	689-699	N	±40	8.46	C	—
—	—	—	—	—	—	—	2002 Apr 12	965-975	N	±57	1.43	A	—
—	—	—	—	—	—	—	—	—	N	±82	4.86	A	—
—	—	—	—	—	—	—	2003 Oct 17	1519-1529	N	±42	8.46	A	4
—	—	—	—	—	—	—	2006 Feb 4	2358-2368	N	±50	22.5	A	298
1999ec	NGC 2207	I7268	Ib	I7269	36	1999 Aug 24 <sup>†</sup>	2003 Oct 17	~ 1515	N	±45	8.46	A	4
1999eh	NGC 2770	I7282	Ib	I7282	28	1999 Jul 27 <sup>†</sup>	2000 Oct 17	~ 447	N	±93	4.86	A	—
—	—	—	—	—	—	—	2003 Oct 17	~ 1543	N	±19	8.46	A	4
1999ex	IC 5179	I7310	Ic/Ibc**	I7310	47	1999 Oct 26-Nov 10	1999 Nov 18	8-23	N	±53	8.46	B	8
—	—	—	—	—	—	—	—	—	N	±71	4.86	B	8
2000C	NGC 2415	I7348	Ic*	I7352	52	1999 Dec 30-2000 Jan 4	2000 Feb 4	31-35	N	≤ 187	4.86	B	8
—	—	—	—	—	—	—	2002 Jul 27	904-909	N	≤ 126	8.46	B	—
—	—	—	—	—	—	—	2003 Oct 17	1382-1387	N	±35	8.46	A	4
2000F	IC 302	I7353	Ic	I7360	78	1999 Dec 30-2000 Jan 10	2003 Oct 17	1376-1387	N	±26	8.46	A	4
2000H	IC 454	I7361	Ia/Ic/Ib**	I7366	53	2000 Jan 26-27	2000 Feb 19	23-24	Y	323 ± 81	8.46	CnB	—
2000S	MCG -1-27-20	I7384	Ic	I7384	89	1999 Dec 19 <sup>†</sup>	2003 Oct 17	~ 1398	N	±30	8.46	A	4
2000cr	NGC 5395	I7443	II/Ic**	I7443	54	2000 Jun 21-26	2000 Jul 3	7-12	N	≤ 420	8.46	CnD	8

Table 4.1—Continued

SN	Host Galaxy	Disc. Ref. (3)	Spec. Type (4)	Spec. Ref. (5)	$d_L$ (Mpc) (6)	$t_0$ (UT) (7)	Date Obs. (UT) (8)	$\Delta t$ (days) (9)	Detected? (10)	$F_\nu$ ( $\mu\text{Jy}$ ) (11)	$\nu$ (GHz) (12)	Array Config. (13)	Ref. (14)
—	—	—	—	—	—	—	2003 Jun 21	1090-1095	N	$\pm 56$	8.46	A	—
—	—	—	—	—	—	—	2004 Sep 18	1544-1549	N	$\pm 48$	8.46	A	—
2000de	NGC 4384	I7478	Ib	I7481	38	2000 Jun 6-Aug 11	2003 Oct 17	1162-1228	Y	$651 \pm 40$	8.46	A	4
2000ds	NGC 2768	I7507	Ibc	I7511	19 <sup>s</sup>	2000 May 28-Oct 10	2000 Oct 29	19-154	N	$\pm 104$	8.46	A	—
—	—	—	—	—	—	—	2001 Feb 19	132-267	N	$\pm 30$	8.46	BnA	—
—	—	—	—	—	—	—	2003 Oct 17	1103-1238	N	$\pm 34$	8.46	A	4
—	—	—	—	—	—	—	2004 Sep 6	1426-1561	N	$\pm 85$	8.46	D	—
—	—	—	—	—	—	—	2006 Jan 3	1910-2045	N	$\pm 23$	8.46	A	—
2000dt	UGC 3411	I7508	Ib	I7511	95	2000 Sep 21-Oct 13	2000 Oct 29	16-38	N	$\pm 66$	8.46	A	—
2000dv	UGC 4671	I7510	Ib	I7511	58	2000 Jul 5 <sup>†</sup>	2000 Oct 29	$\sim 116$	Y	$1032 \pm 89$	8.46	A	—
2000ew	NGC 3810	I7530	Ia/Ic**	I7532	18	2000 Nov 14 <sup>†</sup>	2002 Jun 26	$\sim 589$	N	$\pm 67$	1.43	B	8
2000fn	NGC 2526	I7546	Ib	I7547	65	2000 Oct 31 <sup>†</sup>	2000 Dec 29	$\sim 59$	N	$\pm 45$	8.46	A	8
2001B	IC 391	I7555	Ia/Ib**	I7563	20	2000 Dec 25-2001 Jan 4	2001 Feb 4	31-41	Y	$3500 \pm 29$	8.46	BnA	8
2001M	NGC 3240	I7568	Ic*	I7576	53	2001 Jan 3-21	2001 Feb 4	14-32	N	$\pm 28$	8.46	BnA	8
—	—	—	—	—	—	—	2003 Oct 17	999-1017	N	$\pm 54$	8.46	A	4
2001ai	NGC 5278	I7605	Ic*	I7605	111	2001 Mar 19-28	2001 Mar 31	3-12	N	$\lesssim 172$	8.46	B	8
—	—	—	—	—	—	—	—	—	N	$\lesssim 196$	4.86	B	8
—	—	—	—	—	—	—	—	—	N	$\lesssim 196$	1.43	B	8
2001bb	IC 4319	I7614	Ia/Ic**	I7616	67	2001 Apr 15-29	2001 May 5	6-20	N	$\pm 50$	8.46	B	8

Table 4.1—Continued

SN	Host Galaxy	Disc. Ref.	Spec. Type	Spec. Ref.	$d_L$ (Mpc)	$t_0$ (UT)	Date Obs. (UT)	$\Delta t$ (days)	Detected?	$F_\nu$ ( $\mu$ Jy)	$\nu$ (GHz)	Array Config.	Ref.
(1)	(2)	(3)	(4)	(5)	(6)	(7)	(8)	(9)	(10)	(11)	(12)	(13)	(14)
—	—	—	—	—	—	—	—	—	N	$\pm 60$	4.86	B	8
—	—	—	—	—	—	—	—	—	N	$\pm 120$	1.43	B	8
—	—	—	—	—	—	—	2003 Oct 17	901-915	N	$\pm 35$	8.46	A	4
2001ch	MCG -1-54-16	I7637	Ic	I7637	40	2001 Mar 24 <sup>†</sup>	2003 Oct 17	$\sim 937$	N	$\pm 32$	8.46	A	4
2001ci	NGC 3079	I7618	Ic	I7638	17	2001 Apr 17-25	2001 Jun 6	42-50	N	$\lesssim 900$	8.46	BnA	8
—	—	—	—	—	—	—	2001 Dec 17	244-252	N	$\lesssim 448$	22.5	D	—
—	—	—	—	—	—	—	2003 May 17	752-760	N	$\lesssim 2668$	8.46	D	—
—	—	—	—	—	—	—	2003 Sep 13	871-879	N	$\pm 163$	8.46	A	—
—	—	—	—	—	—	—	2003 Oct 17	905-913	N	$\pm 188$	8.46	A	4
2001ej	UGC 3829	I7719	Ibc/Ic/Ib**	I7721	55	2001 Aug 31 <sup>†</sup>	2001 Sep 27	$\sim 27$	N	$\lesssim 1540$	8.46	CnD	8
—	—	—	—	—	—	—	2002 Jun 16	$\sim 289$	N	$\pm 85$	1.43	B	8
—	—	—	—	—	—	—	2003 Jul 20	$\sim 688$	N	$\pm 74$	4.86	A	—
—	—	—	—	—	—	—	2003 Oct 15	$\sim 775$	N	$\pm 36$	8.46	A	4
2001em	UGC 11794	I7722	Ibc/IIn**	I7737	81	2001 Sep 5-15	2003 Oct 17	762-772	Y	$1151 \pm 51$	8.46	A	9
2001gl	Anon.	I7763	Ibc	I7763	1907	2001 Mar 28-Apr 20	2002 Jun 26	401-424	N	$\pm 176$	1.43	B	—
2001ig	NGC 7424	I7772	Ilb/Ibc**	I7782	11	2001 Dec 4 <sup>u</sup>	2001 Dec 15	$\sim 11$	Y	$2100 \pm 300$	8.64	—	10
2001is	NGC 1961	I7782	Ib	I7787	54	2001 Dec 14-23	2002 Jun 16	175-184	N	$\lesssim 210$	1.43	B	8
—	—	—	—	—	—	—	2003 Jul 20	574-583	N	$\pm 68$	4.86	A	—
—	—	—	—	—	—	—	2003 Oct 15	661-670	N	$\pm 31$	8.46	A	4

Table 4.1—Continued

SN	Host Galaxy	Disc. Ref.	Spec. Type	Spec. Ref.	$d_L$ (Mpc)	$t_0$ (UT)	Date Obs. (UT)	$\Delta t$ (days)	Detected?	$F_\nu$ ( $\mu\text{Jy}$ )	$\nu$ (GHz)	Array Config.	Ref.
(1)	(2)	(3)	(4)	(5)	(6)	(7)	(8)	(9)	(10)	(11)	(12)	(13)	(14)
2002J	NGC 3464	I7800	Ic	I7808	57	2002 Jan 15-21	2002 Jun 15	145-151	N	$\pm 251$	1.43	B	—
—	—	—	—	—	—	—	2002 Jun 18	148-154	N	$\pm 85$	1.43	B	8
—	—	—	—	—	—	—	2002 Nov 22	305-311	N	$\pm 74$	8.46	C	8
—	—	—	—	—	—	—	2002 Nov 26	309-315	N	$\pm 49$	8.46	C	—
—	—	—	—	—	—	—	2003 Oct 17	635-641	N	$\pm 23$	8.46	A	4
2002ap	NGC 628	I7810	Ibc/Ic-BL**	I7811	6.7 <sup>v</sup>	2002 Jan 25-29	2002 Feb 1	3-7	Y	$374 \pm 29$	8.46	A	11
2002bl	UGC 5499	I7845	Ic-BL	I7845	70	2002 Feb 14-Mar 3	2002 Mar 8	5-22	N	$\pm 50$	8.46	A	8
—	—	—	—	—	—	—	—	—	N	$\pm 45$	4.86	A	8
—	—	—	—	—	—	—	2003 Oct 17	593-610	N	$\pm 39$	8.46	A	4
2002bm	MCG -01-32-19	I7845	Ic	I7848	84	2002 Jan 16-Mar 6	2002 Jun 26	112-161	N	$\pm 66$	1.43	B	8
—	—	—	—	—	—	—	2003 Oct 17	590-639	N	$\pm 39$	8.46	A	4
2002eg	UGC 10415	I7877	Ic	I7881	142	2002 Feb 23 <sup>f</sup>	2002 Jun 26	$\sim 123$	N	$\lesssim 740$	1.43	B	8
2002cj	ESO 582-G5	I7882	Ic*	I7894	103	2002 Apr 10-Apr 22	2002 Jun 3	42-54	Y	$121 \pm 33$	8.46	B	8
2002cp	NGC 3074	I7887	Ibc**	I7894	75	2002 Apr 11-28	2002 Jun 2	35-52	N	$\pm 31$	8.46	BnA	8
—	—	—	—	—	—	—	—	—	N	$\pm 35$	4.86	BnA	8
—	—	—	—	—	—	—	—	—	N	$\pm 36$	1.43	BnA	8
—	—	—	—	—	—	—	2003 Oct 17	537-554	N	$\pm 29$	8.46	A	4
2002dn	IC 5145	I7922	Ic	I7922	103	2002 Jun 1-16	2002 Jul 4	18-33	N	$\pm 39$	8.46	B	8
—	—	—	—	—	—	—	—	—	N	$\pm 43$	4.86	B	8

Table 4.1—Continued

SN	Host Galaxy	Disc. Ref.	Spec. Type	Spec. Ref.	$d_L$ (Mpc)	$t_0$ (UT)	Date Obs. (UT)	$\Delta t$ (days)	Detected?	$F_\nu$ ( $\mu$ Jy)	$\nu$ (GHz)	Array Config.	Ref.
(1)	(2)	(3)	(4)	(5)	(6)	(7)	(8)	(9)	(10)	(11)	(12)	(13)	(14)
—	—	—	—	—	—	—	—	—	N	$\pm 72$	1.43	B	8
—	—	—	—	—	—	—	2003 Oct 21	492-507	N	$\pm 37$	8.46	B	8
2002dg	Anon.	I7915	Ib	I7922	197	2002 May 5 - May 31	2002 Jul 10	40-66	Y	$92 \pm 37$	4.86	B	8
2002ge	NGC 7400	I7987	Ia/Ic**	I7990	41	2002 Sep 21 <sup>†</sup>	2002 Oct 12	$\sim 21$	N	$\lesssim 1600$	8.46	C	8
—	—	—	—	—	—	—	—	—	N	$\lesssim 390$	4.86	C	8
2002gy	UGC 2701	I7996	Ibc	I7999	98	2002 Oct 9-16	2002 Oct 28	12-19	N	$\pm 36$	8.46	C	8
—	—	—	—	—	—	—	—	—	N	$\pm 39$	4.86	C	8
2002hf	MCG -05-3-20	I8004	Ic	I8007	75	2002 Oct 2-29	2002 Nov 7	9-36	N	$\pm 40$	8.46	C	8
—	—	—	—	—	—	—	2003 Oct 17	353-380	N	$\pm 48$	8.46	A	4
2002hn	NGC 2532	I8009	Ic	I8009	74	2002 Oct 22-31	2002 Nov 7	7-16	N	$\pm 44$	8.46	C	8
—	—	—	—	—	—	—	2002 Nov 10	10-19	N	$\pm 114$	8.46	C	—
2002ho	NGC 4210	I8011	Ic	I8014	40	2002 Sep 28 <sup>†</sup>	2002 Nov 15	$\sim 48$	N	$\pm 47$	8.46	C	8
—	—	—	—	—	—	—	—	—	N	$\pm 54$	4.86	C	8
—	—	—	—	—	—	—	2003 Oct 17	$\sim 384$	N	$\pm 35$	8.46	A	4
2002hy	NGC 3464	I8016	Ib	I8019	57	2002 Oct 13-Nov 12	2002 Nov 22	10-40	N	$\pm 74$	8.46	C	8
—	—	—	—	—	—	—	2002 Nov 26	14-44	N	$\pm 49$	8.46	C	—
—	—	—	—	—	—	—	2003 Oct 17	339-369	N	$\pm 23$	8.46	A	4
2002hz	UGC 12044	I8017	Ib	I8051	75	2002 Nov 2-12	2003 Jan 21	70-80	N	$\pm 29$	8.46	DnC	8
—	—	—	—	—	—	—	2003 Oct 17	339-349	N	$\pm 29$	8.46	A	4

Table 4.1—Continued

SN	Host Galaxy	Disc. Ref.	Spec. Type	Spec. Ref.	$d_L$ (Mpc)	$t_0$ (UT)	Date Obs. (UT)	$\Delta t$ (days)	Detected?	$F_\nu$ ( $\mu$ Jy)	$\nu$ (GHz)	Array Config.	Ref.
(1)	(2)	(3)	(4)	(5)	(6)	(7)	(8)	(9)	(10)	(11)	(12)	(13)	(14)
2002ji	NGC 3655	I8025	Ic/Ibc**	I8026	25	2002 Oct 11 <sup>†</sup>	2002 Dec 6	~ 56	N	±43	8.46	C	8
—	—	—	—	—	—	—	2003 Oct 17	~ 371	N	±18	8.46	A	4
2002jj	IC 340	I8026	Ic	I8031	54	2002 Oct 1-24	2002 Dec 15	52-75	N	±33	8.46	C	8
—	—	—	—	—	—	—	2003 Oct 15	356-379	N	±30	8.46	A	4
2002jp	NGC 3313	I8031	Ic	I8031	56	2002 Nov 7 <sup>†</sup>	2002 Dec 15	~ 38	N	±38	8.46	C	8
—	—	—	—	—	—	—	2003 Oct 17	~ 344	N	±37	8.46	A	4
2002jz	UGC 2984	I8037	Ic/I Ib**	I8037	16	2002 Nov 26 <sup>†</sup>	2003 Jan 3	~ 38	N	≲ 75	8.46	C	8
2003A	UGC 5904	I8041	Ibc	I8042	95	2002 Nov 23-2003 Jan 5	2003 Jan 8	3-46	N	≲ 140	8.46	C	—
—	—	—	—	—	—	—	2003 Jun 15	161-204	N	±69	8.46	A	4
2003H	NGC 2207	I8045	Ib/Ibc**	I8047	36	2003 Jan 3-5	2003 Jan 14	9-11	N	≲ 438	8.46	DnC	—
2003I	IC 2481	I8046	Ib	I8049	78	2002 Dec 14 <sup>†</sup>	2003 Jan 19	~ 36	Y	171 ± 21	8.46	DnC	—
2003L	NGC 3506	I8048	Ic/Ibc**	I8057	96	2002 Nov 15-Jan 7	2003 Jan 26	19-72	Y	743 ± 39	8.46	DnC	12
2003bg	MCG -05-10-15	I8092	Ic-BL/II/Ibc**	I8084	15	2002 Nov 7-2003 Feb 26	2003 Mar 4	6-117	Y	2510 ± 70	8.46	D	13
2003bm	UGC 4226	I8086	Ibc	I8091	112	2003 Feb 20-Mar 3	2003 Mar 14	11-22	N	±58	8.46	D	—
—	—	—	—	—	—	—	2003 Jun 15	104-115	N	±57	8.46	A	4
2003bp	NGC 2596	I8089	Ib/Ibc**	I8091	85	2003 Feb 19-28	2003 Mar 14	14-23	N	≲ 254	8.46	D	—
—	—	—	—	—	—	—	2003 Jun 15	107-116	N	±66	8.46	A	—
2003bu	NGC 5393	I8092	Ic	I8098	92	2003 Feb 11-Mar 12	2003 Mar 27	15-44	N	≲ 392	8.46	D	—
—	—	—	—	—	—	—	2003 Jun 15	80-124	N	±71	8.46	A	4

Table 4.1—Continued

SN	Host Galaxy	Disc. Ref.	Spec. Type	Spec. Ref.	$d_L$ (Mpc)	$t_0$ (UT)	Date Obs. (UT)	$\Delta t$ (days)	Detected?	$F_\nu$ ( $\mu$ Jy)	$\nu$ (GHz)	Array Config.	Ref.
(1)	(2)	(3)	(4)	(5)	(6)	(7)	(8)	(9)	(10)	(11)	(12)	(13)	(14)
2003cr	UGC 9639	I8103	Ic	I8111	160	2003 Feb 24-Mar 31	2003 Jun 15	76-111	N	$\pm 67$	8.46	A	—
—	—	—	—	—	—	—	2003 Nov 2	216-251	N	$\pm 59$	8.46	B	4
2003dg	UGC 6934	I8113	Ibc	I8159	84	2003 Mar 24-Apr 8	2003 Jul 1	84-99	N	$\pm 57$	8.46	A	—
—	—	—	—	—	—	—	2003 Nov 2	208-223	N	$\pm 90$	8.46	B	4
2003dr	NGC 5714	I8117	Ibc	I8159	36	2003 Apr 8-12	2003 Jul 1	80-84	N	$\pm 46$	8.46	A	—
—	—	—	—	—	—	—	2003 Nov 2	204-208	N	$\pm 58$	8.46	B	4
2003ds	MCG +08-19-17	I8120	Ic	I8158	131	2003 Mar 25-Apr 14	2003 Jul 1	78-98	N	$\pm 49$	8.46	A	—
—	—	—	—	—	—	—	2003 Nov 2	202-222	N	$\pm 67$	8.46	B	4
2003el	NGC 5000	I8135	Ic	I8136	85	2003 Apr 19-May 22	2003 May 28	6-39	N	$\pm 60$	8.46	A	—
—	—	—	—	—	—	—	2003 Jun 10	19-52	N	$\pm 22$	8.46	A	—
—	—	—	—	—	—	—	2003 Jun 15	24-57	N	$\pm 70$	8.46	A	—
—	—	—	—	—	—	—	2003 Nov 2	164-197	N	$\pm 65$	8.46	B	4
2003ev	Anon.	I8140	Ic-BL/Ic**	I8142	103	2003 Apr 9-Jun 1	2003 Jun 10	9-62	N	$\pm 57$	8.46	A	—
—	—	—	—	—	—	—	2003 Jun 15	14-67	N	$\pm 56$	8.46	A	—
—	—	—	—	—	—	—	2003 Nov 2	154-207	N	$\pm 61$	8.46	B	4
2003gf	MCG -04-52-26	I8156	Ic	I8157	35	2003 May 15 <sup>†</sup>	2003 Jul 1	~ 47	N	$\pm 50$	8.46	A	—
2003gk	NGC 7460	I8162	Ib*	I8164	41	2003 May 22 <sup>†</sup>	2003 Jul 14	~ 53	N	$\pm 66$	8.46	A	—
2003hp	UGC 10942	I8088	Ic-BL	I8211	94	2003 Aug 17-25	2003 Oct 7	43-51	N	$\pm 74$	8.46	BnA	—
—	—	—	—	—	—	—	2003 Nov 2	69-77	N	$\pm 66$	8.46	B	—

Table 4.1—Continued

SN	Host Galaxy	Disc. Ref.	Spec. Type	Spec. Ref.	$d_L$ (Mpc)	$t_0$ (UT)	Date Obs. (UT)	$\Delta t$ (days)	Detected?	$F_\nu$ ( $\mu\text{Jy}$ )	$\nu$ (GHz)	Array Config.	Ref.
(1)	(2)	(3)	(4)	(5)	(6)	(7)	(8)	(9)	(10)	(11)	(12)	(13)	(14)
2003id	NGC 895	I8201	Ic*	I8203	26	2003 Sep 8-17	2003 Sep 23	6-15	N	$\pm 89$	8.46	BnA	—
—	—	—	—	—	—	—	2003 Oct 21	34-43	N	$\pm 42$	8.46	B	—
—	—	—	—	—	—	—	2003 Dec 4	78-87	N	$\pm 36$	8.46	B	—
2003ig	UGC 2971	I8207	Ic	I8211	79	2003 Sep 12-23	2003 Oct 7	14-25	N	$\pm 43$	8.46	BnA	—
2003ih	UGC 2836	I8207	Ibc	I8246	66	2003 Sep 8-15	2003 Dec 4	80-87	N	$\pm 38$	8.46	B	—
2003is	MCG +07-40-03	I8224	Ic	I8225	79	2003 Oct 4-14	2003 Oct 18	4-14	N	$\pm 27$	8.46	B	—
—	—	—	—	—	—	—	2003 Nov 2	19-29	N	$\pm 73$	8.46	B	—
2003jd	MCG -01-59-21	I8232	Ic-BL*	I8234	77	2003 Oct 16-25	2003 Oct 29	4-13	N	$\pm 34$	8.46	B	4
—	—	—	—	—	—	—	—	—	N	$\pm 52$	4.86	B	4
—	—	—	—	—	—	—	—	—	N	$\pm 58$	22.5	B	4
—	—	—	—	—	—	—	2003 Nov 4	10-19	N	$\pm 77$	8.46	B	4
—	—	—	—	—	—	—	2003 Nov 15	21-30	N	$\pm 74$	8.46	B	4
—	—	—	—	—	—	—	2005 May 12	564-573	N	$\pm 15$	8.46	B	4
2003jg	NGC 2997	I8235	Ibc	I8241	17	2003 Sep 27-Oct 6	2003 Nov 26	31-40	N	$\pm 70$	8.46	B	—
—	—	—	—	—	—	—	2003 Dec 7	62-71	N	$\pm 48$	8.46	B	—
2003kb	UGC 3432	I8241	Ia/Ic**	I8242	69	2003 Nov 5-19	2003 Nov 26	7-21	N	$\pm 32$	8.46	B	—
—	—	—	—	—	—	—	2003 Dec 7	18-32	N	$\pm 44$	8.46	B	—
2004C	NGC 3683	I8269	Ic	I8269	26	2003 Dec 5 <sup>†</sup>	2004 Jan 24	$\sim 50$	Y	$1633 \pm 54$	8.46	ChB	—
2004ao	UGC 10862	I8299	Ib*	I8304	29	2004 Feb 15 <sup>†</sup>	2004 Mar 20	$\sim 33$	N	$\pm 32$	8.46	C	—

Table 4.1—Continued

SN	Host Galaxy	Disc. Ref.	Spec. Type	Spec. Ref.	$d_L$ (Mpc)	$t_0$ (UT)	Date Obs. (UT)	$\Delta t$ (days)	Detected?	$F_\nu$ ( $\mu$ Jy)	$\nu$ (GHz)	Array Config.	Ref.
(1)	(2)	(3)	(4)	(5)	(6)	(7)	(8)	(9)	(10)	(11)	(12)	(13)	(14)
2004aw	NGC 3997	I8310	Ia/Ic-BL/Ibc/Ic**	I8312	72	2004 Mar 13-20	2004 Mar 23	3-10	N	$\pm 37$	8.46	C	—
—	—	—	—	—	—	—	2004 Nov 14	239-246	N	$\pm 278$	4.86	A	—
2004ax	NGC 5939	I8311	Ibc	I8331	97	2004 Mar 7-21	2004 Apr 27	37-51	N	$\lesssim 176$	8.46	C	—
2004bf	UGC 8739	I8317	Ic	I8324	77	2004 Mar 23-Apr 7	2004 Apr 15	8-23	N	$\lesssim 244$	8.46	C	—
2004bi	UGC 5894	I8321	Ic/I Ib**	I8324	97	2004 Mar 15-Apr 13	2004 Apr 19	6-35	N	$\pm 33$	8.46	C	—
2004bm	NGC 3437	I8335	Ic	I8339	21	2004 Mar 15-Apr 25	2004 May 21	26-67	N	$\lesssim 1900$	8.46	DnC	—
—	—	—	—	—	—	—	2004 Jun 3	39-80	N	$\pm 89$	22.5	DnC	—
2004bs	NGC 3323	I8341	Ib	I8344	77	2004 Apr 25-May 10	2004 May 29	19-34	N	$\pm 75$	22.5	DnC	—
2004bu	UGC 10089	I8343	Ic-BL*	I8345	84	2004 May 14 <sup>w</sup>	2004 May 29	$\sim 15$	N	$\pm 29$	8.46	DnC	—
2004cc	NGC 4568	I8350	Ic	I8353	16 <sup>k</sup>	2004 May 23-Jun 10	2004 Jun 17	7-25	Y	$7350 \pm 180$	22.5	D	—
2004dc	IC 1504	I8372	Ic	I8372	85	2004 May 30 <sup>†</sup>	2004 Jul 15	$\sim 46$	N	$\lesssim 403$	8.46	D	—
—	—	—	—	—	—	—	—	—	N	$\pm 111$	22.5	D	—
—	—	—	—	—	—	—	2004 Aug 7	$\sim 69$	N	$\lesssim 382$	8.46	D	—
2004dk	NGC 6118	I8377	Ic/Ib**	I8379	28	2004 Jul 29-30	2004 Aug 7	8-9	Y	$1304 \pm 48$	8.46	D	—
2004dn	UGC 2069	I8381	Ic	I8381	48	2004 Jul 18 <sup>†</sup>	2004 Aug 8	$\sim 21$	N	$\pm 25$	8.46	D	—
—	—	—	—	—	—	—	2004 Aug 16	$\sim 29$	N	$\pm 46$	8.46	D	—
2004dx	MCG +07-37-36	I8392	Ibc	I8420	133	2004 Jun 27-Aug 20	2004 Oct 28	69-123	N	$\pm 29$	8.46	A	—
2004eh	UGC 1892	I8401	Ib	I8420	138	2004 Aug 28 <sup>†</sup>	2004 Oct 28	$\sim 61$	N	$\pm 24$	8.46	A	—
2004eu	MCG +07-5-39	I8417	Ic*	I8418	88	2004 Sep 15-Oct 6	2004 Oct 18	12-33	N	$\pm 37$	8.46	A	—

Table 4.1—Continued

SN	Host Galaxy	Disc. Ref.	Spec. Type	Spec. Ref.	$d_L$ (Mpc)	$t_0$ (UT)	Date Obs. (UT)	$\Delta t$ (days)	Detected?	$F_\nu$ ( $\mu\text{Jy}$ )	$\nu$ (GHz)	Array Config.	Ref.
(1)	(2)	(3)	(4)	(5)	(6)	(7)	(8)	(9)	(10)	(11)	(12)	(13)	(14)
2004fe	NGC 132	18425	Ic*	18426	71	2004 Oct 22-30	2004 Nov 4	5-13	N	$\pm 35$	8.46	A	—
2004ff	ESO 552-G40	18425	Ic	18428	93	2004 Oct 21-30	2004 Nov 4	5-14	N	$\pm 40$	8.46	A	—
2004ge	UGC 3555	18443	Ic	18453	66	2004 Nov 14-17	2004 Dec 16	29-32	N	$\pm 42$	8.46	A	—
2004gk	IC 3311	18446	Ic	18446	16 <sup>k</sup>	2004 Nov 7 <sup>†</sup>	2004 Dec 1	$\sim 24$	N	$\pm 52$	8.46	A	—
—	—	—	—	—	—	—	—	—	N	$\pm 102$	1.43	A	—
—	—	—	—	—	—	—	2004 Dec 10	$\sim 33$	N	$\pm 42$	8.46	A	—
—	—	—	—	—	—	—	2005 Dec 12	$\sim 400$	N	$\pm 40$	8.46	D	—
2004gq	NGC 1832	18452	Ic/Ib**	18452	23	2004 Dec 4-11	2004 Dec 16	5-12	Y	$2003 \pm 45$	8.46	A	14
2004gt	NGC 4038	18454	Ib/Ic**	18456	14 <sup>x</sup>	2004 Nov 27 <sup>†</sup>	2004 Dec 22	$\sim 25$	N	$\pm 65$	8.46	A	—
—	—	—	—	—	—	—	2005 Dec 12	$\sim 380$	N	$\pm 71$	22.5	D	—
2004gv	NGC 856	18454	Ibc	18456	79	2004 Nov 29-Dec 14	2004 Dec 19	5-20	N	$\pm 50$	8.46	A	—
—	—	—	—	—	—	—	2005 Jan 8	25-40	N	$\pm 49$	8.46	A	—
2005C	Anon.	18468	Ib	18468	219 <sup>y</sup>	2004 Nov 20-2005 Jan 11	2005 Jan 31	20-72	N	$\pm 43$	8.46	BnA	—
2005E	NGC 1032	18465	Ib	18465	32	2004 Dec 24-2005 Jan 13	2005 Jan 21	8-28	N	$\pm 53$	8.46	A	—
2005N	NGC 5420	18470	Ibc	18472	76	2004 Sep 22 <sup>†</sup>	2005 Feb 12	$\sim 143$	N	$\pm 57$	8.46	BnA	—
2005O	NGC 3340	18471	Ib	18472	83	2004 Dec 28-2005 Jan 17	2005 Jan 23	6-26	Y	$301 \pm 61$	8.46	BnC	—
2005V	NGC 2146	18474	Ibc	18474	11	2005 Jan 1 <sup>†</sup>	2005 Feb 3	$\sim 33$	N	$\pm 42$	8.46	BnA	—
—	—	—	—	—	—	—	2005 Feb 12	$\sim 42$	N	$\pm 144$	8.46	BnA	—
2005aj	UGC 2411	18488	Ic	18493	34	2005 Feb 9 <sup>w</sup>	2005 Mar 15	$\sim 34$	N	$\pm 20$	8.46	B	—

Table 4.1—Continued

SN	Host Galaxy	Disc. Ref.	Spec. Type	Spec. Ref.	$d_L$ (Mpc)	$t_0$ (UT)	Date Obs. (UT)	$\Delta t$ (days)	Detected?	$F_\nu$ ( $\mu$ Jy)	$\nu$ (GHz)	Array Config.	Ref.
(1)	(2)	(3)	(4)	(5)	(6)	(7)	(8)	(9)	(10)	(11)	(12)	(13)	(14)
2005ar	CGCG 011-033	I8493	Ib	I8493	113	2005 Feb 10-Mar 10	2005 Mar 17	7-35	N	$\pm 35$	8.46	B	—
2005az	NGC 4961	I8503	Ib/Ic**	A451	41	2005 Mar 20-27	2005 Apr 7	11-18	N	$\pm 24$	8.46	B	—
2005bf	MCG +00-27-5	I8507	Ic/II-Ib/Ib**	I8509	84	2005 Mar 15-30	2005 Apr 13	14-29	N	$\pm 30$	8.46	B	—
—	—	—	—	—	—	—	2005 May 2	33-48	N	$\pm 36$	8.46	B	—
—	—	—	—	—	—	—	2005 May 22	53-68	N	$\pm 50$	8.46	B	—
—	—	—	—	—	—	—	2005 Jun 8	70-85	N	$\pm 41$	8.46	B	—
—	—	—	—	—	—	—	2005 Nov 4	219-234	N	$\pm 20$	8.46	DnC	—
—	—	—	—	—	—	—	2005 Nov 12	227-242	N	$\lesssim 48$	8.46	D	—
—	—	—	—	—	—	—	2005 Dec 7	252-267	N	$\lesssim 90$	8.46	D	—
—	—	—	—	—	—	—	2005 Dec 13	258-273	N	$\pm 63$	22.5	D	—
—	—	—	—	—	—	—	2006 Jan 2	278-293	N	$\pm 49$	8.46	D	—
—	—	—	—	—	—	—	2006 Mar 7	342-357	N	$\pm 31$	8.46	A	—
—	—	—	—	—	—	—	2006 Dec 21	631-646	N	$\pm 31$	8.46	C	—
—	—	—	—	—	—	—	—	—	N	$\pm 62$	4.86	C	—
2005bh	UGC 6495	I8509	Ic	I8513	97	2005 Mar 12 <sup>†</sup>	2005 Apr 19	$\sim 38$	N	$\pm 40$	8.46	B	—
2005bj	MCG +03-43-5	I8511	Ic	I8513	100	2005 Mar 11 <sup>†</sup>	2005 Apr 19	$\sim 39$	N	$\pm 35$	8.46	B	—
2005bk	MCG +07-33-27	I8512	Ic	I8514	109	2005 Mar 20 <sup>†</sup>	2005 Apr 19	$\sim 30$	N	$\pm 33$	8.46	B	—
2005bq	IC 4367	I8515	Ic	I8520	64	2005 Feb 19 <sup>†</sup>	2005 Jun 7	$\sim 108$	N	$\sim 88$	8.46	B	—
2005ce	IC 5233	I8534	Ibc	I8534	103	2005 May 5 <sup>†</sup>	2005 Jun 6	$\sim 32$	N	$\pm 40$	8.46	B	—

Table 4.1—Continued

SN	Host Galaxy	Disc. Ref.	Spec. Type	Spec. Ref.	$d_L$ (Mpc)	$t_0$ (UT)	Date Obs. (UT)	$\Delta t$ (days)	Detected?	$F_\nu$ ( $\mu\text{Jy}$ )	$\nu$ (GHz)	Array Config.	Ref.
(1)	(2)	(3)	(4)	(5)	(6)	(7)	(8)	(9)	(10)	(11)	(12)	(13)	(14)
2005ct	NGC 207	18557	Ic	18564	51	2005 May 29 <sup>w</sup>	2005 Jul 20	~ 52	N	$\pm 39$	8.46	C	—
2005cz	NGC 4589	18569	Ib	18579	21 <sup>C</sup>	2005 Jun 20-Jul 18	2005 Aug 8	21-49	N	$\pm 55$	8.46	C	—
2005da	UGC 11301	18570	Ic-BL	18575	67	2005 Jun 2-Jul 18	2005 Jul 26	8-54	N	$\pm 38$	8.46	C	—
—	—	—	—	—	—	—	2005 Aug 5	18-64	N	$\pm 62$	8.46	C	—
—	—	—	—	—	—	—	2005 Dec 11	146-192	N	$\pm 54$	8.46	D	—
2005dg	ESO 420-3	18581	Ic	18585	54	2005 Jul 20-Aug 5	2005 Aug 28	23-39	N	$\pm 56$	8.46	C	—
2005ek	UGC 2526	18604	Ic	C235	65	2005 Sep 15-25	2005 Sep 29	4-14	N	$\pm 64$	8.46	C	—
2005eo	UGC 4132	18605	Ic	18605	73	2005 Sep 9 <sup>†</sup>	2005 Oct 4	~ 25	N	$\pm 65$	8.46	C	—
2005fk	Anon.	C247	lbc	C247	1193	2005 Jul 13 <sup>†</sup>	2005 Oct 10	~ 89	N	$\pm 24$	8.46	C	—
2005hg	UGC 1394	18623	Ic/lb**	C267	87	2005 Oct 20-25	2005 Oct 29	4-9	N	$\pm 31$	8.46	D	—
—	—	—	—	—	—	—	2005 Nov 3	9-14	N	$\pm 22$	8.46	D	—
—	—	—	—	—	—	—	2006 Jan 2	69-74	N	$\pm 44$	8.46	D	—
2005kf	Anon.	18630	Ic	C301	62	2005 Sep 30 <sup>†</sup>	2005 Nov 28	~ 59	N	$\pm 47$	8.46	D	—
2005kl	NGC 4369	18634	Ic	C305	18	2005 Nov 1 <sup>†</sup>	2005 Nov 28	~ 27	N	$\lesssim 1500$	8.46	D	—
—	—	—	—	—	—	—	2005 Dec 7	~ 36	N	$\lesssim 300$	22.5	D	—
—	—	—	—	—	—	—	2005 Dec 17	~ 46	N	$\lesssim 1600$	8.46	D	—
2005kz	MCG +08-34-32	18639	Ic-BL	18639	119	2005 Nov 1-Dec 1	2005 Dec 6	5-35	N	$\lesssim 91$	8.46	D	—
—	—	—	—	—	—	—	2006 Dec 16	15-45	N	$\lesssim 348$	8.46	D	—
—	—	—	—	—	—	—	2006 Dec 19	18-48	N	$\pm 59$	8.46	D	—

Table 4.1—Continued

SN	Host Galaxy	Disc. Ref.	Spec. Type	Spec. Ref.	$d_L$ (Mpc)	$t_0$ (UT)	Date Obs. (UT)	$\Delta t$ (days)	Detected?	$F_\nu$ ( $\mu$ Jy)	$\nu$ (GHz)	Array Config.	Ref.
(1)	(2)	(3)	(4)	(5)	(6)	(7)	(8)	(9)	(10)	(11)	(12)	(13)	(14)
—	—	—	—	—	—	—	—	—	N	$\pm 209$	15.0	D	—
—	—	—	—	—	—	—	—	—	N	$\pm 127$	22.5	D	—
—	—	—	—	—	—	—	2006 Apr 4	124-154	N	$\pm 66$	8.46	D	—
2005la	Anon.	18639	II-Ib	18639	79 <sup>A</sup>	2005 Jan 16-Dec 1	2005 Dec 7	6-325	N	$\pm 49$	8.46	D	—
—	—	—	—	—	—	—	2005 Dec 17	16-335	N	$\pm 60$	8.46	D	—
2005lr	ESO 492-G2	18641	Ic	C:321	35	2005 Nov 5-Dec 4	2006 Jan 2	29-58	N	$\lesssim 1600$	8.46	D	—
2005mf	UGC 4798	18648	Ic	18650	116	2005 Dec 13-26	2006 Jan 2	7-20	N	$\pm 43$	8.46	D	—
2005nb	UGC 7230	18657	Ic-BL	18657	107	2005 Dec 8 <sup>†</sup>	2006 Jan 14	$\sim 37$	N	$\lesssim 86$	8.46	D	—
2006F	NGC 935	18658	Ib	18658	53	2005 Nov 21-2006 Jan 12	2006 Jan 25	13-65	N	$\lesssim 172$	8.46	D	—
—	—	—	—	—	—	—	2006 Apr 4	82-134	N	$\pm 70$	8.46	A	—
2006ab	PGC 10652	18669	Ic	18677	66	2006 Jan 24-Feb 9	2006 Mar 27	46-62	N	$\pm 62$	8.46	A	—
2006bf	UGC 8093?	18693	Ib/IIb**	C:455	139 <sup>B</sup>	2006 Feb 26 <sup>†</sup>	2006 Apr 3	$\sim 35$	N	$\pm 54$	8.46	A	—
2006cb	NGC 5541	18709	Ib	C:529	115	2006 Feb 23-May 5	2006 Jun 2	28-99	N	$\pm 44$	8.46	BnA	—
2006ck	UGC 8238	18713	Ic	C:519	111	2006 May 2 <sup>†</sup>	2006 Jun 16	$\sim 45$	N	$\pm 57$	8.46	BnA	—
2006dg	IC 1508	18725	Ic	C:562	56	2006 Apr 6 <sup>†</sup>	2006 Jul 5	$\sim 90$	N	$\pm 27$	8.46	B	—
2006dj	UGC 12287	18727	Ib	C:567	72	2006 Apr 1 <sup>†</sup>	2006 Jul 5	$\sim 85$	N	$\pm 30$	8.46	B	—
2006dl	MCG +04-31-5	18727	IIb/Ib**	C:567	99	2006 Jun 19-29	2006 Jul 4	5-10	N	$\pm 56$	8.46	B	—
2006dm	UGC 12188	18728	Ib	A:854	73 <sup>C</sup>	2006 Jun 9-Jul 5	2006 Jul 13	8-34	Y	$395 \pm 82$	8.46	B	—
2006ea	UGC 12134	18736	Ib	C:589	102	2006 Jul 10-25	2006 Aug 2	8-23	N	$\pm 77$	8.46	B	—

Table 4.1—Continued

SN	Host Galaxy	Disc. Ref.	Spec. Type	Spec. Ref.	$d_L$ (Mpc)	$t_0$ (UT)	Date Obs. (UT)	$\Delta t$ (days)	Detected?	$F_\nu$ ( $\mu$ Jy)	$\nu$ (GHz)	Array Config.	Ref.
(1)	(2)	(3)	(4)	(5)	(6)	(7)	(8)	(9)	(10)	(11)	(12)	(13)	(14)
2006ec	MCG -04-55-14	18736	Ib	C599	106	2006 Jul 3-Aug 4	2006 Aug 26	22-54	N	$\pm 110$	8.46	B	—
2006eg	CGCG 462-023	C600	Ibc	C604	51	2006 Aug 1-Aug 21	2006 Aug 27	6-26	N	$\pm 99$	8.46	B	—
2006ei	NGC 735	C600	Ic	C604	61	2006 Aug 4-21	2006 Aug 26	5-22	N	$\pm 166$	8.46	B	—
2006el	UGC 12188	18741	Ib/IIb**	C612	73 <sup>z</sup>	2006 Aug 18-25	2006 Sep 7	13-20	N	$\pm 29$	8.46	B	—
2006ep	NGC 214	18744	Ib/Ibc**	C612	59	2006 Aug 27-30	2006 Sep 7	8-11	N	$\pm 38$	8.46	B	—
2006fo	UGC 2019	18570	Ia/Ic**	18750	81	2006 Aug 31 <sup>P</sup>	2006 Sep 26	$\sim 26$	N	$\pm 64$	8.46	CnB	—
—	—	—	—	—	—	—	—	—	N	$\pm 280$	22.5	CnB	—
—	—	—	—	—	—	—	2007 Jan 21	$\sim 143$	N	$\lesssim 202$	8.46	DnC	—
2006gi	NGC 3147	18751	Ib	C635	48 <sup>E</sup>	2006 Aug 30 <sup>†</sup>	2006 Sep 26	$\sim 26$	Y	$225 \pm 42$	8.46	CnB	—
2006ip	Anon.	C658	Ibc	C658	130 <sup>F</sup>	2006 Aug 1-Sep 19 <sup>G</sup>	2006 Oct 6	17-66	N	$\pm 29$	8.46	CnB	—
2006ir	KUG 2302+073	18758	Ibc	18758	81	2006 Jun 25-Sep 23 <sup>H</sup>	2006 Oct 6	13-103	N	$\pm 37$	8.46	CnB	—
2006jc	UGC 4904	18762	Ib/IIb/Ibc**	C672	23	2006 Sep 22-Oct 10	2006 Dec 16	67-85	Y	$192 \pm 44$	8.46	C	—
2006lc	NGC 7364	C688	Ic/Ibc**	C688	65	2006 Oct 19-24 <sup>I</sup>	2006 Oct 26	2-7	N	$\pm 39$	8.46	C	—
2006ld	UGC 348	18766	Ib	18766	53	2006 Sep 20-Oct 19	2006 Nov 28	40-69	N	$\pm 25$	8.46	C	—
2006lt	Anon.	C714	Ib	C714	64 <sup>J</sup>	2006 Apr 17 <sup>†</sup>	2006 Oct 23	$\sim 189$	Y	$401 \pm 62$	8.46	C	—
2007C	NGC 4981	18792	Ib	C800	30	2006 Dec 24-2007 Jan 9	2007 Jan 11	2-18	Y	$729 \pm 30$	8.46	C	15
2007D	UGC 2653	18794	Ic-BL	C805	94	2006 Dec 6-2007 Jan 9	2007 Jan 14	5-39	N	$\pm 25$	8.46	C	—
—	—	—	—	—	—	—	2007 Jan 16	7-41	N	$\pm 35$	8.46	C	—
2007I	Anon.	18798	Ic-BL	C808	91	2006 Dec 7-2007 Jan 14	2007 Jan 17	3-41	N	$\pm 28$	8.46	C	—

Table 4.1—Continued

SN	Host Galaxy	Disc. Ref.	Spec. Type	Spec. Ref.	$d_L$ (Mpc)	$t_0$ (UT)	Date Obs. (UT)	$\Delta t$ (days)	Detected?	$F_\nu$ ( $\mu\text{Jy}$ )	$\nu$ (GHz)	Array Config.	Ref.
(1)	(2)	(3)	(4)	(5)	(6)	(7)	(8)	(9)	(10)	(11)	(12)	(13)	(14)
—	—	—	—	—	—	—	2007 Jan 18	4-42	N	$\pm 70$	8.46	C	—
—	—	—	—	—	—	—	2007 Jan 19	5-43	N	$\pm 22$	8.46	C	—
2007Y	NGC 1187	I8813	Ibc	C862	14	2007 Jan 26-Feb 15	2007 Feb 24	9-29	N	$\pm 34$	8.46	D	—
—	—	—	—	—	—	—	2007 Mar 11	24-44	N	$\pm 18$	8.46	D	—
2007az	Anon.	I8829	Ib	I8829	147 <sup>K</sup>	2006 Dec 18-2007 Mar 6 <sup>L</sup>	2007 Mar 29	23-102	N	$\pm 25$	8.46	D	—
2007bg	Anon.	C927	Ic	C927	147 <sup>M</sup>	2007 Apr 6-16	2007 Apr 19	3-13	Y	$233 \pm 42$	8.46	D	—

Col (1): SN name. Col (2): host galaxy name. Col (3): circular number for the SN discovery. Entries refer to table references or circular numbers prefaced by “T” (IAUC), “C” (CBET), or “A” (ATEL). Col (4): spectroscopic classification(s) listed in chronological order. SNe with multiple spectroscopic classification references are denoted as “\*\*” or “\*\*\*” depending on whether the references are consistent or inconsistent, respectively. Reference for the initial spectroscopic classification listed in Col 4. Entries refer to table references or circular numbers prefaced by “T” (IAUC), “C” (CBET), or “A” (ATEL). Subsequent classifications are either included in the circular in column 5 or referenced in the Notes section below. Col (6): luminosity distance to the host galaxy calculated using the NED corrected velocities (Virgo + Great Attractor + Shapley Supercluster Infall) and assuming  $H_0 = 71 \text{ km s}^{-1} \text{ Mpc}^{-1}$ ,  $\Omega_M = 0.27$ ,  $\Omega_\Lambda = 0.73$ . When available, luminosity distances for specific hosts are adopted from the NED-1d NASA/IPAC Extragalactic Database of Distances and referenced accordingly. In the cases where the host galaxy is Anonymous, the luminosity distance is calculated from the redshift of the host (referenced accordingly) adopting the cosmological parameters given above. Col (7): Constraints on the SN explosion date. When available, we use the range of dates bracketed by the discovery date and the most recent pre-discovery image in which the SN is not detected. In cases where this range is larger than 3 months, we adopt the spectral age estimate or the date of maximum light and assume a rise time of 21 days. Col (8): Date of radio observations. Col (9): days since explosion. Ranges reflect the uncertainty in explosion date given in col. 7 while rough estimates are preceded by “~” and given in cases where the explosion date is estimated by the spectral age or the date of maximum light. Col (10) whether radio emission was detected. For those SNe with positive detections, only the initial detection is listed; peak fluxes are given in Table 2. Col (11) radio flux density. Non-detections and errors are given as  $\pm 1\sigma$  rms. In the cases where diffuse host galaxy emission dominates the observed flux, an upper limit is given instead. Col (12): radio frequency; Col (13): VLA configuration.

Table 4.2. Radio Observations of SNe Ibc (cont')

SN	Host Galaxy	Disc. Ref.	Spec. Type	Spec. Ref.	$d_L$ (Mpc)	$t_0$ (UT)	Date Obs. (UT)	$\Delta t$ (days)	Detected?	$F_\nu$ ( $\mu\text{Jy}$ )	$\nu$ (GHz)	Array Config.	Ref.
(1)	(2)	(3)	(4)	(5)	(6)	(7)	(8)	(9)	(10)	(11)	(12)	(13)	(14)

<sup>†</sup>Explosion date estimated from spectral age provided by ref in column 5 and assuming a 21 day rise time.

<sup>a</sup>Distance estimate is an average of values reported in Maíz-Apellániz et al. (236), Karachentsev et al. (200), Drozdovsky et al. (104).

<sup>b</sup>Explosion date calculated from date of maximum light given in Wheeler and Harkness (427) and assuming a rise time of 21 days.

<sup>c</sup>Wheeler and Harkness (426) and references within.

<sup>d</sup>Elias et al. (108).

<sup>e</sup>Gaskell et al. (157).

<sup>f</sup>Distance estimate is an average of values reported in Thim et al. (392), Karachentsev et al. (200).

<sup>g</sup>Branch (51).

<sup>h</sup>Kanbur et al. (199).

<sup>i</sup>Filippenko and Sargent (119).

<sup>j</sup>Explosion date calculated from date of maximum light given in Tsvetkov (399) and assuming a rise time of 21 days.

<sup>k</sup>Host galaxy in the Virgo cluster. Distance averaged from Freedman (139), Mould et al. (262).

<sup>l</sup>No redshift available for host. Adopt 150 Mpc based on SN and host luminosities.

<sup>m</sup>Distance and explosion date from Benetti et al. (14) assuming 21 day rise time.

<sup>n</sup>Distance from Tully-Fisher method referenced online by LEDA.

<sup>o</sup>Distance calculated using the recession velocity of the host galaxy reported in I5237.

<sup>p</sup>Distance estimate is an average of values reported in Ciardullo et al. (82), Feldmeier et al. (110), Tonry et al. (396), Karachentsev et al. (200).

Table 4.3. Radio Observations of SNe Ibc (cont')

SN	Host Galaxy	Disc. Ref.	Spec. Type	Spec. Ref.	$d_L$ (Mpc)	$t_0$ (UT)	Date Obs. (UT)	$\Delta t$ (days)	Detected?	$F_\nu$ ( $\mu\text{Jy}$ )	$\nu$ (GHz)	Array Config.	Ref.
(1)	(2)	(3)	(4)	(5)	(6)	(7)	(8)	(9)	(10)	(11)	(12)	(13)	(14)

<sup>a</sup>Explosion date adopted from Richmond et al. (317).

<sup>r</sup>Explosion date estimate adopted from Mazzali et al. (251).

<sup>s</sup>Distance estimate is an average of values reported in Kundu and Whitmore (217), Tonry et al. (396), Blakeslee et al. (39) and the Tully-Fisher value referenced online by LEDA.

<sup>t</sup>Explosion date calculated from date of maximum light given in Gerardy et al. (158) and assuming a rise time of 21 days.

<sup>u</sup>Explosion date estimated from spectral age with respect to shock breakout reported in I7793.

<sup>v</sup>Distance estimate is an average of values reported in Karachentsev et al. (200), Hendry et al. (185), Vinkó et al. (412), and Tully-Fisher method referenced online by LEDA.

<sup>w</sup>Explosion date estimate from private communication with A. Filippenko and R. Foley.

<sup>x</sup>Distance estimate is an average of values reported in Saviane et al. (340).

<sup>y</sup>Distance calculated using the recession velocity of the host galaxy, from private communication with A. Filippenko and R. Foley.

<sup>z</sup>Distance estimate is an average of values reported in Tonry et al. (396), Jensen et al. (197).

<sup>A</sup>Distance calculated using the recession velocity of the host galaxy reported in I8639.

<sup>B</sup>Distance calculated using the recession velocity of the host galaxy reported in C455.

<sup>C</sup>Distance calculated using the recession velocity of the host galaxy reported in A854.

<sup>D</sup>Explosion date estimate from private communication with M. Sako.

<sup>E</sup>Distance estimate is from Reindl et al. (312).

<sup>F</sup>Distance calculated using the recession velocity of the host galaxy reported in C658.

<sup>G</sup>Explosion date estimate from private communication with G. Aldering.

Table 4.4. Radio Observations of SNe Ibc (cont')

SN	Host Galaxy	Disc. Ref.	Spec. Type	Spec. Ref.	$d_L$ (Mpc)	$t_0$ (UT)	Date Obs. (UT)	$\Delta t$ (days)	Detected?	$F_\nu$ ( $\mu\text{Jy}$ )	$\nu$ (GHz)	Array Config.	Ref.
(1)	(2)	(3)	(4)	(5)	(6)	(7)	(8)	(9)	(10)	(11)	(12)	(13)	(14)

<sup>H</sup>Explosion date estimate from private communication with G. Aldering.

<sup>I</sup>Explosion date range from C693.

<sup>J</sup>Distance estimate from recession velocity reported in C714.

<sup>K</sup>Distance estimate from recession velocity reported in C909.

<sup>L</sup>Explosion date range from C872.

<sup>M</sup>Distance estimate from recession velocity reported in C927.

Note. — For SNe with multiple spectroscopic classifications, the initial reference is given in column 5 while the subsequent classifications are referenced below. Entries refer to table references or circular numbers prefaced by “I” (IAUC), “C” (CBET), “A” (ATEL), “G” (GCN). SN 1962L: Wheeler and Harkness (426) and references within; SN 1964L: Wheeler and Harkness (426) and references within; SN 1983I: Wheeler et al. (428); SN 1983V: Wheeler et al. (428); SN 1985F: Gaskell et al. (157), Filippenko and Sargent (120); SN 1987M: I4470, Filippenko et al. (118); SN 1988L: I4597, I4614; SN 1990U: I5111; SN 1990aa: 5111,5129; SN 1991ar: I3348; SN 1994I: I5964,I5966,I5971,I5972,I5981,I6019, Ford et al. (125); SN 1996N: Sollerman et al. (373); SN 1997B: Gómez and López (161), Clocchiatti et al. (83); SN 1997X: I6554; SN 1997dc: I6716; SN 1997dq: Mazzali et al. (248); SN 1997ef: I6798,I6809,I6820,Mazzali et al. (251 248); SN 1997ei: I6800,I6801,I6809; SN 1999bv: I7186; SN 1999dn: I7245, Deng et al. (101); SN 1999ex: Hamuy et al. (173); SN 2000H: I7367,I7375; SN 2000cr: I7444; SN 2000ew: I7547; SN 2001B: I7577; SN 2001M: I7579; SN 2001ai: I7639; SN 2001bb: I7619; SN 2001ej: I7737; SN 2001em: G2586; SN 2001ig: I7781,I7793,I7988; SN 2002ap: I7820, I7825, I7834, I7838, I7860, Mazzali et al. (249), Gal-Yam et al. (149), Kinugasa et al. (207), Kawabata et al. (201), Takada-Hidai et al. (387), Leonard et al. (220), Wang et al. (413), Fox et al. (127); SN 2002cp: I7894, SN 2002ji: I8028; SN 2003H: I8049,I8159; SN 2003L: W. Li, private communication.; SN 2003bg: I8088, M. Hamuy private communication; SN 2003ev: I8158; SN 2003id: I8228; SN 2003jd: I8410, Mazzali et al. (252); SN 2003kb: I8243; SN 2004ac: Gómez et al. (162); SN 2004aw: I8311,I8331,Taubenberger et al. (389); SN 2004bi: I8331; SN 2004bu: I8353; SN 2004dk: I8404; SN 2004gq: I8461; SN 2005az: I8504; SN 2005bf: I8520,I8521,I8522,Anupama et al. (5), Tominaga et al. (395), Folatelli et al. (121); SN 2005hg: C271; SN 2006el: C614, SN 2006ep: C614; SN 2006fo: I8770; SN 2006jc: C674, C677, C676, Foley et al. (123), Pastorello et al. (281); SN 2006lc: C699

Table 4.5. Peak Radio Flux Densities of SNe Ibc

SN	Spec. Type	$d_L$ (Mpc)	$t_0$ (UT)	$t_p$ (UT)	$\Delta t$ (days)	$F_{\nu,p}$ ( $\mu\text{Jy}$ )	$\nu_p$ (GHz)	Ref.
(1)	(2)	(3)	(4)	(5)	(6)	(7)	(8)	(9)
1983N	Ib	4.5	1983 Jun 29 <sup>a</sup>	1983 Jul 28	29	$18500 \pm 1000$	4.86	1
1984L	Ib	15	1984 Aug 12 <sup>a</sup>	$\lesssim 1984$ Oct 2	$\lesssim 51$	$\gtrsim 700 \pm 180$	4.86	2
1990B	Ib/Ic	16	1989 Dec 15 <sup>a</sup>	1990 Mar 7	82	$1480 \pm 110$	1.43	3
1994I	II/IIb/Ia/Ibc	7.9	1994 Mar 30	1994 May 5	36	$14600 \pm 1000$	4.86	4
1996N	Ibc/Ib	15	1996 Feb 29	1996 Apr 8	39	$464 \pm 30$	4.86	—
1996aq	Ic	29	1996 Jul 30	$\lesssim 1996$ Oct 6	$\lesssim 68$	$\gtrsim 709 \pm 40$	4.86	—
1997X	Ic/Ibc	16	1997 Jan 25	1997 Feb 6	12	$2080 \pm 38$	4.86	—
2000H	Ia/Ic/IIb	53	2007 Jan 27	$\lesssim 2000$ Feb 19	$\lesssim 23$	$\gtrsim 323 \pm 81$	8.46	—
2000de	Ib	38	2000 Jul 9	$\lesssim 2003$ Oct 17	$\lesssim 1196$	$\gtrsim 651 \pm 40$	8.46	5
2000dv	Ib	58	2000 Jul 5	$\lesssim 2000$ Oct 29	$\lesssim 116$	$\gtrsim 1032 \pm 89$	8.46	—
2001B	Ia/Ib	20	2000 Dec 30	$\lesssim 2002$ Oct 28	$\lesssim 678$	$\gtrsim 3500 \pm 29$	8.46	6
2001em	Ibc/IIc	81	2001 Sep 15 <sup>a</sup>	2004 Jan 31	868	$1815 \pm 99$	4.86	7
2001ig	IIb/Ibc	11	2001 Dec 3 <sup>a</sup>	2002 Mar 28	116	$21900 \pm 1000$	4.79	8
2002ap	Ibc/Ic-BL	6.7	2002 Jan 28 <sup>b</sup>	2002 Feb 4	7	$410 \pm 41$	1.43	9
2002cj	Ic	103	2002 Apr 16	2002 Jun 18	63	$408 \pm 81$	1.43	6
2002dg	Ib	197	2002 May 18	2002 Jul 10	53	$92 \pm 37$	4.86	6
2003I	Ib	78	2002 Dec 14	$\gtrsim 2003$ Feb 6	$\gtrsim 54$	$\gtrsim 335 \pm 42$	8.46	—
2003L	Ic/Ibc	96	2003 Jan 1 <sup>a</sup>	2003 Mar 10	68	$2081 \pm 52$	8.46	10
2003bg	Ic-BL/II/Ibc	15	2003 Feb 22 <sup>a</sup>	2003 Mar 17	23	$106300 \pm 2160$	22.5	11

Table 4.5—Continued

SN	Spec. Type	$d_L$ (Mpc)	$t_0$ (UT)	$t_p$ (UT)	$\Delta t$ (days)	$F_{\nu,p}$ ( $\mu\text{Jy}$ )	$\nu_p$ (GHz)	Ref.
(1)	(2)	(3)	(4)	(5)	(6)	(7)	(8)	(9)
2004C	Ic	26	2003 Dec 8 <sup>c</sup>	2004 Apr 19	157	$10940 \pm 256$	15.0	—
2004cc	Ic	16	2004 Jun 3 <sup>c</sup>	2004 Jun 30	27	$4596 \pm 85$	8.46	—
2004dk	Ic/Ib	28	2004 Jul 30	2004 Aug 13	14	$2419 \pm 58$	8.46	—
2004gq	Ic/Ib	23	2004 Dec 8 <sup>c</sup>	2005 Jan 8	31	$6404 \pm 57$	8.46	—
2005O	Ib	83	2005 Jan 7	$\lesssim$ 2005 Jan 23	$\lesssim$ 16	$\gtrsim 301 \pm 61$	8.46	—
2006dn	Ib	73	2006 Jun 22	2006 Jul 21	29	$607 \pm 51$	8.46	—
2006gi	Ib	48	2006 Aug 30	2006 Sep 29	30	$626 \pm 71$	8.46	—
2006jc	Ib/IIb/Ibc	23	2006 Oct 1	2006 Dec 20	80	$300 \pm 34$	8.46	—
2006lt	Ib	64	2006 Apr 17	$\lesssim$ 2006 Oct 23	$\lesssim$ 189	$\gtrsim 401 \pm 62$	8.46	—
2007C	Ib	30	2007 Jan 1	2007 Jan 16	15	$800 \pm 65$	8.46	—
2007bg	Ic	147	2007 Apr 2 <sup>d</sup>	2006 Apr 25	23	$1329 \pm 67$	22.5	—

Col. (1): SN name; Col. (2) Spectroscopic classification(s) listed in chronological order and referenced in Table 4.1. Col. (3): luminosity distance adopted from

Table 4.1; Col. (4): explosion date adopted from Table 4.1. For SNe with a range of dates we adopt the median value. For the well-studied SNe, we adopt the explosion date as constrained through optical or radio modeling and reference accordingly. Col. (5): epoch of the observed radio peak flux. Limits are given in the where the peak was not observed. Col. (6): peak time in units of days since explosion; Col. (7): observed peak flux density; Col. (8): radio frequency; Col. (9): reference for the radio data.

<sup>a</sup>Explosion date is further constrained by the radio modeling reported in column 8.

<sup>b</sup>Explosion date is further constrained by optical modeling reported in Mazzali et al. (249).

<sup>c</sup>Explosion date is further constrained by the radio modeling of Soderberg in prep.

References. — 1.Sramek et al. (374); 2. Panagia et al. (276) ; van Dyk et al. (408) ; 4.Weiler et al. (424)

5. Soderberg et al. (367) ; 6. Berger et al. (26) ; 7.18282; 8. Rydler et al. (325); 9. Berger et al. (22); 10. Soderberg et al. (359); 11. Soderberg et al. (356)

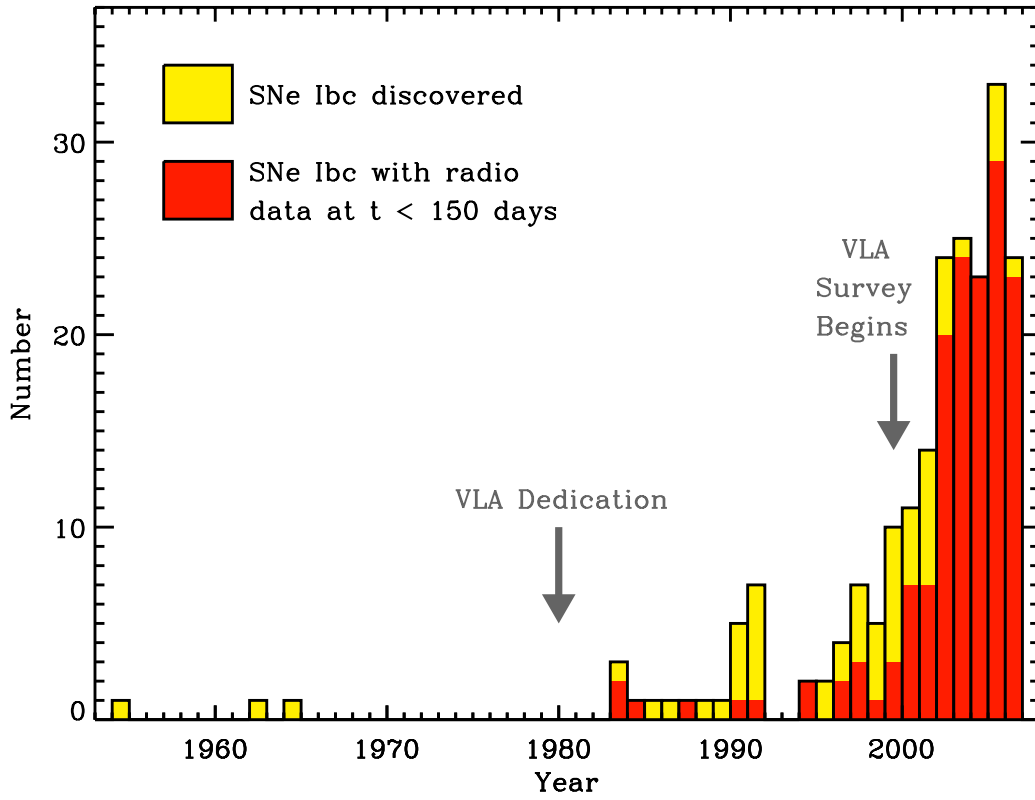


Figure 4.1: The discovery rate of SNe Ibc each year (yellow) is compared with the fraction observed in the radio on timescales less than 150 days (red). Early radio observations are crucial for constraining underluminous and/or off-axis GRBs since they trace the fastest ejecta in the explosion. Since the launch of our VLA survey, nearly every SN Ibc is observed on this timescale.

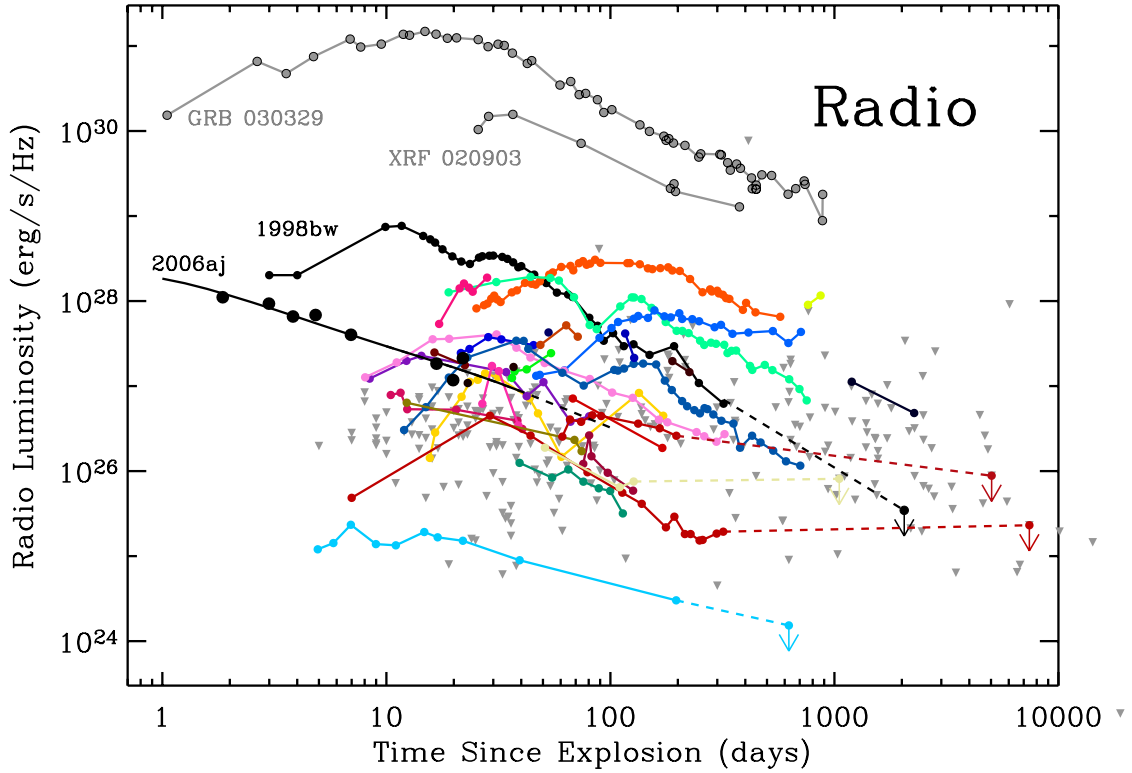


Figure 4.2: To date, 30 local ( $d \lesssim 200$  Mpc) SNe Ibc have been detected at radio wavelengths, the majority of which were found through our dedicated VLA survey. Detections are shown as colored light-curves and  $3\sigma$  upper limits as inverted grey triangles. GRB-SN 1998bw and XRF 2006aj, also within the maximum distance of this sample, are distinguished by their bright early peaking radio emission (black). Both of these events were sub-energetic in comparison with typical GRBs (e.g., GRB 030329; grey) and XRFs (e.g., XRF 020903; grey).

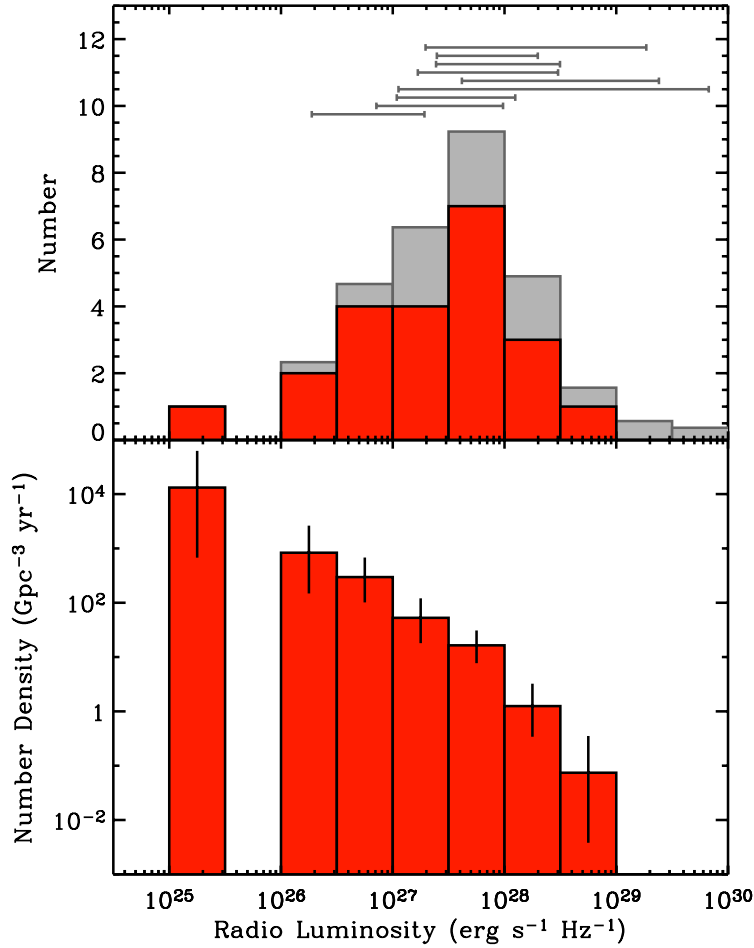


Figure 4.3: Top: The peak radio luminosity distribution for SNe Ibc (Table 2) peaks near  $L_\nu \approx 10^{28} \text{ erg s}^{-1} \text{ Hz}^{-1}$ . For the detected SNe where the spectral peak was not observed directly, we extrapolate the observed flux over the range of observed peak times (2 days to 150 days) to estimate the upper limit on the peak luminosity (horizontal bars). Moreover, we include them in the histogram (grey) by assuming each has an equal probability of having a peak luminosity in the range determined by the observed luminosity to the estimated upper limit. Bottom: The radio luminosity function of SNe Ibc. Low luminosity SNe clearly dominate the intrinsic sample, though they are rarely observed due to their low flux. We emphasize that this analysis includes several biases, including effective monitoring time pre-2002 and efficiency of optical spectroscopic classification.

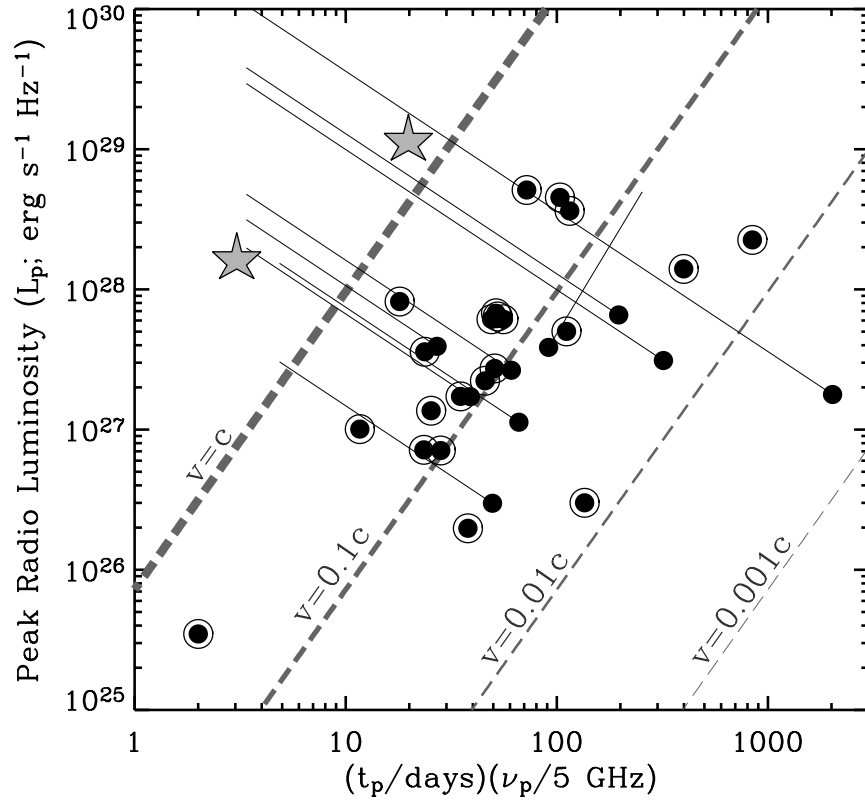


Figure 4.4: The peak radio luminosities of all the SNe Ibc detected to date (Table 2) are plotted against the timescale of peak. SNe with well-constrained peaks are shown as black encircled dots while those where the peak is not well constrained are shown as black dots with lines indicating the extrapolation of the radio light-curves between the range of typically observed peak times. GRB-SN 1998bw and XRF-SN 2006aj were also discovered within this volume and we include them here as grey stars. Dashed lines indicate how the velocity of the fastest ejecta scales with the observed spectral parameters.

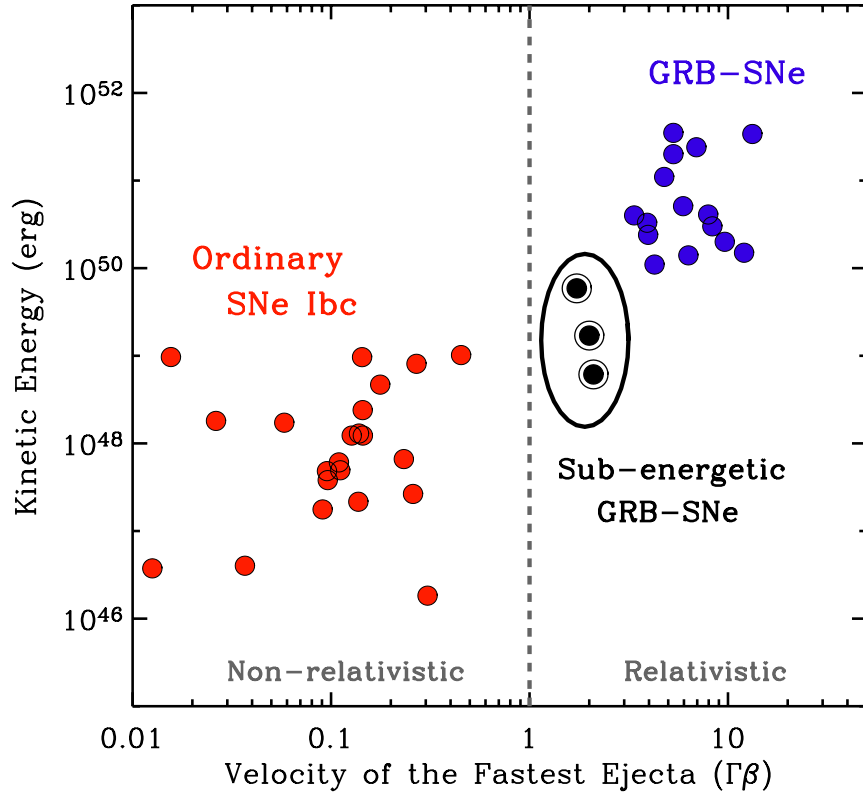


Figure 4.5: The kinetic energy and velocity of the fastest ejecta for radio bright SNe Ibc are compared with those of GRBs, XRFs, and sub-energetic bursts. Ordinary SNe Ibc (red) are distinguished in that they couple  $10^{48}$  erg to non-relativistic ejecta at  $v \approx 0.15c$  while GRBs and XRFs (blue) couple at  $10^{51}$  erg to relativistic material ( $\Gamma \approx 10$ ). Sub-energetic bursts (black) are intermediate between the two classes, coupling at least  $10^{48}$  erg to mildly-relativistic ( $\Gamma \approx 3$ ).

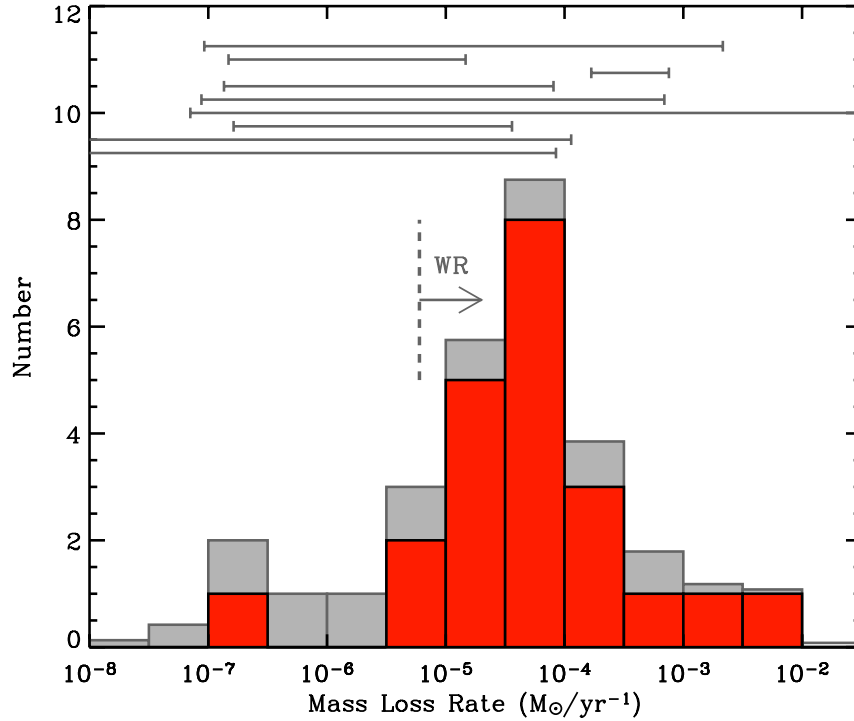


Figure 4.6: Radio observations enable the mass loss rate of the progenitor star to be constrained. The distribution of inferred mass loss rates are shown assuming a progenitor wind velocity of  $v_w = 1000 \text{ km s}^{-1}$ . Those SNe for which the peak radio luminosity is only constrained from below are extrapolated to the range of typical peak times (2–150 days) and the inferred range in mass loss rate is shown as horizontal bars. Moreover, we include them in the total distribution (grey) by assuming they have an equal probability of having a mass loss rate anywhere in the range specified. The lower end of the mass loss rates observed for local Wolf-Rayet (WR) stars is shown as a dashed line for comparison.

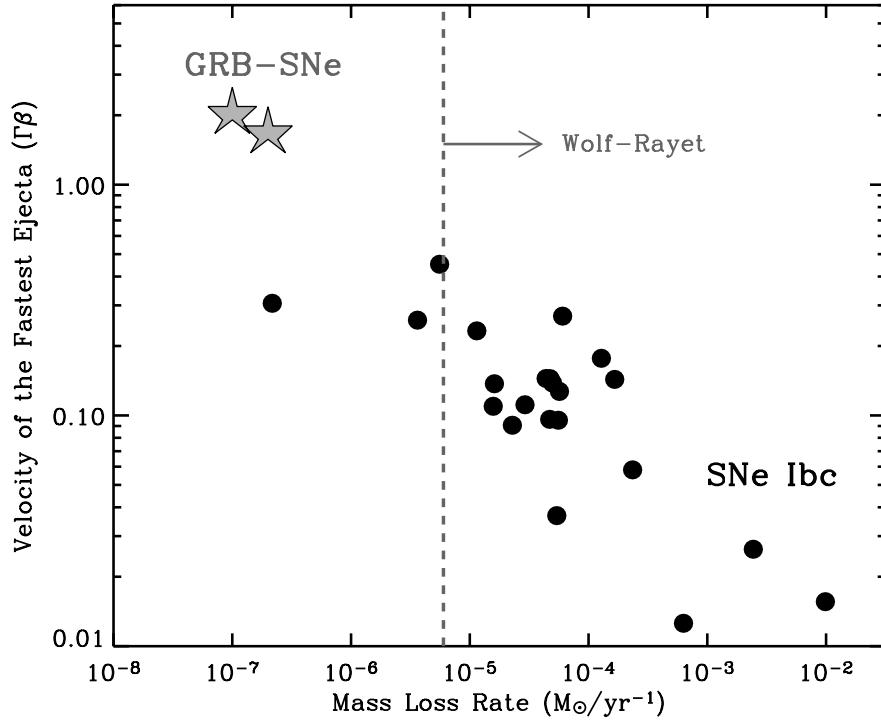


Figure 4.7: The inferred mass loss rates from radio observations (Figure 6) are plotted against the velocity of the fastest ejecta. A general trend is observed such that SNe Ibc with faster ejecta velocities also have lower CSM densities. The mass loss rates for local GRB-SN 1998bw and XRF-SN 2006aj are shown for comparison. In addition, we show the low end of the observed distribution of local WR stars. This plot suggests that single WR stars may not be the progenitors of GRB/XRF-SNe, which may require a binary companion to further strip the star.

## Chapter 5

### Future Directions

#### 5.1 The Progenitors of SNe Ibc

In this thesis, I have highlighted the recent progress made in our understanding of the connection between gamma-ray bursts (GRBs), X-ray flashes (XRFs), sub-energetic bursts, and Type Ibc supernovae (SNe Ibc). Through this effort, the basic properties of these cosmic explosions have been revealed: their distance scale, volumetric rates, ejecta geometry, energetics, Nickel production, and local environments. While it is now clear that these explosions are all associated with the death of massive stars, the fundamental question regarding the nature and relation of their respective progenitor systems (single vs. binary) remains an open question.

Important clues can be obtained from the explosion environment on both local- and large-scales. Numerical simulations suggest that metallicity plays a crucial role in stripping the progenitor star of its outer envelope (437). Along these lines, recent studies suggest that GRBs (including XRFs and sub-energetic bursts) reside almost exclusively in low-metallicity host galaxies (e.g., Stanek et al. 376). On the other hand, the current sample of SNe Ibc are selected primarily through “targeted” optical searches that focus on luminous galaxies and bias against low-metallicity hosts (Figure 5.1). This strong selection effect plagues current attempts to compare the samples and environments of SNe Ibc and GRB explosions.

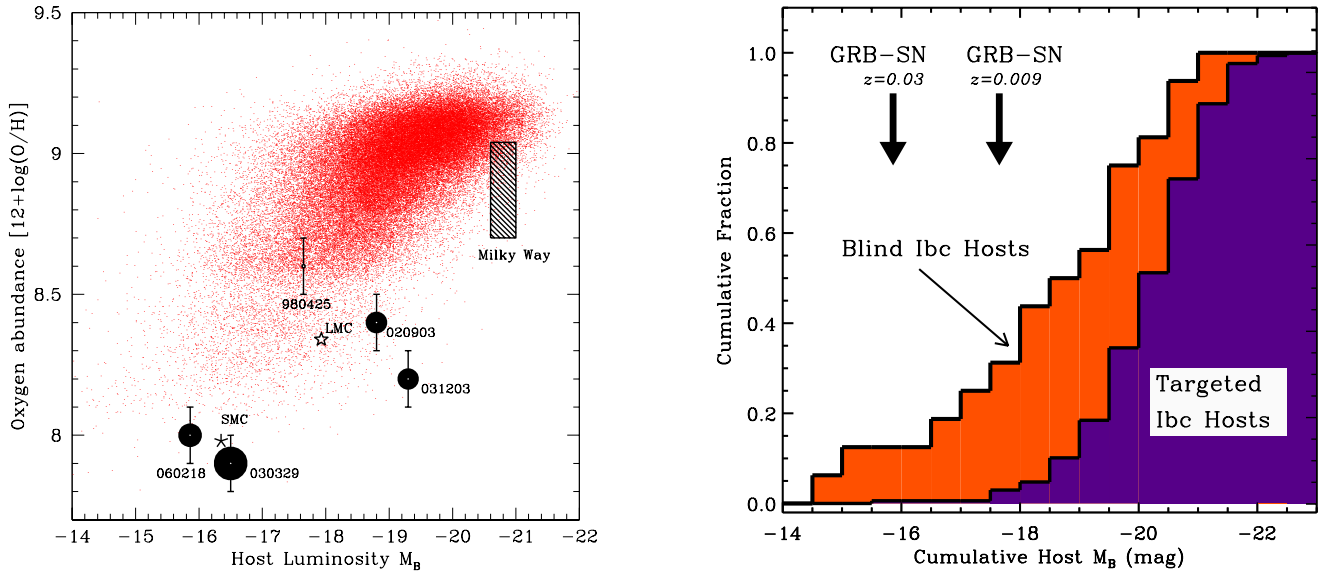


Figure 5.1: Left: Luminosity and metallicity of nearby ( $z < 0.25$ ) GRB host galaxies (labeled) compared to SDSS star-forming galaxies within same redshift range, from (376). GRBs appear to favor low metallicity, low luminosity hosts. Right: Cumulative luminosity distribution of local ( $d < 150$  Mpc) SNe Ibc host galaxies from blind (red) and targeted (blue) search campaigns are compared. Low-luminosity GRB-SN hosts (arrows) are strongly biased against in the targeted SNe Ibc sample and are only accessible through blind surveys.

Fortunately, with the advent of “blind” search campaigns such as the Sloan Digital Sky Survey (SDSS) SN survey (333), an unbiased sample of SN Ibc is now being revealed. These SN surveys, along with future projects (e.g., Pan-STARRS, LSST), are opening a new window to our understanding of SNe Ibc. In parallel to on-going investigations of GRBs, the time is now ripe to study the explosion physics and environments of SNe Ibc - the most numerous of all the stripped-envelope explosions.

Drawing from both targeted and blind SN samples, the following questions must be addressed:

- What is the relation between the progenitors of SNe Ibc and

## GRBs?

- **What is the role of the environment?**

This approach has the promise to enable a mapping between progenitor systems (single vs. binary) and explosion characteristics.

## 5.2 Large-scale Environment

A full investigation into the progenitors of SNe Ibc and their relation to GRBs must include a study of their large-scale host galaxy environments. This study relies exclusively on the unbiased sample of blind SNe Ibc. In this context, host galaxy metallicity is a crucial parameter as a rough proxy for the progenitor metallicity, and in turn, the progenitor system.

The envelope-stripping winds of isolated Wolf-Rayet stars require a significant metallicity since the mass loss is driven by bound-free and metal line opacities; a relation  $\dot{M} \propto Z^{1/2}$  has been found from observations of Wolf-Rayet stars in the Local Group (97, 235). On the other hand, a low metallicity favors the creation of a larger core and the retention of angular momentum, which can lead to an accretion disk powered GRB (234). In the latter case, a companion star is required to strip the massive envelope. Therefore, in comparison with well-studied galaxy samples (e.g., SDSS, Blanton et al. 40), SNe Ibc host metallicities may shed light on the nature of their progenitors (single vs. binary), the size of the remnant core, and perhaps the nature of the post-explosion compact object (NS vs. BH). Moreover, in comparison to GRB host metallicities, this study may reveal the relation between these two channels of stellar death. I underscore that this study relies exclusively on the discovery of SNe Ibc from blind surveys since targeted search campaigns bias against low metallicity hosts.

While an unbiased statistical study of SNe Ibc host galaxy metallicities has not yet been carried out in full, the preliminary results are promising. As shown in Figure 5.2, a spectral analysis of the host galaxy of SN 2005hm, discovered through

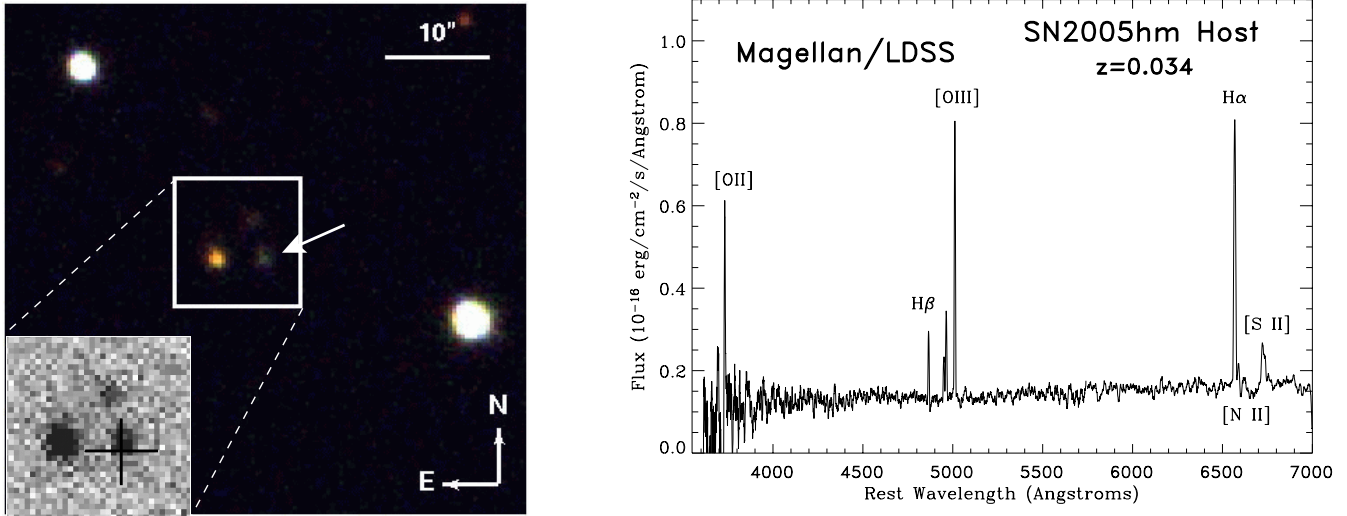


Figure 5.2: Left: Pre-explosion SDSS color imaging of the host galaxy of the blind Type Ibc SN 2005hm ( $z = 0.034$ ) reveals that it is a low-luminosity star-forming dwarf (arrow) with  $M_B \sim -15$  mag. The explosion site (cross) lies less than an arcsec from the host nucleus (inset). Right: A Magellan/LDSS spectrum of the host galaxy reveals that the metallicity at the SN position is low,  $Z \sim 0.5 Z_\odot$ . Thus, the SN host galaxy is similar to those of GRB hosts and only accessible through blind SN search campaigns.

the SDSS SN survey, reveals a low metallicity comparable to those of GRB hosts,  $Z \sim 0.5 Z_\odot$ .

Finally, this study should also include an analysis of host galaxy star-formation rate (SFR) estimates. GRB hosts have been claimed to have high specific SFRs ( $\sim 10 M_\odot \text{ yr}^{-1} L_*^{-1}$ , Christensen et al. 77) and a comparison to the hosts of SNe Ibc will provide additional diagnostics of their relation.

### 5.3 Unique Diagnostics of Ejecta Properties

As discussed throughout this thesis, radio, and X-ray observations of SNe Ibc trace the non-thermal synchrotron emission produced by the dynamical interaction of the fastest ejecta ( $v \gtrsim 0.1c$ ) with the CSM. Since 2002, I have increased the existing

sample of well-studied radio SNe Ibc tenfold (353). Through detailed modeling of the synchrotron emission, the velocity and kinetic energy of the fastest ejecta are robustly constrained. Most importantly, these observations measure the explosion geometry since they are sensitive to ejecta components initially “jetted” away from our line-of-sight (287, 275, 367). Together, these diagnostics represent a powerful tool to search for the presence of collimated and/or relativistic ejecta – the hallmark of a engine-driven explosion. As discussed in the previous chapter, my dedicated radio survey has revealed evidence for central engines in less than 3% of optically-selected SNe Ibc.

It is natural to question if the radio properties of SNe Ibc are tied to those of their large-scale environments: star-formation rate (SFR) and metallicity. Indeed, this is true for SNe Ia, where the most luminous events are found primarily in star-forming galaxies (384). Clearly, this type of investigation requires a statistical sample of SNe Ibc discovered through an unbiased search campaign. The SNe Ibc included in my VLA survey were drawn almost exclusively from targeted surveys which bias heavily towards luminous, metal-rich host galaxies (Figure 5.1).

Looking forward, a radio study of SNe Ibc from blind surveys will enable an unbiased view of the radio properties of SNe Ibc. With the increased sensitivity provided by EVLA<sup>1</sup> (factor of  $\sim 10$ ) starting in late-2008, the faint end of the radio luminosity function of SNe Ibc (Figure 5.3) will finally be accessible. In comparison with their inferred host galaxy properties, the relation between large-scale environment and ejecta properties will be mapped out. This is particularly important in the context of the GRB/XRF-SN connection since it is argued that the low metallicities observed for GRB/XRF host galaxies imply a low metallicity for their progenitors, which in turn may be required for the production of relativistic ejecta.

Next, thanks to the fast response capability of the *Swift* X-ray Telescope (XRT), the sample of early time ( $\lesssim 10$  days) X-ray observations of local SNe Ibc will increase tenfold in the coming years. These data will enable untriggered GRB-

---

<sup>1</sup><http://www.aoc.nrao.edu/evla/>

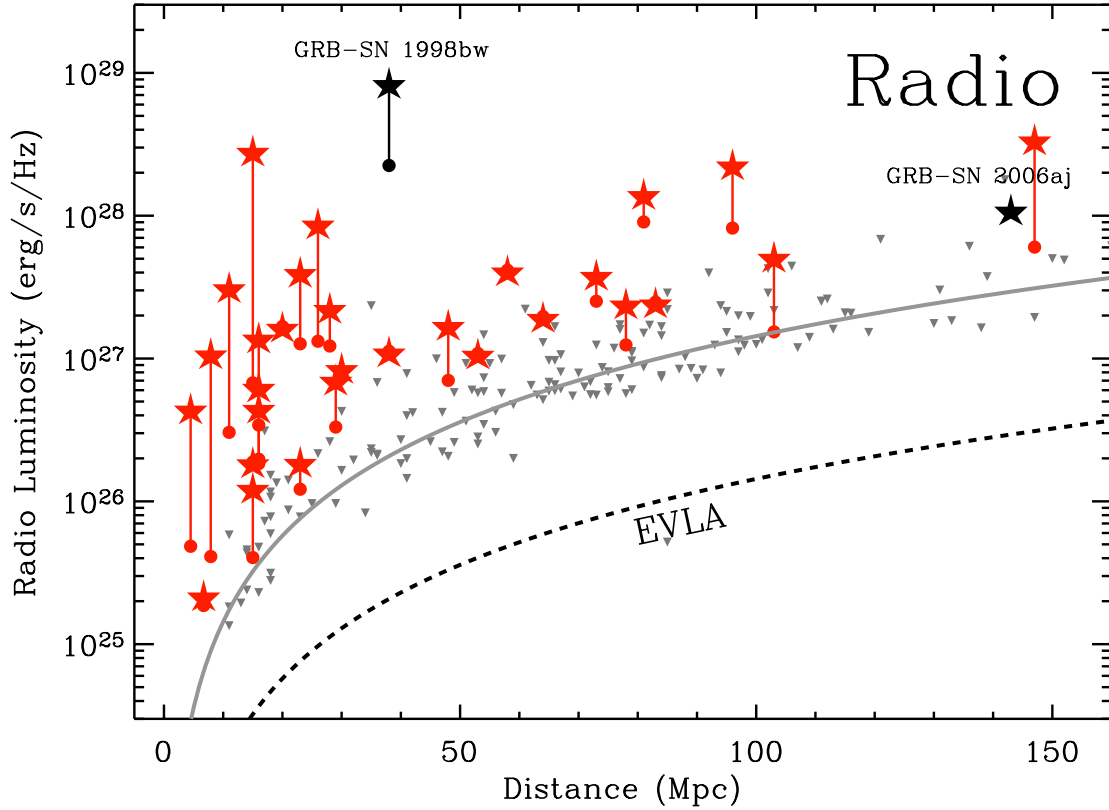


Figure 5.3: A compilation of data from my dedicated VLA survey of nearby ( $d \lesssim 150$  Mpc) GRB-SNe and optically-selected SNe Ibc (353). Circles and stars mark the discovery and peak radio luminosity, respectively. GRB-SNe are labeled (black), SNe Ibc are red, and upper limits (typically 0.1 mJy, solid line) are shown as grey triangles. With the sensitivity of EVLA (dashed line) I will investigate the properties of radio faint SNe Ibc which currently go undetected.

SNe to be recovered, identified by their early, bright X-ray emission (Figure 5.4). By leveraging the early-time XRT data with deep late-time observations from Chandra, the first detailed X-ray light-curves for SNe Ibc will be revealed. In parallel to radio studies, a comparison of the X-ray properties of targeted and blind SNe Ibc may uncover the role of metallicity in the production of relativistic ejecta.

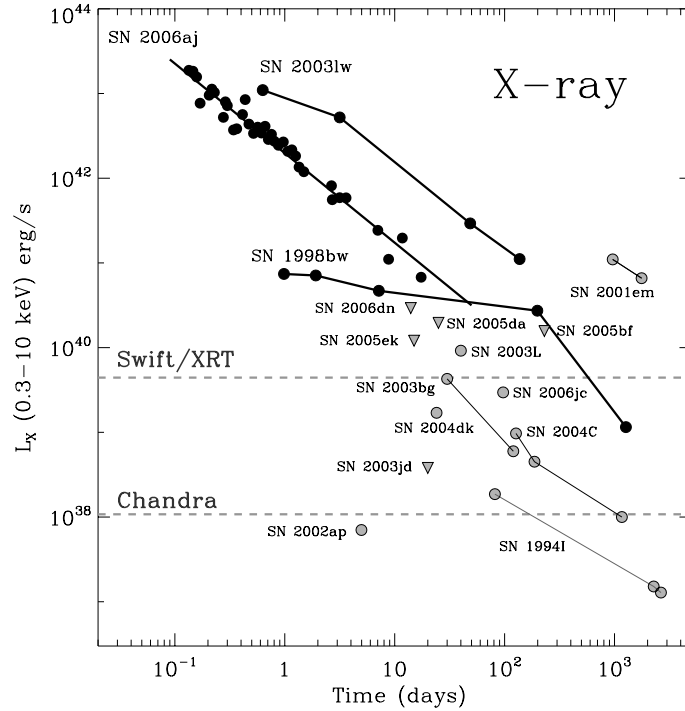


Figure 5.4: GRB-SNe (black) are distinguished from ordinary SNe Ibc (grey) by their luminous X-ray emission. Detections are shown as circles and limits as inverted triangles. Dashed lines show the typical detection threshold for Swift/XRT and Chandra/ACIS-S at a distance of  $z = 0.01$  (dashed lines). By leveraging early-time XRT data with late-time Chandra data, GRB-SNe and SNe Ibc will be both distinguished and well-sampled.

## 5.4 Conclusions

Through my PhD work, the connection between GRBs, XRFs, and SNe Ibc has been established in broad terms. We now know that most (perhaps all) long-duration GRBs and XRFs are accompanied by SNe Ibc, but less than 3% of SNe Ibc produce relativistic ejecta. Next, while GRB/XRF-SNe and ordinary SNe Ibc show similar optical luminosities, their photospheric velocities are typically faster by a factor of 2 to 3. Finally, the recent discovery of a class of sub-luminous bursts suggests a broad continuum between ordinary SNe, sub-energetic GRBs, and typical GRBs/XRFs in terms of volumetric rate and energetics. At the same

time, the essential physical process that enables a small fraction of SNe Ibc to produce GRBs and XRFs remains largely unknown.

Progress requires a deeper understanding of the progenitors of ordinary SNe Ibc. As discussed in this chapter, radio/X-ray follow-up and host-galaxy studies of SNe Ibc discovered through unbiased surveys (SDSS, PanSTARRS, LSST) will shed light on this specific issue and increase our overall understanding of the death of massive stars.

## Bibliography

- [1] C. Alard. Image subtraction using a space-varying kernel. *A&AS*, 144:363–370, June 2000.
- [2] L. Amati. The Ep,i - Eiso correlation in GRBs: updated observational status, re-analysis and main implications. *ArXiv Astrophysics e-prints*, January 2006.
- [3] L. Amati, M. Capalbi, F. Frontera, G. Gandolfi, L. Piro, J. J. M. in't Zand, S. Granata, and F. Reali. GRB(XRF) 020427: X-ray afterglow with BeppoSAX. *GRB Circular Network*, 1386:1–+, 2002.
- [4] L. Amati, F. Frontera, M. Tavani, J. J. M. in't Zand, A. Antonelli, E. Costa, M. Feroci, C. Guidorzi, J. Heise, N. Masetti, E. Montanari, L. Nicastro, E. Palazzi, E. Pian, L. Piro, and P. Soffitta. Intrinsic spectra and energetics of BeppoSAX Gamma-Ray Bursts with known redshifts. *A&A*, 390:81–89, July 2002.
- [5] G. C. Anupama, D. K. Sahu, J. Deng, K. Nomoto, N. Tominaga, M. Tanaka, P. A. Mazzali, and T. P. Prabhu. The Peculiar Type Ib Supernova SN 2005bf: Explosion of a Massive He Star with a Thin Hydrogen Envelope? *ApJ*, 631:L125–L128, October 2005.
- [6] W. D. Arnett. On the early behavior of supernova 1987A. *ApJ*, 331:377–387, August 1988.
- [7] L. Ball, D. Campbell-Wilson, D. F. Crawford, and A. J. Turtle. Radio Observations of SN 1987A at 843 MHz. *ApJ*, 453:864–+, November 1995.

- [8] D. Band, J. Matteson, L. Ford, B. Schaefer, D. Palmer, B. Teegarden, T. Cline, M. Briggs, W. Paciesas, G. Pendleton, G. Fishman, C. Kouveliotou, C. Meegan, R. Wilson, and P. Lestrade. BATSE observations of gamma-ray burst spectra. I - Spectral diversity. *ApJ*, 413:281–292, 1993.
- [9] E. Baron, D. Branch, P. H. Hauschildt, A. V. Filippenko, and R. P. Kirshner. Spectral Models of the Type IC Supernova SN 1994I in M51. *ApJ*, 527:739–745, December 1999.
- [10] E. Baron, T. R. Young, and D. Branch. On the stellar progenitor of the type Ib supernova 1984L. *ApJ*, 409:417–421, May 1993.
- [11] C. Barraud, G. Ricker, J-L. Atteia, N. Kawai, D. Lamb, and S. Woosley. XRF040701 (=U11548): a bright XRF detected by HETE. *GRB Circular Network*, 2620, 2004.
- [12] S. D. Barthelmy, G. Chincarini, D. N. Burrows, N. Gehrels, S. Covino, A. Moretti, P. Romano, P. T. O’Brien, C. L. Sarazin, C. Kouveliotou, M. Goad, S. Vaughan, G. Tagliaferri, B. Zhang, L. A. Antonelli, S. Campana, J. R. Cummings, P. D’Avanzo, M. B. Davies, P. Giommi, D. Grupe, Y. Kaneko, J. A. Kennea, A. King, S. Kobayashi, A. Melandri, P. Meszaros, J. A. Nousek, S. Patel, T. Sakamoto, and R. A. M. J. Wijers. An origin for short  $\gamma$ -ray bursts unassociated with current star formation. *Nature*, 438:994–996, December 2005.
- [13] M. C. Begelman and C. L. Sarazin. SN 1985f - Death of a Wolf-Rayet star. *ApJ*, 302:L59–L62, March 1986.
- [14] S. Benetti, D. Branch, M. Turatto, E. Cappellaro, E. Baron, L. Zampieri, M. Della Valle, and A. Pastorello. The exceptionally bright Type Ib supernova 1991D. *MNRAS*, 336:91–96, October 2002.
- [15] E. Berger. GRB 040812: Optical counterparts of CXO sources. *GRB Circular Network*, 2650, 2004.

- [16] E. Berger. The Afterglows and Host Galaxies of Short GRBs: An Overview. In S. S. Holt, N. Gehrels, and J. A. Nousek, editors, *AIP Conf. Proc. 838: Gamma-Ray Bursts in the Swift Era*, pages 33–42, May 2006.
- [17] E. Berger, L. L. Cowie, S. R. Kulkarni, D. A. Frail, H. Aussel, and A. J. Barger. A Submillimeter and Radio Survey of Gamma-Ray Burst Host Galaxies: A Glimpse into the Future of Star Formation Studies. *ApJ*, 588: 99–112, 2003.
- [18] E. Berger, A. Diercks, D. A. Frail, S. R. Kulkarni, J. S. Bloom, R. Sari, J. Halpern, N. Mirabal, G. B. Taylor, K. Hurley, G. Pooley, K. M. Becker, R. M. Wagner, D. M. Terndrup, T. Statler, D. R. Wik, E. Mazets, and T. Cline. GRB 000418: A Hidden Jet Revealed. *ApJ*, 556:556–561, 2001.
- [19] E. Berger, D. B. Fox, S. R. Kulkarni, W. Krzeminski, and M. Hamuy. GRB 040812: Keck and LCO observations. *GRB Circular Network*, 2644, 2004.
- [20] E. Berger, D. B. Fox, S. R. Kulkarni, W. Krzeminski, A. M. Soderberg, D. A. Frail, D. N. Burrows, S. B. Cenko, E. J. Murphy, P. A. Price, A. Gal-Yam, D. . Moon, N. Gehrels, W. L. Freedman, S. E. Persson, S. Barthelmy, J. E. Hill, J. A. Nousek, and A. Moretti. The Discovery of the Optical and Near-IR Afterglows of the First Swift Gamma-Ray Bursts. *ArXiv Astrophysics e-prints*, February 2005. astro-ph/0502468.
- [21] E. Berger, A. Gal-Yam, D. B. Fox, I. Thompson, B. Schmidt, R. McNaught, and B. Peterson. XRF040701 - optical observations of the decaying Chandra source. *GRB Circular Network*, 2631, 2004.
- [22] E. Berger, S. R. Kulkarni, and R. A. Chevalier. The Radio Evolution of the Ordinary Type Ic Supernova SN 2002ap. *ApJ*, 577:L5–L8, 2002.
- [23] E. Berger, S. R. Kulkarni, and D. A. Frail. A Standard Kinetic Energy Reservoir in Gamma-Ray Burst Afterglows. *ApJ*, 590:379–385, 2003.

- [24] E. Berger, S. R. Kulkarni, and D. A. Frail. The Nonrelativistic Evolution of GRBs 980703 and 970508: Beaming-independent Calorimetry. *ApJ*, 612: 966–973, September 2004.
- [25] E. Berger, S. R. Kulkarni, D. A. Frail, P. A. Price, D. B. Fox, A. M. Soderberg, S. B. Cenko, D.-S. Moon, S. A. Yost, and F. A. Harrison. GRB Host Galaxies. in prep, 2005.
- [26] E. Berger, S. R. Kulkarni, D. A. Frail, and A. M. Soderberg. A Radio Survey of Type Ib and Ic Supernovae: Searching for Engine-driven Supernovae. *ApJ*, 599:408–418, December 2003.
- [27] E. Berger, S. R. Kulkarni, G. Pooley, D. A. Frail, V. McIntyre, R. M. Wark, R. Sari, A. M. Soderberg, D. W. Fox, S. Yost, and P. A. Price. A common origin for cosmic explosions inferred from calorimetry of GRB030329. *Nature*, 426:154–157, November 2003.
- [28] E. Berger, P. A. Price, S. B. Cenko, A. Gal-Yam, A. M. Soderberg, M. Kasliwal, D. C. Leonard, P. B. Cameron, D. A. Frail, S. R. Kulkarni, D. C. Murphy, W. Krzeminski, T. Piran, B. L. Lee, K. C. Roth, D.-S. Moon, D. B. Fox, F. A. Harrison, S. E. Persson, B. P. Schmidt, B. E. Penprase, J. Rich, B. A. Peterson, and L. L. Cowie. The afterglow and elliptical host galaxy of the short  $\gamma$ -ray burst GRB 050724. *Nature*, 438:988–990, December 2005.
- [29] E. Berger, R. Sari, D. Ñ. Frail, S. Ñ. Kulkarni, F. Bertoldi, A. Ñ. Peck, K. Ñ. Menten, D. Ñ. Shepherd, G. Ñ. Moriarty-Schieven, G. Pooley, J. Ñ. Bloom, A. Diercks, T. Ñ. Galama, and K. Hurley. A jet model for the afterglow emission from grb 000301c. *ApJ*, 545:56–62, 2000.
- [30] D. Bersier, A. S. Fruchter, J. E. Rhoads, L.-G. Strolger, A. Levan, J. Gorosabel, I. Burud, J. Hjorth, and GOSH. Optical light curve of the enigmatic X-ray flash XRF 020903. *American Astronomical Society Meeting Abstracts*, 205:–+, December 2004.

- [31] D. Bersier, A. S. Fruchter, L.-G. Strolger, J. Gorosabel, A. Levan, I. Burud, J. E. Rhoads, A. C. Becker, A. Cassan, R. Chornock, S. Covino, R. S. de Jong, D. Dominis, A. V. Filippenko, J. Hjorth, J. Holmberg, D. Malesani, B. Mobasher, K. A. G. Olsen, M. Stefanon, J. M. Castro Cerón, J. P. U. Fynbo, S. T. Holland, C. Kouveliotou, H. Pedersen, N. R. Tanvir, and S. E. Woosley. Evidence for a Supernova Associated with the X-Ray Flash 020903. *ApJ*, 643:284–291, May 2006.
- [32] K. Beuermann, F. V. Hessman, K. Reinsch, H. Nicklas, P. M. Vreeswijk, T. J. Galama, E. Rol, J. van Paradijs, C. Kouveliotou, F. Frontera, N. Masetti, E. Palazzi, and E. Pian. Vlt observations of grb 990510 and its environment. *aa*, 352:L26–L30, 1999.
- [33] M. F. Bietenholz and N. Bartel. An Upper Limit on the Expansion Velocity of Gamma-Ray Burst Candidate SN 2001em. *ApJ*, 625:L99–L102, June 2005.
- [34] M. F. Bietenholz, N. Bartel, and M. P. Rupen. SN 1986J VLBI: The Evolution and Deceleration of the Complex Source and a Search for a Pulsar Nebula. *ApJ*, 581:1132–1147, December 2002.
- [35] M. F. Bietenholz, N. Bartel, and M. P. Rupen. SN 1993J VLBI. III. The Evolution of the Radio Shell. *ApJ*, 597:374–398, November 2003.
- [36] I. Bikmaev, N. Sakhibullin, M. A. Alpar, U. Kiziloglu, S. Balman, Z. Aslan, I. Khamitov, R. Burenin, M. Pavlinsky, and R. Sunyaev. GRB041006: RTT150 Optical Observations. *GRB Circular Network*, 2826, 2004.
- [37] C. Björnsson and C. Fransson. The X-Ray and Radio Emission from SN 2002ap: The Importance of Compton Scattering. *ApJ*, 605:823–829, April 2004.
- [38] G. Björnsson, E. H. Gudmundsson, and G. Jóhannesson. Energy Injection Episodes in Gamma-Ray Bursts: The Light Curves and Polarization Properties of GRB 021004. *ApJ*, 615:L77–L80, November 2004.

- [39] J. P. Blakeslee, J. R. Lucey, B. J. Barris, M. J. Hudson, and J. L. Tonry. A synthesis of data from fundamental plane and surface brightness fluctuation surveys. *MNRAS*, 327:1004–1020, November 2001.
- [40] M. R. Blanton, R. H. Lupton, D. J. Schlegel, M. A. Strauss, J. Brinkmann, M. Fukugita, and J. Loveday. The Properties and Luminosity Function of Extremely Low Luminosity Galaxies. *ApJ*, 631:208–230, September 2005.
- [41] J. S. Bloom, S. G. Djorgovski, S. R. Kulkarni, and D. A. Frail. The Host Galaxy of GRB 970508. *ApJ*, 507:L25–L28, November 1998.
- [42] J. S. Bloom et al. The unusual afterglow of grb 980326: evidence for the gamma-ray burst/supernova connection. *Nature*, 401:453–456, 1999.
- [43] J. S. Bloom, D. Fox, P. G. van Dokkum, S. R. Kulkarni, E. Berger, S. G. Djorgovski, and D. A. Frail. The First Two Host Galaxies of X-ray Flashes: XRF 011030 and XRF 020427. *ArXiv Astrophysics e-prints*, March 2003.
- [44] J. S. Bloom, D. A. Frail, and S. R. Kulkarni. Gamma-Ray Burst Energetics and the Gamma-Ray Burst Hubble Diagram: Promises and Limitations. *ApJ*, 594:674–683, 2003.
- [45] J. S. Bloom, S. R. Kulkarni, and S. G. Djorgovski. The Observed Offset Distribution of Gamma-Ray Bursts from Their Host Galaxies: A Robust Clue to the Nature of the Progenitors. *AJ*, 123:1111–1148, 2002.
- [46] J. S. Bloom, S. R. Kulkarni, F. Harrison, T. Prince, E. S. Phinney, and D. A. Frail. Expected Characteristics of the Subclass of Supernova Gamma-Ray Bursts. *ApJ*, 506:L105–L108, 1998.
- [47] J. S. Bloom, S. R. Kulkarni, P. A. Price, D. Reichart, T. J. Galama, B. P. Schmidt, D. A. Frail, E. Berger, P. J. McCarthy, R. A. Chevalier, J. C. Wheeler, J. P. Halpern, D. W. Fox, S. G. Djorgovski, F. A. Harrison, R. Sari, T. S. Axelrod, R. A. Kimble, J. Holtzman, K. Hurley, F. Frontera, L. Piro,

- and E. Costa. Detection of a Supernova Signature Associated with GRB 011121. *ApJ*, 572:L45–L49, 2002.
- [48] J. S. Bloom, D. A. Perley, H. . Chen, N. Butler, J. X. Prochaska, D. Kocevski, C. H. Blake, A. Szentgyorgyi, and E. E. Falco. A Putative Early-Type Host Galaxy for GRB 060502B: Implications for the Progenitors of Short-Duration Hard-Spectrum Bursts. *ArXiv Astrophysics e-prints*, July 2006.
- [49] J. S. Bloom, J. X. Prochaska, D. Pooley, C. H. Blake, R. J. Foley, S. Jha, E. Ramirez-Ruiz, J. Granot, A. V. Filippenko, S. Sigurdsson, A. J. Barth, H.-W. Chen, M. C. Cooper, E. E. Falco, R. R. Gal, B. F. Gerke, M. D. Gladders, J. E. Greene, J. Hennanwi, L. C. Ho, K. Hurley, B. P. Koester, W. Li, L. Lubin, J. Newman, D. A. Perley, G. K. Squires, and W. M. Wood-Vasey. Closing in on a Short-Hard Burst Progenitor: Constraints from Early-Time Optical Imaging and Spectroscopy of a Possible Host Galaxy of GRB 050509b. *ApJ*, 638:354–368, February 2006.
- [50] T. Boles. Supernovae 2003J, 2003K, 2003L, 2003M. *IAUC*, 8048:1–+, January 2003.
- [51] D. Branch. On the relative frequencies of the kinds of Type I supernovae. *ApJ*, 300:L51–L54, January 1986.
- [52] J. Burket, B. Swift, W. Li, and D. Briggs. Supernovae 2003jb, 2003jc, 2003jd, and 2003je. *IAUC*, 8232:1–+, October 2003.
- [53] B. J. Burn. On the depolarization of discrete radio sources by Faraday dispersion. *MNRAS*, 133:67–+, 1966.
- [54] C. J. Burrows, J. Krist, J. J. Hester, R. Sahai, J. T. Trauger, K. R. Stapelfeldt, J. S. Gallagher, G. E. Ballester, S. Casertano, J. T. Clarke, D. Crisp, R. W. Evans, R. E. Griffiths, J. G. Hoessel, J. A. Holtzman, J. R. Mould, P. A. Scowen, A. M. Watson, and J. A. Westphal. Hubble Space Telescope Observations of the SN 1987A Triple Ring Nebula. *ApJ*, 452:680–+, October 1995.

- [55] D. N. Burrows, D. Grupe, M. Capalbi, A. Panaitescu, S. K. Patel, C. Kouveliotou, B. Zhang, P. Meszaros, G. Chincarini, N. Gehrels, and R. A. M. Wijers. Jet Breaks in Short Gamma-Ray Bursts. II: The Collimated Afterglow of GRB 051221A. *ArXiv Astrophysics e-prints*, April 2006.
- [56] N. R. Butler, T. Sakamoto, M. Suzuki, N. Kawai, D. Q. Lamb, C. Graziani, T. Q. Donaghy, A. Dullighan, R. Vanderspek, G. B. Crew, P. Ford, G. Ricker, J. Atteia, A. Yoshida, Y. Shirasaki, T. Tamagawa, K. Torii, M. Matsuoka, E. E. Fenimore, M. Galassi, J. Doty, J. Villasenor, G. Prigozhin, J. G. Jernigan, C. Barraud, M. Boer, J. Dezalay, J. Olive, K. Hurley, A. Levine, F. Martel, E. Morgan, S. E. Woosley, T. Cline, J. Braga, R. Manchanda, and G. Pizzichini. High Energy Observations of XRF 030723: Evidence for an Off-axis Gamma-Ray Burst? *ArXiv Astrophysics e-prints*, August 2004. astro-ph/0408453.
- [57] N. R. Butler, T. Sakamoto, M. Suzuki, N. Kawai, D. Q. Lamb, C. Graziani, T. Q. Donaghy, A. Dullighan, R. Vanderspek, G. B. Crew, P. Ford, G. Ricker, J.-L. Atteia, A. Yoshida, Y. Shirasaki, T. Tamagawa, K. Torii, M. Matsuoka, E. E. Fenimore, M. Galassi, J. Doty, J. Villasenor, G. Prigozhin, J. G. Jernigan, C. Barraud, M. Boer, J.-P. Dezalay, J.-F. Olive, K. Hurley, A. Levine, F. Martel, E. Morgan, S. E. Woosley, T. Cline, J. Braga, R. Manchanda, and G. Pizzichini. High-Energy Observations of XRF 030723: Evidence for an Off-Axis Gamma-Ray Burst? *ApJ*, 621:884–893, March 2005.
- [58] D. Calzetti, A. L. Kinney, and T. Storchi-Bergmann. Dust extinction of the stellar continua in starburst galaxies: The ultraviolet and optical extinction law. *ApJ*, 429:582–601, July 1994.
- [59] S. Campana, V. Mangano, A. J. Blustin, P. Brown, D. N. Burrows, G. Chincarini, J. R. Cummings, G. Cusumano, M. Della Valle, D. Malesani, P. Meszaros, J. A. Nousek, M. Page, T. Sakamoto, E. Waxman, B. Zhang, Z. G. Dai, N. Gehrels, S. Immler, F. E. Marshall, K. O. Mason,

- A. Moretti, P. T. O'Brien, J. P. Osborne, K. L. Page, P. Romano, P. W. A. Roming, G. Tagliaferri, L. R. Cominsky, P. Giommi, O. Godet, J. A. Kennea, H. Krimm, L. Angelini, S. D. Barthelmy, P. T. Boyd, D. M. Palmer, A. A. Wells, and N. E. White. The shock break-out of GRB 060218/SN 2006aj. *Nature*, submitted, astro-ph/0603279.
- [60] S. Campana and A. Moretti. XRF040812: possible afterglow. *GRB Circular Network*, 2649, 2004.
- [61] S. Campana and A. Moretti. XRF040812: possible afterglow second Chandra observation. *GRB Circular Network*, 2656, 2004.
- [62] C. Cappa, W. M. Goss, and K. A. van der Hucht. A Very Large Array 3.6 Centimeter Continuum Survey of Galactic Wolf-Rayet Stars. *AJ*, 127: 2885–2897, May 2004.
- [63] C. Cappa, W.M. Goss, and K. A. van der Hucht. A Very Large Array 3.6 cm Continuum Survey of Galactic Wolf-Rayet Stars. astro-ph/0401571, 2003.
- [64] E. Cappellaro, R. Evans, and M. Turatto. A new determination of supernova rates and a comparison with indicators for galactic star formation. *ã*, 351: 459–466, November 1999.
- [65] R. Cen. Supernovae, Pulsars, and Gamma-Ray Bursts: A Unified Picture. *ApJ*, 507:L131–L134, 1998.
- [66] P. Chandra and A. Ray. Implications of Aging in Young Supernovae. In M. Turatto, S. Benetti, L. Zampieri, and W. Shea, editors, *1604-2004: Supernovae as Cosmological Lighthouses*, volume 342 of *Astronomical Society of the Pacific Conference Series*, pages 430–+, December 2005.
- [67] R. A. Chevalier. Self-similar solutions for the interaction of stellar ejecta with an external medium. *ApJ*, 258:790–797, July 1982.
- [68] R. A. Chevalier. The radio and X-ray emission from type II supernovae. *ApJ*, 259:302–310, August 1982.

- [69] R. A. Chevalier. Blast waves with cosmic-ray pressure. *ApJ*, 272:765–772, September 1983.
- [70] R. A. Chevalier. The Circumstellar Interaction Model for Radio Supernovae. In *ASP Conf. Ser. 93: Radio Emission from the Stars and the Sun*, pages 125–+, 1996.
- [71] R. A. Chevalier. Synchrotron Self-Absorption in Radio Supernovae. *ApJ*, 499:810–+, May 1998.
- [72] R. A. Chevalier and C. Fransson. Supernova Interaction with a Circumstellar Medium. in *Supernovae and Gamma-ray Bursters*, ed. K. W. Weiler (Berlin: Springer), 171, 2003.
- [73] R. A. Chevalier and C. Fransson. Circumstellar Emission from Type Ib and Ic Supernovae. *ApJ*, 651:381–391, November 2006.
- [74] R. A. Chevalier, Z.-Y. Li, and C. Fransson. The Diversity of Gamma-Ray Burst Afterglows and the Surroundings of Massive Stars. *ApJ*, 606:369–380, May 2004.
- [75] Roger A. Chevalier, Zhi-Yun Li, and Claes Fransson. The diversity of gamma-ray bursts and the surroundings of massive stars. *ApJ*, submitted; astro-ph/0311326, 2003.
- [76] R. Chornock and A. V. Filippenko. GRB 021004 redshift. *GRB Circular Network*, 1605:1–1, 2002.
- [77] L. Christensen, J. Hjorth, and J. Gorosabel. UV star-formation rates of GRB host galaxies. *A&A*, 425:913–926, October 2004.
- [78] Y.-H. Chu. From Wolf-Rayet Stars to Supernovae. In *ASP Conf. Ser. 260: Interacting Winds from Massive Stars*, pages 109–+, 2002.
- [79] N. N. Chugai. The origin of supernovae with dense winds. *Astronomy Reports*, 41:672–681, September 1997.

- [80] N. N. Chugai and R. A. Chevalier. Late Emission from the Type Ib/c SN 2001em: Overtaking the Hydrogen Envelope. *ArXiv Astrophysics e-prints*, October 2005. astro-ph/0510362.
- [81] N. N. Chugai and I. J. Danziger. Supernova 1988Z - Low-Mass Ejecta Colliding with the Clumpy Wind. *MNRAS*, 268:173–+, May 1994.
- [82] R. Ciardullo, J. J. Feldmeier, G. H. Jacoby, R. Kuzio de Naray, M. B. Laychak, and P. R. Durrell. Planetary Nebulae as Standard Candles. XII. Connecting the Population I and Population II Distance Scales. *ApJ*, 577: 31–50, September 2002.
- [83] A. Clocchiatti, B. Leibundgut, J. Spyromilio, S. Benetti, E. Cappellaro, M. Turatto, and M. M. Phillips. SN 1997b and the different types of Type Ic supernovae. In P. Höflich, P. Kumar, and J. C. Wheeler, editors, *Cosmic explosions in three dimensions*, pages 50–+, 2004.
- [84] A. Clocchiatti, M. M. Phillips, N. B. Suntzeff, M. DellaValle, E. Cappellaro, M. Turatto, M. Hamuy, R. Avilés, M. Navarrete, C. Smith, E. P. Rubenstein, R. Covarrubias, P. B. Stetson, J. Maza, A. G. Riess, and C. Zanin. The Luminous Type IC Supernova 1992AR at  $z=0.145$ . *ApJ*, 529:661–674, February 2000.
- [85] A. Clocchiatti, N. B. Suntzeff, M. M. Phillips, A. V. Filippenko, M. Turatto, S. Benetti, E. Cappellaro, R. Avilés, R. Covarrubias, K. DeGioia-Eastwood, M. Dickinson, C. Gouiffes, P. Guhathakurta, M. Hamuy, S. R. Heathcote, B. Leibundgut, T. Matheson, M. Navarrete, M. Perez, A. Phillips, A. Piemonte, M. T. Ruiz, J. C. Shields, C. Smith, H. Spinrad, C. R. Sturch, J. A. Tyson, and L. Wells. The Type IC SN 1990B in NGC 4568. *ApJ*, 553: 886–896, June 2001.
- [86] A. Clocchiatti, J. C. Wheeler, S. Benetti, and M. Frueh. SN 1983N and the Nature of Stripped Envelope–Core Collapse Supernovae. *ApJ*, 459:547–+, March 1996.

- [87] A. Clocchiatti, J. C. Wheeler, M. M. Phillips, N. B. Suntzeff, S. Cristiani, A. Phillips, R. P. Harkness, M. A. Dopita, K. Beuermann, M. Rosa, P. Grosbol, P. O. Lindblad, and A. V. Filippenko. SN 1983V in NGC 1365 and the Nature of Stripped Envelope Core-Collapse Supernovae. *ApJ*, 483:675–+, July 1997.
- [88] B. E. Cobb and C. D. Bailyn. GRB040812, optical/IR observations. *GRB Circular Network*, 2642, 2004.
- [89] J. J. Condon, W. D. Cotton, E. W. Greisen, Q. F. Yin, R. A. Perley, G. B. Taylor, and J. J. Broderick. The NRAO VLA Sky Survey. *AJ*, 115:1693–1716, May 1998.
- [90] E. Costa, F. Frontera, J. Heise, M. Feroci, J. In 't Zand, F. Fiore, M. N. Cinti, D. Dal Fiume, L. Nicastro, M. Orlandini, E. Palazzi, M. Rapisarda, G. Zavattini, R. Jager, A. Parmar, A. Owens, S. Molendi, G. Cusumano, M. C. Maccarone, S. Giarrusso, A. Coletta, L. A. Antonelli, P. Giommi, J. M. Muller, L. Piro, and R. C. Butler. Discovery of an x-ray afterglow associated with the gamma-ray burst of 28 february 1997. *Nature*, 387:783–785, 1997.
- [91] S. Covino, D. Malesani, G. Ghisellini, F. Stefanon, M. andTavecchio, G. Covone, D. Fugazza, A. Di Paola, G. L. Israel, F. Mannucci, N. Masetti, and E. Pian. XRF020903: TNG and Asiago photometry. *GRB Circular Network*, 1563, 2002.
- [92] S. Covino, D. Malesani, G. Tagliaferri, P. D'Avanzo, L. A. Antonelli, G. Chincarini, M. Della Valle, F. Fiore, D. Fugazza, and L. Stella. GRB041006: VLT observations of the afterglow and host galaxy. *GRB Circular Network*, 2803, 2004.
- [93] J. J. Cowan, D. A. Roberts, and D. Branch. Radio observations of M83 and its supernova remnants. *ApJ*, 434:128–135, October 1994.

- [94] G. Da Costa, N. Noel, and P. A. Price. GRB 041006: Optical afterglow candidate. *GRB Circular Network*, 2765, 2004.
- [95] T. Dahlen, L.-G. Strolger, A. G. Riess, B. Mobasher, R.-R. Chary, C. J. Conselice, H. C. Ferguson, A. S. Fruchter, M. Giavalisco, M. Livio, P. Madau, N. Panagia, and J. L. Tonry. High-Redshift Supernova Rates. *ApJ*, 613:189–199, September 2004.
- [96] P. D’Avanzo, A. Cucchiara, G. Tagliaferri, D. Malesani, D. Fugazza, S. Covino, and S. Campana. XRF 040812: optical observation at VLT. *GRB Circular Network*, 2651, 2004.
- [97] C. de Jager, H. Nieuwenhuijzen, and K. A. van der Hucht. Mass loss rates in the Hertzsprung-Russell diagram. *A&AS*, 72:259–289, February 1988.
- [98] A. De Luca. GRB 060218: analysis of the XMM-Newton observation. *GRB Circular Network*, 4853: , 2006.
- [99] A. de Ugarte Postigo, P. Tristram, Sasaka, J. Gorosabel, P. Yock, and A. J. Castro-Tirado. XRF 040701, optical observations. *GRB Circular Network*, 2621, 2004.
- [100] J. Deng, N. Tominaga, P. A. Mazzali, K. Maeda, and K. Nomoto. On the Light Curve and Spectrum of SN 2003dh Separated from the Optical Afterglow of GRB 030329. *ApJ*, 624:898–905, May 2005.
- [101] J. S. Deng, Y. L. Qiu, J. Y. Hu, K. Hatano, and D. Branch. Spectrum Analysis of the Type IB Supernova SN 1999DN: Probable Identifications of C II and H $\alpha$ . *ApJ*, 540:452–455, September 2000.
- [102] C. D. Dermer, J. Chiang, and M. Böttcher. Fireball Loading and the Blast-Wave Model of Gamma-Ray Bursts. *ApJ*, 513:656–668, March 1999.
- [103] J. M. Dickey and F. J. Lockman. "h i in the galaxy". *ARAA*, 28:215–261, 1990.

- [104] I. O. Drozdovsky, R. E. Schulte-Ladbeck, U. Hopp, L. Greggio, and M. M. Crone. The Dwarf Irregular/Wolf-Rayet Galaxy NGC 4214. I. A New Distance, Stellar Content, and Global Parameters. *AJ*, 124:811–827, August 2002.
- [105] C. R. Eck, J. J. Cowan, and D. Branch. A Search for Radio Emission from Supernovae with Ages from about 1 Week to More than 80 Years. *ApJ*, 573:306–323, July 2002.
- [106] D. Eichler and A. Levinson. Shading and Smothering of Gamma-Ray Bursts. *ApJ*, 521:L117–L120, 1999.
- [107] D. Eichler, M. Livio, T. Piran, and D. N. Schramm. Nucleosynthesis, neutrino bursts and gamma-rays from coalescing neutron stars. *Nature*, 340:126–128, July 1989.
- [108] J. H. Elias, K. Matthews, G. Neugebauer, and S. E. Persson. Type I supernovae in the infrared and their use as distance indicators. *ApJ*, 296:379–389, September 1985.
- [109] L. M. Ensmann and S. E. Woosley. Explosions in Wolf-Rayet stars and Type Ib supernovae. I - Light curves. *ApJ*, 333:754–776, October 1988.
- [110] J. J. Feldmeier, R. Ciardullo, and G. H. Jacoby. Planetary Nebulae as Standard Candles. XI. Application to Spiral Galaxies. *ApJ*, 479:231–+, April 1997.
- [111] E. Fenimore, G. Ricker, J. L. Atteia, N. Kawai, D. Lamb, S. Woosley, T. Donaghy, M. Galassi, C. Graziani, and M. Matsuoka. GRB 040924(=H3564): A Short, Bright GRB Localized in Real Time by HETE. *GRB Circular Network*, 2735, 2004.
- [112] P. Ferrero, C. Bartolini, G. Greco, A. Guarnieri, A. Piccioni, E. Mazzotti Epifani, R. Gualandi, and G. Pizzichini. GRB 041006 (=H3570): optical observations. *GRB Circular Network*, 2777, 2004.

- [113] A. V. Filippenko. Optical Spectra of Supernovae. *ARAA*, 35:309–355, 1997.
- [114] A. V. Filippenko and R. Chornock. Supernovae 2001ig, 2002eg, 2002ew, 2002gc. *IAUC*, 7988:3–+, October 2002.
- [115] A. V. Filippenko and R. Chornock. Supernovae 2003aa and 2003bg. *IAUC*, 8084:4–+, February 2003.
- [116] A. V. Filippenko, R. T. Foley, and B. Swift. Supernovae 2003jd, 2003je, and 2003jf. *IAUC*, 8234:2–+, October 2003.
- [117] A. V. Filippenko, T. Matheson, and A. J. Barth. The peculiar type II supernova 1993J in M81: Transition to the nebular phase. *AJ*, 108:2220–2225, December 1994.
- [118] A. V. Filippenko, A. C. Porter, and W. L. W. Sargent. The type IC (helium-poor Ib) supernova 1987M - Transition to the supernebular phase. *AJ*, 100:1575–1587, November 1990.
- [119] A. V. Filippenko and W. L. W. Sargent. The unique supernova (1985f) in NGC 4618. *AJ*, 91:691–696, April 1986.
- [120] A. V. Filippenko and W. L. W. Sargent. Spectroscopic evidence for inhomogeneities in the ejecta of the Type Ib supernova 1985F. *ApJ*, 345:L43–L46, October 1989.
- [121] G. Folatelli, C. Contreras, M. M. Phillips, S. E. Woosley, S. Blinnikov, N. Morrell, N. B. Suntzeff, B. L. Lee, M. Hamuy, S. González, W. Krzeminski, M. Roth, W. Li, A. V. Filippenko, R. J. Foley, W. L. Freedman, B. F. Madore, S. E. Persson, D. Murphy, S. Boissier, G. Galaz, L. González, P. J. McCarthy, A. McWilliam, and W. Pych. SN 2005bf: A Possible Transition Event between Type Ib/c Supernovae and Gamma-Ray Bursts. *ApJ*, 641:1039–1050, April 2006.

- [122] R. J. Foley, M. S. Pappenkova, B. J. Swift, A. V. Filippenko, W. Li, P. A. Mazzali, R. Chornock, D. C. Leonard, and S. D. Van Dyk. Optical Photometry and Spectroscopy of the SN 1998bw-like Type Ic Supernova 2002ap. *PASP*, 115:1220–1235, October 2003.
- [123] R. J. Foley, N. Smith, M. Ganeshalingam, W. Li, R. Chornock, and A. V. Filippenko. SN 2006jc: A Wolf-Rayet Star Exploding in a Dense He-rich Circumstellar Medium. *ApJ*, 657:L105–L108, March 2007.
- [124] S. Folkes, S. Ronen, I. Price, O. Lahav, M. Colless, S. Maddox, K. Deeley, K. Glazebrook, J. Bland-Hawthorn, R. Cannon, S. Cole, C. Collins, W. Couch, S. P. Driver, G. Dalton, G. Efstathiou, R. S. Ellis, C. S. Frenk, N. Kaiser, I. Lewis, S. Lumsden, J. Peacock, B. A. Peterson, W. Sutherland, and K. Taylor. The 2dF Galaxy Redshift Survey: spectral types and luminosity functions. *MNRAS*, 308:459–472, September 1999.
- [125] L. A. Ford et al. Batse observations of gamma-ray burst spectra. 2: Peak energy evolution in bright, long bursts. *ApJ*, 439:307–321, 1995.
- [126] D. Fox. GRB040924: Optical afterglow properties. *GRB Circular Network*, 2741, 2004.
- [127] D. Fox et al. Discovery of early optical emission from GRB 021211. *ApJ* submitted; astro-ph/0301377, 2003.
- [128] D. B. Fox. XRF040701: Second-Epoch Chandra Observations. *GRB Circular Network*, 2630, 2004.
- [129] D. B. Fox, D. A. Frail, P. A. Price, S. R. Kulkarni, E. Berger, T. Piran, A. M. Soderberg, S. B. Cenko, P. B. Cameron, A. Gal-Yam, M. M. Kasliwal, D.-S. Moon, F. A. Harrison, E. Nakar, B. P. Schmidt, B. Penprase, R. A. Chevalier, P. Kumar, K. Roth, D. Watson, B. L. Lee, S. Sheckman, M. M. Phillips, M. Roth, P. J. McCarthy, M. Rauch, L. Cowie, B. A. Peterson, J. Rich, N. Kawai, K. Aoki, G. Kosugi, T. Totani, H.-S. Park, A. MacFadyen, and

- K. C. Hurley. The afterglow of GRB 050709 and the nature of the short-hard  $\gamma$ -ray bursts. *Nature*, 437:845–850, October 2005.
- [130] D. W. Fox, P. A. Price, A. M. Soderberg, E. Berger, S. R. Kulkarni, R. Sari, D. A. Frail, F. A. Harrison, S. A. Yost, K. Matthews, B. A. Peterson, I. Tanaka, J. Christiansen, and G. H. Moriarty-Schieven. Discovery of Early Optical Emission from GRB 021211. *ApJ*, 586:L5–L8, March 2003.
- [131] D. W. Fox, S. Yost, S. R. Kulkarni, K. Torii, T. Kato, H. Yamaoka, M. Sako, F. A. Harrison, R. Sari, P. A. Price, E. Berger, A. M. Soderberg, S. G. Djorgovski, A. J. Barth, S. H. Pravdo, D. A. Frail, A. Gal-Yam, Y. Lipkin, T. Mauch, C. Harrison, and H. Buttery. Early optical emission from the  $\gamma$ -ray burst of 4 October 2002. *Nature*, 422:284–286, 2003.
- [132] D. A. Frail, S. R. Kulkarni, E. Berger, and M. H. Wieringa. A complete catalog of radio afterglows: The first five years. *AJ*, 125:2299–2306, May 2003.
- [133] D. A. Frail, S. R. Kulkarni, R. Sari, S. G. Djorgovski, J. S. Bloom, T. J. Galama, D. E. Reichart, E. Berger, F. A. Harrison, P. A. Price, S. A. Yost, A. Diercks, R. W. Goodrich, and F. Chaffee. Beaming in Gamma-Ray Bursts: Evidence for a Standard Energy Reservoir. *ApJ*, 562:L55–L58, 2001.
- [134] D. A. Frail, A. M. Soderberg, S. R. Kulkarni, E. Berger, S. Yost, D. W. Fox, and F. A. Harrison. Accurate Calorimetry of GRB 030329. *ApJ*, 619:994–998, February 2005.
- [135] D. A. Frail, E. Waxman, and S. R. Kulkarni. A 450 Day Light Curve of the Radio Afterglow of GRB 970508: Fireball Calorimetry. *ApJ*, 537:191–204, 2000.
- [136] C. Fransson and C. Björnsson. Radio Emission and Particle Acceleration in SN 1993J. *ApJ*, 509:861–878, December 1998.

- [137] C. Fransson, P. Lundqvist, and R. A. Chevalier. Circumstellar Interaction in SN 1993J. *ApJ*, 461:993–+, April 1996.
- [138] D. L. Freedman and E. Waxman. On the energy of gamma-ray bursts. *ApJ*, 547:922–928, 2001.
- [139] W. L. Freedman. The Hubble constant and the expansion age of the Universe. *Phys. Rep.*, 333:13–31, 2000.
- [140] A. Fruchter, L. Strolger, B. Mobasher, J. Rhoads, A. Levan, I. Burud, and A. Becker. XRF 020903: r band observations. *GRB Circular Network*, 1557: 1–+, 2002.
- [141] A. S. Fruchter and R. N. Hook. Drizzle: A Method for the Linear Reconstruction of Undersampled Images. *PASP*, 114:144–152, February 2002.
- [142] A. S. Fruchter, A. J. Levan, L. Strolger, P. M. Vreeswijk, S. E. Thorsett, D. Bersier, I. Burud, J. M. Castro Cerón, A. J. Castro-Tirado, C. Conselice, T. Dahlen, H. C. Ferguson, J. P. U. Fynbo, P. M. Garnavich, R. A. Gibbons, J. Gorosabel, T. R. Gull, J. Hjorth, S. T. Holland, C. Kouveliotou, Z. Levay, M. Livio, M. R. Metzger, P. E. Nugent, L. Petro, E. Pian, J. E. Rhoads, A. G. Riess, K. C. Sahu, A. Smette, N. R. Tanvir, R. A. M. J. Wijers, and S. E. Woosley. Long  $\gamma$ -ray bursts and core-collapse supernovae have different environments. *Nature*, 441:463–468, May 2006.
- [143] F. Fugazza, F. Fiore, S. Covino, L. A. Antonelli, P. D’Avanzo, F. Cocchia, D. Malesani, E. Pian, L. Stella, V. Lorenzi, and G. Tassicini. GRB041006: Optical photometry and spectroscopy at TNG. *GRB Circular Network*, 2782, 2004.
- [144] J. P. U. Fynbo, J. Sollerman, J. Hjorth, F. Grundahl, J. Gorosabel, M. Weidinger, P. Møller, B. L. Jensen, P. M. Vreeswijk, C. Fransson, E. Ramirez-Ruiz, P. Jakobsson, S. F. Jørgensen, C. Vinter, M. I. Andersen, J. M. Castro Cerón, A. J. Castro-Tirado, A. S. Fruchter, J. Greiner, C. Kouveliotou,

- A. Levan, S. Klose, N. Masetti, H. Pedersen, E. Palazzi, E. Pian, J. Rhoads, E. Rol, T. Sekiguchi, N. R. Tanvir, P. Tristram, A. de Ugarte Postigo, R. A. M. J. Wijers, and E. van den Heuvel. On the Afterglow of the X-Ray Flash of 2003 July 23: Photometric Evidence for an Off-Axis Gamma-Ray Burst with an Associated Supernova? *ApJ*, 609:962–971, July 2004.
- [145] B. M. Gaensler, N. M. McClure-Griffiths, M. S. Oey, M. Haverkorn, J. M. Dickey, and A. J. Green. A Stellar Wind Bubble Coincident with the Anomalous X-Ray Pulsar 1E 1048.1-5937: Are Magnetars Formed from Massive Progenitors? *ApJ*, 620:L95–L98, February 2005.
- [146] A. Gal-Yam. XRF 020903: archival optical images. *GRB Circular Network*, 1556:1–+, 2002.
- [147] A. Gal-Yam, D. B. Fox, S. R. Kulkarni, K. Matthews, D. C. Leonard, D. J. Sand, D.-S. Moon, S. B. Cenko, and A. M. Soderberg. A High Angular Resolution Search for the Progenitor of the Type Ic Supernova 2004gt. *ApJ*, 630:L29–L32, September 2005.
- [148] A. Gal-Yam, D.-S. Moon, D. B. Fox, A. M. Soderberg, S. R. Kulkarni, E. Berger, B. Cenko, S. Yost, D. A. Frail, M. Sako, W. L. Freedman, S. E. Persson, P. Wyatt, M. M. Phillips, N. B. Suntzeff, and P. A. Mazzali. The near infra-red light curve of sn 2003lw, associated with grb 031203. submitted to *ApJ*, 2004.
- [149] A. Gal-Yam, E. O. Ofek, and O. Shemmer. Supernova 2002ap: the first month. *MNRAS*, 332:L73–L77, June 2002.
- [150] T. J. Galama, P. M. Vreeswijk, E. Pian, F. Frontera, V. Doublier, and J.-F. Gonzalez. GRB 980425, 1998.
- [151] T. J. Galama, P. M. Vreeswijk, J. Van Paradijs, C. Kouveliotou, T. Augusteijn, H. Bohnhardt, J. P. Brewer, V. Doublier, J.-F. Gonzalez, B. Leibundgut, C. Lidman, O. R. Hainaut, F. Patat, J. Heise, J. In 't Zand,

- K. Hurley, P. J. Groot, R. G. Strom, P. A. Mazzali, K. Iwamoto, K. Nomoto, H. Umeda, T. Nakamura, T. R. Young, T. Suzuki, T. Shigeyama, T. Koshut, M. Kippen, C. Robinson, P. De Wildt, R. A. M. J. Wijers, N. Tanvir, J. Greiner, E. Pian, E. Palazzi, F. Frontera, N. Masetti, L. Nicastro, M. Feroci, E. Costa, L. Piro, B. A. Peterson, C. Tinney, B. Boyle, R. Cannon, R. Stathakis, E. Sadler, M. C. Begam, and P. Ianna. An unusual supernova in the error box of the gamma-ray burst of 25 april 1998. *Nature*, 395: 670–672, 1998.
- [152] T. J. Galama and R. A. M. J. Wijers. High column densities and low extinctions of gamma-ray bursts: Evidence for hypernovae and dust destruction. *ApJ*, 549:L209–L213, 2001.
- [153] M. Galassi, G. Ricker, J-L. Atteia, N. Kawai, D. Lamb, and S. Woosley. GRB 041006 (=H3570): An X-Ray Rich GRB Localized in Real Time by HETE. *GRB Circular Network*, 2770, 2004.
- [154] G. Garcia-Segura, N. Langer, and M.-M. Mac Low. The hydrodynamic evolution of circumstellar gas around massive stars. II. The impact of the time sequence O star - RSG - WR star. *A&A*, 316:133–146, December 1996.
- [155] G. Garcia-Segura, M.-M. Mac Low, and N. Langer. The dynamical evolution of circumstellar gas around massive stars. I. The impact of the time sequence Ostar - LBV - WR star. *A&A*, 305:229–+, January 1996.
- [156] A. Garg, C. Stubbs, P. Challis, K. Z. Stanek, and P. Garnavich. GRB041006: VLT observations of the afterglow and host galaxy. *GRB Circular Network*, 2829, 2004.
- [157] C. M. Gaskell, E. Cappellaro, H. L. Dinerstein, D. R. Garnett, R. P. Harkness, and J. C. Wheeler. Type Ib supernovae 1983n and 1985f - Oxygen-rich late time spectra. *ApJ*, 306:L77–L80, July 1986.
- [158] C. L. Gerardy, R. A. Fesen, K. Nomoto, K. Maeda, P. Hoflich, and J. C.

- Wheeler. Carbon Monoxide in the Type Ic Supernova 2000ew. *PASJ*, 54: 905–910, December 2002.
- [159] L. M. Germany, D. J. Reiss, E. M. Sadler, B. P. Schmidt, and C. W. Stubbs. SN 1997CY/GRB 970514: A New Piece in the Gamma-Ray Burst Puzzle? *ApJ*, 533:320–328, April 2000.
- [160] G. Ghirlanda, G. Ghisellini, and D. Lazzati. The Collimation-corrected Gamma-Ray Burst Energies Correlate with the Peak Energy of Their  $\nu F_\nu$  Spectrum. *ApJ*, 616:331–338, November 2004.
- [161] G. Gómez and R. López. Nebular Spectra of the Type Ic Supernovae 1997B and 1997X. *AJ*, 123:328–336, January 2002.
- [162] G. Gómez, R. López, J. Acosta-Pulido, and A. Manchado. LIRIS Observations of SN 2004ao. *The Newsletter of the Isaac Newton Group of Telescopes (ING Newsl.)*, issue no. 9, p. 14–15., 9:14–15, March 2005.
- [163] J. Gorosabel, J. Hjorth, H. Pedersen, B. L. Jensen, J. P. U. Fynbo, M. Andersen, J. M. Castro Cern, and A. J. Castro-Tirado. XRF 020903: flattening of the optical light curve. *GRB Circular Network*, 1631, 2002.
- [164] D. Gotz, S. Mereghetti, M. Beck, J. Borkowski, and N. Mowlavi. GRB 031203: a long GRB detected with INTEGRAL. 2003.
- [165] M. Gotz, S. Mereghetti, N. Mowlavi, M. Beck, and J. Borkowsk. GRB040812: a long GRB detected by INTEGRAL. *GRB Circular Network*, 2640, 2004.
- [166] J. Granot and A. Loeb. Radio Imaging of Gamma-Ray Burst Jets in Nearby Supernovae. *ApJ*, 593:L81–L84, 2003.
- [167] J. Granot, E. Nakar, and T. Piran. The variable light curve of GRB 030329: The case for refreshed shocks. *ApJ*, submitted; astro-ph/0304563, 2003.
- [168] J. Granot, A. Panaitescu, P. Kumar, and S. E. Woosley. Off-Axis Afterglow Emission from Jetted Gamma-Ray Bursts. *ApJ*, 570:L61–L64, 2002.

- [169] J. Granot and E. Ramirez-Ruiz. The Case for a Misaligned Relativistic Jet from SN 2001em. *ApJ*, 609:L9–L12, July 2004.
- [170] J. Granot, E. Ramirez-Ruiz, and R. Perna. Afterglow Observations Shed New Light on the Nature of X-Ray Flashes. *ApJ*, 630:1003–1014, September 2005.
- [171] J. Granot and R. Sari. The Shape of Spectral Breaks in Gamma-Ray Burst Afterglows. *ApJ*, 568:820–829, 2002.
- [172] D. Guetta, T. Piran, and E. Waxman. The Luminosity and Angular Distributions of Long-Duration Gamma-Ray Bursts. *ApJ*, 619:412–419, January 2005.
- [173] M. Hamuy, J. Maza, P. A. Pinto, M. M. Phillips, N. B. Suntzeff, R. D. Blum, K. A. G. Olsen, D. J. Pinfield, V. D. Ivanov, T. Augusteijn, S. Brilliant, M. Chadid, J.-G. Cuby, V. Doublier, O. R. Hainaut, E. Le Floch, C. Lidman, M. G. Petr-Gotzens, E. Pompei, and L. Vanzi. Optical and Infrared Spectroscopy of SN 1999ee and SN 1999ex. *AJ*, 124:417–429, July 2002.
- [174] M. Hamuy, M. Phillips, and J. Thomas-Osip. Supernova 2003bg in MCG -05-10-15. *IAUC*, 8088:3–+, March 2003.
- [175] M. Hamuy, M. M. Phillips, N. B. Suntzeff, J. Maza, L. E. González, M. Roth, K. Krisciunas, N. Morrell, E. M. Green, S. E. Persson, and P. J. McCarthy. An asymptotic-giant-branch star in the progenitor system of a type Ia supernova. *Nature*, 424:651–654, August 2003.
- [176] M. Hamuy, M. Stritzinger, M. M. Phillips, N. B. Suntzeff, J. Maza, and P. A. Pinto. Evidence for Core Collapse in the Type Ib/c SN 1999ex. In *From Twilight to Highlight: The Physics of Supernovae*, pages 222–+, 2003.
- [177] F. A. Harrison, S. Yost, D. Fox, J. Heise, S. R. Kulkarni, P. A. Price, and

- E. Berger. XRF011030: Chandra observations. *GRB Circular Network*, 1143:1+, 2001.
- [178] K. Hatano, D. Branch, K. Nomoto, J. S. Deng, K. Maeda, P. Nugent, and G. Aldering. The Type Ic Hypernova SN 1999as. *Bulletin of the American Astronomical Society*, 33:838, May 2001.
- [179] A. Heger, C. L. Fryer, S. E. Woosley, N. Langer, and D. H. Hartmann. How Massive Single Stars End Their Life. *ApJ*, 591:288–300, July 2003.
- [180] J. Heise, J. in't Zand, R. M. Kippen, and P. M. Woods. X-Ray Flashes and X-Ray Rich Gamma Ray Bursts. In E. Costa, F. Frontera, and J. Hjorth, editors, *Gamma-ray Bursts in the Afterglow Era*, pages 16–+, 2001.
- [181] J. Heise, J. in't Zand, R. M. Kippen, and P. M. Woods. X-Ray Flashes and X-Ray Rich Gamma Ray Bursts. In *Gamma-ray Bursts in the Afterglow Era*, pages 16–21, 2001.
- [182] A. Henden. XRF020903, BVRI field photometry. *GRB Circular Network*, 1571:1–+, 2002.
- [183] A. Henden. XRF040916, optical observations. *GRB Circular Network*, 2727, 2004.
- [184] A. Henden. Recent GRB BVRcIc field photometry. *GRB Coordinates Network*, 3454:1–+, 2005.
- [185] M. A. Hendry, S. J. Smartt, J. R. Maund, A. Pastorello, L. Zampieri, S. Benetti, M. Turatto, E. Cappellaro, W. P. S. Meikle, R. Kotak, M. J. Irwin, P. G. Jonker, L. Vermaas, R. F. Peletier, H. van Woerden, K. M. Exter, D. L. Pollacco, S. Leon, S. Verley, C. R. Benn, and G. Pignata. A study of the Type II-P supernova 2003gd in M74. *MNRAS*, 359:906–926, May 2005.
- [186] D. J. Hillier. Advances in modeling of Wolf-Rayet stars. In *IAU Symposium*, pages 70–+, 2003.

- [187] J. Hjorth, J. Sollerman, P. Møller, J. P. U. Fynbo, S. E. Woosley, C. Kouveliotou, N. R. Tanvir, J. Greiner, M. I. Andersen, A. J. Castro-Tirado, J. M. Castro Cerón, A. S. Fruchter, J. Gorosabel, P. Jakobsson, L. Kaper, S. Kloze, N. Masetti, H. Pedersen, K. Pedersen, E. Pian, E. Palazzi, J. E. Rhoads, E. Rol, E. P. J. van den Heuvel, P. M. Vreeswijk, D. Watson, and R. A. M. J. Wijers. A very energetic supernova associated with the  $\gamma$ -ray burst of 29 March 2003. *Nature*, 423:847–850, 2003.
- [188] S. T. Holland, P. T. Boyd, J. Gorosabel, J. Hjorth, P. Schady, B. Thomsen, T. Augusteijn, A. J. Blustin, A. Breeveld, M. De Pasquale, J. P. U. Fynbo, N. Gehrels, C. Gronwall, S. Hunsberger, M. Ivanushkina, W. Landsman, P. Laursen, K. McGowan, V. Mangano, C. B. Markwardt, F. Marshall, K. O. Mason, A. Moretti, M. J. Page, T. Poole, P. Roming, S. Rosen, and M. Still. Optical, Infrared, and Ultraviolet Observations of the X-Ray Flash GRB 050416A. *ArXiv Astrophysics e-prints*, April 2006. astro-ph/0604316.
- [189] E. Hoversten, K. Chiu, E. Nissen, C. Kelleman, and K. Glazebrook. GRB 041006, optical I observations. *GRB Circular Network*, 2778, 2004.
- [190] D. A. Howell, M. Sullivan, K. Perrett, T. J. Bronder, I. M. Hook, P. Astier, E. Aubourg, D. Balam, S. Basa, R. G. Carlberg, S. Fabbro, D. Fouchez, J. Guy, H. Lafoux, J. D. Neill, R. Pain, N. Palanque-Delabrouille, C. J. Pritchett, J. Rich, R. Taillet, R. Knop, R. G. McMahon, and S. Perlmutter. Gemini Spectroscopy of Supernovae from SNLA: Improving High Redshift SN Selection and Classification. *ApJ*, 2005. submitted.
- [191] K. Hurley, S. E. Boggs, D. M. Smith, R. C. Duncan, R. Lin, A. Zoglauer, S. Krucker, G. Hurford, H. Hudson, C. Wigger, W. Hajdas, C. Thompson, I. Mitrofanov, A. Sanin, W. Boynton, C. Fellows, A. von Kienlin, G. Lichti, A. Rau, and T. Cline. An exceptionally bright flare from SGR 1806-20 and the origins of short-duration  $\gamma$ -ray bursts. *Nature*, 434:1098–1103, April 2005.

- [192] K. Hurley, T. Cline, E. Mazets, S. Golenetskii, D. M. Smith, R. P. Lin, J. McTiernan, R. Schwartz, C. Wigger, W. Hajdas, A. Zehnder, A. von Kienlin, G. Lichti, A. Rau, I. Mitrofanov, D. Anfimov, A. Kozyrev, M. Litvak, A. Sanin, W. Boynton, C. Fellows, K. Harshman, C. Shinohara, R. Starr, G. Ricker, J.-L. Atteia, N. Kawai, D. Lamb, S. Woosley, J. Doty, R. Vanderspek, J. Villasenor, G. Crew, G. Monnelly, N. Butler, J. G. Jernigan, A. Levine, F. Martel, E. Morgan, G. Prigozhin, J. Braga, R. Manchanda, G. Pizzichini, Y. Shirasaki, C. Graziani, M. Matsuoka, T. Tamagawa, K. Torii, T. Sakamoto, A. Yoshida, E. Fenimore, M. Galassi, T. Tavenner, T. Donaghy, M. Boer, J.-F. Olive, and J.-P. Dezalay. IPN upper limit to a GRB associated with SN2003L. *GRB Circular Network*, 1939, 2003.
- [193] K. Iwamoto, P. A. Mazzali, K. Nomoto, H. Umeda, T. Nakamura, F. Patat, I. J. Danziger, T. R. Young, T. Suzuki, T. Shigeyama, T. Augusteijn, V. Dobbler, J.-F. Gonzalez, H. Boehnhardt, J. Brewer, O. R. Hainaut, C. Lidman, B. Leibundgut, E. Cappellaro, M. Turatto, T. J. Galama, P. M. Vreeswijk, C. Kouveliotou, J. Van Paradijs, E. Pian, E. Palazzi, and F. Frontera. A hypernova model for the supernova associated with the gamma-ray burst of 25 april 1998. *Nature*, 395:672–674, 1998.
- [194] K. Iwamoto, T. Nakamura, K. Nomoto, P. A. Mazzali, I. J. Danziger, P. Garnavich, R. Kirshner, S. Jha, D. Balam, and J. Thorstensen. The Peculiar Type IC Supernova 1997EF: Another Hypernova. *ApJ*, 534:660–669, May 2000.
- [195] K. Iwamoto, K. Nomoto, P. Hoflich, H. Yamaoka, S. Kumagai, and T. Shigeyama. Theoretical light curves for the type IC supernova SN 1994I. *ApJ*, 437:L115–L118, December 1994.
- [196] P. Jakobsson, J. Hjorth, J. P. U. Fynbo, M. Weidinger, J. Gorosabel, C. Ledoux, D. Watson, G. Björnsson, E. H. Gudmundsson, R. A. M. J. Wijers, P. Möller, K. Pedersen, J. Sollerman, A. A. Henden, B. L. Jensen,

- A. Gilmore, P. Kilmartin, A. Levan, J. M. Castro Cerón, A. J. Castro-Tirado, A. Fruchter, C. Kouveliotou, N. Masetti, and N. Tanvir. The line-of-sight towards GRB 030429 at  $z = 2.66$ : Probing the matter at stellar, galactic and intergalactic scales. *A&A*, 427:785–794, December 2004.
- [197] J. B. Jensen, J. L. Tonry, B. J. Barris, R. I. Thompson, M. C. Liu, M. J. Rieke, E. A. Ajhar, and J. P. Blakeslee. Measuring Distances and Probing the Unresolved Stellar Populations of Galaxies Using Infrared Surface Brightness Fluctuations. *ApJ*, 583:712–726, February 2003.
- [198] P. Kaaret, S. Corbel, A. H. Prestwich, and A. Zezas. Radio Emission from an Ultraluminous X-ray Source. *Science*, 299:365–368, 2003.
- [199] S. M. Kanbur, C. Ngeow, S. Nikolaev, N. R. Tanvir, and M. A. Hendry. The extra-galactic Cepheid distance scale from LMC and Galactic period-luminosity relations. *A&A*, 411:361–379, December 2003.
- [200] I. D. Karachentsev, V. E. Karachentseva, W. K. Huchtmeier, and D. I. Makarov. A Catalog of Neighboring Galaxies. *AJ*, 127:2031–2068, April 2004.
- [201] K. S. Kawabata, D. J. Jeffery, M. Iye, Y. Ohyama, G. Kosugi, N. Kashikawa, N. Ebizuka, T. Sasaki, K. Sekiguchi, K. Nomoto, P. Mazzali, J. Deng, K. Maeda, H. Umeda, K. Aoki, Y. Saito, T. Takata, M. Yoshida, R. Asai, M. Inata, K. Okita, K. Ota, T. Ozawa, Y. Shimizu, H. Taguchi, Y. Yadoumaru, T. Misawa, F. Nakata, T. Yamada, I. Tanaka, and T. Kodama. Optical Spectropolarimetry of SN 2002ap: A High-Velocity Asymmetric Explosion. *ApJ*, 580:L39–L42, November 2002.
- [202] K. S. Kawabata, K. Maeda, J. Deng, K. Nomoto, P. A. Mazzali, E. Pian, L. Wang, Y. Ohyama, and M. Iye. Supernova 2003jd. *IAUC*, 8410:2–+, September 2004.
- [203] K. I. Kellermann and I. I. K. Pauliny-Toth. Compact radio sources. *ARAA*, 19:373–410, 1981.

- [204] D. D. Kelson, K. Koviak, E. Berger, and D. B. Fox. XRF040701: Magellanian Spectroscopy of Chandra Source 2 Associated Galaxy. *GRB Circular Network*, 2627, 2004.
- [205] R. C. Kennicutt. Star formation in galaxies along the hubble sequence. *ARAA*, 36:131–188, 1998.
- [206] A. L. Kinney, R. C. Bohlin, D. Calzetti, N. Panagia, and R. F. G. Wyse. An atlas of ultraviolet spectra of star-forming galaxies. *ApJS*, 86:5–93, May 1993.
- [207] K. Kinugasa, H. Kawakita, K. Ayani, T. Kawabata, H. Yamaoka, J. S. Deng, P. A. Mazzali, K. Maeda, and K. Nomoto. Early-Phase Spectra of “Hypernova” SN 2002ap. *ApJ*, 577:L97–L101, October 2002.
- [208] A. Klotz, J. L. Atteia, G. Sgratta, and M. Bohr. TAROT Observations of GRB 040916 (HETE 3558). *GRB Circular Network*, 2729, 2004.
- [209] H. A. Kobulnicky, C. L. Fryer, and D. C. Kiminki. A Fresh Look at the Binary Characteristics Among Massive Stars with Implications for Supernova and X-Ray Binary Rates. *ArXiv Astrophysics e-prints*, May 2006.
- [210] H. A. Kobulnicky and L. J. Kewley. Metallicities of  $0.3 < z < 1.0$  Galaxies in the GOODS-North Field. *ApJ*, 617:240–261, December 2004.
- [211] G. Kosugi, N. Kawai, A. Tajitsu, and H. Furusawa. XRF040916: Optical Transient Candidate by Subaru. *GRB Circular Network*, 2726, 2004.
- [212] C. Kouveliotou et al. Chandra observations of the x-ray environs of sn 1998bw/grb 980425. *ApJ* submitted; astro-ph/0401184, 2004.
- [213] C. Kouveliotou, C. A. Meegan, G. J. Fishman, N. P. Bhat, M. S. Briggs, T. M. Koshut, W. S. Paciesas, and G. N. Pendleton. Identification of two classes of gamma-ray bursts. *ApJ*, 413:101–104, 1993.

- [214] S. Kulkarni and D. W. Fox. Supernova 2003L in NGC 3506. *IAUC*, 8073: 2–+, February 2003.
- [215] S. R. Kulkarni, D. A. Frail, R. Sari, G. H. Moriarty-Schieven, D. S. Shepherd, P. Udomprasert, A. C. S. Readhead, J. S. Bloom, M. Feroci, and E. Costa. Discovery of a radio flare from grb 990123. *ApJ*, 522:L97–L100, 1999.
- [216] S. R. Kulkarni, D. A. Frail, M. H. Wieringa, R. D. Ekers, E. M. Sadler, R. M. Wark, J. L. Higdon, E. S. Phinney, and J. S. Bloom. Radio emission from the unusual supernova 1998bw and its association with the gamma-ray burst of 25 April 1998. *Nature*, 395:663–669, 1998.
- [217] A. Kundu and B. C. Whitmore. New Insights from Hubble Space Telescope Studies of Globular Cluster Systems. II. Analysis of 29 S0 Systems. *AJ*, 122: 1251–1270, September 2001.
- [218] D. Q. Lamb, Donaghy, T. Q., and C. Graziani. A Unified Jet Model of X-Ray Flashes and Gamma-Ray Bursts. astro-ph/0309456, 2003.
- [219] E. Le Floch, P.-A. Duc, I. F. Mirabel, D. B. Sanders, G. Bosch, R. J. Diaz, C. J. Donzelli, I. Rodrigues, T. J.-L. Courvoisier, J. Greiner, S. Mereghetti, J. Melnick, J. Maza, and D. Minniti. Are the hosts of gamma-ray bursts sub-luminous and blue galaxies? *A&A*, 400:499–510, March 2003.
- [220] D. C. Leonard, A. V. Filippenko, R. Chornock, and R. J. Foley. Photospheric-Phase Spectropolarimetry and Nebular-Phase Spectroscopy of the Peculiar Type Ic Supernova 2002ap. *PASP*, 114:1333–1348, December 2002.
- [221] A. Levan, A. Fruchter, L. Strolger, I. Burud, and J. Rhoads. XRF 020903 : HST observations. *GRB Circular Network*, 1761:1–+, 2002.
- [222] A. Levan, S. Patel, C. Kouveliotou, A. Fruchter, J. Rhoads, E. Rol, E. Ramirez-Ruiz, J. Gorosabel, J. Hjorth, R. Wijers, W. M. Wood-Vasey, D. Bersier, A. Castro-Tirado, J. Fynbo, B. Jensen, E. Pian, N. Tanvir,

- S. Thorsett, and S. Woosely. A Deep Search with HST for Late Time Supernova Signatures in the Hosts of XRF 011030 and XRF 020427. *ArXiv Astrophysics e-prints*, October 2004. astro-ph/0410560.
- [223] A. J. Levan, J. P. Osborne, N. R. Tanvir, K. L. Page, E. Rol, B. Zhang, M. R. Goad, P. T. O’Brien, R. S. Priddey, D. Bersier, D. N. Burrows, R. Chapman, A. S. Fruchter, P. Giommi, N. Gehrels, M. A. Hughes, S. Pak, C. Simpson, G. Tagliaferri, and E. Vardoulaki. The first Swift X-ray Flash: The faint afterglow of XRF 050215B. *ArXiv Astrophysics e-prints*, May 2006. astro-ph/0605256.
- [224] A. Levinson, E. O. Ofek, E. Waxman, and A. Gal-Yam. Orphan Gamma-Ray Burst Radio Afterglows: Candidates and Constraints on Beaming. *ApJ*, 576:923–931, 2002.
- [225] W. Li, R. Chornock, S. Jha, and A. V. Filippenko. GRB 050416: KAIT observations. *GRB Coordinates Network*, 3270:1–+, 2005.
- [226] Z. Li and R. A. Chevalier. Radio Supernova SN 1998BW and Its Relation to GRB 980425. *ApJ*, 526:716–726, 1999.
- [227] Z. Li and L. M. Song. Late-Time Radio Rebrightening of Gamma-Ray Burst Afterglows: Evidence for Double-Sided Jets. *ApJ*, 614:L17–L20, October 2004.
- [228] Zhi-Yun Li and Roger A. Chevalier. Wind-interaction models for the early afterglows of gamma-ray bursts: The case of grb 021004. *ApJ* in press; astro-ph/0303650, 2003.
- [229] Y. M. Lipkin, E. O. Ofek, A. Gal-Yam, E. M. Leibowitz, D. Poznanski, S. Kaspi, D. Polishook, S. R. Kulkarni, D. W. Fox, E. Berger, N. Mirabal, J. Halpern, M. Bureau, K. Fathi, P. A. Price, B. A. Peterson, A. Frebel, B. Schmidt, J. A. Orosz, J. B. Fitzgerald, J. S. Bloom, P. G. van Dokkum, C. D. Bailyn, M. M. Buxton, and M. Barsony. The Detailed Optical Light Curve of GRB 030329. *ApJ*, 606:381–394, May 2004.

- [230] Y. Lithwick and R. Sari. Lower Limits on Lorentz Factors in Gamma-Ray Bursts. *ApJ*, 555:540–545, July 2001.
- [231] M. Livio and E. Waxman. Toward a model for the progenitors of gamma-ray bursts. *ApJ*, 538:187–191, 2000.
- [232] A. G. Lyne, R. S. Pritchard, F. Graham-Smith, and F. Camilo. Very low braking index for the VELA pulsar. *Nature*, 381:497–498, 1996.
- [233] A. I. MacFadyen and S. E. Woosley. Collapsars: Gamma-Ray Bursts and Explosions in “Failed Supernovae”. *ApJ*, 524:262–289, 1999.
- [234] A. I. MacFadyen, S. E. Woosley, and A. Heger. Supernovae, Jets, and Collapsars. *ApJ*, 550:410–425, 2001.
- [235] A. Maeder. The relative numbers of Wolf-Rayet stars in galaxies with active star formation - The metallicity effect. *A&A*, 242:93–111, February 1991.
- [236] J. Maíz-Apellániz, L. Cieza, and J. W. MacKenty. Tip of the Red Giant Branch Distances to NGC 4214, UGC 685, and UGC 5456. *AJ*, 123:1307–1315, March 2002.
- [237] D. Malesani, G. Tagliaferri, G. Chincarini, S. Covino, M. Della Valle, D. Fugazza, P. A. Mazzali, F. M. Zerbi, P. D’Avanzo, S. Kalogerakos, A. Simoncelli, L. A. Antonelli, L. Burderi, S. Campana, A. Cucchiara, F. Fiore, G. Ghirlanda, P. Goldoni, D. Götz, S. Mereghetti, I. F. Mirabel, P. Romano, L. Stella, T. Minezaki, Y. Yoshii, and K. Nomoto. SN 2003lw and GRB 031203: A Bright Supernova for a Faint Gamma-Ray Burst. *ApJ*, 609:L5–L8, July 2004.
- [238] R. N. Manchester, B. M. Gaensler, V. C. Wheaton, L. Staveley-Smith, A. K. Tzioumis, N. S. Bizunok, M. J. Kesteven, and J. E. Reynolds. Evolution of the Radio Remnant of SN 1987A: 1990-2001. *Publications of the Astronomical Society of Australia*, 19:207–221, 2002.

- [239] V. Mangano, V. La Parola, G. Cusumano, T. Mineo, D. Malesani, J. Dyks, S. Campana, M. Capalbi, G. Chincarini, P. Giommi, A. Moretti, M. Perri, P. Romano, G. Tagliaferri, D. N. Burrows, O. Godet, S. T. Holland, J. A. Kennea, K. L. Page, J. L. Racusin, P. W. A. Roming, and B. Zhang. Swift XRT Observations of the Afterglow of XRF 050416A. *ArXiv Astrophysics e-prints*, March 2006. astro-ph/0603738.
- [240] R. O. Marzke, L. N. da Costa, P. S. Pellegrini, C. N. A. Willmer, and M. J. Geller. The Galaxy Luminosity Function at  $Z < 0.05$ : Dependence on Morphology. *ApJ*, 503:617–+, August 1998.
- [241] T. Matheson, P. Challis, R. P. Kirshner, and P. M. Garnavich. Type Ic SN2003L (SN/GRB?), optical spectrum. *GRB Circular Network*, 1846:1–+, 2003.
- [242] T. Matheson, A. V. Filippenko, W. Li, D. C. Leonard, and J. C. Shields. Optical Spectroscopy of Type IB/C Supernovae. *AJ*, 121:1648–1675, March 2001.
- [243] T. Matheson, P. M. Garnavich, K. Z. Stanek, D. Bersier, S. T. Holland, K. Krisciunas, N. Caldwell, P. Berlind, J. S. Bloom, M. Bolte, A. Z. Bonanos, M. J. I. Brown, W. R. Brown, M. L. Calkins, P. Challis, R. Chornock, L. Echevarria, D. J. Eisenstein, M. E. Everett, A. V. Filippenko, K. Flint, R. J. Foley, D. L. Freedman, M. Hamuy, P. Harding, N. P. Hathi, M. Hicken, C. Hoopes, C. Impey, B. T. Jannuzi, R. A. Jansen, S. Jha, J. Kaluzny, S. Kannappan, R. P. Kirshner, D. W. Latham, J. C. Lee, D. C. Leonard, W. Li, K. L. Luhman, P. Martini, H. Mathis, J. Maza, S. T. Megeath, L. R. Miller, D. Minniti, E. W. Olszewski, M. Papenkova, M. M. Phillips, B. Pindor, D. D. Sasselov, R. Schild, H. Schweiker, T. Spahr, J. Thomas-Osip, I. Thompson, D. Weisz, R. Windhorst, and D. Zaritsky. Photometry and Spectroscopy of GRB 030329 and Its Associated Supernova 2003dh: The First Two Months. *ApJ*, 599:394–407, December 2003.

- [244] T. Matheson, P. M. Garnavich, K. Z. Stanek, D. Bersier, S. T. Holland, K. Krisciunas, N. Caldwell, P. Berlind, J. S. Bloom, M. Bolte, A. Z. Bonanos, M. J. I. Brown, W. R. Brown, M. L. Calkins, P. Challis, R. Chornock, L. Echevarria, D. J. Eisenstein, M. E. Everett, A. V. Filippenko, K. Flint, R. J. Foley, D. L. Freedman, M. Hamuy, P. Harding, N. P. Hathi, M. Hicken, C. Hoopes, C. Impey, B. T. Jannuzi, R. A. Jansen, S. Jha, J. Kaluzny, S. Kannappan, R. P. Kirshner, D. W. Latham, J. C. Lee, D. C. Leonard, W. Li, K. L. Luhman, P. Martini, H. Mathis, J. Maza, S. T. Megeath, L. R. Miller, D. Minniti, E. W. Olszewski, M. Papenkova, M. M. Phillips, B. Pindor, D. D. Sasselov, R. Schild, H. Schweiker, T. Spahr, J. Thomas-Osip, I. Thompson, D. Weisz, R. Windhorst, and D. Zaritsky. Photometry and Spectroscopy of GRB 030329 and Its Associated Supernova 2003dh: The First Two Months. *ApJ*, 599:394–407, December 2003.
- [245] C. D. Matzner and C. F. McKee. The Expulsion of Stellar Envelopes in Core-Collapse Supernovae. *ApJ*, 510:379–403, January 1999.
- [246] J. R. Maund, S. J. Smartt, R. P. Kudritzki, P. Podsiadlowski, and G. F. Gilmore. The massive binary companion star to the progenitor of supernova 1993J. *Nature*, 427:129–131, January 2004.
- [247] J. R. Maund, S. J. Smartt, and F. Schweizer. Luminosity and Mass Limits for the Progenitor of the Type Ic Supernova 2004gt in NGC 4038. *ApJ*, 630:L33–L36, September 2005.
- [248] P. A. Mazzali, J. Deng, K. Maeda, K. Nomoto, A. V. Filippenko, and T. Matheson. Properties of Two Hypernovae Entering the Nebular Phase: SN 1997ef and SN 1997dq. *ApJ*, 614:858–863, October 2004.
- [249] P. A. Mazzali, J. Deng, K. Maeda, K. Nomoto, H. Umeda, K. Hatano, K. Iwamoto, Y. Yoshii, Y. Kobayashi, T. Minezaki, M. Doi, K. Enya, H. Tomita, S. J. Smartt, K. Kinugasa, H. Kawakita, K. Ayani, T. Kawabata, H. Yamaoka, Y. L. Qiu, K. Motohara, C. L. Gerardy, R. Fesen, K. S.

- Kawabata, M. Iye, N. Kashikawa, G. Kosugi, Y. Ohyama, M. Takada-Hidai, G. Zhao, R. Chornock, A. V. Filippenko, S. Benetti, and M. Turatto. The Type Ic Hypernova SN 2002ap. *ApJ*, 572:L61–L65, June 2002.
- [250] P. A. Mazzali, J. Deng, K. Nomoto, E. Pian, N. Tominaga, M. Tanaka, and K. Maeda. A Neutron Star-driven XRF associated with SN 2006aj. *Nature*, submitted, astro-ph/0603567.
- [251] P. A. Mazzali, K. Iwamoto, and K. Nomoto. A Spectroscopic Analysis of the Energetic Type Ic Hypernova SN 1997EF. *ApJ*, 545:407–419, December 2000.
- [252] P. A. Mazzali, K. S. Kawabata, K. Maeda, K. Nomoto, A. V. Filippenko, E. Ramirez-Ruiz, S. Benetti, E. Pian, J. Deng, N. Tominaga, Y. Ohyama, M. Iye, R. J. Foley, T. Matheson, L. Wang, and A. Gal-Yam. An Asymmetric Energetic Type Ic Supernova Viewed Off-Axis, and a Link to Gamma Ray Bursts. *Science*, 308:1284–1287, May 2005.
- [253] S. S. McGaugh. H II region abundances - Model oxygen line ratios. *ApJ*, 380:140–150, October 1991.
- [254] E. H. McKenzie and B. E. Schaefer. The Late-Time Light Curve of SN 1998BW Associated with GRB 980425. *PASP*, 111:964–968, August 1999.
- [255] C. Meegan et al. The spatial distribution of gamma-ray bursts observed by BATSE. *Nature*, 355:143, 1992.
- [256] M. R. Metzger, S. G. Djorgovski, S. R. Kulkarni, C. C. Steidel, K. L. Adelberger, D. A. Frail, E. Costa, and F. Fronterra. Spectral constraints on the redshift of the optical counterpart to the  $\gamma$ -ray burst of 8 may 1997. *Nature*, 387:879, 1997.
- [257] A. J. Mioduszewski, V. V. Dwarkadas, and L. Ball. Simulated Radio Images and Light Curves of Young Supernovae. *ApJ*, 562:869–879, December 2001.

- [258] N. Mirabal, J. P. Halpern, D. An, J. R. Thorstensen, and D. M. Terndrup. GRB 060218/SN 2006aj: A Gamma-Ray Burst and Prompt Supernova at  $z=0.0335$ . *Astrophys. J.*, submitted, astro-ph/0603686.
- [259] M. Modjaz, K. Z. Stanek, P. M. Garnavich, P. Berlind, S. Blondin, W. Brown, M. Calkins, P. Challis, A. M. Diamond-Stanic, H. Hao, M. Hicken, R. P. Kirshner, and J. L. Prieto. Early-Time Photometry and Spectroscopy of the Fast Evolving SN 2006aj Associated with GRB 060218. *ApJ*, 645:L21–L24, July 2006.
- [260] M. J. Montes, S. D. van Dyk, K. W. Weiler, R. A. Sramek, and N. Panagia. Radio Observations of SN 1980K: Evidence for Rapid Presupernova Evolution. *ApJ*, 506:874–879, October 1998.
- [261] M. J. Montes, K. W. Weiler, S. D. Van Dyk, N. Panagia, C. K. Lacey, R. A. Sramek, and R. Park. Radio Observations of SN 1979C: Evidence for Rapid Presupernova Evolution. *ApJ*, 532:1124–1131, April 2000.
- [262] J. R. Mould, J. P. Huchra, W. L. Freedman, R. C. Kennicutt, Jr., L. Ferrarese, H. C. Ford, B. K. Gibson, J. A. Graham, S. M. G. Hughes, G. D. Illingworth, D. D. Kelson, L. M. Macri, B. F. Madore, S. Sakai, K. M. Sebo, N. A. Silbermann, and P. B. Stetson. The Hubble Space Telescope Key Project on the Extragalactic Distance Scale. XXVIII. Combining the Constraints on the Hubble Constant. *ApJ*, 529:786–794, February 2000.
- [263] T. Nakamura. A Model for Non High Energy Gamma Ray Bursts and Sources of Ultra High Energy Cosmic Rays — Super Strongly Magnetized Millisecond Pulsar Formed from a (C + O) Star and a Neutron Star (Black Hole) Close Binary System —. *Progress of Theoretical Physics*, 100:921–929, 1998.
- [264] T. Nakamura, P. A. Mazzali, K. Nomoto, and K. Iwamoto. Light Curve and Spectral Models for the Hypernova SN 1998BW Associated with GRB 980425. *ApJ*, 550:991–999, April 2001.

- [265] E. Nakar. Short-Hard Gamma-Ray Bursts. *ArXiv Astrophysics e-prints*, January 2007.
- [266] E. Nakar and J. Granot. Smooth Light Curves from a Bumpy Ride: Relativistic Blast Wave Encounters a Density Jump. *ArXiv Astrophysics e-prints*, June 2006. astro-ph/0606011.
- [267] J. P. Norris. Implications of the Lag-Luminosity Relationship for Unified Gamma-Ray Burst Paradigms. *ApJ*, 579:386–403, 2002.
- [268] J. P. Norris and J. T. Bonnell. Short Gamma-Ray Bursts with Extended Emission. *ApJ*, 643:266–275, May 2006.
- [269] J. P. Norris, G. F. Marani, and J. T. Bonnell. Connection between Energy-dependent Lags and Peak Luminosity in Gamma-Ray Bursts. *ApJ*, 534:248–257, 2000.
- [270] J. A. Nousek, C. Kouveliotou, D. Grupe, K. L. Page, J. Granot, E. Ramirez-Ruiz, S. K. Patel, D. N. Burrows, V. Mangano, S. Barthelmy, A. P. Beardmore, S. Campana, M. Capalbi, G. Chincarini, G. Cusumano, A. D. Falcone, N. Gehrels, P. Giommi, M. R. Goad, O. Godet, C. P. Hurkett, J. A. Kennea, A. Moretti, P. T. O’Brien, J. P. Osborne, P. Romano, G. Tagliaferri, and A. A. Wells. Evidence for a Canonical Gamma-Ray Burst Afterglow Light Curve in the Swift XRT Data. *ApJ*, 642:389–400, May 2006.
- [271] P. T. O’Brien, R. Willingale, J. Osborne, M. R. Goad, K. L. Page, S. Vaughan, E. Rol, A. Beardmore, O. Godet, C. Hurkett, A. Wells, B. Zhang, S. Kobayashi, D. N. Burrows, J. A. Nousek, J. A. Kennea, A. Falcone, D. Grupe, N. Gehrels, S. Barthelmy, J. Cannizzo, J. Cummings, J. Hill, H. Krimm, G. Chincarini, G. Tagliaferri, S. Campana, A. Moretti, P. Giommi, M. Perri, V. Mangano, and V. LaParola. The early X-ray emission from GRBs. *ArXiv Astrophysics e-prints*, January 2006.
- [272] Y. Oren, E. Nakar, and T. Piran. The apparent size of gamma-ray burst

- afterglows as a test of the fireball model. *MNRAS*, 353:L35–L40, October 2004.
- [273] D. E. Osterbrock. *Astrophysics of gaseous nebulae and active galactic nuclei*. Research supported by the University of California, John Simon Guggenheim Memorial Foundation, University Science Books, University of Minnesota, et al. Mill Valley, CA, 1989.
- [274] B. Paczyński. Gamma-ray bursters at cosmological distances. *ApJ*, 308:L43–L46, 1986.
- [275] B. Paczynski. Gamma-Ray Bursts at Low Redshift. *Acta Astronomica*, 51:1–4, 2001.
- [276] N. Panagia, R. A. Sramek, and K. W. Weiler. Subluminous, radio emitting Type I supernovae. *ApJ*, 300:L55–L58, January 1986.
- [277] A. Panaitescu. The energetics and environment of the short-GRB afterglows 050709 and 050724. *MNRAS*, 367:L42–L46, March 2006.
- [278] A. Panaitescu and P. Kumar. Analytic Light Curves of Gamma-Ray Burst Afterglows: Homogeneous versus Wind External Media. *ApJ*, 543:66–76, 2000.
- [279] A. Panaitescu and P. Kumar. Fundamental Physical Parameters of Collimated Gamma-Ray Burst Afterglows. *ApJ*, 560:L49–L53, 2001.
- [280] A. Panaitescu and P. Kumar. Properties of Relativistic Jets in Gamma-Ray Burst Afterglows. *ApJ*, 571:779–789, 2002.
- [281] A. Pastorello, S. J. Smartt, S. Mattila, J. J. Eldridge, D. Young, K. Itagaki, H. Yamaoka, H. Navasardyan, S. Valenti, F. Patat, I. Agnoletto, T. Augusteijn, S. Benetti, E. Cappellaro, T. Boles, J. . Bonnet-Bidaud, M. T. Botticella, F. Bufano, C. Cao, J. Deng, M. Dennefeld, N. Elias-Rosa, A. Harutyunyan, F. P. Keenan, T. Iijima, V. Lorenzi, P. A. Mazzali, X. Meng,

- S. Nakano, T. B. Nielsen, J. V. Smoker, V. Stanishev, M. Turatto, D. Xu, and L. Zampieri. A giant outburst two years before the core-collapse of a massive star. *ArXiv Astrophysics e-prints*, March 2007.
- [282] F. Patat, E. Cappellaro, J. Danziger, P. A. Mazzali, J. Sollerman, T. Augusteijn, J. Brewer, V. Doublrier, J. F. Gonzalez, O. Hainaut, C. Lidman, B. Leibundgut, K. Nomoto, T. Nakamura, J. Spyromilio, L. Rizzi, M. Turatto, J. Walsh, T. J. Galama, J. van Paradijs, C. Kouveliotou, P. M. Vreeswijk, F. Frontera, N. Masetti, E. Palazzi, and E. Pian. The Metamorphosis of SN 1998bw. *ApJ*, 555:900–917, 2001.
- [283] S. Patel, C. Kouveliotou, S. Mereghetti, D. Gotz, N. Lund, J. Chenevez, P. Ubertini, A. Levan, E. van den Heuvel, and K. Hurley. GRB 040812: Second epoch CXO observations. *GRB Circular Network*, 2655, 2004.
- [284] S. Patel, C. Kouveliotou, S. Mereghetti, D. Gotz, N. Lund, J. Chenevez, P. Ubertini, E. van den Heuvel, and K. Hurley. CXO observation of GRB 040812. *GRB Circular Network*, 2648, 2004.
- [285] E. Pavlenko, V. Rumyantsev, and A. Pozanenko. XRF 020903: optical observations. *GRB Circular Network*, 1535:1–+, 2002.
- [286] Y. C. Pei. Interstellar dust from the Milky Way to the Magellanic Clouds. *ApJ*, 395:130–139, August 1992.
- [287] R. Perna and A. Loeb. Constraining the beaming of gamma-ray bursts with radio surveys. *ApJ*, 509:L85–L88, 1998.
- [288] R. Perna, R. Sari, and D. Frail. Jets in Gamma-Ray Bursts: Tests and Predictions for the Structured Jet Model. *ApJ*, 594:379–384, 2003.
- [289] M. M. Phillips, N. B. Suntzeff, K. Krisciunas, R. Carlberg, M. Gladders, F. Barrientos, T. Matheson, and S. Jha. Supernova 2001ig in NGC 7424. *IAUC*, 7772:2–+, December 2001.

- [290] E. Pian, L. Amati, L. A. Antonelli, R. C. Butler, E. Costa, G. Cusumano, J. Danziger, M. Feroci, F. Fiore, F. Frontera, P. Giommi, N. Masetti, J. M. Muller, L. Nicastro, T. Oosterbroek, M. Orlandini, A. Owens, E. Palazzi, A. Parmar, L. Piro, J. J. M. in't Zand, A. Castro-Tirado, A. Coletta, D. Dal Fiume, S. Del Sordo, J. Heise, P. Soffitta, and V. Torroni. BEPPOSAX Observations of GRB 980425: Detection of the Prompt Event and Monitoring of the Error Box. *ApJ*, 536:778–787, 2000.
- [291] E. Pian, J. Fynbo, U. G. Joergensen, A. Levan, N. Masetti, E. Palazzi, F. Patat, E. Rol, J. Hjorth, B. Lindgren Jensen, P. Mazzali, C. Kouveliotou, K. Nomoto, and E. Cappellaro. XRF040701: Optical Observations at ESO. *GRB Circular Network*, 2638, 2004.
- [292] E. Pian, P. A. Mazzali, N. Masetti, P. Ferrero, S. Klose, E. Palazzi, E. Ramirez-Ruiz, S. E. Woosley, C. Kouveliotou, J. Deng, A. V. Filippenko, R. Foley, J. Fynbo, D. A. Kann, J. Hjorth, K. Nomoto, F. Patat, J. Sollerman, P. M. Vreeswijk, E. W. Guenther, A. Levan, P. O'Brien, N. Tanvir, R. A. M. J. Wijers, C. Dumas, O. Hainaut, L. Amati, E. Cappellaro, A. J. Castro-Tirado, F. Frontera, J. Greiner, K. Kawabata, K. Maeda, P. Moller, L. Nicastro, and E. Rol. Gamma-Ray Burst associated Supernovae: Outliers become Mainstream. *Nature*, submitted, astro-ph/0603530.
- [293] T. Piran. Gamma-ray bursts and the fireball model. *Phys. Rep.*, 1999. in press.
- [294] P. Podsiadlowski. The progenitor of SN 1987 A. *PASP*, 104:717–729, September 1992.
- [295] P. Podsiadlowski, P. C. Joss, and J. J. L. Hsu. Presupernova evolution in massive interacting binaries. *ApJ*, 391:246–264, May 1992.
- [296] P. Podsiadlowski, P. A. Mazzali, K. Nomoto, D. Lazzati, and E. Cappellaro. The Rates of Hypernovae and Gamma-Ray Bursts: Implications for Their Progenitors. *ApJ*, 607:L17–L20, May 2004.

- [297] D. Pooley and W. H. G. Lewin. Supernova 2003bg in MCG -05-10-15. *IAUC*, 8110:2–+, April 2003.
- [298] D. Pooley and W. H. G. Lewin. Supernova 2001em in UGC 11794. *IAUC*, 8323:2–+, April 2004.
- [299] P. Predehl and J. H. M. M. Schmitt. "x-raying the interstellar medium: Rosat observations of dust scattering halos.". *A&A*, 293:889–905, January 1995.
- [300] P. A. Price, S. R. Kulkarni, B. P. Schmidt, T. J. Galama, J. S. Bloom, E. Berger, D. A. Frail, S. G. Djorgovski, D. W. Fox, A. A. Henden, S. Klose, F. A. Harrison, D. E. Reichart, R. Sari, S. A. Yost, T. S. Axelrod, P. McCarthy, J. Holtzman, J. P. Halpern, R. A. Kimble, J. C. Wheeler, R. A. Chevalier, K. Hurley, G. R. Ricker, E. Costa, F. Frontera, and L. Piro. GRB 010921: Strong Limits on an Underlying Supernova from the Hubble Space Telescope. *ApJ*, 584:931–936, February 2003.
- [301] P. A. Price, T. Minezaki, L. Cowie, and Y. Yoshii. GRB 050416: Optical/NIR observations. *GRB Coordinates Network*, 3312:1–+, 2005.
- [302] P. A. Price, B. P. Schmidt, and T. S. Axelrod. XRF 020903: optical observations. *GRB Circular Network*, 1533:1–+, 2002.
- [303] J. X. Prochaska, J. S. Bloom, H. . Chen, R. J. Foley, D. A. Perley, E. Ramirez-Ruiz, J. Granot, W. H. Lee, D. Pooley, K. Alatalo, and K. Hurley. The Galaxy Hosts and Large-Scale Environments of Short-Hard  $\gamma$ -ray Bursts. *ArXiv Astrophysics e-prints*, October 2005. astro-ph/0510022.
- [304] J. X. Prochaska, J. S. Bloom, H. Chen, K. C. Hurley, J. Melbourne, A. Dressler, J. R. Graham, D. J. Osip, and W. D. Vacca. The Host Galaxy of GRB 031203: Implications of its low metallicity, low redshift, and starburst nature. submitted to *ApJ*, February 2004.

- [305] Y. Qiu, C. L. Lu, Y. Q. Lou, K. Y. Huang, and Y. Urata. GRB 050416 : optical observation at XingLong observatory. *GRB Coordinates Network*, 3286:1–+, 2005.
- [306] E. Ramirez-Ruiz, L. M. Dray, P. Madau, and C. A. Tout. Winds from massive stars: implications for the afterglows of  $\gamma$ -ray bursts. *MNRAS*, 327: 829–840, November 2001.
- [307] E. Ramirez-Ruiz, G. García-Segura, J. D. Salmonson, and B. Pérez-Rendón. The State of the Circumstellar Medium Surrounding Gamma-Ray Burst Sources and Its Effect on the Afterglow Appearance. *ApJ*, 631:435–445, September 2005.
- [308] A. Rau, M. Salvato, and J. Greiner. The host of GRB/XRF 030528 - an actively star forming galaxy at  $z = 0.782$ . *A&A*, 444:425–430, December 2005.
- [309] A. C. S. Readhead. Equipartition brightness temperature and the inverse Compton catastrophe. *ApJ*, 426:51–59, May 1994.
- [310] A. C. S. Readhead. Equipartition brightness temperature and the inverse Compton catastrophe. *ApJ*, 426:51–59, May 1994.
- [311] M. J. Rees and P. Mészáros. Refreshed shocks and afterglow longevity in gamma-ray bursts. *ApJ*, 496:L1, 1998.
- [312] B. Reindl, G. A. Tammann, A. Sandage, and A. Saha. Reddening, Absorption, and Decline Rate Corrections for a Complete Sample of Type Ia Supernovae Leading to a Fully Corrected Hubble Diagram to  $v \lesssim 30,000 \text{ km s}^{-1}$ . *ApJ*, 624:532–554, May 2005.
- [313] J. E. Rhoads. How to tell a jet from a balloon: A proposed test for beaming in gamma-ray bursts. *ApJ*, 487:L1–L4, 1997.
- [314] J. E. Rhoads. The dynamics and light curves of beamed gamma-ray burst afterglows. *ApJ*, 525:737–749, 1999.

- [315] J. E. Rhoads. The Dynamics and Light Curves of Beamed Gamma-Ray Burst Afterglows. *ApJ*, 525:737–749, November 1999.
- [316] D. Richardson, D. Branch, D. Casebeer, J. Millard, R. C. Thomas, and E. Baron. A Comparative Study of the Absolute Magnitude Distributions of Supernovae. *AJ*, 123:745–752, February 2002.
- [317] M. W. Richmond, S. D. van Dyk, W. Ho, C. Y. Peng, Y. Paik, R. R. Treffers, A. V. Filippenko, J. Bustamante-Donas, M. Moeller, C. Pawellek, H. Tartara, and M. Spence. UBVRI Photometry of the Type IC SN 1994I in M51. *AJ*, 111:327–+, January 1996.
- [318] G. Ricker, J.-L. Atteia, N. Kawai, D. Lamb, S. Woosley, R. Vanderspek, J. Doty, J. Villasenor, G. Crew, G. Monnelly, N. Butler, T. Cline, J. G. Jernigan, A. Levine, F. Martel, E. Morgan, G. Prigozhin, G. Azzibrouck, J. Braga, R. Manchanda, G. Pizzichini, C. Graziani, Y. Shirasaki, M. Matsuoka, T. Tamagawa, K. Torii, T. Sakamoto, A. Yoshida, E. Fenimore, M. Galassi, T. Tavenner, T. Donaghy, M. Boer, J.-F. Olive, J.-P. Dezalay, and K. Hurley. GRB020903(=H2314): an X-ray flash localized by HETE. *GRB Circular Network*, 1530:1–+, 2002.
- [319] L. Rigon, M. Turatto, S. Benetti, A. Pastorello, E. Cappellaro, I. Aretxaga, O. Vega, V. Chavushyan, F. Patat, I. J. Danziger, and M. Salvo. SN 1999E: another piece in the supernova-gamma-ray burst connection puzzle. *MNRAS*, 340:191–196, March 2003.
- [320] P. Rodriguez-Pascual, M. Santos-Lleo, R. Gonzalez-Riestra, N. ScharTEL, and B. Altieri. XMM-Newton observation of GRB031203. 2003.
- [321] P. Romano, A. Moretti, P. L. Banat, D. N. Burrows, S. Campana, G. Chincarini, S. Covino, D. Malesani, G. Tagliaferri, S. Kobayashi, B. Zhang, A. D. Falcone, L. Angelini, S. Barthelmy, A. P. Beardmore, M. Capalbi, G. Cusumano, P. Giommi, M. R. Goad, O. Godet, D. Grupe, J. E. Hill, J. A. Kennea, V. La Parola, V. Mangano, P. Mészáros, D. C. Morris, J. A.

- Nousek, P. T. O'Brien, J. P. Osborne, A. Parsons, M. Perri, C. Pagani, K. L. Page, A. A. Wells, and N. Gehrels. X-ray flare in XRF 050406: evidence for prolonged engine activity. *A&A*, 450:59–68, April 2006.
- [322] I. Rosenberg. Distribution of brightness and polarization in Cassiopeia A at5 - O Gliz. *MNRAS*, 151:109–+, 1970.
- [323] A. P. Rybicki, G. B. and Lightman. *Radiative Processes in Astrophysics*. Wiley, New York, 1979.
- [324] S. D. Ryder, C. E. Murrowood, and R. A. Stathakis. A post-mortem investigation of the Type IIb supernova 2001ig. *MNRAS*, 369:L32–L36, June 2006.
- [325] S. D. Ryder, E. M. Sadler, R. Subrahmanyan, K. W. Weiler, N. Panagia, and C. Stockdale. Modulations in the radio light curve of the Type IIb supernova 2001ig: evidence for a Wolf-Rayet binary progenitor? *MNRAS*, 349:1093–1100, April 2004.
- [326] T. Sakamoto. Are Short GRBs Really Hard? In S. S. Holt, N. Gehrels, and J. A. Nousek, editors, *AIP Conf. Proc. 838: Gamma-Ray Bursts in the Swift Era*, pages 43–47, May 2006.
- [327] T. Sakamoto, L. Barbier, S. D. Barthelmy, J. R. Cummings, E. E. Fenimore, N. Gehrels, D. Hullinger, H. A. Krimm, C. B. Markwardt, D. M. Palmer, A. M. Parsons, G. Sato, and J. Tueller. Confirmation of the  $E_{\text{peak}} - E_{\text{iso}}$  (Amati) Relation from the X-Ray Flash XRF 050416A Observed by the Swift Burst Alert Telescope. *ApJ*, 636:L73–L76, January 2006. astro-ph/0512149.
- [328] T. Sakamoto, D. Q. Lamb, C. Graziani, T. Q. Donaghy, M. Suzuki, G. Ricker, J. Atteia, N. Kawai, A. Yoshida, Y. Shirasaki, T. Tamagawa, K. Torii, M. Matsuoka, E. E. Fenimore, M. Galassi, J. Doty, R. Vanderspek, G. B. Crew, J. Villasenor, N. Butler, G. Prigozhin, J. G. Jernigan, C. Barraud, M. Boer, J. Dezalay, J. Olive, K. Hurley, A. Levine, G. Monnelly, F. Martel,

- E. Morgan, S. E. Woosley, T. Cline, J. Braga, R. Manchanda, G. Pizzichini, K. Takagishi, and M. Yamauchi. Global Characteristics of X-Ray Flashes and X-Ray-Rich GRBs Observed by HETE-2. *ArXiv Astrophysics e-prints*, September 2004. astro-ph/0409128.
- [329] T. Sakamoto, D. Q. Lamb, C. Graziani, T. Q. Donaghy, M. Suzuki, G. Ricker, J. Atteia, N. Kawai, A. Yoshida, Y. Shirasaki, T. Tamagawa, K. Torii, M. Matsuoka, E. E. Fenimore, M. Galassi, T. Tavenner, J. Doty, R. Vanderspek, G. B. Crew, J. Villasenor, N. Butler, G. Prigozhin, J. G. Jernigan, C. Barraud, M. Boer, J. Dezalay, J. Olive, K. Hurley, A. Levine, G. Monnelly, F. Martel, E. Morgan, S. E. Woosley, T. Cline, J. Braga, R. Manchanda, G. Pizzichini, K. Takagishi, and M. Yamauchi. HETE-2 Observations of the Extremely Soft X-Ray Flash XRF 020903. *ArXiv Astrophysics e-prints*, September 2003.
- [330] T. Sakamoto, D. Q. Lamb, C. Graziani, T. Q. Donaghy, M. Suzuki, G. Ricker, J.-L. Atteia, N. Kawai, A. Yoshida, Y. Shirasaki, T. Tamagawa, K. Torii, M. Matsuoka, E. E. Fenimore, M. Galassi, T. Tavenner, J. Doty, R. Vanderspek, G. B. Crew, J. Villasenor, N. Butler, G. Prigozhin, J. G. Jernigan, C. Barraud, M. Boer, J.-P. Dezalay, J.-F. Olive, K. Hurley, A. Levine, G. Monnelly, F. Martel, E. Morgan, S. E. Woosley, T. Cline, J. Braga, R. Manchanda, G. Pizzichini, K. Takagishi, and M. Yamauchi. High Energy Transient Explorer 2 Observations of the Extremely Soft X-Ray Flash XRF 020903. *ApJ*, 602:875–885, February 2004.
- [331] T. Sakamoto, D. Q. Lamb, C. Graziani, T. Q. Donaghy, M. Suzuki, G. Ricker, J.-L. Atteia, N. Kawai, A. Yoshida, Y. Shirasaki, T. Tamagawa, K. Torii, M. Matsuoka, E. E. Fenimore, M. Galassi, T. Tavenner, J. Doty, R. Vanderspek, G. B. Crew, J. Villasenor, N. Butler, G. Prigozhin, J. G. Jernigan, C. Barraud, M. Boer, J.-P. Dezalay, J.-F. Olive, K. Hurley, A. Levine, G. Monnelly, F. Martel, E. Morgan, S. E. Woosley, T. Cline, J. Braga, R. Manchanda, G. Pizzichini, K. Takagishi, and M. Yamauchi. High Energy

Transient Explorer 2 Observations of the Extremely Soft X-Ray Flash XRF 020903. *ApJ*, 602:875–885, February 2004.

- [332] T. Sakamoto, D. Q. Lamb, N. Kawai, A. Yoshida, C. Graziani, E. E. Fenimore, T. Q. Donaghy, M. Matsuoka, M. Suzuki, G. Ricker, J.-L. Atteia, Y. Shirasaki, T. Tamagawa, K. Torii, M. Galassi, J. Doty, R. Vanderspek, G. B. Crew, J. Villasenor, N. Butler, G. Prigozhin, J. G. Jernigan, C. Barraud, M. Boer, J.-P. Dezalay, J.-F. Olive, K. Hurley, A. Levine, G. Monnelly, F. Martel, E. Morgan, S. E. Woosley, T. Cline, J. Braga, R. Manchanda, G. Pizzichini, K. Takagishi, and M. Yamauchi. Global Characteristics of X-Ray Flashes and X-Ray-Rich Gamma-Ray Bursts Observed by HETE-2. *ApJ*, 629:311–327, August 2005.
- [333] M. Sako, R. Romani, J. Frieman, J. Adelman-McCarthy, A. Becker, F. DeJongh, B. Dilday, J. Estrada, J. Hendry, J. Holtzman, J. Kaplan, R. Kessler, H. Lampeitl, J. Marriner, G. Miknaitis, A. Riess, D. Tucker, J. Barentine, R. Blandford, H. Brewington, J. Dembicky, M. Harvanek, S. Hawley, C. Hogan, D. Johnston, S. Kahn, B. Ketzebach, S. Kleinman, J. Krzesinski, D. Lamenti, D. Long, R. McMillan, P. Newman, A. Nitta, R. Nichol, R. Scranton, E. Sheldon, S. Snedden, C. Stoughton, D. York, and the SDSS Collaboration. The Fall 2004 SDSS Supernova Survey. *ArXiv Astrophysics e-prints*, April 2005.
- [334] J. D. Salmonson. On the Kinematics of GRB 980425 and Its association with SN 1998BW. *ApJ*, 546:L29–L31, 2001.
- [335] M. Santos-Lleo, P. Calderon, and D. Gotz. GRB 031203 XMM-newton observation. 2003.
- [336] R. Sari. Hydrodynamics of gamma-ray burst afterglow. *ApJ*, 489:L37–L40, 1997.
- [337] R. Sari and T. Piran. GRB 990123: The Optical Flash and the Fireball Model. *ApJ*, 517:L109–L112, June 1999.

- [338] Re’Em Sari, Tsvi Piran, and J. P. Halpern. Jets in gamma-ray bursts. *ApJ*, 519:L17–L20, 1999.
- [339] Re’em Sari, Tsvi Piran, and Ramesh Narayan. Spectra and light curves of gamma-ray burst afterglows. *ApJ*, 497:L17, 1998.
- [340] I. Saviane, J. E. Hibbard, and R. M. Rich. The Stellar Content of the Southern Tail of NGC 4038/4039 and a Revised Distance. *AJ*, 127:660–678, February 2004.
- [341] S. Yu Sazonov, A. A. Lutovinov, and R. A. Sunyaev. An apparently normal gamma-ray burst with an unusually low luminosity. submitted to *Nature*, 2004.
- [342] P. Schady, K. O. Mason, J. P. Osborne, M. J. Page, P. W. A. Roming, M. Still, B. Zhang, A. J. Blustin, P. Boyd, A. Cucchiara, N. Gehrels, C. Gronwall, M. De Pasquale, S. T. Holland, F. E. Marshall, K. E. McGowan, and J. A. Nousek. Swift UVOT Observations of X-Ray Flash 050406. *ApJ*, 643:276–283, May 2006.
- [343] D. J. Schlegel, D. P. Finkbeiner, and M. Davis. Maps of dust infrared emission for use in estimation of reddening and cosmic microwave background radiation foregrounds. *ApJ*, 500:525–553, 1998.
- [344] D. J. Schlegel, D. P. Finkbeiner, and M. Davis. Maps of Dust Infrared Emission for Use in Estimation of Reddening and Cosmic Microwave Background Radiation Foregrounds. *ApJ*, 500:525–+, June 1998.
- [345] E. M. Schlegel, S. Ryder, L. Staveley-Smith, R. Petre, E. Colbert, M. Dopita, and D. Campbell-Wilson. Physical Properties of the X-Ray-Luminous SN 1978K in NGC 1313 from Multiwavelength Observations. *AJ*, 118:2689–2704, December 1999.
- [346] M. Schmidt. Luminosity function of gamma-ray bursts derived without benefit of redshifts. *ApJ* in press, astro-ph/0101163, 2001.

- [347] M. E. Sharina, I. D. Karachentsev, and N. A. Tikhonov. Photometric distances to NGC 628 and its four companions. *A&AS*, 119:499–507, November 1996.
- [348] J. Silvey, D. Allen, M. Bayliss, M. Nysewander, T. Tilleman, A. Henden, M. Leake, A. Homewood, R. Cantera, D. Reichart, D. H. Hartmann, and M. Schwartz. GRB 040924: Afterglow Color. *GRB Circular Network*, 2833, 2004.
- [349] M. Sirianni, M. J. Jee, N. Benítez, J. P. Blakeslee, A. R. Martel, G. Meurer, M. Clampin, G. De Marchi, H. C. Ford, R. Gilliland, G. F. Hartig, G. D. Illingworth, J. Mack, and W. J. McCann. The Photometric Performance and Calibration of the Hubble Space Telescope Advanced Camera for Surveys. *PASP*, 117:1049–1112, October 2005.
- [350] S. J. Smartt, J. R. Maund, M. A. Hendry, C. A. Tout, G. F. Gilmore, S. Mattila, and C. R. Benn. Detection of a Red Supergiant Progenitor Star of a Type II-Plateau Supernova. *Science*, 303:499–503, January 2004.
- [351] S. J. Smartt, P. M. Vreeswijk, E. Ramirez-Ruiz, G. F. Gilmore, W. P. S. Meikle, A. M. N. Ferguson, and J. H. Knapen. On the Progenitor of the Type Ic Supernova 2002ap. *ApJ*, 572:L147–L151, June 2002.
- [352] J. A. Smith, D. L. Tucker, S. Kent, M. W. Richmond, M. Fukugita, T. Ichikawa, S.-i. Ichikawa, A. M. Jorgensen, A. Uomoto, J. E. Gunn, M. Hamabe, M. Watanabe, A. Tolea, A. Henden, J. Annis, J. R. Pier, T. A. McKay, J. Brinkmann, B. Chen, J. Holtzman, K. Shimasaku, and D. G. York. The u'g'r'i'z' Standard-Star System. *AJ*, 123:2121–2144, April 2002.
- [353] A. M. Soderberg. A Broader Perspective on the GRB-SN Connection. In S. S. Holt, N. Gehrels, and J. A. Nousek, editors, *Gamma-Ray Bursts in the Swift Era*, volume 836 of *American Institute of Physics Conference Series*, pages 380–385, May 2006.

- [354] A. M. Soderberg, E. Berger, M. Kasliwal, D. A. Frail, P. A. Price, B. P. Schmidt, S. R. Kulkarni, D. B. Fox, S. B. Cenko, A. Gal-Yam, E. Nakar, and K. C. Roth. The Afterglow, Energetics and Host Galaxy of the Short-Hard Gamma-Ray Burst 051221a. *ArXiv Astrophysics e-prints*, January 2006. astro-ph/0601455.
- [355] A. M. Soderberg, R. A. Chevalier, S. R. Kulkarni, and D. A. Frail. The Radio and X-ray Luminous SN 2003bg and Circumstellar Density Variations Around Radio Supernovae. *ArXiv Astrophysics e-prints*, December 2005.
- [356] A. M. Soderberg, R. A. Chevalier, S. R. Kulkarni, and D. A. Frail. The Radio and X-Ray Luminous SN 2003bg and the Circumstellar Density Variations around Radio Supernovae. *ApJ*, 651:1005–1018, November 2006.
- [357] A. M. Soderberg, D. A. Frail, and M. A. Wieringa. Severe constraints on off-axis grb jets in type ibc supernovae from late-time radio observations. astro-ph/0402163, 2004.
- [358] A. M. Soderberg, A. Gal-Yam, and S. R. Kulkarni. Type Ic SN2001em (off-axis GRB jet?), optical spectrum. *GRB Circular Network*, 2586:1–+, 2004.
- [359] A. M. Soderberg, S. R. Kulkarni, E. Berger, R. A. Chevalier, D. A. Frail, D. B. Fox, and R. C. Walker. The Radio and X-Ray-Luminous Type Ibc Supernova 2003L. *ApJ*, 621:908–920, March 2005.
- [360] A. M. Soderberg, S. R. Kulkarni, E. Berger, D. B. Fox, P. A. Price, S. Yost, M. Hunt, D. A. Frail, C. Walker, M. Hamuy, S. Sheckman, J. Halpern, and N. Mirabal. A Redshift Determination for XRF 020903: First Spectroscopic Observations of an X-Ray Flash. *ApJ submitted*, astro-ph/0311050, 2003.
- [361] A. M. Soderberg, S. R. Kulkarni, E. Berger, D. B. Fox, P. A. Price, S. A. Yost, M. P. Hunt, D. A. Frail, R. C. Walker, M. Hamuy, S. A. Sheckman, J. P. Halpern, and N. Mirabal. A Redshift Determination for XRF 020903: First Spectroscopic Observations of an X-Ray Flash. *ApJ*, 606:994–999, May 2004.

- [362] A. M. Soderberg, S. R. Kulkarni, E. Berger, D. W. Fox, M. Sako, D. A. Frail, A. Gal-Yam, D. S. Moon, S. B. Cenko, S. A. Yost, M. M. Phillips, S. E. Persson, W. L. Freedman, P. Wyatt, R. Jayawardhana, and D. Paulson. The sub-energetic  $\gamma$ -ray burst GRB 031203 as a cosmic analogue to the nearby GRB 980425. *Nature*, 430:648–650, August 2004.
- [363] A. M. Soderberg, S. R. Kulkarni, D. B. Fox, E. Berger, P. A. Price, S. B. Cenko, D. A. Howell, A. Gal-Yam, D. C. Leonard, D. A. Frail, D. Moon, R. A. Chevalier, M. Hamuy, K. C. Hurley, D. Kelson, K. Koviak, W. Krzeminski, P. Kumar, A. MacFadyen, P. J. McCarthy, H. S. Park, B. A. Peterson, M. M. Phillips, M. Rauch, M. Roth, B. P. Schmidt, and S. Sheckman. An HST Search for Supernovae Accompanying X-Ray Flashes. *ApJ*, 627:877–887, July 2005.
- [364] A. M. Soderberg, S. R. Kulkarni, and D. A. Frail. GRB 031203: variable radio source. *GRB Circular Network*, 2483, 2003.
- [365] A. M. Soderberg, S. R. Kulkarni, E. Nakar, E. Berger, D. B. Fox, D. A. Frail, A. Gal-Yam, R. Sari, S. B. Cenko, M. Kasliwal, P. B. Cameron, R. A. Chevalier, T. Piran, P. A. Price, B. P. Schmidt, G. Pooley, D. . Moon, B. E. Penprase, N. Gehrels, J. A. Nousek, D. N. Burrows, S. E. Perrson, and P. J. McCarthy. Relativistic ejecta from XRF 060218 and the complete census of cosmic explosions. *ArXiv Astrophysics e-prints*, April 2006. astro-ph/0604389.
- [366] A. M. Soderberg, S. R. Kulkarni, P. A. Price, D. B. Fox, E. Berger, D.-S. Moon, S. B. Cenko, A. Gal-Yam, D. A. Frail, R. A. Chevalier, L. Cowie, G. S. Da Costa, A. MacFadyen, P. J. McCarthy, N. Noel, H. S. Park, B. A. Peterson, M. M. Phillips, M. Rauch, A. Rest, J. Rich, K. Roth, M. Roth, B. P. Schmidt, R. C. Smith, and P. R. Wood. An HST Study of the Supernovae Accompanying GRB 040924 and GRB 041006. *ApJ*, 636:391–399, January 2006.

- [367] A. M. Soderberg, E. Nakar, E. Berger, and S. R. Kulkarni. Late-Time Radio Observations of 68 Type Ibc Supernovae: Strong Constraints on Off-Axis Gamma-Ray Bursts. *ApJ*, 638:930–937, February 2006.
- [368] A. M. Soderberg, E. Nakar, S. B. Cenko, P. B. Cameron, D. A. Frail, S. R. Kulkarni, D. B. Fox, E. Berger, A. Gal-Yam, D. Moon, P. A. Price, G. Anderson, B. P. Schmidt, M. Salvo, J. Rich, A. Rau, E. O. Ofek, R. A. Chevalier, M. Hamuy, F. A. Harrison, P. Kumar, A. MacFadyen, P. J. McCarthy, H. S. Park, B. A. Peterson, M. M. Phillips, M. Rauch, M. Roth, and S. Sheckman. A Spectacular Radio Flare from XRF 050416a at 40 days and Implications for the Nature of X-ray Flashes. *ArXiv Astrophysics e-prints*, July 2006.
- [369] A. M. Soderberg, E. Nakar, and S. R. Kulkarni. Late-time Radio Observations of Type Ibc Supernovae: Strong Constraints on Off-axis Gamma-ray Bursts. *ArXiv Astrophysics e-prints*, July 2005. astro-ph/0507147.
- [370] A. M. Soderberg, E. Nakar, S. R. Kulkarni, and E. Berger. Late-time observations of Type Ibc supernovae. *ApJ*, 2005. in press.
- [371] A. M. Soderberg, P. A. Price, D. W. Fox, S. R. Kulkarni, S. G. Djorgovski, E. Berger, F. Harrison, S. Yost, M. Hamuy, S. Sheckman, N. Mirabal, and J. Halpern. XRF 020903: supernova. *GRB Circular Network*, 1554:1–+, 2002.
- [372] Y. Sohn and T. J. Davidge. Multicolor CCD Photometry of Supergiants in the Disk of NGC 628. *AJ*, 111:2280–+, June 1996.
- [373] J. Sollerman, B. Leibundgut, and J. Spyromilio. SN 1996N - A type Ib supernova at late phases. *A&A*, 337:207–215, September 1998.
- [374] R. A. Sramek, N. Panagia, and K. W. Weiler. Radio emission from a type I supernova - SN 1983.51 IN NGC 5236. *ApJ*, 285:L59–L62, October 1984.
- [375] K. Z. Stanek, P. M. Garnavich, P. A. Nutzman, J. D. Hartman, and A. Garg.

- Deep Photometry of GRB 041006 Afterglow: Hypernova Bump at Redshift  $z=0.716$ . *ArXiv Astrophysics e-prints*, February 2005. astro-ph/0502319.
- [376] K. Z. Stanek, O. Y. Gnedin, J. F. Beacom, A. P. Gould, J. A. Johnson, J. A. Kollmeier, M. Modjaz, M. H. Pinsonneault, R. Pogge, and D. H. Weinberg. Protecting Life in the Milky Way: Metals Keep the GRBs Away. astro-ph/0604113, April 2006.
- [377] K. Z. Stanek, T. Matheson, P. M. Garnavich, P. Martini, P. Berlind, N. Caldwell, P. Challis, W. R. Brown, R. Schild, K. Krisciunas, M. L. Calkins, J. C. Lee, N. Hathi, R. A. Jansen, R. Windhorst, L. Echevarria, D. J. Eisenstein, B. Pindor, E. W. Olszewski, P. Harding, S. T. Holland, and D. Bersier. Spectroscopic Discovery of the Supernova 2003dh Associated with GRB 030329. *ApJ*, 591:L17–L20, 2003.
- [378] C. J. Stockdale, B. Kaster, L. O. Sjouwerman, M. P. Rupen, I. Marti-Vidal, J. M. Marcaide, S. D. van Dyk, K. W. Weiler, B. Paczynski, and N. Panagia. Supernova 2001em in UGC 11794. *IAUC*, 8472:4–+, January 2005.
- [379] C. J. Stockdale, L. A. Maddox, J. J. Cowan, A. Prestwich, R. Kilgard, S. Immler, and M. Krauss. A Radio and X-Ray Study of Historical Supernovae in M83. *ArXiv Astrophysics e-prints*, November 2005. astro-ph/0511202.
- [380] C. J. Stockdale, R. A. Sramek, K. W. Weiler, S. D. Van Dyk, N. Panagia, M. J. Montes, and M. P. Rupen. The Radio Supernova 1994I. In *Cosmic Explosions: On the 10th Anniversary of SN1993J (IAU Colloquium 192)*, 2005.
- [381] C. J. Stockdale, S. D. Van Dyk, R. A. Sramek, K. W. Weiler, N. Panagia, M. P. Rupen, and B. Paczynski. SUPERNOVA 2001em IN UGC 11794. In *International Astronomical Union Circular*, number 8282, page 1, 2004.
- [382] C. J. Stockdale, S. D. Van Dyk, K. W. Weiler, N. Panagia, R. A. Sramek, B. Paczynski, and M. P. Rupen. Late-Time Radio Emission from Type Ib/c

- Supernovae: Testing the Oblique GRB Jet Model. *American Astronomical Society Meeting Abstracts*, 203:–+, December 2003.
- [383] M. Stritzinger, M. Hamuy, N. B. Suntzeff, R. C. Smith, M. M. Phillips, J. Maza, L.-G. Strolger, R. Antezana, L. González, M. Wischnjewsky, P. Candia, J. Espinoza, D. González, C. Stubbs, A. C. Becker, E. P. Rubenstein, and G. Galaz. Optical Photometry of the Type Ia Supernova 1999ee and the Type Ib/c Supernova 1999ex in IC 5179. *AJ*, 124:2100–2117, October 2002.
- [384] M. Sullivan, R. S. Ellis, G. Aldering, R. Amanullah, P. Astier, G. Blanc, M. S. Burns, A. Conley, S. E. Deustua, M. Doi, S. Fabbro, G. Folatelli, A. S. Fruchter, G. Garavini, R. Gibbons, G. Goldhaber, A. Goobar, D. E. Groom, D. Hardin, I. Hook, D. A. Howell, M. Irwin, A. G. Kim, R. A. Knop, C. Lidman, R. McMahon, J. Mendez, S. Nobili, P. E. Nugent, R. Pain, N. Panagia, C. R. Pennypacker, S. Perlmutter, R. Quimby, J. Raux, N. Regnault, P. Ruiz-Lapuente, B. Schaefer, K. Schahmaneche, A. L. Spadafora, N. A. Walton, L. Wang, W. M. Wood-Vasey, and N. Yasuda. The Hubble diagram of type Ia supernovae as a function of host galaxy morphology. *MNRAS*, 340:1057–1075, April 2003.
- [385] F. K. Sutaria, P. Chandra, S. Bhatnagar, and A. Ray. The nature of the prompt X-ray and radio emission from SN 2002ap. *A&A*, 397:1011–1018, January 2003.
- [386] D. A. Swartz, A. V. Filippenko, K. Nomoto, and J. C. Wheeler. Spectra of low-mass helium star models and the type IC supernova SN 1987M. *ApJ*, 411:313–322, July 1993.
- [387] M. Takada-Hidai, W. Aoki, and G. Zhao. Na I D Lines in the SN 2002ap Spectrum. *PASJ*, 54:899–903, December 2002.
- [388] J. C. Tan, C. D. Matzner, and C. F. McKee. Trans-Relativistic Blast Waves in Supernovae as Gamma-Ray Burst Progenitors. *ApJ*, 551:946–972, 2001.

- [389] S. Taubenberger, A. Pastorello, P. A. Mazzali, S. Valenti, G. Pignata, D. N. Sauer, A. Arbey, O. Bärnbantner, S. Benetti, A. Della Valle, J. Deng, N. Elias-Rosa, A. V. Filippenko, R. J. Foley, A. Goobar, R. Kotak, W. Li, P. Meikle, J. Mendez, F. Patat, E. Pian, C. Ries, P. Ruiz-Lapuente, M. Salvo, V. Stanishev, M. Turatto, and W. Hillebrandt. SN 2004aw: confirming diversity of Type Ic supernovae. *MNRAS*, 371:1459–1477, September 2006.
- [390] G. B. Taylor, D. A. Frail, and S. R. Kulkarni. The radio afterglow from the X-ray rich GRB 011030. *GRB Circular Network*, 1136:1–+, 2001.
- [391] H. Terada and M. Akiyama. GRB 040924: Subaru NIR observations. *GRB Circular Network*, 2742, 2004.
- [392] F. Thim, G. A. Tammann, A. Saha, A. Dolphin, A. Sandage, E. Tolstoy, and L. Labhardt. The Cepheid Distance to NGC 5236 (M83) with the ESO Very Large Telescope. *ApJ*, 590:256–270, June 2003.
- [393] A. Tiengo, S. Mereghetti, G. Ghisellini, E. Rossi, G. Ghirlanda, and N. Scharrel. The X-ray afterglow of GRB030329. *ArXiv Astrophysics e-prints*, pages 5564–+, May 2003.
- [394] N. Tominaga, J. Deng, P. A. Mazzali, K. Maeda, K. Nomoto, E. Pian, J. Hjorth, and J. P. U. Fynbo. Supernova Light-Curve Models for the Bump in the Optical Counterpart of X-Ray Flash 030723. *ApJ*, 612:L105–L108, September 2004.
- [395] N. Tominaga, M. Tanaka, K. Nomoto, P. A. Mazzali, J. Deng, K. Maeda, H. Umeda, M. Modjaz, M. Hicken, P. Challis, R. P. Kirshner, W. M. Wood-Vasey, C. H. Blake, J. S. Bloom, M. F. Skrutskie, A. Szentgyorgyi, E. E. Falco, N. Inada, T. Minezaki, Y. Yoshii, K. Kawabata, M. Iye, G. C. Anupama, D. K. Sahu, and T. P. Prabhu. The Unique Type Ib Supernova 2005bf: A WN Star Explosion Model for Peculiar Light Curves and Spectra. *ApJ*, 633:L97–L100, November 2005.

- [396] J. L. Tonry, A. Dressler, J. P. Blakeslee, E. A. Ajhar, A. B. Fletcher, G. A. Luppino, M. R. Metzger, and C. B. Moore. The SBF Survey of Galaxy Distances. IV. SBF Magnitudes, Colors, and Distances. *ApJ*, 546:681–693, January 2001.
- [397] K. Torii. GRB 050416: ART observations. *GRB Coordinates Network*, 3272:1–+, 2005.
- [398] T. Totani. A Failed Gamma-Ray Burst with Dirty Energetic Jets Spirited Away? New Implications for the Gamma-Ray Burst-Supernova Connection from SN 2002ap. *ApJ*, 598:1151–1162, 2003.
- [399] D. Y. Tsvetkov. Lightcurve of the Peculiar Supernova 1985F in NGC4618. *Soviet Astronomy Letters*, 12:328–+, October 1986.
- [400] D. Y. Tsvetkov. Light curves of type Ib supernova: SN 1984l in NGC 991. *Soviet Astronomy Letters*, 13:376–+, October 1987.
- [401] M. Turatto, T. Suzuki, P. A. Mazzali, S. Benetti, E. Cappellaro, I. J. Danziger, K. Nomoto, T. Nakamura, T. R. Young, and F. Patat. The Properties of Supernova 1997CY Associated with GRB 970514. *ApJ*, 534:L57–L61, May 2000.
- [402] P. G. Tuthill, J. D. Monnier, and W. C. Danchi. A dusty pinwheel nebula around the massive star WR 104. *Nature*, 398:487–489, 1999.
- [403] M. Uemura, R. Ishioka, T. Kato, and H. Yamaoka. GRB 021004: Kyoto observation. *GRB Circular Network*, 1566:1–1, 2002.
- [404] V. V. Usov. Millisecond pulsars with extremely strong magnetic fields as a cosmological source of gamma-ray bursts. *Nature*, 357:472–474, 1992.
- [405] S. Valenti, E. Cappellaro, S. Danese, G. Di Pede, H. Navasardyan, A. Pastorello, S. Benetti, and M. Turatto. Supernovae 2003L, 2003M, and 2003O. *IAUC*, 8057:2–+, January 2003.

- [406] P. G. van Dokkum and J. S. Bloom. XRF 020427: gemini-south spectroscopic observations of the host. *GRB Circular Network*, 2380, 2003.
- [407] S. D. van Dyk. Association of supernovae with recent star formation regions in late type galaxies. *AJ*, 103:1788–1803, June 1992.
- [408] S. D. van Dyk, R. A. Sramek, K. W. Weiler, and N. Panagia. The radio emission from the type IC supernova SN 1990B. *ApJ*, 409:162–169, May 1993.
- [409] S. D. van Dyk, K. W. Weiler, R. A. Sramek, M. P. Rupen, and N. Panagia. SN 1993J: The early radio emission and evidence for a changing presupernova mass-loss rate. *ApJ*, 432:L115–L118, September 1994.
- [410] R. Vanderspek et al. Hete observations of the gamma-ray burst grb030329: Evidence for an underlying soft x-ray component. astro-ph/0401311, 2004.
- [411] J. S. Villaseñor, D. Q. Lamb, G. R. Ricker, J.-L. Atteia, N. Kawai, N. Butler, Y. Nakagawa, J. G. Jernigan, M. Boer, G. B. Crew, T. Q. Donaghy, J. Doty, E. E. Fenimore, M. Galassi, C. Graziani, K. Hurley, A. Levine, F. Martel, M. Matsuoka, J.-F. Olive, G. Prigozhin, T. Sakamoto, Y. Shirasaki, M. Suzuki, T. Tamagawa, R. Vanderspek, S. E. Woosley, A. Yoshida, J. Braga, R. Manchanda, G. Pizzichini, K. Takagishi, and M. Yamauchi. Discovery of the short  $\gamma$ -ray burst GRB 050709. *Nature*, 437:855–858, October 2005.
- [412] J. Vinkó, R. M. Blake, K. Sárneczky, B. Csák, G. Furész, S. Csizmadia, L. L. Kiss, G. M. Szabó, R. Szabó, H. DeBond, M. M. De Robertis, J. R. Thomson, and S. W. Mochnacki. Distance of the hypernova SN 2002ap via the expanding photosphere method. *A&A*, 427:453–464, November 2004.
- [413] L. Wang, D. Baade, P. Höflich, and J. C. Wheeler. Spectropolarimetry of the Type Ic Supernova SN 2002ap in M74: More Evidence for Asymmetric Core Collapse. *ApJ*, 592:457–466, July 2003.

- [414] L. Wang and J. C. Wheeler. The supernova-gamma ray burst connection. *ApJ*, 504:L87–L90, 1998.
- [415] D. Watson, J. Hjorth, A. Levan, P. Jakobsson, P. T. O’Brien, J. P. Osborne, K. Pedersen, J. N. Reeves, J. A. Tedds, S. A. Vaughan, M. J. Ward, and R. Willingale. A very low luminosity X-ray flash: XMM-Newton observations of GRB 031203. submitted to *ApJL*, 2004.
- [416] D. Watson, E. Pian, J. N. Reeves, J. Hjorth, and K. Pedersen. SN 2003jd (SN/GRB?) – X-ray observations. *GRB Circular Network*, 2445:1–+, 2003.
- [417] E. Waxman. The nature of GRB980425 and the search for off-axis GRB signatures in nearby type Ib/c supernovae emission. *ApJ*, in press; astro-ph/0310320, October 2003.
- [418] E. Waxman. Does the detection of X-ray emission from SN1998bw support its association with GRB980425? *ApJ*, submitted; astro-ph/0401551, January 2004.
- [419] K. W. Weiler, N. Panagia, and M. J. Montes. SN 1998bw/GRB 980425 and Radio Supernovae. *ApJ*, 562:670–678, December 2001.
- [420] K. W. Weiler, N. Panagia, and R. A. Sramek. Radio emission from supernovae. II - SN 1986J: A different kind of type II. *ApJ*, 364:611–625, December 1990.
- [421] K. W. Weiler, R. A. Sramek, N. Panagia, J. M. van der Hulst, and M. Salvati. Radio supernovae. *ApJ*, 301:790–812, February 1986.
- [422] K. W. Weiler, R. A. Sramek, J. M. van der Hulst, and N. Panagia. Radio supernovae. In *NATO ASIC Proc. 90: Supernovae: A Survey of Current Research*, pages 281–291, November 1982.
- [423] K. W. Weiler, S. D. van Dyk, J. L. Discenna, N. Panagia, and R. A. Sramek. The 10 year radio light curves for SN 1979C. *ApJ*, 380:161–166, October 1991.

- [424] K. W. Weiler, S. D. van Dyk, M. J. Montes, N. Panagia, and R. A. Sramek. Radio Supernovae as Distance Indicators. *ApJ*, 500:51–+, June 1998.
- [425] K. W. Weiler, S. D. van Dyk, J. E. Pringle, and N. Panagia. Evidence for periodic modulation of presupernova mass loss from the progenitor of SN 1979 C. *ApJ*, 399:672–679, November 1992.
- [426] J. C. Wheeler and R. P. Harkness. Physical models of supernovae and the distance scale. In B. F. Madore and R. B. Tully, editors, *NATO ASIC Proc. 180: Galaxy Distances and Deviations from Universal Expansion*, pages 45–54, 1986.
- [427] J. C. Wheeler and R. P. Harkness. Type I supernovae. *Reports of Progress in Physics*, 53:1467–1557, 1990.
- [428] J. C. Wheeler, R. P. Harkness, E. S. Barker, A. L. Cochran, and D. Wills. Supernovae 1983i and 1983v - Evidence for abundance variations in type Ib supernovae. *ApJ*, 313:L69–L73, February 1987.
- [429] J. C. Wheeler and R. Levreault. The peculiar Type I supernova in NGC 991. *ApJ*, 294:L17–L20, July 1985.
- [430] K. Wiersema, S. Savaglio, P. M. Vreeswijk, S. L. Ellison, C. Ledoux, S.-C. Yoon, P. Møller, J. Sollerman, J. P. U. Fynbo, E. Pian, R. L. C. Starling, and R. A. M. J. Wijers. The nature of the dwarf starforming galaxy associated with GRB 060218/SN 2006aj. *A&A*, 464:529–539, March 2007.
- [431] K. Wiersema, R. L. C. Starling, E. Rol, P. Vreeswijk, and R. A. M. J. Wijers. GRB 040924: VLT spectroscopy. *GRB Circular Network*, 2800, 2004.
- [432] R. A. M. J. Wijers. Strange Afterglows from Embedded GRBs: Reconciling Hypernovae with Slow Decays. In E. Costa, F. Frontera, and J. Hjorth, editors, *Gamma-ray Bursts in the Afterglow Era*, pages 306–+, 2001.

- [433] C. L. Williams, N. Panagia, S. D. Van Dyk, C. K. Lacey, K. W. Weiler, and R. A. Sramek. Radio Emission from SN 1988Z and Very Massive Star Evolution. *ApJ*, 581:396–403, December 2002.
- [434] W. M. Wood-Vasey and R. Chassagne. Supernovae 2003bf and 2003bg. *IAUC*, 8082:1–+, February 2003.
- [435] S. E. Woosley and J. S. Bloom. The Supernova/Gamma-Ray Burst Connection. *ARAA*, 44:507–556, September 2006.
- [436] S. E. Woosley, Ronald G. Eastman, and Brian P. Schmidt. Gamma-ray bursts and type ic supernova sn 1998bw. *ApJ*, 516:788–796, May 1999.
- [437] S. E. Woosley, A. Heger, and T. A. Weaver. The evolution and explosion of massive stars. *Reviews of Modern Physics*, 74:1015–1071, November 2002.
- [438] S. E. Woosley, N. Langer, and T. A. Weaver. The Presupernova Evolution and Explosion of Helium Stars That Experience Mass Loss. *ApJ*, 448:315–+, July 1995.
- [439] R. Yamazaki, K. Ioka, and T. Nakamura. Cosmological X-Ray Flashes in the Off-Axis Jet Model. *ApJ*, 593:941–945, August 2003.
- [440] R. Yamazaki, D. Yonetoku, and T. Nakamura. An Off-Axis Jet Model For GRB 980425 and Low-Energy Gamma-Ray Bursts. *ApJ*, 594:L79–L82, 2003.
- [441] R. Yamazaki, D. Yonetoku, and T. Nakamura. An Off-Axis Jet Model For GRB 980425 and Low-Energy Gamma-Ray Bursts. *ApJ*, 594:L79–L82, September 2003.
- [442] T. Yamazaki, G. Ricker, J-L. Atteia, N. Kawai, D. Lamb, and S. Woosley. GRB040916 (=H3558): A Long XRF Localized by HETE. *GRB Circular Network*, 2712, 2004.
- [443] T. Yamazaki, G. Ricker, J-L. Atteia, N. Kawai, D. Lamb, and S. Woosley.

- GRB040916 (=H3558): A Long XRF Localized by HETE. *GRB Circular Network*, 2713, 2004.
- [444] K. Yanagisawa, H. Toda, and N. Kawai. GRB 050416: Mitsume optical observation. *GRB Coordinates Network*, 3287:1–+, 2005.
- [445] S. A. Yost, F. A. Harrison, R. Sari, and D. A. Frail. A Study of the Afterglows of Four Gamma-Ray Bursts: Constraining the Explosion and Fireball Model. *ApJ*, 597:459–473, November 2003.
- [446] M. S. Yun and C. L. Carilli. Radio-to-Far-Infrared Spectral Energy Distribution and Photometric Redshifts for Dusty Starburst Galaxies. *ApJ*, 568: 88–98, March 2002.
- [447] A. Zeh, S. Klose, and D. H. Hartmann. A Systematic Analysis of Supernova Light in Gamma-Ray Burst Afterglows. *ApJ*, 609:952–961, July 2004.
- [448] Y. B. Zel’dovich and Y. P. Raizer. *Physics of Shock Waves and High Temperature Hydrodynamic Phenomena*. Dover, Mineola, NY, 2002.
- [449] Bing Zhang and Peter Meszaros. Gamma-ray bursts: Progress, problems & prospects. Submitted to *Int.J.Mod.Phys.A.*; astro-ph/0311321, 2003.
- [450] W. Zhang, S. E. Woosley, and A. Heger. The Propagation and Eruption of Relativistic Jets from the Stellar Progenitors of Gamma-Ray Bursts. *ApJ*, 608:365–377, June 2004.
- [451] W. Zhang, S. E. Woosley, and A. I. MacFadyen. Relativistic Jets in Collapsars. *ApJ*, 586:356–371, 2003.